Edited by
Matthias Driess, Heinrich Nöth

WILEY-VCH

Molecular Clusters of the Main Group Elements

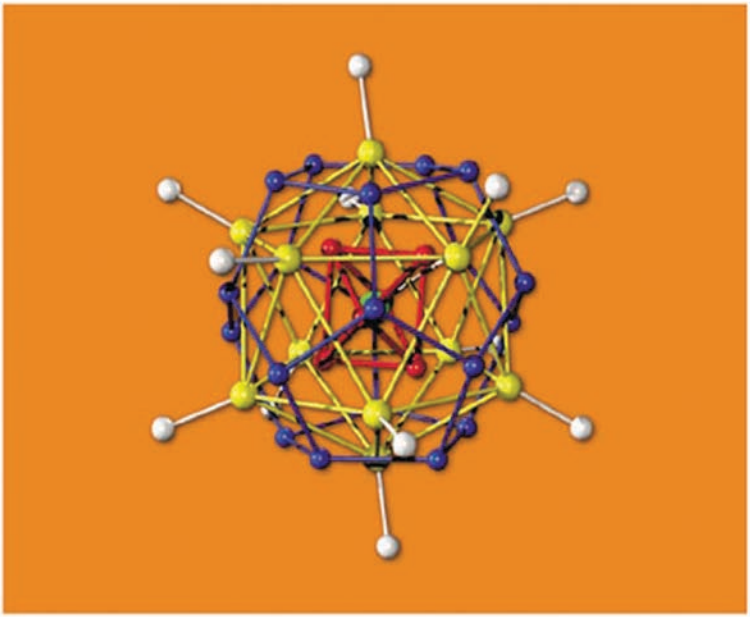

Matthias Driess, Heinrich Nöth (Eds.)
Molecular Clusters of the Main Group Elements

Further Titles of Interest:

G. Schmid (Ed.)

Nanoparticles

From Theory to Application

2003
ISBN 3-527-30507-6

P. Jutzi, U. Schubert (Eds.)

Silicon Chemistry

From the Atom to Extended Systems

2003
ISBN 3-527-30647-1

P. Braunstein, L. A. Oro, P. R. Raithby (Eds.)

Metal Clusters in Chemistry

1999
ISBN 3-527-29549-6

U. Schubert, N. Hüsing

Synthesis of Inorganic Materials

2000
ISBN 3-527-29550-X

P. Comba, T. W. Hambley

Molecular Modeling of Inorganic Compounds

2001
ISBN 3-527-29915-7

Matthias Driess, Heinrich Nöth (Eds.)

Molecular Clusters of the Main Group Elements

WILEY-VCH Verlag GmbH & Co. KGaA

Prof. Matthias Driess
Ruhr-Universität Bochum
Fakultät für Chemie
Lehrstuhl für Anorganische Chemie I:
Cluster- und Koordinations-Chemie
44780 Bochum
Germany

Prof. Heinrich Nöth
Ludwig-Maximilians-Universität München
Department Chemie
Butenandt Str. 5-13 (Haus D)
81377 Munich
Germany

Library of Congress Card No.: applied for
A catalogue record for this book is available from the British Library.
Bibliographic information published by Die Deutsche Bibliothek
Die Deutsche Bibliothek lists this publication in the Deutsche Nationalbibliografie; detailed bibliographic data is available in the Internet at http://dnb.ddb.de

Printed in the Federal Republic of Germany.
Printed on acid-free paper.

Typesetting Asco Typesetters, Hong Kong
Printing Strauss Offsetdruck Gmbh, Mörlenbach
Bookbinding Litges & Dopf Buchbinderei GmbH, Heppenheim

ISBN 3-527-30654-4

Contents


2003

Preface

The past 10 years have witnessed spectacular discoveries in the field of molecular cluster chemistry of the main-group elements: that is the reason for this book! It is timely to provide a survey of a number of important developments in this field, particularly only because the synthesis, functionalization, and theoretical concepts of novel molecular cluster systems are currently one of the most promising challenges in modern inorganic chemistry. Today, molecular clusters are used as one of the profound constituents of a variety of applications, ranging from materials science with nanoscaled atomic aggregates (e.g., metal clusters as molecular transistors) to medical targets (e.g., boron-rich clusters for boron-neutron-capture-therapy, BNCT). Additionally, one can envision that obtaining simple routes to many different element clusters with tunable electronic properties could significantly accelerate the development of molecular electronics and nanorobots, which are aims of a promising future. Clusters of the chemical elements show a tremendous variety of chemical and physical properties even if they consist of identical sorts of atoms. This is due to the fact that atoms can be connected topologically differently by spatially directed chemical bonds, thus leading to a molecular polyhedral skeleton with a different shape. This is particularly evident by the spectacular discovery of the spherically shaped carbon clusters (fullerenes C_{60}, C_{70}, C_{78} etc.), which have inspired many chemists and physicists to investigate related ''naked'' clusters of main-group elements and their chemical functionalization. About 10 years ago, most of the cluster chemistry of the main-group elements was devoted to cluster systems that form very stable atomic aggregates (cluster skeletons). Of prime importance were polyboranes, the prototype for the investigation of cluster formation of the main-group elements. Many boron compounds (boron hydrides, heteroboranes such as carba-, aza-, and metallaboranes, and several subvalent boron halides) inherently possess aggregate (cluster) structures with a deltapolyhedral shape (e.g., tetrahedral, octahedral, or icosahedral skeletons). The secret of the extraordinary properties of these classees of compounds is based on their unusual bonding state, which cannot be described by classical (localized) two-center two-electron covalence bonds but through multiple center bonds. Multiple-center (cluster) bonds lend such systems super stability similar to that in aromatic compounds in organic chemistry. It has been the credit of W.N. Lipscomb (Nobel Price winner 1976) who showed for the first time that deltapolyhedral structures of

polyboranes can be understood on the basis of modified valence rules by using a multiple-center-bonding description. However, more than 20 years passed before the first clusters of the boron-congeners (aluminum, gallium, indium, and thallium clusters) were synthesized. Not only that, unlike the chemistry of polyboron and heteropolyboron compounds, little or nothing was known about the formation, stability, or functionalizability of related homo- and heteronuclear molecular clusters of other heavier main-group elements, e.g., those involving group 14 and 15 elements. Since main-group chemistry has a strong and very successful tradition in Germany, several leading experts in the field of molecular cluster chemistry decided to establish the priority research program "Assembling and Functionalization of Polyhedral Clusters of the Main-Group Elements" in1994 (until 2002) under the auspices of the German Research Council (Deutsche Forschungsgemeinschaft). The research program was devoted to the discovery of unknown territory in cluster chemistry of the main-group element. It was worth the effort: our knowledge of molecular clusters of the main-group elements dramatically increased during that period of time: this is evident when looking at the spectacular discovery of the first Al_{77}- and Ga_{84}-clusters, which represent the largest molecular main-group metal clusters hitherto structurally characterized. We believe that the novel landscape of cluster compounds discussed in this book will lead to new exciting applications in chemistry, physics, biology and materials science in the near future.

We particularly thank the German Research Council ("Deutschen Forschungsgemeinschaft") for generous financial support during the period of the priority-program "Assembling and Functionalization of Polyhedral Clusters of the Main-Group Elements" ("Aufbau und Funktionalisierung von Polyedergerüsten aus Hauptgruppenelementen"), which enabled us to write this book. The priority-program would not have been possible without the commitment and initiatives of Prof. Dr. Walter Siebert (Heidelberg), Prof. Dr. Gottfried Huttner (Heidelberg) and the editors. We also thank Dr. Karlheinz Schmidt for his untiring supreme organizational care of the scientific projects during the priority-program. Last but not least, on behalf of all participants of the priority-program, We would like to express my thanks to the scientific referees of the program, Prof. Dr. Kurt Dehnicke (Marburg), Prof. Dr. Dieter Fenske (Karlsruhe), Prof. Dr. Bernt Krebs (Münster), Prof. Dr. Werner Kutzelnigg (Bochum), Prof. Dr. Michael Lappert (Sussex, U.K.), Prof. Dr. Günter Schmid (Essen) and Prof. Dr. Michael Veith (Saarbrücken), for their scientific advice and helpful discussions.

We hope that this book will be a source of inspiration for many colleagues in molecular and material sciences.

Bochum/München, December 2003

Matthias Driess
Heinrich Nöth

List of Contributors

Prof. Armin Berndt
Berndt@chemie.uni-marburg.de
Phillips-Universität Marburg
Fachbereich Chemie
Hans-Meerwein-Straße
D-35032 Marburg
Germany

Prof. Hans-Jörg Deiseroth
Deiseroth@chemie.uni-siegen.de
Fakultät für Chemie der Universität Siegen
Adolf-Reichwein-Straße 9
D-57068 Siegen
Germany

Prof. Matthias Driess
Matthias.Driess@rub.de
Ruhr-Universität Bochum
Fakultät für Chemie
Lehrstuhl für Anorganische Chemie I:
Cluster- und Koordinations-Chemie
D-44780 Bochum
Germany

Prof. Yasuyuki Endo
yendo@tohoku-pharm.ac.jp
Laboratory of Organic and Medicinical Chemistry
Tohoku Pharmaceutical University
4-4-1, Komatsushima, Aoba-ku,
Sendai 981-8558
Japan

Prof. Detlef Gabel
Gabel@chemie.uni-bremen.de
Institut für Organische Chemie
Universität Bremen
Leobener Straße
D-28359 Bremen
Germany

Dr. Matthias Hofmann
Universität Heidelberg
Institut für Anorganische Chemie
Im Neuenheimer Feld 270
D-69120 Heidelberg
Germany

Prof. Narayan Hosmane
Nhosmane@niu.edu
Department of Chemistry & Biochemistry
Northern Illinois University
De Kalb
IL 60115-2862
USA

Prof. R. Bruce King
Rbking@sunchem.chem.uga.edu
Department of Chemistry
University of Georgia
Athens
GA 30602
USA

Dr. Ingo Krossing
Krossing@achpc9.chemie.uni-karlsruhe.de
Universität Karlsruhe
Institut für Anorganische Chemie
Engesserstraße 15
D-76128 Karlsruhe
Germany

Prof. Gerald Linti
Gerald.linti@urz.uni-heidelberg.de
Universität Heidelberg
Institut für Anorganische Chemie
Im Neuenheimer Feld 270
D-69120 Heidelberg
Germany

Prof. Robert Mulvey
r.e.mulvey@strath.ac.uk
Department of Pure and Applied Chemistry
University of Strathclyde
295 Cathedral Street

Glasgow G1 1XL
UK

Prof. Heinrich Nöth
H.Noeth@lrz-uni-muenchen.de
Ludwig-Maximilians-Universität München
Institut für Anorganische Chemie
Butenandtstraße 5–13 (Haus D)
D-81377 München
Germany

Prof. Peter Paetzold
Peter.Paetzold@AC.RWTH-Aachen.de
Institut für Anorganische Chemie
RWTH Aachen
Professor-Pirlet-Straße 1
D-52074 Aachen
Germany

Prof. Philip P. Power
Pppower@ucdavis.edu
Department of Chemistry
University of California at Davis
One Shield Avenue
Davis
CA 95616
USA

Prof. Herbert W. Roesky
Hroesky@gwdg.de
Institut für Anorganische Chemie
der Georg-August Universität Göttingen
Tammannstraße 4
D-37077 Göttingen
Germany

Prof. Paul v. R. Schleyer
Schleyer@chem.uga.edu
Department of Chemistry
University of Georgia
Athens
GA 30602
USA

Prof. Hansgeorg Schnöckel
Hansgeorg.Schnoeckel@chemie.uni-karlsruhe.de
Universität Karlsruhe
Institut für Anorganische Chemie
Engesserstraße 15
D-76131 Karlsruhe
Germany

Prof. William S. Sheldrick
Shel@anachem.ruhr-uni-bochum.de
Ruhr-Universität Bochum
Fakultät für Chemie
Lehrstuhl für Analytische Chemie
D-44780 Bochum
Germany

Prof. Walter Siebert
Ci5@ix.urz.uni-heidelberg.de
Universität Heidelberg
Institut für Anorganische Chemie
Im Neuenheimer Feld 270
D-69120 Heidelberg
Germany

Prof. Arndt Simon
A.Simon@fkf.mpg.de
Max-Planck-Institut für Festkörperforschung
Heisenbergstraße 1
D-70569 Stuttgart
Germany

Prof. Werner Uhl
Uhl@chemie.uni-marburg.de
Fachbereich Chemie der Philipps-Universität
Marburg
Institut für Anorganische Chemie
Hans-Meerwein-Straße
D-35032 Marburg
Germany

Prof. Lars Wesemann
Lars.wesemann@uni-tuebingen-de
Institut für Anorganische Chemie
Universität Tübingen
Auf der
Morgenstelle 18
D-72076 Tübingen
Germany

Prof. Matthias Westerhausen
Maw@cup.uni-muenchen.de
Ludwig-Maximilians-Universität München
Institut für Anorganische Chemie
Butenandtstraße 5–13 (Haus D)
D-81377 München
Germany

Prof. Nils Wiberg
niw@cup.uni-muenchen.de
Ludwig-Maximilians-Universität München
Institut für Anorganische Chemie
Butenandtstraße 5–13 (Haus D)
D-81377 München
Germany

Prof. Bernd Wrackmeyer
B.Wrack@uni-bayreuth.de
Universität Bayreuth
Lehrstuhl für Anorganische Chemie II
Universitätsstraße 30,
Gebäude NWI
D-95440 Bayreuth
Germany

1
Theory and Concepts in Main-Group Cluster Chemistry

R. Bruce King and Paul v. R. Schleyer

1.1
Introduction

The main group cluster chemistry discussed in this book can be considered to originate from two important, but apparently unrelated developments in inorganic chemistry in the 1930s. The first was the identification of the neutral boron hydrides by Stock [1]. The second was the observation by Zintl and co-workers [2–5] of anionic clusters formed from potentiometric titrations of post-transition metals (i.e., heavy main group elements) with sodium in liquid ammonia.

Understanding the structure and chemical bonding in these new types of inorganic molecules proceeded rather slowly after these original discoveries. In the 1950s, Lipscomb used the fundamental concept of three-center two-electron bonding [6–8] to develop a topological model that explained the structures of the known neutral boron hydrides of the general types B_nH_{n+4} and B_nH_{n+6} (Figure 1-1). Subsequently, Williams [9] recognized that the structures of these neutral boranes could be considered to be fragments of the "most spherical" deltahedra (Figure 1-2) with the most uniformly or most homogeneously connected vertices. Such polyhedra only have triangular faces. As many of their vertices as possible have degrees four or five. The "degree" is the number of edges meeting at a vertex. The degree is the same whether or not an external hydrogen or group is attached. The deltahedral borane dianions [10] $B_nH_n^{2-}$ and isoelectronic carboranes [11] $C_2B_{n-2}H_n$ ($6 \leq n \leq 12$) had just been discovered. Most of these species were considerably more stable than the neutral boron hydrides, B_nH_{n+4} and B_nH_{n+6}. This led to the concept of three-dimensional aromaticity, first suggested explicitly by Aihara [12] in 1978. The particularly favorable icosahedral units found in the very stable $B_{12}H_{12}^{2-}$ and in the three $C_2B_{10}H_{12}$ isomers were predicted computationally by Longuet-Higgins and Roberts in 1955 [13]. Similar B_{12} icosahedral units are also found in the structures of refractory solid state materials such as elemental boron [14] and boron carbide (B_4C) [15]. In 1971 Wade [16] recognized that the stability of the deltahedral boranes $B_nH_n^{2-}$ and isoelectronic species was related to the presence of $2n + 2$ skeletal electrons in such structures. Shortly afterwards these ideas were incorporated by Mingos [17, 18] into his "polyhedral skeletal

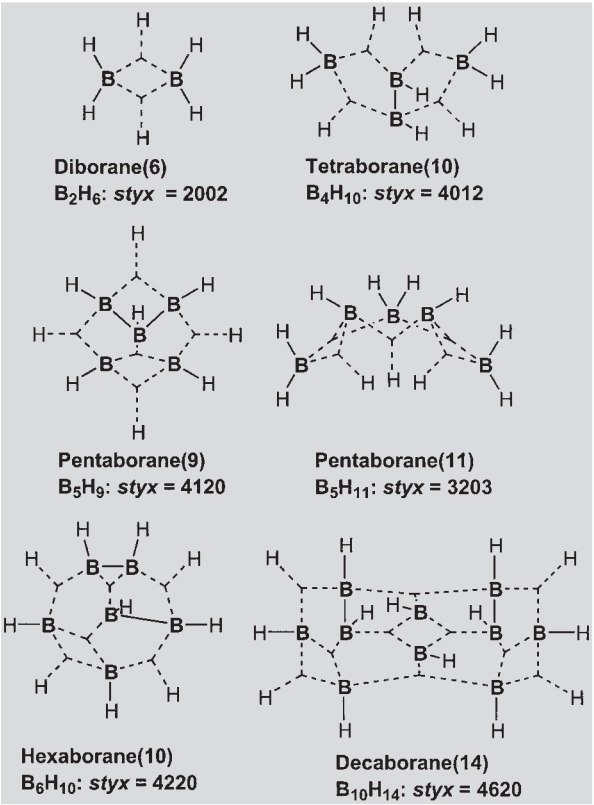

Fig. 1-1. The original neutral boron hydrides (boranes) isolated by Stock along with their *styx* numbers.

electron pair approach'' for the understanding of the structural diversity of polyhedral boranes. Consequently, these theoretical electron-counting schemes are now frequently called the ''Wade-Mingos rules.'' Subsequent work showed that the Wade-Mingos rules are applicable not only to polyhedral boranes but also to clusters both of main group elements and of transition metals.

Understanding the nature of the anionic bare post-transition metal clusters (i.e., the heavier main group elements), first observed by Zintl and co-workers [2–5] in liquid ammonia titrations, was hindered by difficulties in isolating pure crystalline phases whose structures could be determined by X-ray diffraction methods. Corbett and co-workers finally solved this problem in 1975 [19] by complexing the alkali metal counterion with 2,2,2-crypt to obtain crystalline products. Their initial report [19] of the structure of Sb_7^{3-} was followed by the elucidation of the geometries of numerous other bare post-transition metal anions, such as E_9^{2-} and E_9^{4-} (E = Ge, Sn), E_5^{2-} (E = Sn, Pb), and E_4^{2-} (E = Sb, Bi) [20]. In addition, salts of bare post-transition metal cations, such as the subvalent bismuth Bi_5^{3+}, Bi_8^{2+}, and Bi_9^{5+}, were isolated from strongly Lewis acidic reaction mixtures as single

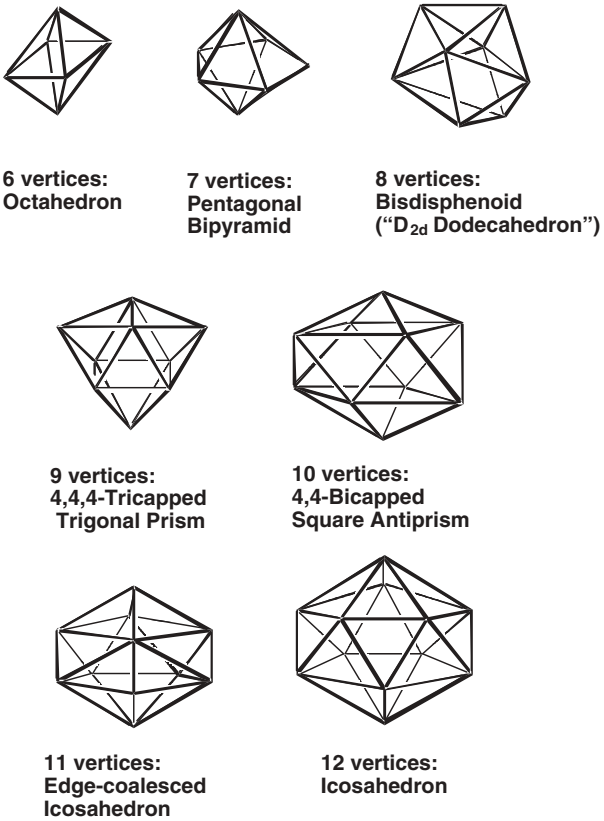

Fig. 1-2. The "most nearly spherical" deltahedra found in the boranes $B_nH_n^{2-}$ ($6 \leq n \leq 12$) and isoelectronic carboranes.

crystals, which could be characterized by X-ray analysis [21]. After sufficient structural data on bare post-transition metal clusters had accumulated, isoelectronic relationships between these clusters and the polyhedral boranes became apparent. Evidently, similar principles of structure and bonding were applicable to both types of molecules.

During the past decade the number and variety of main group element clusters has expanded drastically, particularly with the heavier group 13 metals. Thus, some organometallic group 13 metal analogues of the polyhedral boranes have been isolated and characterized including the icosahedral dianion $[Al_{12}Bu^i_{12}]^{2-}$ and the tricapped trigonal prismatic $Ga_9Bu^t_9$ (both discussed below), as well as more complicated organoaluminum and organogallium clusters that are best interpreted as fused, nested, or capped deltahedra (see Chapter 2.3.3.2) [22]. The larger organometallic clusters include Al_{69} and Al_{77} derivatives with five-fold symmetry that may be considered as icosahedral quasicrystal fragments [23]. A few examples of smaller clusters of heavier group 13 metals are also known, even including triangular

$[Ga_3R_3]^{2-}$ (R = bulky aryl group) [24], isoelectronic with the aromatic cyclopropenium cation. In addition, tin clusters exhibit a variety of interesting cage structures (see Chapter 2.5.4) [25].

1.1.1 Three-center Bonding in Boranes: Lipscomb's Equations of Balance

The unusual compositions and geometries of the neutral boron hydrides (Figure 1-1) stimulated efforts to understand their structure and bonding. In this connection, Lipscomb and co-workers [6–8] recognized that the prevalence of three-center bonds was the particular feature distinguishing three-dimensional boranes (based on the trivalent element, boron) both from the two-dimensional planar hydrocarbons (constituted by trivalent sp^2 carbons) as well as from the alkanes (which require the fourth valence of carbon to be three-dimensional). In the usual two-center two-electron covalent bond, two atoms supply two orbitals, one centered on each atom. These atomic orbitals interact to form one bonding and one antibonding orbital. If two electrons are available, they will just fill the bonding orbital. If the elements have nearly the same electronegativities, as in the typical hydrocarbons, the standard covalent σ-bond results.

Such two-center two-electron bonds accommodate as many electrons as atomic orbitals. Thus, if n atomic orbitals form a bonding network using two-center two-electron bonds exclusively, as in the saturated hydrocarbons, they form $n/2$ bonding (valence) orbitals which accommodate n electrons. For example, ethane C_2H_6 has one C–C and six C–H two-center two-electron bonds formed by the 14 atomic orbitals originating from the eight valence orbitals of the two carbon atoms and the six 1s orbitals of the six hydrogen atoms. These 14 atomic orbitals use the 14 valence electrons (four each from the two carbon atoms and a total of six from the hydrogen atoms) effectively, since all valence MOs are filled and all antibonding virtual orbitals are empty. The same is true of unsaturated hydrocarbons with multiple bonds.

In the cyclic three-center two-electron bonding found in boranes, three atoms supply three orbitals, one on each atom. These atomic orbitals interact to form one bonding and two antibonding orbitals so that only two electrons can be accommodated favorably. These fill the bonding orbital to form a three-center two-electron bond. If n atomic orbitals interact to form three-center two-electron bonds exclusively, only $n/3$ bonding orbitals result and only $2n/3$ electrons can be accommodated. Hence, three-center two-electron bonding (H_3^+ is the simplest example) is utilized in "electron deficient" compounds, which have fewer bonding electrons than atomic orbitals. Diborane, B_2H_6 (Figure 1-1), is a simple example of an electron-deficient compound. The combination of the two boron and the six hydrogen atoms provides the same 14 atomic valence orbitals as the two carbons and six hydrogens of ethane. However, the two boron atoms and six hydrogen atoms provide only 12 valence electrons. Hence, diborane is electron deficient; there are not enough electrons to form seven covalent σ-bonds. This electron deficiency leads to the $B_2H_4(\mu\text{-}H)_2$ diborane structure, consisting of four two-center

two-electron external B–H bonds and two three-center two-electron B–H–B bonds involving the bridging hydrogen atoms (Figure 1-1).

Using completely analogous bonding principles, Lipscomb and co-workers [6–8] delineated the topologies of the distribution of two-center two-electron B–B and three-center two-electron B–B–B bonds in the networks of boron atoms constituting the higher boron hydrides. The following assumptions constitute Lipscomb's bonding analysis:

1. Only the 1s orbital of hydrogen and the four sp^3 orbitals of boron are used.
2. Each external (i.e., terminal) B–H bond is regarded as a typical two-center two-electron single bond requiring the hydrogen 1s orbital, one hybridized boron orbital, and one electron each from the H and the B atoms. Because of the small electronegativity difference between hydrogen and boron, these bonds are assumed to be non-polar. In the polynuclear boron hydrides every boron atom may form zero or one but never more than two such external B–H bonds.
3. Each B–H–B three-center two-electron "bridge" bond corresponds to a filled three-center localized bonding orbital requiring the hydrogen orbital and one hybrid orbital from each boron atom.
4. The orbitals and electrons of any particular boron atom are allocated to satisfy, as first priority, the requirements of the external B–H single bonds and the bridge B–H–B bonds. The remaining orbitals and electrons are allocated to the skeletal molecular orbitals of the boron framework.

The relative numbers of orbitals, electrons, hydrogen, and boron atoms as well as bonds of various types were expressed systematically by Lipscomb [6–8].

Assuming that each boron atom is bonded to at least one hydrogen atom, the hydrogen balance in a neutral boron hydride B_pH_{p+q} containing s bridging hydrogen atoms, x "extra" two-center two-electron B–H bonds in terminal BH_2 groups rather than in BH groups, t three-center two-electron B–B–B bonds, and y 2c2e B–B bonds is given by $s + x = q$. Since each boron atom supplies four orbitals but only three electrons, the total number of three-center two-electron bonds in the molecule is the same as the number of boron atoms, namely $s + t = p$. This leads to the following equations of balance:

$$2s + 3t + 2y + x = 3p \quad \text{(orbital balance with 3 orbitals/BH vertex)} \tag{1a}$$

$$s + 2t + 2y + x = 2p \quad \text{(electron balance with 2 } \textit{skeletal} \text{ electrons/BH vertex)} \tag{1b}$$

Using this approach the structure of a given borane can be expressed by a four-digit *styx* number corresponding to the numbers of B–H–B, B–B–B, and B–B bonds, and BH_2 groups, respectively. For example the *styx* numbers for the structures for the boranes originally discovered by Stock (Figure 1-1) are 2002 for B_2H_6, 4012 for B_4H_{10}, 4120 for B_5H_9, 3203 for B_5H_{11}, 4220 for B_6H_{10}, and 4620 for $B_{10}H_{14}$.

"Resonance" was a central idea in the historical development of the aromaticity concept. The combination of two (or more) hypothetical "classical" Lewis contributors [26] gave a weighted-average "resonance hybrid." This "real" structure has lower energy due to the "aromatic resonance stabilization" [27, 28]. Further examples of resonance stabilization are found in triangular molecules. Thus the cyclopropenylium ion ($C_3H_3^+$, D_{3h}) is a simple example with a 3c–2e π bond. There are three equivalent resonance contributors, each with a different placement of the C=C double bond. An even simpler example is H_3^+ (also D_{3h}) where the three resonance contributors have H–H single bonds. The two-electron two-center B–B bonds and the three-center two-electron B–B–B bonds in polyhedral boranes have a similar relationship to the alternating single C–C and double C=C bond Kekulé structures of benzene.

Consider the *closo*-$B_nH_n^{2-}$ ($6 \leq n \leq 12$) boranes (Figure 1-2). Such deltahedral boranes cannot have any terminal BH_2 groups or three-center two-electron B–H–B bonds but acquire two "extra" electrons from the −2 charge on the ion. Therefore $s = x = 0$ in the equations of balance (1a) and (1b); these reduce to (2a) and (2b) in which n is the number of boron atoms in the deltahedron corresponding to p in (1a) and (1b):

$$3t + 2y = 3n \quad \text{(orbital balance for } B_nH_n^{2-}\text{)} \tag{2a}$$

$$2t + 2y = 2n + 2 \quad \text{(electron balance for } B_nH_n^{2-}\text{)} \tag{2b}$$

Solving the simultaneous equations (2a) and (2b) leads to $y = 3$ and $t = n - 2$, implying the presence of three B–B bonds and $n - 2$ B–B–B bonds in the boron skeleton. Since a deltahedron with n vertices has $2n - 4$ faces, the $n - 2$ B–B–B bonds cover exactly half of the faces. In this sense a Kekulé-type structure for the deltahedral boranes $B_nH_n^{2-}$ has exactly half of the faces covered by B–B–B bonds just as a Kekulé structure for benzene has half of its edges covered by C=C double bonds. In 1977 Lipscomb and co-workers [29] reported a variety of such Kekulé-type localized bonding structures with the lowest energies for deltahedral boranes. These structures were computed using wave functions in the differential overlap approximation.

1.1.2
Polyhedral Skeletal Electron Pair Theory: The Wade-Mingos Rules

Structural information on the boranes $B_nH_n^{2-}$ ($6 \leq n \leq 12$) shows all of these ions to have the "most spherical" deltahedral structures (Figure 1-2) as suggested by Williams in 1971 [9]. In addition Williams [9] also recognized that the loss of boron vertices from these most spherical *closo* deltahedra generates the structures of the known boranes B_nH_{n+4} and B_nH_{n+6} (Figure 1-1). Thus the *nido* boranes B_nH_{n+4} (Figure 1-3) and isoelectronic carboranes have structures which can be derived from the corresponding $B_{n+1}H_{n+1}^{2-}$ structure by the loss of the vertex with the highest degree (i.e., the most highly connected vertex). Similarly, the *arachno*

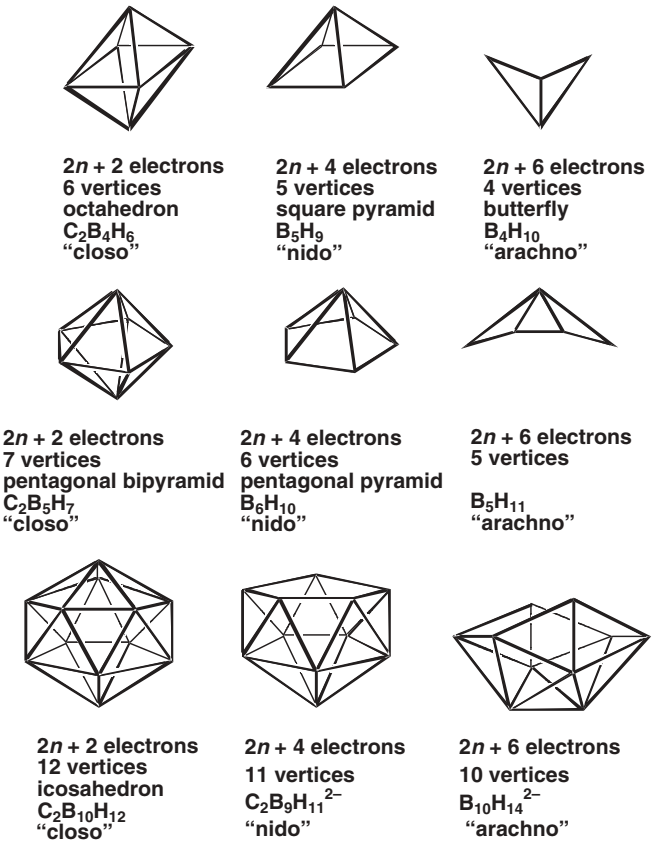

Fig. 1-3. Examples of *nido* and *arachno* boranes obtained by removal of vertices from the octahedron, pentagonal bipyramid, and icosahedron.

boranes B_nH_{n+6} (Figure 1-3) are related to those of the corresponding $B_{n+2}H_{n+2}^{2-}$ structure by the loss of a pair of adjacent vertices of relatively high degree. The role of the most spherical deltahedra (Figure 1-2) in all of these structures suggest that they are particularly stable structural units in borane chemistry, similar to the planar benzenoid rings in the chemistry of aromatic hydrocarbons and their derivatives.

The next important contribution in this area was made shortly thereafter by Wade [16], who recognized that this structural relationship could be related to the number of valence electrons associated with skeletal bonding in the boranes. Thus deprotonation of all of the bridging hydrogens from the related series of boranes $B_nH_n^{2-}$, $B_{n-1}H_{(n-1)+4}$, and $B_{n-2}H_{(n-2)+6}$ gives the ions $B_nH_n^{2-}$, $B_{n-1}H_{n-1}^{4-}$, and $B_{n-2}H_{n-2}^{6-}$. All of these ions can readily be seen to have the same number of skeletal electron pairs, namely $n + 1$, corresponding to $2n + 2$ skeletal electrons.

Consequently, Wade [16] provided an electronic rationale for the observations of Williams [9], namely that the *closo*, *nido*, and *arachno* structures are related because they share a common number of bonding molecular orbitals associated with the boron skeleton. Rudolph and Pretzer [30, 31] subsequently provided the first attempt to account for the structural and electronic relationships proposed by Williams and Wade using semi-empirical molecular orbital calculations. Finally, Mingos [17, 18] incorporated these ideas into his "polyhedral skeletal electron pair approach," which provides a simple way of understanding the structural diversity shown by polynuclear molecules. Because of the seminal work of Wade and Mingos in understanding electron counting in polyhedral molecules, the rules assigning $2n + 2$ skeletal electrons to deltahedral boranes (Figure 1-2) and related *nido* and *arachno* derivatives (Figure 1-3) as well as other similar polyhedral molecules (e.g., certain transition metal carbonyl clusters) are frequently called the "Wade-Mingos Rules."

Balakrishnarajan and Jemmis [32, 33] have very recently extended the Wade-Mingos rules from isolated borane deltahedra to fused borane ("*conjuncto*") deltahedra. They arrive at the requirement of $n + m$ skeletal electron pairs corresponding to $2n + 2m$ skeletal electrons for such fused deltahedra having n total vertices and m individual deltahedra. Note that for a single deltahedron (i.e., $m = 1$) the Jemmis $2n + 2m$ rule reduces to the Wade-Mingos $2n + 2$ rule.

1.1.3 Aromaticity in Three-dimensional Clusters

1.1.3.1 From Polygonal Aromatics to Deltahedral Boranes

The *closo* boranes $B_nH_n^{2-}$ ($6 \leq n \leq 12$), along with their isoelectronic counterparts, the carboranes, $CB_{n-1}H_n^-$ and $C_2B_{n-2}H_n$, as well as the newly computed azaboranes $NB_{n-1}H_n$ [34], exemplify three-dimensional aromatics. These comprise the most nearly spherical deltahedra (Figure 1-2) in which all vertices have degrees 4 or larger and the vertex degrees are as nearly equal as possible. In such structures, BH vertices provide two skeletal electrons each. Similarly, CH vertices and their isoelectronic equivalents (e.g., BH^- and N) provide three skeletal electrons each. Each vertex atom can be considered to have four valence orbitals, but, because of the coordination higher than four, these can not be arranged tetrahedrally. One orbital forms a conventional two-center two-electron bond to a hydrogen atom or other external group (or a lone pair) leaving only three "internal" orbitals for the skeletal bonding to four or more adjacent vertices. For three-dimensional structures, these three orbitals are partitioned into two p-like, degenerate "tangential" orbitals and a unique "radial" orbital extending towards the interior. Pairwise overlap of the $2n$ twin tangential orbitals results in n bonding and n antibonding MO combinations. In the three-dimensional deltahedral systems, the tangential orbitals contribute to the bonding over the two-dimensional surface of the deltahedron, which may be regarded as topologically homeomorphic to the sphere [35]. Note that the conventional polygonal aromatics, like benzene, utilize the perpendicular set of their tangential orbitals for π bonding.

The bonding and antibonding tangential orbitals are supplemented, when allowed by symmetry, by additional bonding and antibonding orbitals formed by the overlap of the n radial orbitals. Graph–theoretical methods have been used to describe the global overlap of these n unique internal orbitals [36]. The vertices of this graph correspond to the vertex atoms of the polygon or deltahedron and the edges represent pairs of overlapping unique internal orbitals [36, 37]. The adjacency matrix [38] **A** of such a graph can be defined as follows:

$$A_{ij} = \begin{cases} 0 & \text{if } i = j \\ 1 & \text{if } i \text{ and } j \text{ are connected by an edge} \\ 0 & \text{if } i \text{ and } j \text{ are not connected by an edge} \end{cases} \tag{3}$$

The eigenvalues of the adjacency matrix are obtained from the following determinantal equation:

$$|\mathbf{A} - x\mathbf{I}| = 0 \tag{4}$$

in which **I** is the unit matrix ($I_{ij} = 1$ and $I_{ij} = 0$ for $i \neq j$). These topologically derived eigenvalues are closely related to the energy levels as determined by Hückel theory which uses the secular equation

$$|\mathbf{H} - E\mathbf{S}| = 0 \tag{5}$$

Note the general similarities between Eqs. (4) and (5). In equation (5) the energy matrix **H** and the overlap matrix **S** can be resolved into the identity matrix **I** and the adjacency matrix **A** as follows:

$$\mathbf{H} = \alpha\mathbf{I} + \beta\mathbf{A} \tag{6a}$$

$$\mathbf{S} = \mathbf{I} + S\mathbf{A} \tag{6b}$$

The energy levels of the Hückel molecular orbitals [Eq. (5)] are thus related to the eigenvalues x_k of the adjacency matrix **A** (equation 4) by the following equation:

$$E_k = \frac{\alpha + x_k\beta}{1 + x_k\mathrm{S}} \tag{7}$$

In Eq. (7) α is the standard Coulomb integral, assumed to be the same for all atoms, β is the resonance integral taken to be the same for all bonds, and S is the overlap integral between atomic orbitals on neighboring atoms. Because of the relationship of the set of the eigenvalues of a graph to the energy levels of the molecular orbitals of a structure represented by the graph in question as indicated by Eqs. (4) to (7), the set of eigenvalues of a graph is called the *spectrum* of the graph, even by mathematicians solely concerned with graph theory with no interest in its chemical applications.

First consider planar polygonal aromatic systems, where the twin internal orbitals (a degenerate set of tangential orbitals on each vertex atom) are related to the π MOs. These systems include benzene and its non-carbon analogues like the N_5^- [39] and P_5^- pentagons [40], the Bi_4^{2-} [41a] and Al_4^{2-} squares [40b], and the $[Ga_3R_3]^{2-}$ (R = 2,6-dimesityl-phenyl) triangle [24]. In such structures, a cyclic graph, C_n, corresponding to the geometry of the polygon, describes the overlap of the unique internal (''radial'') orbitals, where n is the number of polygonal vertices. Regardless of n, the spectra of the cyclic graphs C_n [Eqs. (3) and (4)] all have odd numbers of positive eigenvalues [42] leading to the familiar Hückel $4N + 2$ (N = integer) π-electrons [43] (corresponding to $2N + 1$ π bonding MOs) for planar aromatic hydrocarbons. Thus, the carbon skeleton of benzene has nine bonding orbitals (six σ and three π) occupied by the 18 skeletal electrons arising from the contributions of three skeletal electrons from each CH vertex. Twelve of these 18 skeletal electrons are used for the σ CC bonding and the remaining six electrons for the π-bonding.

These same principles can be extended to systems, such as H_3^+, with delocalized multicenter σ-bonding derived solely from the radial s-orbital combinations. The descriptive term, ''in-plane aromaticity,'' [44] includes such cases (see Chapter 3.2.1 for further discussion).

In three-dimensional deltahedral boranes and their relatives, the overlap among the n internal radial orbitals forms n-center core bonding and antibonding combinations. In graph theory, the complete graph, K_n, has an edge between every pair of vertices. This leads to a total of $n(n-1)/2$ edges and best represents the corresponding overlap topology [45] as well as providing a description of an n-center 2-electron bond. In this graph–theoretical method, the underlying symmetry group is S_n of order $n!$ and corresponds to all possible permutations of the n radial orbitals rather than to the actual symmetry point group of the deltahedron.

For any value of n, the corresponding complete graph K_n has only one positive eigenvalue, namely $n - 1$, and $n - 1$ negative eigenvalues, namely -1 each, as obtained from Eq. (3), which refers to an $n \times n$ matrix, and Eq. (4). The single positive eigenvalue of the K_n complete graph corresponds to *only* one core bonding orbital. The remaining $n - 1$ orbitals arising from the negative eigenvalues of the graph–theoretical spectrum [Eq. (3)] of a deltahedron become antibonding. Combining the single bonding core orbital with the n surface bonding orbitals leads to $n + 1$ bonding orbitals for a deltahedron with n vertices. Filling each of these $n + 1$ bonding orbitals with electron pairs leads to the $2n + 2$ skeletal electrons required by the Wade-Mingos rules [16–18] for deltahedral clusters.

Furthermore, the combination of the n surface and the single core bonding orbitals in globally delocalized deltahedra corresponds to the n σ-bonding ring orbitals and the $2N + 1$ π-bonding orbitals, respectively, in polygonal aromatic systems such as benzene. Since N is always zero for globally delocalized deltahedra in this graph theoretical method, the Hückel $4N + 2$ electron rule for planar polygons is followed, just as it is for the cyclopropenylium ion $C_3H_3^+$ and related triangular species such as $[Ga_3R_3]^{2-}$ [24]. Until recently the largest deltahedral metal-free boranes following the $2n + 2$ skeletal electron rule were the icosahedral derivatives

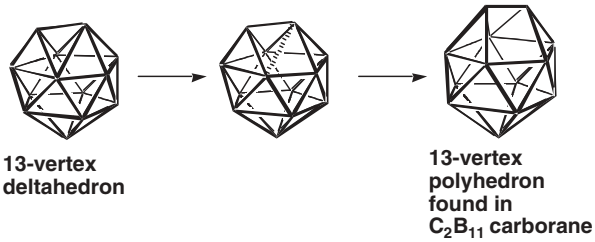

Fig. 1-4. Generation of the 13-vertex polyhedron found in 1,2-μ-[$C_6H_4(CH_2)_2$]-1,2-$C_2B_{11}H_{10}$-3Ph by breaking a single edge (hashed line) in a 13-vertex deltahedron.

$B_{12}R_{12}^{2-}$ (R = H, halogen, alkyl, etc.) and their isoelectronic carboranes $CB_{11}R_{12}^{-}$ and $C_2B_{10}R_{10}$. However, very recently [46, 47] the 13-vertex supraicosahedral carborane 1,2-μ-[$C_6H_4(CH_2)_2$]-1,2-$C_2B_{11}H_{10}$-3Ph was reported. The key to the successful synthesis of this supraicosahedral carborane was to force the two carbon vertices to remain adjacent by bridging them with the *o*-phenylene group $C_6H_4 \cdot (CH_2)_2$. Interestingly enough the 13-vertex polyhedron found for this carborane was not the expected deltahedron but instead a polyhedron derived from a 13-vertex deltahedron by breaking one of its 33 edges to give a single trapezoidal face (Figure 1-4).

More advanced mathematical aspects of the graph–theoretical models for aromaticity are given in other references [36, 48, 49]. Some alternative methods, beyond the scope of this chapter, for the study of aromaticity in deltahedral molecules include tensor surface harmonic theory [51–53] and the topological solutions of non-linear field theory related to the Skyrmions of nuclear physics [54].

1.1.3.2 Interstitial Polygonal Aromatic–Deltahedral Borane Relationships

The graph–theoretical $4N + 2$ Hückel rule analogy with the aromaticity of two-dimensional polygons requires that $N = 0$ in all the three-dimensional deltahedra. The Jemmis-Schleyer interstitial electron rule [55], originally introduced for *nido* "half-sandwich" species, also relates the $4N + 2$ Hückel rule to the delocalized deltahedra directly. In this treatment, N is typically 1.

In order to apply the Jemmis-Schleyer interstitial electron rule, the *closo* $B_nH_n^{2-}$ dianions (their isoelectronic analogues are treated similarly) are dissected conceptually into two BH^- "caps" and one or two constituent $(BH)_n$ rings. The BH^- caps contribute three interstitial electrons each but the rings (which, formally, have zero electrons in the π MOs), contribute none. Hence, six electrons, described as "interstitial," link the bonding symmetry-adapted cap and ring orbitals together perfectly.

The bonding analysis of the 50 $B_{12}H_{12}^{2-}$ valence electrons is illustrative. After the conceptual dissection into two BH caps and two $(BH)_5$ rings, two electrons each are assigned to the 12 BH bonds and to the 10 BB ring bonds. This leaves six electrons $(4N + 2)$ for the interstitial bonding, which holds the rings and caps together. Icosahedral symmetrization then completes the description.

Each of the two methods, namely the graph–theory and interstitial electron methods, has its advantages and disadvantages. The Jemmis-Schleyer interstitial electron rules are directly applicable to 5, 6, and 7-vertex deltahedra (which have one ring), and to 10, 11, and 12-vertex deltahedra (which have two rings) but are less obvious for 8- and 9-vertex deltahedra. (Two $B_2H_2^-$ caps supply three interstitial electrons each to the central D_{2d}-puckered B_4H_4 ring of $B_8H_8^{2-}$, whereas the six interstitial electrons are provided by the three, widely separated central BH "caps" in D_{3h} $B_9H_9^{2-}$. In the latter, the electrons from the −2 charge on the ion can be assigned to a weak 3c2c bond involving the three BH "caps.")

The interstitial electron rule can be applied more directly to pyramidal clusters than the graph–theoretical approximation since the latter breaks down by giving zero eigenvalues in Eq. (3) when applied to pyramids. The same ideas as those in the Jemmis-Schleyer method are needed to treat *nido* pyramids graph–theoretically.

1.1.3.3 Aromaticity Evaluations of Three-dimensional Structures: Nucleus-Independent Chemical Shift (NICS)

Chemical nomenclature and the usage of descriptive terms evolve over the years. "Aromaticity" was employed only to describe planar fully π conjugated organic and isoelectronic inorganic systems for well over a century, until it became increasingly apparent that some degree of out-of-plane distortion, for example in Vogel's bridged [10]annulenes, could be tolerated. In such structures the p-orbitals are twisted somewhat, but π overlap is still effective. Ferrocene (and its relatives) are fundamentally different geometrically from arenes. Half-sandwich, sandwich, and multi-sandwich molecules are also clearly "aromatic" but their electronic structures involve the third dimension. Nevertheless, it can be argued that their theoretical essence is still two-dimensional, since the maximum possible molecular orbital degeneracy of such systems is only two. Likewise, Möbius systems with undulating electronic topologies provide further examples of "aromatic three dimensional molecules." Rzepa has described inorganic examples with undulating Möbius MOs [56].

Aihara introduced the term, "three dimensional aromaticity" (featured in the title of his paper), to discuss *closo*-borane dianions in 1978 [12]. Jemmis and Schleyer applied the term to *nido* systems with six interstitial electrons [55], but their treatment emphasized the Hückel analogy, rather than the spherical character.

The fullerenes illustrate further conceptual and also practical problems, common to main group clusters generally. Clearly, fullerenes are physically three-dimensional and are aromatic (at least to some extent). But how does one know? How can one deduce the extent of aromaticity quantitatively? Is C_{60} best regarded as an assembly of interconnected planar rings, aromatic six-membered and anti-aromatic five-membered, or does it have "global" aromatic character involving the whole ensemble? C_{60}^{6-}, for example, can be regarded as just such a "super-aromatic," where the total aromaticity is more than the sum of the contributions of the constituent rings.

The fullerene, C_{60}, as an example of a main-group element cluster, shows very few properties of benzene, the aromatic paradigm. Fullerene derivatives are not pleasantly odoriferous. C_{60} does not undergo typical aromatic reactions. There are no hydrogens to substitute or to display arene-type NMR chemical shifts. C_{60} undergoes addition reactions more readily than benzene. The bond lengths are not all equal and some are significantly longer than in benzene. C_{60} is highly persistent (''stable'') but the geometrical distortion (''strain'') precludes reliable, quantitative estimation of the aromatic stabilization energy (ASE), which is less than 1% of the total bonding (atomization) energy. While these ''classical'' aromaticity criteria can be applied to some main group clusters (e.g., the cage boranes [57], see below), most other inorganic cluster families (e.g., the Zintl and other elemental cages) are unsuitable. Fortunately, magnetic criteria provide general evaluation methods for all these species.

Local circulations of electrons in molecules are induced by external magnetic fields. When a molecule has a cyclically delocalized electronic structure, ''ring currents'' of larger magnitude than the local contributions are generated. These result from behavior resembling that of electrons free to move in a circular wire. These ''ring currents'' generate a secondary magnetic field, which opposes the applied field. Hence, the substance is repelled ''diatropically'' in a magnetic field gradient. Consequently, the ''magnetization'' or ''magnetic susceptibility'' of aromatic molecules is ''exalted'' (larger than normal, based on increment schemes or non-aromatic models). Conversely, anti-aromatic molecules exhibit temperature-independent paramagnetic susceptibilities. Unfortunately, not many magnetic susceptibility measurements have been carried out experimentally on closed-shell main group clusters, and exaltation evaluations are very rare. Because the three principal axes are the same or nearly so, magnetic susceptibility anisotropy is not applicable to clusters.

Although magnetic susceptibilities and NMR chemical shifts have been computed routinely by quantum mechanics programs for well over a decade, ''ring current'' theory applied to chemical shifts has been employed far more widely as an aromaticity criterion. As every organic chemist knows, ^{1}H NMR signals (and those of other elements) located in the ''shielding cone'' above or even inside the ring are shifted upfield, whereas nuclei outside the ring plane are ''deshielded'' to positions downfield [58]. Does such behavior also pertain to globular clusters endohedrally and exohedrally?

Saunders et al. were the first to measure the chemical shift of a ^{3}He as an ''aromaticity probe atom'' inside C_{60} (-6.3 ppm) and C_{70} (-28.8 ppm) in 1994 [59]. Reliable computations reproducing and extending these findings, which showed C_{60} to be weakly and C_{70} to be more strongly aromatic, followed quickly [59b]. Li^+ behaved like He computationally. Logically, the next step would be to compute just the magnetic shielding (without any atom) at key points, e.g., in the center of rings and clusters. This is the basis of NICS, introduced in 1996 [60].

Many electronic structure programs, widely used to compute chemical shifts of atoms [61], can be used routinely to compute NICS employing ''ghost atoms'' at chosen points. The sign of absolute shieldings obtained in this manner are merely

reversed to conform to the chemists' sign convention (negative upfield, positive downfield). Since NICS, like chemical shifts, are influenced by the local magnetic effects of 2c2e bonds, it is useful interpretively to "dissect" the total NICS values into contributions of localized orbitals [62] (which are like chemical bonds, lone pairs, and core electrons) or contributions of the individual canonical MOs [63]. This not only gives the π contributions of an arene, but the other MOs also provide instructive and often surprising insights [64]. These LMO and MO analyses provide complimentary interpretive information, and will be widely used in future, not just for NICS interpretations, but also for the analysis of element chemical shifts.

The problem of distinguishing "aromaticity" in species, which merely have three-dimensional geometries, from situations where the "aromaticity" requires or at least strongly depends on the special nature or characteristics of three-dimensional systems, can be addressed easily by NICS evaluations. The circulation of "mobile electrons" in a more conventional aromatic system involves a single circuit (either in a plane or traversing an undulating geometry). The "mobile electrons" in a strictly defined three-dimensional aromatic system utilize three circuits, representing the principal dimensions for their delocalization.

Each 3c–2e deltahedral bonding component in boranes, carboranes, nonclassical carbocations, cyclopropenyl cation, etc., is "aromatic" in the sense of involving a ring current and giving diatropic NICS, magnetic susceptibility exaltation, energetic stabilization, etc. Since three centers define a plane, the 3c–2e deltahedral units in an *arachno* or a *nido* borane may be regarded individually (as in a *styx* assignment), or, alternatively, two or more such units also might combine in forming canonical molecular orbitals. B_2H_6 is a simple example. The nonclassical bonding is often explained as involving two 3c–2e BHB units. The alternative MO picture uses two orbitals ($1B_{2u}$ and $3A_g$). Since the two boron and the two bridging hydrogen atoms participate in each, a "4c–4e" (or a double 4c–2e) bonding description is equally valid. Larger boranes with non-planar geometries offer similar interpretive alternatives, also with regard to the contributions to the total aromaticity of a molecule.

As examples of the behavior of *arachno* and *nido* species, B_2H_6, B_4H_{10}, and $B_{10}H_{14}$ with a number of NICS points are shown in Figure 1-5, along with a picture of *closo*-$B_{12}H_{12}^{2-}$ for comparison. Note that the sizes of the points (which indicate the numerical NICS values) are large in the centers of the triangles (BBB faces and bridged BHB components), and then fall off in magnitude away from these centers. However, the NICS point in the center of the icosahedron in *closo*-$B_{12}H_{12}^{2-}$ (shown by the arrow) is larger than expected considering the distance from the deltahedral faces. The *nido*-$B_{10}H_{14}$ behavior provides calibration; the NICS point in its center (shown by the arrow) is significantly smaller than in $B_{12}H_{12}^{2-}$. The larger NICS in the center of $B_{12}H_{12}^{2-}$ can possibly be ascribed to the operation of "true three-dimensional aromaticity" in such *closo* clusters, that is, a global effect involving all the cage borons instead of a local effect involving the sum of effects from the individual deltahedral BBB faces. However, this distinction is not clear, as $B_{10}H_{14}$ offers fewer contributing faces than $B_{12}H_{12}^{2-}$. Species which do not exhibit special global effects may be better described as "aromatic three dimensional molecules," rather than as "true three dimensional aromatics."

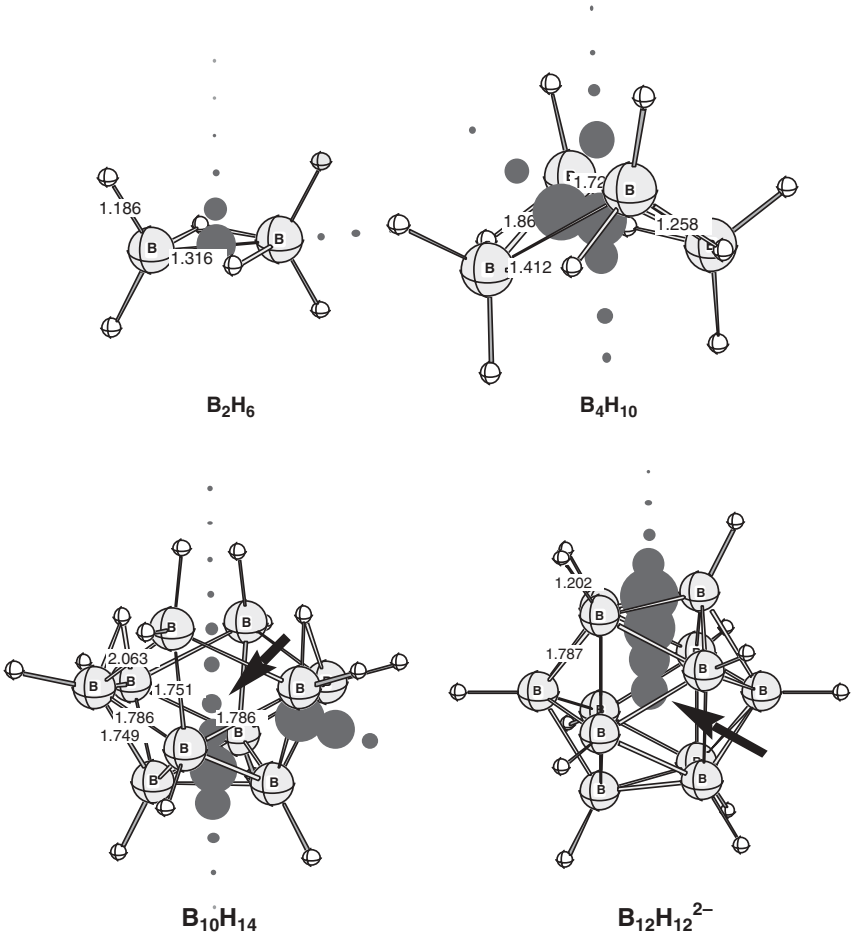

Fig. 1-5. Comparisons of NICS for various boranes. The size of the points depends on the magnitude of NICS, and the dark grey color signifies diatropic (shielding) behavior.

However, *nido* clusters, such as the capped-ring $C_4B_2H_6$ to B_6H_{10} family (which follow the six interstitial electron rule) also may exhibit three-dimensional aromaticity. The values of centrally-located NICS points are generally quite large. Although such species also have deltahedral faces, they can be regarded as having a higher degree (e.g., 6c–6e) of delocalized multicenter bonding. However, like the [*n*]annulenes, the maximum orbital degeneracy considered in the treatment is two.

Building on and extending earlier studies, Schleyer, Najafian, et al. [57] employed computed geometric, energetic, and magnetic properties to quantify the aromaticity of the *closo* boranes $B_nH_n^{2-}$ $(6 \leq n \leq 12)$, and their isoelectronic counterparts, the $CB_{n-1}H_n^-$ and $C_2B_{n-2}H_n$ carboranes, and the $NB_{n-1}H_n$ azaboranes [34]. All possible heteroatom placements were considered. The most stable iso-

mers showed striking parallels in the behavior of the various criteria (variation in bond lengths, NICS, magnetic susceptibility exaltation, and energy progression). In general, earlier conclusions were confirmed: the 6- and 12-vertex species were the most aromatic, followed by those with 10 vertices. However, the NICS values did not mirror the energies of the various positional isomers, owing to other influences.

An important distinction concerning spherical aromaticity was emphasized: the aromatic stabilization energies (ASE) of these three-dimensional *closo* cages increase *per vertex* with cluster size, in contrast to two-dimensional aromatics. Polycyclic benzenoid hydrocarbon ASE/carbon values generally decrease slightly with the number of rings and the monocyclic [*n*]annulene ASE/carbon energies fall off rapidly with ring size [65].

1.1.3.4 Spherical Aromaticity

Hirsch has developed a $2(n+1)^2$ electron rule based on the spherical harmonics of atoms (K_h symmetry). With his co-workers, Hirsch has applied this rule specifically to globular molecules with very high symmetry, e.g., T_d, O_h, I_h, etc. [60]. These "spherical aromatics" exhibit global delocalization of mobile electrons in molecular orbitals often of higher degeneracy (three, four, and five) involving all of the principal skeletal cluster atoms. However, the applicable electron count (which includes the hydrogen) is not restricted to a single 2(s), 8(s,p), 18(s,p,d), 32(s,p,d,f), 50(s,p,d,f,g) ... set, but may involve two such sets interleaved (radial and tangential), for example $8+2=10$, $18+2=20$, $18+8=26$, $32+8=40$ electrons. Thus, the most stable *closo* borane dianions, octahedral $B_6H_6^{2-}$ and icosahedral $B_{12}H_{12}^{2-}$, have 26 and 50 valence electrons, respectively. Other examples are considered below. The theoretical essence of such systems is three-dimensional. As the typical molecular orbital degeneracy is three (as well as four and five in larger systems), the Hückel rule, which is based on an MO degeneracy of two, does not apply to spherical aromatic systems (except in the context of the restricted Jemmis-Schleyer "interstitial electron" rule) [55].

Hirsch's rule has more limited applicability than the Hückel rule. However, the $2(n+1)^2$ concept has been used very successfully to interpret relative fullerene stabilities [66], and to suggest new systems, including neutral and charged non-fullerene carbon [67] and homoaromatic cages [68]. All these species have large NICS values in their centers and satisfy other criteria of aromaticity.

The Hirsch, Chen, Jiao analysis of inorganic clusters of main group elements [69] are of special interest in the context of this chapter. They showed that the 20 electron group 15 element tetrahedra (N_4, P_4, As_4, and Bi_4), as well as their protonated and isoelectronic T_d Si_4^{4-}, Ge_4^{4-}, Sn_4^{4-}, and Pb_4^{4-} counterparts typically had very large NICS values in the centers (see Chapter 1.1.4). The recently described T_d cation [70] S_4^{4+} can be added to this set, along with the other analogous chalcogen tetrahedral tetracations (see Chapter 2.7.2.1). The MOs confirm the interleaved $18+2=20$ electron sets for all of these tetrahedral clusters.

A large number of nine-vertex Zintl ions are known (see details in the next section). Those having electron counts of $32+8=40$ (E_9^{4-}, E = Si, Ge, Sn, Pb), do

not follow Wade's rule, but have very large NICS(0) values (−87 to −68) which do not depend on the D_{3h} or C_{4v} symmetry. However, the Bi_9^{5+} NICS(0) is much smaller (−28), and no explanation was offered. Species having only 38 valence electrons, Bi_9^{7+} and E_9^{2-} (E = Ge, Sn, Pb), do not satisfy the $2(n+1)^2$ rule and have more modest NICS(0) values (−43 to −27) than the corresponding species with 40 valence electrons. This illustrates the function of the Hirsch rule: to identify and predict the (''most aromatic'') species with the best electronic structure.

While Hirsch conceived his $2(n+1)^2$ electron rule for ''spherical aromatics,'' subsets of three-dimensionally aromatic molecules having very high symmetries (T_d, O_h, I_h, etc.), it can be applied to lower symmetry clusters such as the nine-vertex examples above. In cluster molecules the highest degeneracy MOs of a spherically harmonic atom set split into related, but lower degeneracy (or even non-degenerate) components.

There are similarities and differences between the Hirsch rule and those developed by physicists, originally to rationalize the ''magic numbers'' observed experimentally for simple metal clusters. The reader is referred to the excellent review by de Heer for more information [71]. The magic numbers for sodium clusters, 8, 20, 40, 58, are consistent with treatments, such as the Jellium model, which assume that the electrons are nearly free and are confined to a potential well. This gives 2, 8, 20, 40, 70, 112 ... for a spherical potential, but a square well potential also results in further breakdown into 18, 34, 58, 68, 90 ... electrons. Note that neither 26 and 50, the numbers of $B_6H_6^{2-}$ and $B_{12}H_{12}^{2-}$ valence electrons, respectively, nor 14 and 26, their $2n+2$ skeletal electron counts, are foreseen.

Such ''electron gas'' models also do not predict the geometrical structures of the clusters. The many computations of the structures of alkali and alkaline earth metal clusters will not be reviewed here [72], except to point out that the ''magic number'' Na_{20}, surprisingly said to prefer a peculiar, lower symmetry C_{2v} structure [73], actually is 2.7 kcal mol^{-1} *less* stable (at B3LYP/6-311+G*) than the alternative high-symmetry T_d minimum (Figure 1-6) [74]. However, the corresponding C_{2v} Li_{20} form is 22.5 kcal mol^{-1} *more* stable than the T_d minimum. Both the I_h Li_{20} and Na_{20} dodecahedra are very unfavorable.

1.1.4
Bare Ionic Post-transition Metal Clusters: The Zintl Phases

The polyhedral boranes and carboranes discussed above may be regarded as boron clusters in which the single external orbital of each vertex atom helps to bind an external hydrogen or other monovalent atom or group. Post-transition main group elements are known to form clusters without external ligands bound to the vertex atoms. Such species are called ''bare metal clusters'' for convenience. Anionic bare metal clusters were first observed by Zintl and co-workers in the 1930s [2–5]. The first evidence for anionic clusters of post-transition metals such as tin, lead, antimony, and bismuth was obtained by potentiometric titrations with alkali metals in liquid ammonia. Consequently, such anionic post-transition metal clusters are often called Zintl phases.

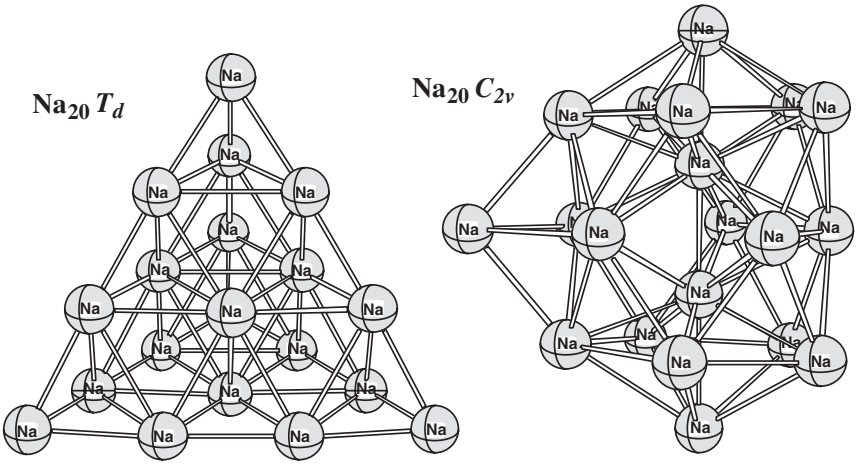

Fig. 1-6. Alternative structures for the Na_{20} cluster.

As mentioned in the Introduction, no structural information on these species was available for more than 40 years after the discovery of the first Zintl metal cluster anions, since no pure crystalline phases could be isolated and characterized structurally. Nevertheless, early efforts to rationalize the observed formulas and chemical bonding of these intermetallics and related molecules utilized the Zintl-Klemm concept [75, 76] and the Mooser-Pearson [77] extended $(8 - N)$ rule. In this rule N refers to the number of valence electrons of the more electronegative metal (and thus anionic metal) in the intermetallic phases.

The intermetallic phase, $[Na_2Tl]$ [78], illustrates a simple application of the Zintl-Klemm concept to a group 13 metal cluster. Complete electron transfer from Na to Tl leads to the $[(Na^+)_2Tl^{2-}]$ formulation. The Tl^{2-} dianion is isovalent with group 15 5/12/03 elements and thus should form similar structures with three two center-two electron bonds. Indeed, the Tl^{2-} anions in the $[Na_2Tl]$ phase form Tl_4^{8-} tetrahedra, similar to the isoelectronic P_4 and As_4 units in white phosphorus and yellow arsenic [78]. For a general formulation, consider an intermetallic A_mX_n phase, where A is the more electropositive element (typically an alkali or an alkaline earth metal). Both A and X, viewed as individual atoms, are assumed to follow the octet rule due to electron transfer $A \rightarrow A^{p+}$, $X \rightarrow X^{q-}$ so that $|mp| = |nq|$. The anionic unit X^{q-} arising from this electron transfer is considered to be a pseudoatom, which exhibits a structural chemistry closely related to that of the isoelectronic elements [76]. Since bonding is also possible in the cationic units, the numbers of electrons involved in A–A and X–X bonds of various types (e_{AA} and e_{XX}, respectively) as well as the number of electrons e* not involved in localized bonds, can be generated from the numbers of valence electrons on A and X, namely e_A and e_X, respectively, by the following equations of balance:

$$me_A + ne_X + k = 8n \tag{8a}$$

$$k = -\sum e_{AA} + \sum e_{XX} - \sum e^* \tag{8b}$$

Such equations vaguely resemble Lipscomb's equations of balance for the polyhedral boranes [Eqs. (1) and (2)].

Extensive definitive structural information on anionic post-transition metal clusters was obtained by Corbett [20] only in the 1970s. His group discovered that complexation with 2,2,2-crypt gave crystals of molecular alkali metal ion pairs (called "Zintl compounds") of such clusters suitable for structure determination by X-ray diffraction. Somewhat earlier, Corbett [21] had used X-ray crystallography to obtain definitive structural information on cationic post-transition metal clusters obtained as halometalate salts, particularly with $AlCl_4^-$ counterions, from highly acidic melts. After sufficient structural information on the bare post-transition metal clusters became available, the resemblance of their polyhedra to the known polyhedral boranes became apparent. The simple Zintl-Klemm concept has been largely superseded by newer, more advanced descriptions of chemical bonding in such clusters, in particular those applied to the polyhedral boranes. The Wade-Mingos rules [16–18] appear to apply to most post-transition metal clusters.

The limitations of the simple Zintl-Klemm concept can be illustrated by differences in the two [MTl] intermetallics (M = Na [79] and Cs [80]). Complete electron transfer from M to Tl leads to $[M^+Tl^-]$, where the Tl^- anion with four valence electrons is isoelectronic with a neutral group 14 atom and four bonds and needed to attain the octet configuration. Hence, the Tl^- anion should form structures similar to allotropes of carbon or heavier group 14 elements. Indeed, [NaTl] has a "stuffed diamond" structure [79] with internal Na and an anionic $(Tl^-)_\infty$ lattice similar to diamond. However, the Tl^- anions in [CsTl] form tetragonally compressed octahedra [80] unlike any structures of the allotropes of carbon or its heavier congeners.

Rules for counting the number of skeletal electrons provided by each vertex atom need to be established in order to determine the number of skeletal electrons in polygonal and polyhedral clusters of the post-transition elements. The rules discussed above for polyhedral boranes can be adapted to bare post-transition metal vertices as follows:

1. The post-transition metals utilize a four-orbital sp^3 valence orbital manifold. The inner shell d orbitals are assumed not to be involved in the bonding but instead comprise non-bonding electron pairs.
2. If the clusters exhibit either two- or three-dimensional aromaticity as discussed in Chapter 1.1.3, three orbitals of each bare metal vertex atom are required for the internal orbitals (two twin internal orbitals and one unique internal orbital). This leaves an external orbital for a non-bonding lone pair.

Application of this procedure to post-transition metal clusters indicates that bare Ga, In, and Tl vertices contribute one skeletal electron; bare Ge, Sn, and Pb vertices contribute two skeletal electrons; bare As, Sb, and Bi vertices contribute three skeletal electrons; and bare Se and Te vertices contribute four skeletal electrons in two- and three-dimensional aromatic systems (see Chapter 1.1.3). Thus, Ge, Sn, and Pb vertices are isoelectronic with BH vertices and As, Sb, and Bi vertices are isoelectronic with CH vertices.

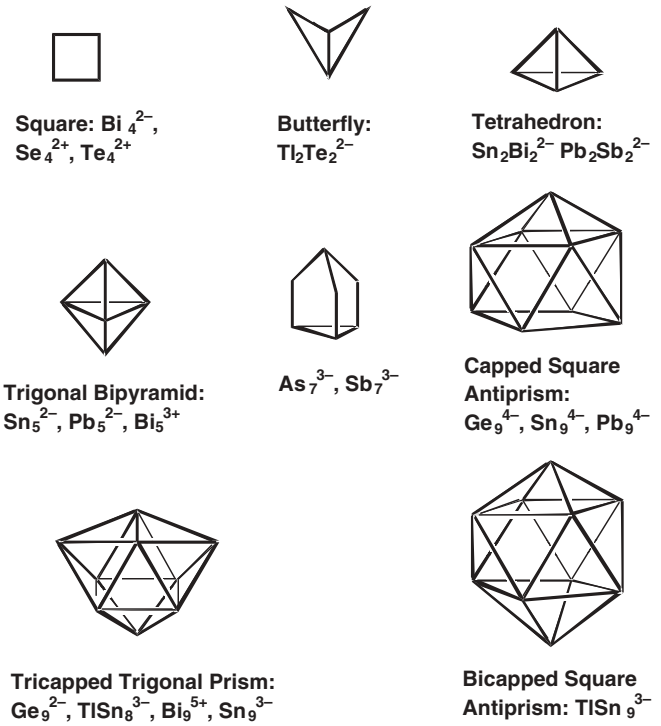

Fig. 1-7. Examples of the shapes of bare post-transition metal clusters.

Some examples of bare ionic post-transition metal clusters are depicted in Figure 1-7. Their chemical bonding topologies can be analyzed as follows:

1. *Square.* Bi_4^{2-}, Se_4^{2+}, and Te_4^{2+} are isoelectronic and isolobal with the delocalized planar cyclobutadiene dianions. There are 14 skeletal electrons [e.g., for Bi_4^{2-}: $(4)(3) + 2 = 14$] corresponding to 8 electrons for the 4 σ-bonds and 6 electrons for the π-bonding (see Chapter 2.7.2.1).
2. *Butterfly.* While $Tl_2Te_2^{2-}$ has a $(2)(1) + (2)(4) + 2 = 12$ skeletal electron count isoelectronic and isolobal with *neutral* cyclobutadiene, it undergoes a different Jahn-Teller-like distortion to the butterfly structure discussed by Burns and Corbett [81].
3. *Tetrahedron.* $Sn_2Bi_2^{2-}$ and $Pb_2Sb_2^{2-}$ have $(2)(2) + (2)(3) + 2 = 12$ skeletal electrons for tetrahedra analogous to P_4 and organic C_4R_4 tetrahedrane derivatives (see Section 1.1.3.4).
4. *Trigonal Bipyramid.* Sn_5^{2-}, Pb_5^{2-}, and Bi_5^{3+} have 12 skeletal electrons [e.g., $(5)(2) + 2 = 12$ for Sn_5^{2-} and Pb_5^{2-}] and are analogous to the trigonal bipyramidal $C_2B_3H_5$ carborane.
5. *Seven-vertex Structures.* As_7^{3-} and Sb_7^{3-} have the C_{3v} structure depicted in Figure 1-7 and the correct $(4)(3) + (3)(1) + 3 = 18$ skeletal electron count for

bonds along the 9 edges derived by considering the three vertices of degree 2 to use two internal orbitals each and the four vertices of degree 3 to use three internal orbitals each.

6. *Capped Square Antiprism.* Ge_9^{4-}, Sn_9^{4-}, and Pb_9^{4-} have the $(9)(2) + 4 = 22 = 2n + 4$ skeletal electrons required for an $n = 9$ vertex C_{4v} *nido* polyhedron having 12 triangular faces and one square face. Hirsch et al. [69] computed these species and their isoelectronic counterparts to prefer D_{3h} symmetry slightly, but these clusters exhibit nearly identical, very large NICS values in both D_{3h} and C_{4v} symmetries (see Chapter 1.1.3.4).
7. *Tricapped Trigonal Prism.* Ge_9^{2-} and $TlSn_8^{3-}$ have the $2n + 2 = 20$ skeletal electrons required for an $n = 9$ vertex globally delocalized D_{3h} deltahedron analogous to $B_9H_9^{2-}$ (Ref. [82]). Bi_9^{5+} anomalously has $(9)(3) - 5 = 22$ rather than the expected 20 skeletal electrons suggesting [83] incomplete overlap of the unique internal orbitals directed towards the core of the deltahedron. Sn_9^{3-} has $(9)(2) + 3 = 21$ skeletal electrons including one extra electron for a low-lying antibonding orbital analogous to radical anions formed by stable aromatic hydrocarbons such as naphthalene and anthracene.
8. *Bicapped Square Antiprism.* $TlSn_9^{3-}$ has the $(1)(1) + (9)(2) + 3 = 22 = 2n + 2$ skeletal electrons required for an $n = 10$ vertex globally delocalized D_{4d} deltahedron (*cf.* the bicapped square antiprism in Figure 1-7) analogous to that found in the $B_{10}H_{10}^{2-}$ anion [84].

The results of illustrative NICS computations of a few arsenic clusters representing types of species discussed in this review are illustrated in Figure 1-8. The magnetic shielding is sampled in the centers of the cages and cage faces, as well as outside the molecules. Note that the Hückel aromatic, As_5^-, has been included. In all but one case, the clusters are highly diatropic with large negative NICS values (red dots). The exception, cubic As_8, is a hypothetical species included to show that some clusters could be, in principle, anti-aromatic (paratropic, green NICS dots). However, this is unlikely since unstable species would probably rearrange during formation. Very recently, the gas phase observation of an "all-metal aromatic molecule," $Al_4Li_3^-$, has been claimed [85], but the NICS values computed for this species disagree. The last structure shown below for the proposed lowest energy isomer shows only diatropic (aromatic) shielding.

1.1.5 Clusters of the Heavier Group 13 Metals

1.1.5.1 Apparently Hypoelectronic Deltahedra in Bare Clusters of Indium and Thallium: Polyhedra with Flattened Vertices

Bare group 13 metal vertices (e.g., Ga, In, Tl) provide, as noted above, only one skeletal electron each to polyhedral cluster structures. Thus it is not surprising that the bare metal cluster ions E_n^{z-} (E = group 13 element) found in homonuclear alkali-metal/group 13 intermetallic phases [86–89] (mainly for In and Tl) have charges less negative than the $-(n + 2)$ (i.e., $z < n + 2$) required by the Wade-

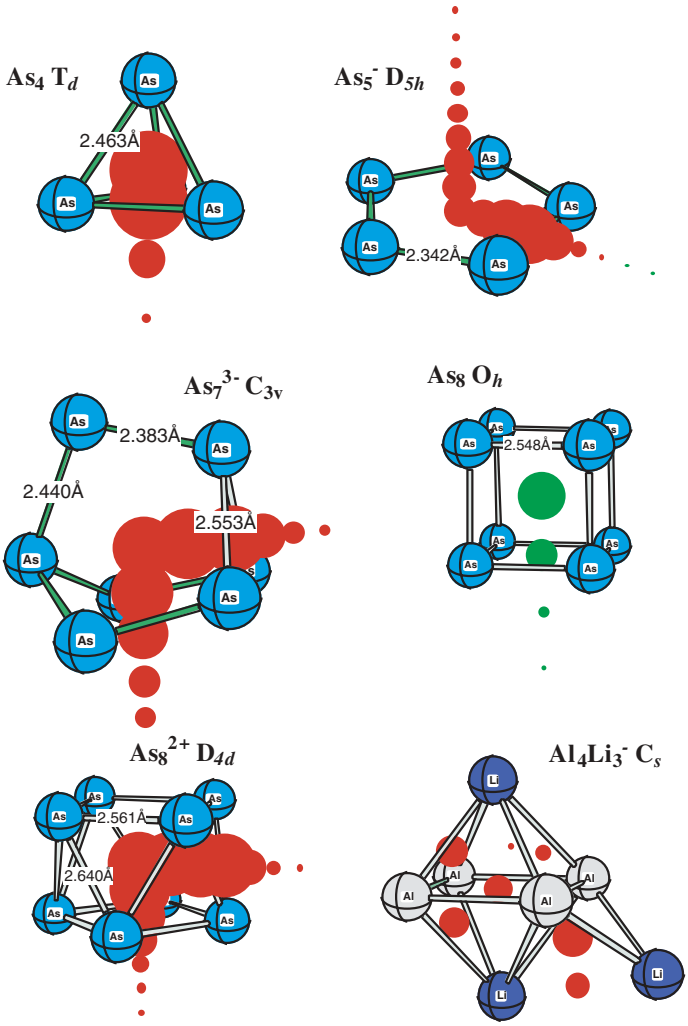

Fig. 1-8. Comparison of NICS for various arsenic clusters.

Mingos rules. This hypoelectronicity or electron poverty (fewer than the Wade-Mingos $2n + 2$ skeletal electrons) in the bare metal cluster anions E_n^{z-} ($z < n + 2$) leads to deltahedra not only different from those in the deltahedral boranes but also different from those in hypoelectronic metal carbonyl clusters of metals such as osmium.

The shapes of the deltahedra in the apparently hypoelectronic clusters of the heavier group 13 metals bear an interesting relationship to their electron counts. All such hypoelectronic deltahedra can be derived formally from the standard *closo*-borane structures (Figure 1-2) by "flattening" one or more vertices towards

the center [91, 92]. The deltahedral vertices particularly susceptible to flattening are degree 4 vertices surrounded by vertices of degree 5 or higher. Among the borane deltahedra the nine-vertex tricapped trigonal prism has three such degree 4 vertices and the ten-vertex bicapped square antiprism has two such vertices. The flattening process distorts the vertex in question towards the center of the deltahedron so that its otherwise external lone pair can become involved in the skeletal bonding. For the apparently hypoelectronic E_n^{z-} clusters with nine, ten, and eleven vertex atoms the numbers of flattened vertices correspond to exactly the same number of additional skeletal electrons from the otherwise external lone pairs required to make these clusters no longer hypoelectronic, i.e., to have the $2n + 2$ skeletal electrons for globally delocalized deltahedra (Figure 1-9). The "wheels" predicted by Wang and Schleyer [92] (Figure 1-10) as well as their Al_n precedent from Schnöckel and co-worker [93] are further examples of flattened polyhedra in which opposite vertex hydrogen atoms are removed.

The E_n^{z-} clusters become isoelectronic with the corresponding $B_nH_n^{2-}$ deltahedral boranes albeit with highly distorted, flattened geometries. The eleven-vertex In_{11}^{7-} moiety in the intermetallic K_8In_{11}, the first homoatomic group 13 cluster to be discovered [94], has three flattened vertices. This distortion influences the relative energetics of the ideal 11-vertex deltahedra significantly. Thus, while the 11-vertex boron cluster $B_{11}H_{11}^{2-}$ is based on the so-called "edge-coalesced" icosahedron of C_{2v} symmetry (Figure 1-2), the In_{11}^{7-} cluster geometry is derived from a pentacapped trigonal prism of D_{3h} symmetry (Figure 1-9) by flattening the three vertices capping the rectangular prism faces.

1.1.5.2 Organometallic Deltahedral Clusters of the Heavier Group 13 Metals and More Complicated Structures Derived from Deltahedra

The heavier group 13 metals E = Al, Ga, In, Tl form much weaker E–H than B–H bonds. Thus, the deltahedral hydrides $E_nH_n^{2-}$ remain unknown. However, hydrides of these elements are well known to be less stable, i.e., to have lower decomposition temperatures than the corresponding alkyls. Consequently, replacement of the relatively weak E–H bonds with stronger E–C bonds has been shown recently to give stable deltahedral clusters of the general type $E_nR_n^{z-}$ (E = Al and Ga; $z = 0$, 1, and 2 in the known examples).

The first deltahedral cluster of a heavier group 13 element to be prepared was the icosahedral aluminum cluster $K_2[i\text{-}Bu_{12}Al_{12}]$ (*i*-Bu = *iso*-butyl) [95], which is isoelectronic and isostructural with the icosahedral borane anion $B_{12}H_{12}^{2-}$. No further simple deltahedral clusters of the heavier group 13 metals were known until the recent discovery [96] of the nine-vertex gallium cluster $Ga_9(CMe_3)_9$ (see Chapter 2.3.3.2). This tricapped trigonal prismatic deltahedral cluster is an 18 skeletal electron cluster corresponding to $2n$ rather than $2n + 2$ skeletal electrons for $n = 9$. This anomalous electron count is analogous to that found in the stable neutral boron halides B_9X_9 (X = Cl, Br, I) [97].

An unusual type of deltahedral cluster found in organoindium chemistry but not in deltahedral borane chemistry is the eight-vertex $In_8[Si(CMe_3)_3]_6$ (see Chapter 2.3.4.2); its structure is based on a bicapped octahedron with idealized D_{3d} sym-

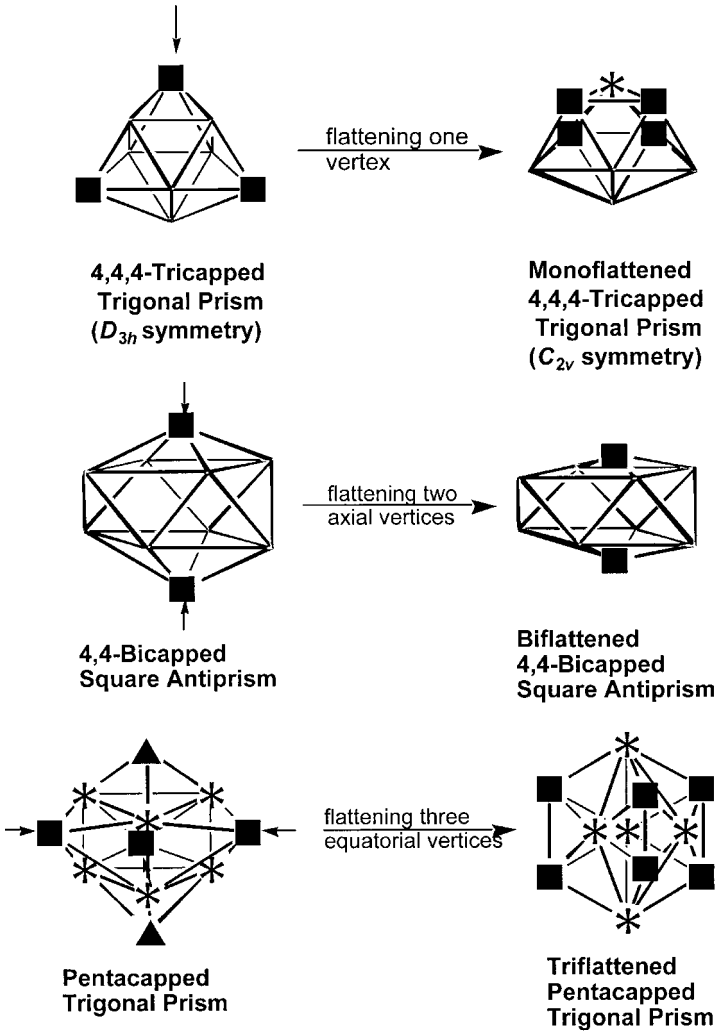

Fig. 1-9. Flattening one to three vertices in 9-, 10-, and 11-vertex deltahedra to give the deltahedra found in apparently hypoelectronic group 13 metal clusters. Vertices of degrees 3, 4, and 6 are indicated by ▲, ■, and ✳, respectively. Vertices of degree 5 are unmarked.

metry of the underlying polyhedron (Figure 1-11, top) [98]. If the six $(Me_3C)_3SiIn$ vertices donate two skeletal electrons each and the two "bare" In vertices have an external lone pair and, hence, donate only a single skeletal electron, then $In_8[Si(CMe_3)_3]_6$ (see Chapter 2.3.4.2) has a $(6 \times 2) + (2 \times 1) = 14$ skeletal electron structure in accord with its central In_6 octahedron. Thus $In_8[Si(CMe_3)_3]_6$ may be regarded as an "electron-poor" or hypoelectronic cluster related to hypoelectronic

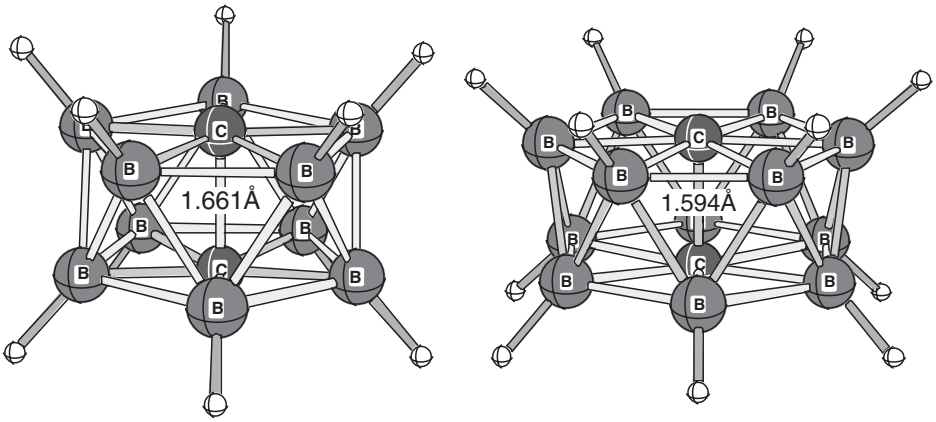

Fig. 1-10. Examples of prismatic C_2B_n ($n = 10, 12$) "wheels".

osmium carbonyl clusters based on capped octahedra [98]. No boron analogues of such hypoelectronic polyhedra are known.

Two reported examples of heavier group 13 metal clusters consist of two fused deltahedra, $Ga_{10}[Si(SiMe_3)_3]_6$ [100] and $In_{12}[Si(CMe_3)_3]_8$ [101]. These two clusters have closely related structures (Figure 1-11, bottom) with edge-sharing pairs

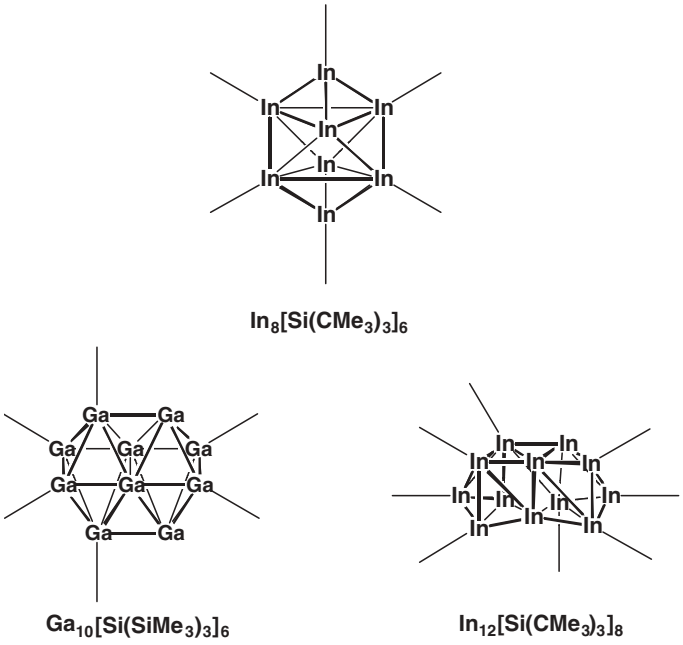

Fig. 1-11. The structures of $In_8[Si(CMe_3)_3]_6$, $Ga_{10}[Si(SiMe_3)_3]_6$, and $In_{12}[Si(CMe_3)_3]_8$. The pendant $(Me_3C)_3Si$ and $(Me_3Si)_3Si$ groups are omitted for clarity in Figures 1-11, 1-12, and 1-13.

of deltahedra, octahedra for $Ga_{10}[Si(SiMe_3)_3]_6$ and bisdisphenoids for $In_{12}[Si(CMe_3)_3]_8$. A known aluminum cluster radical anion [102] $Al_{12}[N(SiMe_3)_2]_8^-$ has a structure closely related to that of $In_{12}[Si(CMe_3)_3]_8$. In both cases the two vertices of the shared edge and two other vertices are bare, that is with no terminal groups. For electron-counting purposes, the bare group 13 metal vertices can be assumed to donate three skeletal electrons. Hence, both of these cluster types follow the Jemmis $2n + 2m$ electron counting rule for fused polyhedral clusters [32, 33]. Thus $Ga_{10}[Si(SiMe_3)_3]_6$ receives $6 \times 2 = 12$ skeletal electrons from the six RGa groups and $4 \times 3 = 12$ skeletal electrons from the four "bare" Ga atoms with four internal orbitals. The resulting 24 skeletal electrons correspond to the $2n + 2m$ skeletal electrons required by the ten gallium atoms ($n = 10$) and the two polyhedra ($m = 2$). Similarly, $In_{12}[Si(CMe_3)_3]_8$ receives $8 \times 2 = 16$ skeletal electrons from the eight RIn groups and $4 \times 3 = 12$ skeletal electrons from the four "bare" In atoms. The resulting 28 skeletal electrons again follow the Jemmis rule by corresponding to $2n + 2m$ for $n = 12$ and $m = 2$.

Some recently prepared larger gallium clusters may be interpreted as containing gallium supraicosahedra with a single gallium atom in the center analogous to the centered $Tl@Tl_{12}$ icosahedron found in the intermetallic $Na_3K_8Tl_{13}$ [103]. All the structures of such clusters can be derived by the following procedure:

1. Start with a 12- or 13-vertex gallium polyhedron containing some quadrilateral and/or pentagonal faces. This polyhedron is conveniently called the core polyhedron.
2. Cap each of the non-triangular faces of the core polyhedron with one or more additional gallium atoms. This leads to a supraicosahedral deltahedron since the capping process removes all of the non-triangular faces.
3. Place an additional gallium atom in the center of the core polyhedron.
4. Place bulky organic substituents [typically $-C(SiMe_3)_3$ or $-Si(SiMe_3)_3$] on the outermost gallium atoms.

Electron counting in these supraicosahedral gallium clusters consisits of ambiguities since it is not clear which of the bare vertex atoms of the core polyhedra provide the usual three internal orbitals and which vertex atoms provide four internal orbitals. Typically the Wade-Mingos [16–18] or the Jemmis [32, 33] skeletal electron rule is obeyed if about half of the bare vertex gallium atoms use all four orbitals of their sp^3 manifolds as internal orbitals, and thus are donors of three skeletal electrons, and the other half of the bare vertex gallium atoms use only three orbitals of their sp^3 manifolds and thus are donors of only a single skeletal electron each.

The following supraicosahedral organogallium clusters have been characterized structurally (Figures 1-12 and 1-13; see also Chapters 2.3.4.2.5 and 2.3.4.2.6):

1. *The $[Ga_{19}\{C(SiMe_3)_3\}_6]^-$ anion* (Figure 1-12): This anion has a structure based on a centered $Ga@Ga_{18}$ deltahedron [104]. The structure of this 18-vertex del-

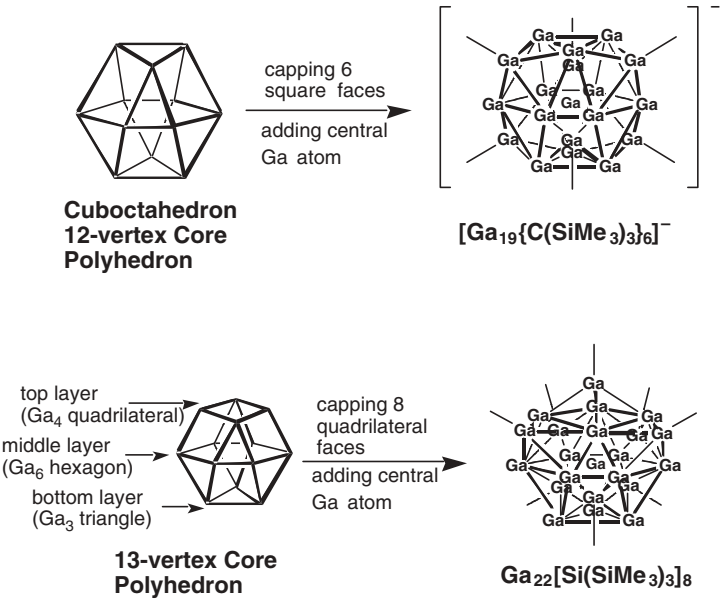

Fig. 1-12. Derivation of the structures of $[Ga_{19}\{C(SiMe_3)_3\}_6]^-$ and $Ga_{22}[Si(SiMe_3)_3]_8$ from 12- and 13-vertex core polyhedra, respectively.

tahedron can be derived from a cuboctahedron by capping its six square faces with $(Me_3Si)_3CGa$ vertices.

2. *Neutral $Ga_{22}[Si(SiMe_3)_3]_8$* (Figure 1-12): In this cluster the gallium atoms form a centered $Ga@Ga_{21}$ 21-vertex deltahedron [105]. This deltahedron can be derived from a 13-vertex Ga_{13} polyhedron with eight quadrilateral faces and six triangular faces by capping all eight of the quadrilateral faces with $(Me_3Si)_3SiGa$ vertices [22]. The underlying 13-vertex polyhedron in $Ga_{22}[Si(SiMe_3)_3]_8$ may be regarded as a three-layer structure with a Ga_4 quadrilateral in the top layer, a Ga_6 hexagon in the middle layer, and a Ga_3 triangle in the bottom layer.
3. *The $Ga_{26}[Si(SiMe_3)_3]_8^{2-}$ dianion* (Figure 1-13): The underlying polyhedral structure of this dianion [106] may be regarded as a fusion of a central Ga-centered $Ga@Ga_{17}$ polyhedron with two side bicapped trigonal prisms. The core polyhedron of the $Ga_{26}[Si(SiMe_3)_3]_8^{2-}$ structure is a 13-vertex polyhedron with eight triangular faces, six quadrilateral faces, and two pentagonal faces. Capping the two pentagonal faces and two of the quadrilateral faces of the core polyhedron leads to a 17-vertex polyhedron, which still has two quadrilateral faces. Capping each of these two remaining quadrilateral faces with Ga_4 units combined with the central Ga atom forms a nine-vertex tricapped trigonal prismatic cavity on each side. The four gallium atoms, corresponding to outer caps in each of these trigonal prismatic cavities, each bear external $Si(SiMe_3)_3$ groups to provide the remaining two $(Me_3Si)_3Si$ vertices.

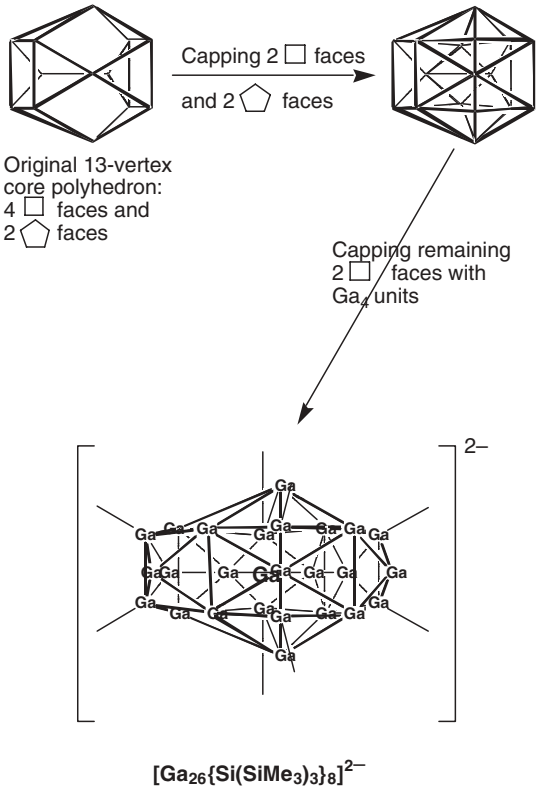

Fig. 1-13. Derivation of the structure of $[Ga_{26}\{Si(SiMe_3)_3\}_8]^{2-}$ from a 13-vertex core polyhedron.

1.1.5.3 Giant Aluminum Clusters with Shell Structures Consisting of Nested Polyhedra: Pieces of Icosahedral Quasicrystals

The supraicosahedral clusters discussed above are not the largest structurally characterized molecular group 13 metal clusters. Thus Schnöckel and co-workers have prepared giant aluminum clusters of the stoichiometries $[Al_{69}\{N(SiMe_3)_2\}_{18}]^{3-}$ (Ref. 107) and $[Al_{77}\{N(SiMe_3)_2\}_{20}]^{2-}$ (see Chapter 2.3.4.1.3) [108]. These clusters have structures consisting of nested polyhedra with the shells, counting from the inside out, consisting of $1 + 12 + 38 + 18$ Al atoms for the Al_{69} cluster and $1 + 12 + 44 + 20$ Al atoms for the Al_{77} cluster [23]. The aluminum atoms in the outer shell are bonded to the external $N(SiMe_3)_2$ groups. The inner $Al@Al_{12}$ shell is a centered icosahedron in the Al_{77} cluster but a centered bicapped pentagonal prism in the Al_{69} cluster. The five-fold symmetries of the inner polyhedra in both of these giant clusters suggest that these clusters might be pieces of an icosahedral quasicrystal similar to that found in certain aluminum alloys [109–111]. These layer structures appear to be related to the Mackay icosahedron [112] used to construct such quasicrystal structures.

1.1.6
Conclusion and Outlook

Many rules have been developed to rationalize the stoichiometry and structures of main group element clusters, but these are only applicable to sets of related molecules. The most recent is the $6m + 2n$ electron rule, developed by Wang and Schleyer [113] to predict a new family of high symmetry borane and carborane cages. The protruding hydrogen atoms of $B_{92}H_{92}{}^{8-}$ (I_h) and other large cages resemble the prickly spines of sea urchins.

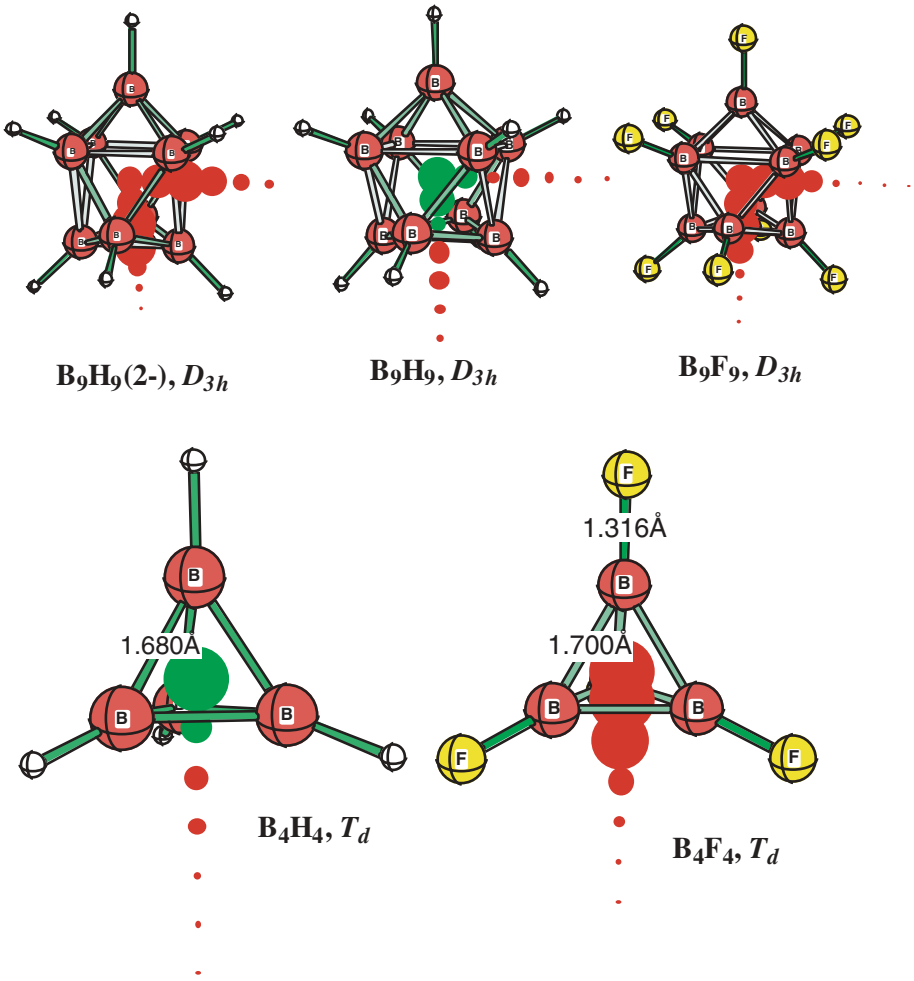

Fig. 1-14. Comparison of NICS for boron clusters: top row, nine-vertex D_{3d} tricapped trigonal prismatic clusters; bottom row, four-vertex T_d tetrahedral clusters.

The existing rules are useful, not only to categorize existing examples, but also to predict new structures. However, they quite frequently are contradictory and break down, especially when explored systematically. Computational investigations reveal unexpected problems, as two related illustrations from our current research [114] show.

Icosahedral Si_{12}^{2-} and Ge_{12}^{2-} are isoelectronic with I_h $B_{12}H_{12}^{2-}$, the most stable *closo* borane dianion. All three follow the Wade-Mingos and the Hirsch rules. As expected, $B_{12}H_{12}^{2-}$ fulfills the various aromaticity criteria and has a large diatropic NICS(0) value [57]. In sharp contrast, the NICS(0) values in the centers of Si_{12}^{2-} and Ge_{12}^{2-} are large and *paratropic*. These 50 valence electron bare element clusters are thus indicated to be *anti-aromatic*, at least according to their magnetic properties.

Different substituents also can influence the *same* cluster decisively. Neutral B_8Cl_8 and B_9Cl_9 are well known [97], but B_8H_8 and B_9H_9 have not been observed. As illustrated by the comparison below for D_{3h} B_9F_9 and $B_9H_9^{2-}$ (both diatropic, red dots) with B_9H_9 (paratropic, green dots), NICS shows the halo derivatives to be aromatic, but the neutral hydrides to be anti-aromatic (Figure 1-14, top). Tetrahedral B_4H_4 and B_4F_4 behave analogously (Figure 1-14, bottom).

MO-NICS analysis reveals that some of the cage orbitals are strongly paratropic (like the HOMO of cyclobutadiene) [63]. The hydrogens of $B_{12}H_{12}^{2-}$ and the halogens of B_8Cl_8 and B_9Cl_9 withdraw skeletal electrons [115] and reduce the paratropicity of these MOs substantially and selectively, thus allowing the influence of the diatropic MOs to dominate [114].

The full understanding of the nature of main-group element clusters will be very difficult to achieve.

References

1 Stock, A., *Hydrides of Boron and Silicon*, Cornell University Press, Ithaca, NY, **1933**.

2 Zintl, E., Goubeau, J., Dullenkopf, W., *Z. Phys. Chem., Abt. A*, **1931**, *154*, 1.

3 Zintl, E., Harder, A., *Z. Phys. Chem., Abt. A*, **1931**, *154*, 47.

4 Zintl, E., Dullenkopf, W., *Z. Phys. Chem., Abt. B*, **1932**, *16*, 183.

5 Zintl, E., Kaiser, H., *Z. Anorg. Allgem. Chem.*, **1933**, *211*, 113.

6 Dickerson, R. E., Lipscomb, W. N., *J. Chem. Phys.*, **1957**, *27*, 212.

7 Lipscomb, W. N., *Boron Hydrides*, W. A. Benjamin, New York, **1963**.

8 Lipscomb, W. N., in *Boron Hydride Chemistry*, Muetterties, E. L., ed., Academic Press, New York, **1975**, pp. 30–78.

9 Williams, R. E., *Inorg. Chem.*, **1971**, *10*, 210.

10 Muetterties, E. L., Knoth, W. H., *Polyhedral Boranes*, Marcel Dekker, New York, **1968**.

11 Grimes, R. N., *Carboranes*, Academic Press, New York, 1970.

12 Aihara, J., *J. Am. Chem. Soc.*, **1978**, *100*, 3339.

13 Longuet-Higgins, H. C., Roberts, M. de V., *Proc. R. Soc. (London)*, **1955**, *230A*, 110.

14 Hoard, J., Hughes, R. E., in *The Chemistry of Boron and its Compounds*, Muetterties, E. L., ed., Wiley, New York, **1967**, p. 25.

15 Clark, K. H., Hoard, J. L., *J. Am. Chem. Soc.*, **1943**, *65*, 2115.
16 Wade, K., *Chem. Commun.*, **1971**, 792.
17 Mingos, D. M. P., *Nature Phys. Sci.*, **1972**, *99*, 236.
18 Mingos, D. M. P., *Acc. Chem. Res.*, **1984**, *17*, 311.
19 Corbett, J. D., Adolphson, D. G., Merryman, D. J., Edwards, P. A., Armatic, F. J., *J. Am. Chem. Soc.*, **1975**, *67*, 6267.
20 Corbett, J. D., *Chem. Rev.*, **1985**, *85*, 383.
21 Corbett, J. D., *Prog. Inorg. Chem.*, **1976**, *21*, 129.
22 King, R. B., *J. Organometal. Chem.*, **2002**, *646*, 146.
23 Schnöckel, H., Köhnlein, H., *Polyhedron*, **2002**, *21*, 489.
24 Li, X.-W., Pennington, W. T., Robinson, G. H., *J. Am. Chem. Soc.*, **1995**, *117*, 7578.
25 Sita, L., *Acc. Chem. Res.*, **1994**, *27*, 191.
26 King, R. B., *Croat. Chim. Acta*, **1995**, *68*, 293.
27 Gutman, I., Cyvin, S. J., *Introduction to the Theory of Benzenoid Hydrocarbons*, Springer, Berlin, **1989**.
28 Gutman, I., *Topics Curr. Chem.*, **1992**, *153*, 1–18.
29 Dixon, D. A., Kleier, D. A., Halgren, T. A., Hall, J. H., Lipscomb, W. N., *J. Am. Chem. Soc.*, **1977**, *99*, 6226.
30 Rudolph, R. W., Pretzer, W. R., *Inorg. Chem.*, **1972**, *11*, 1974.
31 Rudolph, R. W., *Acc. Chem. Res.*, **1976**, *9*, 446.
32 Baslakrishnarajan, M. M., Jemmis, E. D., *J. Am. Chem. Soc.*, **2000**, *122*, 4516.
33 Jemmis, E. D., Balakrishnarajan, M. M., Pancharatna, P. D., *J. Am. Chem. Soc.*, **2001**, *123*, 4313.
34 Najafian, K., Schleyer, P. v. R., Tidwell, T. T., *Inorg. Chem.*, **2003**, *42*, 4190.
35 Mansfield, M. J., *Introduction to Topology*, Van Nostrand, Princeton, New Jersey, **1963**, p. 40.
36 King, R. B., Rouvray, D. H., *J. Am. Chem. Soc.*, **1977**, *99*, 7834.
37 King, R. B., *Chem. Rev.*, **2001**, *101*, 1119.
38 Biggs, N. L., *Algebraic Graph Theory*, Cambridge University Press, London, 1974.
39 Vij, A., Pavolich, J. G., Wilson, W. W., Vij, V., Christie, K. O., *Angew. Chem. Int. Ed. Engl.*, **2002**, *41*, 3051–3054.
40 Baudler, M., Akpapoglou, M., Ouzounis, D., Wasgestian, F., Meinigke, B., Budzikiewicz, H., Münster, H., *Angew. Chem., Int. Ed. Engl.*, **1988**, *27*, 280–281.
41 (a) Cisar, A., Corbett, J. D., *Inorg. Chem.*, **1977**, *16*, 2482. (b) Li, X., Kutznetsov, A. E., Zhang, H.-F., Boldyrev, A. I., Wang, L.-S., *Science*, **2001**, *291*, 859.
42 Biggs, N. L., *Algebraic Graph Theory*, Cambridge University Press, London, **1974**.
43 Hückel, E., *Z. Physik*, **1932**, *76*, 628.
44 (a) Chandrasekhar, J., Jemmis, E., Schleyer, P. v. R., *Tetrahedron Lett.*, **1979**, 3707. (b) McEwen, A. B., Schleyer, P. v. R., *J. Org. Chem.*, **1986**, *51*, 4357–4368. (c) Schleyer, P. v. R., Jiao, H., Glukhovtsev, M. N., Chandrasekhar, J., Kraka, E., *J. Am. Chem. Soc.*, **1994**, *116*, 10129–10134.
45 Beinecke, L. W., Wilson, R. J., *Selected Topics in Graph Theory*, Academic Press, New York, **1978**, Chapter 1.
46 Burke, A., Ellis, D., Giles, B. T., Hodson, B. E., Macgregor, S. A., Rosair, G. M., Welch, A. J., *Angew. Chem., Int. Ed. Engl.*, **2003**, *42*, 225.
47 Grimes, R. N., *Angew. Chem., Int. Ed. Engl.*, **2003**, *42*, 1198.
48 King, R. B., in *Chemical Applications of Topology and Graph Theory*, King, R. B., ed., Elsevier, Amsterdam, **1983**, pp. 99–123.
49 King, R. B., in *Molecular Structure and Energetics*, Liebman, J. F., Greenberg, A., ed., VCH, Deerfield Beach, Florida, **1976**, pp. 123–148.
50 Stone, A. J., *Inorg. Chem.*, **1981**, *20*, 563.
51 Stone, A. J., *Mol. Phys.*, **1980**, *41*, 1339.

52 Stone, A. J., Alderton, M. J., *Inorg. Chem.*, **1982**, *21*, 2297.

53 Stone, A. J., *Polyhedron*, **1984**, *3*, 1299.

54 King, R. B., *Chem. Phys. Lett.*, **2001**, *338*, 237.

55 Jemmis, E. D., Schleyer, P. v. R., *J. Am. Chem. Soc.*, **1982**, *104*, 4781–4788.

56 Martin-Santamaría, S., Carroll, M. A., Carroll, C. M., Carter, C. D., Rzepa, H. S., *Chem. Commun.*, **2000**, 1089–1090.

57 (a) Schleyer, P. v. R., Subramanian, G., Jiao, J., Najafian, K., Hofmann, M., in *Advances in Boron Chemistry*, Siebert, W., ed., The Royal Society of Chemistry, Cambridge, **1997**, pp. 3–14. (b) Schleyer, P. v. R., Najafian, K., in *The Borane, Carborane and Carbocation Continuum*, Casanova, J., ed., John Wiley & Sons, New York, **1998**, pp. 169–190. (c) Schleyer, P. v. R., Najafian, K., *Inorg. Chem.*, **1998**, 37, 3455–3470.

58 But see Ref. 61 for a modern reinterpretation.

59 (a) Saunders, M., Jiménez-Vázques, H. A., Cross, R. J., Mroczkowski, S., Freedberg, D., Anet, F. A. L., *Nature*, **1994**, *367*, 256. (b) Bühl, M., Thiel, W., Jiao, H., Schleyer, P. v. R., Saunders, M., Anet, F. A. L., *J. Am. Chem. Soc.*, **1994**, *116*, 6005–6006. (c) Cioslowski, J., *J. Am. Chem. Soc.*, **1994**, *116*, 3919–3920.

60 Schleyer, P. v. R., Maerker, C., Dransfeld, A., Jiao, H., van Eikema Hommes, N. J. R., *J. Am. Chem. Soc.*, **1996**, *118*, 6317–6318.

61 See Kutzelnigg, W., Fleischer, U., Schindler, M., in *NMR Basic Principles and Progress*, Diehl, P., Fluck, E., Gunter, H., Kosfeld, R., Seelig, J., eds., Springer Verlag, New York, **1991**, Vol. 23.

62 Schleyer, P. v. R., Jiao, H., van Eikema Hommes, N. J. R., Malkin, V. G., Malkina, O., *J. Am. Chem. Soc.*, **1997**, *119*, 12669–12670.

63 (a) Corminboeuf, C., Heine, T., Weber, J., *Phys. Chem. Chem. Phys.*, **2003**, 5, 246–251. (b) Bohmann, J., Weinhold, F. A., Farrar, T. C., *J. Chem. Phys.*, **1997**, *107*, 1173–1184.

64 Wannere, C. S., Schleyer, P. v. R., *Org. Lett.*, **2003**, *5*, 605–608.

65 Wannere, C. S., Schleyer, P. v. R., *Org. Lett.*, **2003**, *5*, 865–868.

66 Hirsch, A., Chen, Z., Jiao, H., *Angew. Chem., Int. Ed. Engl.*, **2000**, *37*, 3915–3917.

67 Hirsch, A., Chen, Z., Jiao, H., Thiel, W., *J. Mol. Model.*, **2001**, *7*, 161–163.

68 Chen, Z., Jiao, H., Hirsch, A., Schleyer, P. v. R., *Angew. Chem., Int. Ed. Engl.*, **2002**, *39*, 4309–4312.

69 Hirsch, A., Chen, Z., Jiao, H., *Angew. Chem., Int. Ed. Engl.*, **2001**, *38*, 834–2838.

70 Song, M. Y., Kim, Y., Seff, K., *J. Phys. Chem. B*, **2003**, *107*, 3117–3123.

71 de Heer, W. A., *Rev. Modern Phys.*, **1993**, *65*, 611–676.

72 Koutecky, J., Fantucci, P., *Chem. Rev.*, **1986**, *86*, 539–587.

73 See Aguado, A., López, J. M., Alonso, J. A., Scott, M. J., *J. Chem. Phys.*, **1999**, *111*, 6026–6035.

74 Schleyer, P. v. R., King, R. B., Chen, Z., in preparation.

75 Zintl, E., *Angew. Chem.*, **1939**, *52*, 1.

76 Klemm, W., *Proc. Chem. Soc. (London)*, **1958**, 329.

77 Mooser, E., Pearson, W. B., *Phys. Rev.*, **1956**, *101*, 1608.

78 Hansen, D. A., Smith, J. F., *Acta Crystallogr.*, **1967**, *22*, 836.

79 Zintl, E., Dullenkopf, W., *Z. Phys. Chem.*, **1932**, *B16*, 195.

80 Dong, Z.-C., Corbett, J. D., *Inorg. Chem.*, **1996**, *35*, 2301.

81 Burns, R. C., Corbett, J. D., *J. Am. Chem. Soc.*, **1981**, *103*, 2627.

82 Guggenberger, L. J., *Inorg. Chem.*, **1968**, *7*, 2260.

83 King, R. B., *Inorg. Chim. Acta*, **1982**, *57*, 79.

84 Dobrott, R. D., Lipscomb, W. N., *J. Chem. Phys.*, **1962**, *37*, 1779.

85 Kuznetsov, A. E., Birch, K. A., Boldyrev, A. I., Li, X., Zhai, H.-J., Wang, L.-S., *Science*, **2003**, *300*, 622–625.

86 Corbett, J. D., *J. Chem. Soc., Dalton Trans.*, **1996**, 575.

87 Corbett, J. D., *Struct. Bonding*, **1997**, *87*, 157.

88 Corbett, J. D., *Inorg. Chem.*, **2000**, *39*, 5178.

89 Corbett, J. D., *Angew. Chem., Int. Ed. Engl.*, **2000**, *39*, 670.

90 King, R. B., *Inorg. Chim. Acta*, **1995**, *228*, 219.

91 King, R. B., *Inorg. Chim. Acta*, **1996**, *252*, 115.

92 Wang, Z. X., Schleyer, P. v. R., *Angew. Chem., Int. Ed. Engl.*, **2002**, *41*, 4082–4085.

93 Kohnlein, H., Stösser, G., Baum, E., Möllhausen, E., Huniar, U., Schnökel, H., *Angew. Chem., Int. Ed. Engl.*, **2000**, *39*, 799.

94 Sevov, S. C., Corbett, J. D., *Inorg. Chem.*, **1991**, *30*, 4875.

95 Hiller, W., Klinkhammer, K.-W., Uhl, W., Wagner, J., *Angew. Chem., Int. Ed. Engl.*, **1991**, *30*, 789.

96 Uhl, W., Cuypers, L., Harms, K., Kaim, W., Wanner, M., Winter, R., Koch, R., Saak, W., *Angew. Chem., Int. Ed. Engl.*, **2001**, *40*, 566.

97 Hönle, W., Grin, Y., Burckhardt, A., Wedig, U., Schultheiss, M., von Schnering, H. G., Kallner, R., Binder, H., *J. Solid State Chem.*, **1997**, *133*, 59.

98 Wiberg, N., Blank, T., Purath, A., Stößer, G., Schnöckel, H., *Angew. Chem., Int. Ed. Engl.*, **1999**, *38*, 2563.

99 King, R. B., *Inorg. Chim. Acta*, **1986**, *116*, 99.

100 Kehrwald, M., Köstler, W., Rodig, A., Linti, D., Blank, T., Wiberg, N., *Inorg. Chem.*, **2001**, *20*, 860.

101 Wiberg, N., Blank, T., Nöth, H., Ponikwar, W., *Angew. Chem., Int. Ed. Engl.*, **1999**, *38*, 839.

102 Parath, A., Koppe, R., Schnöckel, H., *Chem. Commun.*, **1999**, 1933.

103 Dong, Z., Corbett, J. D., *J. Am. Chem. Soc.*, **1995**, *117*, 6447.

104 Schnepf, A., Stösser, G., Schnöckel, H., *J. Am. Chem. Soc.*, **2000**, *122*, 9178.

105 Schnepf, A., Weckert, E., Linti, G., Schnöckel, H., *Angew. Chem., Int. Ed. Engl.*, **1999**, *38*, 3381.

106 Rodig, A., Linti, G., *Angew. Chem., Int. Ed. Engl.*, **2000**, *39*, 2952.

107 Köhnlein, H., Purath, A., Klemp, C., Baum, R., Krossing, I., Stößer, G., Schnöckel, H., *Inorg. Chem.*, **2001**, *40*, 4830.

108 Ecker, A., Weckert, E., Schnöckel, H., *Nature*, **1997**, *387*, 379.

109 Shechtman, D., Blech, I., Gratias, D., Cahn, J. W., *Phys. Rev. Lett.*, **1984**, *53*, 1951.

110 Shechtman, D., Blech, I. A., *Metall. Trans.*, **1985**, *16A*, 1005.

111 Janot, C., *Quasicrystals: a Primer*, Clarendon Press, Oxford, **1994**.

112 Mackay, A. L., *Acta Crystallogr.*, **1962**, *15*, 916.

113 Wang, Z.-X., Schleyer, P. v. R., *J. Am. Chem. Soc.*, **2003**, *125*, 10484.

114 King, R. B., Schleyer, P. v. R., Heine, T., in preparation.

115 McKee, M. J., *Inorg. Chem.*, **2002**, *41*, 1299.

2.1
Homonuclear Boron Clusters

H. Nöth

2.1.1
Introduction

The structural chemistry of boron hydrides and the interpretation of the bonding became one of the great challenges of inorganic chemistry after characterization by analysis, determination of physical constants and molecular weights by Alfred Stock [1]. Bonding in the smallest isolated member, diborane B_2H_6, could not be explained by normal covalent bonds as the simplest borane should have had the formula BH_3 having only an electron sextet, and this would be a high energy species. Because the hydrogen atoms of BH_3 have no lone pairs, a dimerization to the stable molecule B_2H_6 could not be explained by normal two center two electron covalent bonds (2c2e bonds). It has been suggested that the structure of diborane can be considered as a diprotonated $H_2B{=}BH_2^{2-}$ or as a resonance hybrid between two BH_3 units. After the structure of diborane had been determined, resonance formulae were put forward and this culminated in the ''banana bond'' description (three center two electron bonds, 3c2e-B–H–B bonds), as well as for polyboranes to the general acceptance of 3c2e bonds for the bonding between boron atoms (Figure 2.1-1). These bonding schemes have since then be proven to be very useful for describing the bonding in the polyboranes, once their structure had been determined.

Today the chemistry of diborane and the polyboranes is well understood [2] and much of it is textbook knowledge. Therefore, after a brief survey, emphasis will focus on the development of polyhedral borane chemistry within recent decades, and even restricting discussions to homopolyboranes only certain areas can be dealt with. This incorporates synthetic procedures, the chemistry of some polyboranes and particularly polyborane anions. Other chapters of this book are devoted to heteropolyboranes such as the carbaboranes (see Chapter 3.1), azaboranes and related heteropolyboranes (see Chapter 3.3) of the main group elements. In these areas enormous progress has been achieved within the last two decades.

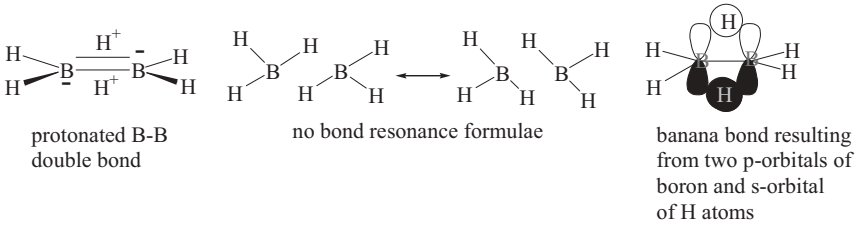

Fig. 2.1-1. Several bonding representations for diborane.

2.1.2
General Principles and Systematic Naming

In the early days of polyborane chemistry the chemical bonding in these molecular compounds posed great problems because there were too few electrons available to connect the atoms by the conventional covalent two center two electron bonds. This problem has been alleviated by the introduction of the 3c2e bonds of which there are two types in polyboranes, BHB-3c2e bonds and BBB-3c2e bonds. We will use here three center two electron bonds in localized descriptions although more sophisticated MO and *ab initio* methods, nowadays especially DFT methods, allow a more precise but less visual description of the bonding for deltahedral cluster compounds. In particular, these methods are so powerful that today they are indispensable to check and verify structural results obtained by X-ray diffraction analysis and high end NMR studies, as well as for predicting stability and structures of unknown polyboranes. An example is that the unknown $B_{13}H_{13}$ is expected to be a stable boron hydride and this would be the first *hypercloso*-polyborane (*vide infra*) [3]. Therefore, all these methods are today essential in polyborane cluster chemistry.

In general, polyboranes can be considered to be composed of structural fragments of small boranes which by themselves may not be stable, but their existence has either been deduced from kinetic data or they have been detected as intermediates. For instance, B_4H_{10} can be considered to be built from two BH_3 and one B_2H_4 units, and these are indeed easily recognizable in the structure of this borane. So far, four series of polyboranes are known:

B_nH_{n+4}: B_2H_6, $[B_3H_7]$, $[B_4H_8]$, B_5H_9, B_6H_{10}, B_8H_{12}, $[B_9H_{13}]$, $B_{10}H_{14}$, $B_{11}H_{15}$, $B_{12}H_{16}$, $B_{14}H_{18}$, $B_{16}H_{20}$, $B_{20}H_{26}$

B_nH_{n+6}: $[B_3H_9]$, B_4H_{10}, B_5H_{11}, B_6H_{12}, B_7H_{13}, B_8H_{14}, $B_{10}H_{16}$, $B_{13}H_{19}$, $B_{14}H_{20}$, $B_{20}H_{26}$

B_nH_{n+8}: B_6H_{14}, B_8H_{16}, $B_{10}H_{18}$, $B_{14}H_{22}$, $B_{15}H_{23}$

B_nH_{n+10}: B_8H_{18}, $B_{26}H_{36}$, $B_{40}H_{50}$

In addition there exists a boron rich polyborane such as $B_{20}H_{16}$, and this suggests that other boron rich polyboranes can be detected. Those polyboranes which are presented in square brackets have not been isolated but were either characterized

as fragments in addition products or postulated as reaction intermediates such as B_3H_9 in the pyrolysis of diborane. It should, however, be noted, that these series of polyboranes are strictly a formalism and say nothing about their stability and their structures, although expected structures can now be deduced from the composition by the so called Wade rules [4] (see Chapters 1.1.2 and 2.1.5.7). Moreover, cations and anions also exist which can be derived from neutral polyboranes. This extends the scope of polyborane chemistry enormously.

One might expect that a large number of isomers of polyboranes should exist as the number of boron atoms increases, similar to hydrocarbon chemistry. This, however, is not the case in borane chemistry. There are indeed only a few examples of proven isomerism, for instance for the $B_{20}H_{18}^{2-}$ anions (see Section 5.8). However, this point has been addressed in many theoretical papers, and energy differences between various isomers of a polyborane are, in general, larger than in hydrocarbons.

All hydrogen compounds of boron are known as boranes. In order to denote the number of boron atoms in a borane a Greek prefix is used, while the number of hydrogen atoms are given in Arabic numbers in parentheses at the end of the name. Thus, B_4H_{10} is known as tetraborane(10). Anions derived from boranes are named according to the rules for complexes, i.e., the hydrogen atoms are considered as ligands. $B_{12}H_{12}^{2-}$ is named as dodecahydro-dodecaborate(2−). Cations are characterized similarly, e.g., $B_6H_{11}^{+}$ is known as undecahydro-hexaborane(1+).

2.1.2.1 Structures and Bonding

The information on the structures of polyboranes that has so far accumulated shows that the boron atoms are present as edge sharing deltahedra. The neutral poylboranes have structures that are basket-like and can be derived from an icosahedron by removing one or more adjacent corners. The icosahedron with I_h symmetry is realized in the anion $B_{12}H_{12}^{2-}$. However, it is better not to describe the structure of B_5H_9 as a fragment of an icosahedron but rather as a tetragonal pyramid derived from octahedral $B_6H_6^{2-}$ by removing one corner.

The constituting boron atoms of the polyboranes, the carbaboranes (see Chapter 3.2) and other heteropolyboranes (see Chapters 3.3 and 3.4), including metallaboranes, are also characterized by the *connectivitiy c* of the skeletal atoms. The connectivity defines the number of atoms next to the atom in question within the cluster framework. Each atom within the cluster carries one exopolyhedral atom, in the case of the polyboranes a hydrogen atom. All other atoms build the cluster. For instance, $B_{12}H_{12}^{2-}$ has only exopolyhedral B–H bonds. Each atom has a connectivity $c = 5$, as each boron atom has five boron atoms next to it in the cluster. In $B_{10}H_{10}^{2-}$, which has the structure of a bicapped Archimedian antiprism, there are two boron atoms with $c = 4$ for the apical boron atoms, and eight boron atoms of $c = 5$ for the "belt" region (see Figure 2.1-2). Thus in B_5H_9, with its tetragonal pyramidal structure the apical boron atom has $c = 4$, while the basal boron atoms have $c = 3$ (neighboring B atoms) or $c = 5$ if we include the bridging hydrogen

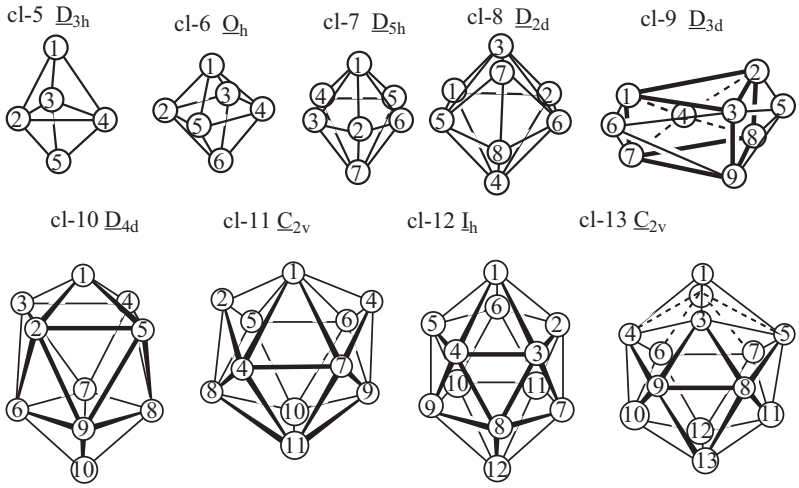

Fig. 2.1-2. Parent *closo*-$B_nH_n^{2-}$ structures [$n = 5$ to 13; *cl(oso)*-5 to *cl*-13].

atoms (see Figure 2.1-2). Most boron atoms of polyboranes have $c = 5$, but $c = 4$ is also quite common. However, $c = 6$ or 7 is not often observed, but it is found for boron atoms with $c = 6$ in $B_{11}H_{11}^{2-}$ or $c = 7$ in $B_{20}H_{16}$. It can be deduced that the more boron atoms of higher connectivity that are present in a polyborane the more stable will be the compound (see Figures 2.1-2, 2.1-3 and 2.1-4, which show structural relationships).

As previously indicated the bonding in the polyboranes will be described by localized bonds that is 2c2e, 3c2e and 4c2e bonds, the last being for protonated B_3 faces. B–H single bonds result from a combination of an sp-orbital of a boron and an s-orbital of a hydrogen atom. The 3c2e BHB bridge bond results from a combination of two sp^2-orbitals of two boron atoms and an s-orbital of a hydrogen atom. On the other hand, there are two types of 3c2e BBB bonds: the *open* one results from the combination of one sp^2-orbital, one each of two boron atoms, and a p-orbital of the third boron atom while the *closed (deltahedral)* 3c2e bond is a result of an overlap of three sp^2 orbitals, one for each boron atom. This is schematically depicted in Figure 2.1-5.

For many representations of the structures an open circle will denote a BH group with an exohydrogen atom, i.e., a hydrogen atom pointing radially away from the center of the deltahedron. A black circle represents an EH group, i.e., CH or NH, PH etc., and apart from CH the element E in question will be stated in the figure. Bridging hydrogen atoms of a BHB 3c2e bond will either be depicted by a small black circle on the line joining two boron atoms or by a bent line joining two boron atoms with the H atom located on top. Hydrogen atoms bound by a 4c2e bond to three boron atoms will be represented by dashed lines from the H atom to three boron atoms. The lines in structural formulae represent no bonding description but their connectivity both in planarized structural projections as well as

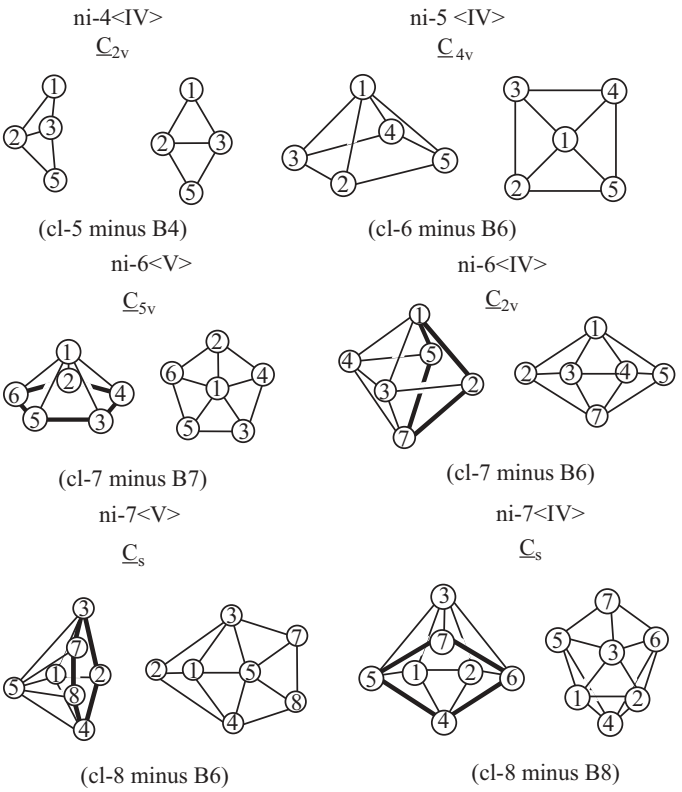

Fig. 2.1-3. Hypothetical parent *nido*-$B_nH_n^{4-}$ structures [$n = 4$–12: *ni(do)*-4 to *ni*-12] in perspective and planarized representation; bold lines mark the apertures (Roman numbers). The perspective representations are fragments of the corresponding *closo*-structures (see Figure 2.1-2). The connectivity of the removed vertex gives the polygon aperture to which the numbering corresponds. In the case of *ni*-9⟨V⟩, a second, more common arrangement is presented.

in ''three dimensional drawings''. *Closed* three center bonds will be shown as triangles or by three lines joining in the center of a triangle while *open* three center bonds will be represented by a bent line connecting three boron atoms in three dimensional representations or by dashed lines in planarized projections.

From the structural information one can derive allowed combinations of bonding in which one boron atom is involved from those which are forbidden for geometrical reasons. These are shown in Figure 2.1-6.

As is to be expected, all valence electrons and valence orbitals of the boron (4 orbitals) and hydrogen atoms (1 orbital) in the polyboranes and their derivatives are involved in bonding. (H atoms with 1 electron, H^- ions with two electrons, B atoms with 3 electrons, NR_3 molecules with two electrons, etc.). Then the following equations have to be satisfied:

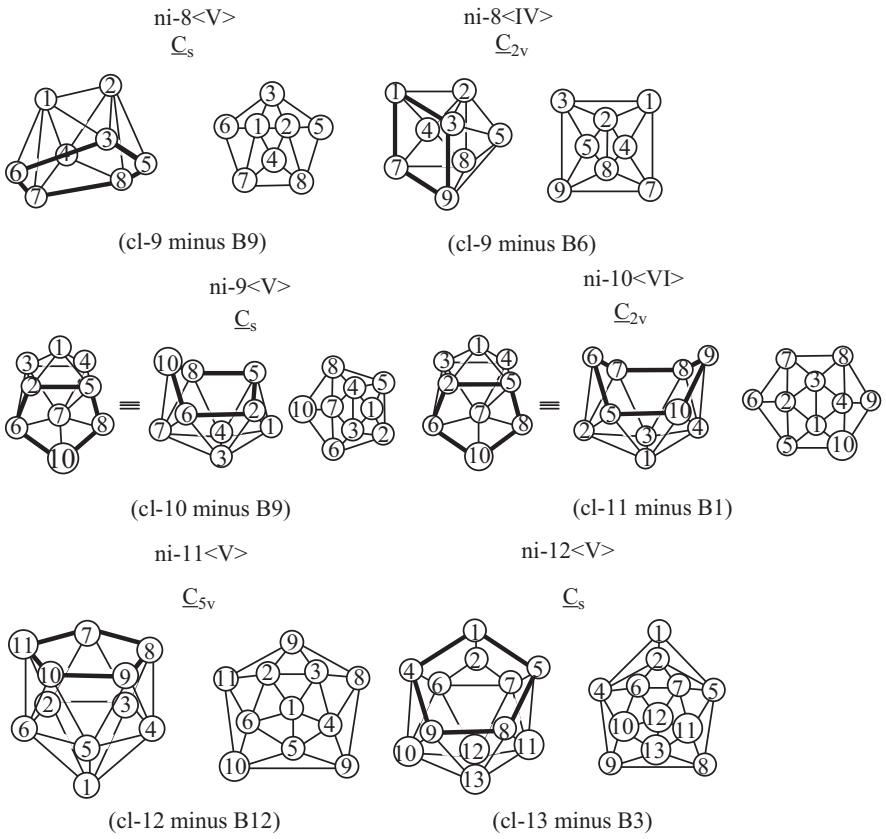

Fig. 2.1-3 *(continued)*

- Valence orbital balance: $o = 3t + 2\gamma$
- Valence electron balance: $e = 3t + 2\gamma + l$

Here t represents the number of 3c2e bonds, γ the number of 2c2e bonds and l the charge in the case of hydridopolyborate anions (l is negative in the case of polyborane cations). (see Chapter 1.1.1) So, it follows for B_4H_{10}:

- Sum of valence orbitals: $o = 4 \times 4 + 10 \times 1 = 26 = 3t + 2\gamma$
- Sum of valence electrons: $e = 4 \times 3 + 10 \times 1 + 0 = 22 = 2t + 2\gamma$

Therefore, the number of 3c2e bonds t for B_4H_{10} is 4, represented by four BHB bridge bonds. Similarly for B_5H_9 we have $o = 29$ and $e = 24$. It follows that there must be five 3c2e bonds which are realized by four BHB bonds and one BBB three center bond.

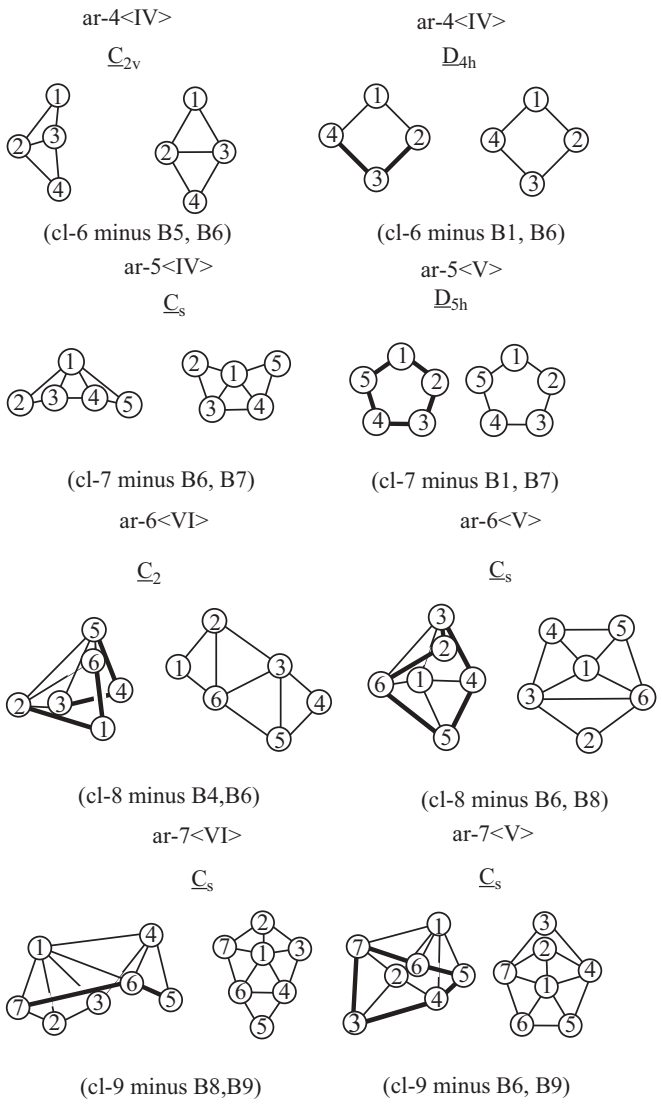

Fig. 2.1-4. Hypothetical parent *arachno*-$B_nH_n^{6-}$ structures [$n = 4$ to 11: *ar(achno)*-4 to *ar*-11] in perspective and planarized representation. Bold lines mark the apertures (Roman numbers); numbering in accord with IUPAC rules (as far as possible) or in accord with traditional *ni*-10(VI) numbering (in the case of *ar*-10⟨VI⟩, *ar*-11⟨VII⟩, *ar*-11⟨V, V⟩) or in accord with *ni*-11⟨V⟩ numbering (for *ar*-11⟨VI⟩). The perspective representations are fragments of the parent *closo* compound (see Figure 2.1-2). In the case of *ar*-11⟨VII⟩ and *ar*-11⟨VI⟩ a second more common arrangement is depicted.

ar-8<VI>

$\underline{C}_{2v}$

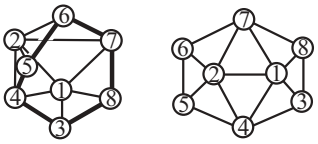

(cl-10 minus B5, B9)

ar-8<V>

$\underline{C}_{s}$

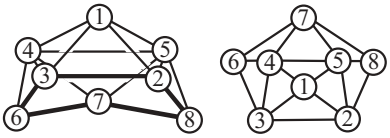

(cl-10 minus B9, B10)

ar-9<VII>

$\underline{C}_{s}$

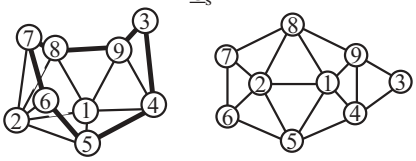

(cl-11 minus B1, B7)

ar-9<VI>

$\underline{C}_{3v}$

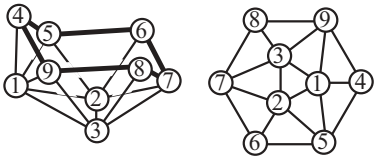

(cl-11 minus B1, B3)

ar-10<VI>

$\underline{C}_{2v}$

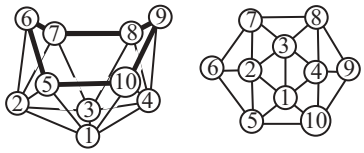

(cl-12 minus B11, B12)

ar-10<V,V>

$\underline{C}_{2v}$

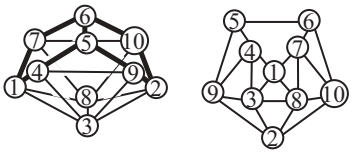

(cl-12 minus B6, B12)

ar-11<VII>

$\underline{C}_{1}$

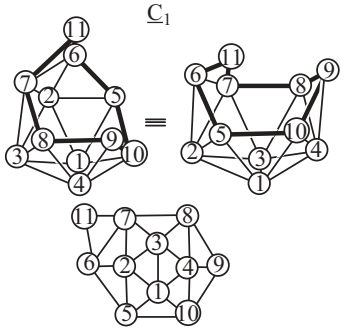

(cl-13 minus B3, B5)

ar-11<VI>

$\underline{C}_{s}$

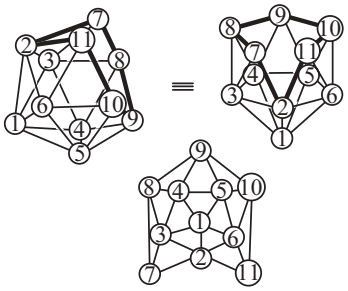

(cl-13 minus B1, B5)

ar-11<V,V>

$\underline{C}_{2v}$

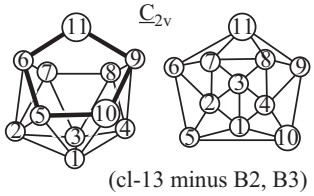

(cl-13 minus B2, B3)

Fig. 2.1-4 *(continued)*

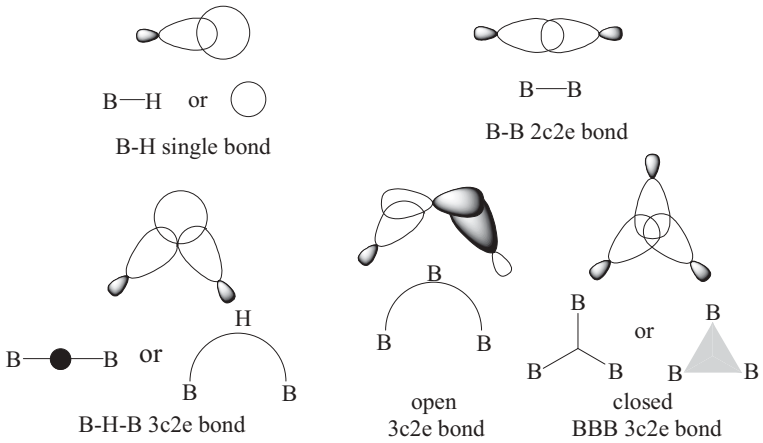

Fig. 2.1-5. Formal description of the bonding in polyboranes, and various representations used in depicting formulae.

Another very useful rule for classifying the structures of polyboranes and heteroboranes as well as many metal boron cluster compounds and their derivatives has been developed by Rudolph, Williams, Mingos and Wade (see Chapter 1.1.2) [4]. Today these are generally termed the Wade rules. They can be derived from the structures and electronic requirements of closed polyhedral boranes, such as an octahedron or an icosahedron, which are present in the anions $B_6H_6^{2-}$ and $B_{12}H_{12}^{2-}$. Since there are only exopolyhedral B–H bonds the number of electron

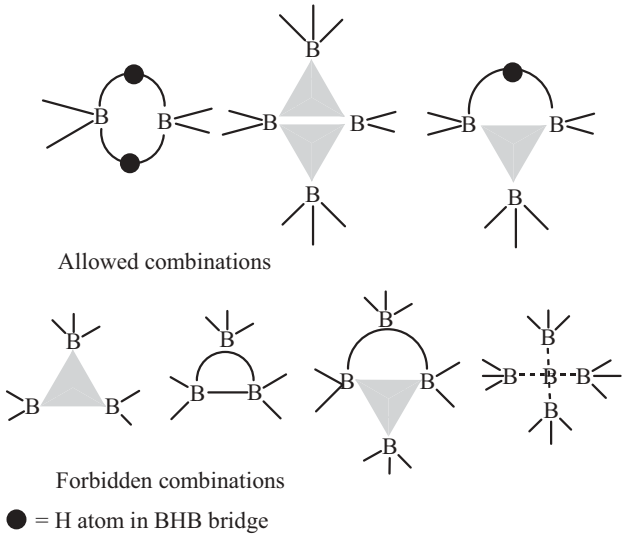

Fig. 2.1-6. Allowed and forbidden bonding combinations.

pairs available for bonding the boron cluster atoms in $B_nH_n^{2-}$ is $n+1$ electron pairs. On removal of a neutral BH group (as a three electron unit) from the $B_{12}H_{12}^{2-}$ icosahedron we arrive at $B_{11}H_{11}^{2-}$. This process makes five valence orbitals on an open pentagonal face of an icosahedron available for bonding. Compensating the charge with two protons we will have a boron hydride $B_{11}H_{13}$. If we now count electrons, we have $33 + 13 = 46$ electrons, of which 22 are used for 11 exopolyhedral BH bonds, leaving 24 electrons or 12 electron pairs for cluster bonding, i.e., $n+1$ electron pairs. If we add two negative charges by reducing $B_{11}H_{13}$ to $B_{11}H_{13}^{2-}$ we get an $n+2$ electron species with a more open structure. Boranes with this more open (nest) structure are called *nido*-polyboranes. In analogy, if we remove two adjacent BH groups we get, by the same procedure, polyboranes having $n+3$ electron pairs available for cluster bonding. These are called *arachno*-boranes (from spider like) which have an even more open structure than the *nido*-boranes. Boranes having $n+4$ cluster electron pairs are called *hypho*-boranes. Figures 2.1-2 to 2.1-4 show this relationships:

- *closo*-boranes: $n+1$ cluster electron pairs
- *nido*-boranes: $n+2$ cluster electron pairs
- *arachno*-boranes: $n+3$ cluster electron pairs
- *hypho*-boranes: $n+4$ cluster electron pairs

These counting rules can also be applied to heterosubstituted boranes. The two electron BH species can be replaced by an isoelectronic and isolobal EX group. Although the symmetry of the heteroborane will be different to the parent borane, its structural features will be retained. So BH can be replaced by LiH^{2-}, BeH^{-}, CH^{+}, NH^{2+} and OH^{3+}. In the case of *closo*-$B_{12}H_{12}^{2-}$ this generates an isoelectronic series of *closo*-compounds $B_{11}LiH_{12}^{4-}$, $B_{11}BeH_{12}^{3-}$, $B_{11}CH_{12}^{-}$, $B_{11}NH_{12}$ and $B_{11}(O)H_{12}^{+}$. Substitution of two BH groups in *closo*-$B_{12}H_{12}^{2-}$ by two CH^{+} groups generates the neutral *closo*-dicarbadodecaborane(12), $B_{10}C_2H_{12}$, or by replacement of two BH units from *nido*-$B_{11}H_{11}^{4-}$ by two CH^{+} groups the anion *nido*-$B_9C_2H_{11}^{2-}$. Both of these dicarbapolyboranes are important building blocks for organic derivatives as well as for main group and transition metal complexes. The latter with the $B_9C_2H_{11}^{2-}$ ligand are called metal carbollides. On the other hand, if we replace a BH group lets say by NH_3, NH_2, NH or N (one lone pair pointing outside of the cluster) then these groups supply two, three, four and three electrons. So in case of $B_{11}(NH)H_{11}^{2-}$ we have 14 electron pairs for cluster bonding, and, according to Wade rules, the compound is of the *nido*-type with an open face. In Figure 2.1-7 planarized structures for a number of polyboranes showing the 2c2e and 3c2e bonds are depicted.

In addition to these polyhedral boranes there exist polyboranes where two (or more) polyboranes are connected by single B–B bonds or by sharing three or four boron atoms of two (or more) borane units by 3c2e bonds. In the case of $B_{10}H_{16}$ there are two B_5H_8 units where the apical boron atoms of B_5H_9 are joined by a B–B bond (1,1′-isomer) or by a B–B bond between the apical boron atom of one pentaborane unit with a basal boron atom of a second pentaborane fragment

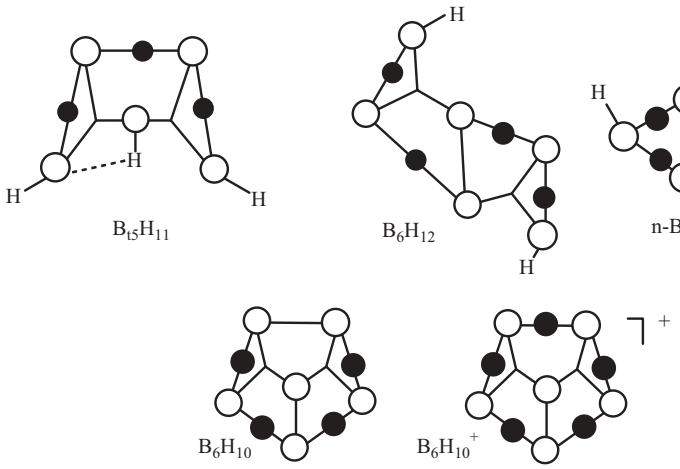

Fig. 2.1-7. Localized bonding description of some selected polyboranes.

(1,2′-isomer). The third possibility, a 2,2′-bis(pentaboranyl) has not yet been observed. The polyboranes that result on joining smaller borane fragments are called *conjuncto*-polyboranes. These belong formally to one of the B_nH_{n+m} series: $B_8H_{18} = 1,1'\text{-}(B_4H_9)_2$, $B_9H_{17} = 1,2'\text{-}(B_4H_9)(B_5H_8)$, $B_{10}H_{16} = 1,1'\text{-}(B_5H_8)_2$, $B_7H_{13} = \mu\text{-}2\text{-}(B_5H_8)(B_2H_5)$, $B_{20}H_{18}{}^{2-*} = 1,1'\text{-}(B_{10}H_9)_2{}^{4-}$.

More recently a rule has been proposed for finding the correct number of cluster electrons for condensed polyhedral boranes [5]. For a stable *closo*-borane with n vertices we need $n + 1$ electron pairs. For condensed polyboranes we need $m + n$ electron pairs, where m represents the number of polyhedral borane units in the condensed system, and n the number of boron vertices (atoms). Take as an example $B_{20}H_{16}$. Here we have two condensed icosahedrons and 20 vertices. Therefore, to bind the skeleton, $2 + 20 = 22$ electron pairs are required. The total number of electrons for $B_{20}H_{16}$ is $20 \times 3 + 16 \times 1 = 76$. So we have 38 electron pairs, with six electron pairs being supplied from the four *shared* boron atoms. Of these, 16 electron pairs out of the 38 are used for B–H bonding leaving $m + n = 22$ electron pairs for cluster bonding. Thus $B_{20}H_{16}$ should be (and is) a stable species. A similar calculation for $B_{21}H_{18}$, where two icosahedrons share three common boron atoms, shows that there are two polyhedrons and 21 vertices. So 23 electron pairs are required for bonding of the skeleton. However, the total number of electron pairs is only 22.5 (18 for BH groups and 4.5 for the three shared boron atoms). This suggests the $B_{21}H_{18}$ should carry a negative charge ($B_{21}H_{18}{}^-$) [6] to be a stable species, as is found experimentally [7].

Geometrically it is impossible for polyhedral boranes where two *closo*-polyboranes share two common boron atoms, i.e., a common edge, to exist, because the hydrogen atoms of the neighboring BH groups would interfere sterically. For instance, if two $B_{12}H_{12}$ units are joined by a common edge this would result in H–H distances of less than 1.5 Å, well below the van der Waals contacts. However,

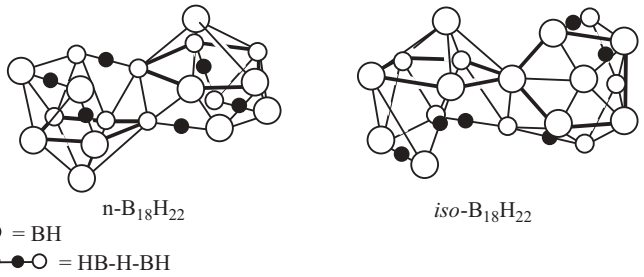

Fig. 2.1-8. The structure of the two isomeric condensed octadecaboranes (22).

in more open condensed *nido*-boranes, where one vertex is removed from a polyhedron, edge sharing is possible. However, an additional electron pair is needed to compensate for the loss of one BH group. Indeed, several molecules are known that are built from two *nido*-boranes joined by a common edge such as $B_{12}H_{16}$, $B_{13}H_{19}$, $B_{16}H_{20}$, $B_{18}H_{20}^{2-}$, and the isomeric pair $B_{18}H_{22}$ (see Figure 2.1-8) [7–9]. For $B_{18}H_{22}$, which is derived from $B_{10}H_{14}$, $n = 18$, $m = 2$, so a total of $n + m + p = 18 + 2 + 2 = 22$ electron pairs are required [p is the number of electron pairs resulting from the number (p) of removed BH units] for skeletal bonding. These are supplied from 16 BH units, six bridging H atoms (electrons) and six electrons from the two shared boron atoms. Table 2.1-1 shows several examples.

2.1.3 Synthetic Methods

In principle, several general methods are available for the synthesis of polyboranes and their derivatives, and only three will be discussed in more detail:

Tab. 2.1-1. Electron pair counts for condensed *nido*-boranes.

Borane	*n*	*m*	*p*	$\sum$	*BH*	*B*[a)]	H_{bridge}	$\sum$	*Q (charge)*
$B_{12}H_{12}$	12	1	0	13	12	0	0	12	−2
$B_{12}H_{16}$	12	2	2	16	10	3	3	16	0
$B_{13}H_{19}$	13	2	2	17	12	1.5	3.5	17	0
$B_{16}H_{20}$	16	2	2	20	14	3	3	20	0
$B_{18}H_{20}$	18	2	2	22	16	3	2	21	−2
$B_{18}H_{22}$[b)]	18	2	2	22	16	3	3	22	0
$B_{19}H_{20}$[c)]	19	2	2	23	17	3	1.5	21.5	−3
$B_{20}H_{16}$	20	2	0	22	16	6	0	22	0
$B_{21}H_{18}$	21	2	0	23	18	4.5	0	22.5	−1
$B_{22}H_{20}$	22	2	0	24	20	3	0	2	−2

[a)] Number of boron atoms at shared positions. [b)] Tow isomers. [c)] This anion was suggested to be $B_{19}H_{20}^-$ [9] but should be $B_{19}H_{20}^{3-}$ by these counting rules [5, 6]. The anion was prepared from $Na_2B_{18}H_{20}$ and $H_2BCl{\cdot}SMe_2$ [10].

1. Pyrolysis of diborane and other boron hydrides.
2. Preparation of hydridopolyborates followed by subsequent protonation or substitution reactions (cluster expansion).
3. Platinum-catalyzed dehydrocoupling.

2.1.3.1
Diborane Pyrolysis

Diborane, B_2H_6, which can be readily prepared by a number of routes from alkali metal tetrahydroborates, MBH_4 [11], as shown in Eqs. (1) and (2), is a metastable gas which decomposes with hydrogen evolution at temperatures >50 °C producing various polyboranes. Depending on the reaction conditions such as temperature, pressure, presence of hydrogen gas and time the following polyboranes were isolated: B_4H_{10}, B_5H_9, B_5H_{11}, B_6H_{10}, B_6H_{12}, B_8H_{12}, B_9H_{15}, $B_{10}H_{14}$, and $B_{20}H_{16}$.

$$3LiBH_4 + BF_3 \rightarrow 3LiF + 2B_2H_6 \quad (1)$$

$$3NaBH_4 + 4BF_3 \rightarrow 3NaBF_4 + 2B_2H_6 \quad (2)$$

It was shown that the rate of decomposition of diborane follows a rate law that corresponds to $d(B_2H_6) = k[B_2H_6]^{3/2}$. This is consistent with the dissociation of diborane into BH_3 as the rate determining step with formation of $\{B_3H_9\}$. This intermediate then decomposes with hydrogen evolution to give unstable B_3H_7 which on reaction with further BH_3 produces B_4H_{10} as the first isolable polyborane:

$$B_2H_6 \rightleftarrows 2BH_3 \quad (3)$$

$$B_2H_6 + BH_3 \rightleftarrows \{B_3H_9\} \quad (4)$$

$$\{B_3H_9\} \rightleftarrows \{B_3H_7\} + H_2 \quad (5)$$

$$\{B_3H_7\} + \{BH_3\} \rightleftarrows B_4H_{10} \quad (6)$$

$$B_4H_{10} \rightleftarrows \{B_4H_8\} \quad (7)$$

$$\{B_4H_8\} + \{B_3H_7\} \rightleftarrows B_5H_{11} + B_2H_6 \quad (8)$$

$$3B_5H_{11} \rightarrow 2B_5H_9 + B_2H_6 \quad (9)$$

$$B_6H_{10} + 2B_2H_6 \rightarrow B_{10}H_{14} + 4H_2 \quad (10)$$

$$B_6H_{10} + \{B_3H_7\} \rightarrow B_9H_{15} + H_2 \quad (11)$$

$$B_9H_{15} \rightarrow B_8H_{12} + \{BH_3\} \quad (12)$$

$$B_8H_{12} + \{B_3H_7\} \rightarrow B_9H_{13} + B_2H_6 \quad (13)$$

$$B_9H_{13} + \{B_3H_7\} \rightarrow B_{10}H_{14} + B_2H_6 \quad (14)$$

Most of these reactions are reversible. Thus, heating tetraborane(10) in the presence of a large excess of hydrogen reforms diborane. Pentaborane(11) is thermally

unstable and decomposes to B_5H_9 with diborane formation as shown in Eq. (9) in a first-order reaction. Processes of these types continue to form the higher polyboranes such as B_6H_{10} that reacts with diborane involving once again the species $\{B_3H_7\}$, which finally produces decaborane(14) as shown in Eq. (10). However there are several intermediate steps involved as depicted in Eqs. (11–14). For instance, B_9H_{15} is another intermediate [Eq. (11)], and the pyrolysis leads finally to the thermally quite stable, solid decaborane(14) as depicted in Eqs. (12–14). Thus, the species $\{B_3H_7\}$ plays a decisive role in the pyrolysis of the boron hydrides [12]. Pentaborane(5) and decaborane(14) were produced on a large scale by pyrolysis of diborane [13].

2.1.3.2 The Anionic Route

The synthesis of hydropolyborates proceeds in a similar way to the formation of polyboranes from diborane or other boranes. These reactions all start from an alkali metal tetrahydroborate, in most cases from the commercially available $NaBH_4$ or tetraalkylammonium tetrahydroborates $R_4N[BH_4]$. Although several routes are available and specifically designed for the preparation of a particular hydropolyborate, e.g., $B_3H_8^-$, $B_5H_8^-$, $B_9H_{11}^{2-}$, $B_{10}H_{10}^{2-}$, $B_{11}H_{14}^-$, $B_{12}H_{12}^{2-}$, the routes to produce them have only been explored systematically more recently. Similar to the build-up reactions of polyboranes starting from diborane, thermolysis of tetrahydroborates leads to the formation of hydropolyborates. In a first step the reactive species BH_3 is formed in a stabilized form either by a donor molecule L as in $H_3B{\cdot}L$, L being usually an ether molecule such as diglyme or BH_4^- (which forms $B_2H_7^-$) as an intermediate.

It should be noted that BH_4^- is not a typical Lewis base (such as the O atoms of ethers or N atoms of amines are). However, it is well known that Lewis acids add BH_4^- via 3c2e bonds. Thus, $B_2H_7^-$ is formed readily by the interaction of diborane (or $BH_3{\cdot}L$) with $NaBH_4$ in the presence of a polyether or, even better, in the presence of a large cation such as tetrabutylammonium as shown in Eqs. (15) and (16) [14]. In the latter case, the heptahydrodiborate $B_2H_7^-$ can also be prepared in a non-polar solvent such as hexane. The diborane that is required for these reactions can be generated from the tetrahydroborates with either BCl_3, BF_3-etherates or iodine. The structure of the $B_2H_7^-$ anion in the $[(Ph_3P)_2N]^+$ salt shows a single hydrogen bridge $[H_3B\cdots H\cdots BH_3]^-$ with a bent B–H–B bond [angle 136.6(2)°] [15].

$$2NaBH_4 + B_2H_6 \rightarrow 2NaB_2H_7 \quad (15)$$

$$2Bu_4N(BH_4) + B_2H_6 \rightarrow 2Bu_4N(B_2H_7) \quad (16)$$

$$2MBH_4 + I_2 \rightarrow 2MB_2H_7 + 2MI + H_2 \quad (17)$$

$$2MB_2H_7 + I_2 \rightarrow 2B_2H_6 + 2MI + H_2 \quad (18)$$

$(M = Li^+, Na^+, R_4N^+, R_4P^+)$

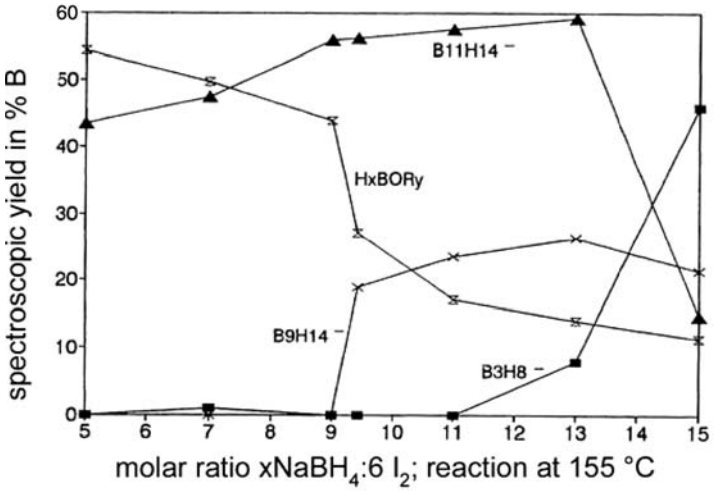

Fig. 2.1-9. Formation of $B_9H_{14}^-$ and $B_{11}H_{14}^-$ by oxidation of $NaBH_4$ with iodine in diglyme.

A conversion of $NaBH_4$ into NaB_2H_7 in better than 95% yield has been achieved in diglyme using iodine. The best results were obtained with an $NaBH_4$:I_2 ratio of 3.72:1, and byproducts being small amounts of BH_3·L and NaB_3H_8 (<3%) [16]. Similarly, the salts $Ph_4P[B_2H_7]$, $Ph_3MeP[B_2H_7]$ or $Et_4N[B_2H_7]$ can be prepared from the corresponding tetrahydroborates and iodine in solvents such as CH_2Cl_2 or $CHCl_3$ [16].

The reaction proceeds according to Eq. (17). An additional equivalent of iodine reacts at ambient temperature to produce diborane. If this reaction is performed with $Et_4N[B_2H_7]$ in CH_2Cl_2 then the unstable anion H_3BI^-, and the more stable anions $H_2BI_2^-$ and HBI_3^- can be detected by ^{11}B NMR spectroscopy in small amounts.

Figure 2.1-9 shows that the iodine oxidation of $NaBH_4$ also leads to $B_9H_{14}^-$ and $B_{11}H_{14}^-$. The best yield (55%) of the former is obtained at 115 °C in diglyme solution within 5 h at a ratio of $NaBH_4$:I_2 = 9:4. This corresponds to the theoretical requirement as shown in Eq. (19).

$$9NaBH_4 + 4I_2 \rightarrow NaB_9H_{14} + 1H_2 + 8NaI \quad (19)$$

$$11NaBH_4 + 5I_2 \rightarrow NaB_{11}H_{14} + 15H_2 + 10NaI \quad (20)$$

However, even then, about 30% of the BH_4^- is already converted into $B_{11}H_{14}^-$. The yield of the undecahydroundecaborate(−1) reaches a maximum (75%) at 135 °C when a 26% excess of I_2 as demanded by Eq. (20) is employed due to loss of HI at this temperature, and this is achieved within 2.5 h [16]. The B_{11} anion can be precipitated from an aqueous solution as $Ph_4As[B_{11}H_{14}]$ or $Bu_4N[B_{11}H_{14}]$. Yields of up to 62% were observed by a similar reaction using $NaBH_4$ and BF_3·OEt_2 [17, 18].

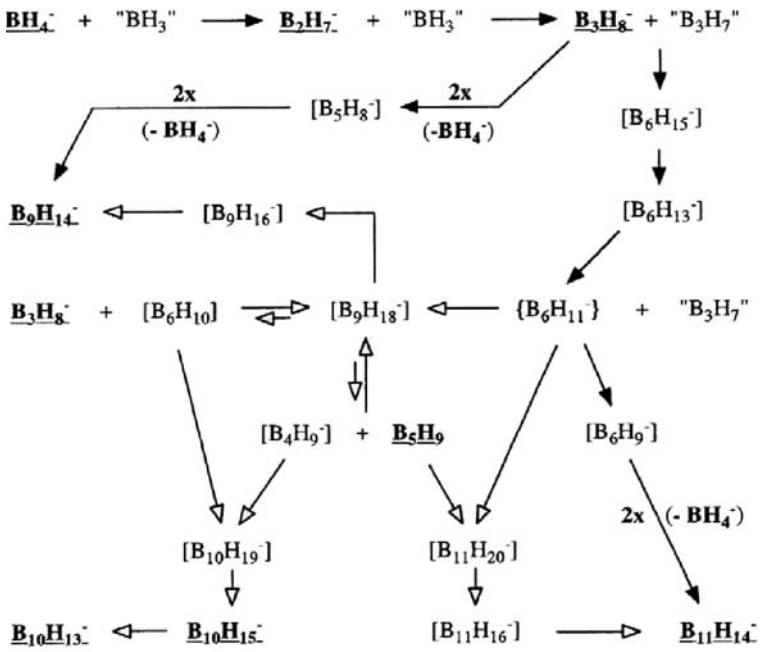

Scheme 2.1-1. Hydropolyborate formation by oxidation of $NaBH_4$. Anions in parentheses are possible intermediates.

Scheme 2.1-1 summarizes the most likely steps in the oxidative formation of hydridopolyborate anions from $NaBH_4$ and iodine. Anions in bold face have been detected by ^{11}B-NMR spectroscopy and bold arrows show the main reaction pathways. The formation of $B_9H_{14}^-$ from $B_3H_8^-$ and $B_5H_8^-$ or $B_6H_9^-$ as well as $B_{11}H_{14}^-$ from $B_5H_8^-$ and $B_6H_9^-$ has also been established [19]. This route supplies no *closo*-hydropolyborates, which require higher temperatures in order that ether cleavage may occur.

Another, quite versatile, route to hydropolyborates is based on the thermal decomposition of tetraorganylammonium tetrahydroborates, $R_4N[BH_4]$. Here, the products formed depend on temperature and time. For each hydropolyborate reaction conditions have to be optimized.

A systematic study using the thermolysis of $Et_4N[BH_4]$ has shown that within the first 20 h at 155 °C the reaction proceeds principally as described by Eq. (21):

$$3Et_4N[BH_4] \rightarrow Et_4N[B_3H_8] + 2Et_3N + H_2 + 2EtH \quad (21)$$

$$3Et_4N[B_3H_8] + BH_3{\cdot}NEt_3 \rightarrow [Et_4N]_2[B_{10}H_{10}] + EtH + 2Et_3N \quad (22)$$

On further heating the formation of $B_{10}H_{10}^{2-}$ dominates reaching 70% after 200 h. An additional anion, $B_9H_9^{2-}$, is also formed (up to 10%) after 125 h, as well as $B_{12}H_{12}^{2-}$ (20% yield) after 200 h (see Figure 2.1-10) [16].

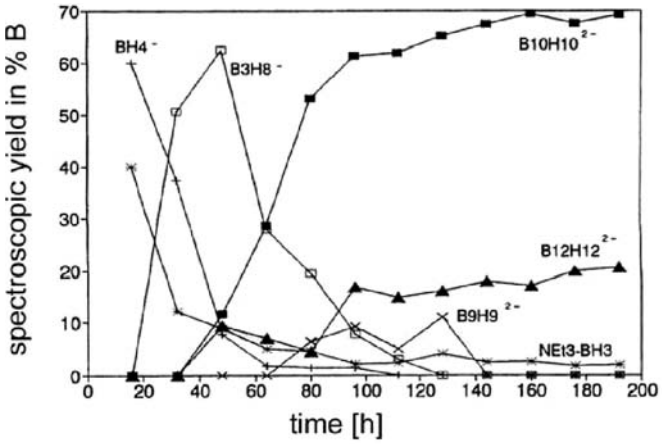

Fig. 2.1-10. Time dependent *closo*-hydropolyborate formation from $Et_4N[BH_4]$ at 155 °C.

Thermolysis of $Et_4N[BH_4]$ at 185 °C leads to a 50–60% yield of $B_{10}H_{10}^{2-}$ with an increasing amount of $B_{12}H_{12}^{2-}$ up to 40–45% after 190 h. In addition an 18% yield of $B_{11}H_{11}^{2-}$ is indicated within 20 h and this amount decreases with time to about 5% (190 h). At 200 °C the dominating product is $B_{12}H_{12}^{2-}$ (about 60% after 190 h) while the amount of $B_{10}H_{10}^{2-}$ decreases continuously from 55% (within 20 h) to about 20% (within 190 h). The increase of the *closo*-dodecaborate ion concentration matches the decrease of the *closo*-decaborate concentration while an almost constant, but low, level of $B_9H_9^{2-}$ is retained (around 3%). In the initial stages, the $B_{11}H_{11}^{2-}$ anion concentration is about 17% and decreases to about 7%. It is obvious from these data that the cluster expansion reaction to B_{12} proceeds by a process that allows the transfer of BH units from the $B_9H_9^{2-}$ unit to $B_{11}H_{11}^{2-}$. This is formally represented by the Eqs. (21–23):

$$2B_{10}H_{10}^{2-} \rightarrow B_9H_9^{2-} + B_{11}H_{11}^{2-} \quad (21)$$

$$2B_{11}H_{11}^{2-} \rightarrow B_{10}H_{10}^{2-} + B_{12}H_{12}^{2-} \quad (22)$$

$$B_9H_9^{2-} + nB_{11}H_{11}^{2-} \rightarrow nB_{12}H_{12}^{2-} + [B_{9-n}H_{9-n}]^{2-} \quad (23)$$

The pyrolysis of $[Et_4N][BH_4]$ demonstrates that the stability of the *closo*-hydropolyborates increases along the series $B_9H_9^{2-} < B_{11}H_{11}^{2-} < B_{10}H_{10}^{2-} < B_{12}H_{12}^{2-}$, and this is in accord with calculated stabilities [20].

2.1.3.3
Platinum-catalyzed Dehydrocoupling

Boron hydrides are reducing agents and reduce many metal cations to the metal. However, it is also known that noble metal complexes, particularly those of rho-

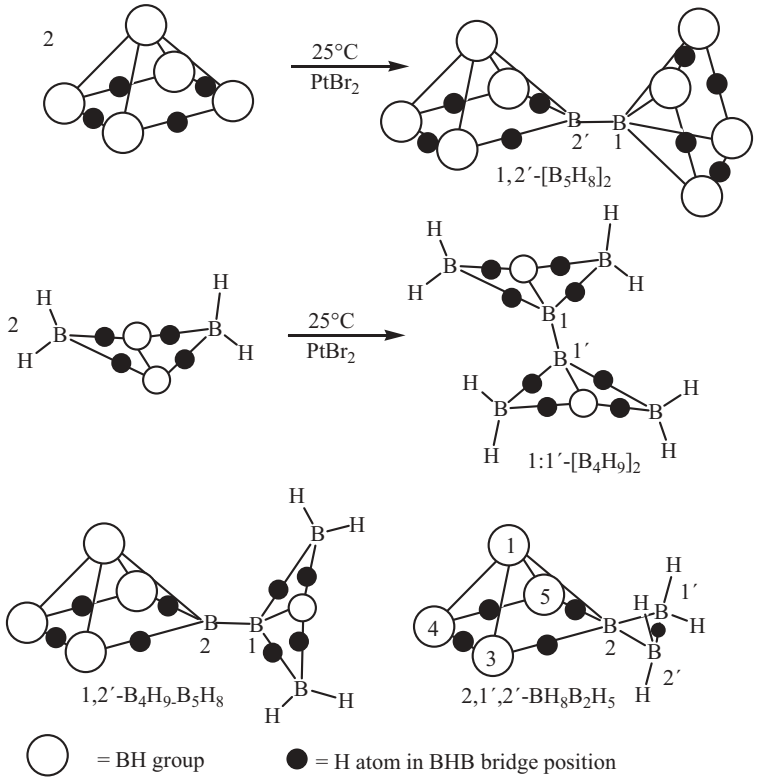

Fig. 2.1-11. Some dehydrocoupling reactions and products thereof.

dium and platinum, catalyze hydroboration reactions. It has been shown that boryl transition metal complexes are reaction intermediates. Therefore, it is not really surprising that $PtBr_2$ can be used to synthesize new polyboranes by a dehydrocoupling reaction with generation of a boron to boron bond. Some typical examples are shown in Figure 2.1-11:

For instance, the *conjuncto*-1,2′-$(B_5H_8)_2$ isomer is formed with high selectivity. Similarly, tetraborane(10) reacts at room temperature to give *conjuncto*-1,1′-$(B_4H_9)_2$. This is an unstable polyborane which decomposes above −30 °C. This method has also been used to synthesize "mixed" polyboranes. For instance, B_5H_9 reacts with B_4H_{10} in the presence of $PtBr_2$ to give 1,2′-$(B_4H_9)(B_5H_8)$. There is even evidence that a polyborane $B_7H_{13} = (B_5H_8)(B_2H_5)$ is generated when pentaborane(9) is allowed to react with diborane in the presence of $PtBr_2$. This borane can be derived from diborane by replacing one of its bridging hydrogen atoms by a B_5H_8 fragment generating a BBB 3c2e bond with a basal boron atom of the pentaborane molecule [21].

2.1.3.4
Cluster Expansion and Cluster Contraction Reactions

In general the deprotonation of a polyborane B_nH_{n+m} ($m = 4, 6$) leads to the anions $[B_nH_{n+m-1}]^-$ or $[B_nH_{n+m-2}]^{2-}$ by removal of one or two protons from a BHB 3c2e bridge with formation of a B–B single bond. Cluster expansion with a BH_3 unit, usually offered as diborane in diethyl ether or tetrahydrofuran, produces borane anions $[B_{n+1}H_{n+m+2}]^-$ or $[B_{n+1}H_{n+m+1}]^{2-}$ and these in turn on protonation give the polyboranes $B_{n+1}H_{n+m+3}$. These may be stable species. However, in most cases they loose H_2 which results in a cluster expansion by one BH unit. Several examples of this method are described in the following sections.

2.1.4
Chemistry of Selected Polyboranes

2.1.4.1
Chemistry of Triborane B_3H_7

Triborane B_3H_7 can be readily generated from $B_3H_8^-$ by reaction with a non-oxidizing protic acid in the presence of an ether. Under these conditions it must be stabilized as a Lewis acid base adduct. The 1:1 THF adduct of B_3H_7 is quite stable and is most often used for further reactions. The ether may be readily replaced by stronger bases such as dimethylamine [22]:

$$B_3H_8^- + H^+ + THF \rightarrow B_3H_7{\cdot}THF \tag{24}$$

$$B_3H_7{\cdot}THF + HNMe_2 \rightarrow B_3H_7{\cdot}NHMe_2 + THF \tag{25}$$

Amines, phosphines, acetonitrile, and many other neutral Lewis bases as well as anions such as hydride, halides (F^- to I^-), cyanide or thiocyanate add readily to B_3H_7. The latter can be used to make anionic adducts of B_3H_7 which are derived from the octahydridotriborate(1–) by replacement of a hydride ion or by another monovalent anion. It is interesting that $B_3H_7NCS^-$ is know in two isomeric forms, an ambient temperature form and a low temperature form as established by X-ray crystallography (see Figure 2.1-12). Although triborane(7) cannot be isolated, MO calculations show that a single BHB bridged species is more stable than alternatives with two hydrogen bridges (Figure 2.1-12) [23]. The anion $B_3H_8^-$ in the solid state shows three types of hydrogen atoms, however, in solution, only one type of proton and boron atom is seen in its NMR spectrum, indicating fluxional character.

Aminoiminoboranes $R_2N{-}B{\equiv}NR$ are readily hydroborated by either $H_3B{\cdot}THF$ or $H_3B{\cdot}SMe_2$. Therefore, one could expect that the triborane adduct $B_3H_7{\cdot}THF$ would behave similarly. This is indeed the case. Owing to the basic character of tmp-$B{\equiv}N{-}t$Bu (tmp = 2,2,6,6-tetramethylpiperidino group) the first step is the replacement of THF to give tmp $B{=}NBu^t{\cdot}B_3H_7$ followed by hydroboration at the

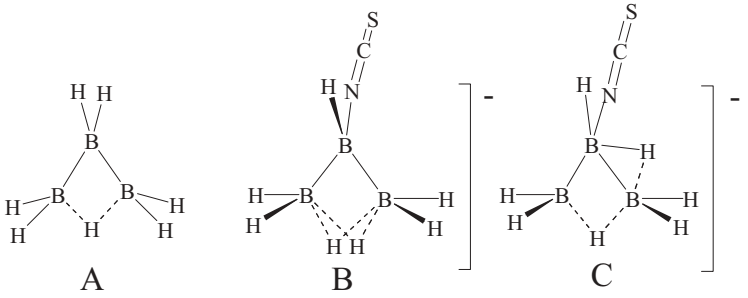

Fig. 2.1-12. Structural representations of triborane B_3H_7 and its thiocyanate anion. (A) Calculated ground state structure of B_3H_7; (B) *ambient temperature* structure of the B_3H_7·NCS anion; (C) *low temperature* structure of the B_3H_7NCS anion.

B=N–CMe_3 double bond. This generates a diazatetraborane derivative [24] (Figure 2.1-13). In contrast, B_3H_7·THF reacts with the iminoborane Bu^t–B≡N–Bu^t to give a μ-amino-diborane in which the Bu^t groups stand *trans* to each other [25].

The thallium salt or the tetramethylammonium salt of $B_3H_8^-$ open the route to transition metal octahydrotriborates by metathesis with transition metal complex monohalides. Examples are $CpFe(CO)(B_3H_8)$, $FeH(CO)_2(B_3H_8)$ [26] or $(Ph_3P)_2CuB_3H_8$ [27], and, according to spectral data, the triborate anion binds to the metal atom of the complexes with two of its hydrogen atoms (Figure 2.1-14). This is also the case for $ClCuB_3H_8$ obtained from $Et_4N[B_3H_8]$ and CuCl [28]. However, the reaction of $Me_4N[B_3H_8]$ with $Mn(CO)_5Br$ yields $Mn(CO)_4(\mu_2\text{-}B_3H_8)$

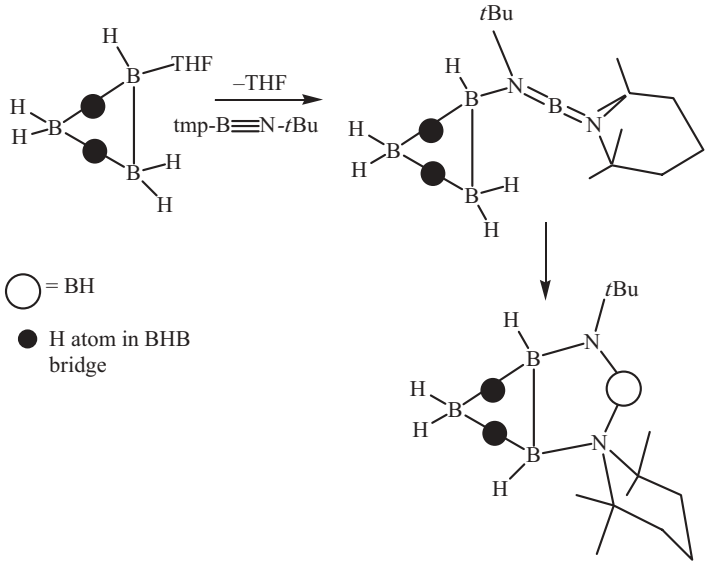

Fig. 2.1-13. Reactions of B_3H_7·THF with the iminoborane tmp B≡NBu^t.

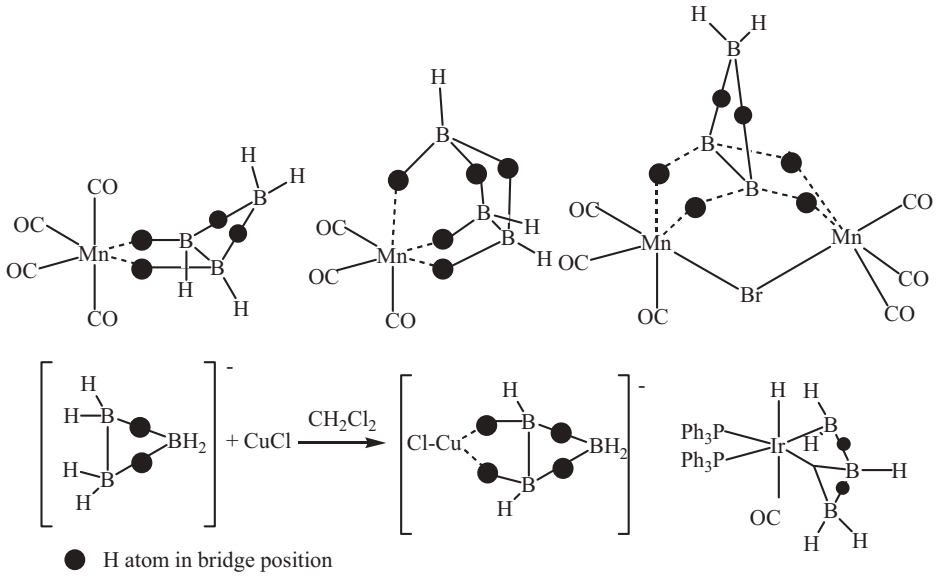

Fig. 2.1-14. Structures of some transition metal octahydrotriborates.

[29], which on thermolysis at 180 °C gives $(CO)_3Mn(\mu_3\text{-}B_3H_8)$ with formation of three Mn···H–B bonds [30]. Reaction of this compound with bromine leads to the binuclear manganese complex having a MnBrMn bridge and a $B_3H_8^-$ ligand which binds to the two Mn atoms by *four* of its hydrogen atoms. On the other hand, the reaction between TlB_3H_8 and *trans*-$Ir(CO)(PPh_3)_2$ yields a complexed triborane(7) with formation of an Ir–B bond [31]. In this case, a hydrogen atom has been moved from the boron to the iridium atom, a behavior that is not uncommon for metal boryl complexes.

2.1.4.2 Chemistry of Tetraboranes

2.1.4.2.1 *arachno*-Tetraborane(10)

arachno-Tetraborane(10) (Figure 2.1-15) was one of the first polyboranes to be discovered by A. Stock. It is formed by acid hydrolysis (HCl or H_3PO_4) of magnesium boride. It has a butterfly boron skeleton with C_{2v} symmetry, and there are seven electron pairs available for the skeletal atom bonding. As can be seen from the description by localized bonds, there are four 3c2e BHB bonds and one B–B single bond besides two extra terminal H atoms:

B_4H_{10} forms slowly by decomposition of diborane, B_2H_6, in a slightly exothermic reaction ($\Delta H = -14$ kJ mol^{-1}) and it is produced in a hot-cold-reactor (120 °C/−78 °C). At present the best method is to react $Bu_4N[B_3H_8]$ with BCl_3 or $AlCl_3$ in the presence of toluene as shown in Eq. (26):

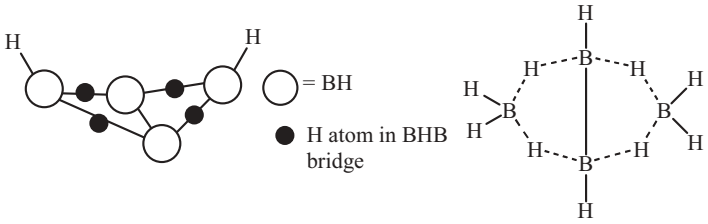

Fig. 2.1-15. Two representations of the structure of *arachno*-tetraborane(10).

$$2Bu_4N[B_3H_8] + ECl_3 \rightarrow B_4H_{10} + \{B_2H_4\} + 2Bu_4N[EHCl_3] \quad (26)$$

$E = B, Al$

It is most likely that unstable B_3H_7 is generated in a first step. Its dimerization leads to unstable B_6H_{14} [32] which decomposes to tetraborane(10) and non-characterized additional boron compounds, denoted in Eq. (26) as $\{B_2H_4\}$.

Pure tetraborane(10) hydrolyzes readily, decomposes at slightly elevated temperatures with hydrogen evolution and formation of higher boron hydrides (particularly *arachno*-B_5H_{11}). The structure of tetraborane(10) B_4H_{10} reveals that it can be considered to be built from two molecules of BH_3 and one molecule of B_2H_4. This suggests that Lewis bases may remove BH_3 groups as adducts $H_3B{\cdot}L$ with formation of adducts $B_3H_7{\cdot}L$ and/or $B_2H_4{\cdot}2L$. Moreover, one can also note in the structure the fragment BH_4. Removal of BH_4^- would leave a fragment $B_3H_6^+$. Moreover, heterolysis may also occur with formation of the fragment BH_2^+ and $B_3H_8^-$. Both cations will not exist freely but must be stabilized by Lewis bases. Moreover, *arachno*-B_4H_{10} may loose H_2 to produce B_4H_8 or B_4H_6. The former would be a *nido*-species, the latter a *closo*-compound. All these types of reactions and compounds have been observed.

Tetraborane(10) is a very weak acid. Therefore, deprotonation requires a very strong base:

$$B_4H_{10} \underset{+HCl,\,-MCl}{\overset{+MH,\,-H_2}{\rightleftharpoons}} B_4H_9^- \quad (27)$$

$M = Na, K$

Reactions according to Eq. (27) are achieved with hydrides such as NaH or KH in THF, or with lithiumorganyls, e.g., LiMe. The formation of gases such as hydrogen or methane shifts the equilibrium to the right hand side. Reprotonation of the $B_4H_9^-$ anion can be achieved with liquid HCl. Instead of a protic acid the Lewis acid diborane (formally BH_3) also adds to $B_4H_9^-$ with cluster expansion to give *hypho*-$B_5H_{12}^-$.

Lewis bases such as NMe_3, PMe_3, Me_2S react with tetraborane(10) readily but not with formation of adducts $B_4H_{10}{\cdot}L$ or $B_4H_{10}{\cdot}2L$ but rather by removing BH_3 units in a so-called symmetrical cleavage reaction as shown in Figure 2.1-16.

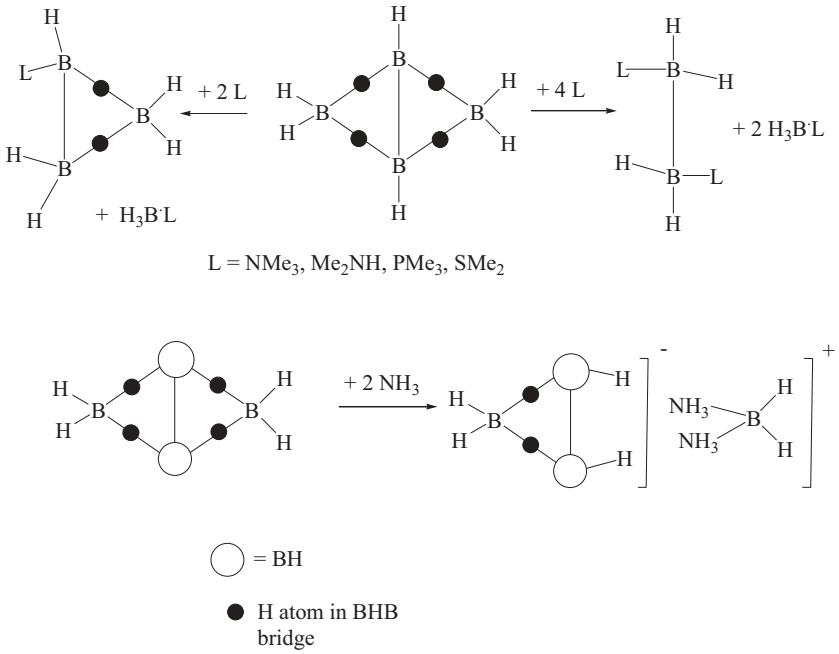

Fig. 2.1-16. Some typical reactions of B_4H_{10} with ammonia and amines.

Symmetrical cleavage also occurs with alkali metal hydrides MH (MH = LiH, NaH) in diethyl ether. The products are MBH_4 and MB_3H_8. In the case of Br^- one obtains $B_3H_7Br^-$ [33] and MBH_4. In addition to these "symmetrical" cleavages the "asymmetrical" cleavage has been found with ammonia as a base. However, this splitting of B_4H_{10} into a B_1 and a B_3 fragment is also observed when a boron hydride is offered as a hydride source. The borane reacts with *hypho*-$B_4H_8L_2$ according to Eqs. (28) and (29) [34]. Similarly, *arachno*-$B_2H_4L_2$ and *arachno*-B_4H_{10} react by transfer of a BH_2^+ unit from B_4H_{10} thus generating the salt $[B_3H_6L_2][B_3H_8]$ [35]. The adduct $B_2H_4(PMe_3)_2$ shows an even more interesting behavior. It reacts readily with diborane or tetraborane(10) to generate cations derived from triborane as shown in Eqs. (30–32) [36]:

$$\textit{hypho}\text{-}B_4H_8L_2 + B_4H_{10} \rightarrow \textit{arachno}\text{-}[B_4H_7L_2][B_3H_8] + \tfrac{1}{2}B_2H_6 \quad (28)$$

$$\textit{arachno}\text{-}B_2H_4L_2 + B_4H_{10} \rightarrow \textit{arachno}\text{-}[B_3H_6L_2][B_3H_8] \quad (29)$$

$$B_2H_4(PMe_3)_2 + 1.5B_2H_6 \rightarrow [B_3H_6(PMe_3)_2][B_2H_7] \quad (30)$$

$$B_2H_4(PMe_3)_2 + B_4H_{10} \rightarrow [B_3H_6(PMe_3)_2][B_3H_8] \quad (31)$$

$$2B_2H_4(PMe_3)_2 + Ph_3C^+ \rightarrow [B_3H_4(PMe_3)_3]^+ + Me_3P{\cdot}BH_3 + Ph_3CH \quad (32)$$

$$2B_4H_8(PMe_3)_2 + Ph_3C^+ \rightarrow [B_5H_8(PMe_3)]^+ + Me_3P{\cdot}B_3H_7 + Ph_3CH \quad (33)$$

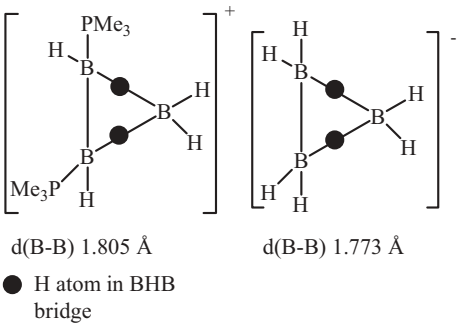

Fig. 2.1-17. Valence bond description of the *arachno*-$[B_3H_6(PMe_3)_2][B_3H_8]$.

$$B_2H_4(PMe_3)_2 + Ph_3C^+ \rightarrow [B_2H_3(PMe_3)_2]^+ + Ph_3CH \quad (34)$$

$$[B_2H_3(PMe_3)_2]^+ + B_2H_4(PMe_3)_2 \rightarrow [B_3H_4(PMe_3)_3]^+ + Me_3P{\cdot}BH_3 \quad (35)$$

These reactions are typical asymmetric cleavage reactions in which $B_2H_4(PMe_3)_2$ acts as a base and as a BH_2^+ scavenger. On the other hand, if strong hydride abstracting reagents are used then rather unexpected cations are formed as shown in Eqs. (32–33) [36]. These reactions probably proceed in two steps as suggested in Eqs. (34) and (35). The *arachno* structures of the salt $[B_3H_6(PMe_3)_2][B_3H_8]$ is depicted in Figure 2.1-17. Similar cations have been prepared with B_4, B_5, and B_6 species [36]. The relationship between these cations, the isoelectronic neutral and anionic species is shown in Figure 2.1-18.

Tetraborane(10) reacts, as does diborane, readily with unsaturated hydrocarbons. Alkenes give access to B2,B4-alkylene bridged $B_4H_8(RCH{-}CHR)$ organoboranes [37] while alkynes, allenes and 1-ene-3-ynes lead to a variety of carbaboranes [38–40].

The reaction of CO with B_5H_{11} yields volatile B_4H_8CO which in turn can be used to prepare adducts of type B_4H_8L ($L = PF_3$, PF_2Cl, PF_2NMe_2, PF_2tBu, PH_3, NH_3) [41–45]. In most cases two isomers are formed which are present in a temperature dependent equilibrium (see Figure 2.1-19). However $B_4H_8(PF_2H)$ exists solely in the form of the *endo*-isomer [42] while B_4H_8CO is present as an *endo*:*exo* mixture in the gas phase with proportions of 62:38 [43]. On the other hand, $B_4H_8(PF_3)$ like $B_4H_8(PF_2NMe_2)$ strongly prefers the *endo* form [46].

2.1.4.2.2 Derivatives of *nido*-Tetraborane(8), B_4H_8, and *closo*-Tetraborane(6), B_4H_6

Formally, the transformation of B_4H_{10} by loss of H_2 leads to B_4H_8, which is expected to have a *nido*-structure, and to B_4H_6, which has to be considered a *closo*-tetraborane(6). The existence of the last two of these classes of tetraboranes has only recently been verified. While B_4H_{10} is still the only known and well characterized *arachno*-tetraborane(10) it is only one member out of five possible ones that are feasible, and that are now known in the form of derivatives. The series of tetraboranes comprise B_4H_4, B_4H_6, B_4H_8, B_4H_{10}, and B_4H_{12}, belonging to the

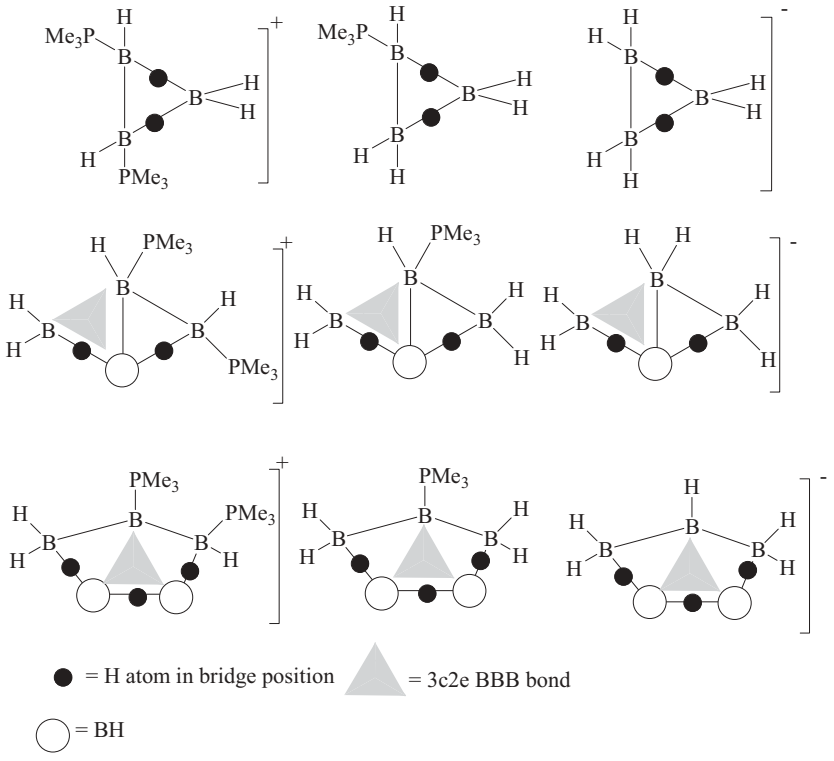

Fig. 2.1-18. Relationships between isoelectronic neutral, cationic and anionic polyborane bis(trimethylphosphine) compounds.

hypercloso-, *closo-*, *nido-*, *arachno-* and *hypho*-series. Derivatives of the *hypercloso*-B_4H_4 compound will be discussed in Chapter 2.1.6.

Organo derivatives of composition $B_4R_4H_2$ result as byproducts in the dehalogenation of RBX_2 (X = F, Cl, Br) by alkali metals in a hydrocarbon solvent [47]. The hydrogen atom is generated by the organic group R and does not originate

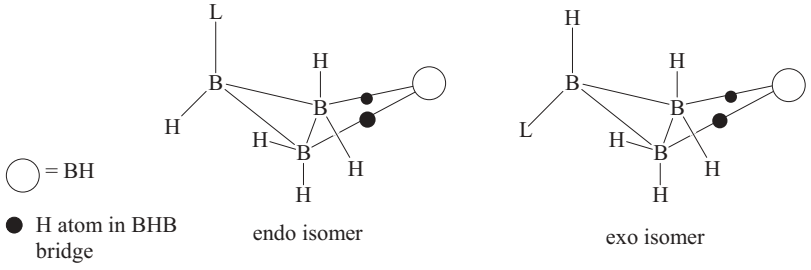

Fig. 2.1-19. The two isomers of B_4H_8L.

from the solvent. B_4R_4 compounds are intermediates in the formation of *closo*-$B_4R_4H_2$, and there is good evidence that the anion $B_4R_4H^-$ is also an intermediate as shown in Eqs. (36–38).

$$4RBX_2 + 8K \xrightarrow{-8KX} B_4R_4 \quad (36)$$

$$B_4R_4 + 2K + 2L + H^+ \rightarrow [KL][B_4R_4H] + [KL]^+ \quad (37)$$

$$[KL][B_4R_4H] + HCL \rightarrow B_4R_4H_2 + [KL]Cl \quad (38)$$

$L = 18\text{-crown-6}$

^{11}B NMR spectra allow an easy distinction between the *hypercloso*- and *closo*-species: the former show a resonance in the range of 134–140 ppm, the latter having boron nuclei that are better shielded than the former by 125 ppm.

The *hypercloso*-tetraboranes B_4R_4 are reduced to the *closo*-anions $B_4R_4H^-$ by elemental lithium. If potassium is used in tetrahydropyrane (thp), the reduction not only leads to the anion $B_4R_4H^-$ but also to $B_4R_3H_4^-$. This latter anion can be generated more effectively by reducing $B_4R_4H_2$ with potassium in thp as a solvent using hexamethyldisilazane as the proton source [48]. The potassium salt can be quantitatively converted into the *nido*-tetraborane $B_4R_4H_4$ as shown in Eq. (40) [49].

$$B_4R_4H_2 + 2K + HN(SiMe_3)_2 + 6thp \rightarrow [K(thp)_6][B_4R_4H_3] + KN(SiMe_3)_2 \quad (39)$$

$$[K(thp)_6][B_4R_4H_3] + HCl \rightarrow B_4R_4H_4 + KCl + 6thp \quad (40)$$

NMR data are in accord with a bicyclobutane-type structure for $B_4R_4H_3^-$ and the presence of two bridging hydrogen atoms. At elevated temperature the atoms B2 and B3 become equivalent and also the bridging hydrogen atoms. This enantiomerization is shown in Figure 2.1-20.

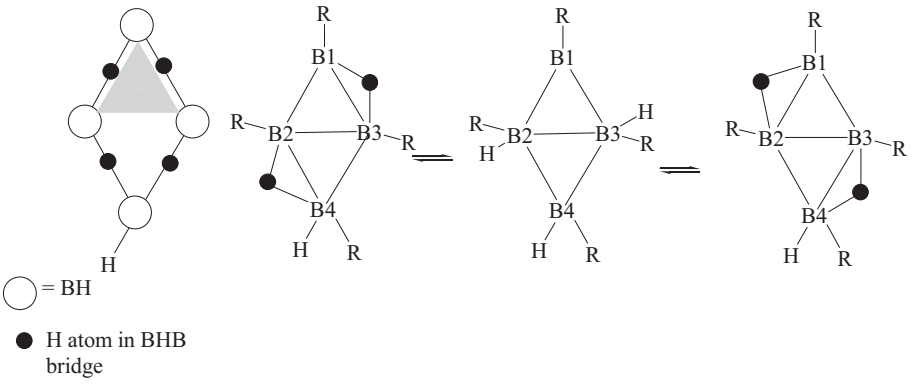

Fig. 2.1-20. Valence bond structure of the calculated ground state for *nido*-tetra-borane(8) and a suggested mechanism for the enantiomerization of $B_4H_3R_4^-$ (R = H or alkyl).

2.1.4.3
Chemistry of Pentaborane(9)

nido-Pentaborane(9) can be prepared by passing a stream of diborane diluted with hydrogen gas through a tube at 250 °C [Eq. (41)]. The presence of hydrogen suppresses the formation of higher boranes:

$$5B_2H_6 \rightarrow 2B_5H_9 + 6H_2 \quad (41)$$

$$Bu_4N[B_3H_8] + HX \rightarrow Bu_4N[B_3H_7X] + H_2 \quad (42)$$

$$5Bu_4N[B_3H_7X] \rightarrow 3B_5H_9 + 4H_2 + 5[Bu_4N]X \quad (43)$$

A modern laboratory procedure for the synthesis of pentaborane(9) is a variation of a process [50] that starts from tetraalkylammonium salts of $B_3H_8^-$. Reactions with HX (X = Br, I) produce monohalogeno heptahydrotriborates $B_3H_7X^-$ [Eq. (42)] [51], which on thermal decomposition at 100 °C, give excellent yields of B_5H_9 [Eq. (50)]. The anion $B_3H_7X^-$ is even better prepared by the reaction of $B_3H_8^-$ with one equivalent of either Br_2 or I_2 [16].

Pentaborane(9) is a volatile, colorless liquid, m.p. −46.9 °C, b.p. 60.1 °C, which ignites in contact with air. It is fairly stable hydrolytically, but reacts rapidly with hot water. It has a tetragonal pyramidal structure with four 3c2e BHB bridge bonds at the basal boron atoms.

Its valence bond description requires six resonance structures. Three are shown in Figure 2.1-21. The molecule posses C_{4v} symmetry. There is a higher negative charge at the apical hydrogen atom than on the basal ones. Therefore, reactions with electrophiles occur at the apical B1 atom, while nucleophiles will attack at one of the basal boron atoms. These have preformed BH_3 groups which may be removed from the B_5 unit by reactions with Lewis bases generating a B_4H_6 fragment. Removal of two BH_3 units leads formally to a B_3H_3 fragment. Neither B_3H_3 nor B_4H_6 are known as free molecules and need stabilization by electron pair donors.

Strong bases such as alkali metal hydrides deprotonate B_5H_9 at −78 °C in ether solution to the octahydropentaborate(1−) which not only is a strong base but also an important reagent for the synthesis of derivatives [52]. The anion itself is not

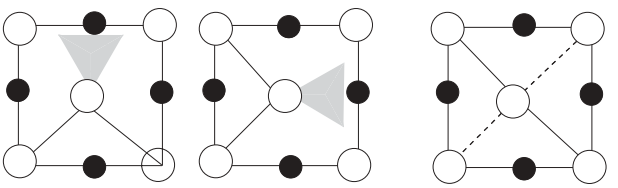

Fig. 2.1-21. Bonding description of pentaborane(9) by localized bonds: two resonance formula with closed 3c2e bonds and one with an open BBB 3c2e bond are shown.

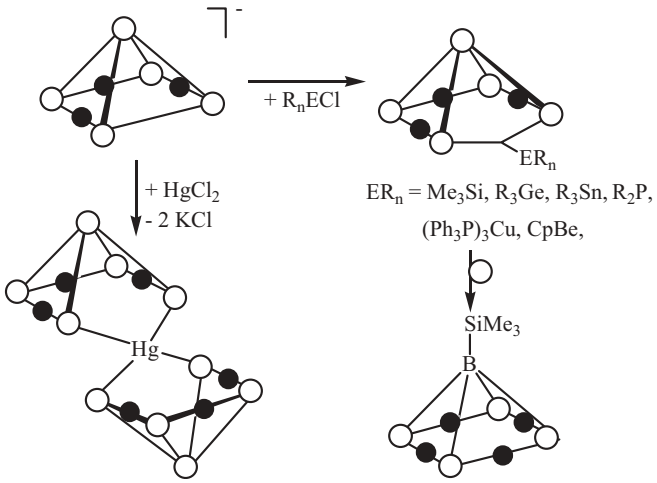

Fig. 2.1-22. Some reactions of the $B_5H_8^-$ anion with organyl element halides.

stable and decomposes at ambient temperature into BH_4^-, $B_3H_8^-$, as well as $B_9H_{14}^-$ and $B_{11}H_{14}^-$. Many metathetical reactions of KB_5H_8 have been studied with main group and transition metal halides. These reactions lead to B_5H_9 derivatives in which one of the bridging hydrogen atoms is replaced by a bridging main group or transition metal fragment via a 3c2e bond. μ-$Me_3SiB_5H_8$ rearranges thermally or by base catalysis to the isomer 1-$Me_3SiB_5H_8$ giving a 1:4 mixture of both isomers in which the 1-isomer is favored (see Figure 2.1-22). Two B_5H_9 units may be joined with the Ph_2Sn fragment via 3c2e bonds with B atoms B2 and B3 of each B_5 unit:

Obviously, the basic site in KB_5H_8 is its basal B–B single bond and, therefore, reactions with Lewis acids are to be expected. A typical example is the reaction with diborane in ether at −78 °C which generates via its μ-adduct (3c2e-BBB bond) the *nido*-undeca-hexaborate(1−), $B_6H_{11}^-$, by cluster expansion. This anion can be protonated to B_6H_{12} [53].

While the μ-dichloroboryl-pentaborane(9) obtained from KB_5H_8 and BCl_3 is stable only up to 0 °C [54], the 1-dichloroboryl isomer is a comparatively stable liquid. It is obtained from B_5H_9 and BCl_3 in the presence of $AlCl_3$ as a catalyst in a Friedel-Crafts type reaction [55]:

$$B_5H_9 + BCl_3 \rightarrow 1\text{-}Cl_2B\text{-}B_5H_8 + HCl \quad (44)$$

$$B_5H_9 + RCl \rightarrow 1\text{-}RB_5H_8 + HCl \quad (45)$$

$$B_5H_9 + Cl_2 \rightarrow 1\text{-}ClB_5H_8 + HCl \quad (46)$$

This type of reaction has also been used to prepare 1-alkylpentaboranes [Eq. (45)]. Similarly, liquid 1-chloropentaborane(9) is obtained from pentaborane(9) and chlo-

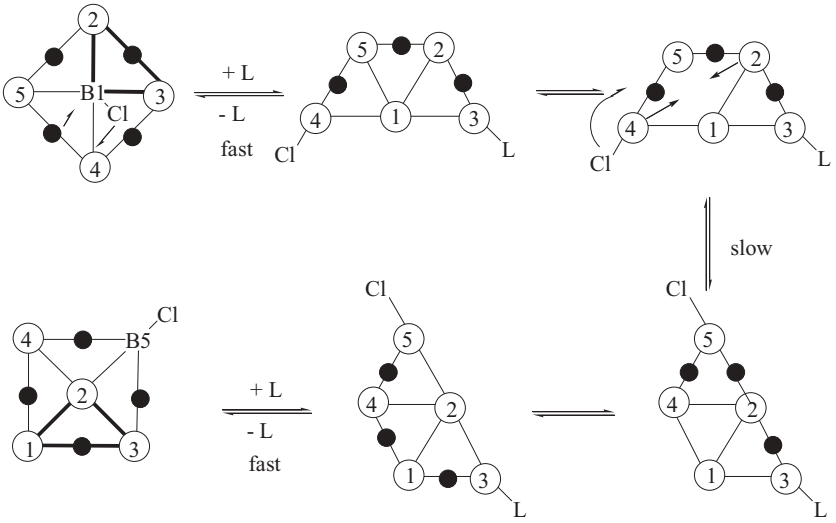

Fig. 2.1-23. Rearrangement of *nido*-ClB_5H_8 via an *arachno*-structure in the presence of an ether L.

rine in the presence of $AlCl_3$ [Eq. (46)]. Bromination and iodination is achieved in the same way. 1-ClB_5H_8 rearranges to the 2-isomer either thermally or by base catalysis. NMR studies showed that catalysis by an ether leads to rapid scrambling of the hydrogen atoms at the base, whereas it takes longer to achieve the rearrangement from the 1-ClB_5H_9 isomer to the 2-ClB_5H_8 isomer. The initial step in the rearrangement is the opening of one of the basal hydrogen bridges by addition of the ether to generate an *arachno*-pentaborane(11) as shown in Figure 2.1-23 [56].

Similar to the $PtBr_2$ catalyzed B–B bond formation between pentaborane(9) and other polyboranes, B–C bond formation is observed in the presence of $PtBr_2$ between pentaborane(9) and alkenes leading to a mixture of 1- and 2-alkenylpentaboranes(9). On the other hand, only the 2-butyl-derivative results when B_5H_9 is reacted with $Li[Bu_3BH]$. This alkyl/hydrogen exchange is specific for this reagent as the reaction with $Li[Et_3BH]$ leads to 2,3,4-$Et_3B_5H_6$ [57].

$$B_5H_9 + Li[Bu_3BH] \rightarrow 2\text{-}BuB_5H_8 + Li[Bu_2BH_2] \qquad (47)$$

The opening of a 3c2e-BHB bond by a base can be verified by the action of trimethylamine or trimethylphosphine on B_5H_9. Ammonia reacts in an analogous manner with B_4H_{10} with asymmetrical cleavage, while trimethylamine removes one or two BH_3 groups as $H_3B{\cdot}NMe_3$. On the other hand, when PMe_3 is allowed to react with B_5H_9 stable adducts are formed such as *hypho*-$B_5H_9(PMe_3)_2$ (see Figure 2.1-24) [58, 59].

While the THF adduct of triborane(7) reacts with $Bu^t{-}B{\equiv}N{-}Bu^t$ by hydroboration to produce a μ-aminodiborane (see Section 2.1.4.1) the analogous reaction

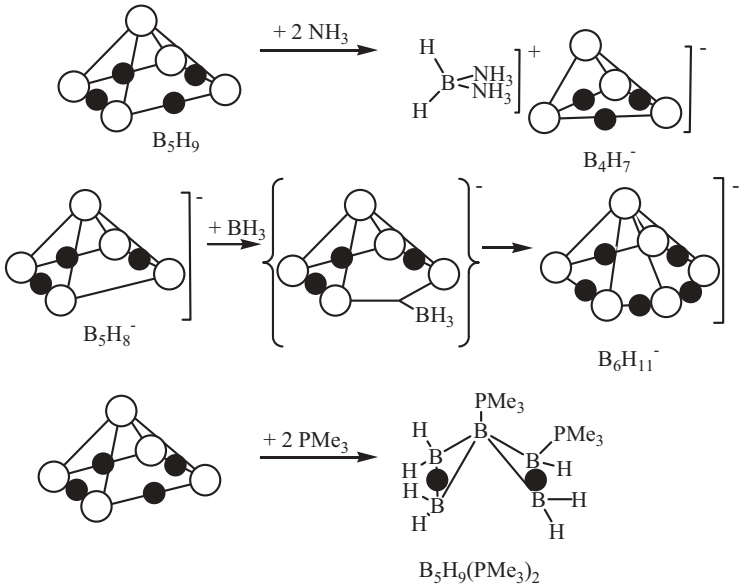

Fig. 2.1-24. Reactions of pentaborane(9) with ammonia, trimethylphosphine and diborane.

with pentaborane(9) in the presence of lutidine leads to the *arachno*-nonaborane anion $B_9H_{14}^-$ [60]. This reaction is well known in pentaborane(9) chemistry when proton abstraction from B_5H_9 is possible [61] because $B_9H_{14}^-$ is formed by the interaction of $B_5H_8^-$ with B_5H_9 to give the intermediate $B_{10}H_{17}^-$, which loses "BH_3" to give the anion $B_9H_{14}^-$:

$$Bu^t{-}B{\equiv}N{-}Bu^t + 2B_5H_9 + 2L \rightarrow [Bu^t(L)B{=}NHBu^t][B_9H_{14}] \qquad (48)$$

$$L = 2,6\text{-}NC_5H_3Me_2$$

2.1.4.4

Chemistry of Decaborane(14)

nido-Decaborane(14) is a colorless, air stable, typically smelling, sublimable solid of m.p. 99.7 °C. It is fairly stable thermally (in the absence of air), and burns when heated, with a green flame. It hydrolyzes in hot basic solutions slowly, and its aqueous solutions are strongly acidic. $B_{10}H_{14}$ is prepared by decomposing diborane at 160 to 200 °C. Me_2O catalyzes reaction (49).

$$5B_2H_6 \rightarrow B_{10}H_{14} + 8H_2 \qquad (49)$$

$$B_{10}H_{14} + OH^- \rightarrow B_{10}H_{13}^- + H_2O \qquad (50)$$

$$B_{10}H_{14} + 2L^- \rightarrow B_{10}H_{12}{\cdot}2L + H_2 \qquad (51)$$

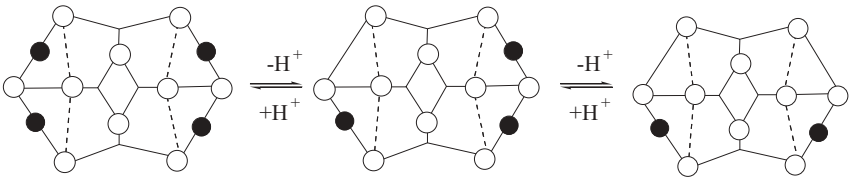

Fig. 2.1-25. Dodecaborane(14) and its anions $B_{10}H_{13}^-$ and $B_{10}H_{12}^{2-}$, representation by localized bonding (only one of 24 resonance structures is shown).

As is to be expected from its structure (see Figure 2.1-25), which has C_{2v} symmetry, the molecule has a significant dipole moment ($\mu = 3.4$ Debye). This is one of the reasons why decaborane(14) dissolves in alcohols and water. One of its four bridging protons can readily be removed by a base in aqueous solution ($pK_a = 2.7$) according to Eq. (50). The yellow anion $B_{10}H_{13}^-$ in not very stable in solution. The deprotonation of $B_{10}H_{14}$ leads to a shortening of the B6-B7-bond.

$B_{10}H_{14}$ is a *nido*-polyborane, therefore, it is expected that it forms adducts with Lewis bases. This is indeed the case but with concomitant loss of hydrogen as shown in Eq. (51). These adducts of the type $B_{10}H_{12}{\cdot}2L$ (L = amines, pyridine, phosphines, nitriles, dialkylsulfides *inter alia*) proved to be versatile reagents. For instance, when triethylamine is used to replace acetonitrile from the adduct not only does the expected replacement occur but in preference also a proton shift (most likely prior to the base displacement reaction) with cluster closure to the decahydro-*closo*-decaborate(2−) (Eq. 52):

$$B_{10}H_{12}{\cdot}2NCMe + 2Et_3N \rightarrow [Et_3NH]_2[B_{10}H_{10}] + 2MeCN \qquad (52)$$

Calculations show that the highest negative charge in $B_{10}H_{14}$ is located at atoms 1 to 4, while there is less negative charge at atoms 6 and 9. Hence, nucleophilic substitutions occur preferentially at boron atoms 6 and 9. Thus, the halogenation of decaborane(14) to $B_{10}H_{14-n}X_n$ ($n = 1$ to 4, X = Cl, Br, I) occurs under Friedel-Crafts condition at the 1 to 4 positions, and up to 4 atoms of Br or I can readily be introduced.

Alkylation reactions lead to mono-, di-, and even higher alkylated products in various ratios. The products formed depend on the nature of the alkylation reagent. For instance, the nucleophilic LiEt reacts with $B_{10}H_{14}$ to give 6-ethyldecaborane(14), while most other LiR compounds produce a mixture of 5- and 6-alkyldecaboranes [62]. Grignard reagents, on the other hand, deprotonate decaborane(14) to the "borane-Grignard" $B_{10}H_{13}MgX$, and only small amounts of 6-alkyl-decaboranes are observed in this reaction. Thus, there is competition between deprotonation and alkylation. $B_{10}H_{13}MgBr$, on the other hand, reacts with triethyloxonium tetrafluoroborate or diethylsulfate selectively to 5-ethyldecaborane, while dimethyl sulfate produces a 1:1 mixture of the 5- and 6-methyldecaboranes [63]. An alternative route to monoalkyl decaboranes uses the reaction of $B_{10}H_{13}^-$

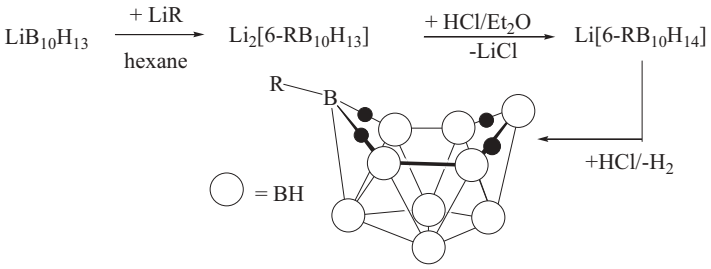

Fig. 2.1-26. The route to 6-alkyl-decaboranes.

with dialkyl sulfates or benzylchloride. 6-Alkyldecaboranes(14) are formed according to the reaction outlined in fig. 2.1-26, but this is not a generally applicable route. A more general as well as regioselective alternative starts from *nido*-$B_{10}H_{13}^-$. Alkylation with LiR leads to *arachno*-6-$RB_{10}H_{13}^{2-}$. This anion on protonation with HCl in diethyl ether yields *arachno*-6-$RB_{10}H_{14}^-$ which on further protonation gives 6-$RB_{10}H_{13}$, with hydrogen evolution (see Figure 2.1-25) [64]. Hydroboration of olefins by 6,9-$(Me_2S)_2B_{10}H_{12}$, which provide isolable decaboranes of type 6-R-8-$(Me_2S)B_{10}H_{11}$, opens a new route to 6-alkyldecaboranes 6-R-$B_{10}H_{13}$ by treating 6-R-8-$(Me_2S)B_{10}H_{11}$ with $Li[Et_3BH]$ in diethyl ether. This generates, by hydride transfer, the yellow anion 6-R-$B_{10}H_{12}^-$, which in turn can be converted by strong acids into *nido*-6-$RB_{10}H_{13}$ (see Figure 2.1-27) [64].

More important than the hydroboration of olefins with decaborane is its reaction with alkynes. Decaborane, in the form of the adduct $(Me_2S)_2B_{10}H_{12}$ or is acetonitrile adduct reacts with alkynes by insertion across the B6, B9 positions closing the open face to an icosahedral 1,2-dicarba-*closo*-dodecaborane $(CR)_2B_{10}H_{10}$ (R = H, Me, Ph, etc.) at slightly elevated temperatures [65–67] (Figure 2.1-28). This is one of the most important reactions of decaborane because it allows an entry into many new areas of polyborane chemistry (*closo*-hydropolyborates, carbaborane chemistry, complex chemistry with the dicarbollide ligand $C_2B_9H_{11}^{2-}$, etc.).

In contrast, reaction of *nido*-decaborane(14) with iminoboranes RB≡NR did not result in the formation of *closo*-azadodecaboranes $(RN)(RB)B_{10}H_{10}$ because the iminoborane dimerized more rapidly and, therefore, does not insert into the B_{10} cluster [68]. On the other hand, the aminoiminoborane tmp-B≡N-Bu^t reacted readily with $B_{10}H_{14}$ to give 6-$(tmpH)(Bu^t)$B-$B_{10}H_{13}$. Most likely, the fist step in this

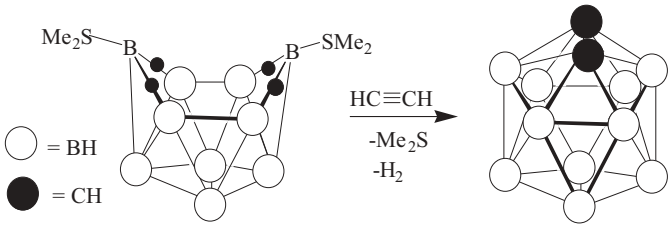

Fig. 2.1-27. Formation of dodecahydro-*closo*-1,2-dicarbadodecaborane.

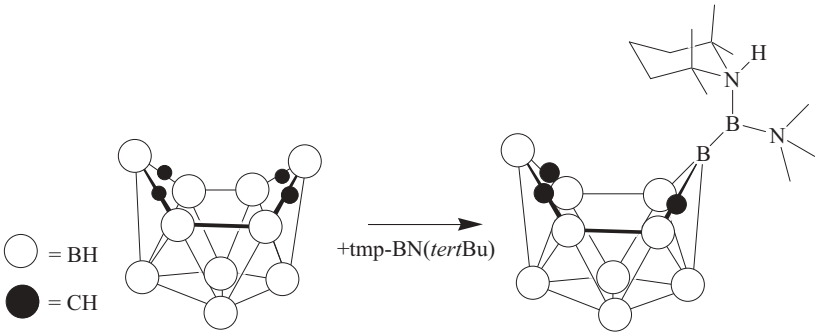

Fig. 2.1-28. Reaction of decaborane(14) with the aminoiminoborane tmp-B≡N-Bu^t.

reaction is an acid/base reaction by monodeprotonation of $B_{10}H_{14}$ to $B_{10}H_{13}^-$ and formation of the cation $[tmpB{=}NH\text{-}Bu^t]^+$ (see Figure 2.1-28) [69].

A similar behavior as found for alkynes could be expected for the unknown silaalkynes RSi≡CR. However, a phosphaalkyne might react differently due to the Lewis basicity of its P atom. This has indeed been observed, but there are two notable differences in the resulting product compared with alkynes. First, the reaction proceeds in a 2:1 stoichiometry, and secondly no *closo*-product is formed. The terminal hydrogen atom at position B6 of the decaborane unit migrates to the P atom with formation of a PH bond, and concomitant formation of a B–C bond at the 6-position of a $B_{10}H_{13}$ unit while the other B_{10} cluster unit is expanded by the P atom of the phosphaalkyne with formation of two B–P bonds (to atoms B6 and B5) generating a CPB three membered ring (Figure 2.1-29) [70].

While RB≡NR compounds did not react "properly" with $B_{10}H_{12}(SMe_2)_2$ an entry into the class of *arachno*-azadecaboranes (see Chapter 3) is provided by the reaction of hydrazoic acid with $B_{10}H_{12}(SMe)_2$ which occurs as shown in Eq. (53) [71].

$$B_{10}H_{12}(SMe_2)_2 + 2HN_3 \rightarrow B_{10}H_{12}(N_3)NH_2 + N_2 + 2SMe_2 \qquad (53)$$

The structure of this compound (Figure 2.1-30) shows the decaborane cluster with

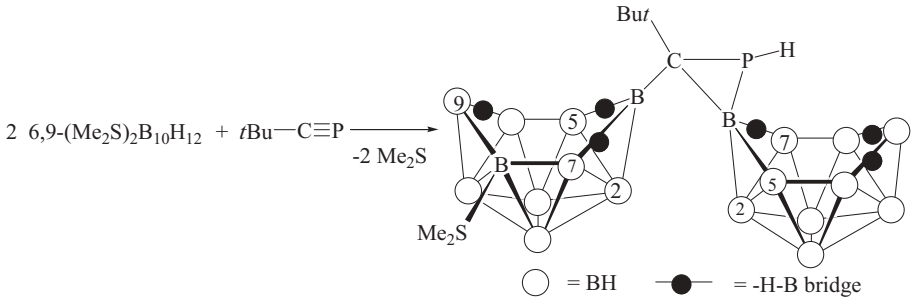

Fig. 2.1-29. Reaction of Bu^{t}C≡P with 6,9-$B_{10}H_{12}(SMe_2)$.

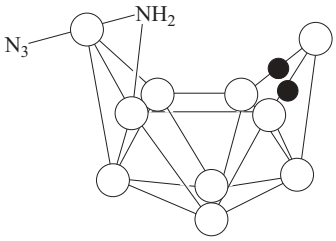

Fig. 2.1-30. Representation of the structure of $B_{10}H_{12}(N_3)NH_2$.

the B6 atom carrying the azido group. The amino group bridges the B6–B5 positions, and there are two 3c2e-BHB bonds involving the atoms B8–B9 and B9–B10.

2.1.5
Chemistry of Selected *nido*- and *closo*-Polyborane Anions

Amongst the *closo*-hydroborate anions the *closo*-dodecaborate $B_{12}H_{12}^{2-}$ is the best known because many derivatives can be made by maintaining its icosahedral structure in substitution reactions. Thus the replacement of its hydrogen atoms by other groups such as OH, Me, $CHCl_2$, F, Cl, Br, I, CF_3, OC(O)Me, OC(O)Ph, OCH_2Ph, and others is possible [72]. Moreover, these anions can be oxidized to radical anions and even to *hypercloso* species [73]. Radical monoanions are known for X = Me, and OCH_2Ph, and neutral $B_{12}X_{12}$ species for X = OCH_2Ph (see Section 2.1.6). While the polyhedral dianions $B_{12}H_{12-n}X_n^{2-}$ are all stable, the neutral decaboranes $B_{12}X_{12}$ can not usually be isolated. Computations show, however, that their stability increases as the group electronegativity of the substituent X increases, and the corresponding dianion is also more readily oxidized as the Hammet parameter of the substituents becomes more negative, corresponding to an increase of the electron donating ability of the substituent. Oxidation is usually accompanied by a lengthening of the B–B bonds of the cage [72]. Many of the redox processes that are schematically shown in Eq. (54) are reversible, particularly the formation of the radical anion.

$$B_{12}X_{12}^{2-} \underset{+e^-}{\overset{-e^-}{\rightleftharpoons}} B_{12}X_{12}^{\bullet -} \underset{+e^-}{\overset{-e^-}{\rightleftharpoons}} B_{12}X_{12} \qquad (54)$$

Amongst the hydro-*closo*-polyborates $B_nH_n^{2-}$ members with $n = 6$ to 12 are known. All hydro-*closo*- but also hydro-*nido*-polyborates act as bases; they are, however, not typical Lewis-bases as they miss free electron pairs. However, the negative charge at the hydrogen atoms allows for an interaction with Lewis acids **A** by formation of hydride bridge bonds (3c2e bonds):

$$\mathbf{A} + H{-}B< \rightarrow \mathbf{A}\cdots H{-}B< \qquad (55)$$

In most cases the Lewis acid **A** is a transition metal or main group element fragment. Because the hydrogen atoms bear a negative charge, the hydropolyborates are reducing agents.

2.1.5.1 Chemistry of *closo*-$B_6H_6^{2-}$

The *closo*-$B_nH_n^{2-}$ anions can all be considered as three dimensional aromatic systems [74, 75], all of them being characterized by an $n+1$ electron pair count. Amongst these the $B_6H_6^{2-}$ is the smallest unit, and, therefore, the partial negative charge associated with the hydrogen atoms exceeds that of the larger polyborate dianions such as $B_{10}H_{10}^{2-}$ or $B_{12}H_{12}^{2-}$. Consequently, one can expect that $B_6H_6^{2-}$ will be a stronger base and reducing reagent, and will therefore readily be attacked by electrophiles. This has, in principle, been observed experimentally.

$Na_2[B_6H_6]$, a colorless solid, results in low yield (as a byproduct) by heating $NaBH_4$ in the presence of diborane in diglyme solution for several hours at 160 °C. The anion is isolated as the Cs or tetraalkylammonium salt by precipitation from aqueous solution.

The anion $B_6H_6^{2-}$ can readily be protonated to $B_6H_7^-$ but further protonation to neutral B_6H_8 has never been achieved. Aqueous solutions of alkali metal hexahydro-*closo*-hexaborates give basic solutions due to hydrolysis as described by Eq. (56):

$$B_6H_6^{2-} + H_2O = B_6H_7^- + OH^- \tag{56}$$

The pK_a is 7.0 corresponding to the H_2S/SH^- acid base pair [76]. For this reason salts of the anion can be readily generated by strong acids, and salts $M[B_6H_7]$ with large cations M can be isolated.

The basic site of the $B_6H_6^{2-}$ anion is one of its B_3 faces. A proton adds to this face forming a 4c2e B_3H bond (facially bonded hydrogen atom). While the structure in the solid state is well established, in solution the anion shows fluxional behavior on the NMR time scale. Only a single ^{11}B and ^1H NMR signal is observed at ambient temperature. From temperature dependent NMR data an activation energy of 10 kcal mol^{-1} has been determined for the proton exchange processes. The mechanism of the proton migration involves a face-edge-face migration of the facial hydrogen atom [77] as depicted in Figure 2.1-31.

The introduction of substituents into the $B_6H_6^{2-}$ unit changes its O_h symmetry to C_{4v} on mono-substitution and to C_{4h} on *trans*-disubstitution or to C_{2h} for *cis*-disubstitution. Therefore, the protonation of $[B_6H_5X]^{2-}$ to $[1\text{-}B_6H_6X]^-$ can occur in the case of monosubstitution at one of the upper faces of the octahedron or on one of the lower faces. In the case of a regiospecific addition of the proton, one of two isomers can be generated as shown in Figure 2.1-32.

Structures of type **A** result on protonation of monoalkyl-pentahydro-*closo*-hexaborate ions $B_6H_5R^{2-}$ while type **B** anions are observed for the halogeno derivatives $[B_6H_5X]^{2-}$ (X = Cl, Br, I) [78]. This regiospecificity results from inductive

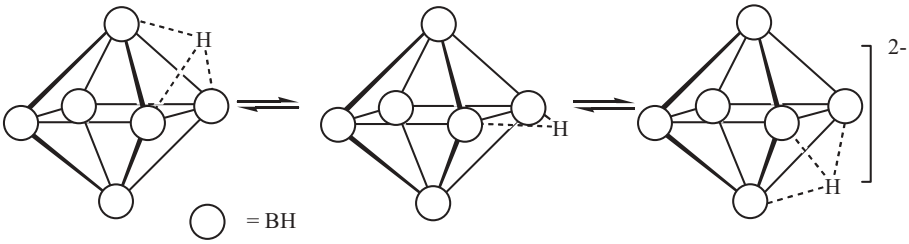

Fig. 2.1-31. Proposed mechanism for the fluctuation of the facial proton in $B_6H_7^-$.

effects of the substituents. The alkyl groups increase electron density at the upper part of the B_6 octahedron, while the electron withdrawing effect of the halogens decrease electron density in this region. In consonance with this is the decreased basicity of the $[B_6H_5X]^{2-}$ anions as shown by pK_a values of 5.35, 5.00 and 4.65 for the chloro-, bromo- and iodo-derivatives. On the other hand, the compound $CpCo(C_5H_4B_6H_5)^-$, prepared from cobaltocene Cp_2Co and $B_6H_7^-$ is protonated at the lower part of the octahedron in spite of the presence of a B–C bond [79]. While alkylation of $B_6H_6^{2-}$ is normally performed with alkyl iodides under mild conditions [80] arylation requires activated haloaromatics such as *p*-bromo-nitrobenzene and higher temperatures (Eq. 57) [81].

Fluorination of $B_6H_6^{2-}$ is difficult in contrast to halogenation by Cl, Br, and I. However, $B_6H_5F^{2-}$ is obtained by using the tetrafluoroborate of 1-chlormethyl-4-fluoro-1,4-diazabicyclo[2.2.2]-octane, a reaction that is described formally in Eq. (58) [82].

$$[Bu_4N]_2[B_6H_6] + p\text{-Br-}C_6H_4\text{-}NO_2 \rightarrow [Bu_4N]_2[B_6H_5\text{-}C_6H_4\text{-}NO_2] + HBr \qquad (57)$$

$$B_6H_6^{2-} + >N\text{-}F \rightarrow B_6H_5F^{2-} + >NH \qquad (58)$$

The fluoro derivate can be readily iodinated by KI/I_2 up to $B_6I_5F^{2-}$ [83], and this anion is isotypic with $B_6I_5H^{2-}$ [84]. On the other hand $B_6H_6^{2-}$ reacts with $NaOH/I_2$ to form $B_6H_4I_2^{2-}$ and $B_6H_3I_3^{2-}$. Further iodination is achieved with KI_3 where

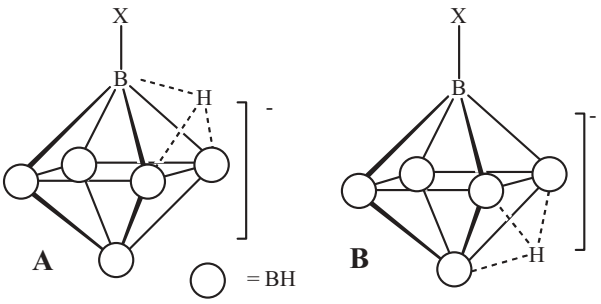

Fig. 2.1-32. The two possible isomers of protonated monosubstituted *closo*-hexaborate.

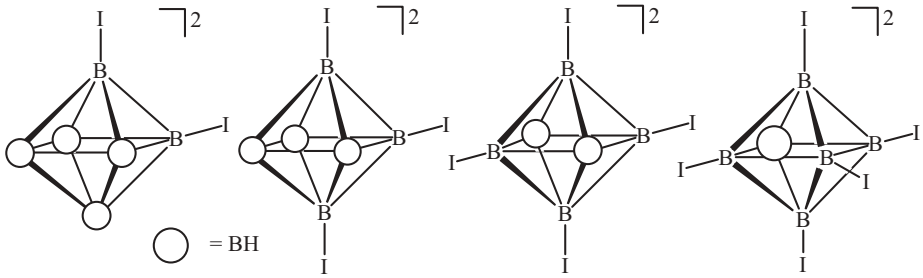

Fig. 2.1-33. The structure of iodinated *closo*-hexaborates.

a mixture of $B_6H_3I_4^{2-}$ and $B_6HI_5^{2-}$ results. The geometry of the anions are shown in Figure 2.1-33, and it interesting to note that only the *cis*-diiodohexaborate isomer is formed as well as the *mer*-triiodo-*closo*-hexaborate on iodination.

The perhalogenated anions $B_6X_6^{2-}$ are formed on reacting $B_6H_6^{2-}$ with an excess of halogen in aqueous solutions [85]. Also, the SCN and SeCN group can be introduced into the B_6 cage by reacting $B_6H_6^{2-}$ with $(SCN)_2$ or $(SeCN)_2$. In the resulting anions, $B_6H_5XCN^{2-}$, the sulfur and selenium atoms, respectively, bind to a boron atom suggesting that the hexahydro-*closo*-hexaborate behaves as a soft base [81] in analogy with $B_{10}H_{10}^{2-}$ and $B_{12}H_{12}^{2-}$. The SC bond in $Cs_2[B_6H_5SCN]$ can be cleaved by elemental Na. The product after hydrolysis is the anion $[B_6H_5(H_{fac})SH]^-$ which on deprotonation with 1,8-diazabicyclo[5.4.0]-undecen-7-ene yields the anion $[B_6H_5S]^{3-}$. On the other hand the SeC bond in $[Ph_4P]_2[B_6H_5SeCN]$ can already been cleaved by CsOH in ethanol, and the isolated product is $Cs_3B_6H_5Se$ [86].

Also nitro groups can be introduced into the B_6 cluster. This is done by electrochemical oxidation in the presence of nitrite ions. $B_6H_5Me^{2-}$ gives a pair of isomers, *cis*- and *trans*-$B_6H_4Me(NO_2)^{2-}$ as well as *fac*- and *mer*-$B_6H_3Me(NO_2)_2^{2-}$ [87]. In contrast, a benzyl group activates the *cis*-positions as only the *cis*-isomer $B_6H_4(CH_2Ph)NO_2^{2-}$ is found [88]. In addition the blue anion B_6H_5-NO-$B_6H_5^{3-}$ is formed [89] which is isoelectronic with R_2NO^+ cations.

As might be expected, the $B_6H_6^{2-}$ anion has ligand properties. It forms transition metal complexes which are usually obtained by metathesis from a transition metal complex halide and $M_2[B_6H_6]$ (M = Na, Cs, R_4N). Examples are $Ph_4P[PhHg(\eta^3\text{-}B_6H_6)]$ [90] and $[(Ph_3)M(\mu\text{-bis-}\eta^3\text{-}B_6H_6)_2M(PPh_3)]$ (M = Cu, Au) [91]. However, in $[Bu_4N]_2[Cd(\eta^3\text{-}B_6H_6)_2]$ the Cd ion is coordinated to six boron atoms of two B_3 faces from two hexapolyborate anions but not to its hydrogen atoms because the Cd–H distances are significantly longer than the Cd–B distances [92]. Such a cluster expansion has also been observed for η^5-$CpNiB_6H_6$ and $[(\eta^5\text{-}CpNi)_3B_6H_6]^-$, which are therefore considered to be an NiB_6 cluster or a trinickela derivative of $B_9H_9^{2-}$, respectively [93]. However, in attempts to prepare a silver complex of $B_6H_6^{2-}$ by reacting $ClAg(PPh_3)_2$ with $(Bu_4N)_2[B_6H_6]$ colorless crystals of $B_6H_{10}(PPh_3)_2$ were obtained, which is a *hypho*-hexaborane derived from B_6H_{12} (Figure 2.1-34) [94].

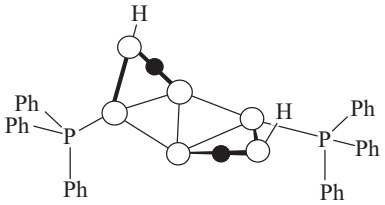

Fig. 2.1-34. Structure of the *hypho*-hexaborane $B_6H_{10}(PPh_3)_2$.

2.1.5.2

Chemistry of the Nonahydro-*closo*-nonaborate(2−)

In contrast to $B_7H_7^{2-}$ and $B_8H_8^{2-}$, which are not readily available (*vide infra*), the chemistry of $B_9H_9^{2-}$ has been studied in some detail, however, not as extensively as the chemistry of $B_{10}H_{10}^{2-}$ and $B_{12}H_{12}^{2-}$. The $B_9H_9^{2-}$ anion results from the decomposition of $Na_2B_3H_8$ at 230 °C. It can be isolated as tetralkylammonium salts in yields up to about 60%. It has the structure of a tricapped trigonal prism (point group symmetry C_{2v}).

Substitution chemistry has not yet been investigated intensively. However, the perhalo derivatives $B_9X_9^{2-}$ are important intermediates for the preparation of perhalo-*hypercloso*-nonaboranes B_9X_9 (X = Cl, Br, I). These di-anions are obtained by reacting $B_9H_9^{2-}$ with sulfuryl chloride, *N*-halosuccinimide or with iodine [95]. The salts $[R_4N]_2[B_9X_9]$ are air stable, and in contrast to $B_9H_9^{2-}$ also hydrolytically stable even in basic or acid solution. However, when a ratio of $Na_2[B_9H_9]$:*N*-halosuccinimide of 1:3 is used in a 0.7 M solution of NaOH then only partial halogenation occurs. Precipitation with $[Ph_4P]Cl$ gives access to $[Ph_4P]_2[B_9H_8X]$, which crystallizes from acetonitrile in single crystals as $[Ph_4P]_2[B_9H_8X]\cdot MeCN$. Substitution occurred at the 1-position of the trigonal face of the tricapped trigonal prism. The bonds B2–B3 and B1–B7 are exceptionally long (2.0 Å) [96]. The directing effect of substituents is not yet well understood within the series of $B_9H_{9-n}X_n^{2-}$ anions. The structure of the 1-monohalo-octahyro-*closo*-nonaborate(2−) is shown in Figure 2.1-35.

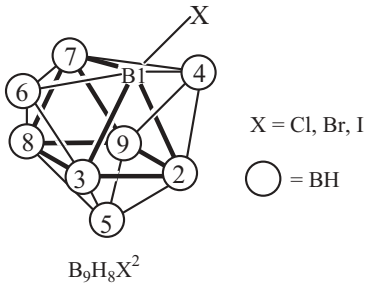

Fig. 2.1-35. Structure of the 1-$B_9H_8X^{2-}$ anions.

2.1.5.3
Reaction of Decahydro-*closo*-decaborate(2−)

The $B_{10}H_{10}^{2-}$ anion is best obtained by heating $[Et_3NH]_2[B_{10}H_{12}]$ to 160 °C. Its alkali metal salts are soluble in water, while the thallium salt is insoluble. The white alkali metal salts are stable up to 500 °C. Their aqueous solutions react neutral because the corresponding acid is a strong acid. It can be isolated as $[H_3O]_2[B_{10}H_{10}]$ (m.p. 202 °C) from its aqueous solutions obtained by ion exchange from the alkali metal salts.

The anion of $Na_2[B_{10}H_{10}]$ has the structure of a bicapped square antiprism (point group symmetry D_{4d}, see Figure 2.1-36). This induces an uneven charge distribution. The boron atoms at the capping positions have a connectivity of 4, all others a connectivity of 5. It was shown both by experiments as well as calculations that the hydrogen atoms bound to the apical boron atoms carry a higher negative charge than the hydrogen atoms at the two belt regions. Therefore, electrophilic reactions occur predominantly at the apical boron atoms. $B_{10}H_{10}^{2-}$ shows basic properties. In non-aqueous solutions (e.g., acetonitrile) protonation by fairly strong acids, such as formic acid [97], leads to the $B_{10}H_{11}^{-}$ anion provided that the cationic counter ion is large such as Bu_4N^+, Ph_4P^+ or Ph_4As^+. Protonation occurs at one of the trigonal faces of the $B_{10}H_{10}^{2-}$ anion. The resulting $B_{10}H_{11}^{-}$ is fluxional on the NMR time scale (see Figure 2.1-36) similar to $B_6H_7^{-}$.

Halogens attack preferentially at the apical boron atoms to give 1-$B_{10}H_9X^{2-}$ anions. The 2-$B_{10}H_9X^{2-}$ isomer is not formed. Further halogenation leads to dihalodecaborates(2−) and even perhalogenation is possible. There are 6 possible isomers for disubstituted *closo*-decaborates(2−), and 13 for $B_{10}H_7X_3^{2-}$ species, however, only a few of them have been structurally characterized. Fluorination is best achieved with HF. OH and NH_2 derivatives are also accessible, e.g., the 2-OH-$B_{10}H_9^{2-}$ anon results from base catalyzed hydrolysis of $[Me_4N]_2[2\text{-}(CH_2)_4S(O)\text{-}O\text{-}B_{10}H_9]$, the product of the reaction of $[Me_4N]_2[B_{10}H_{10}]$ with tetramethylene-sulfone.

One of the most interesting derivatives of $B_{10}H_{10}^{2-}$ is the inner diazonium salt 1,10-$(N_2)_2B_{10}H_8$, obtained by reacting $B_{10}H_{10}^{2-}$ with $NaNO_2$ followed by reduction

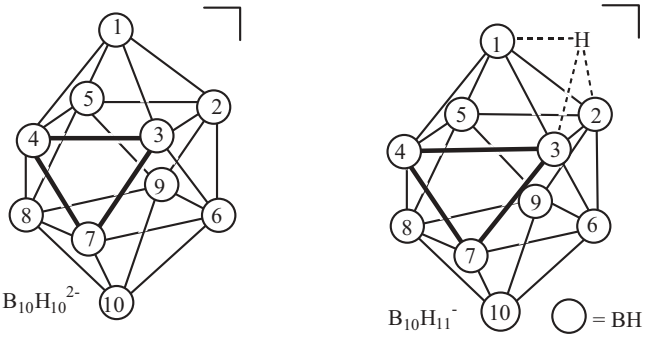

Fig. 2.1-36. Structure of the $B_{10}H_{10}^{2-}$ and the $B_{10}H_{11}^{-}$ anion.

with $NaBH_4$ in methanol. It can be further reduced to the 1,10-diamino derivative 1,10-$(H_2N)_2B_{10}H_8$. The nitrogen atoms of $B_{10}H_8(N_2)_2$ can be replaced by pyridine, acteonitrile and even by CO. This last reaction leads to the dicarbonyl 1,10-$(CO)_2B_{10}H_8$ [98].

Oxidation of the $B_{10}H_{10}^{2-}$ anion in aqueous solution either by Fe^{3+} or Ce^{4+} joins two of the B_{10} clusters to the *conjuncto*-icosaborate $B_{20}H_{18}^{2-}$ (see Section 2.1.5.8).

2.1.5.4
Chemistry of the *nido*-Decaborate $B_{10}H_{13}^-$

An entry into the chemistry of *nido*-decaborates is provided by *nido*-$B_{10}H_{14}$. As already mentioned, decaborane $B_{10}H_{14}$ is easily deprotonated even in aqueous medium to yellow $B_{10}H_{13}^-$ and with strong bases, such as alkali metal hydrides, even further to the colorless anion $B_{10}H_{12}^{2-}$. This is summarized in the reversible reactions shown in Eq. (59).

$$B_{10}H_{14} \underset{+H^+}{\overset{-H^+}{\rightleftharpoons}} B_{10}H_{13}^- \underset{+H^+}{\overset{-H^+}{\rightleftharpoons}} B_{10}H_{12}^{2-} \tag{59}$$

Reactions of $NaB_{10}H_{13}$ with alkyl halides give access to monoalkylated decaboranes $B_{10}H_{13}R$. Alkylation occurs at the 6-position. When $NaB_{10}H_{13}$ is allowed to react with R_2BHal compounds, the question is, will an exopolyhedral B–B bond be formed or will there be a cluster expansion? For the case of 9-BBN-halides [9-BBN = 9-bora-(3.3.0)-bicyclononyl] this question has been tested. In fact none of the two possibilities are realized, rather a "partial" insertion of the 9-BBN unit into the *nido*-framework of the B_{10} cluster occurs with formation of a highly asymmetric bridge between the boron atom of the 9-BBN unit and the atoms B5 and B6 of the B10 unit with distances of 1.740 and 2.079 Å (see Figure 2.1-37). The compound reacts with "proton sponge" [PS = 1,8-bis(dimethylamino)-naphthalene] to give [PSH][9-BBN-$B_{10}H_{13}$]. The anion of this salt has a structure similar to $B_{11}H_{14}^-$. However, the B(BBN)-B6 distance is abnormally long with 2.142 Å, indicating that the BBN unit is not fully accommodated into the B_{10} framework. This is a good example that cluster formation may be in between an exopolyhedral B–B bond and a true cluster expansion [99].

2.1.5.5
Chemistry of Undecahydro-*closo*-undecaborate $B_{11}H_{11}^{2-}$

The *closo*-anion $B_{11}H_{11}^{2-}$ anion is accessible by the thermal decomposition of $B_{11}H_{13}^{2-}$ at about 250 °C [100]. A more efficient route is given in Eq. (60) [101]:

$$B_{10}H_{13}(SMe_2) + 2LiBu^t + 6thp \rightarrow [Li(thp)_3]_2[B_{11}H_{11}] + 2HBu^t \tag{60}$$

In analogy, K[$BHEt_3$] can be used to prepare the potassium salt. Metathesis is employed for preparing tetraalkyl ammonium salts. The Li cation in $[Li(thp)_3]_2$-

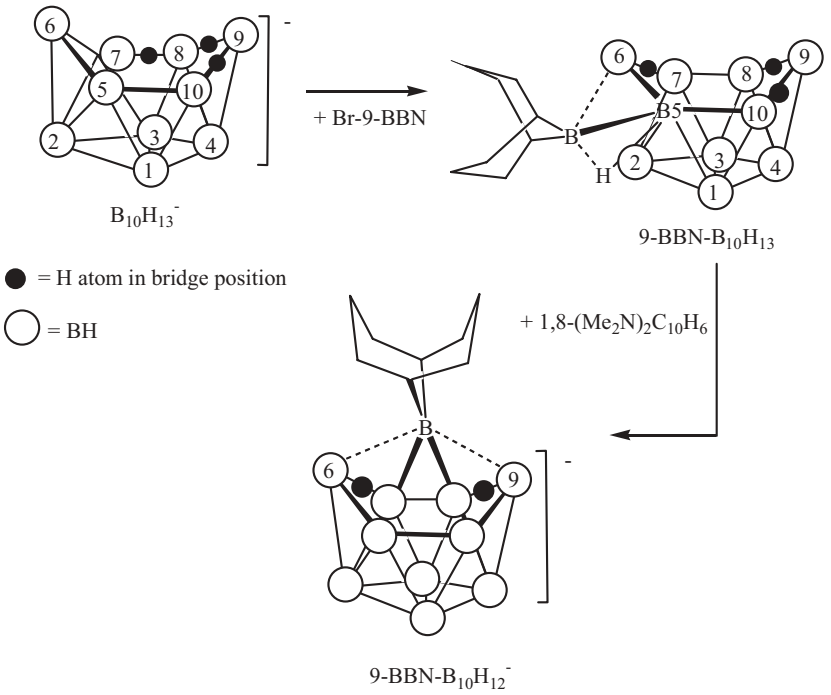

Fig. 2.1-37. Insertion of a 9-BBN unit into the B_{10} cluster of $B_{10}H_{13}^-$.

$[B_{11}H_{11}]$ interacts with the $B_{11}H_{11}$ anionic unit as shown in Figure 2.1-38. This leads to a distortion of the B_{11} cluster while the anion of the ammonium salt $[N(bzl)Et_3]_2[B_{11}H_{11}]$ (bzl = benzyl) has almost perfect C_{2v} symmetry [101].

The *closo*-anion $B_{11}H_{11}^{2-}$ reacts with acids. In the case of CF_3COOH the $B_{11}H_{11}^{2-}$ is not only protonated to $B_{11}H_{12}^-$ but this anion also adds one molecule of the carboxylic acid according to Eq. (61) [101] by restoring the pentagonal face of the $B_{11}H_{13}$ anion as shown in Figure 2.1-39. Addition of water, ethanol or pyridine to $B_{11}H_{12}^-$ at low temperature yields the *nido*-anions $B_{11}H_{13}(OH)^-$, $B_{11}H_{13}(OEt)^-$ and $B_{11}H_{13}py^-$ [103].

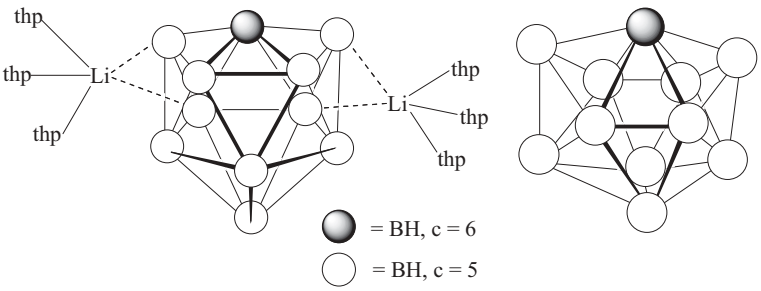

Fig. 2.1-38. Structure of $[Li(thp)_3]_2[B_{11}H_{11}]$ and of the $B_{11}H_{11}^{2-}$ anion.

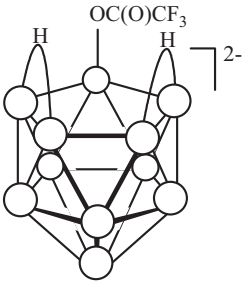

Fig. 2.1-39. Structure of the anion $[B_{11}H_{13}(OC(O)CF_3)]^-$.

$$[B_{11}H_{11}]^{2-} + 2F_3C\text{-}C(O)OH \rightarrow [B_{11}H_{13}(OC(O)CF_3)]^- + F_3C(O)O^- \quad (61)$$

Cluster expansion of the $B_{11}H_{11}$ cluster is possible on heating with triethylamine borane to give the dodecahydro-*closo*-dodecaborate (Eq. 62) [104]:

$$B_{11}H_{11}{}^{2-} + Et_3N{\cdot}BH_3 \rightarrow B_{12}H_{12}{}^{2-} + Et_3N + H_2 \quad (62)$$

Moreover, in analogy with several other hydropolyborates such as $B_{10}H_{10}{}^{2-}$ or $B_{12}H_{12}{}^{2-}$ the anion $B_{11}H_{11}{}^{2-}$ can be oxidized to *conjunto*-polyborates. In the case of $B_{11}H_{11}{}^{2-}$ the reaction with Fe^{3+} ions leads to the $B_{22}H_{22}{}^{2-}$ anion (Figure 2.1-40), which consists structurally of a *closo*-$B_{12}H_{10}$ unit fused to a *nido*-$B_{10}H_{12}$ unit [101].

The $B_{11}H_{11}{}^{2-}$ anion can be transformed into hydrido-halogeno-*closo*-undecaborates. Reaction with OBr^- yields $B_{11}H_9Br_2{}^{2-}$ [105] while Br_2 in NaOH (ratio $B_{11}H_{11}{}^{2-}$:Br_2 = 1:3.8) gives $B_{11}H_7Br_4{}^{2-}$ [106]. However, with Cl_2 the anion

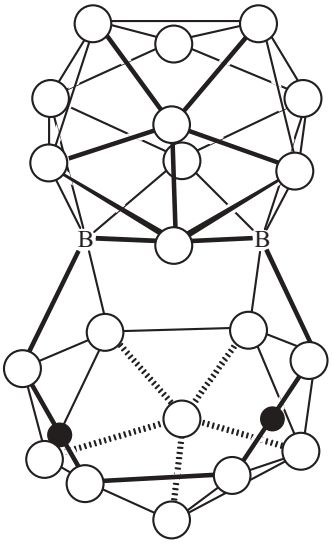

Fig. 2.1-40. Structure of the $B_{22}H_{22}{}^{2-}$ anion.

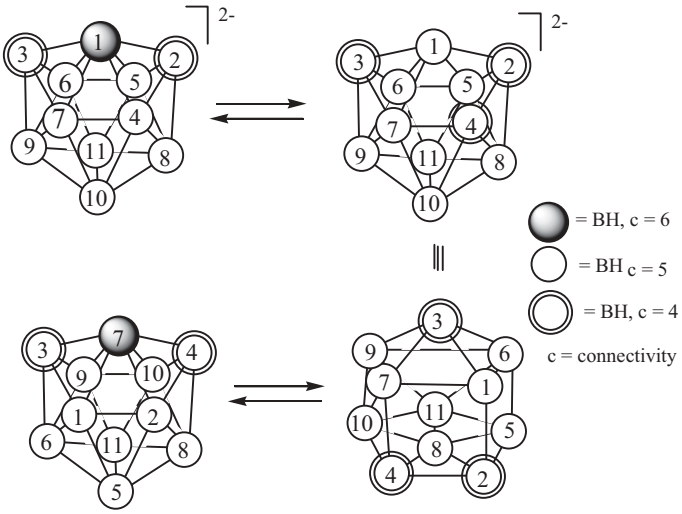

Fig. 2.1-41. Diamond-square-diamond mechanism for $B_{11}H_{11}^{2-}$.

$B_{11}HCl_{10}^{2-}$ is obtained and with an excess of Br_2 or I_2 the perhalo-*closo*-enneaborates $B_{11}X_{11}^{2-}$ result [107]. The anion $B_{11}Cl_{11}^{2-}$ is accessible from $B_{11}H_{11}^{2-}$ and *N*-chlorosuccinimide [108]. In solution, all boron atoms of these anions are equivalent as shown by ^{11}B NMR spectroscopy, as is also the case also for $B_{11}H_{11}^{2-}$. This suggests a degenerate cluster atom rearrangement of the B_{11} skeleton (which shows three different types of boron atoms in its cluster) by the diamond-square-diamond mechanism as depicted in Figure 2.1-41 [107]. This is also supported by DFT calculations. Typical for this type of mechanism is the least migration of boron atoms on the surface of a circumscribed sphere covering all boron atoms of the anion. While $B_{11}H_{11}^{2-}$ can be oxidized to $B_{22}H_{22}^{2-}$ the oxidation of the $B_{11}X_{11}^{2-}$ species starts with a one electron transfer to the radical anion $B_{11}X_{11}^{-}$, but no $B_{22}X_{22}^{2-}$ anion is formed on further oxidation [109].

Within the series of hydroundecaborates there exists the *nido*-species $B_{11}H_{15}$, $B_{11}H_{14}^{-}$, $B_{11}H_{13}^{2-}$, $B_{11}H_{12}^{3-}$ and *closo*-$B_{11}H_{11}^{2-}$. The $B_{11}H_{15-n}^{n-}$ series can be generated from the parent borane $B_{11}H_{15}$ by deprotonation. To obtain the anion $B_{11}H_{12}^{3-}$ a strong base such as $LiBu^t$ is needed as shown in Eq. (63). The deprotonations are reversible as observed for many other highly charged hydropolyborate anions:

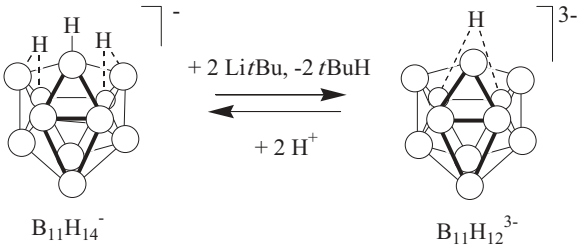

(63)

As a consequence, $B_{11}H_{12}^{3-}$ could not be further deprotonated to $B_{11}H_{11}^{4-}$ as this anion should be an extremely strong base. The boron skeleton of $B_{11}H_{12}^{3-}$ is not fluxional, but the bridging proton migrates along the open pentagonal face [107].

Heating a suspension of $[Li(thp)_x]_3[B_{11}H_{12}]$ to 80 °C leads to elimination of LiH, while thermolysis of $B_{11}H_{13}^{2-}$ salts occur with hydrogen evolution. In both cases *closo*-$B_{11}H_{11}^{2-}$ is formed [110]:

$$B_{11}H_{12}^{3-} \rightarrow B_{11}H_{11}^{2-} + H^- \quad (64)$$

$$B_{11}H_{13}^{2-} \rightarrow B_{11}H_{11}^{2-} + H_2 \quad (65)$$

2.1.5.6 Chemistry of the Dodecahydro-*closo*-dodecaborate

2.1.5.6.1 Protonation and Alkylation of $B_{12}H_{12}^{2-}$

The $B_{12}H_{12}^{2-}$ anion is a very weak base as $[H_3O]_2[B_{12}H_{12}]$ is a very strong acid in aqueous medium. One reason for this is that the anion has icosahedral symmetry, I_h, and the negative charge is distributed over a large volume. So, protonation is certainly not possible in aqueous solution, but it is in a non-aqueous medium. Indeed, trifluoroacetic acid reacts in acetone, acetonitrile or diethyl ether solution with the $B_{12}H_{12}^{2-}$ anion, however with hydrogen evolution. In this process a new anion is formed, $B_{24}H_{23}^{3-}$. Its formation is considered to proceed in two steps: the first one leads to unstable $B_{12}H_{13}^-$ which decomposes with H_2 evolution, and the resulting $B_{12}H_{11}^-$ anion adds to $B_{12}H_{12}^{2-}$ generating $B_{24}H_{23}^{2-}$ [111]:

$$B_{12}H_{12}^{2-} + H^+ \rightarrow \{B_{12}H_{13}^-\} \rightarrow \{B_{12}H_{11}^-\} + H_2 \quad (66)$$

$$\{B_{12}H_{11}^-\} + B_{12}H_{12}^{2-} \rightarrow B_{24}H_{23}^{3-} \quad (67)$$

According to calculations, this new anion should have a structure where two $B_{12}H_{11}$ units are joined by a 3c2e B–H bond.

Permethylation of the anion $B_{12}H_{12}^{2-}$ is achieved by reacting its R_4N^+ salts (R = Et, Bu) with a an excess of MeI in trimethylaluminum [112, 113]. An intermediate anion $[B_{12}Me_{11}I]^{2-}$ can be isolated as an R_4N^+ salt. When it is heated to reflux with additional $AlMe_3$ for 1 week permethylation to $B_{12}Me_{12}^{2-}$ is achieved. The colorless alkali metal salts of $B_{12}Me_{12}^{2-}$ are readily accessible by ion exchange methods while $[Ph_4As]_2[B_{12}Me_{12}]$ is obtained from $[Et_4N]_2B_{12}Me_{12}$ and $[Ph_4As]Cl$. The structure of the anion in $[Ph_4As]_2B_{12}Me_{12}$ is almost a perfect icosahedron (Figure 2.1-42). The salt with a dipyridinomethane cation is red due to a charge transfer interaction between the cation and the $B_{12}Me_{12}^{2-}$ anion. While the one electron oxidation of $B_{12}Me_{12}^{2-}$ with Ce^{4+} yields the blue radical anion $B_{12}Me_{12}^{\bullet-}$ [114] the electrochemical oxidation of $B_{12}H_{12}^{2-}$ gives the *conjuncto*-anion $B_{24}H_{23}^{3-}$, where two B_{12} units are bridged by a hydrogen atom [111].

2.1.5.6.2 Halogeno-, Hydroxo-, Alkoxo- and Amine *closo*-dodecaborates

Halogenation of the $B_{12}H_{12}^{2-}$ ion with *N*-halosuccinamide leads to mono- and dihalosubstituted dodecaborates, while reaction with elemental halogens finally led

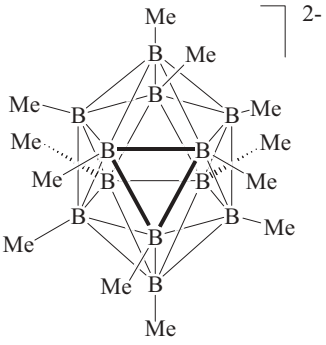

Fig. 2.1-42. Structure of the anion $B_{12}Me_{12}^{2-}$.

to the perhalo derivatives. The substitution of the hydrogen atoms by fluorine atoms occurs in liquid HF according to Eq. (68) [115]. To achieve $B_{12}HF_{11}^{2-}$ a melt of K_2HF (290 °C) is necessary. The fluorination proceeds stereoselectively, and it was shown that the F atoms have a pronounced *meta*-orienting effect. The sequence of fluorination is: $B_{12}H_{11}F^{2-}$, 1,7-$B_{12}H_{10}F_2^{2-}$, 1,7,9-$B_{12}H_9F_3^{2-}$, 1,7,9,10-$B_{12}H_8F_4^{2-}$, 1,7,8,9,10-$B_{12}H_7F_5^{2-}$, 1,7,8,9,10,11-$B_{12}H_6F_6^{2-}$, 1,2,7,8,9,10-$B_{12}H_6F_6^{2-}$, 1,2,7,8,9,10,11-$B_{12}H_5F_7^{2-}$, 1,2,4,7,8,9,10,11-$B_{12}H_4F_8^{2-}$, 1,2,4,5,7,8,9,10,11-$B_{12}H_3F_9^{2-}$, 1,2,3,4,5,6,8,9,10,11-$B_{12}H_2F_{10}^{2-}$, and 1,3,4,5,6,7,8,9,10,11-$B_{12}HF_{11}^{2-}$.

$$B_{12}H_{12}^{2-} + n\mathrm{HF} \rightarrow B_{12}H_{12-n}F_n^{2-} + n\mathrm{H_2} \qquad (68)$$

The dodecahalogeno-*closo*-dodecaborates $B_{12}X_{12}^{2-}$ can be oxidatively transformed into polyboranes B_nX_n. However, the anions proved not to be suitable for developing a chemistry of their own, e.g., polymers based on B_{12} units or dendrimers. Therefore, functional hydro-*closo*-dodecaborates carrying reactive substituents are needed.

One possibility is the replacement of hydrogen atoms by OH groups whose hydrogen atom can be substituted by more reactive, more versatile and even multifunctional groups. One of the main problems is to generate a synthesis with high selectivity, because as the number of substituent n in $B_{12}H_{12-n}R_n^{2-}$ change from 1 to 12 the number of possible isomers i increases up to $n = 6$ ($n = 1$, $i = 1$; $n = 2$, $i = 3$; $n = 3$, $i = 5$; $n = 4$, $i = 16$; $n = 5$, $i = 24$; $n = 6$, $i =$).

Mono- and 1,2-dihydroxohydro-*closo*-dodecaborates are obtained by hydrolysis of the corresponding carboxylato-*closo*-dodecaborates [116]. The 1,7-$B_{12}H_{10}(OH)_2^{2-}$ isomer is obtained by reacting $[H_3O]_2[B_{12}H_{12}]$ with glycole at 160 °C followed by hydrolysis with an aqueous sodium carbonate solution. The anion precipitates from the aqueous solution with tetrabutylammonium ions [116]. These hydroxy derivatives of $B_{12}H_{12}^{2-}$ are of great utility as they allow the synthesis of many derivatives with, e.g., different solubility properties. Thus the reaction of $B_{12}H_{11}$-$(OH)^{2-}$ with thionyl or sulfuryl chloride leads to anions, where two $B_{12}H_{11}$ units are bridged by SO and SO_2 groups, respectively. Similarly, oxalylchloride, or ter-

ephthaloylchloride give anions of the type $[B_{12}H_{11}O\text{-}C(O)\text{-}R\text{-}C(O)\text{-}O\text{-}B_{12}H_{11}]^{4-}$. On the other hand, when 1,2-$B_{12}H_{10}(OH)_2^{2-}$ is allowed to react with oxalylchoride or sulfurylchloride the "chelate" complex anions $B_{12}H_{10}[O(O)C\text{-}C(O)O]^{2-}$ and $B_{12}H_{10}(O_2SO_2)^{2-}$ are formed [117].

When hydrogen peroxide is used as an oxidizing reagent the total replacement of the hydrogen atoms of $Na_2B_{12}H_{12}$ via a number of intermediates occurs. At room temperature oxidation by 30% H_2O_2 leads to *closo*-1,4,5,8,9,10,11-heptahydroxo-pentahydro-*closo*-dodecaborate $B_{12}H_5(OH)_7^{2-}$, and at reflux temperature (24 hours) the hydroxo-hydro-*closo*-dodecaborate $B_{12}H(OH)_{11}^{2-}$ resulted [118]. By the same method but by using $Cs_2B_{12}H_{12}$ and 3 days at reflux the perhydroxylated compound $Cs_2B_{12}(OH)_{12}$ was obtained [119]. Astonishingly, all alkali metal salts (Li to Cs) of the $B_{12}(OH)_{12}^{2-}$ anion are almost insoluble at ambient temperature in water, in spite of the many hydrophilic OH groups. One reason for the low solubility may be that the OH groups of the anion interact strongly with the alkali metal cations. The OH groups can be acylated by acetic acid anhydride or benzoyl chloride. However, it is necessary to increase the solubility of the $B_{12}(OH)_{12}^{2-}$ salts, and this can be done by using the tetrabutylammonium salts. The benzoate was isolated (after chromatography and recrystallization from acetonitrile/water) as $[H_3O]_2[B_{12}(OC(O)Ph)_{12}]$ [see Eqs. (69) to (71)] [120]:

$$B_{12}H_{12}^{2-} + 12H_2O_2 \rightarrow B_{12}(OH)_{12}^{2-} + 12H_2O \tag{69}$$

$$B_{12}(OH)_{12}^{2-} + 12(MeCO)_2O \rightarrow B_{12}[O\text{-}C(O)\text{-}Me]_{12}^{2-} + 12Me\text{-}C(O)OH \tag{70}$$

$$B_{12}(OH)_{12}^{2-} + 12PhC(O)Cl + 12NEt_3 \rightarrow B_{12}[O\text{-}C(O)Ph]_{12}^{2-} + 12[Et_3NH]Cl \tag{71}$$

Moreover, $B_{12}(OH)_{12}^{2-}$ can also perbenzylated with benzylchloride in the presence of $EtNPr^i_2$ under reflux in acetonitrile. The alkylation requires 6 days [see Eq. (72)]. Shorter reaction times result in incomplete reaction, longer ones in the formation of larger quantities of the purple radical anion $[B_{12}(OCH_2Ph)_{12}]^{\bullet-}$. This radical can also be generated by a one electron oxidation with Fe^{3+}, and it is even possible to further oxidize the radical anion to the dark orange neutral *hyper-closo*-$B_{12}(OCH_2Ph)_{12}$ [121]:

$$B_{12}(OH)_{12}^{2-} + 12PhCH_2Cl + 12EtNPr^i_2 \rightarrow B_{12}(OCH_2Ph)_{12}^{2-} + 12[EtPr^i_2H]Cl \tag{72}$$

$$B_{12}(OCH_2Ph)_{12}^{2-} \underset{+NaBH_4}{\overset{+Fe^{3+}}{\rightleftharpoons}} B_{12}(OCH_2Ph)_{12}^{\bullet-} \underset{+NaBH_4}{\overset{+Fe^{3+}}{\rightleftharpoons}} B_{12}(OCH_2Ph)_{12} \tag{73}$$

While the structure of the B_{12} radical anion is slightly more distorted (B–B bonds 1.768–1.840 Å) than the parent $B_{12}(OCH_2Ph_{12})^{2-}$ (B–B 1.781–1.824 Å) the *hyper-closo*-$B_{12}(OCH_2Ph_{12})$ has only D_{3d} symmetry (see Figure 2.1-42). This is attributed to a Jahn-Teller distortion. There are six long bonds (1.910–1.918 Å) of two opposite triangles while all the others are shorter (1.755–1.864 Å). There are also six short and six longer B–O bonds, the shorter ones are found at the boron atoms with the

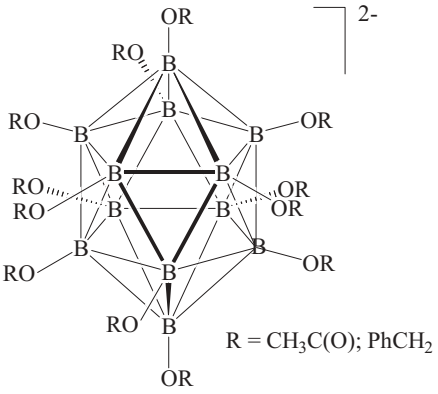

Fig. 2.1-42a. Structure of $B_{12}(OR)_{12}$ anions.

long bonds. This indicates that these B–O bonds have a larger π-bond character than the others [121].

Amination of $B_{12}H_{12}^{2-}$ requires the electrophile hydroxylamine-O-sulfonic acid. Besides $B_{12}H_{11}(NH_3)$, the main product is 1,7-$B_{12}H_{10}(NH_3)_2$ [122]. In both compounds, the B–N bond lengths are shorter than in $B_{12}H_{11}NEt_3$.

2.1.5.7 Chemistry of $B_{20}H_{18}^{2-}$ Anions

As already outlined, the anion $B_{20}H_{18}^{2-}$ can be synthesized by oxidizing $B_{10}H_{10}^{2-}$ with Fe^{3+}. In principle this anion can form three geometrical isomers: the 1,1-isomer with a B–B bond between two axial boron atoms of two B_{10} clusters (*a,a-isomer*), the 1,2-isomer with a B–B bond between axial boron atoms and a B atom from the equatorial region of the second B_{10} unit (*a,e*-isomer), and a 2,2-isomer (*e,e*-isomer). These are shown in Figure 2.1-43.

The reduction of $[Et_3NH]_2[B_{20}H_{18}]$ with elemental sodium in liquid ammonia leads to e^2-$B_{20}H_{18}^{4-}$ where the two B_{10} clusters are linked via equatorial–equatorial boron–boron bonds [123, 124]. The high negative charge suggests a substantial basicity for this anion. Indeed, the anion can be readily protonated to $B_{20}H_{19}^{3-}$, but this leads to a mixture of isomers, which on treatment with KOH gives $K_4[ae$-$B_{20}H_{18}]$ where the B_{10} clusters are linked through an apical and equatorial boron–boron bond. The isomerizations observed on protonation/deprotonation reactions of the anionic B_{20} species are not well understood but seem to be promoted by acid catalysis (see Figure 2.1-44) [124]. These clusters are potential candidates for BNCT (see Chapter 2.2) provided that the "double" cluster can be functionalized. This is possible with oxalyl chloride which reacts with $[Et_4N]_2[B_{20}H_{18}]$ in dichloromethane to produce $[Et_4N][a^2$-$B_{20}H_{17}(CO)_2]$ [see Figure 2.1-45 and Eq. (73)]:

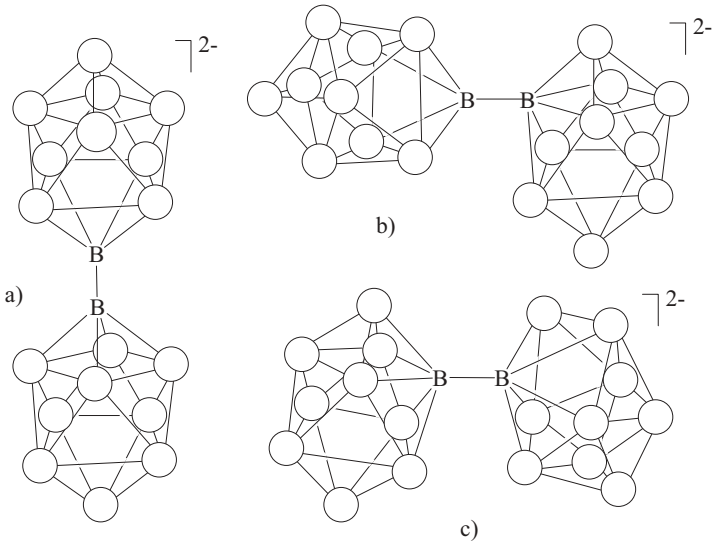

Fig. 2.1-43. The three isomers of $B_{20}H_{18}^{2-}$: (a) *a*,*a*-isomer, (b) *a*,*e*-isomer, and (c) *e*,*e*-isomer.

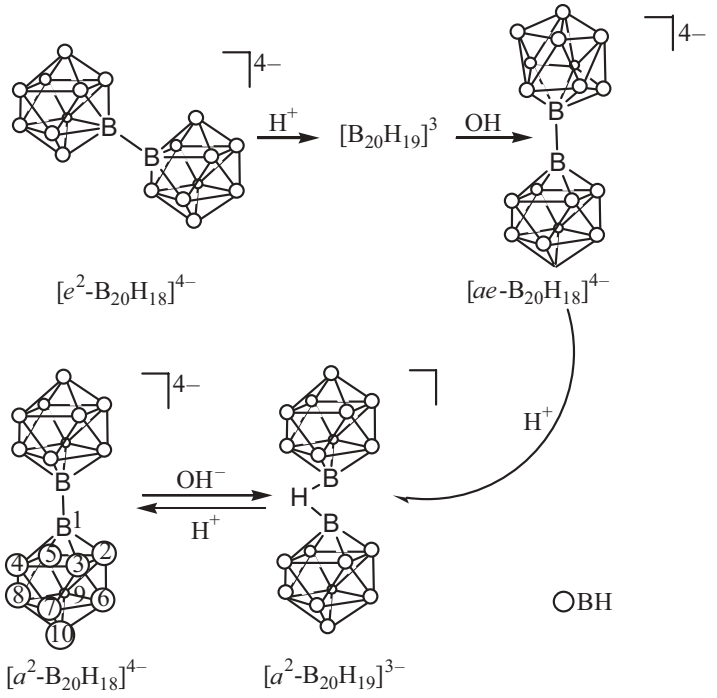

Fig. 2.1-44. Isomerization induced by protonation and deprotonation reactions of $B_{20}H_{18}^{4-}$.

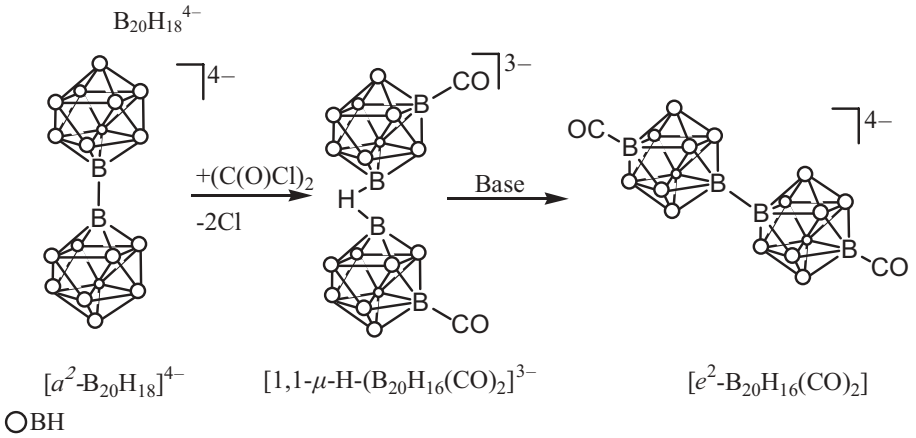

Fig. 2.1-45. Carbonylation of $B_{20}H_{18}^{4-}$ to isomers of $B_{20}H_{16}(CO)_2$ anions.

$$[B_{20}H_{18}]^{4-} + 2Cl(O)C\text{-}C(O)Cl \rightarrow [B_{20}H_{17}(CO)_2]^{-} + HCl + 3Cl^{-} + 2CO \qquad (74)$$

The CO groups are in the B6 positions of each of the two *closo*-$B_{10}H_8(CO)$ units which are linked by a 3c2e-BHB-bond involving their B1 boron atoms. This anion on deprotonation with non-aqueous, non-nucleophilic bases ($CaCO_3$ or $NaHCO_3$ in CH_3CN) gives $[e^2\text{-}B_{20}H_{16}(CO)_2]^{2-}$ (isolated as the Ph_3PMe^+ salt).

Reaction of $[Et_4N]_3[a^2\text{-}B_{20}H_{17}(CO)_2]$ with NaN_3 yields the cyanate $[Et_4N]_3[a^2\text{-}B_{20}H_{17}(NCO)_2]$ which on addition of isopropylamine gives a urea derivative $[Et_4N]_2[a^2\text{-}B_{20}H_{16}(NH)_2\text{-}C(O)\text{-}N(iPr)_2]$ or on hydrolysis the carbonic acid derivative $[a^2\text{-}B_{20}H_{17}(C(O)OH)_2]^{3-}$ [125].

The oxidation of *ae*-$B_{20}H_{18}^{-}$ leads to μ-$B_{20}H_{18}OH^{2-}$ anions [126]. Therefore, a similar behavior was expected for the amino derivative of $B_{20}H_{17}NH_3^{3-}$. Because benzoquinone oxidizes $B_{10}H_{10}^{2-}$ and $B_{20}H_{18}^{4-}$ readily to $B_{20}H_{18}^{2-}$ [127] a similar behavior can be expected for the oxidation of a^2-$B_{20}H_{18}NH_3^{3-}$. However, when the oxidation was performed in acetonitrile the solvent interacted leading to a^2-[μ-$MeC(NH)_2B_{20}H_{16}]^{3-}$ where the two B_{10} clusters are bridged by an amidinium ion [128]. Reaction of this ion with hydrochloric acid leads to a B_{20} anion where the B–B bond between the two B_{10} clusters is protonated. This proton can be easily removed with a base (Figure 2.1-47). However, if the protonation is carried out in the presence of benzoquinone then a μ-amidinium-$B_{20}H_{16}^{-}$ anion is formed where the two B_{10} clusters are joined by 3c2e bonds involving the atoms B2 and B3 of the B_{10} units. Similarly, the oxidation of a^2-$B_{20}H_{17}OH^{4-}$ with benzoquinone leads to a^2-μ-(2,2′-O)$B_{20}H_{15}^{4-}$, which on protonation produces μ-H, μ-OH-$B_{20}H_{16}^{2-}$ (see Figure 2.1-46). The amino derivative are of particular interest for BNCT [129, 130].

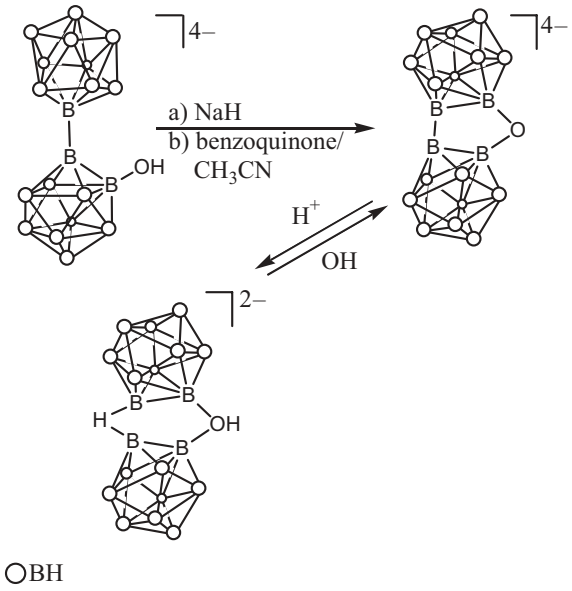

Fig. 2.1-46. Protonation/deprotonation of derivatives of the anion $B_{20}H_{18}^{4-}$.

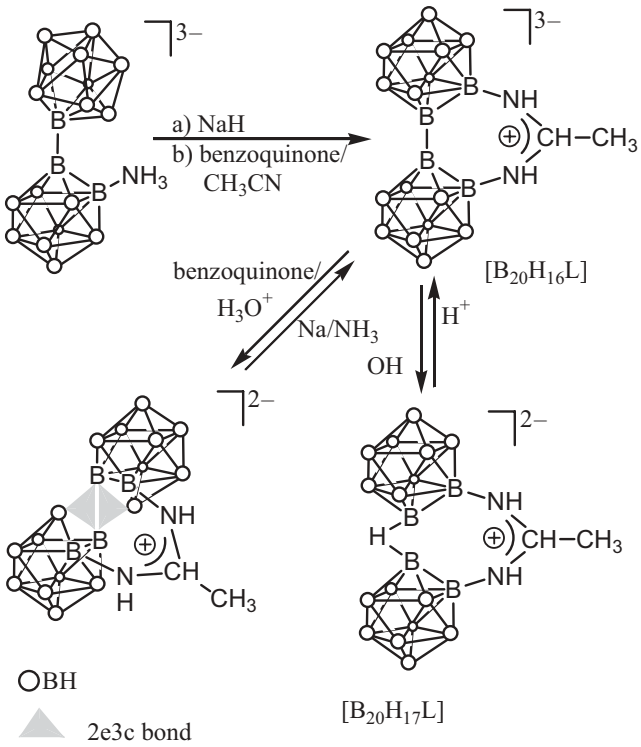

Fig. 2.1-47. Amidine bridged $B_{20}H_{18}$ anions.

2.1.6 Substituted Neutral Polyboranes of Type B_yX_y

2.1.6.1 Overview

In contrast to the polyhedral boranes B_nH_{n+m} there exist a number of neutral boron cluster molecules B_nX_n (X = Cl, Br, I, NR_2, R) all of them having closed deltahedral structures in spite of the fact that the number of bonding electron pairs is only *n*. For this reason these homonuclear cluster compounds of boron are called *hypercloso* polyboranes. However, there also exist anions of type $B_nX_n^{2-}$ which fit Wade's rules.

Table 2.1-2 lists some of these uncharged cluster compounds. Many more actually exist, but so far these have not yet been isolated or fully characterized. Some of these are mentioned in the footnote to the table, most of them were only detected by mass spectrometry. For a review see Ref. [131].

In addition to $B_4(tmp)_4$ [132] there exist several other $B_n(NR_2)_n$ compounds but these have ring structures (v.i.). Astonishingly no fluorides B_nF_n are yet known, and all attempts to synthesize B_4F_4, e.g., by fluorination of B_4Cl_4 have failed [133]. However, some boron fluorides of the type B_nF_{n+x} have been reported, one of them shows a distorted tetrahedral B_4 skeleton [134]. More recently the first *hypercloso*-alkoxy-icosahedrane $B_{12}(OCH_2Ph)_{12}$ has been prepared [120].

Tab. 2.1-2. Some physical data of *hypercloso*-polyboranes.[a)]

	X = Cl	***X = Br***	***X = I***
B_4X_4	yellow, m.p. 95 °C subl. 30 °C/31 mbar		
B_8X_8	purple, m.p. 185 °C		dark brown
B_9X_9		dark red solid not sublimable	dark brown solid
	X = tmp	X = Bu^t	X = mes
B_4X_4	yellow, m.p. 292 °C	colorless, m.p. 45 °C	orange solid

[a)] Other reported compounds: $B_{10}Cl_9$ (orange brown, m.p. >35 °C, $B_{11}Cl_{11}$ usually in mixture with $B_{10}Cl_{10}$, B_9Cl_8H, $B_9Cl_7H_2$, B_9Cl_8Me, B_9Br_8Me.

2.1.6.2 Structures

Common to the structures of B_4Cl_4, $B_4(tmp)_4$, $B_4(mes)_4$ (mes = 2,4,6-trimethylphenyl) are (slightly distorted) tetrahedral skeletons. Closest to T_d symmetry is B_4Cl_4 in the gas phase. The B–B bond lengths of $B_4(mes)_4$ vary from 1.695 to 1.704(4) Å and of $B_4(tmp)_4$ from 1.695(6) to 1.765(5) Å where the two opposite edges are shorter than all other B–B distances. The core structure of B_8Cl_8 is a dodecahedron [135], while B_9Cl_9 is isotypic with B_9Br_9 [136]. The skeleton of these

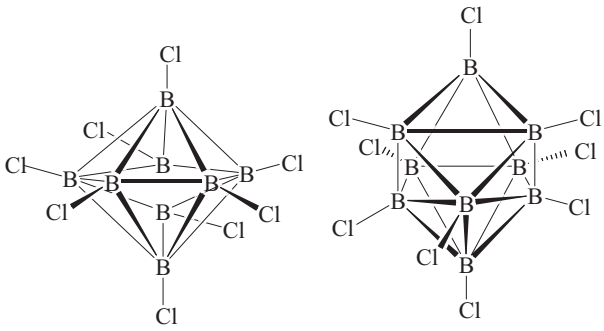

Fig. 2.1-48. Structures of B_8Cl_8 and B_9Cl_9.

latter two molecules is best described as being a tricapped trigonal prism of boron atoms. In all cases the B–X bonds are directed towards the centers of the cluster core (see Figure 2.1-48).

The lengths of the B–B bonds in the tetraboron tetrahedranes are particularly influenced by the substituents, although in $B_4(tmp)_4$ there are two significantly longer and two significantly shorter bonds. The reason for this is probably due to the bulky amino groups. However, the B–B bonds of B_8Cl_8 vary considerably from 1.707 to 2.048 Å while those of the B_9Cl_9 molecule are much more uniform spanning only a range of from 1.721 to 1.748 Å. Because the infrared spectrum of B_9I_9 [137] is similar to those of B_9Cl_9 and B_9Br_9 one expects that this iodide has the same structure as the other two nonaboron nonahalides.

Although the boron atoms in B_9Cl_9 are not equivalent (three B atoms are of connectivity four, and six atoms of connectivity five), the ^{11}B NMR spectrum shows only one signal. This indicates that the compound is fluxional in solutions making all boron atoms on the NMR time scale equivalent [138].

$B_4(Bu^t)_4$ has C_2 symmetry in the solid state [139] with B–B bonds lengths ranging from 1.699 to 1.714 Å while in the gas phase T_d symmetry is achieved, the B–B bond lengths being 1.704(4) Å [140]. $B_4(mes)_4$ has a tetrahedral structure for the B_4C_4 core with an average B–B bond length of 1.696(4) Å in the solid state [141].

2.1.6.3 Synthesis

B_4Cl_4 is best prepared by passing B_2Cl_4 vapor through a mercury discharge [142], but more conveniently by the use of a radiofrequency discharge through a stream of BCl_3 vapor at low pressure by using Hg for scavenging Cl atoms [135]:

$$4BCl_3 + 8Hg \xrightarrow{\text{electr. discharge}} B_4Cl_4 + 4Hg_2Cl_2 \qquad (75)$$

B_8Cl_8, B_9Cl_9, $B_{10}Cl_{10}$ and $B_{11}Cl_{11}$ are formed in small yield by thermolysis of B_2Cl_4 but no B_4Cl_4 results in this process. B_8Cl_8 can be removed from B_9Cl_9 by

fractional sublimation *in vacuo*, while B_9Cl_9 is obtained by heating the red mixture of $B_{10}Cl_{10}$ and $B_{11}Cl_{11}$ in the presence of chlorine [143]. Today, the best route to B_9Cl_9 is the chlorination of $[Bu_4N]_2[B_9H_9]$ with an excess of S_2Cl_2 in methylene chloride. Moreover, it is also formed by the oxidation of $B_9Cl_9^{2-}$ or $B_9Cl_9^{\bullet -}$ with $Tl(OCOCF_3)_3$ [144]. This is also the best route to B_9Br_9 and B_9I_9 [145].

Polyboron fluorides B_nF_{n+m} are obtained by passing BF_3 over elemental boron at a temperature of 1000 °C and co-condensing the generated BF with BF_3. This yields B_2F_4 and B_3F_5 besides B_8F_{12}. The ^{11}B NMR spectrum of the last compound is consistent with a diborane like structure $(F_2B)_2B(\mu\text{-}BF_2)_2B(BF_2)_2$ (see Figure 2.1-47) where the hydrogen atoms in B_2H_6 are replaced by BF_2 groups. This was confirmed by X-ray structure determination [136]. In addition, another polyboron-fluoride was isolated as a crystalline material and proved to be $B_{10}F_{12}$. This compound has a central distorted tetrahedral B_4 core whereby each of these boron atoms are bound to a BF_2 group. In addition, there are two more BF_2 groups, each of them bridging one B–B distance on opposite edges (see Figure 2.1-49). Therefore, these are bonded to the core by 3c2e bonds. The B–B edges are short [1.605(3) Å] with longer B–B distances to the bridging boron atoms [1.758(1), 1.807(2) Å]. Moreover, the B–F bond lengths are indicative of the presence of B–F π-bonding. As a result, the BF_2 groups are obviously less electron deficient than BH_2 groups. The molecule $B_{10}F_{12}$ has S_4 symmetry [134].

Dehalogenation of appropriate boron halides by alkali metals provides another route to compounds of type B_nX_n. Using dialkylamino boron dihalides R_2NBX_2 (X = Cl, Br) compounds of the type $B_n(NR_2)_n$ are formed such as $B_4(NEt_2)_4$ and $B_6(NMe_2)_6$ (see Figure 2.1-50). This latter compound has a six-membered ring with chair conformation. The synthesis of compounds with bulky R_2N groups requires $B_2(NR_2)_2Cl_2$ as a starting material, and in this case it was a surprise that the resulting $B_4[N(Pr^i{}_2)]_4$ is blue having a folded four-membered structure while $B_4(tmp)_4$ is yellow and a representative of the *closo*-tetrahedranes [132]. The differ-

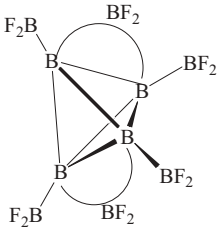

The structure of $B_{10}F_{12}$has S_4 symmetry. The inner core B-B bond lengths of the bridged B atoms are shorter than the other four B-B bonds. Those to the bridging BF_2 groups are the longest 1.703(1) Å.

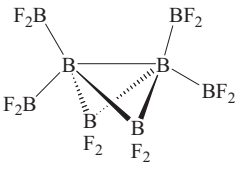

B_8F_{12} has C_{2v} symmetry and a non planar B_4 core with different B-B bond lengths. This structure is 8.77 kJ/mol^{-1} more stable than with equal B-B bond lengths.

Fig. 2.1-49. The structures of B_8F_{12} and $B_{10}F_{12}$.

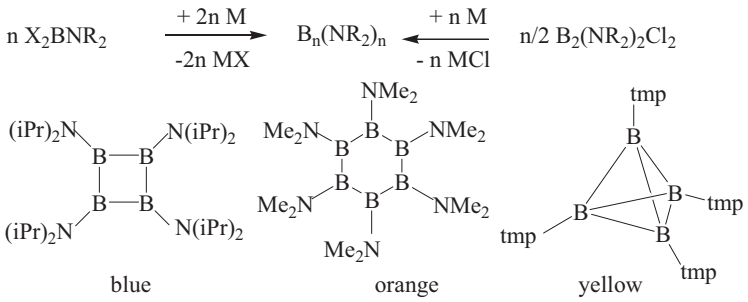

Fig. 2.1-50. Synthesis of dialkylaminopolyboranes $B_n(NR_2)_n$.

ence in color between the ring compound and the tetrahedrane is due to a different HOMO/LUMO gap.

Obviously B–N π-bonding is not a decisive factor as to whether a $B_4(NR_2)_4$ compound is tetrahedral or adopts a classical ring structure. Calculation on model compounds $B_n(NH_2)_n$ ($n = 3$, 4, 5 and 6) by using the B32YP(6-31-G/A) level reveal that the all-planar $B_3(NH_2)_3$ with C_s symmetry is 4.8 kcal mol^{-1} more stable than the compound with D_{3h} symmetry (amino groups perpendicular to the B_3 plane). The most stable structure of $B_4(NH_2)_4$ compounds is the bent four-membered ring structure with D_{2d} symmetry while the planar ring with D_{4h} symmetry is 4.8 kcal mol^{-1} less stable. Tetrahedral alternatives with D_{2d} symmetries are even less favorable by 11.5 and 12.0 kcal mol^{-1}. However, these energy differences are not significantly different, so it can be understood that the sterically encumbered $B_4(tmp)_4$ has a tetrahedral structure. Similarly, the planar $B_5(NH_2)_5$ with D_2 symmetry is more stable by 12.6 kcal mol^{-1} compared with a tetragonal pyramidal structure of C_{2v} symmetry, and for the six B atom species the chair conformation for $B_6(NH_2)_6$ (D_{3d}) is more stable by 15.2 kcal mol^{-1} than the planar structure (D_{6h}). Structures based on a B_6 octahedron with C_2, C_{2v}, D_2 and D_{3d} symmetry are higher in energy by 15.7 to 15.0 kcal mol^{-1} [146].

In addition to $(BNR_2)_n$ compounds a variety of other aminopolyboranes of type $B_n[B(NR_2)_2]_n$ may exist, and a first member of this type is $B_4(NMe_2)_2[B(NMe_2)_2]_2$ [147]. It was obtained by co-dehalogenation of a 1:1 mixture of Me_2NBCl_2 and $B_2Cl_2(NMe_2)_2$ with sodium potassium alloy in hexane (see Figure 2.1-51).

$$Me_2NBCl_2 + B_2(NMe_2)_2Cl_2 \xrightarrow[-KCl]{+NaK_{2.8}} \text{A or B or C or D or E} \qquad (76)$$

Neither the three membered cyclotriborane **A**, the elusive cyclotetraborane **B** [148], the hexakis(dimethylamino)octahedrahexaborane **D** [all of which could result from dechlorination of MeN_2BCl_2 as well as from $B_2Cl_2(NMe_2)_2$] nor the cyclopentaborane **C** were obtained but, rather unexpectedly, the hexakis(dimethylamino-hexaborane **E**, an isomer of the six-membered ring $B_6(NMe_2)_6$. One could have imagined that its central B_4 unit of **E** would adopt a tetrahedral array. However, the four-membered ring is planar and of rhombohedral shape. Particularly interesting

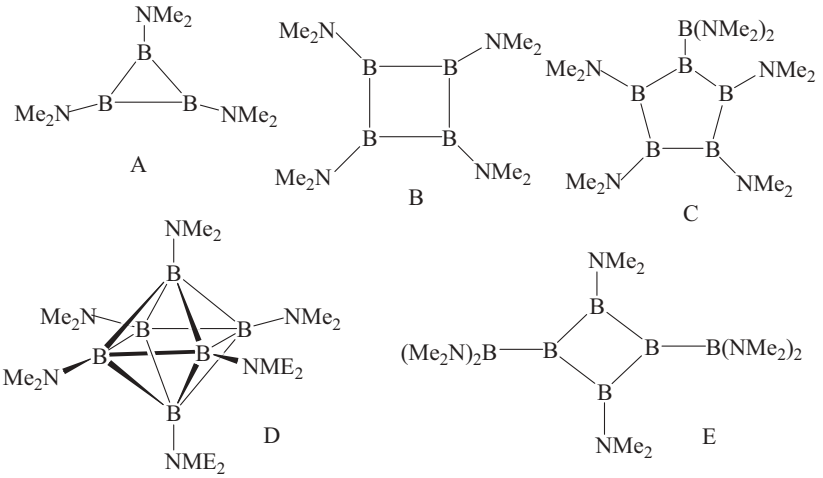

Fig. 2.1-51. Various dimethylaminopolyboranes.

is the short B–B distance between the boron atoms that carry a bis(dimethylamino)boryl group (1.605 Å), which is 0.03 Å shorter than the other B–B distances in the four-membered ring. The exocyclic B–B bond lengths are even longer (1.691 Å). While the ring bonded Me_2N groups are almost coplanar with the B_4 ring, the BN_2 planes of the $B(NMe_2)_2$ units stand almost perpendicular to the B_4 ring plane. A theoretical analysis of possible bonding modes suggests that there is a B–B interaction in the B_4 ring, making two boron atoms tetracoordinated. Thus, there are then only four electron pairs for five B–B bonds. In simple terms, the rhombohedral unit in **E** can be described as having 4σ-B–B bonds besides a 4c2e π bond [147].

Another unusual tetraborane is the tetraalkyl tetraborane **B** with a B4 core similar to $B_6(NMe_2)_6$ shown in Figure 2.1-51. It results from the reduction of the tricyclic system **A** with lithium naphthalide in tetrahydrofuran. **B** is astonishingly stable (m.p. 140 °C). It reacts with $H_3B{\cdot}SMe_2$ to a tetraalkyl derivative of the very rare *closo*-pentaborane(7) [149]. DFT calculations show that a planar B_4Me_4 (model compound for **B**) is 18.4 kcal mol^{-1} less stable than the tetrahedral B_4Me_4 while the $(CH_2CH_2CH_2)$ bridged planar tetraborane **B** is 39.9 kcal mol^{-1} more stable than the tetrahedral tetraborane derivative.

Also $B_4(Bu^t)_4$, $B_4(CH_2Bu^t)_4$ and $B_4(CMe_2Et)_4$ can be obtained by dehalogenation of the respective organylboron dihalides, RBX_2 (X = F, Cl, Br) with alkali metals [150]. In this case minor amounts of the tetraboranes $B_4R_4H_2$ (R = organyl) are always formed. Higher reaction temperature, longer reaction times, more polar solvents and heavier halogen atoms (e.g., Br) favor the formation of $B_4R_4H_2$ over B_4R_4. On the other hand, the preparation of $B_4(mes)_4$ requires the iodide $B_2(mes)_2I_2$ for a successful dehalogenation [143]. $B_4(Bu^t)_4$ can also be obtained from B_4Cl_4 by nucleophilic substitution of its Cl atoms by Bu^tLi.

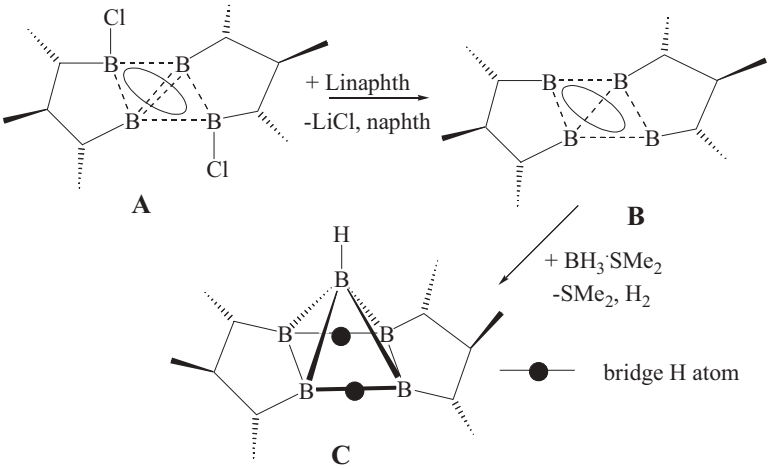

Fig. 2.1-52. An unusual tetraalkyl tetraborane and its transformation into a derivative of *closo*-B_4H_7.

2.1.6.4 Reactions

The chemistry of the *hypercloso*-polyboranes has received comparatively little attention. While B_4Cl_4 is pyrophoric in contact with air, the other polyboron halides B_nX_n are only attacked slowly by air and even hydrolyze quite slowly. This behavior is also observed for all the other tetraboratetrahedranes.

The thermal stability of the chlorides B_nCl_n decreases with $n = 9 > 10 > 11 > 12 > 8$. B_4Cl_4 can be attacked by nucleophiles and electrophiles. Lithiumorganyls such as LiEt allow a stepwise substitution of its Cl atoms to produce B_4EtCl_3, $B_4Et_2Cl_2$ and B_4ClEt_3. With $LiBu^t$ all four Cl atoms can be substituted to generate $B_4(Bu^t)_4$. Weak bases such as PCl_3 form unstable adducts with B_4Cl_4. These dissociate in solution. In contrast, strong bases L such as PMe_3, NMe_3, or SMe_2 react with B_4Cl_4 to give adducts $Cl_3B{\cdot}L$ with destruction of the *hypercloso*-tetraboron cluster. As a consequence, species having a B:Cl ratio less than 1:1 must form. Indeed, in the case of the reaction of B_4Cl_4 with PMe_3 a *hypercloso*-heptaborane cluster $B_7Cl_5(PMe_3)_2$ is formed whose structure was deduced from ^{11}B NMR spectra to be pentagonal bipyramidal (Figure 2.1-53) [151].

Trimethylaluminum degrades B_9Br_9 to BMe_3 while a partial methylation can be achieved with $SnMe_4$ or $PbMe_4$. The chlorine atoms of B_nCl_n can be stepwise and even totally replaced by bromine atoms using Br_2 (at 115 °C), BBr_3 (room temperature for B_4Cl_4, 250 °C for B_9Cl_9), or $AlBr_3$ (at 260 °C for B_8Cl_8). B_9Cl_9 and B_9Br_9 can be reduced to the anions $B_9X_9^{\cdot -}$ and $B_9X_9^{2-}$ by tetrabutylammonium iodide, and this is particularly easy for B_9I_9 which readily forms the blue radical anion $B_9I_9^{\cdot -}$ in reactions with organic solvents having donor properties.

The mixture of $B_{10}Cl_{10}$ with $B_{11}Cl_{11}$ reacts with Cl_2 with contraction of the cluster size to B_9Cl_9, and this occurs also with hydrogen where B_9Cl_8H and $B_9Cl_7H_2$

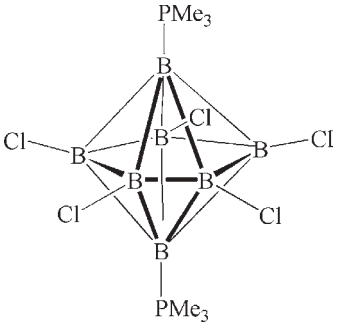

Fig. 2.1-53. Structure of $B_7Cl_5(PMe_3)_2$.

are produced. Similarly B_9Br_9 oxidizes HI to give HB_9Br_9 and $H_2B_9Br_9$ according to Eqs. (77) and (78). Both compounds show fluxional behavior in solution as observed by ^{11}B NMR spectroscopy, and it is assumed that the hydrogen atoms are capping triangular faces of the B_9 core [152].

$$B_9Br_9 + HI \rightarrow B_9HBr_9 + 0.5I_2 \quad (77)$$

$$B_9HBr_9 + HI \rightarrow B_9H_2Br_9 + 0.5I_2 \quad (78)$$

References

1 A. Stock, *The Hydrides of Boron and Silicon*, Cornell University Press, New York, **1933**.

2 General references: W. N. Lipscomb, *Recent Studies of the Boron Hydrides*, in *Adv. Inorg. Radiochem.*, **1959**, *1*, 117; *Boron Hydride Chemistry*, Academic Press, New York, **1975**; E. L. Muetterties, W. H. Knoth, *Polyhedral Boranes*, Marcel Dekker, New York, **1968**; J. F. Liebmann, A. Greenberg, R. E. Williams, eds., *Advances in Boron and the Boranes*, VCH Publishers, Weinheim, New York, **1988**.

3 M. L. McKee, Z.-X. Wang, P. v. R. Schleyer, *J. Am. Chem. Soc.*, **2000**, *122*, 4781.

4 K. Wade, *Adv. Inorg. Radiochem.*, **1976**, *18*, 1. R. E. Williams, page 67 and lit. cited therein.

5 M. M. Balakrishnarajan, E. D. Jemmis, *J. Am. Chem. Soc.*, **2000**, *122*, 4516.

6 E. D. Jemmis, M. M. Balakrishnarajan, P. D. Pancharata, *Inorg. Chem.*, **2001**, *40*, 1731.

7 A. R. Pitochelli, M. F. Hawthorne, *J. Am. Chem. Soc.*, **1962**, *84*, 3218.

8 P. G. Simpson, K. Folting, W. N. Lipscomb, *J. Chem. Phys.*, **1963**, *39*, 26.

9 P. G. Simpson, W. N. Lipscomb, *J. Chem. Phys.*, **1963**, *39*, 2339.

10 J. A. Dopke, D. R. Powell, D. F. Gaines, *Inorg. Chem.*, **2000**, *39*, 463.

11 J. V. B. Kanth, H. C. Brown, *Inorg. Chem.*, **2000**, *39*, 1795.

12 *Gmelins Handbuch der Anorganischen Chemie*, 8th Edn., *Boron Compounds*, Part 18, *Boron Hydrogen Compounds*, **1978** Springer Publ. Heidelberg.

13 A. Dequasie, *The Green Flame*, American Chemical Society, Washington, DC, **1991**.

14 E. B. Baker, R. B. Ellis, W. S. Wilcox, *J. Inorg. Nucl. Chem.*, **1961**, *23*, 41; H. Nöth, M. Ehemann, *Chem.*

Commun., **1966**, 765; L. V. Titov, L. A. Gavrilova, V. Ya. Rosolovski, *Isv. Akad. Nauk, Ser. Khim*., **1971**, 2830.

15 S. G. Shore, S. H. Lawrence, W. I. Watkins, R. Ba, *J. Am. Chem. Soc*., **1982**, *104*, 7669.

16 H. Nöth, B. Brellochs, S. Werner, unpublished work; see S. Werner, *PhD Thesis*, University of Munich, **1994**.

17 G. Dunks, K. Palmer-Ordonez, *Inorg. Chem*., **1978**, *17*, 1514.

18 G. Dunks, K. Palmer-Ordonez, E. Hedaya, *Inorg. Synth*., **1983**, *22*, 202.

19 V. C. Brice, H. D. Johnson, H. D. L. Denton, S. G. Shore, *Inorg. Chem*., **1972**, *11*, 1135.

20 D. A. Dixon, D. A. Kleier, T. Halgren, J. H. Hall, W. N. Lipscomb, *J. Am. Chem. Soc*., **1977**, *99*, 6226.

21 E. W. Corcoran, Jr., L. G. Sneddon, *Advances in Boron and the Boranes*, F. Liebman, A. Greenberg, R. E. Williams, eds., VCH, New York, Weinheim, **1988**, 71.

22 A. R. Dodds, G. Kodama, *Inorg. Chem*., **1976**, *15*, 741.

23 M. L. McKee, W. N. Lipscomb, *Inorg. Chem*., **1982**, *21*, 2846; S. J. Andrews, J. Welch, G. B. Jacobsen, J. H. Morris, *J. Chem. Soc., Chem. Commun*., **1982**, 749; S. J. Andrews, A. J. Welch, *Inorg. Chim. Acta*, **1984**, *88*, 153.

24 G. Geisberger, H. Nöth, *Chem. Ber*., **1992**, *125*, 2169.

25 S. Küppers, P. Paetzold, R. Boese, *Chem. Ber*., **1993**, *126*, 1787.

26 S. H. Lawrence, J. R. Werner, S. K. Boocock, M. A. Banks, P. C. Keller, S. G. Shore, *Inorg. Chem*., **1986**, *25*, 367.

27 M. A. Beckett, P. W. Jones, *Synth. React. Inorg. Met.-Org. Chem*., **1997**, *27*, 41.

28 C. Serrar, A. Es-Sofi, A. Boutalib, A. Ouasses, A. Jarid, *Inorg. Chem*., **2000**, *39*, 2224.

29 S. J. Hildebrandt, D. F. Gaines, J. C. Calabrese, *Inorg. Chem*., **1978**, *17*, 790.

30 D. F. Gaines, S. J. Hildebrandt, *Inorg. Chem*., **1978**, *17*, 794; M. G. Chen, D. F. Gaines, C. G. Hoard, *Inorg. Chem*., **1980**, *19*, 2989.

31 N. N. Greenwood, J. D. Kennedy, D. Reed, *J. Chem., Soc. Dalton Trans*., **1980**, 196.

32 B. Brellochs, H. Binder, *Angew. Chem., Int. Ed. Engl*., **1988**, *27*, 262.

33 G. E. Ryschkewitz, H. V. Miller, *J. Am. Chem. Soc*., **1975**, *97*, 6258.

34 M. Kameda, G. Kodama, *Inorg. Chem*., **1985**, *24*, 2871; R. E. dePoy, G. Kodama, *Inorg. Chem*., **1985**, *24*, 1116.

35 M. Kameda, R. E. dePoy, G. Kodama, *Boron Chemistry*, S. Heřmánek, ed., World Scientific, Singapore, New Jersey, Hong Kong, **1987**, 104.

36 G. Kodama, *Advances in Boron Chemistry and the Boranes*, J. F. Liebman, A. Greenberg, R. E. Williams, eds., VCH Publishers, Weinheim, New York, **1988**, 105; see also [31].

37 P. T. Brain, M. Buehl, M. A. Fox, R. Greatrex, E. Leuschner, M. J. Picton, D. W. H. Rankin, H. E. Robertson, *Inorg. Chem*., **1995**, *34*, 2841.

38 C. L. Bramlet, R. N. Grimes, *J. Am. Chem. Soc*., **1996**, *88*, 4269 and literature cited therein.

39 M. A. Fox, R. Greatrex, M. Hofmann, P. R. von Schleyer, *Angew. Chem., Int. Ed. Engl*., **1994**, *33*, 2298.

40 M. A. Fox, R. Greatrex, M. Hofmann, P. von R. Schleyer, R. E. Williams, *Angew. Chem., Int. Ed. Engl*., **1997**, *36*, 1498.

41 R. T. Paine, R. W. Parry, *Inorg. Chem*., **1972**, *11*, 1237.

42 L. F. Centofani, G. Kodama, R. W. Parry, *Inorg. Chem*., **1969**, *8*, 2072.

43 M. D. LaPrade, C. E. Nordman, *Inorg. Chem*., **1969**, *8*, 1669.

44 J. D. Odom, T. Moore, *Inorg. Chem*., **1980**, *19*, 2651.

45 S. J. Cranson, P. M. Davis, R. Greatrex, D. W. Frankin, H. E. Robertson, *J. Chem. Soc., Dalton Trans*., **1990**, 101.

46 P. T. Brain, D. W. H. Rankin, H. E. Robertson, M. A. Fox, R. Greatrex, A. Nikrahi, M. Bühl, *Inorg. Chem*., **1997**, *36*, 1048.

47 P. Paetzold, *Contemporary Boron Chemistry*, M. G. Davidson, A. K. Hughes, T. B. Marder, K. Wade, eds., Special Publication, The Royal Society of Chemistry, Cambridge, **2000**, 187.

48 A. Neu, T. Menekes, U. Englert, P. Paetzold, M. Hofmann, P. von R. Schleyer, *Angew. Chem., Int. Ed. Engl.*, **1997**, *36*, 2117.

49 A. Neu, T. Menekes, U. Englert, P. Paetzold, M. Hofmann, P. von R. Schleyer, *Inorg. Chim. Acta*, **1999**, *289*, 58.

50 V. H. Miller, G. E. Ryschkewitsch, *Inorg. Synth.*, **1974**, 118.

51 G. E. Ryschkewitsch, V. H. Miller, *J. Am. Chem. Soc.*, **1975**, 6258.

52 H. D. Johnson, R. A. Geanangel, S. G. Shore, *Inorg. Chem.*, **1970**, *4*, 980.

53 S. G. Shore, *Advances in Boron Chemistry and the Boranes*, J. F. Liebman, A. Greenberg, R. E. Williams, eds., VCH Publishers, Weinheim, New York, **1988**, 164.

54 M. A. Nelson, M. Kameda, S. A. Snow, G. Kodama, *Inorg. Chem.*, **1982**, *21*, 2898.

55 D. F. Gaines, J. A. Heppert, D. E. Coons, M. W. Jorgenson, *Inorg. Chem.*, **1982**, *21*, 3662.

56 J. A. Hepper, D. F. Gaines, *Inorg. Chem.*, **1983**, *22*, 3155.

57 D. F. Gaines, G. A. Steehler, *J. Chem. Soc., Chem. Comm.*, **1984**, 1127.

58 C. G. Savory, M. G. H. Wallbridge, *J. Chem. Soc., Dalton Trans.*, **1973**, 179.

59 R. J. Remmel, H. D. Johnson II, I. S. Jaworiwski, S. G. Shore, *J. Am. Chem. Soc.*, **1975**, *907*, 6395.

60 P. Paetzold, S. Küpper, *Chem. Ber.*, **1989**, *122*, 179.

61 S. H. Lawrence, J. R. Werner, S. K. Boocock, M. A. Banks, P. C. Keller, S. G. Shore, *Inorg. Chem.*, **1986**, *25*, 367.

62 R. L. Williams, I. Dunstan, N. Blay, *J. Chem. Soc.*, **1960**, 5012.

63 R. L. Williams, I. Dunstan, N. Blay, *J. Chem. Soc.*, **1960**, 5016.

64 A. N. Bridges, D. R. Powell, J. A. Dopke, J. M. Hesper, D. F. Gaines, *Inorg. Chem.*, **1998**, *37*, 503.

65 J. A. Dupont, M. F. Hawthorne, *Chem. Ind.*, **1962**, 405.

66 T. L. Heying, J. W. Ager, Jr., S. L. Clark, D. J. Mangold, H. L. Goldstein, M. Hillman, R. J. Polak, J. W. Szymanski, *Inorg. Chem.*, **1963**, *2*, 1089.

67 L. I. Zahkarkin, V. I. Stanko, V. A. Brattsev, Y. A. Chapovskii, Y. T. Struchkov, *Isz. Akad. Nauk SSSR, Ser. Khim.*, **1963**, 2069.

68 P. Paetzold, *Adv. Inorg. Chem.*, **1987**, *31*, 123.

69 G. Geisberger, H. Nöth, *Chem. Ber.*, **1992**, *125*, 2691.

70 F. Meyer, P. Paetzold, U. Englert, *Chem. Ber.*, **1994**, *127*, 93.

71 J. Müller, P. Paetzold, R. Boese, *Heteroatom Chem.*, **1990**, *1*, 461.

72 A review of the literature is given in M. L. McKee, *Inorg. Chem.*, **2002**, *41*, 1299 in addition to results of DFT calculations.

73 M. L. McKee, Z.-X. Wang, P. v. R. Schleyer, *J. Am. Chem. Soc.*, **2000**, *122*, 4781.

74 J. Aihara, *J. Am. Chem. Soc.*, **1978**, *100*, 339.

75 K. A. Solntsev, A. M. Mebel, N. A. Votinaova, N. T. Kuznestov, O. P. Charkin, *Koord. Khim.*, **1992**, *18*, 340.

76 W. Preetz, A. Heinrich, J. Thesing, *Z. Naturforsch.*, **1988**, *43b*, 1319.

77 K. A. Solntsev, Yu. A. Buslaev, N. T. Kuznetsov, *Russ. J. Inorg. Chem.*, **1986**, *31*, 1113.

78 A. Heinrich, W. Preetz, H. C. Marsmann, *Z. Naturforsch.*, **1988**, *43b*, 1647.

79 W. Preetz, D. Sonnah, *Z. Naturforsch.*, **1994**, *49b*, 1809.

80 T. Schaper, W. Preetz, *Z. Naturforsch.*, **1998**, *53b*, 819.

81 A. Heinrich, W. Preetz, *Z. Naturforsch.*, **1988**, *43b*, 1327.

82 S. Zander, W. Preetz, *Z. Naturforsch.*, **2000**, *55b*, 1031.

83 H. Thomson, W. Preetz, *Z. Naturforsch.*, **1998**, *53b*, 829.

84 D. Sonnak, W. Preetz, *Z. Naturforsch.*, **1998**, *53b*, 206.

85 N. A. Kutz, W. N. Lipscomb, *Inorg. Chem.*, **1982**, *19*, 3295.

86 B. Steuer, S. Zander, W. Preetz, *Z. Anorg. Allg. Chem.*, **1998**, *624*, 1829.

87 C. Drewes, W. Preetz, *Z. Naturforsch.*, **1999**, *54b*, 349.

88 C. Drewes, W. Preetz, *Z. Naturforsch.*, **1999**, *54b*, 1219.

89 A. Franken, W. Preetz, *Z. Naturforsch.*, **1994**, *49b*, 1263.

90 T. Schaper, W. Preetz, *Z. Naturforsch.*, **1997**, *52b*, 57.

91 T. Schaper, W. Preetz, *Chem. Ber.*, **1997**, *130*, 405.

92 T. Schaper, W. Preetz, *Inorg. Chem.*, **1998**, *37*, 363.

93 D. M. Vinitski, V. C. Lagun, K. A. Solntsev, N. T. Kuznetsov, K. N. Manishkin, R. Yanoushek, K. Bashi, *Zh. Neorg. Khim.*, **1984**, *29*, 1719.

94 T. Schaper, W. Preetz, *Z. Naturforsch.*, **1998**, *53b*, 1326.

95 E. H. Wong, R. M. Kabani, *Inorg. Chem.*, **1980**, *19*, 451.

96 K. Siegburg, W. Preetz, *Inorg. Chem.*, **2000**, *39*, 3280.

97 V. N. Mustyatsa, N. A. Votinova, L. V. Goeva, K. Yu. Zhizhin, E. A. Malinia, N. T. Kuznetsov, *Russ. J. Coord. Chem.*, **2001**, *27*, 662.

98 W. H. Knoth, J. C. Sauer, H. C. Miller, E. L. Muetterties, *J. Am. Chem. Soc.*, **1964**, *86*, 1115; W. H. Knoth, ibid. **1966**, *88*, 935.

99 A. N. Bridges, J. Liu, R. G. Kultyshev, D. F. Gaines, S. G. Shore, *Inorg. Chem.*, **1998**, *37*, 3276.

100 F. Klanberg, E. L. Muetterties, *Inorg. Synth.*, **1968**, *11*, 24.

101 O. Volkov, W. Dirk, U. Englert, P. Paetzold, *Z. Anorg. Allg. Chem.*, **1999**, *625*, 1193.

102 O. Volkov, K. Radacki, P. Paetzold, X. Zheng, *Z. Anorg. Allg. Chem.*, **2001**, *627*, 1185.

103 O. Volkov, P. Paetzold, C. Hu, U. Kölle, *Z. Anorg. Allg. Chem.*, **2001**, *627*, 1029.

104 F. Klanberg, E. L. Muetterties, *Inorg. Chem.*, **1966**, *5*, 1955.

105 F. Klanberg, E. L. Muetterties, *Inorg. Chem.*, **1964**, *3*, 159.

106 E. I. Tolpin, W. N. Lipscomb, *J. Am. Chem. Soc.*, **1973**, *95*, 2384.

107 O. Volkov, P. Paetzold, C. Hu, U. Kölle, *Z. Anorg. Allg. Chem.*, **2001**, *627*, 1029.

108 O. Volkov, K. Radacki, P. Paetzold, X. Zheng, *Z. Anorg. Allg. Chem.*, **2001**, *627*, 1185.

109 G. Volkov, W. Dirk, U. Englert, P. Paetzold, *Contemporary Boron Chemstry*, M. G. Davidson, A. K. Hughes, T. B. Marder, K. Wade, eds., Special Publication 253, Royal Society of Chemistry, Cambridge, **2000**, 159.

110 W. Dirk, P. Paetzold, K. Radacki, *Z. Anorg. Allg. Chem.*, **2001**, *627*, 2615.

111 V. N. Mustyatsa, N. V. Votinova, I. V. Dudenko, K. A. Solntsev, N. T. Kuznetsov, *J. Coord. Chem.*, **1998**, *24*, 905.

112 T. Peymann, C. B. Knobler, S. I. Khan, M. F. Hawthorne, *Inorg. Chem.*, **2001**, *40*, 1291.

113 T. Peymann, C. B. Knobler, M. F. Hawthorne, *J. Am. Chem. Soc.*, **1999**, *121*, 5601.

114 T. Peymann, C. B. Knobler, M. F. Hawthorne, *Chem. Commun.*, **1999**, 2039.

115 K. A. Solntsev, S. V. Ivanov, S. G. Skharov, S. B. Katser, A. S. Chernyavskii, N. A. Volinova, E. A. Klyushishche, N. T. Kuznetsov, *Russ. J. Coord. Chem.*, **1997**, *23*, 403.

116 U. Krause, W. Preetz, *Z. Anorg. Allg. Chem.*, **1995**, *621*, 516.

117 O. Hackel, W. Preetz, *Z. Anorg. Allg. Chem.*, **1998**, *624*, 1089.

118 S. Semioschkin, W. Brellochs, unpublished work, see *PhD Thesis*, S. Semioschkin, University of Munich, 1994.

119 T. Peymann, A. Herzog, C. B. Knobler, M. F. Hawthorne, *Angew. Chem., Int. Ed. Engl.*, **1999**, *38*, 1062.

120 A. Maderna, C. B. Knobler, M. F. Hawthorne, *Angew. Chem., Int. Ed. Engl.*, **2001**, *40*, 1661.

121 T. Peymann, C. B. Knobler, S. I. Khan, M. F. Hawthorne, *Angew. Chem., Int. Ed. Engl.*, **2001**, *40*, 1664.

122 C. Nachtigall, W. Preetz, *Z. Anorg. Allg. Chem.*, **1997**, *623*, 1385.

123 I. V. Dudenkov, K. Yu. Thizhin, A. S. Chernyavskii, S. B. Katser, L. V. Goeva, V. S. Sergienko, K. A.

Solntsev, N. T. Kuznetsov, *Russ. J. Inorg. Chem.*, **2000**, *45*, 1864.
124 M. F. Hawthorne, R. L. Pilling, P. F. Stoely, *J. Am. Chem. Soc.*, **1965**, *87*, 1893.
125 L. Ng, B. K. Ng, C. B. Knobler, M. F. Hawthorne, *Inorg. Chem.*, **1992**, *31*, 3669.
126 R. A. Watson-Clark, C. B. Knobler, M. F. Hawthorne, *Inorg. Chem.*, **1996**, *35*, 1963.
127 R. A. Watson-Clark, K. Shelly, M. F. Hawthorne, *Inorg. Chem.*, **2000**, *9*, 1901.
128 F. Li, K. Shelly, R. R. Kane, C. B. Knobler, M. F. Hawthorne, *J. Am. Chem. Soc.*, **1996**, *118*, 6506.
129 F. Li, K. Shelly, C. B. Knobler, M. F. Hawthorne, *Angew. Chem., Int. Ed. Engl.*, **1998**, *37*, 1868.
130 F. Li, K. Shelly, C. B. Knobler, M. F. Hawthorne, *Angew. Chem., Int. Ed. Engl.*, **1998**, *37*, 1865.
131 A. G. Massey, *Adv. Inorg. Radiochem.*, **1983**, *26*, 1–51; J. A. Morrison, *Advances in Boron and the Boranes*, J. F. Liebmann, A. Greenberg, R. E. Williams, eds., VCH Publishers, Weinheim, New York, **1988**, 151.
132 G. J. Maier, H. Pritzkow, W. Siebert, *Angew. Chem., Int. Ed. Engl.*, **1999**, *38*, 1666.
133 T. Davan, J. A. Morrision, *J. Chem. Soc., Chem. Commun.*, **1981**, 250.
134 J. A. Pardoe, N. C. Norman, P. L. Timms, S. Parson, I. Mackie, C. R. Pulham, D. W. H. Rankin, *Angew. Chem.*, **2003**, *115*, 591.
135 M. Atoji, W. N. Lipscomb, *J. Chem. Phys.*, **1959**, *31*, 601; G. S. Pawley, *Acta Crystallogr.*, **1966**, *20*, 631.
136 W. Hönle, Y. Quin, A. Burkhardt, U. Wedig, M. Schultheiss, H. G. von Schnering, P. Kellner, H. Binder, *J. Solid State Chem.*, **1997**, *133*, 59.
137 E. H. Wong, *Inorg. Chem.*, **1981**, *20*, 1300.
138 N. A. Kutz, J. A. Morrison, *Inorg. Chem.*, **1980**, *19*, 3295.
139 T. Mennekes, P. Paetzold, R. Boese, D. Bläser, *Angew. Chem., Int. Ed. Engl.*, **1991**, *30*, 173.
140 D. Hynk, *Polyhedron*, **1996**, *16*, 603.
141 W. Ponikwar, *PhD Thesis*, University of Munich, **2000**.
142 J. Kane, A. G. Massey, *Chem. Comm.*, **1970**, 1195.
143 G. F. Lanthier, A. G. Massey, *J. Inorg. Nucl. Chem.*, **1971**, *32*, 1807.
144 R. M. Kabbani, E. H. Wong, *J. Chem. Soc., Chem. Commun.*, **1978**, 462.
145 E. H. Wong, R. M. Kabbani, *Inorg. Chem.*, **1980**, *19*, 451.
146 M. L. McKee, *Inorg. Chem.*, **1999**, *38*, 321.
147 A. Maier, M. Hofmann, H. Pritzkow, W. Siebert, *Angew. Chem.*, **2003**, *114*, 1600.
148 G. Urry, A. G. Gerret, H. I. Schlesinger, *Inorg. Chem.*, **1963**, *2*, 396.
149 C. Präsang, M. Hofmann, G. Geiseler, W. Massa, A. Berndt, *Angew. Chem.*, **2003**, *115*, 1079.
150 T. Mennekes, A. Neu, P. Paetzold, *Contemporary Boron Chemistry*, M. Davidson, A. K. Hughes, T. B. Marder, K. Wade, eds., Royal Society of Chemistry, Cambtidge, **2000**, 187.
151 W. Einholz, *Advances in Boron Chemistry*, W. Siebert, ed., **1997**, 441. Royal Soc. Chem. Cambridge.
152 H. Binder, *Advances in Boron Chemistry*, W. Siebert, ed., **1997**, 38. Royal Soc. Chem. Cambridge.

2.2
Boron Clusters in Medical Applications

Detlef Gabel and Yasuyuki Endo

2.2.1
Introduction

The element boron has two stable isotopes, boron-10 and boron-11. Whereas ^{11}B constitutes the majority of the boron found naturally (around 80%), ^{10}B has one property which distinguishes it from most other elements: it has a very high cross section for thermal (slow) neutrons. (The cross section is a measure of the probability that a nucleus captures a neutron, and its units are given in barn, where 1 barn $= 10^{-24}$ cm^2. When referring to the reaction, the reacting nuclide is written first, followed in parentheses by the impinging particle, here a neutron, and the lighter particle or photon generated, and the resulting nuclide is given after the parenthesis.) Whereas other elements occurring in living tissue have small cross sections [for the reaction $^{1}H(n,\gamma)^{2}H$, it is 0.333 barn; for $^{16}O(n,\gamma)^{17}O$, 0.00019 barn; for $^{14}N(n,p)^{14}C$, 1.83 barn; for $^{12}C(n,\gamma)^{13}C$, 0.0035 barn], the cross section for the $^{10}B(n,\alpha)^{7}Li$ reaction is 3843 barn. The high cross section of ^{10}B is used in the control rods of nuclear reactors; as a consequence, ^{10}B-enriched material is commercially available, usually as boric acid. In addition, in most other neutron capture reactions a γ photon is emitted (such as for ^{1}H and ^{16}O), but the reaction with ^{10}B yields two charged particles, a helium-4 nucleus and a lithium-7 nucleus, both of which are able to kill cells. Therefore, the reaction of neutrons with boron has since long been suggested for the treatment of cancer [1]. Today, several clinical investigations are aimed at demonstrating the efficacy of the treatment for brain tumors, melanomas, and other malignancies by boron neutron capture therapy (BNCT) [2–5].

The two charged particles carry a total of 2.3 MeV (corresponding to around $2.2 \cdot 10^{8}$ kJ mol^{-1}) of kinetic energy. They give off their energy on a track which is about the same size as a cell (see Figure 2.2-1), and as a consequence, many chemical bonds are broken along the track. The passage of one particle through a cell nucleus is sufficient to prevent further growth of the cell [6].

Because of the high linear energy transfer (LET) of the particles produced by the $^{10}B(n,\alpha)^{7}Li$ reaction, the production of secondary ions is not enhanced in the presence of oxygen; with low-LET radiation such as external photon irradiation, tissues

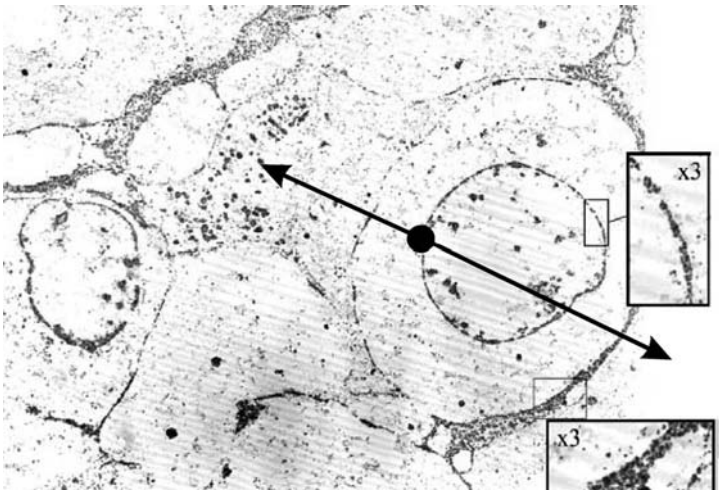

Fig. 2.2-1. A neutron capture event seen in relation to the size of the target. Electron microscopic image of uncontrasted tumor tissue, stained for boron by antibodies. The smaller structure surrounded by clusters of dots is the nucleus. The thin structure lined with dots is the cell membrane. The dots are gold particles attached to the antibodies which are specifically directed against the $B_{12}H_{11}SH^{2-}$ cluster. The tissue was obtained during surgery of a glioblastoma patient to whom $Na_2B_{12}H_{11}SH$ had been administered prior to the operation. The inserts are magnified three times. The boron atom reacting is indicated by the large dot, and the two particles travel approximately the distances indicated by the arrow.

with high oxygen tension (i.e., most healthy tissues) experience a higher degree of damage than tissues with poor oxygen supply through the blood system, such as the central near-necrotic parts of tumors. For a discussion of LET, oxygen effect, etc., see any textbook on radiobiology, e.g., [82].

Other elements with higher cross sections for thermal neutrons are known, such as ^{157}Gd [^{157}Gd(n,γ)^{158}Gd, 2.25×10^5 barn], which give off the reaction energy mainly as γ photons. Whereas they have been discussed for NCT, the long range of the γ radiation in tissue makes it difficult to deliver a tumor-killing dose selectively. This situation changes only when the nucleus in question is in molecular contact with the target, e.g., the DNA; then, electrons set free from the inner electron shells due to the nuclear transition can damage the target.

The amount of boron required for BNCT can be estimated using the neutron capture cross sections, which are atomic properties, and thus pertain to the number, and not the mass, of the atoms present. Conservative estimates for successful therapy result in boron concentrations of around 20 ppm in tumor tissue, to at least match the dose liberated by neutron capture reactions in the other elements of biological tissue. This would correspond to around 10^9 boron-10 atoms per cell, assuming that one cell corresponds to 10^{-9} g.

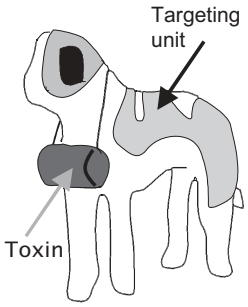

Fig. 2.2-2. Device for targeting and destruction.

For BNCT, it is therefore the goal to prepare boron compounds which seek their targets (the cells to be destroyed) and carry with them enough boron for destruction. This can be seen as a dog finding (sniffing) its way to the "villain", and carrying or dragging the necessary equipment in order to take the "villain" out of action. Obviously, in order to be successful, the dog must not be hindered when finding the way (e.g., by covering his nose), and he must not be hindered in his movements (e.g., by having him drag too heavy a load, or a load so bulky that it prevents him from entering the holes where the "villain" might be hiding). It is the task for the chemist to design such compounds. Usually, the "dog" will be a molecule which is a known tumor-seeking substance, and the "equipment" will be a boron-containing fragment (Figure 2.2-2). These two entities must be joined.

With the capture event in boron, a large amount of energy is liberated (2.79 MeV, corresponding to 2.69×10^8 kJ mol^{-1}). Some of the energy is emitted as γ photons, which can be used to measure quantitatively the amount of boron in a sample [7], or can serve to generate *in vivo* distribution maps of boron [8]. Most of the energy is, however, preserved as kinetic energy of the two particles produced. The lithium and alpha particles emitted during neutron capture travel about 7–10 μm in biological material, i.e., about the same dimensions as those of a mammalian cell, and on this short track they give off the total energy to the surrounding material, resulting in a great number of broken bonds. In order to kill a cell, a direct hit to the cell nucleus is most efficient [6]. Boron present in the cell nucleus is therefore most effective in killing this cell, whereas boron attached to the cell membrane might be up to a factor of ten less effective (depending on the size of the cell and the nucleus).

For compounds to be useful in BNCT, they must allow administration to a patient (usually through the blood stream), accumulate or be retained in the tumor, be of low toxicity, and on the basis of the required accumulation, carry as many boron atoms as possible. To achieve the latter, boron clusters are of great value. In this chapter, the chemistry of some clusters is described that have found application in BNCT (see Scheme 2.2-1). The focus is on the *o*-carborane system dicarba-*closo*-dodecaborane, $C_2B_{10}H_{12}$, and its degradation product *nido*-carborate,

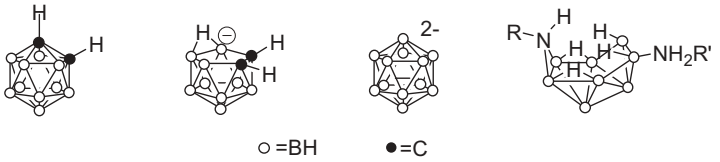

Scheme 2.2-1. Clusters discussed in this chapter. Notes on the formulae representation in this chapter: In clusters, each corner represents one boron atom. Every boron atom carries one *exo*-hydrogen atom, which is not shown for clarity. The hydrogen atoms shown are *endo*- or bridge hydrogen atoms. Carbon atoms in the cluster are indicated by filled circles. For carbon and nitrogen, all hydrogen atoms are shown. *o*-, *m*-, and *p*-Carborane will be abbreviated to *o*-, *m*-, and *p*-C_2B_{10}, respectively.

$C_2B_9H_{12}$, the isomers *m*- and *p*-carborane (see Chapter 3.2), the *closo*-dodecaborate system $B_{12}H_{12}^{2-}$ (see Chapter 2.1.5.6), and an *arachno*-azanonaborane system B_8NH_{13} (see Chapter 3.4.4.3). All these clusters have in common the fact that they are stable in aqueous solution, and thereby would allow administration to patients via the blood stream. Their chemistry, and thus the way in which they can be attached to organic molecules, as well as their physiologically relevant parameters of hydrophobicity, vary considerably, however. For a review of the chemistry of BNCT, see Refs. [9–11].

The sizes of the clusters discussed are similar, and their diameters are slightly larger than that of a benzene ring. Therefore, it might be expected that they do not add too many additional steric demands to an organic molecule when they are covalently bound to structures such as porphyrins or sugars, or replace aromatic structures such as a phenyl ring in amino acids.

However, the cluster compounds differ greatly in their water solubility. Whereas *closo*-dodecaborate (as the sodium salt) is readily water soluble, *o*-carborane and its thermal rearrangement products *m*-carborane and *p*-carborane show poor water solubility. The *nido*-carborane system, because of its negative charge, is water soluble. The azanonaborane cluster is neutral, but still shows a certain degree of water solubility.

The low degree of hydrophilicity of the *o*-carborane unit might be used in its own right, to give analogues of compounds where the carborane moiety replaces a benzene ring, and thereby adds hydrophobicity and results in slightly greater filling of the space. This property has been used to design new, and more specific, analogues of steroid hormones.

When specific compounds for BNCT are to be prepared, the cluster compounds must be covalently attached to organic moieties. The chemistry of such reactions will be the focus of this chapter. It should be borne in mind, however, that the boron species might in themselves already constitute suitable candidates for selective accumulation or retention in tumors, and perhaps also possess other pharmacological properties. Thus, $Na_2B_{12}H_{11}SH$ (BSH) (see Section 2.2.5.1), which is clinically used for BNCT of glioblastoma [2], and its thiocyanate derivative $Na_2B_{12}H_{11}SCN$ [12], are both taken up in tumor tissue without additional targeting units.

2.2.2
Dicarba-*closo*-dodecaborane, $C_2B_{10}H_{12}$, and Derivatives

2.2.2.1
Preparation and Reactions of C_2B_{10} Cage Compounds

The *closo*-cluster containing two carbon atoms, i.e., *o*-, *m*- or *p*-dicarba-*closo*-dodecaborane $C_2B_{10}H_{12}$, is electronically neutral (see Chapter 3.2). Therefore, the cages are thermally and chemically stable, and extremely hydrophobic. The C_2B_{10} cages are advantageous for boron neutron capture therapy (BNCT) because of their high boron content and ease of chemical transformation.

The *o*-C_2B_{10} cage is readily prepared (Scheme 2.2-2) from acetylene by Lewis base-catalyzed reaction with *nido*-decaborane(14) ($B_{10}H_{14}$), which is produced in-

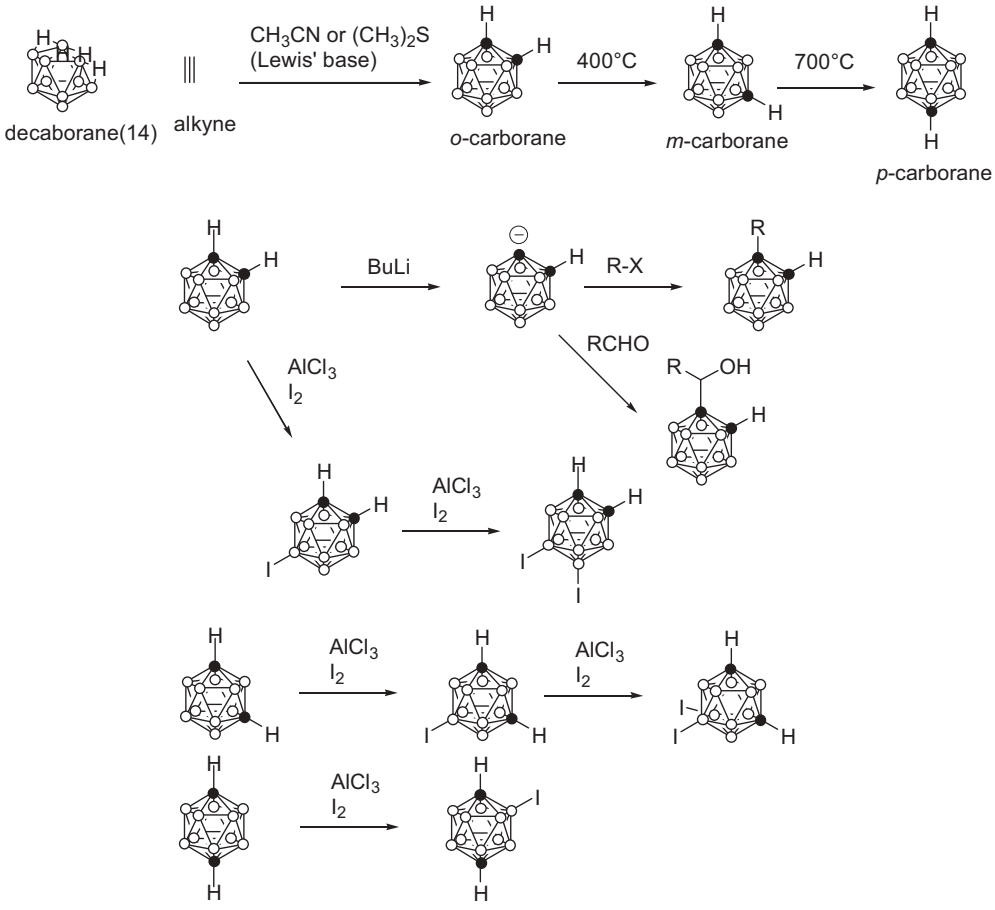

Scheme 2.2-2. Preparation of the C_2B_{10} cage and typical functionalization.

dustrially. Mono- and disubstituted alkynes can also be converted into mono- and di-C-substituted *o*-C_2B_{10}, and this is an effective method for the synthesis of carborane C_2B_{10}-containing compounds for BNCT. Unsubstituted *o*-C_2B_{10} can be isomerized into thermodynamically stable *m*- and *p*-C_2B_{10}. All three isomers are also commercially available. The two carbon atoms of *o*-C_2B_{10} bear relatively acidic protons and transformation to the lithiate readily allows reaction with electrophiles such as alkyl halides and aldehydes to give C-alkyl or C-(1-hydroyalkyl)-*o*-C_2B_{10} (for a review see Ref. [13]). C-Copper reagent derived from the lithium salt is useful to prepare C-aryl, alkenyl and alkynyl-*o*-C_2B_{10} [14]. Similarly, substitution can also be conducted at the two carbon atoms on the *m*- and *p*-C_2B_{10} cages.

Electrophilic substitution on the cage, e.g., Friedel-Crafts halogenation, proceeds regioselectively at the most electronegative boron atoms, i.e., the 9- and 12-positions in the case of *o*-carborane. The resulting B-iodides can be converted into alkyl, alkenyl, and phenyl groups by employing the Grignard reaction or palladium-catalyzed coupling reaction [15, 16]. The positions of the iodination are the 9- and 10-positions in *m*-carborane, and the 3-position in *p*-carborane [17].

2.2.2.2 Design and Classification of BNCT Reagents Containing C_2B_{10} Cages

As described in the introduction, incorporation of 1×10^{-9} g of ^{10}B per cell is required for effective cytotoxicity with BNCT therapy. This concentration is much higher than that usually required for pharmacological activity. The high boron contents and non-toxicity make the C_2B_{10} unit suitable for use as BNCT agents, but they must be delivered in effective ^{10}B concentration selectively into tumor cells. Of course, selective delivery of drugs into tumor cells is also an important requirement of general antitumor chemotherapeutic drugs. One approach is to develop compounds that interfere with DNA (DNA alkylating agents, modified nucleic bases, antisense oligonucleotides, etc.) or protein synthesis within the rapidly growing tumor cells. Therefore, various compounds have been designed and synthesized by adding C_2B_{10} units to cellular building blocks (amino acids, DNA precursors, DNA binders and lipids). C_2B_{10} analogues that are selectively taken up into tumor cells (porphyrins and amino acids) have also been developed. Recently, C_2B_{10} compounds with improved water-solubility (polyols) [18] and C_2B_{10} compounds containing gadolinium [19], which is another promising element for NCT, have been reported.

2.2.2.3 Amino Acids

Amino acids and their derivatives may be accumulated selectively in tumors by becoming incorporated into proteins synthesized in the rapidly growing tumor cells. This strategy has been successfully applied with *p*-boronophenylalanine (*p*-dihydroxyboryl phenylanaline, BPA), which is one of the two clinically used BNCT agents. [The other is $Na_2B_{12}H_{11}SH$ (BSH); see Section 2.2.5.1.] BPA, an analog of

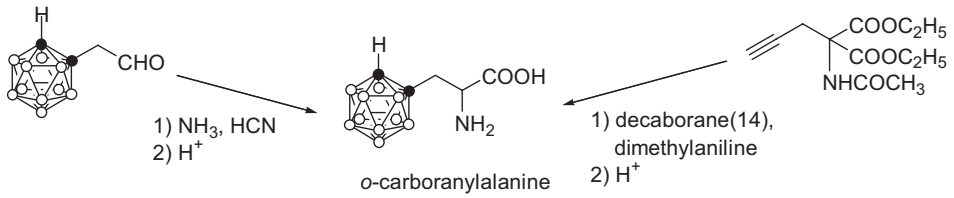

Scheme 2.2-3. Early synthesis of *o*-carboranylalanine.

phenylalanine, accumulates well in melanoma cells, which biosynthesize large amounts of melanin from phenylalanine [20]. However, BPA has only one boron atom in the molecule. C_2B_{10}-containing compounds should be more effective than the boronic acid derivative due to their high boron content. As the C_2B_{10} group is only slightly larger than the phenyl group, a reasonable approach would be to replace the phenyl group of phenylalanine with a C_2B_{10} cage. The first syntheses of racemic *o*-carboranylalanine were reported independently by Brattsev and Zakharkin, employing Strecker amino acid synthesis from *o*-carboranylacetaldehyde or construction of the *o*-C_2B_{10} cage from acetamidomalonate bearing an alkyne moiety and decaborane(14) (see Scheme 2.2-3) [21, 22].

The *S*- form of *o*-carboranylalanine was first synthesized in 1979 by the reaction of an optically active ethynylalanine derivative, obtained by enzymatic resolution, with decaborane(14), followed by hydrolysis (see Scheme 2.2-3) [23]. Since then, several asymmetric syntheses of *S*- and *R*-enantiomers of *o*-carboranylalanine have been reported, including the use of stereoselective propargylation [24] and stereoselective introduction of an amino group [25].

A number of other C_2B_{10}-containing amino acids, such as 4-carboranylphenylalanine, *O*-(*o*-carboranylmethyl)tyrosine and 5-*o*-carboranyl-3,4-dihydroxyphenylalanine (DOPA analogue) have been synthesized and are undergoing biological evaluation (see Scheme 2.2-5) [26]. Amino acids in which the amino and carboxyl groups are located at the two carbon atoms of *o*-, *m*- and *p*-C_2B_{10} have been synthesized by Kahl and Kaser [27] by means of modified Curtius rearrangement from carboranedicarboxylic acids. These amino acids may useful tools for the design of carborane-containing bioactive compounds.

2.2.2.4 Nucleic Acid Precursors

From the viewpoint of targeting the cell nuclei in rapidly growing tumor cells and subjecting the tumor cells to fatal neutron irradiation, nucleic acid bases, nucleosides and nucleotides bearing C_2B_{10} are among the most promising BNCT agents. It might be expected that C_2B_{10}-containing nucleosides [28], in which the C_2B_{10} cage is comparatively large and hydrophobic, would not be incorporated as surrogates in oligomeric DNA. However, intranuclear phosphorylation of a C_2B_{10}-containing nucleoside may serve to immobilize the resulting monophosphate

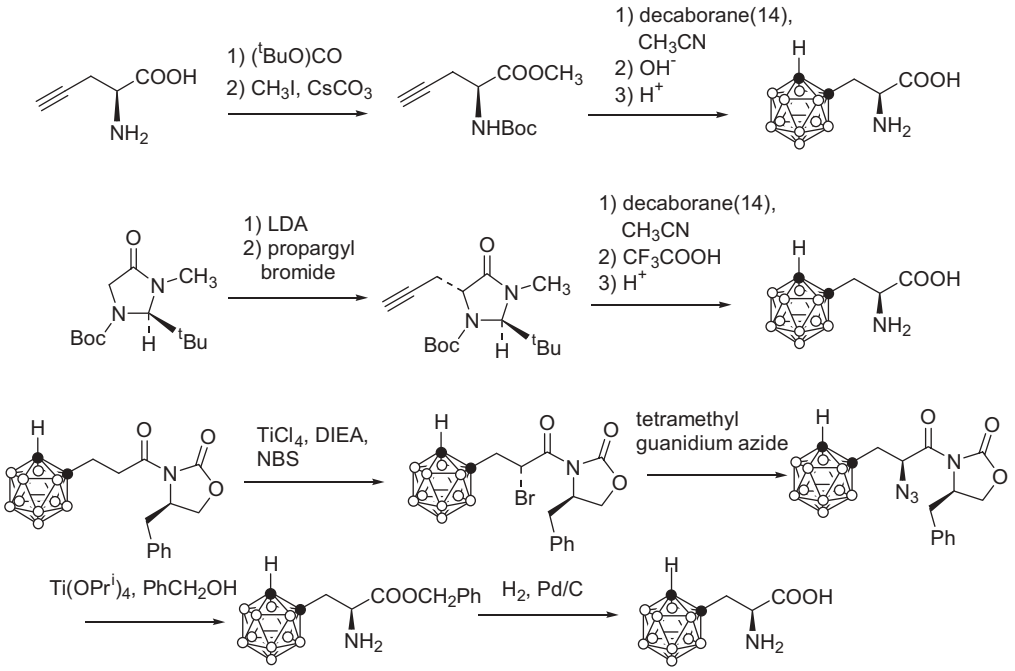

Scheme 2.2-4. Asymmetric syntheses of *S-o*-carboranylalanine.

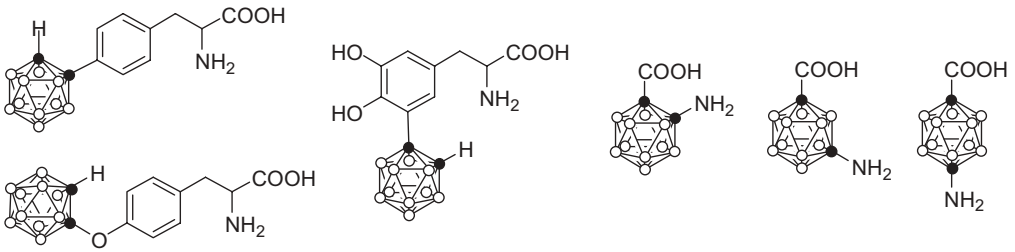

Scheme 2.2-5. C_2B_{10}-containing amino acid derivatives.

within the nucleus. The first synthesis of C_2B_{10}-containing nucleosides was performed by adding the C_2B_{10} cage to the sugar unit of nucleosides (Scheme 2.2-6) [29].

Another synthetic method for the introduction of the C_2B_{10} cage onto the pyrimidine nucleus using palladium-catalyzed coupling of 5-iodonucleoside derivatives with alkynes was developed [30]. A polyol unit increases water solubility, and this allows the synthesis of a water-soluble uracil bearing an *o*-C_2B_{10} cage (Scheme 2.2-7) [31].

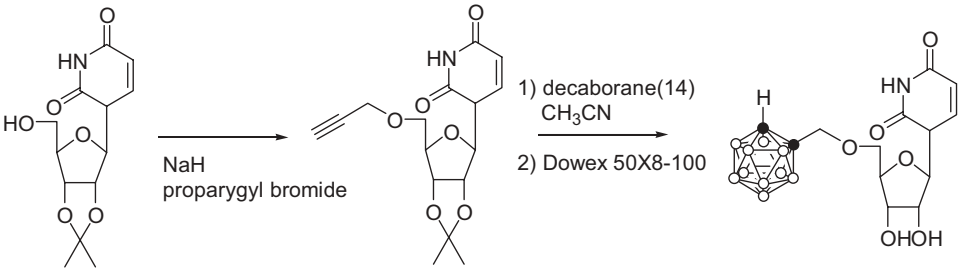

Scheme 2.2-6. The first synthesis of C_2B_{10}-containing nucleoside.

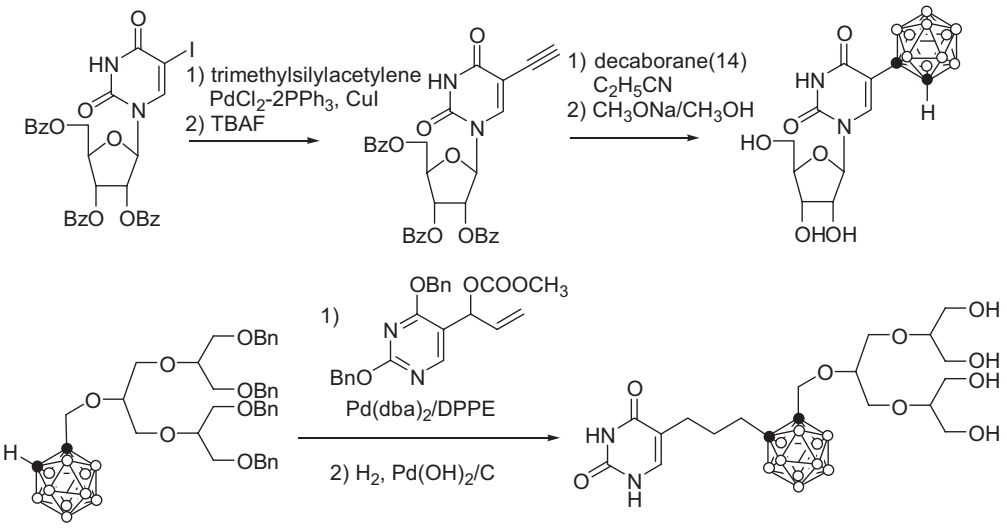

Scheme 2.2-7. Synthesis of a nucleoside with *o*-C_2B_{10} directly on the pyrimidine ring, and a related water-soluble nucleic base with *o*-C_2B_{10}.

2.2.2.5
DNA Binders

The binding of substances to DNA has been used for the treatment of cancer. Such compounds might intercalate into the DNA (such as doxorubicin) or bind to the minor groove of the DNA helix (see Figure 2.2-3), thereby disturbing either duplication of DNA or transcription into mRNA.

Attempts have been made to prepare carborane-containing DNA binders by adding carborane units to representative DNA intercalators (acridine, ethidium) and a DNA groove binder (distamysine), which have high binding affinity with DNA (Scheme 2.2-8). The intercalators insert themselves into a gap between the base pairs of double-helical DNA [32, 33].

Other compounds with strong affinity to DNA are groove binders such as ne-

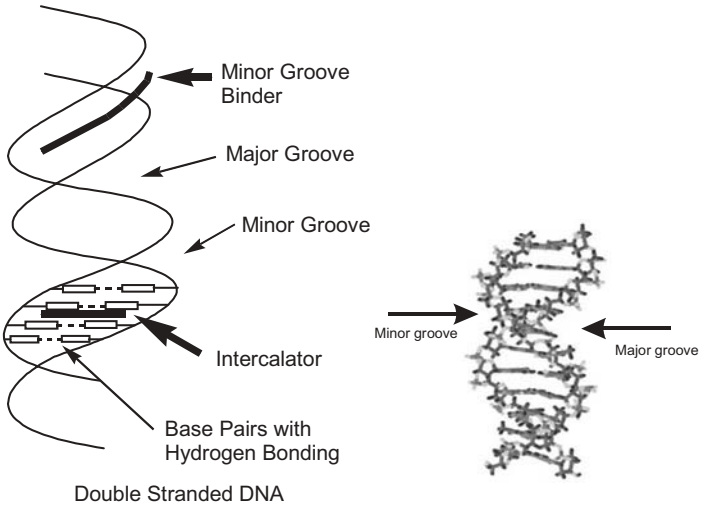

Fig. 2.2-3. DNA and the binding sites for targeting molecules.

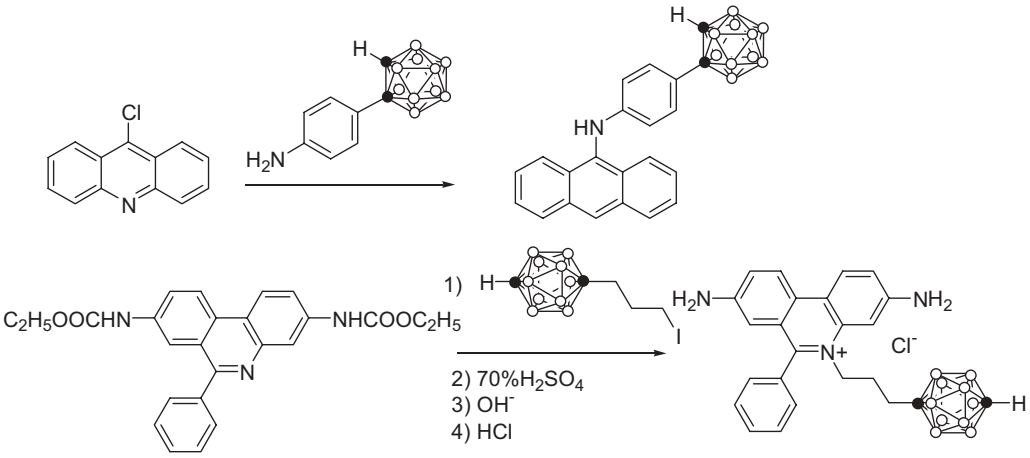

Scheme 2.2-8. C_2B_{10}-containing DNA intercalators.

tropsin and distamycin, which bind in the minor groove of double-helical DNA at adenine–thymine base pair-rich regions. C_2B_{10}-containing analogues of distamycin have been reported (Scheme 2.2-9) [34]. In the design of these compounds, polyols were inserted to increase the water solubility.

2.2.2.6
Porphyrins

Porphyrins and related structures have long been used in photodynamic therapy (PDT). In PDT, the photo-induced production of singlet oxygen is the toxifying

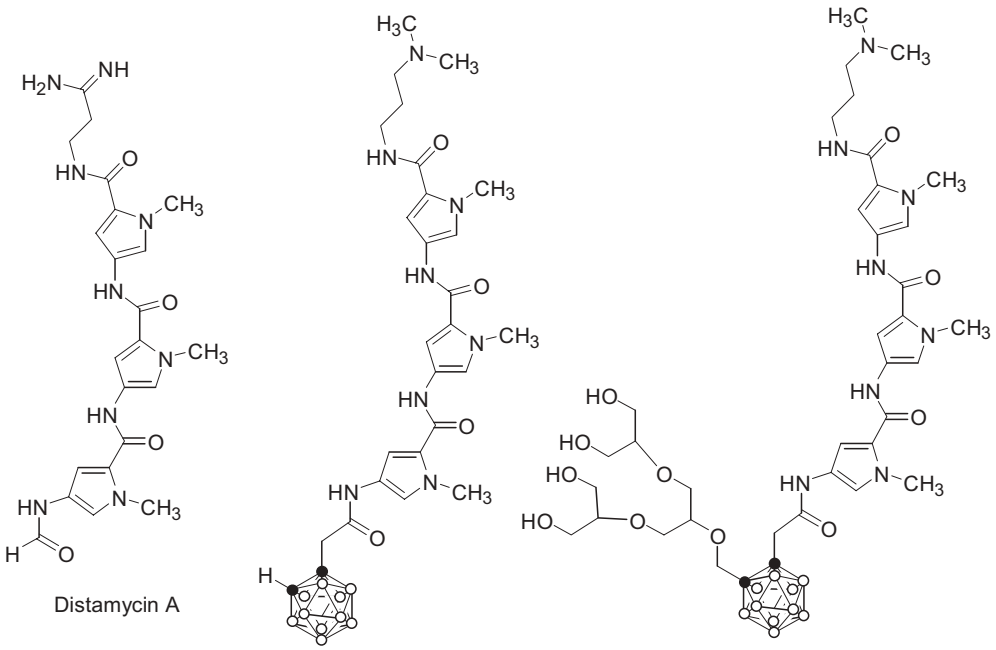

Scheme 2.2-9. C_2B_{10}-containing DNA minor groove binders.

event. Therefore, it is necessary that the porphyrinoids have a high molar extinction coefficient in the red (preferentially around 650 nm or longer), low fluorescence, a high quantum yield of singlet oxygen production, and a high stability to the exciting light. In addition, the tumor parts most effectively treated by PDT are those with high oxygen tension; however, most tumors contain, areas in which the oxygen supply is markedly reduced. For BNCT, the photophysics of the porphyrins is of no consequence for the potential use in therapy. Also, low oxygen tension in parts of the tumor has no influence on the neutron capture reaction, and it does not negatively influence the production of secondary radicals, as the particles produced are high-LET particles. Porphyrins bearing C_2B_{10} cages have therefore attracted interest for possible application in BNCT (for a review, see Ref. [35]). Porphyrins having four *closo*- or *nido*-C_2B_{10} moieties attached via aromatic linkages, methylene or ester have been prepared (Scheme 2.2-10) [36, 37].

2.2.2.7
Combination of C_2B_{10} and Gadolinium-containing Species

Recently, the potential of ^{157}Gd, which has a much higher cross sectional value than ^{10}B for thermal neutrons has been of interest. Chelating agents, diethylenetriaminepentaacetic acid (DTPA) derivatives bearing carborane, were synthesized by the reaction of carboranyl allyl carbonate with DTPA ester. Treatment of

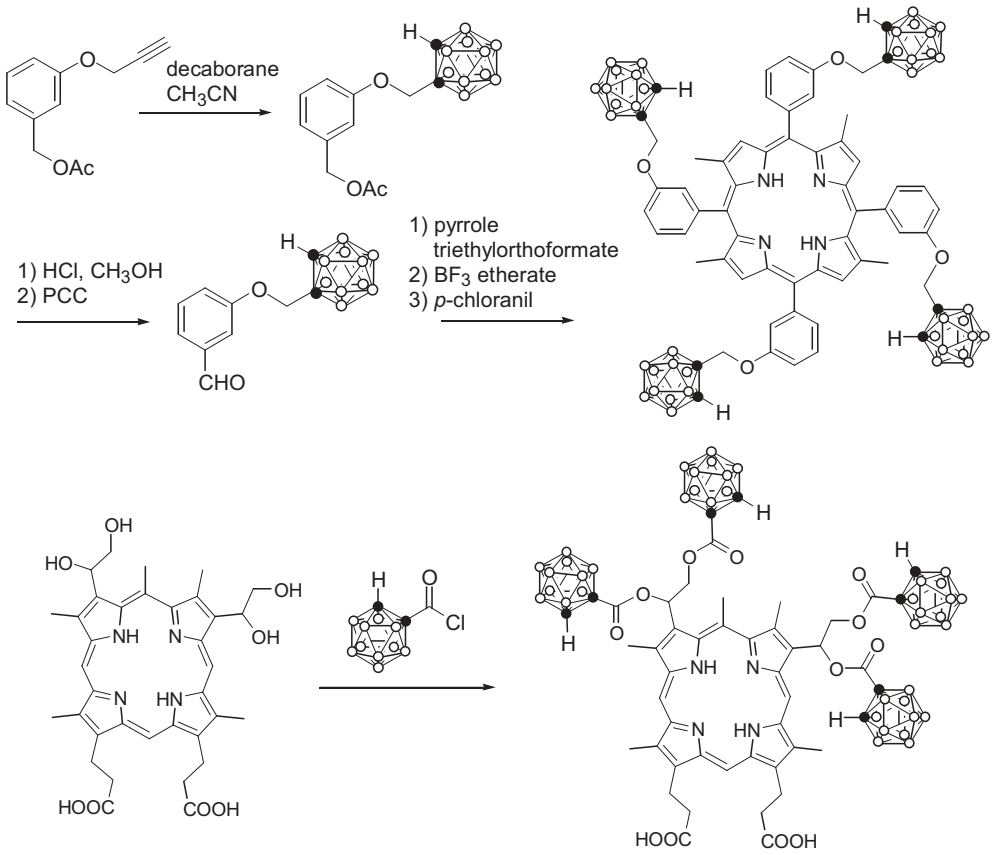

Scheme 2.2-10. C_2B_{10}-containing porphyrin derivatives.

carborane-containing DTPA with gadolinium(III) chloride hexahydrate gave the Gd–DTPA carborane complex shown in Scheme 2.2-11 [38]. These compounds are attractive not only because they contain two neutron capture elements, but also because of the MRI-contrast property of Gd. It may be possible to monitor the distribution of the BNCT agent *in vivo*.

2.2.3
Derivatives of the *nido*-carborane $C_2B_9H_{12}^{2-}$

The extreme hydrophobicity, or in other words, the low water solubility, of the carborane cage is a major disadvantage in terms of biodistribution. However, *o*-C_2B_{10} can be readily converted into a water-soluble degradation product. *o*-C_2B_{10} reacts with strong nucleophiles such as alkoxides, aliphatic amines and fluoride anion to

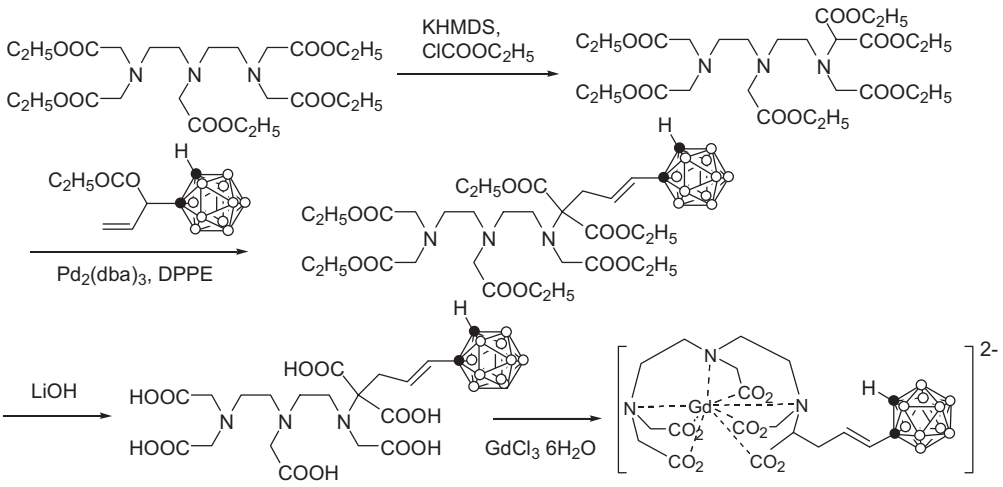

Scheme 2.2-11. Synthesis of gadolinium-chelating molecule with an *o*-C_2B_{10} moiety.

afford the negatively charged *nido*-7,8-$C_2B_9H_{12}^-$ by loss of one boron atom [83]. The nucleophilic attack occurs at one of the equivalent boron atoms 3 or 6, since these are the most electron-deficient boron atoms in the C_2B_{10} cage (Scheme 2.2-12). Although the deboronation also proceeds in the case of *m*-C_2B_{10}, the reaction rate is much lower than that in the case of *o*-C_2B_{10}, and the deboronation of *p*-C_2B_{10} does not proceed.

Therefore, the simplest strategy to increase the water solubility of C_2B_{10}-containing compounds is degradation of the *closo*-cage to the *nido*-anion, and this has been applied to C_2B_{10}-containing amino acids and porphyrins (see Scheme 2.2-13).

Oligonucleotides bearing *nido*-carborane have been synthesized as phosphodiesters using an automated DNA synthesizer (see Scheme 2.2-14) [39]. These oligophosphates are homogeneous, very hydrophilic and are readily taken up into cells. Fluorescein-labeled *nido*-carboranyl oligomeric phosphate diesters accumulate in the cell nucleus [40].

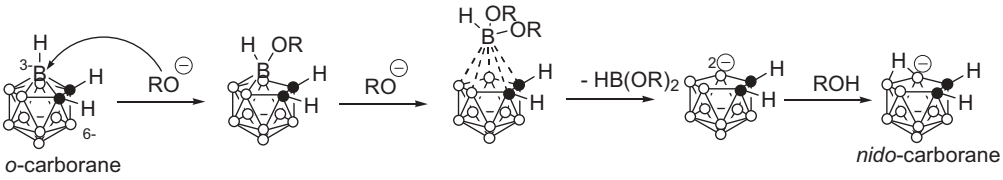

Scheme 2.2-12. Deboronation of *o*-C_2B_{10} derivatives to the *nido*-anion.

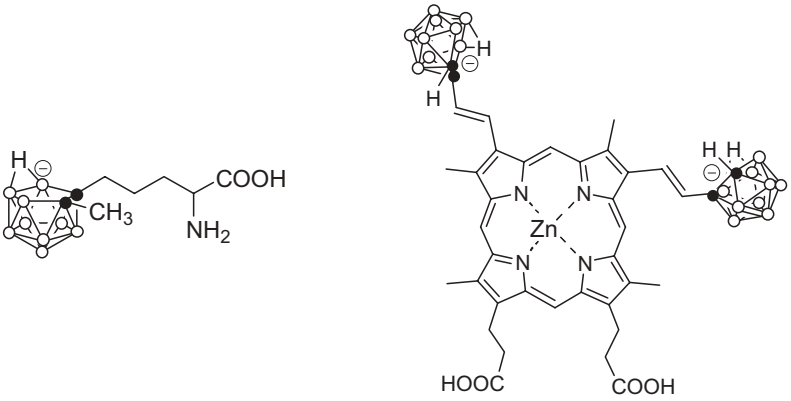

Scheme 2.2-13. Examples of an amino acid and a porphyrin with *nido*-carborane moieties.

2.2.4
Application of C_2B_{10} for Drug Design

2.2.4.1
Properties of C_2B_{10} for Drug Design

The *closo*-C_2B_{10} cages have characteristic properties, such as high boron content, remarkable thermal and chemical stability, spherical geometry and exceptional hydrophobic character (see Section 3.2.3.6). Among the properties of C_2B_{10}, the high boron content and chemical stability are useful for BNCT. However, the highly hydrophobic character of these molecules sometimes prevents their incorporation into tumor cells. The strongly hydrophobic nature of the C_2B_{10} cage can, however, be used directly to incorporate the cage into molecules in those places where, e.g., a hydrophobic residue would increase the binding to the receptor of the molecule. This aspect of the C_2B_{10} cages has so far received little attention.

Quantitative analysis of the hydrophobicity of the *o*-C_2B_{10} group has been done by partitioning amino acid derivatives between octanol and water [41]. The hydrophobic parameter π of *o*-C_2B_{10} is comparable to that of the spherical hydrocarbon, adamantane. Recent analysis of various isomers of *o*-C_2B_{10} using *o*-C_2B_{10}-substituted phenols also concluded that the values were within the range of those of hydrocarbons [42].

In modern medicinal chemistry, the targets of most of the drugs are specific receptors, and two types of contact, hydrogen bonding and hydrophobic interaction, are often utilized. Although hydrogen bonding is well known to be an important factor for recognition of a biologically active molecule at a receptor, hydrophobic interaction is also important for the stability of the ligand–receptor complex. The fit between the shape of a ligand molecule and that of a receptor, in other words, the interaction between the hydrophobic structure of a ligand molecule and a hydrophobic domain of a receptor, plays an important role in determining the affinity

Scheme 2.2-14. *nido*-carboranyl oligomeric phosphate diester.

of a ligand to a receptor. In fact, the ratio of binding constants between a ligand having a suitable hydrophobic group and a ligand without such a group is sometimes higher than 1000. The hydrophobic interaction is important for recognition of the shape of the ligand molecule by a receptor and is dependent on the physical properties of the molecular surface of the ligand. The *closo*-C_2B_{10} cages may therefore be useful as a hydrophobic pharmacophore or structural element in biologically active molecules which interact hydrophobically with receptors. The molecular size of the C_2B_{10} cage is slightly larger than that of a phenyl ring, as mentioned above; this might also make it suitable for drug applications.

2.2.4.2 Nuclear Receptor Ligands Bearing C_2B_{10} Cages

Nuclear receptors are different from the usual membrane-bound receptors present in the cytoplasm or the nucleus of cells. These receptors are particularly important in regulating gene transcription, and the ligands of the receptors are required to pass through the cell membrane. These ligands, which include steroid hormones, are indispensable for cell differentiation, growth and reproduction of animals. The first step in the appearance of these activities is mediated by the binding of hormonal ligands to the receptors. The hormone-bound receptor undergoes a conformational change, allowing the receptor to dimerize. The dimer functions as a transcription factor that mediates biological response by binding to specific promoter elements of DNA to initiate gene transcription. A more detailed description of hormones and their receptors, as well as of the way the DNA is recognized, can be found in advanced textbooks on biochemistry.

For BNCT application, several estrogen-related compounds [43] bearing carboranes have been reported. However, it is difficult to obtain a sufficient concentration of these compounds to be effective for BNCT. These compounds do not exhibit biological activities because of their design, in that the carborane cage is linked directly to the steroid skeleton. For medicinal application of carboranes as nuclear receptor (hormone) ligands, C_2B_{10} analogues of hormones might, however, be feasible and possible. An example of the new approach is the design and synthesis of retinoid receptor modulators. Retinoids, i.e., *all-trans*-retinoic acid and its analogues, are of particular interest as chemopreventive and therapeutic agents in the fields of dermatology and oncology. Retinoids can induce differentiation of a wide spectrum of cell types, such as embryonal carcinoma cells, promyelocytic leukemia cells, and normal and malignant keratinocytes through the retinoic acid receptors RAR, of which three subclasses are known (RAR-α, β, γ). High binding affinity for RAR requires a carboxylic acid moiety and an appropriate bulky hydrophobic group, such as in *all-trans*-retinoic acid and the synthetic retinoid, Am80 (Scheme 2.2-15) [44]. The design of C_2B_{10}-containing retinoids is based on control of the distance between the carboxylic acid and the bulky hydrophobic group by using a diphenylamine skeleton with *o*-C_2B_{10} substituted at the *para*- or *meta*-position of one aromatic nucleus as a hydrophobic region. Compounds bearing *o*-C_2B_{10} at the 4-position exhibited potent differentiation-inducing activity toward cells (a charac-

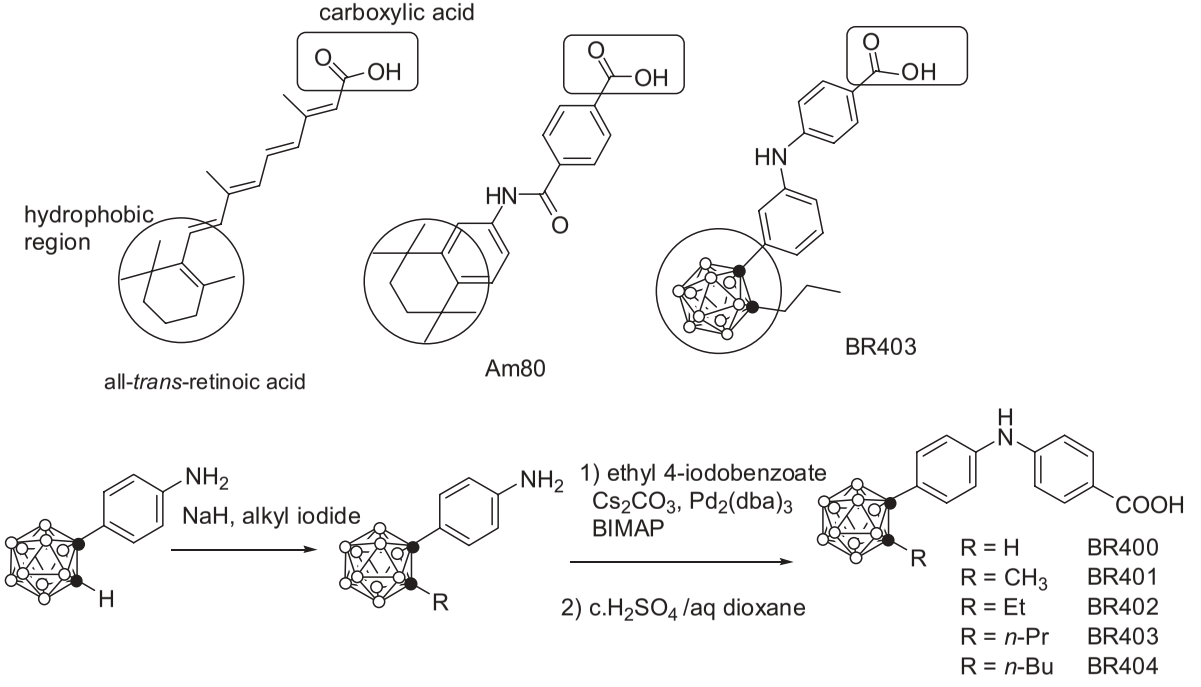

Scheme 2.2-15. Synthesis of retinoic acid receptor agonists.

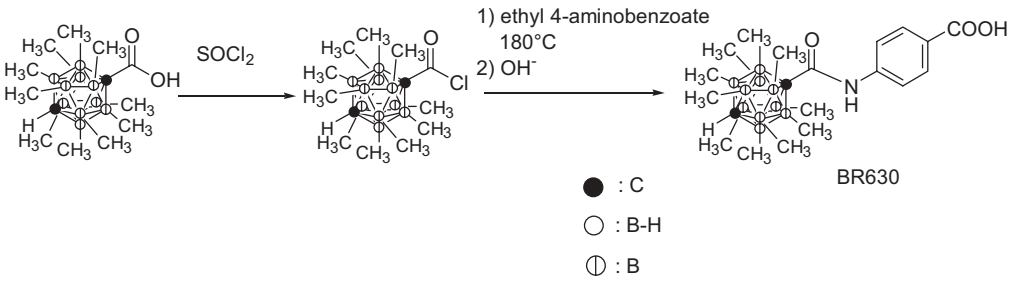

Scheme 2.2-16. Synthesis of retinoic acid receptor antagonist.

teristic retinoidal action). The agonistic activity was increased by introduction of an *n*-propyl or *n*-butyl group on the C_2B_{10} cage. For example, the concentration of BR403 in order to reach 50% of its maximum effect is 1.5×10^{-9} M. This activity is comparable to that of the native ligand for RAR, *all-trans*-retinoic acid. Compounds bearing an *o*-C_2B_{10} at the 3-position also exhibited potent retinoidal activity [45, 46].

In general, introduction of too bulky a hydrophobic group at an appropriate position of the agonist molecule results in a conformational change of the receptor–ligand complex to afford antagonistic activity (Scheme 2.2-16). Polymethylcarborane-containing molecules (BR630) with potent retinoidal antagonistic activity have been reported [47]. The polymethyl-C_2B_{10} has approximately the size of a fullerene.

Another example of a medicinal application of C_2B_{10} is the design and synthesis of estrogen receptor modulators. Estrogens play an important role in the female and male reproductive systems, and also in bone maintenance, in the central nervous system and in the cardiovascular system. Estrogen influences the growth, differentiation, and functioning of many target tissues through the estrogen receptors (ER-α, β). High binding affinity for ER requires two hydrogen-bonding groups such as a phenolic hydroxyl group and another hydroxyl group located at a suitable position on the molecule, and an appropriate bulky hydrophobic group linking the two hydroxyl groups (see Scheme 2.2-17). The size of the C_2B_{10} cage seems to be appropriate for a hydrophobic skeletal structure in place of the C and D ring structure of estradiol. Substitution of the two carbon atoms of the *p*-C_2B_{10} should allow suitable fixation of the direction of the functional groups. The designed C_2B_{10}-containing estrogen (BE120) contains all of the essential molecular recognition components for ER. The estrogenic activities of the synthesized compounds were examined by luciferase reporter gene assay. Surprisingly, the potency of BE120 was at least 10-fold greater than that of estradiol. The simple carboranylphenol BE100 also exhibits activity comparable to that of estradiol [48]. ERα binding data for the compound were consistent with the results of luciferase reporter gene assay (in which the increased expression of a gene by the hormone is measured). The high estrogenic activity of BE120 suggests that the C_2B_{10} cage works as a hydrophobic group for binding to the hydrophobic cavity of ER, and

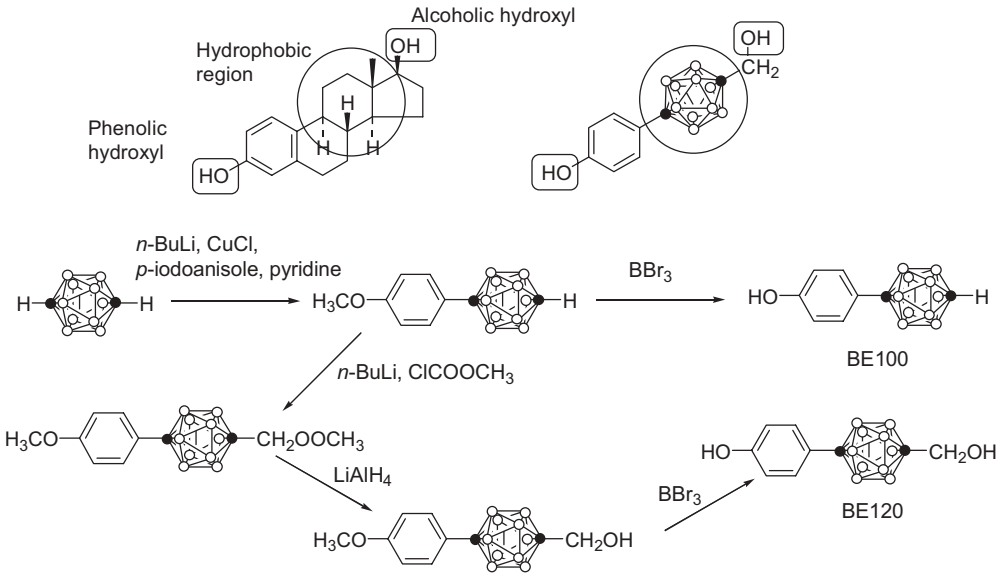

Scheme 2.2-17. Synthesis of estrogen receptor agonists.

the hydrophobic van der Waals contacts along the spherical C_2B_{10} cage produce a stronger interaction than that in the case of estradiol. The compound also showed potent *in vivo* effects on the recovery of uterine weight and bone loss in ovariectomized (OVX) mice [49].

Tamoxifen and raloxifene are representative estrogen antagonists, which have been developed for clinical use. In view of the high ER affinity of BE120, it should be possible to design new estrogen antagonists on the basis of the C_2B_{10} skeleton. C_2B_{10}-containing molecules (BE360 and BE362) exhibit estrogen antagonistic activity (Scheme 2.2-18) [50]. Further, BE360 binds to ERα and exhibits estrogenic action in bone to prevent bone loss *without* inducing estrogenic action in the uterus, suggesting its possible application to osteoporosis as a new type of selective estrogen receptor modulator, which might be useful as a therapeutic agent.

2.2.5 *closo*-Boranes

The *closo*-clusters $B_{12}H_{12}^{2-}$, $B_{10}H_{10}^{2-}$, and $B_6H_6^{2-}$ are stable entities. Their alkali salts are very water soluble. Cesium as a counter-ion reduces the water solubility considerably, and ammonium ions (especially quaternary ammonium ions) precipitate the cluster anions quantitatively from aqueous solutions. The resulting tri- and tetraalkylammonium salts are usually soluble in organic solvents. This allows chemistry to be performed under conditions which are standard for organic

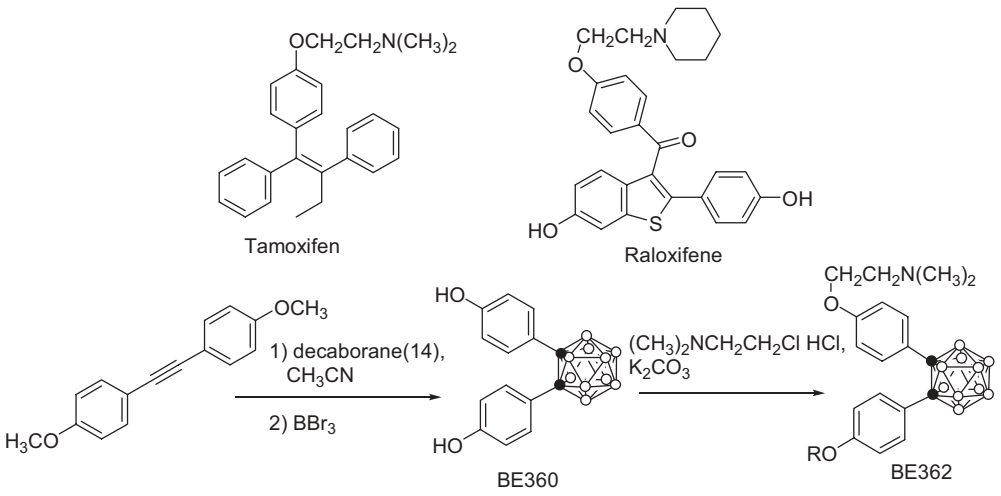

Scheme 2.2-18. Synthesis of estrogen receptor antagonists.

chemistry, without resorting to aqueous solvents. Of the three above-mentioned clusters, only the $B_{12}H_{12}^{2-}$ cluster has been studied intensively with respect to modification with organic substituents, and its application in BNCT.

2.2.5.1 $B_{12}H_{12}^{2-}$

The formation of boron–carbon bonds between the boron atoms of the clusters and carbon atoms of substituents has been described [51, 52]. These reactions have, however, not been used for the preparation of compounds useful for BNCT. Rather, the connection between the cluster and organic moieties via heteroatoms such as S, O, and N, has been achieved, and several compounds of interest to BNCT have been prepared by subsequent reactions on these heteroatoms.

2.2.5.1.1 Introduction of Heteroatoms as Substituents of $B_{12}H_{12}^{2-}$

The heteroatoms S, O, and N can be introduced as substituents of the cluster under acidic conditions (see Scheme 2.2-19). For S and O, the reaction of the hydrochlorides of thiopyrrolidone or pyrrolidone, with the non-protonated form of the pyrrolidone as solvent, is the method used by most workers. The amino group can be introduced with hydroxylamine *O*-sulfonic acid.

The reaction to the SH derivative also proceeds electrochemically [53, 54]. It is also possible to introduce isothiocyanate groups [12, 54].

Oxonium salts can be obtained directly by reaction of $B_{12}H_{12}^{2-}$ with cyclic and open ethers and BF_3 (added as etherate) [55].

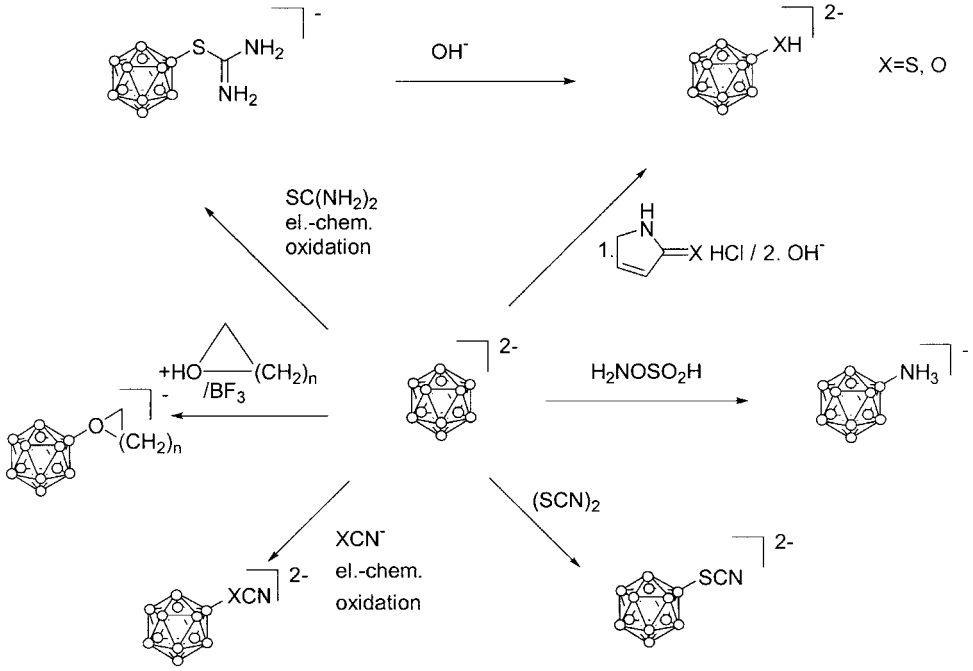

Scheme 2.2-19. Introduction of heteroatoms into $B_{12}H_{12}^{2-}$.

2.2.5.1.2 Reactivity of $B_{12}H_{11}SH^{2-}$

It is expected that the sulfur atom in $B_{12}H_{11}SH^{2-}$ can easily be deprotonated, and that the sulfur atom can be substituted nucleophilicly to thioethers and sulfonium salts, such that the $B_{12}H_{11}SH^{2-}$ cluster can form thioesters, and be susceptible to oxidation, in analogy with organic thiols. Although all these reactions also occur with $B_{12}H_{11}SH^{2-}$, the presence of the cluster changes the properties of the SH-group considerably. The p*K* value of $B_{12}H_{11}SH^{2-}$ is around 13 [56], revealing this cluster anion as a strong electron donor. As a consequence, sulfonium salts are formed readily by nucleophilic substitution of the sulfur atom with alkyl halides (the intermediate thioethers can usually not be isolated), and even sulfonium glycosides have sufficient stability to allow their isolation and characterization. Thioethers can be prepared with the cyanoethyl group as an intermediate protecting group (see Scheme 2.2-20), removal of one of the groups, re-alkylation, and removal of the second cyanoethyl group.

Thioesters can be formed by reacting the thiol of $B_{12}H_{11}SH^{2-}$ with chlorides or anhydrides of carboxylic acids, without prior abstraction of the proton of the thiol [56]. The ester anions $B_{12}H_{11}SCOR^{2-}$ show a high degree of stability toward hydrolysis and nucleophiles, as would be expected from the strong electron-donating ability of the cage. The thioesters formed posses at least the same stability toward hydrolysis as those of esters of alcohols with carboxylic acids.

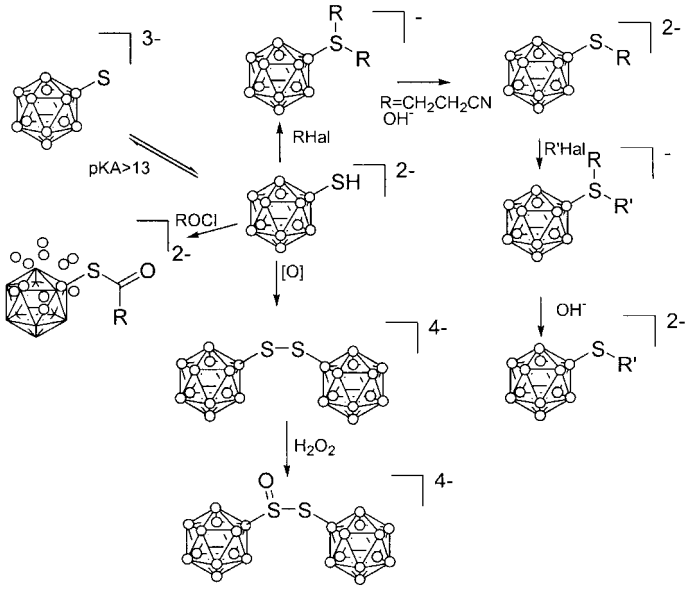

Scheme 2.2-20. Reactions of $B_{12}H_{11}SH^{2-}$.

The SH group of $B_{12}H_{11}SH^{2-}$ can be oxidized to disulfides linking two clusters, and further to the disulfide monoxide [57]. The disulfide has tumor-localizing properties superior to $Na_2B_{12}H_{11}SH$ [58]. In acidic conditions, a free radical with intense blue color is obtained as an intermediate, which can be reduced by $NaBH_4$ or $Na_2S_2O_3$ to $B_{12}H_{11}SH^{2-}$.

2.2.5.1.3 Reactivity of $B_{12}H_{11}OH^{2-}$

The oxygen can be alkylated to form stable oxonium salts, as expected from the electron-donating property of the cluster. With 1,5-dibromopentane, a tetrahydropyrane ring attached to the boron via the oxygen can be obtained in which the oxygen is in a planar environment. The reason for the steric property of the oxygen is probably not due to any orbital interaction of the oxygen π orbital, as the $-NH_2$ group of $B_{12}H_{11}NH_2{}^{2-}$ is a strong base (see below). The tetrahydropyrane ring can undergo ring-opening reactions with a large variety of O-, N-, and C-centered nucleophiles [55, 59], where the O–B bond remains intact. Even with OH^-, no Hofmann-type elimination is observed [59].

2.2.5.1.4 Reactivity of $B_{12}H_{11}NH_2{}^{2-}$

The strong electron-donating property of the cage makes $B_{12}H_{11}NH_2{}^{2-}$ a very strong base. Removal of a hydrogen from $B_{12}H_{11}NH_3{}^-$ requires very strong bases such as NaH [60]. Alkylation will proceed to quaternary ammonium groups unless steric influence limits the substitution. The length of the B–N bond is not unusual, indicating no major orbital interaction of the amine moiety with the cluster.

The anion $B_{12}H_{11}NH_2^{2-}$ can form Schiff bases with aldehydes, which in turn can be reduced to amines, opening the way to both secondary amine derivatives of the $B_{12}H_{12}^{2-}$ cluster and tertiary amines and quaternary ammonium salts after further alkylation [61].

The reaction of $B_{12}H_{11}NH_2^{2-}$ with chlorides of carboxylic acids proceeds not to carboxamides, as would have been expected, but to carboximido acids. Reaction of the amine takes place only when deprotonated with strong base. The high pK_a value of the ammonium group makes reactions with CH-acidic compounds difficult, as the latter might be stronger acids than the $B_{12}H_{11}NH_3^-$.

2.2.5.1.5 Analytical and Chromatographic Properties

Mass spectrometry of the charged clusters proceeds well with electrospray ionization, and results in characteristic "mountains" of peaks due to the presence of both ^{11}B and ^{10}B isotopes in the clusters. Even with doubly negatively charged clusters, however, there is no evidence of signals from any doubly charged molecule; rather, these clusters easily undergo protonation, usually followed by the loss of molecular hydrogen, to give clusters (again with a boron-driven isotope distribution) with a mass of $(M-1)^-$. Chromatography of compounds containing the cluster is usually achieved with reversed-phase material (such as RP-18), using tertiary or quaternary ammonium salts as ion pair reagents [62]. Only occasionally can conventional chromatography be applied successfully, as can be expected for such ionic and polar compounds.

2.2.5.1.6 Compounds for BNCT Derived from the $B_{12}H_{12}^{2-}$ Cluster

$B_{12}H_{11}SH^{2-}$ was the first compound to be used successfully in BNCT. Its synthesis by Soloway [63] was followed by testing in a mouse model, where uptake in a brain tumor model was found. As was discovered much later, the majority of this compound had been oxidized to the disulfide, which in mice has much better tumor accumulation than $B_{12}H_{11}SH^{2-}$ [58]. Retention in and binding to tumor cells was observed quite early on [64], but a plausible mechanism for the observed cellular uptake, firm retention, and localization in the nuclei of tumor cells [65, 66] remains to be elucidated.

A series of *S*-monosaccharides of $B_{12}H_{11}SH^{2-}$ have been prepared, including galactose, glucose, and mannose as sugars [67]. The reaction occurs readily under Koenigs-Knorr conditions with $B_{12}H_{11}SH^{2-}$ as well as with $B_{12}H_{11}S(CH_2)_2CN^{2-}$. The latter results in the formation of sulfonium glycosides, which are stabilized by the electron-donating properties of the cluster and therefore show only slow loss of the cyanoethyl group upon standing (Scheme 2.2-21).

It is of interest to note that the anomeric effect directs the boron substituent into the α-configuration in the case of mannose, despite the considerable steric demand. NMR studies in solution indicate that the usual $^4C_1$ conformation of the pyranose is retained, with the boron substituent in the axial position. Depending on the sugar moiety, tumor uptake is observed when the compounds are given to tumor-bearing animals. Accumulation is, however, only transient, and within a fairly short time, the boron is lost from the tumor, and from other tissues. Even at

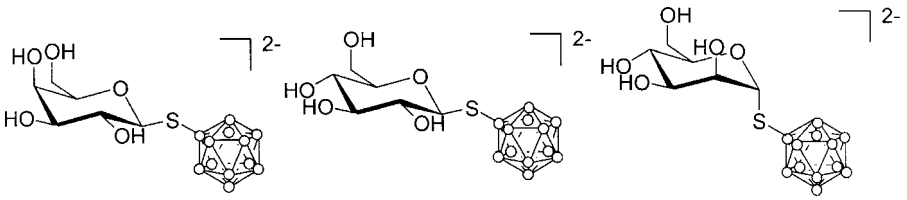

Scheme 2.2-21. *S*-Glycosides with $B_{12}H_{12}^{2-}$.

dosages of 300 mg per kg body weight, the derivatives showed no sign of acute toxicity.

Porphyrins containing carboxyl groups have been esterified with $B_{12}H_{11}SH^{2-}$ (Scheme 2.2-22). The compounds show rather long retention times in the body, as is anticipated from other porphyrins. The toxicity of porphyrins is, however, a problem [68].

2.2.5.2 Azanonaboranes

The azanonaborane cluster $R_2N\text{-}B_8H_{11}NHR$ has properties which distinguish it from other neutral clusters. First of all, the cluster is reasonably stable to water, especially under neutral and alkaline conditions, and its rate of decomposition when exposed to water and oxygen proceeds sufficiently slow to allow recrystallization from boiling water. Secondly, despite the absence of charge, the cluster has a moderate hydrophilicity. Thus, it offers alternatives to the neutral C_2B_{10} and charged $B_{12}H_{12}^{2-}$ clusters described previously.

The azanonaborane cluster allows the introduction of substituents initially through the nitrogen atoms. Two different amines can be introduced, the first RNH_2 forming the bridge in the final cluster [70] (see Scheme 2.2-23). The second

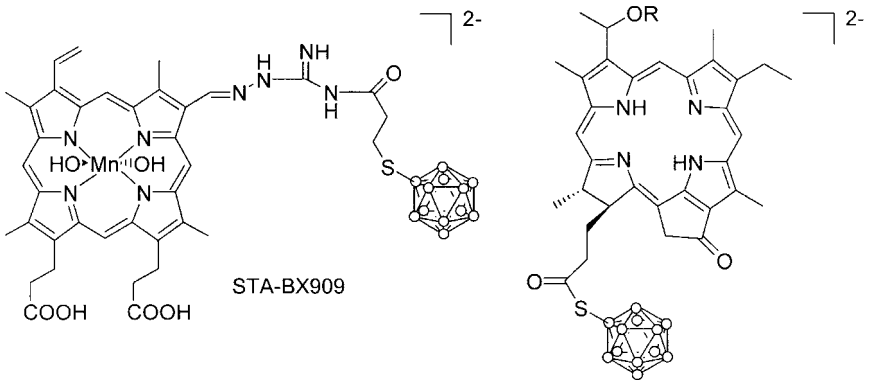

Scheme 2.2-22. Porphyrins [69] and chlorins with $B_{12}H_{11}SH^{2-}$ as boron carrier.

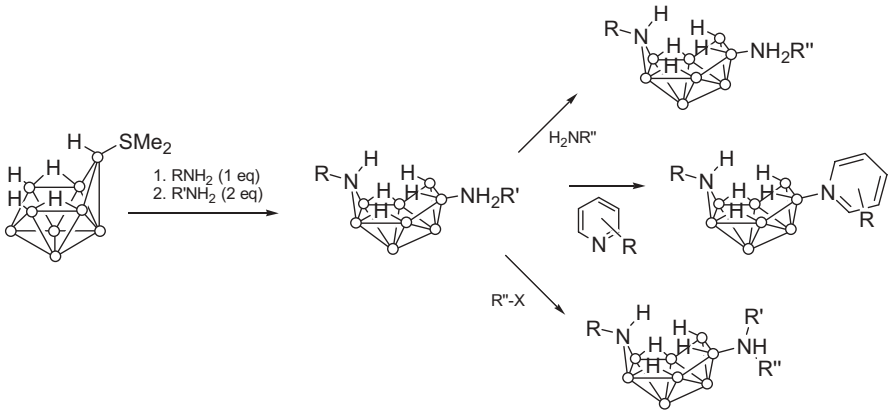

Scheme 2.2-23. Reactions of azanonaborane.

R_2NH, which is a ligand to the cluster, can be replaced by other aliphatic amines [70, 71] or pyridine [72]. The exo amine can be alkylated [70].

Water solubility is achieved through the presence of primary amines (which are protonated to ammonium groups under physiological pH) as well as other groups carrying a net charge at physiological pH, and by hydroxy groups. When the substituents of the amines are 3-hydroxypropyl groups, two of these groups (being R, R′ or R″ in Scheme 2.2-23) are required to ensure good water solubility.

2.2.6 Testing of Compounds for BNCT

Once a new potentially pharmaceutically active drug has been synthesized, it must be tested as to whether it is suitable for the intended purpose. Clearly, it is not possible to test a compound in patients without having gained, from preparatory investigations, prior information about its possible effects on the tumor, and on the health of the patient. Whereas regulations about the initial trial of new drugs in patients vary from country to country, it is obvious, on ethical grounds, that the compounds must be tested pre-clinically. This pre-clinical testing is usually carried out in animals (mice, and sometimes other animals). The testing must yield information about the maximum tolerated dose, and the dose-limiting toxicity, as well as information about the effectiveness of the new drug.

Despite the fact that a pharmacological activity on its own is not necessary for a BNCT drug, information about possible side effects is required. For boron-containing drugs, the investigation of the distribution in tumor models in animals usually gives some information on whether side effects are induced after administration of amounts sufficient for therapy. Toxicity in animals might, however, not be directly transferable to patients, as has been shown for one boronated porphyrin, one among many examples [68, 73].

In contrast to many chemotherapeutic agents in cancer therapy, boron compounds for BNCT do not require a tumoricidal action in their own right. For their successful application in the therapy of patients, it is important to deliver, to the tumor, a radiation dose which is higher than the radiation dose to the surrounding tissue. The demonstration that this is actually achieved lies ultimately in the treatment of the tumor in question. Because of the short range of the particles produced in the $^{10}B(n,\alpha)^{7}Li$ reaction, it is very important where, on a cellular and subcellular dimension, the neutron capture reaction takes place. Different methods for boron detection and quantification give different resolution of the boron distribution. It is instructive to compare these methods, both for their precision and lower detection limits, as well as for their ability to yield an image of the boron distribution in tissue (Table 2.2-1).

Bulk methods, such as inductively coupled plasma optical emission spectrometry (ICP-OES) and other techniques [74], analyze samples of 10–1000 mg. The detection limit is well below the minimum amount of boron required for BNCT. The boron concentration values pertain, however, to the average of the sample, and give no indication about the heterogeneity within the sample. Neutron capture radiography can give resolution down to about 30–100 μm. In this technique, boron (actually only the ^{10}B nuclide) is traced by the very same reaction which is used for its effect in BNCT. When thin tissue sections are placed against a detector sensitive to α-particles (such as CR-39 polycarbonate plates or nitrocellulose films) and exposed to neutrons, the resulting tracks in the detector can be made visible by etching, and can be evaluated quantitatively [75, 76]. This method is sensitive enough to detect boron well below the limit suitable for BNCT, and gives quantitative values for the boron concentration, although with reduced precision. (For non-boronated compounds, a similar method, whole-body autoradiography, is often used to investigate the fate of compounds in the body by tracing, radioactively, labels introduced chemically into the compound.) A major advantage is that all organs of animals can be investigated directly, without tedious preparation of the organs, and their separate preparation for analysis. Also, heterogeneities within one organ can be detected. Light microscopic techniques require either fluorescent molecules (such as porphyrins or other heterocyclic structures), or antibodies which can be made visible by immunohistochemistry. Only small organs can be analyzed in full detail. For immunohistochemistry, the compound in question must remain in the tissue even during the numerous staining and washing steps to which the sample must be exposed. BSH has been visualized by this technique [65]. Immunohistochemistry can also be used for electron microscopic detection of BSH [66]. Quantification is almost impossible with this technique.

Other localization methods rely on mass spectrometry in vaporized parts of the sample such as secondary ion mass spectrometry, SIMS, and other techniques [77, 78]. Here, atomic boron is detected. In addition, the specific electron shell energy of boron (usually the K shell) can be used for visualization [66, 79]. A combination of quantitative techniques with suboptimal spatial resolution and the high-resolution detection methods can give an indication about the radiation response to be expected. All these techniques require, however, that the compound in ques-

Tab. 2.2-1. Selected methods for boron detection and quantification in tissue.

Method	*Amount of tissue required*	*Spatial resolution*	*Requirements for sample preparation*	*Lower detection limit (approximate)*	*Pictorial representation*	*Quantification possible*	*Precision*
ICP-OES	100–1000 mg	0.1–1 cm	Digestion	0.1 ppm	no	yes	good
ICP-MS	10–100 mg	0.3–3 mm	Digestion	0.01 ppm	no	yes	good
Neutron capture radiography	10–100 mg	100 µm	Cryosectioning	0.5 ppm	yes	yes	medium
Immunohisto-chemistry	10–100 mg	1–2 µm	Boron must stay during fixation and staining Antibodies must be available	20 ppm	yes	no	–
Secondary ion mass spec-trometry	10–100 mg	1–2 µm	Cryopreparation	30 ppm	yes	no	–
Electron energy loss spectroscopy	1–10 mg	0.1 µm	Boron must stay during fixation and embedding or sample must be cryoprepared	30 ppm	yes	yes	medium–poor

Tab. 2.2-2. Comparison of BSH and BPA as boron carriers for BNCT.

	BSH	***BPA***
Animals		
Therapeutic effectiveness	yes	yes
Tumor/blood ratio	0.5	3
Firm binding to tumor	yes, but only a fraction	(probably not)
Cell culture		
Firm binding	no	no
Intracellular uptake	low	high
Radiobiological effectiveness	low	high (due to intracellular uptake)

tion is given to animals bearing suitable tumor models. Cell culture studies will in most cases not suffice to give appropriate answers to the question of selective, and quantitatively sufficient, accumulation in the tumor tissue.

Eventually, however, therapy experiments are the only way to demonstrate the effectiveness of a given compound [80]. This is illustrated by the different properties of the two drugs which are used at present for therapy with BNCT in patients (Table 2.2-2). Both drugs are effective in the therapy of animal tumors. It is not clear, from the comparison of all properties of these drugs, that one could have pointed to one of them as the drug which would probably be more effective than the other. The tumor-to-blood ratio of the drugs is different in animal tumors, but it is compensated by the fact that BPA is also taken up in normal cells, thereby limiting the amount of radiation that can be delivered without damaging the healthy tissue. In addition, because tumors do not consist of only one type of cell (blood vessels, e.g., are an important part of the tumor architecture), and because not all cells are equally sensitive to radiation or not equally able to take up a compound, different drugs might exert their effect through different target cells [81]. Therefore, combinations of drugs might be more effective than a single drug, just as in chemotherapy where cocktails of drugs are administered for effective therapy.

References

1 G. L. Locher, *Am. J. Roentgenol. Radium Ther.*, **1936**, *36*, 1–13.
2 Y. Nakagawa, H. Hatanaka, *J. Neuro-Oncol.*, **1997**, *33*, 105–115.
3 M. Chadha, J. Capala, J. A. Coderre, E. H. Elewitz, J.-I. Iwai, D. D. Joel, H. B. Liu, L. Wielpolski, A. D. Chanana, *Int. J. Radiat. Oncol., Biol., Phys.*, **1998**, *40*, 829–834.
4 Y. Mishima, C. Honda, M. Ichibashi, H. Obara, J. Hiratsuka, H. Fukuda, H. Karashima, T. Kobayashi, K. Kanda, K. Yoshino, *Lancet*, **1989**, *II*, 388–389.
5 W. Sauerwein, K. Hideghéty, D. Gabel, R. L. Moss, *Nuclear News*, **1998**, *41*, 54–56.
6 D. Gabel, S. Foster, R. G. Fairchild, *Radiat. Res.*, **1987**, *111*, 14–25.
7 R. G. Fairchild, D. Gabel, B. Laster, D. Greenberg, W. Kiszenick, P. L. Micca, in *Proc. 1st Intern. Symp. NCT*, Fairchild, R. G. and Brownell, G. L., ed., 1983, p. 106.

8 W. F. A. R. Verbakel, F. Stecher-Rasmussen, *Phys. Med. Biol.*, **2001**, *46*, 687–701.

9 M. F. Hawthorne, *Angew. Chem., Int. Ed. Engl.*, **1993**, *32*, 950–984.

10 C. Morin, *Tetrahedron*, **1994**, *50*, 12521–12569.

11 A. H. Soloway, W. Tjarks, B. A. Barnum, F.-G. Rong, R. F. Barth, I. M. Codogni, J. G. Wilson, *Chem. Rev.*, **1998**.

12 R. A. Spryshkova, E. Y. Grigorieva, M. G. Naidenov, J. H. Morris, V. A. Brattsev, G. I. Borisov, V. I. Riabkova, A. S. Halansky, in *Advances in Neutron Capture Therapy, Volume II, Chemistry and Biology*, B. Larsson, J. Crawford, R. Weinreich, eds., Elsevier, Amsterdam, **1997**, p. 253.

13 V. I. Bregadze, *Chem. Rev.*, **1992**, *92*, 209–223.

14 R. Coult, M. A. Fox, W. R. Gill, P. L. Herbertson, J. A. H. MacBride, K. Wade, *J. Organomet. Chem.*, **1993**, *462*, 19–29.

15 L. I. Zakharkin, A. I. Koveredou, V. A. Ol'Shevskaya, S. Shaugumbekova, *J. Organomet. Chem.*, **1982**, *226*, 217–226.

16 Z. Zheng, W. Jiang, A. A. Zinn, C. B. Knobler, M. F. Hawthorne, *Inorg. Chem.*, **1995**, *34*, 2095–2100.

17 W. Jiang, C. B. Knobler, C. E. Curtis, M. D. Mortimer, M. F. Hawthorne, *Inorg. Chem.*, **1995**, *34*, 3491–3498.

18 H. Nemoto, J. G. Wilson, H. Nakamura, Y. Yamamoto, *J. Org. Chem.*, **1992**, *57*, 435.

19 H. Nemoto, J. P. Cai, Y. Yamamoto, *Tetrahedron. Lett.*, **1996**, *57*, 539–542.

20 M. Ichihashi, T. Takanishi, Y. Mishima, *J. Invest. Dermatol.*, **1982**, *78*, 215.

21 V. A. Brattsev, V. I. Stanko, *Zh. Obshch. Khim.*, **1969**, *39*, 1175–1176.

22 L. I. Zakharkin, A. V. Grebinnikov, A. I. L'ov, *Akad. Nauk. SSSR. Ser. Khim.*, **1970**, 106–107.

23 J. L. Fauchere, O. Leukart, A. Eberle, R. Schwyzer, *Helv. Chim. Acta*, **1979**, *62*, 1385–1395.

24 A. H. Soloway, R. F. Barth, D. E. e. Carpenter, *Advances in Neutron Capture Therapy*, Plenum Press, New York, **1993**.

25 P. A. Radel, S. B. Kahl, *J. Org. Chem.*, **1996**, *61*, 4582–4588.

26 A. H. Soloway, W. Tjarks, B. A. Barnum, F. G. Rong, R. F. Barth, I. M. Codogni, J. G. Wilson, *Chem. Rev.*, **1998**, *98*, 1515–1562.

27 S. B. Kahl, R. A. Kasar, *J. Am. Chem. Soc.*, **1996**, *118*, 1223–1224.

28 W. Tjarks, *J. Organomet. Chem.*, **2000**, *614–615*, 37–47.

29 W. Tjarks, A. K. M. Anisuzzaman, L. Liu, A. H. Soloway, R. F. Barth, D. J. Perkins, D. M. Adams, *J. Med. Chem.*, **1992**, *35*, 1628–1633.

30 Y. Yamamoto, T. Seko, H. Nakamura, H. Nemoto, H. Hojo, N. Mukai, Y. Hashimoto, *J. Chem. Soc., Chem. Commun.*, **1992**, 157–158.

31 H. Nemoto, J. Cai, Y. Yamamoto, *J. Chem. Soc., Chem. Commun.*, **1994**, 577–578.

32 M. A. Davis, A. H. Soloway, *J. Med. Chem.*, **1967**, *10*, 730–732.

33 W. Tjarks, H. Ghaneolhosseini, C. L. A. Henssen, J. Malmquist, S. Sjöberg, *Tetrahedron Lett.*, **1996**, *37*, 6905–6908.

34 Y. Yamamoto, J. Cai, H. Nakamura, N. Sadayori, N. Asao, H. Nemoto, *J. Org. Chem.*, **1995**, *60*, 3352–3357.

35 V. I. Bregadze, I. B. Sivaev, D. Gabel, D. Wöhrle, *J. Porphyrins Phthalocyanines*, **2001**, *5*, 767–781.

36 M. Miura, D. Gabel, G. Oenbrink, R. G. Fairchild, *Tetrahedron Lett.*, **1990**, 2247–2250.

37 S. B. Kahl, M.-S. Koo, *J. Chem. Soc., Chem. Commun.*, **1990**, 1769–1771.

38 H. Nemoto, J. Cai, H. Nakamura, M. Fujiwara, Y. Yamamoto, *J. Organomet. Chem.*, **1999**, *58*, 170–175.

39 R. R. Kane, K. Drechsel, M. F. Hawthorne, *J. Am. Chem. Soc.*, **1993**, *115*, 8853–8854.

40 A. Nakanishi, L. Guan, R. R. Kane, H. Kasamatsu, M. F. Hawthorne, *Proc. Natl. Acad. Sci. USA*, **1999**, *96*, 238–241.

41 J. L. Fauchere, K. Q. Do, P. Y. Jow, D. Hansch, *Experimentia*, **1980**, *36*, 1203–1204.

42 K. Yamamoto, Y. Endo, *BioMed. Chem. Lett.*, **2001**, *11*, 2389–2392.

43 L. Schneiderova, O. Strouf, B. Gruner, V. Pouzar, P. Drasar, R. Hampl, I. Kimlova, *Collect. Czech. Chem. Commun.*, **1992**, *57*, 463–471.

44 H. Fukasawa, T. Iijima, H. Kagechika, Y. Hashimoto, K. Shudo, *Biol. Pharm. Bull.*, **1993**, *16*, 343–348.

45 Y. Endo, T. Iijima, K. Ohta, H. Kagechika, E. Kawachi, K. Shudo, *Chem. Pharm. Bull.*, **1999**, *47*, 585–587.

46 Y. Endo, T. Iijima, K. Yaguchi, E. Kawachi, H. Kagechika, *BioMed. Chem. Lett.*, **2001**, *11*, 1307–1311.

47 Y. Endo, A. Yaguchi, E. Kawachi, H. Kagechika, *BioMed. Chem. Lett.*, **2000**, *10*, 1733–1736.

48 Y. Endo, T. Iijima, Y. Yamakoshi, M. Yamaguchi, H. Fukusawa, K. Shudo, *J. Med. Chem.*, **1999**, *42*, 1501–1504.

49 Y. Endo, T. Iijima, Y. Yamakoshi, H. Fukasawa, C. Miyaura, M. Inada, A. Kubo, A. Itai, *Chem. Biol.*, **2001**, *8*, 341–355.

50 Y. Endo, T. Yoshimi, T. Iijima, Y. Yamakoshi, *BioMed. Chem. Lett.*, **1999**, *9*, 3387–3392.

51 D. Gabel, S. Mai, O. Perleberg, *J. Organomet. Chem.*, **1999**, *581*, 45–50.

52 T. Peymann, C. B. Knobler, M. F. Hawthorne, *Inorg. Chem.*, **1998**, *37*, 1544–1548.

53 V. A. Brattsev, J. H. B. A. B. Morris, A. M. Orlova, I. B. Sivaev, A. A. Semioshkin, V. I. Bregadze, S. Sjöberg, in *Advances in Neutron Capture Therapy, Volume II, Chemistry and Biology*, B. Larsson, J. Crawford, R. Weinreich, eds., Elsevier, Amsterdam, **1997**, p. 51.

54 V. Brattsev, J. H. Morris, Patent 6143264, **2000**.

55 I. B. Sivaev, A. A. Semioshkin, B. Brellochs, S. Sjöberg, V. I. Bregadze, *Polyhedron*, **2000**, *19*, 627–632.

56 D. Gabel, D. Moller, S. Harfst, J. Rösler, H. Ketz, *Inorg. Chem.*, **1993**, *32*, 2276–2278.

57 E. I. Tolpin, G. R. Wellum, S. A. Berley, *Inorg. Chem.*, **1978**, *17*, 2867–2873.

58 D. N. Slatkin, D. D. Joel, R. G. Fairchild, P. L. Micca, M. M. Nawrocky, B. H. Laster, J. A. Coderre, G. C. Finkel, C. E. Poletti, W. H. Sweet, *Basic Life Sci.*, **1989**, *50*, 179–91.

59 T. Peymann, K. Kück, D. Gabel, *Inorg. Chem.*, **1997**, *36*, 5138–5139.

60 T. Peymann, E. Lork, M. Schmidt, H. Nöth, D. Gabel, *Chem. Ber.*, **1997**, *130*, 795–799.

61 I. B. Sivaev, A. B. Bruskin, V. V. Nesterov, M. Y. Antipin, V. I. Bregadze, S. Sjöberg, *Inorg. Chem.*, **1999**, *38*, 5887–5893.

62 S. Harfst, D. Moller, H. Ketz, J. Rösler, D. Gabel, *J. Chromatogr. A*, **1994**, *678*, 41–48.

63 A. H. Soloway, H. Hatanaka, M. S. Davis, *J. Med. Chem.*, **1967**, *10*, 714–717.

64 K. Amano, in *Boron-Neutron Capture Therapy for Tumors*, H. Hatanaka, ed., Nishimura, Niigata, **1986**, pp. 107–115.

65 B. Otersen, D. Haritz, F. Grochulla, M. Bergmann, W. Sierralta, D. Gabel, *J. Neuro-Oncol.*, **1997**, *33*, 131–139.

66 M. Neumann, U. Kunz, H. Lehmann, D. Gabel, *J. Neuro-Oncol.*, **2002**, *57*, 97–104.

67 T. Peymann, D. Preusse, D. Gabel, in *Advances in Neutron Capture Therapy, Volume II, Chemistry and Biology*, B. Larsson, J. Crawford, R. Weinreich, eds., Elsevier, Amsterdam, **1997**, p. 35.

68 M. A. Rosenthal, B. Kavar, J. S. Hill, D. J. Morgan, R. L. Nation, S. S. Stylli, R. L. Basser, S. Uren, H. Geldard, M. D. Green, S. B. Kahl, A. H. Kaye, *J. Clinical Oncol.*, **2001**, *19*, 519–524.

69 A. Matsumura, Y. Shibata, T. Yamamoto, F. Yoshida, T. Isobe, K. Nakai, Y. Hayakawa, M. Kiriya, N. Shimojo, K. Ono, I. Sakata, S. Nakajima, M. Okumura, T. Nose, *Cancer Lett.*, **1999**, *141*, 203–209.

70 U. Dörfler, C. Bauer, D. Gabel, N. P. Rath, L. Barton, J. D. Kennedy,

J. Organomet. Chem., **2000**, *614–615*, 215–222.

71 M. El-Zaria, U. Dörfler, D. Gabel, *J. Med. Chem.*, **2002**, *45*, 5817–9.

72 C. Bauer, D. Gabel, T. Borrmann, J. D. Kennedy, C. A. Kilner, M. Thornton-Pett, U. Dörfler, *J. Organomet. Chem.*, **2002**, *657*, 205–216.

73 J. Tibbitts, J. R. Fike, K. R. Lamborn, A. W. Bollen, S. B. Kahl, *Photochem. Photobiol.*, **1999**, *69*, 587–594.

74 T. U. Probst, N. G. Berryman, P. Lemmen, L. Weissfloch, T. Auberger, D. Gabel, J. Carlsson, B. Larsson, *J. Anal. At. Spectrom.*, **1997**, *12*, 1115–1122.

75 D. Gabel, H. Holstein, B. Larsson, L. Gille, G. Ericson, D. Sacker, P. Som, R. G. Fairchild, *Cancer Res.*, **1987**, *47*, 5451–5456.

76 D. Haritz, D. Gabel, R. Huiskamp, *Int. J. Radiat. Oncol., Biol., Phys.*, **1994**, *28*, 1175–1181.

77 K. Haselsberger, H. Radner, W. Gössler, C. Schlagenhaufen, G. Pendl, *J. Neurosurgery*, **1994**, *81*, 741–744.

78 D. R. Smith, S. Chandra, J. A. Coderre, G. H. Morrison, *Cancer Res.*, **1996**, *56*, 4302–4306.

79 B. Gilbert, L. Perfetti, O. Fauchoux, J. Redondo, P.-A. Baudat, R. Andres, M. Neumann, S. Steen, D. Gabel, D. Mercanti, M. T. Ciotto, P. Perfetti, G. Margaritondo, G. De Stasio, *Phys. Rev. E*, **2000**, *62*, 1110–1118.

80 J. A. Coderre, G. M. Morris, P. L. Micca, C. D. Fisher, G. A. Ross, *Radiat. Res.*, **1995**, *144*, 310–317.

81 K. Ono, S.-I. Masunaga, M. Suzuki, Y. Kinashi, M. Takagaki, M. Akaboshi, *Int. J. Radiat. Oncol., Biol., Phys.*, **1999**, *43*, 431–436.

82 E. J. Hall, *Radiobiology for the Radiologist*, 3rd Edn., Lippincott, Philadelphia, **1988**.

83 F. Tebbe, P. M. Garrett, M. F. Hawthorne, *J. Amer. Chem. Soc.* **1964**, *86*, 4222–4223.

2.3
Clusters of the Heavier Group 13 Elements

Gerold Linti, Hansgeorg Schnöckel, Werner Uhl and Nils Wiberg

2.3.1
Introduction

A metal atom cluster as defined by Cotton [1] is still a very broad term, because non-metal atoms can also be part of the cluster core. In this chapter mainly two types of metal atom clusters are presented: the polyborane analogous polyhedral and the metalloid clusters E_nR_r of group 13 elements E. The structures and bonding of the polyhedral clusters with $n \leq r$ are similar to those in the well-known polyboranes.

In a *metalloid cluster* [2] more metal–metal bonds than metal–ligand bonds are involved, which means $n > r$. The largest structurally characterized compounds of this type contain 77 Al or 84 Ga atoms, respectively [3, 4]. Metal–metal bonds dominate these clusters and the framework of the resulting metal–metal bonds exhibits a geometry similar to the bulk metal itself. With respect to the Greek word ειδος (idea, prototype) the suffix *-oid* indicates that the bulk metal element is actually visible in the metal atom core of the metalloid or more generally, elementoid clusters.

The E_n *topologies* of clusters E_nR_r of the heavier group 13 elements E which, as a rule, are electron deficient compounds, are derived for medium sized clusters from the Wade-Mingos rules [5] by counting the E_n skeleton electrons. $2n + m$ cluster electrons (calculated by assuming that each ER group/E atom contributes two electrons/one electron; $n =$ number of cluster atoms) with $m = 2$ lead to *closo*-clusters. This means that the atoms E are at the corners of a trigonal-bipyramid, an octahedron, a pentagonal-bipyramid and so on. With $m = 4, 6, 8, \ldots$, clusters that are missing one, two, three or more corners with respect to a *closo*-cluster are predicted, the so-called *nido*-, *arachno*-, *hypho*-clusters. For $m = 0, -2, -4, \ldots$, one-fold, two-fold, three-fold, ... capped clusters are to be expected.

We will first comment on metal–metal bonds (see Section 2.3.2) and then discuss (see Section 2.3.3) the polyhedral clusters [6], followed by the second central subject, the metalloid clusters in Section 2.3.4 (for recently published reviews see e.g., Refs. [7–11]).

In part, the success with this chemistry of group 13 is based on a technique

called *cryochemistry*, which means trapping of the high temperature monohalides, e.g., AlCl, and generating a low temperature meta-stable solution of the monohalides [12]. This technique has been developed from matrix isolation spectroscopy, where monohalides of Al and Ga are shown to be reactive species that form rare compounds with double bonds (O=AlF) [13] or unexpected oxidation products ($FAlO_2$, $FAlO_4$) [14].

This account summarizes some novel aspects of metal cluster chemistry demonstrating that these clusters are intermediates on the way to the bulk metal. Recent advances have gained insight into one of the oldest processes of mankind, the dissolution and the precipitation of metals from solution. The preparation of these clusters as well as their structure is discussed mainly in comparison with the structures of the bulk elements. Finally, some physical properties of the metalloid clusters containing metal cores of Al and Ga at the nanometer scale are presented, which could possibly be the starting point of a better understanding of the electron conductivity up to superconductivity within metalloid substances. In fact, the compounds E_nR_r, which are at the borderline between molecular and solid state chemistry, are only isolable as meta-stable products with bulky R groups. In the following sections, in the main four substituents are used for stabilizing the clusters: $(Me_3Si)_2N$ [bis(trimethylsilyl)amino], $(Me_3Si)_3Si$ [tris(trimethylsilyl)silyl], $(Me_3C)_3Si$ [tris(*t*-butyl)silyl] and $(Me_3Si)_3C$ [tris(trimethylsilyl)methyl].

2.3.2 The Metal–Metal Bond

Before describing polymetal atom clusters of the heavier group 13 elements that contain several metal–metal bonds one should consider the roots of the metal–metal bonding of these elements [6, 12]. Molecular organometallic compounds R_4E_2 (E = Al, Ga) **1** containing the first Al–Al and Ga–Ga 2c2e bonds were synthesized only about 14 years ago (Figure 2.3-1) [15, 16].

In a pure, "unspoiled" metal–metal bond each of the metal atoms should exclusively be neighboured by other atoms of the same type without any influence

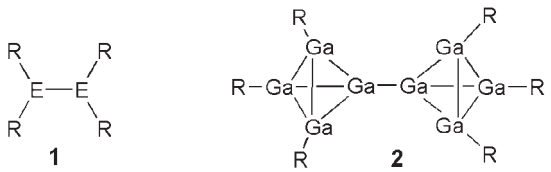

Fig. 2.3-1. Schematic representation of the first dialuminum and digallium derivatives **1**, and the $Ga_8[C(SiMe_3)_3]_6$ cluster **2**.

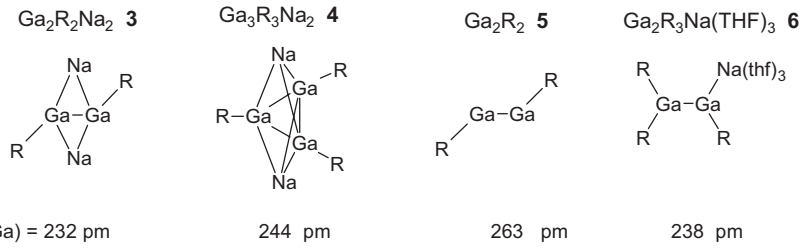

Fig. 2.3-2. Schematic representation of **3** (R = 2,6-Trip$_2$C$_6$H$_3$; Trip = 2,4,6-*i*Pr$_3$C$_6$H$_2$), **4** (R = 2,4,6-*t*Bu$_3$C$_6$H$_2$), **5** (R = 2,6-Dipp-C$_6$H$_3$, Dipp = 2,6-*i*Pr$_2$-C$_6$H$_3$ and **6** (R = Si*t*Bu$_3$). The lines represent connecting of atoms only and do *not* express the bond order.

from bridging atoms. In this sense, the only prototypical compound known so far is **2**, a Ga_8R_6 cluster (Figure 2.3-1) [17] in which two tetrahedral Ga_4R_3 units are joined by a Ga–Ga single bond. This cluster is presented here as an example of the fundamental aspects of metal–metal bonding. The central Ga–Ga bond within this cluster could be viewed as a model for connections between metal atom clusters, independent of their size. Its strength is in-between that of 2c2e and 3c2e bonds [18].

Although at the present time there is no indication of the existence of a compound with a real Ga–Ga double bond, a discussion regarding the "Ga–Ga triple bond" has raged for several years. This was initiated by a remarkable experimental result in which a compound with an anionic Ga_2R_2 unit **3** and bridging Na^+ cations was structurally elucidated (Figure 2.3-2) [19] and interpreted on the basis of quantum chemical calculations [20].

As a result of the short Ga–Ga distance (232 pm) it was suggested that **3** contains a Ga–Ga triple bond. It is unlikely that a triple bond is responsible for the observed bond contraction, because there are other examples where short Ga–Ga distances are observed, e.g.: (1) the Ga_2 dumbbell [d(Ga–Ga) = 235 pm] in the Ga_{84} cluster (cf. Section 2.3.4.2.7) [4]; (2) the Ga_2 unit in α-Ga [7] (cf. 2.3.4.2.1), which despite a coordination number of seven for each Ga atom, exhibits an unexpectedly short bond distance of 245 pm; and (3) the digallanes $[(Me_3SiC)_2B_4]_2$-Ga_2 [21] and $[CH_2(NtBu)]_2Ga_2$ [22], which have short Ga–Ga distances of 234 and 233 pm, respectively. Obviously, the Ga–Ga bond is very variable in length. Therefore, critical assessment of the interpretation of the bonding in the $Ga_2R_2^{2-}$ unit is necessary.

In our view, the expression "triple bond" is fairly misleading, since, if the term is used literally, a bond should be an attractive interaction between atoms and therefore a triple bond should be considerably stronger than the corresponding single bond. Since the restoring forces during bond elongations are a good measure of the bond strength, the force constant can be used to compare the bonding in different molecules. On the basis of an analysis of the force constants it is shown, however, that the so-called Ga–Ga triple bond [18] with respect to the increase in the force constant f compared with that of a Ga–Ga single bond can at most be

described as a strong single bond: f"Ga–Ga"/f"Ga=Ga"/f"Ga≡Ga" = 0.75/0.98/1.01 mdyn Å^{-1} [10, 18]. It is apparent that the contribution of each of the six electrons contributing to the total bond strength is very different.

In addition to the force constant, there are other indications that the short distance of the "Ga–Ga triple bond" is influenced significantly by the bridging Na^+ cations, so that we may be dealing in fact with an $RGaNa_2GaR$ cluster. In theoretical studies the response of the free anion $[HGaGaH]^{2-}$ and the neutral species $[Na^+]_2[HGaGaH]^{2-}$ to hydrogenation reactions has been probed [23]; in the past the enthalpy of hydrogenation was used to clarify multiple bonding in organic compounds. According to these calculations, the reactivities of the free anion and the neutral species are very different, showing that the Na^+ ions exert a significant influence on the Ga–Ga bonding. A similar description is valid for $Na_2Ga_3R_3$, **4**, which contains a central $Ga_3R_3^{2-}$ ring, forming an aromatic 2π-electron system [24]. Very recently, this interpretation has been proved with the synthesis of a neutral Ga_2R_2 compound **5** containing a very large GaGa distance [25] and of the digallanide $R_2GaGaR[Na(thf)_3]$ **6** [26] featuring a short Ga–Ga bond. The parent compound Ga_2H_2 has also been generated and characterized recently using the matrix-isolation technique [27]. The bond strength in HGaGaH has also been analyzed in quantum chemical calculations by looking at the fragmentation leading to two HGa fragments either in their singlet electronic ground states or their triplet excited electron states, and with the unrelaxed Ga–H distance [28]. Extending these calculations to a number of binary subvalent main group element compounds it was possible to classify the bonding: classical versus "non-classical" or donor-acceptor type [28].

From a simple point of view both compounds (**5** and **6**) should exhibit a Ga–Ga double bond. The non-linearity of the R_2Ga_2 entity in **3** and **5** and the non-planarity of the R_3Ga_2 core in **6** demonstrate the "non-classical" bonding. One should keep in mind that the terms of multiple bonding should be used with care when applied to the field of heavy main group cluster compounds [29]. A comparison with Ge_2R_2, being formally isoelectronic with the Ga_2R_2-group in **3**, which has been structurally characterized recently (cf. Chapter 2.5.3.1), may also help to improve the understanding of the bonding situation in these subvalent molecular compounds.

2.3.3
Boron Analogous Clusters of the Type $[E_nR_n]^{x-}$ ($x = 0,1,2$)

This section will focus on homonuclear neutral or anionic clusters of the elements aluminum, gallium, indium, and thallium, which have an equal number of cluster atoms and substituents. Thus, they may clearly be distinguished from the metalloid clusters described below, which in some cases have structures closely related to the allotropes of the elements and in which the number of the cluster atoms exceeds the number of substituents. The compounds described here possess only a single non-centered shell of metal atoms. With few exceptions, their structures resemble those of the well-known deltahedral boron compounds such as $B_4(CMe_3)_4$ [30], B_9Cl_9 [31] or $[B_nH_n]^{2-}$ [32]. The oxidation numbers of the elements in these

clusters are +1 or deviate only slightly from this value. In particular with aluminum and gallium these unusual low oxidation states are liable to disproportionation, and one of the most important tasks in this chemistry is the kinetic stabilization of these compounds by steric shielding.

2.3.3.1 Tetrahedral Cluster Compounds E_4R_4

2.3.3.1.1 Syntheses

The tetrahedral cluster compounds can be synthesized by three methods: (1) reaction of the monohalides EX (X = Cl, Br, I) with alkyllithium or Grignard reagents, (2) reduction of suitable organoelement halides of trivalent aluminum, gallium or indium, and (3) thermolysis of $R_2E\text{-}ER_2$ compounds.

Starting from EX compounds Reactions of aluminum(I) halides with alkali metal silyl derivatives afforded the cluster compounds $Al_4(SiR_3)_4$ **7** and **8** ($R = CMe_3$, $SiMe_3$) in moderate yield [Eq. (1), Figure 2.3-3] [33, 34]. Similarly, the tetrameric (η^5-pentamethylcyclopentadienyl)aluminum(I) $(AlCp^*)_4$ **9** ($Cp^* = C_5Me_5$, Figure 2.3-3) was obtained by the reaction of AlCl with the corresponding dicyclopentadienylmagnesium derivative [35].

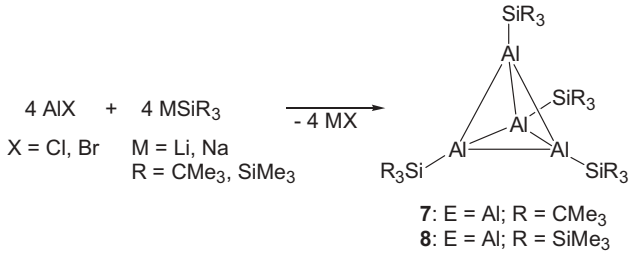

(1)

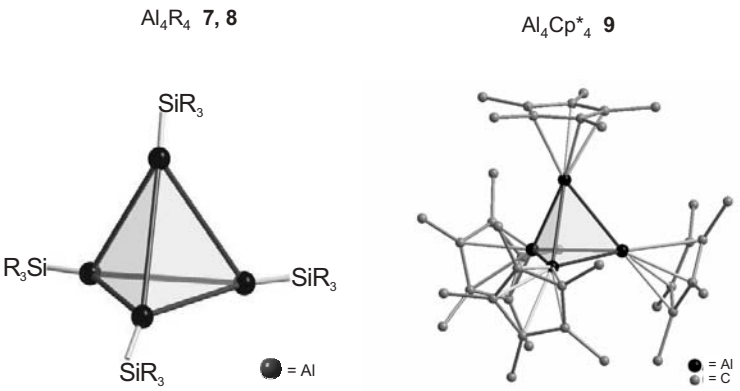

Fig. 2.3-3. Molecular structures of $Al_4(SiR_3)_4$ ($R = CMe_3$, $SiMe_3$) (**7**, **8**) and $Al_4Cp^*_4$ **9**.

Ultrasonic treatment of a mixture of elemental gallium and iodine in toluene yields a light green insoluble product described as gallium(I) iodide [36]. However, it now seems to be clear, as a result of several experimental observations, that a mixture of subiodides of gallium is actually formed. Nevertheless, the green powder behaves like "GaI" in many reactions and has also been employed for the synthesis of tetrahedral tetragallium clusters [Eq. (2)] [37, 38].

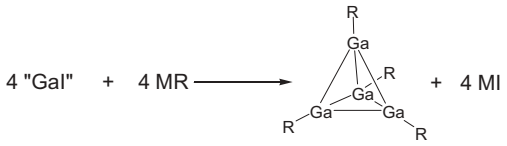

(2)

10: R = $Si(CMe_3)_3$
11: R = $Si(SiMe_3)_3$
12: R = $Ge(SiMe_3)_3$

However, mixtures of these products with some gallium rich metalloid clusters were formed so that this method is rather inadequate, and compounds **10**–**12** were isolated in very low yields.

In contrast to the non-trivial routes for the syntheses of pure aluminum(I) or gallium(I) subhalides, indium(I) chloride or bromide can simply be prepared by melting mixtures of elemental indium and indium trihalides [39]. When these indium(I) halides were treated with bulky alkyllithium compounds, deep violet organoelement indium clusters (**13**–**18**) were obtained [Eq. (3)] [40, 41].

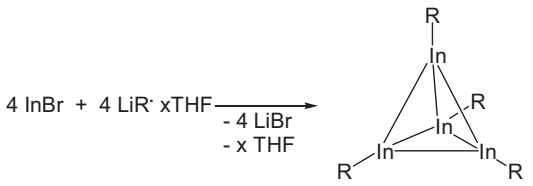

(3)

13: R = $C(SiMe_3)_3$
14: R = $C(SiMe_2Et)_3$
15: R = $C(SiMe_2n\text{-}Bu)_3$
16: R = $C(SiMe_2i\text{-}Pr)_3$
17: R = $C(SiMe_2Ph)_3$
18: R = $C(SiMeEt_2)_3$

As far as single crystals are available, **13**–**18** possess tetrahedral structures in the solid state. Smaller substituents than those given in Eq. (3) led to decomposition by disproportionation [3 In(+1) → 2 In(0) + In(+3)].

Organoelemental thallium(I) compounds were prepared by similar routes starting with thallium(I) cyclopentadienide, for instance [Eq. (4)]. In contrast to the clusters described so far, the metal–metal interactions in the tetrahedral clusters of compound **19** [42] or of the related pyrazolato derivative **20** [43] (Figure 2.3-4) are quite weak; their bonding situation and stability are discussed in Section 2.3.3.1.2.

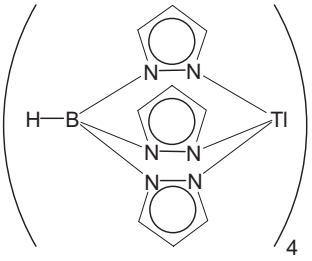

20

Fig. 2.3-4. Schematic drawing of compound **20**.

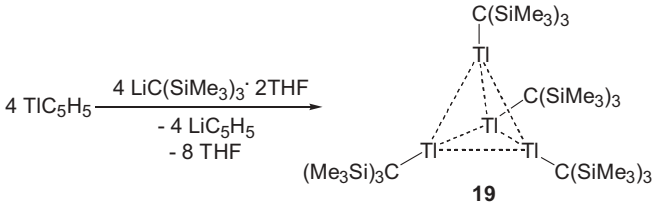

19 (4)

Tetraalkyl- or tetrasilyltetragallium(I) compounds were also obtained by the reactions of the dioxane adducts of Ga_2X_4 (X = Cl, Br) with bulky alkyl- or silyllithium compounds [Eq. (5)], which were accompanied by disproportionation of Ga(+2) to Ga(+1) and Ga(+3) [44, 45]. In particular the yield of the alkyl derivative **21** was very poor and several unknown byproducts were detected by NMR spectroscopy. Furthermore, the reaction requires the employment of a solvent-free lithium compound, which is not readily available. The reaction of tris(trimethylsilyl)silyl lithium yielded the expected product of the disproportionation $[(Me_3Si)_3Si]_2GaCl_2Li(THF)_2$ besides compound **11**.

$$2\ Ga_2X_4(\text{dioxane})_2 \xrightarrow[-\text{dioxane}]{6\ LiE(SiMe_3)_3} Ga_4[E(SiMe_3)_3]_4 + \text{various products} \qquad (5)$$

X = Cl, Br

21: E = C

11: E = Si

Starting from REX_2 compounds Another method for the synthesis of tetrahedral cluster compounds of the heavier elements of the third main-group consists of the reduction of monoalkylelement(III) halides. $Al_4Cp^*_4$ **9**, which was generated originally by the reaction of $MgCp^*_2$ with AlCl according to Eq. (1), was subsequently prepared by reduction of Cp^*AlCl_2 with potassium [46]. Through a similar route $Al_4[C(SiMe_3)_3]_4$ **22** was obtained by reduction of the corresponding alkylaluminum diiodide [Eq. (6)] [47].

$$4(Me_3Si)_3C\text{-}All_2(THF) + 8\ K \xrightarrow[-4\ THF]{} \underset{\mathbf{22}}{Al_4[C(SiMe_3)_3]_4} + 8\ Kl \qquad (6)$$

The low yield of **21** [Eq. (5)] prevented investigations of its reactivity for many years. A facile new method for its synthesis was published only recently. The latter starts from alkyltrichlorogallates [Eq. (7)], which are readily available by the reaction of $GaCl_3$ with the corresponding alkyllithium derivatives in THF [48]. Reduction of sterically highly shielded compounds with activated magnesium (Rieke magnesium) gave the clusters in yields of up to 80% [49]. Clusters possessing smaller substituents than those given in Eq. (7) could not be obtained by this route, because disproportionation occurred under the conditions required. Tetraneopentyltetraalane $[Al\text{-}CH_2CMe_3]_4$ **24** is understood to be formed by the reaction of dineopentylaluminum chloride with potassium [50].

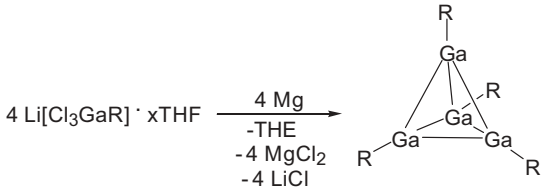

(7)

21: R = $C(SiMe_3)_3$
23: R = $C(SiMe_2Et)_3$

Starting from $R_2E\text{-}ER_2$ compounds The dialane $R_2Al\text{-}AlR_2$ **25** (R = Si*t*Bu_3) decomposes by heating at 100 °C for 10 h via the unusual radical $R_2Al\text{-}AlR$ **27** (isolable at 50 °C) to yield the radical Al_3R_4 **29** and the tetrahedro-tetraalane Al_4R_4 **7** (Scheme 2.3-1) [51].

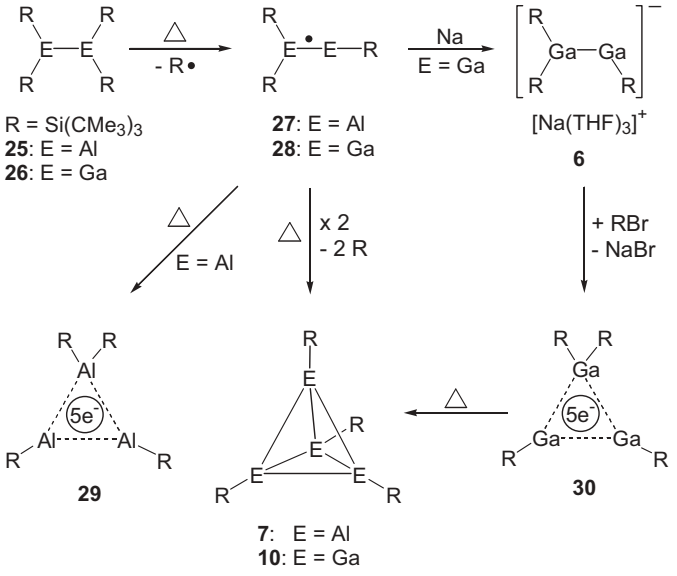

Scheme 2.3-1. Reaction pathways for the decomposition of Al_2R_4 and Ga_2R_4 compounds [R = $Si(CMe_3)_3$].

The starting dielement compounds $R_2E\text{-}ER_2$ (E = Al, Ga) are prepared from EX_3 (X = halogen) and NaR in THF. The corresponding indium and thallium derivatives are also available by treatment of the monohalides EX with NaR [51]. Owing to steric and/or electronic effects the digallane $R_2Ga\text{-}GaR_2$ **26** is unstable under the reaction conditions and gives the radical R_3Ga_2 **28** directly. The latter transforms on heating in heptane at 100 °C to yield exclusively the tetrahedro-tetragallane Ga_4R_4 (**10**, Scheme 2.3-1). This reaction represents the most effective route for the synthesis of **10** [51]. The radical Ga_3R_4 **30** which in contrast to the aluminum derivative **29** is not formed by thermolysis of $R_2Ga\text{-}GaR_2$ **26** was obtained by the reduction of Ga_2R_3 **28** with sodium in THF via the digallenide $R_2GaGaR[Na(THF)_3]$ **6** intermediate in the presence of RBr. Both radicals, Al_3R_4 **29** and Ga_3R_4 **30** decompose on heating to yield the tetrahedranes **7** and **10**, respectively. Ga_4R_4 **10** was also obtained by the reaction of the digallane RClGa-GaClR with Na [52]. The corresponding tetrasilyldiindium compound $R_2In\text{-}InR_2$ decomposes to form the larger cluster $In_{12}R_8$ (Section 2.3.4.1), whereas $R_2Tl\text{-}TlR_2$ gives a black insoluble precipitate.

2.3.3.1.2 **Bonding**

The bonding situation of the tetrahedral clusters may be described by the qualitative MO scheme that is depicted in Figure 2.3-5 and in which the orbitals involved in the bonding of the terminal ligands are ignored [33, 35, 53]. The monomeric fragments M–X have a lone electron pair in a σ-orbital as the HOMO and a degenerate set of two orbitals of π-symmetry as the lowest unoccupied state. Linear

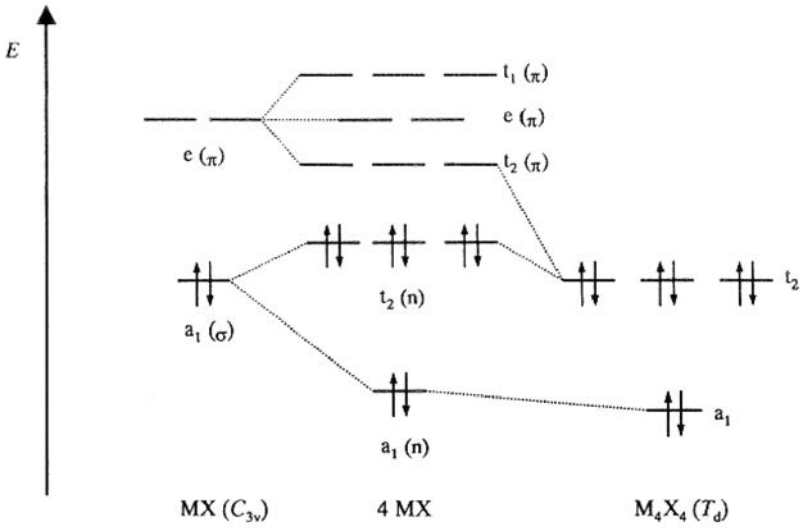

Fig. 2.3-5. Qualitative MO scheme of tetrahedral clusters with elements of Group 13 and their monomeric fragments (the energy of the occupied t_2 orbital depends on the degree of interaction with the empty π-orbitals; see text).

Tab. 2.3-1. Tetramerization energies of EX compounds (E = B, Al, Ga, In; X = H, SiH_3, C_5H_5, CH_3) obtained by quantum chemical calculations on an MP2 level.

	$\Delta E_{tetr.}$ (kJ mol^{-1})	Ref.
B_4H_4	−1153	[53]
Al_4H_4	−571	[53]
$Al_4(SiH_3)_4$	−604	[53]
$Al_4(SiMe_3)_4$	−655	[53]
$Al_4(\eta^5\text{-}C_5H_5)_4$	−160	[53, 54]
Ga_4H_4	−556	[45]
$Ga_4(CH_3)_4$	−528	[45]
$Ga_4(SiH_3)_4$	−596	[45]
In_4H_4	−337	[41]
$In_4(CH_3)_4$	−290	[41]

combination of the lone pair orbitals give one bonding orbital and three degenerate orbitals (t_2) which are essentially anti-bonding with respect to the cluster formation. The last ones become stabilized by an interaction with the empty π-orbitals which form the LUMO in the monomers. Only this interaction causes the formation of stable tetrameric molecules and gives four bonding states occupied by the eight electrons delocalized in the cluster. The anti-bonding orbitals of the clusters are formed by three sets of degenerate orbitals (t_1, t_2 and e).

The tetramerization energies obtained by quantum chemical calculations and their dependency on the type of substituents gives a very good insight into the stability of these clusters (Table 2.3-1). As expected, the energy decreases on going down the third main-group, the most stable clusters being formed with boron. Methyl groups attached to the aluminum, gallium or indium atoms give a slightly lower energy than hydrogen atoms, while a significant increase of the cluster stability was observed with silyl substituents. The smallest tetramerization energy of the aluminum compounds was calculated with the cyclopentadienyl ligand and, indeed, the monomeric $AlCp^*$ species could be structurally characterized in the gas phase by electron diffraction at 120 °C [55, 56].

In particular the last observation is easily understood by the molecular orbital picture given above. The π-orbitals of the monomers are required for a stabilization of the otherwise anti-bonding cluster orbitals of t_2 symmetry which must accept six electrons. If this mixing is prevented because these orbitals adopt the electron density of the ligands, e.g., π-electrons of the side-on coordinated cyclopentadienyl groups, their contribution to the cluster stability is minimized or in particular cases the formation of clusters does not occur at all. Thus, the substituents attached terminally to the clusters strongly influence their stability by the different donor or acceptor capabilities. A further effect may result from the different steric demand of the substituents which will be discussed below.

Tab. 2.3-2. Experimentally determined E–E distances for tetrameric organoelement(I) compounds.

	E–E (pm)	*Ref.*
$Al_4[C(SiMe_3)_3]_4$ **22**	273.9	[47]
$Al_4(\eta^5\text{-}C_5Me_5)_4$ **9**	276.9	[35]
$Al_4[Si(CMe_3)_3]_4$ **7**	260.4	[33]
$Al_4[Si(SiMe_3)_3]_4$ **8**	260.2	[34]
$Ga_4[C(SiMe_3)_3]_4$ **21**	268.8	[44]
$Ga_4[C(SiMe_2Et)_3]_4$ **23**	271.0	[49]
$Ga_4[Si(SiMe_3)_3]_4$ **11**	258.4	[45]
$Ga_4[Si(CMe_3)_3]_4$ **10**	257.2	[51]
$Ga_4[Ge(SiMe_3)_3]_4$ **12**	258.7	[38]
$In_4[C(SiMe_3)_3]_4$ **13**	300.2	[40]
$In_4[C(SiMe_2Et)_3]_4$ **14**	300.4	[41]
$In_4[C(SiMeEt_2)_3]_4$ **18**	300.6; 304.0	–
$In_4[C(SiMe_2iPr)_3]_4$ **16**	315.2	[41]
$Tl_4[C(SiMe_3)_3]_4$ **19**	333.5; 357.5	[42]
$Tl_4[HBpyr_3]_4$ **20**	364.7	[43]

2.3.3.1.3 **Structures**

The tetranuclear clusters $(EX)_4$ (E = Al, Ga, and In) possess virtually undistorted tetrahedral cores. Selected bond lengths of those compounds which were characterized by crystal X-ray diffraction analysis are summarized in Table 2.3-2. The Al–Al separations are longer than the Ga–Ga distances of compounds with identical ligands, similar differences were obtained for localized E–E single bonds. These observations reflect the particular properties of gallium in comparison with aluminum or indium with a small covalent radius and a high electronegativity, which owing to a smaller charge separation in the terminal Ga–C or Ga–Si bonds leads to a weaker electrostatic repulsion in the E–E interactions and hence to a smaller elongation of the bond lengths. As to be expected, the In–In distances are the longest ones in this series. At a rough estimate, the E–E distances are longer than single bonds by about 5% on average, which is caused by the delocalized bonding situation in these clusters. The terminal ligands influence the stability of the clusters greatly and as a consequence the E–E distances. In the series of the aluminum compounds for instance, the pentamethylcyclopentadienyl ligand causes the longest Al–Al separation, the alkyl group is intermediate, and the shortest separations were observed for the silyl substituents. In addition, the size of the substituents influences the E–E distances to a considerable extent, as is shown impressively by the series of four tetraalkyltetraindium derivatives In_4R_4 (Table 2.3-2). On going from trimethylsilyl to dimethyl(isopropyl)silyl groups the In–In distances are lengthened from 300.2 to 315.2 pm. Thus, consideration of a cooperative effect between steric and electronic interactions may give the most consistent insight into the properties of these compounds.

The clusters discussed so far contain almost regular tetrahedra with the E–E separations in a very narrow range and the E–C as well as the E–Si bonds located on the three-fold rotation axes. In contrast, the thallium(I) compounds (**19** and **20**) form only weakly bonded clusters with rather long Tl–Tl distances [42, 43]. Most significant are the changes in the homologous series of alkyl derivatives $[E\text{-}C(SiMe_3)_3]_4$ for which only the thallium compound shows a strong distortion with three Tl–Tl distances at 334 and three further ones at about 358 pm. Furthermore, the Tl–C bonds do not point to the center of the cluster as expected for regular structures, but are tilted with one almost linear Tl–Tl–C group per substituent. The bonding situation in the thallium cluster may best be described in terms of weak van der Waals interactions between monomeric Tl–R units.

2.3.3.1.4 **Physical Properties**

The E_4R_4 cluster compounds are deeply colored and show the expected correlation between the color and the strength of the bonding interaction in the clusters, e.g., $(AlCp^*)_4$ **9** is yellow [35], $[Al\text{-}C(SiMe_3)_3]_4$ **22** adopts an orange color [47], the silyl substituted clusters $[Al\text{-}Si(CMe_3)_3]_4$ **7** and $[Al\text{-}Si(SiMe_3)_3]_4$ **8** are violet [33, 34]. The tetraalkyl compounds with gallium (**21** and **23**) [44, 49] and indium (e.g., **13**) [40, 41] are red and violet, respectively. This trend together with ^{27}Al NMR shifts has been investigated thoroughly [54].

The stability of these clusters in solution or in the gas phase strongly reflects their bonding situation as discussed earlier on the basis of quantum-chemical calculations and crystal structure determinations. The tetraalkyltetragallium compounds **21** and **23** dissociate upon dissolution in benzene to give the unique monomers $Ga\text{-}C(SiMe_2R)_3$ in dilute solutions, which have with respect to coordination and electronically highly unsaturated gallium atoms. The structure of $Ga\text{-}C(SiMe_3)_3$ was determined by electron diffraction in the gas phase at 250 °C, which shows impressively the exceptional thermal stability of this alkylgallium(I) compound [56]. A high thermal stability was also observed for monomeric $GaCp^*$ in the gas phase, which could be heated up to 600 °C without decomposition. The electron diffraction of this molecule exhibits a longer Ga–Cp* distance [57] than in the hexameric aggregate detected in the solid state (Figure 2.3-11).

In contrast, the corresponding tetraindium clusters **13** and **14** remained tetrameric in benzene, which, owing to the longer In–C bonds, may be caused by the weaker repulsive interaction between the substituents. The dissociation into the monomers occurred by employing very bulky groups such as $SiMe_2Ph$ **17**, $SiMe_2iPr$ **16** and $SiMeEt_2$ **18** [40, 41]. A monomeric arylindium(I) compound stabilized by a bulky aryl substituent [InR, $R = C_6H_3(Trip)_2$, $Trip = C_6H_3iPr_2$] has been characterized by crystal structure determination [58]. The thallium analogue **19** which has a distorted Tl_4 cluster with long Tl–Tl distances dissociates completely upon dissolution in accordance with the weak Tl–Tl interaction. In contrast to the gallium or indium clusters, **19** is rather unstable and decomposes rapidly at room temperature in solution with the formation of tris(trimethylsilyl)methane and the precipitation of thallium [42].

Dissociation also occurred with the pentamethylcyclopentadienylaluminum(I)

cluster **9** which had relatively long Al–Al distances and in which the bonding is weakened by the side-on coordination of the cyclopentadienyl groups. The clusters bearing silyl substituents showed the shortest element–element distances in the solid state. A dissociation was not reported, and even in the mass spectra the tetramers were detected.

2.3.3.1.5 **Reactivity**

The tetrahedral cluster compounds show an unprecedented chemical reactivity which led to the syntheses of a broad variety of fascinating products [59]. Some of these will be discussed in the Chapters 3.5. Only a short summary will be given here.

Oxidations Reaction of the tetragallium compound **21** with P_4 resulted in the insertion of monomeric fragments GaR into three P–P bonds of the P_4 tetrahedron and the formation of the cage compound **31** (Figure 2.3-6) [60]. A different species

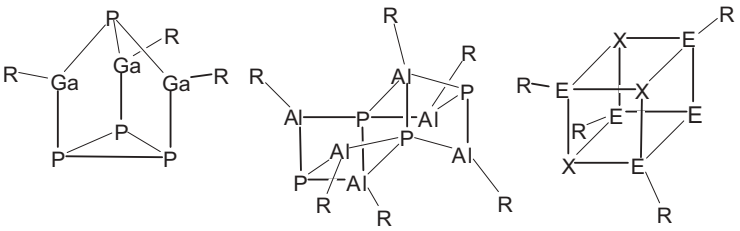

31: R = $C(SiMe_3)_3$ **32**: R = Cp* **33**: E = Al, Ga, In; X = O, S, Se, Te

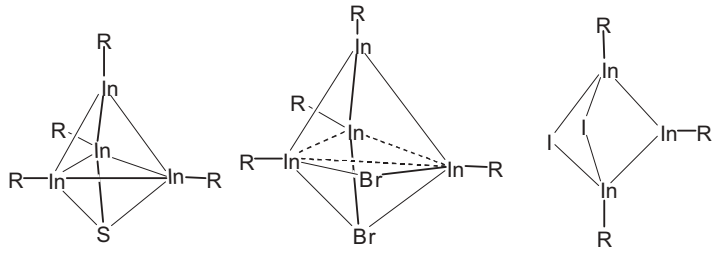

34: R = $C(SiMe_3)_3$ **35**: R = $C(SiMe_3)_3$ **36**: R = $C(SiMe_3)_3$

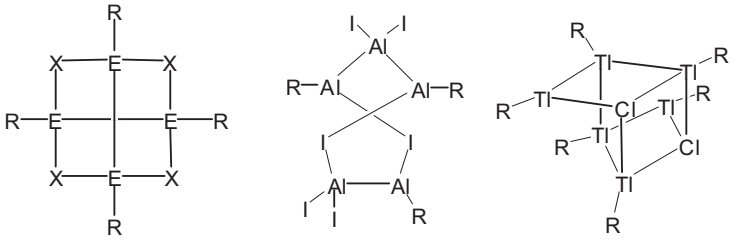

37: E = Ga, In; X = Cl, Br **38**: R = Cp* **39**: R = $Si(CMe_3)_3$

Fig. 2.3-6. Oxidation products of the tetrahedral $(ER)_4$ clusters.

32 was obtained in a similar reaction between $(AlCp^*)_4$ **9** and P_4 [61]. Complete oxidation of $(ER)_4$ clusters with chalcogens yielded the heterocubanes **33** [37, 40, 46, 62], while the partial oxidation of $(InR)_4$ **13** [R = $C(SiMe_3)_3$] with propylenesulfide furnishes the novel cluster **34** in which only one face of the In_4 tetrahedron is bridged by a sulfur atom [63]. Halogens or halogen donors gave the interesting series of products (**35** to **37**) which may be suitable as starting materials for the synthesis of novel secondary products of the clusters by salt elimination reactions [52, 64]. $(AlCp^*)_4$ **9** reacted with Al_2I_6 to yield the unusual $Al_5I_6Cp^*_3$ species **38** [65]. A similar thallium–halogen cluster **39** was formed by the reaction of TlCl with $NaSi(CMe_3)_3$ [66].

Reductions The disodium derivative of the tetragallium cluster **10** {$Na_2Ga_4[Si(CMe_3)_3]_4(THF)_2$ **40**} was obtained by reduction of **10** or $(Me_3C)_3SiGaCl_2(THF)$ with elemental Na [Eq. (8)] [52]. If we assume a complete electron transfer from Na to Ga, the compound may be described as a dianion of the corresponding tetrahedral Ga_4 cluster. The additional two electrons cause a considerable distortion, which can be understood by the particular bonding situation in the Ga_4 tetrahedra with a three-fold degenerate set of the lowest unoccupied molecular orbitals. A four-membered butterfly shaped ring resulted which has long transannular Ga···Ga distances of 321 pm, the endocyclic Ga–Ga distance is 243 pm. Compound **40** is an analogue of 1,2-dihydro-1,3-diborets for which a delocalized, nonplanar 2e-aromatic system was verified by quantum-chemical calculations [67]. Alternatively, **40** may be described as an Na_2Ga_4 cluster in which the sodium atoms make an important contribution to the overall stability (see Section 2.3.2).

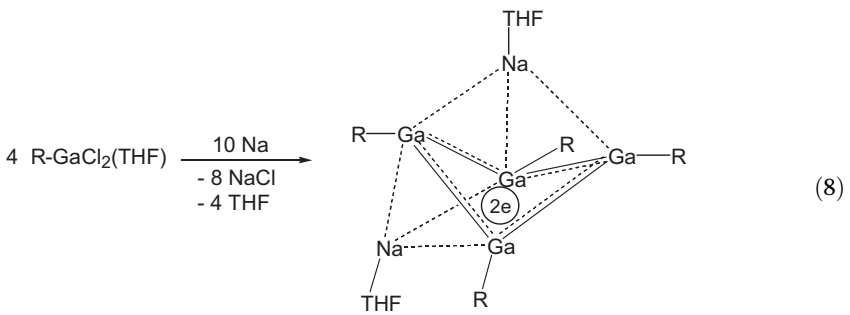

(8)

40: R = $Si(CMe_3)_3$

Coordination chemistry of ER The monomeric fragments E–R are isolobal to carbon monoxide, and many complexes analogous to transition metal carbonyls have been synthesized (**41** to **43**, see Figure 2.3-7) [68]. In most cases these reactions started with those clusters which have a high tendency to dissociate and to form monomers, such as pentamethylcyclopentadienylaluminum(I) or the alkylgallium(I) or alkylindium(I) derivatives. Often the products are isostructural to the respective metal carbonyls, but exceptions are the gallium compounds **44** and **45**.

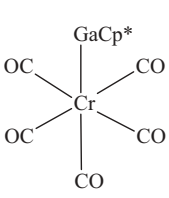

41

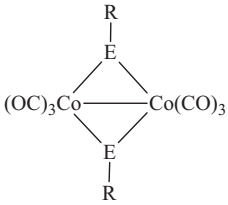

42: E = Al, Ga, In;
R = $C(SiMe_3)_3$, Cp*

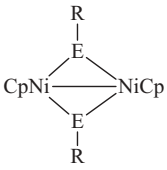

43

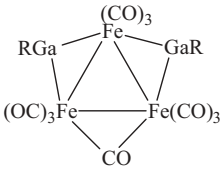

44: R = $C(SiMe_3)_3$

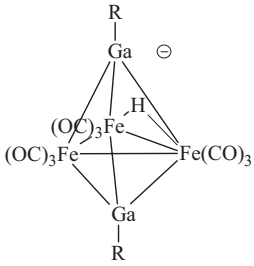

45: R = $Si(SiMe_3)_3$

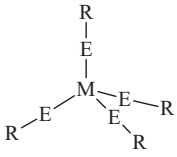

46: M = Ni, E = Ga, R = $C(SiMe_3)_3$
47: M = Ni, E = In, R = $C(SiMe_3)_3$
48: M = Pt, E = In, R = $C(SiMe_3)_3$
49: M = Ni, E = Ga, R = Cp*

Fig. 2.3-7. Representative complexes containing ER ligands.

The cluster **44** formally is an analogue of $Fe_3(CO)_{12}$, in which, however, all edges of the Fe_3 triangle are bridged [69], while **45** is a *closo*-type Fe_3Ga_2 cluster [70].

Particularly interesting are the homoleptic complexes **46** to **49** (Figure 2.3-7) in which Ni or Pt atoms are tetrahedrally coordinated by four Ga–R or In–R ligands [71, 72]. These compounds are analogues of $Ni(CO)_4$. They have relatively short M–Ga or M–In bond lengths, and quantum-chemical calculations verify an effective π-back bonding of electron density from the transition metal atom into the empty p-orbitals of the E-R groups.

Substitutions A substituent exchange has been observed on the treatment of $(AlCp^*)_4$ **3** with lithium bis(trimethylsilyl)amid leading to $(AlCp^*)_3[Al\text{-}N(SiMe_3)_2]$ **50** [73]. The Al–Al distances in the tetrahedron became different, with the shorter ones being to the aluminum atom that is attached to the amido group. This observation is in accordance with the bonding situation in these clusters and reflects

$Ga_8R_8^{2-}$ **51**

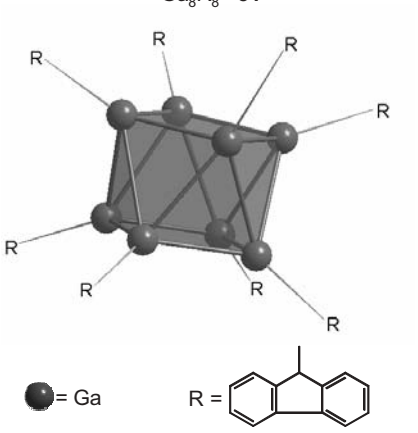

Fig. 2.3-8. Molecular structure of the cluster **51**.

the lower donor capability of the amido group with a less effective transfer of electron density into the LUMOs of the Al–R fragments.

2.3.3.2

Miscellaneous (Neutral and Anionic) Cluster Compounds E_6R_6, E_8R_8, E_9R_9, $E_{12}R_{12}$

Only a few neutral or anionic clusters of the heavier elements of the third main-group are known that have analogues in polyboron chemistry and which do not exhibit a tetrahedral structure. The dianion $[Ga_8R_8]^{2-}$ **51** (R = fluorenyl) was obtained in low yield by the reaction of fluorenyllithium with a metastable GaBr solution (Figure 2.3-8) [74]. Although **51** seems to obey the Wade rules and may be described as a *closo*-cluster, it does not adopt a deltahedral dodecahedric structure similar to the corresponding octaborane compound, but a square antiprismatic structure of the cluster was observed. Quantum-chemical calculations revealed that the antiprismatic structure is the energetically most favorable one. The Ga–Ga distances differ considerably, short ones (252 pm) were observed on the edges of the squares, longer ones (271 pm) resulted for the remaining edges.

The reaction of $GaCl_3$ with $LiCMe_3$ has long been known as a facile method for the synthesis of $Ga(CMe_3)_3$ [75]. Only recently, the dark green Ga_9 cluster compound **52** was isolated as a byproduct in 5% yield [76]. $Ga_9(CMe_3)_9$ **52** possesses a Ga_9 cluster core which adopts a tricapped trigonal prismatic structure (Figure 2.3-9). The shortest Ga–Ga distances were observed to the bridging gallium atoms (259 pm), the longest ones (299 pm) were found in the trigonal prism parallel to the three-fold rotation axis of the cluster and indicate only weak Ga–Ga interactions in that direction.

Cyclovoltammetry revealed a reversible one electron reduction of **52** at −1.74 V referenced to $[Fe(C_5H_5)_2]^{0/+}$. The resulting radical anion **53** was obtained on a

Ga_9R_9 **52**

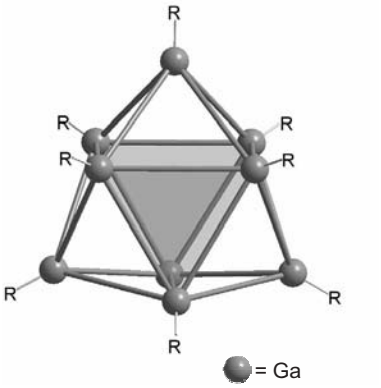

Fig. 2.3-9. Molecular structure of the cluster **52**.

preparative scale in about 80% yield by the treatment of the neutral nonagallium cluster **52** with decamethylcobaltocene [Eq. (9)] [77].

$$\underset{\mathbf{52}}{Ga_9(CMe_3)_9} + Co(C_5Me_5)_2 \rightarrow \underset{\mathbf{53}}{[Co(C_5Me_5)_2]^+[Ga_9(CMe_3)_9]^{\bullet -}} \qquad (9)$$

The overall structure remained almost unchanged with an intact tricapped trigonal prism in the molecular center. However, the transfer of one electron to the cluster resulted in a significant alteration of the Ga–Ga distances, the most important one is the shortening of the long edges of the trigonal prism parallel to the three-fold rotation axis of the molecule from 299 pm in **52** to 282 pm in **53**. Owing to the delocalization of the unpaired electron in the cluster the radical anion is fairly stable and decomposes only at about 190 °C. The bright green crystals can be handled even in air for a short period. A radical anion of an octahedral aluminum cluster, $[Al_6(CMe_3)_6]^-$ **54**, has been detected by means of EPR spectroscopy [78].

One of the first published cluster compounds of the heavier group 13 elements was the *closo*-dodecaaluminate $K_2[Al_{12}iBu_{12}]$ **54** (Figure 2.3-10) [79], which possesses an almost undistorted icosahedron of 12 aluminum atoms with short Al–Al distances (268–270 pm). Up until today, it remained the only homonuclear cluster compound of the elements aluminum to indium which, with respect to structure and cluster electron count, is completely analogous to any boronhydride (see Chapters 1.1.2, 1.1.3, 1.1.5.2, and 2.1.5.6) (in this case: *closo*-$[B_{12}H_{12}]^{2-}$). Compound **54** was formed in small quantities by the reaction of di(isobutyl)aluminum chloride with potassium and was isolated as dark red crystals (Figure 2.3-10).

Compounds similar to B_4Cl_4 or higher boronsubhalides could be stabilized with aluminum or gallium by the formation of adducts with Lewis-bases. Examples are $Al_4X_4(NEt_3)_4$ **55** (X = Br, I) [80] or $Ga_8I_8(PEt_3)_6$ **56** [81]. In contrast to the

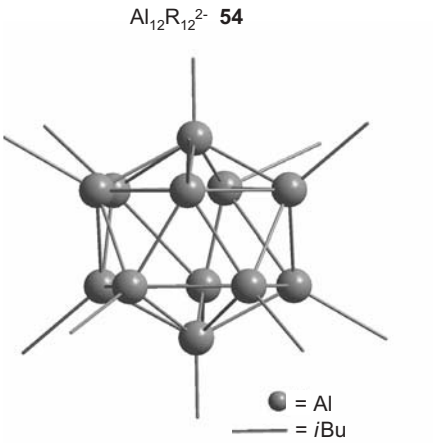

Fig. 2.3-10. Molecular structure of the cluster **54**.

boron compounds, they did not form clusters with delocalized bonding electrons. Instead, rings (Figure 2.3-11) resulted with localized single bonds and aluminum and gallium atoms saturated through coordination. Further subhalides such as $Ga(GaCl_2)_3(GaCl)(Et_2O)_5$ **57** [82] and the similar Al compound $Al_5Cl_7(THF)_5$ [83] (Figure 2.3-11) may also be described by 2e2c bonds.

The reduction of di(neopentyl)gallium chloride with lithium naphthalide was reported to afford the gallium clusters $(Ga\text{-}CH_2CMe_3)_n$, but their structures are hitherto unknown. It was assumed that different species with up to 12 gallium

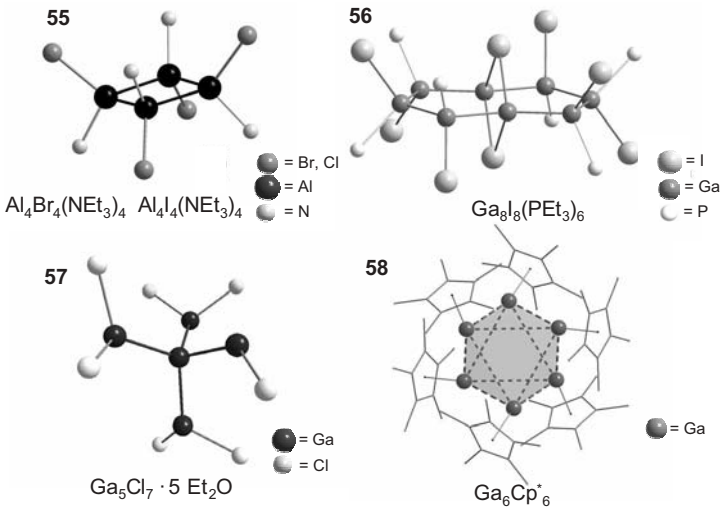

Fig. 2.3-11. Molecular structures of **55**, **56** (only those atoms of the donor molecules are shown that are directly attached to the Ga atoms), **57** (ether molecules omitted) and **58**.

atoms are present. Evidence for the cluster configuration came from some specific reactions [84]. Furthermore, the compounds pentamethylcyclopentadienylgallium(I) **58** [85] and -indium(I) [86] should be mentioned, which adopt an octahedral arrangement of six Ga or In atoms in the solid state (Figure 2.3-11). In contrast to the Al–Al distances in the corresponding tetrameric aluminum derivative **9**, the E–E distances (E = Ga, In) in **58** and its In analogue are rather long and indicate only weak van der Waals interactions. Accordingly, complete dissociation was observed upon dissolution or in the gas phase [57].

2.3.4
Metalloid (Neutral and Anionic) Clusters $E_nR_{m<n}$

Since the large majority of metalloid clusters $E_nR_{<n}$ is observed for the two elements Al and Ga, this section is divided in two parts, including the few clusters for In hitherto known. For many of the metalloid clusters discussed in this section (for a definition of *metalloid* cf. Section 2.3.1, Introduction) the technique of cryochemistry is essential, i.e., trapping of a high-temperature species together with an excess of a suitable solvent in order to obtain a metastable solution. Detailed descriptions and discussions of this technique have been presented recently [7–12].

Ligand-free ''naked'' metalloid clusters detected in the gas phase under high-vacuum conditions present the first step in the development of understanding the size dependence on the physical properties of metals from atoms via nanoparticles to the bulk phase. However, in the main, no structural experimental investigations are available, but quantum chemical calculations have proven useful to supplement such investigations particularly on the questions of topology [87] (see also Chapter 1.1.5.2). In order to obtain experimental details of the structure and to determine the physical properties of structurally known metal atom clusters, such clusters must be protected by ligands and be available in the crystalline form. With the help of such metalloid clusters as intermediates between the metal salt solution and the bulk metal, it should be possible to obtain initial insights into the elementary processes of dissolution and precipitation of metals from solution. To clarify such fundamental questions, however, detailed information on many metalloid clusters with different numbers of ''naked'', non-ligand bearing metal atoms in the cluster core is imperative. Further physical data on compounds with nanostructured metalloid clusters can only be reliably interpreted when a uniform and known arrangement of the metal atoms in the cluster framework is present. Therefore crystalline compounds of metalloid clusters are the primary prerequisite for all investigations.

The next step in the direction of a deeper understanding of nanostructured materials depends on being able to isolate the individual structurally determined cluster units from the crystal lattice and then determine the physical properties of the single clusters in question. This long-term objective has been partially achieved in the gas phase investigation of a structurally determined $Ga_{19}R_6^-$ cluster [$R = C(SiMe_3)_3$] in an FT mass spectrometer (cf. Section 2.3.4.2.5, Ga clusters)

[88]. Further investigations on isolated nanoscale species, for example with microscopic methods on Al and Ga clusters or with the help of quantum mechanical calculations are important tasks for the near future.

2.3.4.1 Metalloid Clusters $Al_nR_{m<n}$

After the first synthesis of tetrahedral clusters of Al (cf. Section 2.3.3.1), the objective was to synthesize metalloid aluminum cluster compounds Al_nR_m with as many "naked" Al atoms, i.e., atoms with no attached groups R, as possible ($n \gg m$). The group $N(SiMe_3)_2$ as R bonded by a 2c2e bond to Al proved to be a particularly favorable species in this endeavor, since it was apparent that the substitution of the halogen atoms X in AlX ($AlX + LiR \rightarrow LiX + AlR$) and the disproportionation of AlX ($3AlX \rightarrow 2Al + AlX_3$) occur in the same temperature range. Reactions in which substitution is favored tend to the formation of oligomeric AlR species [e.g., $(AlCp^*)_4$] **9**, whereas, when substitution is strongly hindered, the formation of aluminum metal through disproportionation of the AlX species is observed.

The size of the Al_n core of metalloid Al clusters is determined by the reactivity of the AlX solution with respect to disproportionation. Therefore for a particular halide X the cluster size can be increased by an increase in temperature. Adding an $LiN(SiMe_3)_2$ solution drop by drop into AlCl solutions for example, the cluster size progresses from the $Al_7R_6^-$ cluster **59** [89] at −7 °C via the $Al_{12}R_6^-$ cluster **60** [90] at room temperature through the $Al_{69}R_{18}^{3-}$ cluster **61** [91] after warming briefly to 60 °C. When, however, adding an $LiN(SiMe_3)_2$ solution into less reactive AlI solutions at room temperature, the partially substituted Al_{14} cluster **62** [92] appears, whereas after warming briefly to 60 °C the $Al_{77}R_{20}^{2-}$ cluster **63** [3] is formed. The clusters mentioned **59**, **60**, **61**, **62**, **63** are extremely sensitive to moisture and air and may even ignite spontaneously after only brief exposure to the atmosphere. Therefore handling these compounds for all physical measurements can be exceptionally difficult (see below). This behavior contrasts dramatically with that of the metalloid noble metal clusters (e.g., ligand-shell bearing Au_{55} and Pd_{145} clusters (cf. Section 2.3.4.1.3) [93, 94]), some of which can be handled in aqueous solution and in contact with air. This different behavior is not surprising since it reflects the difference between precious and base metals.

2.3.4.1.1 Al_7^-, Al_{12}^-, and In_{12} Clusters

The clusters **59** and **60** (Figure 2.3-12) form an Al_n cluster framework, which, amongst others, can be described as a distorted section from the structure of solid aluminum, as is shown in addition in Figure 2.3-12 ("molecular nanostructured element modifications"). The alternative description of cluster **59** as a sandwich compound, wherein an Al^{3+} ion is coordinated by two aromatic $Al_3R_3^{2-}$ rings (cf. $Ga_3R_3^{2-}$, Section 2.3.2), is not confirmed by quantum chemical calculations [89].

A similar arrangement of 12 metal atoms as in **60** is observed in the $In_{12}R_8$ cluster (R = Si*t*Bu$_3$) **60a** (Figure 2.3-12) [95]. **60a** is prepared by thermolysis of

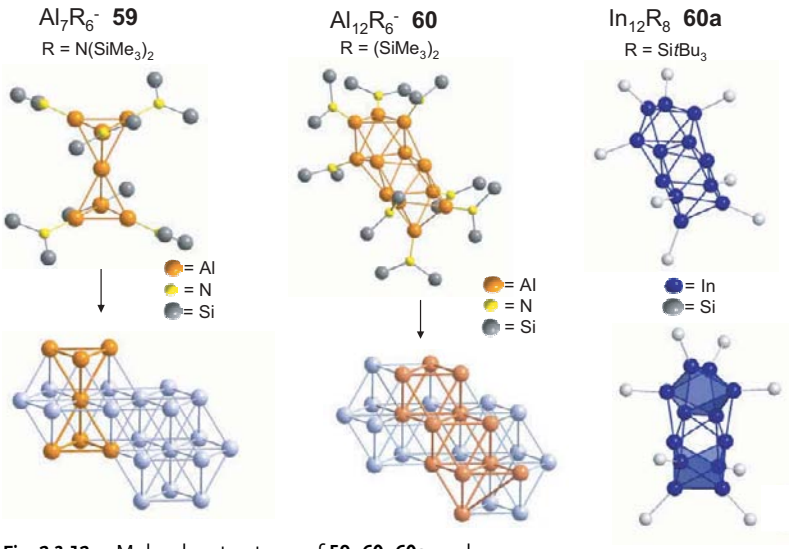

Fig. 2.3-12. Molecular structures of **59**, **60**, **60a**, and topological relationships of **59** and **60** to the corresponding sections from the solid-state structure of elemental aluminum, and structural similarities of the clusters $Al_{12}R_6^-$ and $In_{12}R_8$. In the latter cluster the octahedral sections are highlighted.

In_2R_4 (cf. Section 2.3.3.1). It seems plausible that the larger substituent $SitBu_3$ protects the larger In_{12} entity in contrast to the situation between the Al_{12} core and the $N(SiMe_3)_2$-ligand in **60**. The bonding in **60a** is also described as metalloid since the structure of elemental In exhibits a distorted close packing. Nevertheless, the Wade-Mingos rules can also be applied for the rationalization of the cluster arrangement [5, 95].

2.3.4.1.2 Al_{14} Cluster

The relationship of the "wheel-rim-type" structure of **62** to the metal can be demonstrated by a 30° rotation of the two centered Al_6 rings followed by a shift of the six rings towards each other (cf. Figure 2.3-13) [92]. The other possibility of the formation of an Al_{14} polyhedron with D_{6d} point symmetry by displacement of the two "naked" central atoms in the direction of a polyhedral entity has been shown to be energetically unfavorable by quantum chemical calculations: i.e., the observed metalloid structure (Figure 2.3-13) is favored over the anticipated polyhedral structure as described by Wade-Mingos [5, 96] (see Chapter 1.1.2).

2.3.4.1.3 Al_{69} and Al_{77} Clusters

The principle and the significance of metalloid clusters for the understanding of the formation of metals are made clear by the two largest Al clusters **61** and **63**, which have almost the same size as the 69 and 77 Al atoms and 18 and 20 $N(SiMe_3)$ groups [3, 91]. In both cases the Al atoms are arranged in "shells" (Fig-

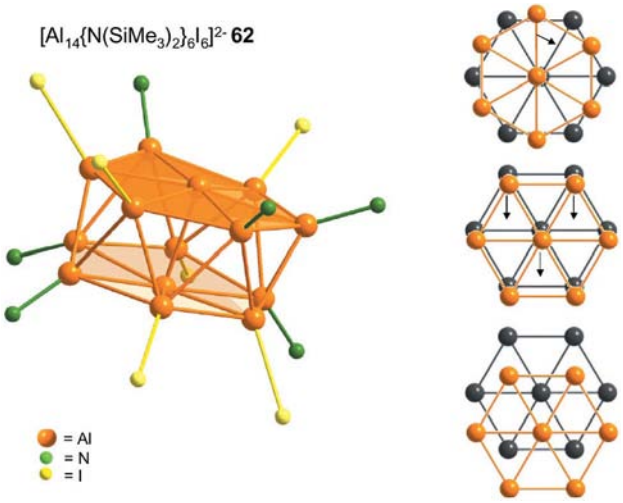

Fig. 2.3-13. Molecular structure of **62** and relationships to Al metal (transformation of the position of the Al atoms of **62** in the direction of the closest packing in the bulk metal).

ure 2.3-14), whereas a central Al atom is surrounded by 12 nearest Al neighbors. The coordination number of the Al atoms and the mean Al–Al distances in a shell decrease from the center to the periphery, indicating that the Al–Al bonds have become more localized and have more molecular character from the inside to the outside. Despite these similarities, the coordination spheres of the central Al atoms of both clusters are significantly different. The Al_{13} core of **61** can be described as distorted D_{5h} (this geometry is often described as decahedral) [96] whereas the central Al atom in the Al_{77} cluster **63** has been shown to have an icosahedral coordination sphere that is distorted in the direction of a cuboctahedron. In both clus-

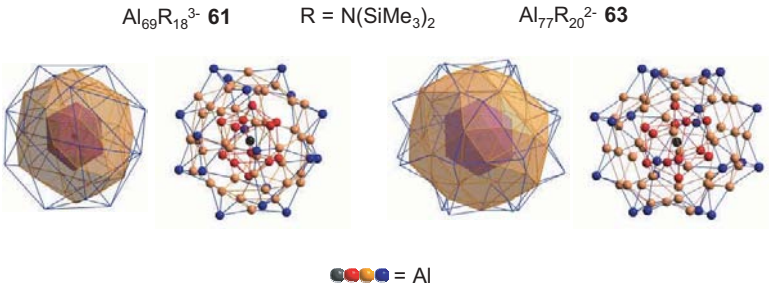

Fig. 2.3-14. Arrangement of the Al atoms in the metalloid clusters **61** and **63** in a stick-and-ball and a shell-like representation with different colors for the different shells: **61** (1 + 12 + 38 + 18 Al atoms); **63** (1 + 12 + 44 + 20 Al atoms). The blue-colored outer shell Al atoms form 2c2e bonds connected with 18 and 20 $N(SiMe_3)_2$ groups, respectively, (not shown for clarity).

ters the Al–Al distances from the center to the first Al_{12} shell and those within this shell are nearly identical [9].

Therefore both cases show a different geometry if compared with noble metal clusters [97]: in the case of $[Au_{55}Cl_6(PR_3)_{12}]$ [93] a cuboctahedral and icosahedral environment was postulated for the central Au atom (an experimental structural analysis of this cluster species has not been reported so far) and for the Pd_{55} framework of "naked" Pd atoms in the center of the $[Pd_{145}(CO)_{60}(PR_3)_{30}]$ cluster [94] a virtually undistorted icosahedral Pd_{13} unit was observed; i.e., the Pd–Pd distances between the central Pd atom to the first Pd_{12} shell is about 5% smaller than within this shell. This demonstrates that these large metalloid clusters (Al_{69}, Pd_{145}, Al_{77}, and a larger Ga_{84} cluster that will be described in Section 2.3.4.2.4), for which structural data are available, exhibit significant differences in the core-shells both amongst the clusters themselves and to the corresponding bulk metals. However, in all cases the distance of the 12 nearest neighbors to the central atom is shorter than that in the bulk metal, indicating that the bonding in these clusters has shifted away from being predominantly delocalized in the metal in the direction of localized molecular bonding (see Chapter 1.1.5.3).

Interestingly, even small changes in the cluster shells of the Al_{69} and Al_{77} clusters, which are probably too small to be observed with common nanoscopic methods (e.g., AFM: atomic force microscopy), lead to changes in the topology of the metal framework at the center, which, consequently, should then affect the electronic properties [91, 98]. These observations also imply that different surface reactions may lead to different topological changes within the interior of the metal down to the nanometer ranges.

In order to understand the topology and the packing density of **61** and **63** with respect to metallic aluminum which is formed in every experiment, the atomic volume of the "naked" Al atoms in **61** and **63** was calculated and compared with the volume of a hypothetical molecular Al_{55} section of the fcc Al metal lattice. For a better comparison the same charge of -3 was assumed for the naked Al_{51} (**61a**: $1 + 12 + 38$ Al atoms from **61**) and Al_{57} (**63a**: $1 + 12 + 44$ Al atoms from **63**) species and for an Al_{55} species (**64**: $1 + 12 + 42$ Al atoms from α-Al) (Figure 2.3-15).

For **61a** and **63a** the topology within the experimentally determined structures of **61** and **63**, and for **64** the coordinates of Al metal, were the basis for single point SCF calculations [9, 91]. As a result, the atomic volume decreases in the order **61a** (29.61 Å^3), **63a** (29.51 Å^3), and **64** (29.21 Å^3). This means that the driving force for the formation of the bulk metal and for **64** is the energy gained by the most compact arrangement with the highest possible coordination number of 12 even if the distances are large (2.86 Å for **64** as in the metal). The hypothetical naked clusters **61a** and **63a** are less compact with shorter (more molecular) Al–Al distances and lower coordination numbers.

2.3.4.1.4 Hypothetical β-Aluminum

All previously discussed metalloid Al clusters show that the favored arrangement of Al atoms is a close packing as in the metal, whereby the observed distortions reflect the adaptation of the cluster core to the $(AlR)_n$ "corset". Since the packing

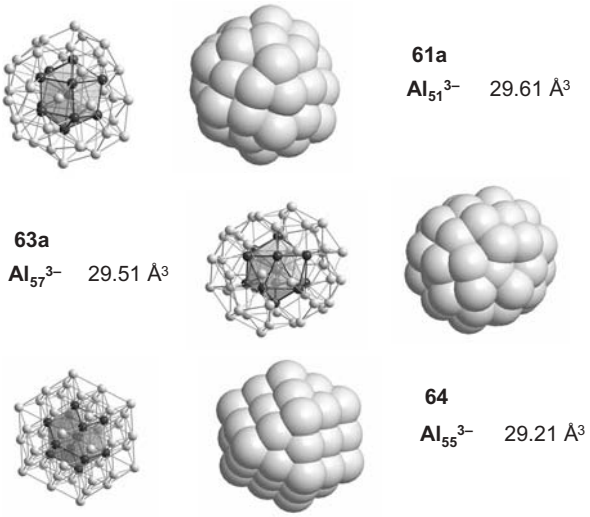

Fig. 2.3-15. Ball-and-stick models and space-filling representations of the Al_n clusters **61a**, **63a**, and **64**.

density comes even closer to that of the metal with increasing cluster size (cf. Section 2.3.4.1.3), it is conceivable that there is an alternative pathway during the early stages of cluster formation that could lead to a less compact modification of aluminum. This hypothesis may not be so unlikely since the other group 13 elements boron and gallium (cf. Section 2.3.4.2.1) also exist in several modifications. An experimental indication for a hypothetical non-metallic β-aluminum modification is given by the results discussed below.

Directly after the condensation of AlX species (X = halogen), for example in the presence of strong donors, the donor-stabilized $Al_4Br_4 \cdot 4NEt_3$ **55** (cf. Section 2.3.3.2) is obtained in which the bonding can be described by means of classical 2c2e bonds [80]. With weaker donors such as THF or THP, the clusters $Al_{22}X_{20} \cdot 12THF$ **65** and $Al_{22}X_{20} \cdot 12THP$ **66** (X = Cl, Br) [99, 100] were obtained which represent the first polyhedral Al subhalides with a unique cluster core (Figure 2.3-16).

The icosahedral Al_{12} core in **65** and **66** is reminiscent of the polyhedral boron subhalides (such as B_4X_4, B_8X_8, B_9X_9, and $B_{12}X_{12}^{2-}$) [101], in which each halogen atom X is directly bonded to a boron atom of the polyhedral framework. In contrast, in the Al_{22} halides **65** and **66**, ten more Al atoms are directly bonded to an Al atom of the icosahedral Al_{12} cluster core, each presenting a unique configuration.

Additionally, the outer ten Al atoms are bonded to two bromine atoms each and saturated by a donor molecule (THF, THP). The apex and base atoms in the Al_{12} icosahedron are not "naked"; they are shielded by one donor molecule each. Despite the great sensitivity of these Al_{22} subhalides **65** and **66**, it was possible to obtain solid-state ^{27}Al NMR spectra and XPS measurements, which showed indeed that three electronically different types of Al atoms are present [100]. The type of

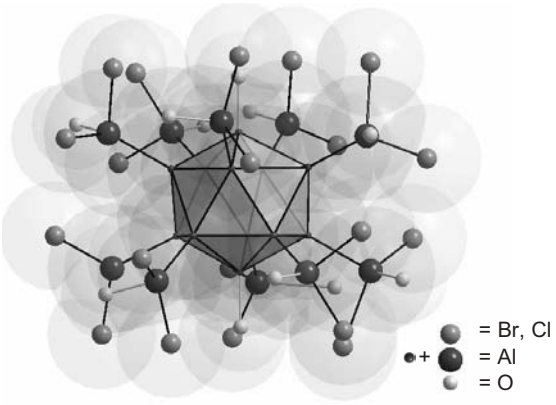

$Al_{22}X_{20} \cdot 12$ THF **65**, $Al_{22}X_{20} \cdot 12$ THP **66**

Fig. 2.3-16. Molecular structure of **65** and **66**. The hydrocarbon framework of the THF and THP ligands has been omitted for clarity.

metal atom topology in **65** and **66** is surprising and has no precedent in molecular chemistry. However, the α-boron structure, which consists of a network of molecular icosahedral cluster units connected by boron–boron bonds, has a similar topologically motif. In order to check the possibility of **65**/**66** of being precursor molecules for a hypothetical non-metallic Al modification with the structure of α-boron, *ab initio* calculations were carried out. The calculations revealed that with an energy-consuming expansion of the closest packed Al atoms in elemental aluminum of about 30% (ca. 33 kJ mol^{-1}) a structure analogous to that of α-boron would be energetically more stable than an expanded fcc lattice [100].

Since contraction in the direction of the bulk metal actually takes place during disproportionation [99, 100], as shown in the discussion of the Al_{69} and Al_{77} clusters **61** and **63** (cf. Section 2.3.4.1.3), the intermediate existence of a β-Al modification with a larger atom volume cannot be excluded.

2.3.4.2
Metalloid Gallium Clusters $Ga_nR_{m<n}$ and Related Indium Clusters

2.3.4.2.1 The Modifications of Elemental Ga

The structurally proven existence of seven modifications for elemental gallium gives rise to the expectation of a larger diversity of metalloid clusters than observed for aluminum, for which only one element modification is hitherto known. In order to classify the topologies of the Ga atoms in all the Ga clusters described below, the most prominent structural features of six of the seven modifications are described in Figure 2.3-17, namely the normal-pressure modifications α-, β-, γ-, and δ-Ga and the high-pressure modifications Ga(II) and Ga(III). Recently, at very high pressure, also Ga(IV) with fcc packing of the Ga atoms has been detected [102].

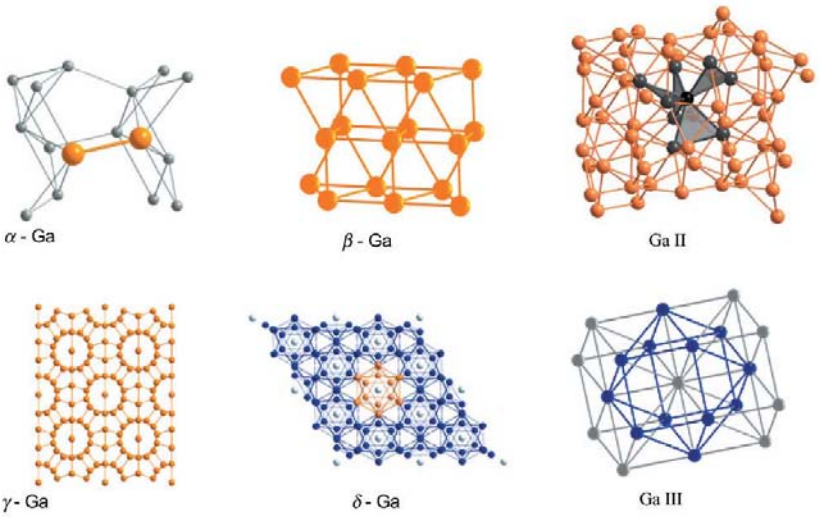

Fig. 2.3-17. Sections of the normal-pressure solid-state modifications α-, β-, γ- and δ-gallium and the high-pressure modifications Ga(II) and Ga(III).

For α-Ga (coordination number $1 + 2 + 2 + 2$) the short Ga–Ga bond distance of 2.45 Å of every Ga atom with one of its seven neighbors is characteristic, so that α-Ga is also described as a molecular metal with Ga_2 dumbbells. For the low-temperature phases β-, γ-, and δ-Ga the following characteristic units are observed: the ladder structure (coordination number $2 + 2 + 2 + 2$) for β-gallium, Ga_7-rings that stack to form tubes and a centered Ga_n "wire", observed for γ-Ga, and interpenetrating Ga_{12} icosahedra for δ-Ga.

In these cases pseudomolecular units can be discerned that indicate a degree of covalent bonding, and therefore similarity to the neighboring element boron. In contrast, in the three high-pressure modifications Ga(II), Ga(III), and Ga(IV) high coordination numbers of Ga atoms are observed (Figure 2.3-17) that point to analogies with packing schemes of "true" metals such as its homologues aluminum [103] and indium [104]. This diversity of bonding options for Ga atoms to each other that is apparent from the different modifications can also be observed in the metalloid or, more comprehensive, elementoid clusters. Thus, the special features of elemental gallium in comparison with elemental boron, aluminum, and indium indicate that it would be less than helpful to describe the metal-rich compounds $E_nR_{m<n}$ of all four elements on the basis of a single rule even though all three have the same number of valence electrons [5].

The lack of a single ordering principle is a shortcoming particularly for the gallium clusters, since there are a larger number of them compared with the corresponding aluminum clusters as a result of their improved synthesis procedures (cf. Section 2.3.3). A purely formal means of classification for the gallium clusters

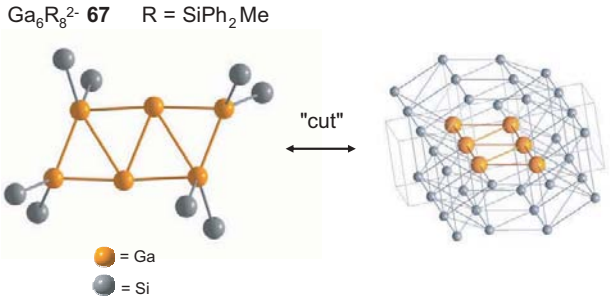

Fig. 2.3-18. Molecular structure of **67** (omitting Ph and Me groups) and the corresponding section from the solid-state structure of β-gallium.

is to take the total number of gallium atoms and their average oxidation number in order to demonstrate analogies to the topologies of the elemental state in the corresponding element modification.

2.3.4.2.2 Ga_6 Cluster

We recently reported on the cluster $Ga_6R_8^{2-}$ (R = $SiPh_2Me$) **67** in which the mean oxidation state of the gallium atoms is +1 [105] (Figure 2.3-18). After cleavage of two R^- groups the formation of an octahedral Ga_6R_6 *precloso* unit analogue to the tetrahedral Ga_4R_4 cluster (cf. Section 2.3.3.1) could be assumed. Model calculations have shown however that a rhomboid Ga_6 unit with two "naked" Ga atoms would be favored over the *precloso* cluster [105].

Similar calculations for the corresponding B_6 and Al_6 compounds, for which the octahedral units are favored, show that the Ga_6 cluster is indeed a special case. The similarity of the arrangement of the Ga atoms to that in β-Ga shows that, in contrast to aluminum and boron, specific connectivity principles predetermined by the element will be favored. The absence of a Ga_6 compound with an octahedral Ga_6 framework [in $Ga_6Cp^*_6$ (Figure 2.3-11) [85] the very long Ga–Ga distances (4.07 und 4.17 Å) show that these bonds must described differently] and the contrast to the many compounds with octahedral B_6 (e.g., $B_6I_6^{2-}$) [106] or Al_6 frameworks ($Al_6R_6^-$, R = *t*Bu) **54** (cf. Section 2.3.3.2) [78] indicate that the topology in certain element modifications and the similar topology in clusters are a result of the special bonding options available to Ga atoms. The description of the cluster $Ga_6R_8^{2-}$ therefore seems appropriate, even though it contains more R groups than Ga atoms as a *metalloid*, or in this case preferably as an *elementoid* (in relation to β-gallium).

2.3.4.2.3 Ga_8, Ga_9 and Related In Clusters

The cluster Ga_8R_6 (R = Si*t*Bu_3) **68** [107] shows a completely different geometry from the antiprismatic $Ga_8R_8^{2-}$ species (R = fluorenyl) **51** [74] and the Ga_8R_6 molecule [R = $C(SiMe_3)_3$] **2** [17] depicted in Figures 2.3-8 and 2.3-1. The Ga cluster framework in **68** is illustrated in Figure 2.3-19 together with the analogue $Ga_8R_6^{2-}$

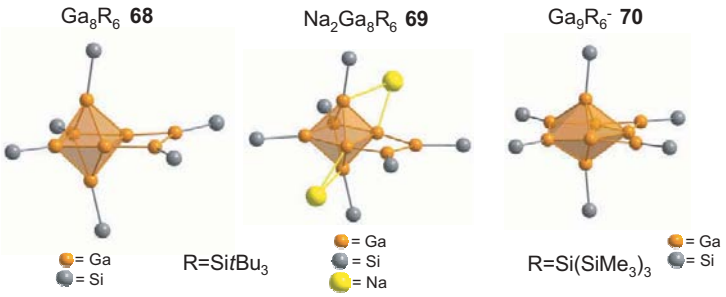

Fig. 2.3-19. Molecular structures of **68**, **69**, and **70** (the Bu^t and $SiMe_3$ groups are omitted for clarity).

dianion in $Na_2Ga_8R_6$ (R = Si*t*Bu$_3$) **69** and the topologically related cluster $Ga_9R_6^-$ [R = Si(SiMe$_3$)$_3$] **70**. Concerning the preparation of **68**, it is to be said that the thermolysis of Ga_3R_4 (R = Si*t*Bu$_3$) **30** in heptane leads not only, according to Scheme 2.3-1 (cf. Section 2.3.3.1.1), to Ga_2R_3 **28** and Ga_4R_4 **10**, but in addition to the octagallane **68** (thermolysis with formation of **10** among others), which with Na in THF may reversibly be reduced to **69**. The nonagallanide **70** on the other hand is prepared from "GaI" [108].

The unexpected Ga_8 framework in the clusters Ga_8R_6 **68** and $Ga_8R_6^{2-}$ **69** can be explained by changing **68** and **69** into the clusters Ga_6R_6 and $Ga_6R_6^{2-}$ in which two R groups are substituted by RGa–GaR. The mentioned hexagallanes can be described by means of the Wade-Mingos rules [5] (cf. Introduction and Chapter 1.1.2) as a *precloso*-hexagallane (Ga_6R_6: $2n \pm 0 = 12$ cluster electrons; one bond in the base of a Ga_5 trigonal-bipyramide capped) and a *closo*-hexagallane ($Ga_6R_6^{2-}$: $2n + 2 = 14$ cluster electrons). In fact, the Ga_6 octahedron in **68** is severely distorted [107].

It is also evident that the planar Ga_6 unit in these two clusters, in particular due to the two "naked" Ga atoms, bears a similarity to that in the above-mentioned $Ga_6R_8^{2-}$ cluster **67**, which is also described as metalloid in relation to β-Ga. The oxidation state of Ga of 0.75 in **68** and 0.50 in **69** in contrast to +1 for $Ga_6R^*{}_8^{2-}$ **67** shows however that reduction has already proceeded extensively in the direction of a three-dimensional connectivity of the Ga atoms as found in elemental Ga (in this case β-Ga). For $Na_2Ga_8R^*{}_6$ **69**, the Ga–Na bond distances of almost 3.00 Å (approximately the sum of the metal radii) indicate that the sodium atoms may be included as part of the cluster framework (cf. $Na_2Ga_3R_3$, **4**, Figure 2.3-2). With an oxidation state of 0.56 for the Ga atom and a structural motif like the icosahedral capped metalloid Ga_{84} cluster [4] (cf. Section 2.3.4.2.4) the cluster $Ga_9R_6^-$ **70** can also be described by means of the Wade-Mingos rules with $2n - 2 = 16$ cluster electrons. Hereafter, the Ga_9 framework is derived from a *closo*-Ga_7 pentagonal-bipyramidal cluster with two bonds of the Ga_5 ring capped by GaR units (cf. Figure 2.3-19).

A completely different arrangement of the metal atoms is observed for the corresponding cluster In_8R_6 (R = Si*t*Bu$_3$) **71** (Figure 2.3-20), which is obtained from

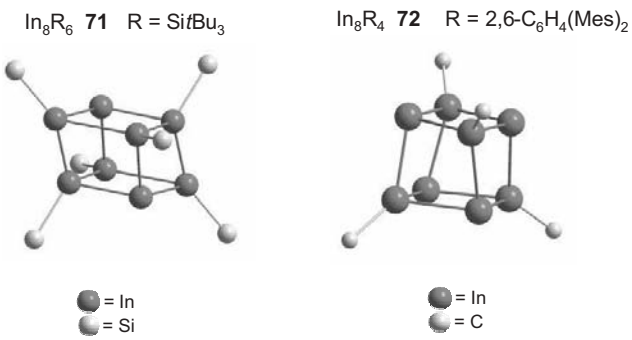

Fig. 2.3-20. Structures of **71** and **72**. Only the C or Si atoms directly bonded to the In atoms are shown for clarity.

$InCp^*$ and NaR [109]. Its structure is described as a cube of eight In atoms lengthened on one space diagonal. Two In atoms on opposite sides are non ligand bearing. According to the Wade-Mingos rules, the octaindane may be described as *hypoprecloso* [95, 109] (In_8R_6: $2n - 2 = 14$ cluster electrons, two capped In_6 octahedranes, cf. Figure 2.3-20). With the bulky 2,6-$C_6H_4(Me_3)_2$ substituent R an octaindane cluster In_8R_4 **72** (Figure 2.3-20) with a cubic array of the In atoms was obtained [110].

2.3.4.2.4 Ga_{12} Clusters

With an increasing number of total Ga atoms and particularly with an increasing number of "naked" gallium atoms it is expected that the topology of the atomic configuration will approach that of the element modifications, which means that metalloid, or often more appropriately elementoid, Ga clusters with mean oxidation states for the Ga atoms decreasing from +1 to 0 will result. In fact, there are obviously no strict limits for the total number of gallium atoms in the metalloid topology. The previous sections described metalloid partial structures for several smaller Ga clusters. Here, we will start with a Ga_{12} cluster for which the distorted icosahedral Ga_{12} unit is reminiscent of analogous *closo*-type compounds discussed in Section 2.3.3 (e.g., $Ga_8R_8^{2-}$, R = fluorenyl **51**; Section 2.3.3.2, Figure 2.3-8).

There is no gallium cluster analogue known which corresponds to the icosahedral $Al_{12}R_{12}^{2-}$ cluster (R = *i*Bu) **54** [79]. However the cluster $Ga_{12}R_{10}^{2-}$ (R = fluorenyl) **73** [111] was recently synthesized which has an icosahedral Ga_{12} framework (Figure 2.3-21). This cluster is formed together with the antiprismatic $Ga_8R_8^{2-}$ cluster **51** during the reaction of GaBr with fluorenyl lithium.

Quantum chemical calculations show that, in contrast to the model compound $Al_{12}H_{10}^{2-}$, the HOMO in a $Ga_{12}H_{10}^{2-}$ cluster is at a particularly unfavorable level for oxidation to the $Ga_{12}H_{12}^{2-}$ species so that the absence of a corresponding $Ga_{12}R_{12}^{2-}$ cluster appears to be plausible. On the other hand for aluminum and indium the metalloid clusters $Al_{12}R_8^-$ **60** and $In_{12}R_8$ **60a** exist in which a section from the close packing of metallic aluminum and indium is realized. Apparently

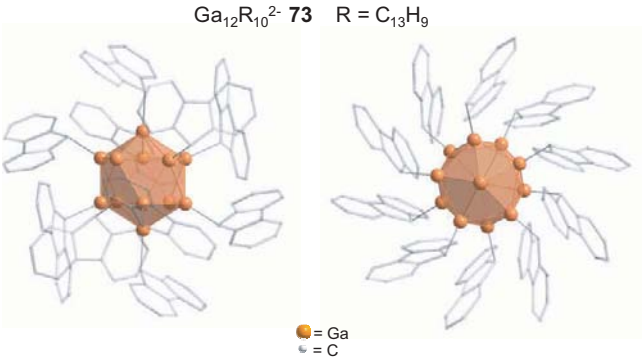

Fig. 2.3-21. Molecular structure **73**.

the formation of a similar structure for a Ga_{12} cluster after the cleavage of two R^- groups ($[Ga_{12}R_{10}]^{2-} \rightarrow [Ga_{12}R_8] + 2R^-$) and rearrangement of the Ga_{12} core is not favorable. The absence of a normal pressure modification with closest packed Ga atoms (in contrast to closest packed structures of elemental aluminum and indium) on the one hand and the realization of the δ-modification for gallium with its interpenetrating Ga_{12} icosahedra on the other, makes this finding of an icosahedrally distorted $Ga_{12}R_{10}^{2-}$ cluster **73** plausible. From this viewpoint the designation metalloid for this cluster is reasonable. The similarity of many Ga cluster compounds to the basic icosahedral framework in α-boron (e.g., the Ga_{84} cluster, Section 2.3.4.2.7) yields the first experimental indications that, in addition to the δ-modification, there may be a hypothetical modification for gallium that resembles α-boron. The most recent quantum chemical band structure calculations [112] based on related previous results [103] revealed that this new phase should be much easier to realize than the above-mentioned β-aluminum phase (cf. Section 2.3.4.1.4) and that the method of disproportionation under mild conditions could enable possible experimental access to this new gallium nonmetallic modification.

2.3.4.2.5 Ga_{10}, Ga_{13}, and Ga_{19} Clusters

Recently two Ga_{10} clusters $Ga_{10}R_6$ [R = $Si(SiMe_3)_3$] **74**, $Ga_{10}R_6^-$ (R = $SitBu_3$) **75** [37] (Figure 2.3-22), and two Ga_{13} clusters $Ga_{13}R_6^-$ **76a** (R = $SitBu_3$) [37] (Figure 2.3-23), $Ga_{13}R_6^-$ [R = $Si(SiMe_3)_3$] **76b** [113] (Figure 2.3-23) and $Ga_{19}R_6^-$ [R = $C(SiMe_3)_3$] **78** [2] (Figure 2.3-24), each of which has six ligands, have been synthesized.

Concerning the preparation of the clusters, it should be noted that "GaI" in toluene/THF with $LiSi(SiMe_3)_3$ or $NaSitBu_3$ gives the decagallane **74** or decagallanide **75** as well as the tridecagallanide **76**. Preparations of **78** start with metastable GaBr solutions (cf. Section 2.3.4).

In the neutral cluster **74** there are two different octahedra (with 4 or 2 ligand-bearing Ga atoms, respectively) connected by a shared edge. On the other hand, in the cluster anion **75** two triangular faces of ligand-bearing Ga atoms, $(GaR)_3$, are

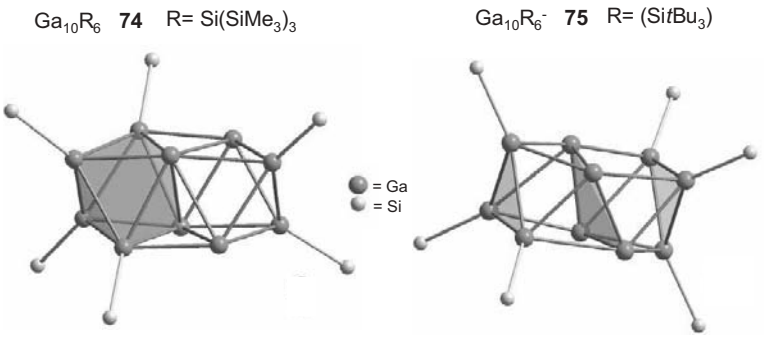

Fig. 2.3-22. Molecular structures of **74** and **75**. Only the Si atoms directly bonded to the Ga atoms are shown.

connected over a rhomboid Ga_4 group. Since both Ga_{10} clusters contain the same number of ligands as the Ga_{13} clusters **76** and in the case of **75** and **76a** even the same type of ligand ($SiBu^t_3$), a detailed comparison of the structures would appear to be appropriate. Unfortunately the structural data for **76a** were only rudimentary so that they could not be included in a database, but the same is not true for isostructural **76b** [113] (Figure 2.3-23).

The seven ''naked'' Ga atoms in **76** form a cube with one missing corner. The three complete square faces of the cube are capped with GaR groups. The three incomplete square faces are shielded by a $(GaR)_3$ group, with the center of the Ga_3 group pointing towards the missing corner of the cube. Schematically, **76** can be regarded, according to the Wade-Mingos rules ($20 = 2n - 6$ cluster electrons), as a four-fold capped *closo*-Ga_9 cluster which is represented by a cube with a Ga_4 face being replaced by a Ga_5 face, whereby three Ga_4 faces and the Ga_5 face are each capped by GaR. The arrangement in **76** is reminiscent of the unique structure of an $SiAl_{14}$ cluster **77** in which a central Si atom is surrounded by a cube of ''naked''

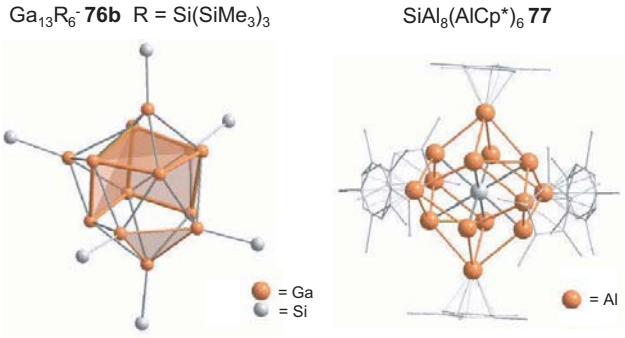

Fig. 2.3-23. Molecular structure of **76b** (only the Si atoms directly bonded to the Ga atoms are shown) and of the metalloid cluster **77**.

Al atoms, the faces of which are each capped by AlR groups (R = Cp*) [114]. In contrast to **76** there is a central atom in the $SiAl_{14}$ cluster **77** (Figure 2.3-23).

In order to determine the atomic volume of the Ga_n framework of the Ga_{10} and Ga_{13} clusters and thereby trace the progress of the formation of the metal, single point SCF calculations were carried out for the anions **75** and **76**, in analogy with the Al clusters (Section 2.3.4.1.3), both containing six $Si(CMe_3)_3$ or $Si(SiMe_3)_3$ groups. The calculations were made on the basis of the experimentally determined geometry of the cluster core and enable the volume of the outer cluster shell to be determined, which is formed by a surface of constant electron density. As anticipated the atomic volume decreases from the Ga_{10} cluster (Ga_{10}^-: 36.9 Å^3 per Ga atom) to the Ga_{13} cluster (Ga_{13}^-: 35.0 Å^3 per Ga atom) by ca. 5% [7]. Since in neither case is there a centered structure, in contrast to $Ga_{22}R_8$ and $Ga_{26}R_8^{2-}$ clusters (see Section 2.3.4.2.6), and since the ratio of the naked to the ligand-bearing Ga atoms is still low (0.66 for **75** and 1.17 for **76**; in contrast to $Ga_{22}R_8$: 1.75 and $Ga_{26}R_8$: 2.2) the mean atomic volumes for **75** and **76** are still about 10% larger than those of the Ga_{22} and Ga_{26} cluster units (cf. Section 2.3.4.2.6). To summarize, it can be concluded that for **75** and **76** with a shell of six GaR groups [$Ga_4(GaR)_6^-$ **75** and $Ga_7(GaR)_6^-$ **76** (Figures 2.3-22 and 2.3-23)] a larger number of "naked" gallium atoms in the core leads to a higher density and therefore a closer resemblance to the bulk material. This principle will become more apparent for clusters with a larger shell of eight GaR groups (cf.: Ga_{18}, Ga_{22} and Ga_{26} clusters, Section 2.3.4.2.6).

Ga_{19} cluster The cluster $Ga_{19}R_6^-$ [R = $C(SiMe_3)_3$] **78** (Figure 2.3-24) in this instance is remarkable for many reasons [2]: (1) it is the only metalloid gallium cluster for which a ^{71}Ga NMR spectrum in solution has been obtained [2]; (2) it is a centered cluster in which the central gallium atom has the same coordination number 12 as in "real" metals [2] and (3) it is the only metalloid gallium cluster

$Ga_{19}R_6^-$ **78** R = $C(SiMe_3)_3$

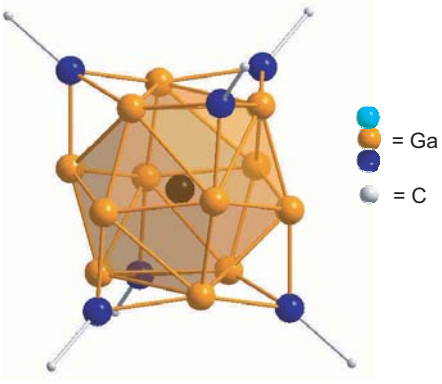

Fig. 2.3-24. Molecular structure of **78** (only the C atoms directly bonded to the Ga atoms are shown).

and, to our knowledge, the largest metalloid cluster ever for which MALDI and ESI mass spectra have been obtained [88]. These experimental findings are fundamental since they mark differences from the large number of investigations on naked metal atom clusters under high vacuum conditions. The first observation of the NMR shift of a central metal atom in a metalloid cluster demonstrates the completely different electronic situation in comparison with naked metal atom clusters, for which more high field shifted NMR signals have only been calculated [2, 88]. Also, the first observation of a structurally known metalloid cluster in the gas phase and its stepwise collision-induced removal of six GaR groups exhibits in a unique way the stabilization of the naked Ga_n cluster core by GaR and not by R substituents. The remarkable stability of the final Ga_{13} anion (**78** $\rightarrow$ 6GaR + Ga_{13}^-) is evident from the large value of the electron affinity of the neutral Ga_{13} cluster (3.35 eV), which is nearly identical to that of the fluorine atom (3.45 eV). Furthermore, this behavior illustrates the electron deficiency of the metalloid Al and Ga clusters and of the formation of several Ga_n Zintl ions [115].

2.3.4.2.6 Ga_{18}, Ga_{22}, and Ga_{26} Clusters

While the above mentioned Ga_{10}, Ga_{13}, and Ga_{19} clusters **74**, **75**, **76**, **78** contain six ligands each, the clusters $Ga_{18}R_8$ (R = Si*t*Bu$_3$) **79** [116] (Figure 2.3-25), $Ga_{22}R_8$ [R = Si*t*Bu$_3$/Si(SiMe$_3$)$_3$/Ge(SiMe$_3$)$_3$] **80** [116, 117, 38, respectively] (Figure 2.3-25), and $Ga_{26}R_8^{2-}$ [R = Si(SiMe$_3$)$_3$] **81** [118] (Figure 2.3-26) have eight R substituents. Concerning the preparation, it should be noted that GaBr in toluene/THF with NaSi*t*Bu$_3$ gives the black Ga_{18} cluster **79** as well as the black Ga_{22} clusters **80**. The Ga_{22} cluster **80** containing Ge(SiMe$_3$)$_3$ ligands and the Ga_{26} cluster **81** were syn-

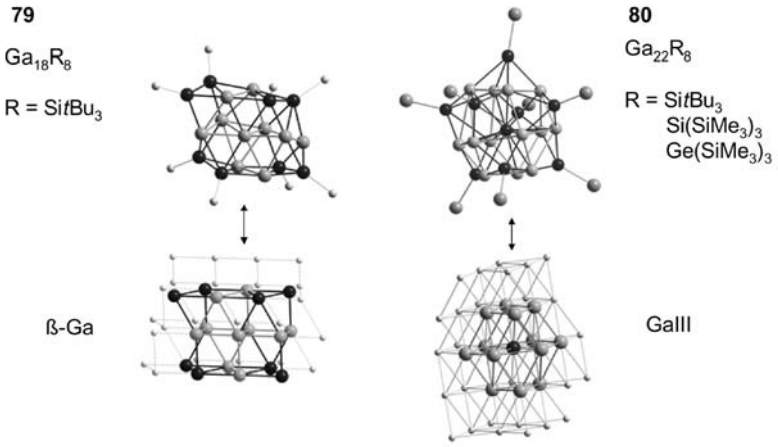

Fig. 2.3-25. Molecular structures of **79** and **80** (only the Si/Ge atoms directly bonded to Ga are shown) and the corresponding sections from the solid-state structures of *β*-gallium and Ga(III).

$Ga_{26}R_8^{2-}$ **81** R = $Si(SiMe_3)_3$

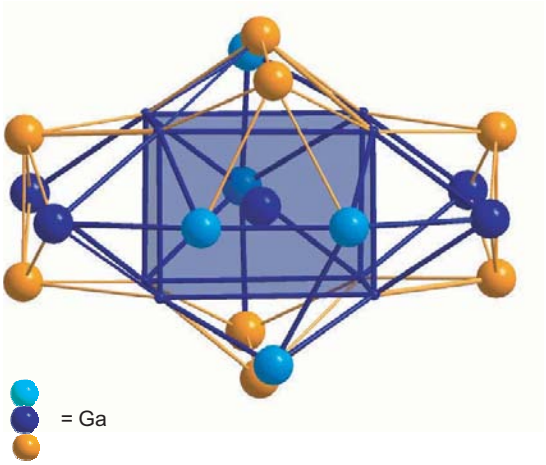

Fig. 2.3-26. Arrangement of the 26 Ga atoms in **81**. The first coordination sphere around the central Ga atom is shown as a polyhedral representation and the Ga atoms attached to a ligand are colored orange.

thesized from "GaI" in the form of black crystals that show, like **79** and **80**, metal luster in reflected light.

Analogous to the results for the Ga_{10}, Ga_{13}, and Ga_{19} clusters (cf. Section 2.3.4.2.5), **79** and **80** should be described as $Ga_{10}(GaR)_8$ and $Ga_{14}(GaR)_8$, which means that inside a cage of eight GaR groups are either 10 or 14 "naked" Ga atoms. A higher packing density was expected for **80** and a smaller mean atomic volume than for **79**. The above-mentioned single point SCF calculations indeed showed that the mean atomic volume decreases from **79** to **80** by about 5%. As a result of the topological similarity of **79** to β-gallium and that of **80** nearly to the high-pressure modification Ga(III) (Figure 2.3-26) and consequently it is not surprising that the experimentally determined density increases by ca. 5% between these two gallium modifications. These considerations are only possible here because a different number of "naked" metal atoms in **79** and **80** are, in our opinion, unique in that they are surrounded by the same number and type of ligands. Since the supersilyl group ($SitBu_3$) is obviously less extended than the hypersilyl group [$Si(SiMe_3)_3$], eight $GaSitBu_3$ groups lead to a cluster pair with 18 or 22 gallium atoms, whereas eight $GaSi(SiMe_3)_3$ ligands lead to a pair with 22 or 26 gallium atoms in **80** and **81**. The cluster core in $Ga_{18}(GaR)_8^{2-}$ cluster **81** (Figure 2.3-26) is particularly reminiscent of the high-pressure modification Ga(III) with its $(4 + 8)$ coordination.

The Ga_{26} cluster **81** can be described as being built up of a Ga_{18} unit, existing as a central Ga atom which is surrounded by a pseudo cubooctahedron of $(8 + 3 + 2 = 13)$ Ga atoms. The remaining four "naked" Ga atoms are part of two Ga_4R_2 units that are located over two Ga_4 faces of the Ga_{14} core [118].

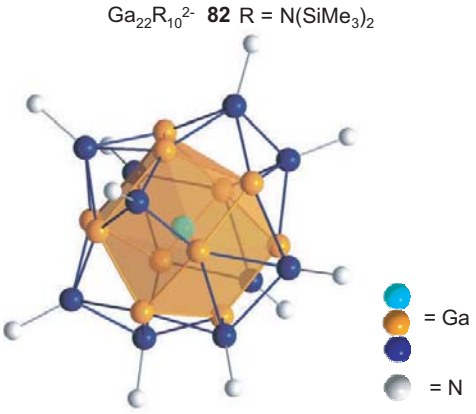

Fig. 2.3-27. Molecular structure of **82** (only the N atoms directly bonded to the Ga atoms are shown). The first coordination sphere around the central Ga atom is shown in a polyhedral representation.

A further Ga_{22} cluster Since it was possible to obtain the Ga_{22} cluster compounds **80** discussed in the above subsection with three different ligands, it is apparent that this electronic configuration is particularly stable, which can be assigned, among others, to the closed jellium configuration with 58 electrons ($14 \times 3 + 8 \times 2$) [117]. Recently we were able to isolate another Ga_{22} compound for which this stability criterion also applies, but where despite the same mean oxidation state of the gallium atoms a different arrangement of the 22 gallium atoms is observed. The use of "slender" $N(SiMe_3)_2$ ligands means that ten instead of eight ligands can fit in the outer shell so that the $Ga_{22}R_{10}^{2-}$ cluster [R = $N(SiMe_3)_2$] **82** results [119]. The shell construction Ga–$Ga_{11}(GaR)_{10}$ in **82** is depicted in Figure 2.3-27.

Quantum chemical single point calculations for the Ga_{22} cluster cores of **82** and **80** show that in the transition from **82** to **80** the atomic volume in the Ga_{22} unit decreases by 2% [119]. Perhaps this shrinkage in volume signalized an intermediate packing on the way from the β-modification ($2 + 6$ coordination) to the high-pressure Ga(III) modification ($4 + 8$ coordination). This "phase transition" of a Ga_{22} unit is associated with an energy increase of 9 ± 5 kJ mol^{-1} (calculated from single point SCF calculations) and is therefore in agreement with the relationship of the high-pressure fcc gallium phase [Ga(IV)], which is only a few kJ higher in energy, to the β-gallium modification [103].

2.3.4.2.7 The Ga_{84} Cluster

Under similar reaction conditions used for the synthesis of the above-mentioned $Al_{77}R_{20}^{2-}$ cluster **63**, the Ga_{84} cluster $Ga_{84}R_{20}^{4-}$ [R = $N(SiMe_3)_2$] **83** [4], is obtained from a metastable GaBr solution and $LiN(SiMe_3)_2$. The molecular structure of **83** is illustrated in a similar fashion to that of **63** in Figure 2.3-28(a).

$Ga_{84}R_{20}^{4-}$ **83** R = $N(SiMe_3)_2$

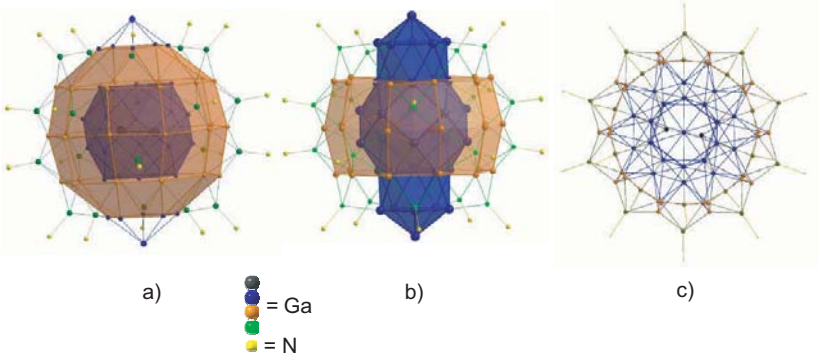

Fig. 2.3-28. Molecular structure of **83** [only the N atoms (yellow) directly bonded to the Ga atoms are shown]. (a) Layered representation analogous to the representation of the Al_{77} cluster, (cf. Figure 2.3-14). (b) Representation corresponding to the relationship of the bond lengths within the Ga_{84} cluster. (c) View along the axis through the top and bottom Ga atom (a, b) and orthogonal to the central Ga_2 unit.

With respect to the "naked" metal atoms, this is the largest metalloid cluster that has ever been structurally determined by diffraction methods. The Ga_2 unit in the center of the 64 "naked" Ga atoms is remarkable and unique in this entire field of chemistry [Figure 2.3-28(c)]. The Ga_2 unit, which contains a bond that is almost as short (2.35 Å) as the above-mentioned Ga–Ga triple bond (2.32 Å) and resembles the Ga_2 unit of α-Ga (2.45 Å), is surrounded by a Ga_{32} shell in the form of a football with icosahedral caps [see δ-Ga (Figure 2.3-17)]. The apex and base atoms of this Ga_{32} unit are "naked" and are oriented towards each other in the crystal in an unusual fashion (see below). The Ga_2Ga_{32} unit is surrounded by a "belt" of 30 Ga atoms that are also "naked". Finally the entire Ga_{64} framework is protected by 20 GaR groups.

The high pseudosymmetry of the cluster molecule **83**, clearly shown in Figure 2.3-28(c), which resembles the approximate five- and ten-fold symmetry of quasicrystals, points to molecular bonding such as that found in the fullerenes. A relationship with the recently published cadmium–gallium phases can also be perceived [120]. On the other hand the spherical layered construction [Figure 2.3-28(a)] shows the analogy with metalloid clusters (e.g., $Al_{77}R_{20}^{2-}$ **63**), so that the bonding in **83** can be described as intermediate between the two extremes.

The arrangement of the Ga_{84} clusters in the crystal is illustrated in Figure 2.3-29. The Ga_{84} clusters are lined up in "tubes".

The distance between two cluster molecules is 1.3 nm, i.e., between the "naked" base and apex of gallium atoms of two clusters, whereby two parallel oriented toluene molecules bridge the intermediate space. Although four-point measurements for electrical conductivity in the temperature range 350 K to 2 K have been carried out, the mechanism of electron conductivity cannot be conclusively explained: **83** is

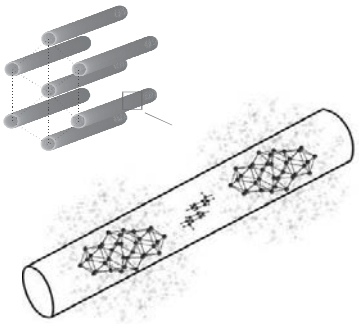

Fig. 2.3-29. Arrangement of the Ga_{84} cluster units **83** in the crystal with two bridging toluene molecules per cluster. The cations are omitted for clarity.

a semiconductor (or a "bad" metal) at room temperature with a small band gap of 0.03 eV; below 7 K **83** becomes superconducting; from recent solid state NMR measurements a metallic conductivity is concluded above 10 K [121, 122]. This question is currently the subject of quantum chemical and experimental investigations. In addition, with the help of synchrotron radiation we hope to clarify the question of the possible rotation of the central Ga_2 unit and finally for the very first time for a metalloid cluster to determine the electron density distribution by experimental methods. The prerequisites for such fundamental investigations are given, since excellent crystals containing **83** can be obtained in good yields using all methods outlined above.

2.3.5 Summary and Outlook

All the results presented here for the heavier elements of group 13 show that there are large differences in the atomic arrangement of aluminum, gallium, indium, thallium, and boron clusters despite the same number of valence electrons. These differences are clearly obvious in the many connectivity possibilities for the atoms in the elements themselves, which means that the element modifications readily show that the bonding in compounds of these elements would be difficult to evaluate according to a single principle (e.g., Wade-Mingos' rules) [5].

Despite this, proven rules for boron clusters can be applied to the smaller metalloid Al, Ga, and In clusters with certain additional assumptions, as recent DFT calculations have shown [87]. In addition, counting rules for smaller Ga and Al metalloid clusters have been developed [123], which will, however, probably not be transferable to the larger clusters. Therefore the first assignment principle presented here for the larger metalloid clusters incorporates the structures of the elements in the various modifications, which means that the metalloid or elementoid clusters are described as nanostructured element modifications.

The development of the synthesis concept described here for metalloid clusters should ultimately be capable of extension to element combinations and therefore molecular nanostructured alloys, as several results on metalloid SiAl and SiGa clusters have shown [114, 88, respectively]. Such mixed clusters resemble the Zintl-type compounds that are under intense investigation by Corbett et al. [115, 124–126].

Many experimental and quantum chemical investigations are required before the final objective of a deeper understanding between the ever-increasing molecular cluster units and the bulk phase can be approached. It is therefore important that as many intermediates as possible are investigated in detail spectroscopically with the nanoscopic methods now available. Since investigations on such sensitive samples as the Al, Ga, and In clusters described here are associated with a large experimental effort, it cannot be expected that results will emerge quickly from the investigations currently in progress. For the near future detailed structural investigations as before on new metalloid clusters, supported by quantum chemical calculations, will provide the main contribution to an understanding of the bonding.

References

1 F. A. Cotton, *Q. Rev. Chem. Soc.*, **1966**, *20*, 397.
2 A. Schnepf, G. Stößer, H. Schnöckel, *J. Am. Chem. Soc.*, **2000**, *122*, 9178.
3 A. Ecker, E. Weckert, H. Schnöckel, *Nature*, **1997**, *387*, 379.
4 A. Schnepf, H. Schnöckel, *Angew. Chem.*, **2001**, *113*, 734; *Angew. Chem., Int. Ed. Engl.*, **2001**, *40*, 711.
5 (a) K. Wade, *Adv. Inorg. Chem. Radiochem.*, **1976**, *18*, 1. (b) R. W. Rudolph, *Acc. Chem. Res.*, **1976**, *9*, 446. (c) R. E. Williams, *Adv. Inorg. Chem. Radiochem.*, **1976**, *18*, 67. (d) D. M. P. Mingos, *Nature*, **1972**, *336*, 99.
6 W. Uhl, *Angew. Chem.*, **1993**, *105*, 1449; *Angew. Chem., Int. Ed. Engl.*, **1993**, *32*, 1386.
7 A. Schnepf, H. Schnöckel, *Angew. Chem.*, **2002**, *114*, 3683; *Angew. Chem., Int. Ed. Engl.*, **2002**, *41*, 3532.
8 H. Schnöckel, A. Schnepf, *Group 13 Chemistry: ACS Symp. Ser.* ACS, Washington, DC, **2002**, *822*.
9 H. Schnöckel, H. Köhnlein, *Polyhedron*, **2002**, *21*, 489.
10 H. Schnöckel, A. Schnepf, *Adv. Organomet. Chem.*, **2001**, *47*, 235.
11 G. Linti, H. Schnöckel, *Coord. Chem. Rev.*, **2000**, *206–207*, 285.
12 C. Dohmeier, D. Loos, H. Schnöckel, *Angew. Chem.*, **1996**, *108*, 141; *Angew. Chem., Int. Ed. Engl.*, **1996**, *35*, 129.
13 H. Schnöckel, *J. Mol. Struct.*, **1978**, *50*, 267.
14 J. Bahlo, H.-J. Himmel, H. Schnöckel, *Angew. Chem.*, **2001**, *113*, 4820; *Angew. Chem., Int. Ed. Engl.*, **2001**, *40*, 4696.
15 W. Uhl, *Z. Naturforsch.*, B **1988**, *43*, 1113.
16 W. Uhl, M. Layh, T. Hildebrand, *J. Organomet. Chem.*, **1989**, *364*, 289.
17 A. Schnepf, R. Köppe, H. Schnöckel, *Angew. Chem.*, **2001**, *113*, 1287; *Angew. Chem., Int. Ed. Engl.*, **2001**, *40*, 1241.
18 R. Köppe, H. Schnöckel, *Z. Anorg. Chem.*, **2000**, *626*, 1095.
19 J. Su, X.-W. Li, R. C. Crittendon, G. H. Robinson, *J. Am. Chem. Soc.*, **1997**, *119*, 5471.

20 (a) Y. Xie, R. S. Grev, J. Ga, H. F. Schäfer III, P. von R. Schleyer, J. Su, X.-W. Li, G. H. Robinson, *J. Am. Chem. Soc.*, **1998**, *120*, 3773. (b) N. Takagi, M. W. Schmidt, S. Nagase, *Organometallics*, **2001**, *20*, 1646. (c) A. J. Bridgeman, L. R. Ireland, *Polyhedron*, **2001**, 2841.

21 A. Saxena, H. Zhang, J. A. Maguire, N. S. Hosmane, A. H. Cowley, *Angew. Chem.*, **1995**, *107*, 378; *Angew. Chem., Int. Ed. Engl.* **1995**, *34*, 332.

22 D. S. Brown, A. Decken, A. H. Cowley, *J. Am. Chem. Soc.*, **1995**, *117*, 5421.

23 H.-J. Himmel, H. Schnöckel, *Chem. Eur. J.*, **2002**, *8*, 2397.

24 X.-W. Li, W. T. Pennington, G. H. Robinson, *J. Am. Chem. Soc.*, **1995**, *117*, 7578.

25 N. J. Hardman, R. J. Wright, A. D. Phillips, P. P. Power, *Angew. Chem.*, **2002**, *114*, 2966; *Angew. Chem., Int. Ed. Engl.*, **2002**, *41*, 2842.

26 N. Wiberg, T. Blank, K. Amelunxen, H. Nöth, J. Knizek, T. Habereder, W. Kaim, M. Wanner, *Eur. J. Inorg. Chem.*, **2001**, 1719.

27 (a) H.-J. Himmel, L. Manceron, A. J. Downs, P. Pullumbi, *Angew. Chem.*, **2002**, *114*, 829; *Angew. Chem., Int. Ed. Engl.*, **2002**, *41*, 796. (b) H.-J. Himmel, L. Manceron, A. J. Downs, P. Pullumbi, *J. Am. Chem. Soc.*, **2002**, *124*, 4448.

28 H.-J. Himmel, H. Schnöckel, *Chem. Eur. J.*, **2003**, *9*, 748.

29 M. Driess, H. Grützmacher, *Angew. Chem.*, **1996**, *108*, 900; *Angew. Chem., Int. Ed. Engl.*, **1996**, *36*, 828.

30 T. Mennekes, P. Paetzold, R. Boese, D. Bläser, *Angew. Chem.*, **1991**, *103*, 199; *Angew. Chem., Int. Ed. Engl.*, **1991**, *30*, 173.

31 M. L. McKee, Z.-X. Wang, P. von R. Schleyer, *J. Am. Chem. Soc.*, **2000**, *122*, 4781; H. Binder, R. Kellner, K. Vaas, M. Hein, F. Baumann, M. Wanner, R. Winter, W. Kaim, W. Hönle, Y. Grin, U. Wedig, M. Schultheiss, R. K. Kremer, H. G. von Schnering, O. Groeger, G. Engelhardt, *Z. Anorg. Allg. Chem.*, **1999**, *625*, 1059.

32 J. Casanova (ed.), *The Borane, Carborane, Carbocation Continuum*, Wiley, New York, **1998**.

33 N. Wiberg, K. Amelunxen, H. Nöth, M. Schmidt, H. Schwenk, *Angew. Chem.*, **1996**, *108*, 110; *Angew. Chem., Int. Ed. Engl.*, **1996**, *35*, 65; A. Purath, C. Dohmeier, A. Ecker, H. Schnöckel, K. Amelunxen, T. Passler, N. Wiberg, *Organometallics* **1998**, *17*, 1894.

34 A. Purath, H. Schnöckel, *J. Organomet. Chem.*, **1999**, *579*, 373.

35 C. Dohmeier, C. Robl, M. Tacke, H. Schnöckel, *Angew. Chem.*, **1991**, *103*, 594; *Angew. Chem., Int. Ed. Engl.*, **1991**, *30*, 564.

36 M. L. H. Green, P. Mountford, G. J. Smout, S. R. Speel, *Polyhedron*, **1990**, *9*, 2763.

37 M. Kehrwald, W. Köstler, A. Rodig, G. Linti, T. Blank, N. Wiberg, *Organometallics*, **2001**, *20*, 860.

38 G. Linti, A. Rodig, *Chem. Commun.*, **2000**, 127.

39 T. Staffel, G. Meyer, *Z. Anorg. Allg. Chem.*, **1987**, *552*, 113; G. Meyer, T. Staffel, *Z. Anorg. Allg. Chem.*, **1989**, *574*, 114.

40 W. Uhl, R. Graupner, M. Layh, U. Schütz, *J. Organomet. Chem.*, **1995**, *493*, C1; R. D. Schluter, A. H. Cowley, D. A. Atwood, R. A. Jones, J. L. Atwood, *J. Coord. Chem.*, **1993**, *30*, 25.

41 W. Uhl, A. Jantschak, W. Saak, M. Kaupp, R. Wartchow, *Organometallics*, **1998**, *17*, 5009.

42 W. Uhl, S. U. Keimling, K. W. Klinkhammer, W. Schwarz, *Angew. Chem.*, **1997**, *109*, 64; *Angew. Chem., Int. Ed. Engl.*, **1997**, *36*, 64.

43 G. B. Deacon, E. E. Delbridge, C. M. Forsyth, B. W. Skelton, A. H. White, *J. Chem. Soc., Dalton Trans.*, **2000**, 745; A. L. Rheingold, L. M. Liable-Sands, S. Trofimenko, *Chem. Commun.*, **1997**, 1691. Further examples for weak Tl–Tl interactions: C. H. Galka, L. H. Gade, *Inorg. Chem.*, **1999**, *38*, 1038; K. W. Hellmann, L. H. Gade, R. Fleischer, T. Kottke, *Chem. Eur. J.*, **1997**, *3*, 1801.

44 W. Uhl, W. Hiller, M. Layh, W.

Schwarz, *Angew. Chem.*, **1992**, *104*, 1378; *Angew. Chem., Int. Ed. Engl.*, **1992**, *31*, 1364.

45 G. Linti, *J. Organomet. Chem.*, **1996**, *520*, 107.

46 S. Schulz, H. W. Roesky, H. J. Koch, G. M. Sheldrick, D. Stalke, A. Kuhn, *Angew. Chem.*, **1993**, *105*, 1828; *Angew. Chem., Int. Ed. Engl.*, **1993**, *32*, 1729.

47 C. Schnitter, H. W. Roesky, C. Röpken, R. Herbst-Irmer, H.-G. Schmidt, M. Noltemeyer, *Angew. Chem.*, **1998**, *110*, 2059; *Angew. Chem., Int. Ed. Engl.*, **1998**, *37*, 1952.

48 J. L. Atwood, S. G. Bott, P. B. Hitchcock, C. Eaborn, R. S. Shariffudin, J. D. Smith, A. C. Sullivan, *J. Chem. Soc., Dalton Trans.*, **1987**, 747.

49 W. Uhl, A. Jantschak, *J. Organomet. Chem.*, **1998**, *555*, 263.

50 E. P. Schram, N. Sudha, *Inorg. Chim. Acta*, **1991**, *183*, 213.

51 N. Wiberg, K. Amelunxen, H.-W. Lerner, H. Nöth, W. Ponikwar, H. Schwenk, *J. Organomet. Chem.*, **1999**, *574*, 246; N. Wiberg, T. Blank, W. Kaim, B. Schwederski, G. Linti, *Eur. J. Inorg. Chem.*, **2000**, 1475; N. Wiberg, K. Amelunxen, T. Blank, H. Nöth, J. Knizek, *Organometallics.*, **1998**, *17*, 5431.

52 N. Wiberg, T. Blank, M. Westerhausen, S. Schneiderbauer, H. Schnöckel, I. Krossing, A. Schnepf, *Eur. J. Inorg. Chem.*, **2002**, 351; G. Linti, W. Küstler, *Angew. Chem.*, **1996**, *108*, 593; *Angew. Chem., Int. Ed. Engl.*, **1996**, *35*, 550.

53 R. Ahlrichs, M. Ehrig, H. Horn, *Chem. Phys. Lett.*, **1991**, *183*, 227; U. Schneider, R. Ahlrichs, H. Horn, A. Schäfer, *Angew. Chem.*, **1992**, *104*, 327; *Angew. Chem., Int. Ed. Engl.*, **1992**, *31*, 353.

54 J. Gauss, U. Schneider, R. Ahlrichs, C. Dohmeier, H. Schnöckel, *J. Am. Chem. Soc.*, **1993**, *115*, 2402.

55 A. Haaland, K.-G. Martinsen, S. A. Shlykov, H. V. Volden, C. Dohmeier, H. Schnöckel, *Organometallics*, **1995**, *14*, 3116.

56 A. Haaland, K.-G. Martinsen, H. V. Volden, W. Kaim, E. Waldhör, W. Uhl, U. Schütz, *Organometallics*, **1996**, *15*, 1146.

57 A. Haaland, K.-G. Martinsen, H. V. Volden, D. Loos, H. Schnöckel, *Acta Chem. Scand.*, **1994**, *48*, 172.

58 S. T. Haubrich, P. P. Power, *J. Am. Chem. Soc.*, **1998**, *120*, 2202; M. Niemeyer, P. P. Power, *Angew. Chem.*, **1998**, *110*, 1291; *Angew. Chem., Int. Ed. Engl.*, **1998**, *37*, 1277.

59 W. Uhl, *Rev. Inorg. Chem.*, **1998**, *18*, 239.

60 W. Uhl, M. Benter, *Chem. Commun.*, **1999**, 771.

61 C. Dohmeier, H. Schnöckel, C. Robl, U. Schneider, R. Ahlrichs, *Angew. Chem.*, **1994**, *106*, 225; *Angew. Chem., Int. Ed. Engl.*, **1994**, *33*, 199.

62 W. Uhl, M. Benter, W. Saak, P. G. Jones, *Z. Anorg. Allg. Chem.*, **1998**, *624*, 1622; W. Uhl, R. Graupner, M. Pohlmann, S. Pohl, W. Saak, *Chem. Ber.*, **1996**, *129*, 143; W. Uhl, M. Pohlmann, *Chem. Commun.*, **1998**, 451; N. Wiberg, T. Blank, K. Amelunxen, H. Nöth, H. Schnöckel, E. Baum, A. Purath, D. Fenske, *Eur. J. Inorg. Chem.*, **2002**, 341.

63 W. Uhl, R. Graupner, W. Hiller, M. Neumayer, *Angew. Chem.*, **1997**, *109*, 62; *Angew. Chem., Int. Ed. Engl.*, **1997**, *36*, 62.

64 W. Uhl, S. Melle, G. Geiseler, K. Harms, *Organometallics*, **2001**, *20*, 3355; W. Uhl, S. Melle, *Chem. Eur. J.*, **2001**, *7*, 4216; W. Uhl, F. Schmock, G. Geiseler, *Z. Anorg. Allg. Chem.*, **2002**, *628*, 1963.

65 C. Üffing, E. Baum, R. Köppe, H. Schnöckel, *Angew. Chem.*, **1998**, *110*, 2488; *Angew. Chem. Int. Ed. Engl.*, **1998**, *37*, 2397.

66 N. Wiberg, T. Blank, H.-W. Lerner, D. Fenske, G. Linti, *Angew. Chem.*, **2001**, *113*, 1275; *Angew. Chem., Int. Ed. Engl.*, **2001**, *40*, 1232.

67 M. Hildenbrand, H. Pritzkow, W. Siebert, *Angew. Chem.*, **1985**, *97*, 769; *Angew. Chem., Int. Ed. Engl.*, **1985**, *24*, 759; S. M. van der Kerk, P. H. M. Budzelaar, A. L. M. van Eekeren,

G. J. M. van der Kerk, *Polyhedron*, **1984**, *3*, 271.

68 C. Dohmeier, H. Krautscheid, H. Schnöckel, *Angew. Chem.*, **1994**, *106*, 2570; *Angew. Chem., Int. Ed. Engl.*, **1994**, *33*, 2482; C. Üffing, A. Ecker, R. Köppe, H. Schnöckel, *Organometallics*, **1998**, *17*, 2373; P. Jutzi, B. Neumann, G. Reumann, H.-G. Stammler, *Organometallics*, **1998**, *17*, 1305; J. Weiß, D. Stetzkamp, B. Nuber, R. A. Fischer, C. Boehme, G. Frenking, *Angew. Chem.*, **1997**, *109*, 95; *Angew. Chem., Int. Ed. Engl.*, **1997**, *36*, 70; D. Weiß, M. Winter, R. A. Fischer, C. Yu, K. Wichmann, G. Frenking, *Chem. Commun.*, **2000**, 2495; P. Jutzi, B. Neumann, L. O. Schebaum, A. Stammler, H.-G. Stammler, *Organometallics*, **2000**, *19*, 1445; D. Weiss, T. Steinke, M. Winter, R. A. Fischer, N. Fröhlich, J. Uddin, G. Frenking, *Organometallics*, **2000**, *19*, 4583; W. Uhl, M. Pohlmann, *Organometallics*, **1997**, *16*, 2478; W. Uhl, S. U. Keimling, M. Pohlmann, S. Pohl, W. Saak, W. Hiller, M. Neumayer, *Inorg. Chem.*, **1997**, *36*, 5478; W. Uhl, S. U. Keimling, W. Hiller, M. Neumayer, *Chem. Ber.*, **1995**, *128*, 1137; W. Uhl, S. U. Keimling, W. Hiller, M. Neumayer, *Chem. Ber.*, **1996**, *129*, 397; W. Uhl, S. Melle, G. Frenking, M. Hartmann, *Inorg. Chem.*, **2001**, *40*, 750.

69 W. Uhl, M. Benter, M. Prött, *J. Chem. Soc., Dalton Trans.*, **2000**, 643.

70 G. Linti, W. Köstler, *Chem. Eur. J.*, **1998**, *4*, 942.

71 W. Uhl, M. Benter, S. Melle, W. Saak, G. Frenking, J. Uddin, *Organometallics*, **1999**, *18*, 3778; W. Uhl, S. Melle, *Z. Anorg. Allg. Chem.*, **2000**, *626*, 2043; W. Uhl, M. Pohlmann, R. Wartchow, *Angew. Chem.*, **1998**, *110*, 1007; *Angew. Chem., Int. Ed. Engl.*, **1998**, *37*, 961.

72 P. Jutzi, B. Neumann, L. O. Schebaum, A. Stammler, H.-G. Stammler, *Organometallics*, **1999**, *18*, 4462.

73 H. Sitzmann, M. F. Lappert, C. Dohmeier, C. Üffing, H. Schnöckel, *J. Organomet. Chem.*, **1998**, *561*, 203.

74 A. Schnepf, G. Stößer, H. Schnöckel, *Z. Anorg. Allg. Chem.*, **2000**, *626*, 1676.

75 R. A. Kovar, H. Derr, D. Brandau, J. O. Callaway, *Inorg. Chem.*, **1975**, *14*, 2809.

76 W. Uhl, L. Cuypers, K. Harms, W. Kaim, M. Wanner, R. Winter, R. Koch, W. Saak, *Angew. Chem.*, **2001**, *113*, 589; *Angew. Chem., Int. Ed. Engl.*, **2001**, *40*, 566.

77 W. Uhl, L. Cuypers, W. Kaim, B. Schwederski, R. Koch, *Angew. Chem.*, **2003**, *115*, 2524; *Angew. Chem., Int. Ed. Engl.*, **2003**, *42*, 2422.

78 C. Dohmeier, M. Mocker, H. Schnöckel, A. Lötz, U. Schneider, R. Ahlrichs, *Angew. Chem.*, **1993**, *105*, 1491; *Angew. Chem., Int. Ed. Engl.*, **1993**, *32*, 1428.

79 W. Hiller, K.-W. Klinkhammer, W. Uhl, J. Wagner, *Angew. Chem.*, **1991**, *103*, 182; *Angew. Chem., Int. Ed. Engl.*, **1991**, *30*, 179.

80 A. Ecker, H. Schnöckel, *Z. Anorg. Allg. Chem.*, **1998**, *624*, 813; A. Ecker, H. Schnöckel, *Z. Anorg. Allg. Chem.*, **1996**, *622*, 149; M. Mocker, C. Robl, H. Schnöckel, *Angew. Chem.*, **1994**, *106*, 1860; *Angew. Chem., Int. Ed. Engl.*, **1994**, *33*, 1754.

81 C. U. Doriat, M. Friesen, E. Baum, A. Ecker, H. Schnöckel, *Angew. Chem.*, **1997**, *109*, 2057; *Angew. Chem., Int. Ed. Engl.*, **1997**, *36*, 1969.

82 D. Loos, H. Schnöckel, D. Fenske, *Angew. Chem.*, **1993**, *105*, 1124; *Angew. Chem., Int. Ed. Engl.*, **1993**, *32*, 1059.

83 C. Klemp, G. Stößer, I. Krossing, H. Schnöckel, *J. Am. Chem. Soc.*, **2000**, *122*, 9181.

84 O. T. Beachley (Jr.), J. C. Pazik, M. J. Noble, *Organometallics*, **1994**, *13*, 2885; O. T. Beachley (Jr.), M. J. Noble, R. D. Allendoerfer, *J. Organomet. Chem.*, **1999**, *582*, 32.

85 D. Loos, E. Baum, A. Ecker, H. Schnöckel, A. J. Downs, *Angew. Chem.*, **1997**, *109*, 894; *Angew. Chem., Int. Ed. Engl.*, **1997**, *36*, 860; P. Jutzi, B. Neumann, G. Reumann, H.-G.

Stammler, *Organometallics*, **1998**, *17*, 1305.

86 O. T. Beachley (Jr.), R. Blom, M. R. Churchill, K. Faegri (Jr.), J. C. Fettinger, J. C. Pazik, L. Victoriano, *Organometallics*, **1989**, *8*, 346.

87 R. Ahlrichs, S. D. Elliot, *Phys. Chem. Chem. Phys.*, **1999**, *1*, 13; W. H. Lam, Z. Lin, *Polyhedron*, **2002**, *21*, 503.

88 K. Weiss, R. Köppe, H. Schnöckel, *Int. J. Mass Spectrom.*, **2002**, *214*, 383; K. Weiss, H. Schnöckel, *Z. Anorg. Allg. Chem.*, **2003**, *629*, 1175.

89 A. Purath, R. Köppe, H. Schnöckel, *Angew. Chem.* **1999**, *111*, 3114; *Angew. Chem. Int. Ed.*, **1999**, *38*, 2926.

90 A. Purath, R. Köppe, H. Schnöckel, *Chem. Commun.*, **1999**, 1933.

91 H. Köhnlein, A. Purath, C. Klemp, E. Baum, I. Krossing, G. Stößer, H. Schnöckel, *Inorg. Chem.*, **2001**, *40*, 4830.

92 H. Köhnlein, G. Stößer, E. Baum, E. Möllhausen, U. Huniar, H. Schnöckel, *Angew. Chem.*, **2000**, *112*, 828; *Angew. Chem., Int. Ed. Engl.*, **2000**, *39*, 799.

93 G. Schmid, *Inorg. Synth.*, **1990**, *7*, 214.

94 N. T. Tran, D. R. Powell, L. F. Dahl, *Angew. Chem.*, **2000**, *112*, 4287; *Angew. Chem., Int. Ed. Engl.*, **2000**, *39*, 4121.

95 N. Wiberg, T. Blank, H. Nöth, W. Ponikwar, *Angew. Chem.*, **1999**, *111*, 887; *Angew. Chem., Int. Ed. Engl.*, **1999**, *38*, 839.

96 J.-Y. Yi, *Phys. Rev. B*, **2000**, *61*, 7277.

97 G. Schmid (ed.), *Cluster and Colloids*, VCH, Weinheim, **1994**; P. Braunstein, L. A. Oro, P. R. Raithby, *Metal Clusters in Chemistry*, VCH, Weinheim, New York, **1999**.

98 X. G. Gong, D. Y. Sun, X.-Q. Wang, *Phys. Rev. B*, **2000**, *62*, 15 413.

99 C. Klemp, R. Köppe, E. Weckert, H. Schnöckel, *Angew. Chem.*, **1999**, *111*, 1852; *Angew. Chem., Int. Ed. Engl.*, **1999**, *38*, 1740.

100 C. Klemp, M. Bruns, J. Gauss, U. Häussermann, G. Stößer, L. van Wühlen, M. Jansen, H. Schnöckel, *J. Am. Chem. Soc.*, **2001**, *123*, 9099.

101 J. A. Morrison, *Chem. Rev.*, **1991**, *91*, 35; W. Hönle, Y. Grin, A. Burkhardt, U. Wedig, M. Schultheiss, H. G. v. Schnering, R. Keller, H. Binder, *J. Solid. State Chem.*, **1997**, *133*, 59.

102 O. Schulte, W. B. Holzapfel, *Phys. Rev. B*, **1997**, *55*, 8122.

103 H. v. Schnering, R. Nesper, *Acta Chem. Scand.*, **1991**, *45*, 870; U. Häusermann, S. Simak, I. Abrikosov, S. Lidin, *Chemistry*, **1997**, *3*, 904; X. G. Gong, G. Chiarotti, M. Parinello, E. Tosatti, *Phys. Rev. B*, **1991**, *43*, 14 277.

104 U. Häussermann, S. I. Simak, R. Ahuja, B. Johansson, S. Lidin, *Angew. Chem.*, **1999**, *111*, 2155; *Angew. Chem., Int. Ed. Engl.*, **1999**, *38*, 2017.

105 A. Donchev, A. Schnepf, E. Baum, G. Stößer, H. Schnöckel, *Z. Anorg. Allg. Chem.*, **2002**, *628*, 157.

106 J. Thesing, J. Baumeister, W. Preetz, D. Thiery, H. G. v. Schnering, *Z. Naturforsch. B*, **1991**, *46*, 800; A. Heinrich, H.-L. Keller, W. Preetz, *Z. Naturforsch. B*, **1990**, *45*, 184; B_6X_6-: V. Lorensen, W. Preetz, F. Baumann, W. Kaim, *Inorg. Chem.*, **1998**, *37*, 4011.

107 N. Wiberg, T. Blank, H. Nöth, M. Suter, M. Warchold, *Eur. J. Inorg. Chem.*, **2002**, *4*, 929.

108 W. Köstler, G. Linti, *Angew. Chem.*, **1997**, *109*, 2758; *Angew. Chem., Int. Ed. Engl.*, **1997**, *36*, 2644.

109 N. Wiberg, T. Blank, A. Purath, G. Stößer, H. Schnöckel, *Angew. Chem.*, **1999**, *111*, 2745; *Angew. Chem., Int. Ed. Engl.*, **1999**, *38*, 2563.

110 B. E. Eichler, N. J. Hardman, P. P. Power, *Angew. Chem.*, **2000**, *112*, 391–393; *Angew. Chem., Int. Ed. Engl.*, **2000**, *39*, 383–385.

111 A. Schnepf, G. Stößer, R. Köppe, H. Schnöckel, *Angew. Chem.*, **2000**, *112*, 1709; *Angew. Chem., Int. Ed. Engl.*, **2000**, *39*, 1637.

112 U. Häussermann, S. I. Simak, R. Ahuja, B. Johansson, *Phys. Rev. Lett.*, **2003**, *90*, 65701–1.

113 J. Steiner, E. Baum, G. Linti, H. Schnöckel, unpublished results on **76b**. Structural data documented: CCDC 180407.

114 A. Purath, C. Dohmeier, A. Ecker, R. Köppe, H. Krautscheid, H.

Schnöckel, R. Ahlrichs, C. Stoermer, J. Friedrich, P. Jutzi, *J. Am. Chem. Soc.*, **2000**, *122*, 6955.

115 J. D. Corbett, *Angew. Chem.*, **2000**, *112*, 682; *Angew. Chem., Int. Ed. Engl.*, **2000**, *39*, 692.

116 A. Donchev, A. Schnepf, G. Stößer, E. Baum, H. Schnöckel, T. Blank, N. Wiberg, *Chemistry*, **2001**, *7*, 3348.

117 A. Schnepf, E. Weckert, G. Linti, H. Schnöckel, *Angew. Chem.*, **1999**, *111*, 3578; *Angew. Chem., Int. Ed. Engl.*, **1999**, *38*, 3381.

118 A. Rodig, G. Linti, *Angew. Chem.*, **2000**, *112*, 3076; *Angew. Chem., Int. Ed. Engl.*, **2000**, *39*, 2952.

119 A. Schnepf, G. Stößer, H. Schnöckel, *Angew. Chem.*, **2002**, *114*, 1959; *Angew. Chem., Int. Ed. Engl.*, **2002**, *41*, 1882.

120 C. P. Gomez, S. Lidin, *Angew. Chem.*, **2001**, *113*, 4161; *Angew. Chem., Int. Ed. Engl.*, **2001**, *40*, 4037.

121 O. N. Bakharev, N. Zelders, H. B. Brom, A. Schnepf, H. Schnöckel, Jos de Jong, *Eur. Phys. J.*, **2003**, *D24*, 101.

122 J. Hagel, M. T. Kelemen, G. Fischer, B. Pilawa, J. Wosnitza, E. Dormann, H. v. Löhneysen, A. Schnepf, H. Schnöckel, U. Neisel, J. Beck, *J. Low Temp. Phys.*, **2002**, *129*(*314*), 133.

123 We have been able to demonstrate that in $E_nX_{n+\gamma}$ subhalides or in the partially substituted subhalide clusters $n - 1/2\gamma$ MOs for E–E bonding are available, which means that 2e2c bonds are only available for $\gamma \leq 0$ (e.g., in ring-shaped Al_4X_4) [80]; C. Klemp, *Dissertation*, Karlsruhe **2000**.

124 Although there are many cases of topological similarity between the Zintl clusters and the metalloid clusters described here, e.g., in the fullerene-type In_{74} cluster of the $Na_{96}In_{97}Ni_2$ phase [114], the differences cannot be overlooked: Zintl-type clusters usually carry a large negative charge (e.g., Tl_{13}^{10-} in $Na_4K_6Tl_{13}$ [115]), and therefore can only be stabilized by the lattice energy from a sea of positive charge. The preparation conditions of these phases show that the great "electron hunger" of group 13 elements can only be satisfied by the strong reductive strength of the alkali metals, and as a result the mean oxidation state for all Zintl-type clusters is negative which is why these clusters are to be found above the Fermi level. In contrast the mean oxidation state of all metalloid Al and Ga clusters described here is positive which means these are compounds that are on the way from the oxidized species (here Al^{1+}, Ga^{1+}) to the metal and the HOMOs of these molecular clusters lie below the Fermi level.

125 C. Sevor, J. D. Corbett, *Science*, **1993**, *262*, 880.

126 G. Cordier, V. Müller, *Z. Naturforsch.*, **1994**, *49b*, 935; Z.-C. Dong, J. D. Corbett, *J. Am. Chem. Soc.*, **1995**, *117*, 6447; Z.-C. Dong, J. D. Corbett, *J. Am. Chem. Soc.*, **1995**, *117*, 6447.

2.4
Discrete and Extended Metal Clusters in Alloys With Mercury and Other Group 12 Elements

Hans-Jörg Deiseroth

2.4.1
Introduction

Covalent metal–metal bonding in clusters is no longer a chemical curiosity as it was in "ancient" times when the dumbbell shaped cation $[Hg_2]^{2+}$ was one of the rare known examples.

Although the number of well characterized cluster compounds with transition metals dominates by far the main group elements, the latter became of increasing importance as materials in basic research due to their unusual structure and bonding properties, which differ significantly from transition metal compounds. Interestingly, however, there has not much attention paid to the cluster chemistry of the group 12 elements, which are formally transition metals but are well known to show typical main group properties too (e.g., closed shell configuration, reduced spectrum of oxidation numbers). It is the main purpose of this chapter to summarize some essential aspects of the present knowledge of clusters with group 12 metals, in particular "anionic mercury clusters" in polar alloys with electropositive metals.

Metal–metal bonded cations of Hg and other group 12 elements, e.g., $[Cd_2]^{2+}$ and $[Hg_3]^{2+}$ are nowadays standard members of inorganic chemistry textbooks [1]. Their existence suggests a certain chemical relationship with subsequent main group elements as the isoelectronic or isosteric species $[In_2]^{4+}$, $[In_3]^{5+}$ and others demonstrate [2]. Based on simple considerations one can rationalize the chemical bonding in these *cationic clusters* by removing electrons from anti-bonding and non-bonding states of the corresponding neutral molecules into appropriate electronic states of the counter anions. On the other hand, a recent theoretical paper [3] based on MO calculations claimed the existence of *anionic ("aromatic") clusters* $[Hg_4]^{6-}$ in the "ancient amalgam" Na_6Hg_4. This compound is one example of a group of related alkali and alkaline earth amalgams with different chemical compositions but comparable structural properties [4]. A basic assumption for the bonding in these solids is an electron transfer *from* the alkali metal *to* the mercury atoms resulting in a (weak!) covalent bond Hg–Hg due to an occupation of low lying bonding p-states [Hg(6p)].

Because the group of *cationic* mercury clusters represents salt like, transparent semiconducting solids (with the exception of the unusual "Alchemist's Gold" $Hg_{2.85}[AsF_6]$ [5]) the ionic description assuming localized electrons in the cations and anions seems appropriate for these compounds. Na_6Hg_4, however, and the above mentioned related solids with "anionic mercury" clusters show metallic properties (luster, magnetism, conductivity). Hence the ionic picture can only be an idealized one and complete electron localization is most unlikely. Keeping in mind this restriction, however, the term "mercurides" is a good approximation for a basic characterization of this group of solids.

The respective alloys treated in the subsequent sections contain alkali metals (in some cases alkaline earth metals) and mercury (Table 2.4-1). From a general viewpoint they are "amalgams" in a classical sense being, however, characterized by well defined chemical compositions and small homogeneity ranges in contrast to alloys in general. Their common structural features are discrete or extended Hg_n clusters (in some cases single mercury atoms) separated by electropositive atoms. In other cases Hg_n polyhedra with single electropositive atoms in the center are a more appropriate basis for the structural description. In any case strong evidence for a *partial* electron transfer from the electropositive atoms to the Hg atoms is present. As a consequence and depending on the respective composition, an ionic bonding contribution between $M^{\delta+}$ and $(Hg_n)^{\delta-}$ results, which is responsible for some special features of the chemical and physical properties. Among these the significant volume contraction (20–30%) upon compound formation and the pronounced increase in the melting points for nearly all compositions M_xHg_y compared with the elemental components M and Hg should be mentioned here. The latter behavior is indicative of a strong heteronuclear interaction between M and Hg atoms compared with the weaker homonuclear one between M and M or Hg and Hg, respectively.

It is known from a variety of crystal structure determinations that the typical interatomic distances d(Hg–Hg) in cationic mercury clusters are significantly smaller (≈250 pm) than in neutral (≈330 pm) and anionic ones (≈300 pm). In a first approximation this is due to a preferred covalent σ_s bonding (strong) in the cationic, a preferred van der Waals bonding in the neutral (weak) and a preferred σ_p bonding (medium) in the anionic forms.

2.4.2
Mercuride Clusters in Amalgams – Conflicts With Zintl's Concept?

2.4.2.1
General

At a first glance the above mentioned electron transfer would require the application of the Zintl concept (designated in a later version as the Zintl-Klemm-Busmann concept [10]) as a tool for understanding the structural properties of alkali and alkaline earth amalgams. In simple words the Zintl concept says that the

Tab. 2.4-1. Summary of alkali metal (M) amalgams containing "anionic" mercury clusters, extended mercury partial structures and/or high coordination number polyhedra.

Li_3Hg	Li_3Bi-type structure, ccp-arrangement of Hg [4]
LiHg	CsCl-type structure [4]
$LiHg_3$	Ni_3Sn-type structure [4]
α-Na_3Hg	Na_3As-type structure, eutactical[a] hcp arrangement of $Hg^{\delta-}$ [4]
β-Na_3Hg	Modified Li_3Bi type, eutactical[a] ccp arrangement of $Hg^{\delta-}$ [4]
α-Na_8Hg_3	Isotypic to Au_8Al_3, stacking variant of an eutactical close packing of $Hg^{\delta-}$ [4]
β,γ-Na_8Hg_3	Similar to β-Na_3Hg, defect variant, disordered [4]
Na_3Hg_2	Unique structure type, square planar $[Hg_4]^{\delta-}$ clusters [4]
α-NaHg	Unique structure type, zigzag chains of condensed rectangular Hg_4 [4]
β,γ-NaHg	NaTl type, diamond-like Hg partial structures [4]
$NaHg_2$	Modified AlB_2 type, graphite-like Hg layers [4]
KHg	KHg type, square planar $[Hg_4]^{\delta-}$ clusters [4]
K_5Hg_7	Unique structure type, extended Hg partial structure [4]
α-KHg_2	KH_2 type, extended partial structure of Hg [4]
β-KHg_2	High pressure phase ($p > 3$GPa) modified AlB_2 type [4]
K_3Hg_{11}	Defect $BaAl_4$ type, extended Hg partial structure [6]
K_2Hg_7	Unique structure type, extended Hg partial structure [7]
K_7Hg_{31}	Isotypical to Ba_7Hg_{31}, extended Hg partial structure [4]
KHg_{11}	Isotypical to $BaHg_{11}$, similar α-Hg, high coordination number polyhedra KHg_{20} [4]
$Rb_{15}Hg_{16}$	Unique structure type with square planar Hg_4 and cube shaped Hg_8 [4]
RbHg	Isotypical to KHg [4]
$RbHg_2$	Isotypical to KHg_2 [4]
Rb_5Hg_{19}	Defect $BaAl_4$ type, extended Hg partial structure [8]
Rb_7Hg_{31}	Isotypical to K_7Hg_{31} [8]
$RbHg_{11}$	Isotypical to $BaHg_{11}$ [4]
CsHg	Isotypical to KHg [4]
$CsHg_2$	Isotypical to KHg_2 [4]
Cs_5Hg_{19}	Isotypical to Rb_5Hg_{19} [6]
Cs_3Hg_{20}	Unique structure type [6]
$NaK_{29}Hg_{48}$	Unique structure type, $NaHg_{12}$ icosahedra, KHg_{12} hexagonal antiprisms [9]

[a] "Eutactical" means topologically equivalent to a close packing of Hg, however, with significantly greater interatomic distances than expected for neutral Hg atoms.

electron accepting atoms in the respective alloys are transferred into a new electronic configuration ("pseudo-atoms") being able to form a partial anionic covalent lattice actually existing or at least reasonable for the respective "pseudo-element" (see Chapter 1.1.4). Limitations, restrictions and sophisticated extensions of this concept are discussed in detail in Refs. [11] and [12] and earlier papers cited therein. Although a consequent validity of the Zintl-Klemm-Busmann concept for group 12 elements was never claimed, it turned out that it is quite useful as a background reference in order to achieve some sensibility for peculiarities of the crystal structures, cluster geometries, and bonding models discussed subsequently.

In amalgams with a high alkali metal content (e.g., Na_3Hg) the electron transfer

to mercury causes a partial population of Hg(6p) states and the formation of either isolated $Hg^{\delta-}$ or small "anionic clusters" $Hg_n^{\delta-}$ embedded in a matrix of $M^{\delta+}$ (M = alkali metal) with bonding angles for Hg–Hg–Hg of around 90°, thus suggesting predominantly σ_p bonding.

With increasing Hg content Hg(6s) states are more and more involved in the homonuclear bonding between Hg atoms. Thus bonding angles Hg–Hg–Hg of around 109° and 120° appear resulting from sp-hybridization. At the same time extended interpenetrating cationic and anionic partial structures and thus a high Coulomb contribution to the overall bonding (e.g., $Na^{\delta+}Hg_2^{\delta-}$) are observed. This shows up predominantly in a significant increase in the melting points of the respective compounds [4].

With further increasing Hg content the transferred charge has to be distributed over more and more Hg atoms thus decreasing the effective charge per Hg and the Coulomb contribution to the lattice energy. The respective compounds become more and more similar to elemental mercury in structure, bonding and chemical properties. Figure 2.4-1 illustrates schematically the gradual change of the bonding properties by showing how the electronic states in selected amalgams of different mercury contents contribute to the "density of states" (DOS). The DOS reflects the energetic sequence of electronic states in a solid very similar to a "molecular orbital" (MO) diagram for molecules. In contrast to the MO levels in an MO diagram each DOS peak, however, consists of a number of narrow (nearly continuous) states determinative for width and height of the respective peak.

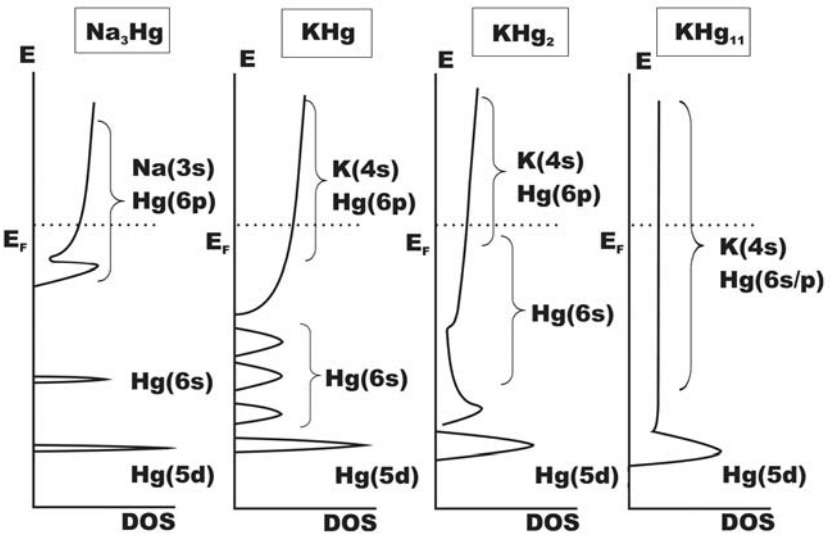

Fig. 2.4-1. A schematic view of the gradual change of the density of states (DOS) with increasing mercury contents (from left to right) for selected alkali metal amalgams. The participation of the respective valence states is marked approximately.

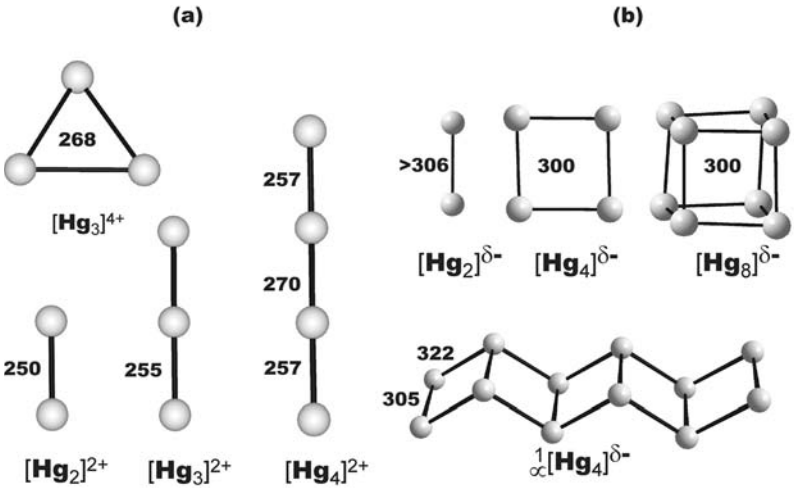

Fig. 2.4-2. A comparison between (a) cationic and (b) small anionic mercury clusters in alkali and alkaline earth amalgams (distances in pm).

2.4.2.2
Small Mercuride Clusters

Up till now anionic mercury clusters have only existed as clearly separable structural units in alloys obtained by highly exothermic reactions between electropositive metals (preferably alkali and alkaline earth metals) and mercury. There is, however, weak evidence that some of the clusters might exist as intermediate species in liquid ammonia [13]. Cationic mercury clusters on the other hand are exclusively synthesized and crystallized by solvent reactions. Figure 2.4-2 gives an overview of the shapes of small monomeric and oligomeric anionic mercury clusters found in alkali and alkaline earth amalgams in comparison with a selection of cationic clusters. For "isolated single mercury anions" and extended network structures of mercury see Section 2.4.2.4.

The smallest possible cluster unit, the dumbbell shaped $[Hg_2]^{\delta-}$, occurs only in the two *alkaline earth* amalgams Ca_5Hg_3 and Sr_3Hg_2 [14, 15]. The $[Hg_2]^{\delta-}$ must not be confused with the $[Hg_2]^{2+}$ cation mentioned in the Introduction (see Figure 2.4-2). Neutral $[Hg_2]^0$ is known as a weakly bonded (van der Waals) gas phase species [16]. The distances d(Hg–Hg) in the anionic $[Hg_2]^{\delta-}$ are somewhat different for Sr_3Hg_2 (341 pm) and Ca_5Hg_3 (306 pm) but significantly greater than in $[Hg_2]^{2+}$ ($\approx$250 pm). An electron transfer into empty p states of the Hg_2 species seems reasonable, at least in Ca_5Hg_3. The amount of electron transfer per mercury atom, however, must be different for both compounds and lower than one, because the bond order of the Hg_2 units was estimated to be only 0.5 in Ca_5Hg_3 and 0.13 in Sr_3Hg_2 [14, 15]. A certain correspondence between $[Hg_2]^{\delta-}$ and the existence of $[Ga_2]$ pairs [d(Ga–Ga) = 247 pm] in elemental gallium may be seen on the background of Zintl's concept.

In contrast to the cationic $[Hg_3]^{2+}$ (linear) [2] and $[Hg_3]^{4+}$ (triangular) [17] isosteric *anionic* $[Hg_3]^{\delta-}$ clusters are unknown.

The *square planar* mercury cluster $[Hg_4]^{\delta-}$ with $d(Hg–Hg) \approx 300$ pm has no correspondence on the cationic side ($[Hg_4]^{2+}$ is linear [2]) and occurs as a discrete cluster unit with nearly ideal D_{4h} symmetry (Figure 2.4-2) in the amalgams MHg (M: K, Rb, Cs [4]) and in Na_3Hg_2. As mentioned in the Introduction, the electronic structure of the latter compound with special focus on the Hg_4 unit was studied recently [3] by MO calculations (Figure 2.4-3). An important result of these calculations was the assumption of three bonding HOMOs formed predominantly by Hg(6p) states ($2 \times \sigma_p$ and $1 \times \pi_p$) and filled with electrons donated by the Na atoms. These MOs are located above the four MOs resulting from a combination of the completely filled Hg(6s) states, which do not provide a net bonding. Based on this idealized ionic formulation for $(Na^+)_6[Hg_4]^{6-}$ a σ/π-aromaticity was claimed for the Hg_4 units in Na_3Hg_2 and compared with the σ/π-aromaticity postulated for $[Al_4]^{2-}$ and others in an earlier publication [18].

Band structure and molecular orbital calculations for CsHg and other compounds [4], however, show the actual electronic situation to be more complicated than described in Ref. [3]. A typical result for CsHg is given in Figure 2.4-4. One can see that the energy levels based predominantly on Hg(6s) combinations are localized (small bandwidth of DOS peaks) and completely filled. On the other hand, the conduction band around the Fermi level originates from a mixing of Hg(6p) *and* Cs(6s) and thus reflects the metallic properties of CsHg. A pseudo gap below the Fermi level is present (between -3 and -1 eV approximately) indicating a ''near-ionic'' bonding situation.

In general an evaluation of the DOS calculations for various amalgams with respect to an electron transfer from alkali metal to mercury shows a net transfer of approximately 0.5 electrons per mercury atom for alkali metal rich amalgams [4, 19]. This value is the result of a donation from the alkali metal atoms to mercury (major component) and a simultaneous back donation (minor component).

The amalgam $Rb_{15}Hg_{16}$ [4] is a unique example of the *simultaneous* occurrence of *square planar* Hg_4 and slightly distorted *cube shaped* Hg_8 clusters (Figures 2.4-2 and 2.4-5). Concerning the model of ''aromaticity'' mentioned above and assuming a complete transfer of electrons from Rb to Hg, it seems that there is no obvious electron counting rule for this compound as it is for Na_6Hg_4. The tetragonal unit cell ($Z = 4$) contains eight square planar Hg_4 and four cube shaped Hg_8, structurally isolated from each other by 60 Rb atoms [intra-cluster $d(Hg–Hg) \approx 300$ pm, inter-cluster $d(Hg–Hg) > 400$ pm).

A special situation occurs for the amalgam NaHg which crystallizes completely different from the MHg alloys mentioned above and occurs as a function of temperature in three modifications [4]. In the room temperature modification α-NaHg the mercury atoms form one-dimensional zigzag chains of condensed rectangular Hg_4 units [$d(Hg–Hg) \approx 300$ pm, Figure 2.4-2] isolated by Na atoms from each other. The structural relation to the CsCl type based on a group–subgroup relation is discussed elsewhere [18]. Neglecting for a moment the obvious metallic properties of α-NaHg and regarding the Na–Hg interaction as purely ionic (Na^+Hg^-) one

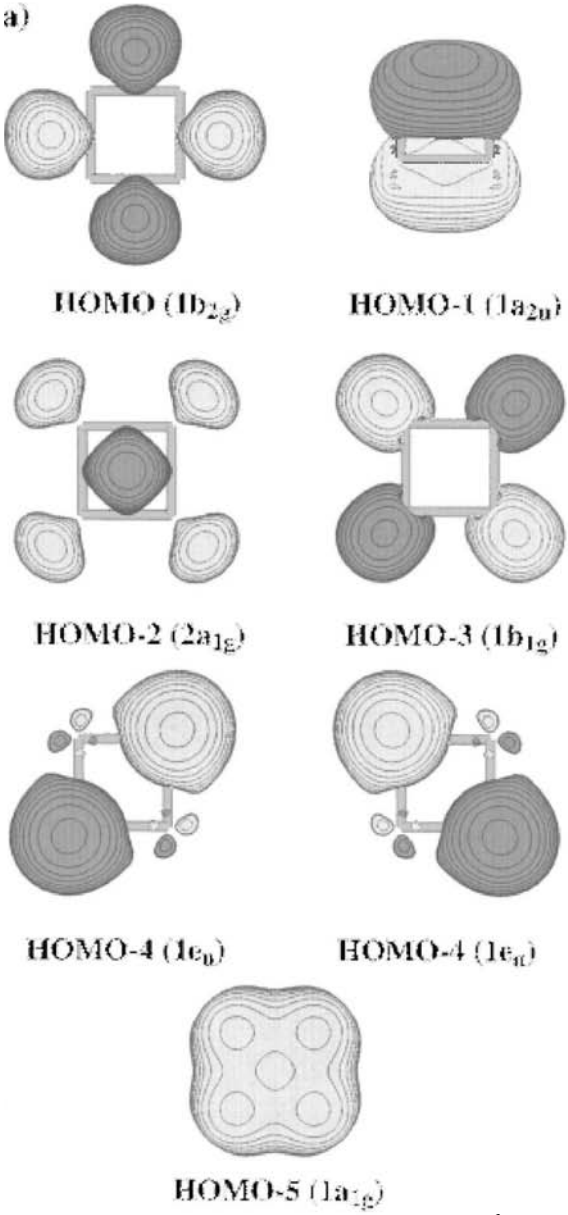

Fig. 2.4-3. Molecular orbitals for the "aromatic" $[Hg_4]^{6-}$ (taken from [3]).

could treat the Hg atoms as formally *three bonded* and thus as atoms of an electron deficient "pseudo-element" of group 13 with the formal charge −1. There is, however, no such crystal structure of a group 13 element known! Even more puzzling is the situation for the high temperature modification γ-NaHg which crystal-

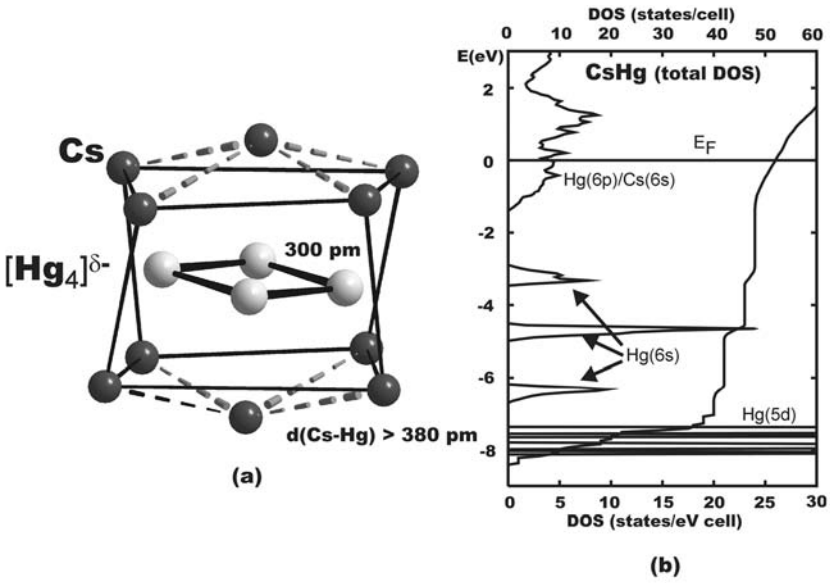

Fig. 2.4-4. (a) Typical first coordination sphere surrounding of square planar Hg_4 clusters in CsHg and (b) a density of states (DOS) representation for this compound.

lizes in the undistorted cubic NaTl type structure with *seemingly four-coordinated* mercury. β-NaHg is a slightly distorted rhombohedral variant of γ-NaHg with more or less the same structure. The reason for the distortion is unknown.

2.4.2.3 Single "Mercuride" Ions?

Unlike CsAu (Cs^+Au^-, CsCl type structure) and others [20] which are "aurides" with well defined Au^- ions, CsHg and similar amalgams are not simple "mercurides" but have more complicated structure and bonding properties, as was shown in Section 2.4.2.2.

Na_3Hg (α, β) and Na_8Hg_3 (α, β, γ), however, constitute a small group of sodium rich solids, which could be termed "mercurides" in a good approximation. They were studied in detail in the course of a series of single crystal structure investigations as a function of temperature [4]. In these solids "isolated" mercury atoms are exclusively surrounded by alkali metal atoms in their first coordination sphere (Figure 2.4-6), with the shortest distances d(Hg–Hg) greater than 500 pm and thus longer than in elemental mercury or typical small mercury clusters ($\approx$300 pm, see Section 2.4.2.2). Without stressing too many details of the crystal structures and phase transitions of these low melting solids, it is remarkable that they crystallize in structures which are characteristic for small gap ionic semiconductors (such as $Na_3As = 3Na^+As^{3-}$ and $Li_3Bi = 3Li^+Bi^{3-}$). Indeed DOS calculations for α-Na_3Hg

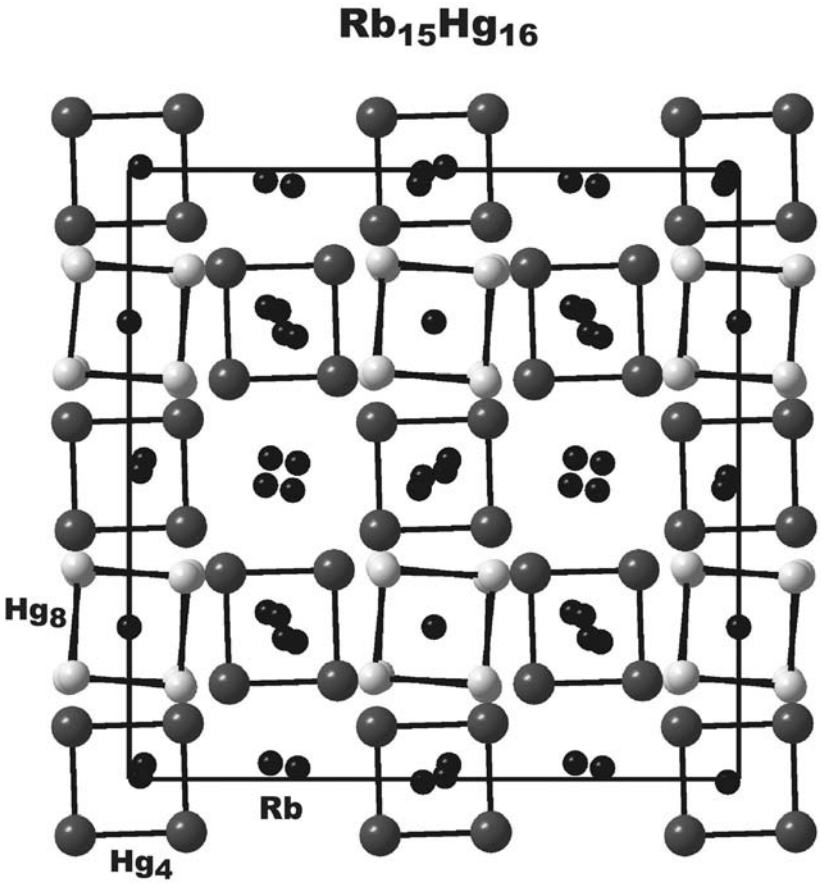

Fig. 2.4-5. The crystal structure of $Rb_{15}Hg_{16}$ projected along [001] (Hg_8: cubes, Hg_4: squares).

show this amalgam to be ''near-ionic'' with a pseudo gap below the Fermi level (-5 eV $< E < -2$ eV, Figure 2.4-6). The electronic states around the Fermi level result from interactions between Hg(6p) and alkali metal valence states. Furthermore, the low lying completely filled Hg(6s) appear as localized states hardly participating in the heteronuclear bonding between Na and Hg. As partial DOS calculations show, the pronounced peak at about -1.5 eV results from partly localized Hg(6p) and Na(3s) electrons [21]. It must be emphasized again at this point that the charge per Hg atoms is far from -3 (as for As in Na_3As) but in the order of -0.5.

The picture just outlined for α-Na_3Hg (Na_3As type) can be transferred to β-Na_3Hg (Li_3Bi type) and to the three modifications of Na_8Hg_3 which crystallize in an ordered defect variant of an A_3B structure [4].

LiHg is one of the MHg amalgams (together with SrCd, BaCd, SrHg, and BaHg [22]) which crystallizes in an undistorted CsCl structure. The term ''mercuride'' is

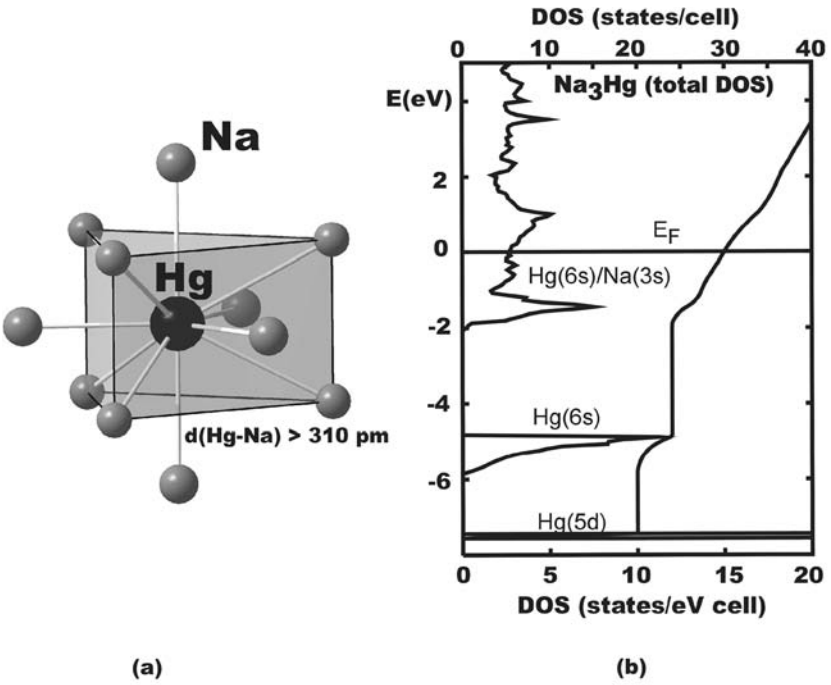

Fig. 2.4-6. (a) The typical first coordination sphere of "isolated" Hg atoms in α-Na_3Hg and (b) a DOS representation for this compound.

again an idealization and does not account for the metallic properties of LiHg. The shortest distances d(Hg–Hg) are 332 pm, being slightly longer than in most of the cluster units discussed above (e.g., $[Hg_4]^{\delta-}$, $[Hg_8]^{\delta-}$) but significantly shorter than in Na_3Hg with isolated $Hg^{\delta-}$.

2.4.2.4 Extended Anionic Partial Structures of Mercury

There is a group of alkali metal amalgams with medium mercury content which contain extended mercury partial structures. As mentioned previously, although an electron transfer plays an important role for the existence of and the chemical bonding in these amalgams, they can only be discussed partly with respect to Zintl's concept. Their structures are related to those of other intermetallics from main group metals exhibiting typical s,p-bonding properties, in a sense as discussed in [11].

γ-NaHg, the high temperature modification of this compound (see Section 2.4.2.3), is a typical example of a compound with s,p-hybridized mercury atoms. It crystallizes in an undistorted cubic NaTl structure, hence as a classical Zintl phase with mercury forming a diamond like three-dimensional network [d(Hg–Hg) =

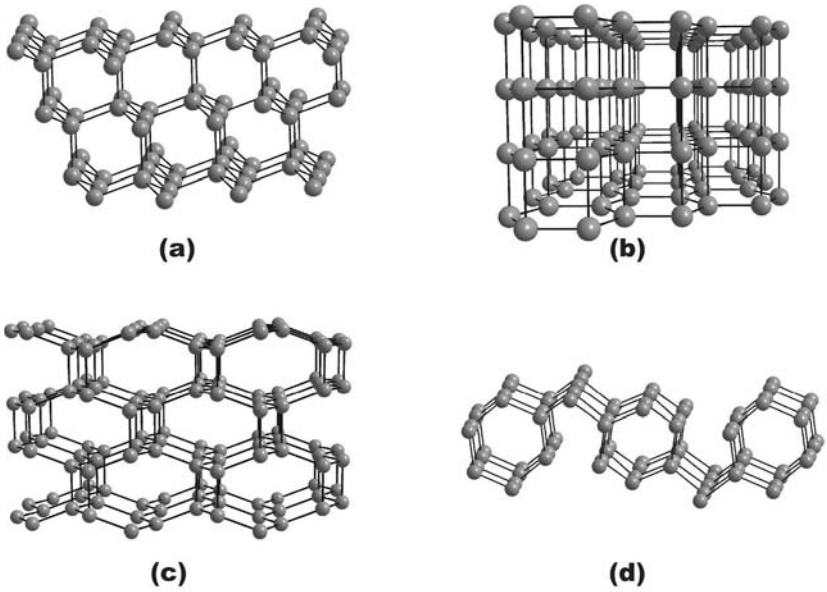

Fig. 2.4-7. Anionic mercury partial structures for (a) γ-NaHg (NaTl type), (b) $NaHg_2$ (AlB_2 type), (c) α-KHg_2 (KHg_2 type) and (d) K_5Hg_7 (unique structure type).

314 pm, Figure 2.4-7(a)]. Thus Hg in γ-NaHg behaves structurally like a pseudo-element of main group 14, although the electron counting clearly shows that, even under the unlikely assumption of a complete electron transfer from Na to Hg (Na^+Hg^-), the latter would only be a pseudo-element of main group 13 (see Section 2.4.2.2 for α-NaHg). LiZn and LiCd are further alloys with group 12 elements crystallizing in the NaTl type structures (see Chapter 1.1.4). All three compounds are good examples of the ambiguous behavior initially mentioned (main group or transition metal?) of group 12 elements.

Additional examples containing extended mercury partial structures with typical s,p-metal structures are the amalgams, with the composition MHg_2, of Na, K, Rb and Cs ($LiHg_2$ is unknown). $NaHg_2$ crystallizes in a modified AlB_2 structure with an exceptionally small c/a ratio (0.64). Graphite-like hexagonal layers of Hg atoms [d(Hg–Hg) = 300 pm] are stacked in a primitive way with short interlayer distances [d(Hg–Hg) = 323 pm, Figure 2.4-7(b)]. The unusually high melting temperature of $NaHg_2$, compared with other sodium amalgams, seems to coincide with its crystal structure, which is possibly optimal for a high ionic interaction between the Hg partial lattice and the incorporated Na atoms (for details see Ref. [4]). The results of band structure calculations for $NaHg_2$ show a particularly high dispersion of Hg(6s) states below the Fermi level. This may be taken as evidence for a strong participation of Hg(6s) states in the homonuclear Hg–Hg bond in addition to the above mentioned ionic Na–Hg interaction.

The heavier alkali metal amalgams $RbHg_2$ and $CsHg_2$ crystallize in a more open variant of the $NaHg_2$ structure [d(Hg–Hg) ≈ 300 pm, Figure 2.4-7(c)]. A fragmented version of a similar mercury arrangement is found in K_5Hg_7 [4] [Figure 2.4-7(d)].

Rb_5Hg_{19} [8] and Cs_5Hg_{19} [6] are isotypic amalgams with complex three-dimensional mercury partial structures [d(Hg–Hg) ≥ 300 pm, Figure 2.4-8(a)]

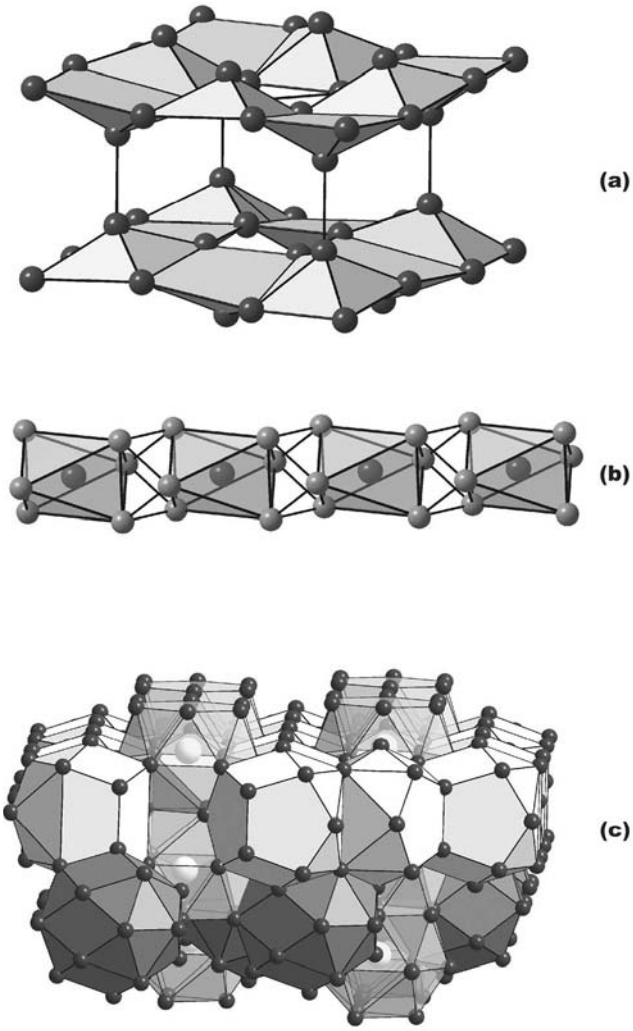

Fig. 2.4-8. More complex anionic and polyhedral mercury partial structures in amalgams with intermediate compositions: (a) Rb_5Hg_{19} (Cs_5Hg_{19}), (b) Rb_2Hg_7 and (c) K_7Hg_{31} (Rb_7Hg_{31}).

based on an ordered defect variant of the $BaAl_4$ type. The structure of K_3Hg_{11}, not among those shown in Figure 2.4-8, however, is fairly similar to Rb_5Hg_{19} and Cs_5Hg_{19} [6] and represents an alternative ordered defect variant of the $BaAl_4$ type. The complex crystal structures of these alloys show different facets which can either be discussed on the basis of extended anionic Hg arrangements or high coordination number polyhedra around the alkali metal atoms.

K_2Hg_7 has a unique structure [7] characterized by chains of alternating empty and filled face sharing octahedra of Hg atoms [d(Hg–Hg) $\geq$ 300 pm, Figure 2.4-8(b)].

K_7Hg_{31}, which is not too far from K_2Hg_7 in chemical composition, is better characterized by an interpenetrating complex arrangement of K-centered high coordination number polyhedra [d(Hg–Hg) $\geq$ 300 pm, Figure 2.4-8(c)] than by its mercury partial structure alone [4], thus leading into the essential aspects of Section 2.4.2.5.

2.4.2.5
MHg_n Clusters With High Coordination Numbers

In particular, the family of group 12 alloys with a minor content of alkali or alkaline earth elements (e.g., $RbHg_{11}$, $NaZn_{13}$, $BaCd_{11}$, Cs_3Hg_{20}) need specific discussion due to the existence of an unusual high coordination number (CN) and high symmetry polyhedra MHg_n (typically CN $\geq$ 12). Covalent Hg–Hg bonding (although inevitably present) seems to be no longer a prominent feature of these amalgams. The MHg_n are three-dimensionally condensed in such a way that face-corner- or edge-sharing polyhedra occur, keeping the large electropositive metals M away from each other. Critical aspects of simplifications by ''cutting down'' extended crystal structures to smaller cluster units are discussed in ref. [23].

KHg_{11} is a typical example which has a crystal structure closely related but readily distinguishable from that of elemental mercury. Dominating structural units are KHg_{20} polyhedra (four-capped tetragonal hexagon prisms) fused together to a highly symmetrical three-dimensional arrangement [d(Hg–Hg) $\geq$ 300 pm, Figure 2.4-9(a),(b)]. Together with additional ''isolated'' Hg atoms in holes located in the space between the KHg_{20} polyhedra, the principal arrangement of polyhedral centers and isolated Hg atoms corresponds topologically to the pattern of the classical alloy Cu_3Au.

The spatial arrangements of atoms in alloys such as KHg_{11}, and related examples, offers fascinating esthetical aspects if it is analyzed further topologically, neglecting the logics of chemical bonding restrictions for a moment. From this aspect the crystal structure of KHg_{11} can also be seen [Figure 2.4-9(c)] as an arrangement of square planar Hg_4, cube shaped Hg_8, both present in alkali metal rich amalgams, (see above) and centered Hg_{13} cuboctahedra (not known in other amalgams). Which one of the views offered in Figure 2.4-9 for the structure of KHg_{11} is ''chemically correct'' must remain an open question and depends on the focus of the scientific questions associated with the description of the structure. A more

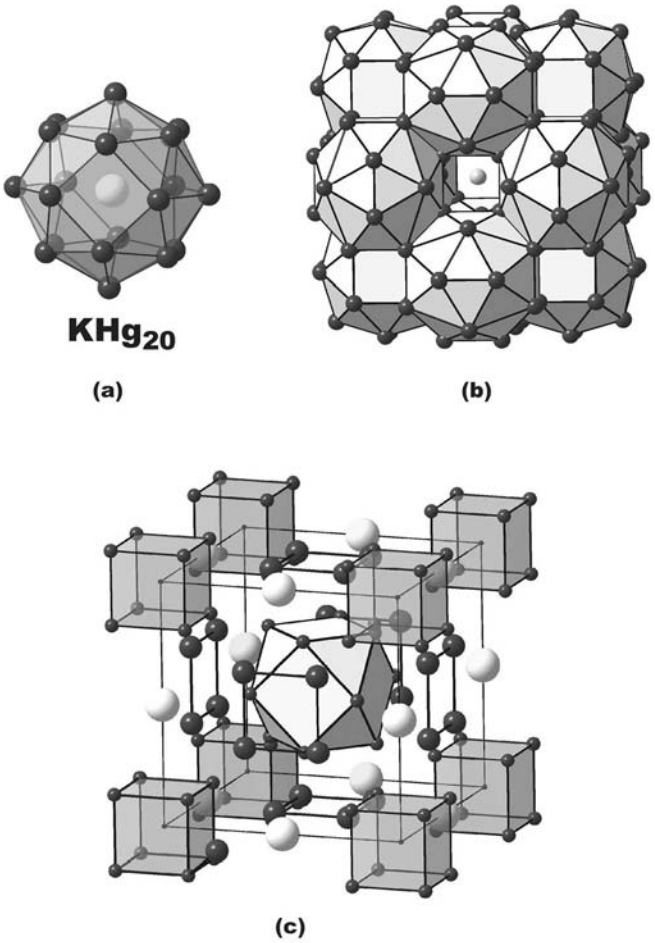

Fig. 2.4-9. Different views of the crystal structure of KHg_{11}: (a) KHg_{20} polyhedra, (b) three-dimensional arrangement of single Hg atoms (small white ball) and KHg_{20} polyhedra, (c) another view of the structure emphasizing the occurrence of a centered cuboctahedra (white), square planar Hg_4 (dark grey) and cube shaped Hg_8 (medium grey), K atoms (big white balls).

detailed discussion based on an additional third view for the structure of KHg_{11} is given in Ref. [24].

The recently [25] published $Mg(NH_3)_6Hg_{22}$ is an outstanding new member of this group of amalgams. It is characterized by a coordination polyhedron of 32 Hg atoms around each cationic $Mg(NH_3)_6$ group.

Figure 2.4-10 shows a selection of high coordination polyhedra in alloys with group 12 elements ranging between CN 15 [one type of polyhedron around K in K_7Hg_{31}, Figure 2.4-10(a)] and CN 32 [the polyhedron in the above mentioned $Mg(NH_3)_6Hg_{22}$, Figure 2.4-10(f)].

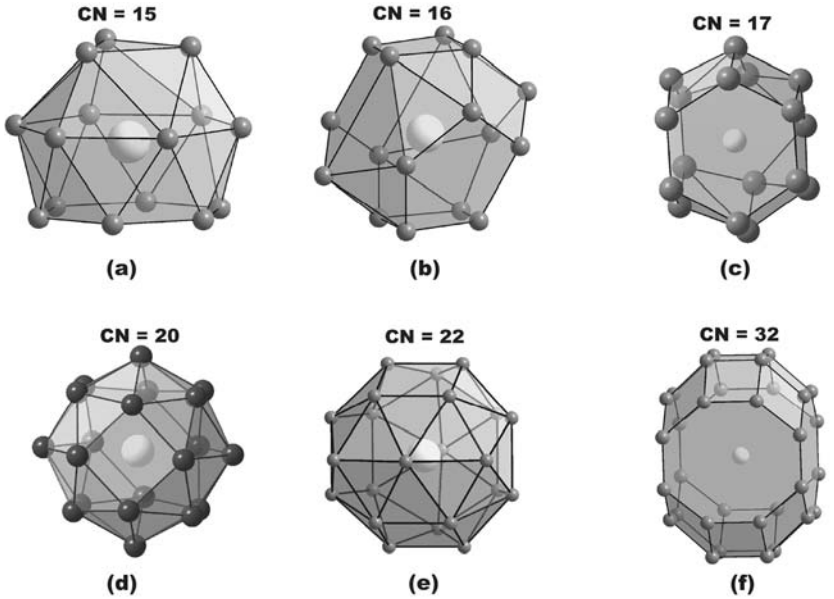

Fig. 2.4-10. High coordination number (CN) polyhedra around alkali (alkaline earth) atoms in different mercury rich amalgams and in $BaCd_{11}$: (a) CN 15 and (b) CN 16 around K in K_7Hg_{31}, (c) CN 17 around Rb in Rb_5Hg_{19}, (d) CN 20 around K in KHg_{11}, (e) CN 22 around Ba in $BaCd_{11}$ and (f) CN 32 around $Mg(NH_3)_6$ in $Mg(NH_3)_6Hg_{22}$.

2.4.2.6

$NaK_{29}Hg_{48}$ A Complex Ternary Amalgam With Mercury Acting as a Pseudo Group 13 Element [9]

To date the unique alloy $NaK_{29}Hg_{48}$ is the only well defined ternary alkali metal amalgam. Although its chemical composition is nearer to MHg_2 than to MHg_{11} its structural topology is more comparable to MHg_{11} (or related examples) due to the occurrence of high coordination number polyhedra [Figure 2.4-11(a)].

The most surprising aspect, however, is for $NaK_{29}Hg_{48}$ to be isotypical to $M_3Na_{26}In_{48}$ (M: K, Rb, Cs, [26–28]). Except for the excess Na atom, $NaK_{29}Hg_{48}$ can be seen as an additional example of Hg behaving as a main group element, in this case like indium. This is particularly interesting because $M_3Na_{26}In_{48}$ was discussed at the time of its discovery as a striking example of the validity of cluster concepts, which were originally designed for boranes as classical examples of electron deficient cluster compounds and *not* for its heavier analogues. The topology of the mercury clusters in $NaK_{29}Hg_{48}$ [d(Hg–Hg) $\geq$ 300 pm, Figure 2.4-11(b),(c)] is, in principal, similar to that of the clusters in $M_3Na_{26}In_{48}$. Both solids contain In_{12}/Hg_{12}-icosahedra, centered by Na in the mercury compound and empty in the indium case, and In_{12}/Hg_{12} hexagonal antiprisms, centered by K in both cases. Furthermore, the interatomic distances Hg–Hg in $NaK_{29}Hg_{48}$ are in general a little longer than the corresponding In–In distances in $M_3Na_{26}In_{48}$. More detailed dis-

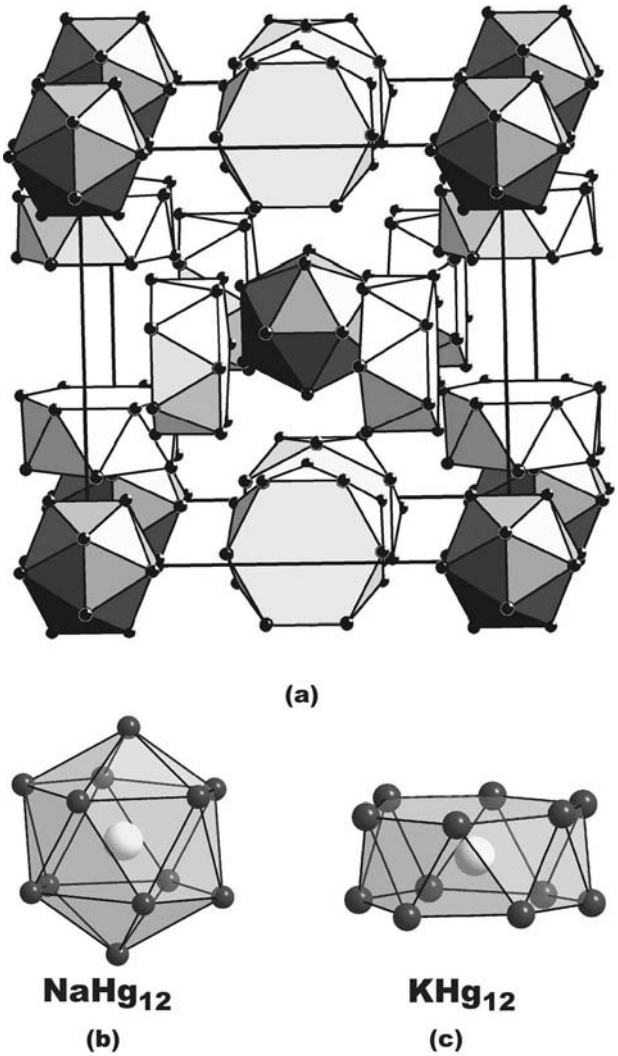

Fig. 2.4-11. The crystal structure of $NaK_{29}Hg_{48}$: (a) view of the structure emphasizing the centered icosahedral (dark grey) and hexagonal antiprismatic mercury clusters, K atoms outside the clusters are neglected, (b) icosahedral $NaHg_{12}$, (c) hexagonal antiprismatic KHg_{12}.

cussions of the chemical bonding and further topological aspects, e.g., relations to clathrate type structures, in both compounds have been described previously [9].

Details of Cs_3Hg_{20}, which is a beautiful new example of an amalgam with high coordination number polyhedra, have been published recently. It can be described simply as being built up by linked octa-capped icosahedra of mercury or as a framework structure related to the clathrate-I type [6].

2.4.2.7
Electric and Magnetic Properties of Amalgams

In spite of their almost ionic properties discussed in the preceeding sections, amalgams basically behave as classical alloys with respect to their electrical and magnetic properties. DC measurements of the electrical resistivity (ρ) based on pressed powder pellets of $RbHg_2$, CsHg and others [29] show the typical increase in the specific electrical resistivity with increasing temperature and specific resistivity values in the order of magnitude of elemental alkali metals and mercury ($\approx 10^2$ $\mu\Omega$ cm). Relatively low residual resistivity ratios [ρ(293 K)/ρ(0 K)] of 10^1 to 10^2 indicate, however, high concentrations of imperfections (e.g., grain boundaries) or contaminations due to a high chemical reactivity of the samples [e.g., perfect single crystals of Cu show a ρ(293 K)/ρ(0 K) of 10^6].

Measurements of the magnetic properties based on a selection of alkali metal rich and alkali metal poor amalgams show a different behavior at higher temperatures.

Na_3Hg, as a typical example of the first group, exhibits Pauli paramagnetism ($\chi_{mol} \approx 3 \times 10^{-5}$) at higher temperatures with a weak but significant temperature dependence [4]. In particular the α/β phase transition for Na_3Hg at 309 K is reflected in a χ change of about 5%.

All magnetic measurements of mercury rich amalgams at low temperatures ($0\ K < T < 10\ K$) indicate a superconductivity below 3.5 K by a sharp magnetic phase transition resulting in a strong diamagnetic susceptibility [4, 7, 9, 24]. Although this temperature is very close to the superconducting phase transition of elemental mercury ($T = 4.2$ K) it is an intrinsic property of the particular amalgam and not due to traces of unreacted Hg.

2.4.3
Conclusions

Although formally a transition metal the structural chemistry of mercury as a group 12 element in amalgams shows typical features close to those of main group 13 and 14 metals.

In particular alloys with the electropositive alkali and alkaline earth elements reflect this ambiguous behavior in various facets, not only for amalgams but also for other group 12 alloys. One example is the occurrence of s,p-bonded Zintl type structures (e.g., Hg acts as a "pseudo-element" of group 13 or 14) although the valence electron counting for the respective compounds is not in accordance with this model (γ-NaHg, LiZn, LiCd). Another example is the ternary amalgam $NaK_{29}Hg_{48}$ where Hg seemingly acts as group 13 element (indium-like).

Moreover in certain amalgams low dimensional anionic mercury partial structures are found (MHg, M_3Hg_2, $M_{15}Hg_{16}$, M'_3Hg_2, M'_5Hg_3, M = alkali metal, M′ = alkaline earth metal) extending down to structures with single isolated $Hg^{\delta-}$ atoms (Na_3Hg, Na_8Hg_3) coordinated only by alkali metal atoms. These alloys re-

semble, to a certain extent, ''aurides'' with Au^-, however, never with an integral electron transfer as is the case for Au.

Extended anionic partial structures of mercury occur in some high melting amalgams (MHg_2 and related examples) with medium Hg content. Significant ionic bonding contributions between M and Hg in addition to covalent Hg–Hg contributions can be assumed to be responsible for the properties of these solids.

In mercury rich alloys such as MHg_{12} (M = K, Rb), a particular situation occurs due to high coordination number (CN) polyhedra (up to CN 22) in their structures. In these compounds the electropositive atoms are located in the centers of these polyhedra and are thus spatially separated from each other. The covalent Hg–Hg interaction, as discussed above, is of minor importance in these amalgams.

The basic aspects of the structural systematic and the chemical bonding are discussed as well as ambiguous topological aspects and selected physical properties (magnetism, conductivity) of the respective alloys.

Acknowledgements

The author is grateful to his coworkers especially to H. Hirth, H. Otterbach, Drs. Erik Biehl, C. Reiner, M. Rochnia, A. Strunck and D. Toelstede, and would like to thank the ''Deutsche Forschungsgemeinschaft'' and the ''Fonds der Chemischen Industrie'' for their continuous financial support.

References

1 A. F. Wells, *Structural Inorganic Chemistry*, 5th Edn., Clarendon Press, Oxford, **1993**, p. 1156.
2 N. N. Greenwood, A. Earnshaw, *Chemie der Elemente*, 1st Edn., VCH Verlagsgesellschaft, Weinheim, **1988**, p. 298.
3 E. E. Kuznetsov, J. D. Corbett, L. Wang, A. I. Boldyrev, *Angew. Chem.*, **2001**, *113*, 3473–3476.
4 H. J. Deiseroth, *Prog. Solid State Chem.*, **1997**, *25*, 74–119.
5 I. D. Brown, B. D. Cutforth, C. G. Davies, R. J. Gillespie, P. R. Ireland, J. E. Vekris, *Can. J. Chem.*, **1974**, *52*, 791–793.
6 E. Todorov, S. C. Sevov, *J. Solid State Chem.*, **2000**, *149*, 419–427.
7 E. Biehl, H. J. Deiseroth, *Z. Anorg. Allg. Chem.*, **1999**, *625*, 1337–1342.
8 E. Biehl, H. J. Deiseroth, *Z. Anorg. Allg. Chem.*, **1999**, *625*, 389–394.
9 H. J. Deiseroth, E. Biehl, *J. Solid State Chem.*, **1999**, *147*, 177–184.
10 W. Klemm, E. Busmann, *Z. Anorg. Allg. Chem.*, **1963**, *319*, 297–305.
11 H. Schäfer, B. Eisenmann, *Rev. Inorg. Chem.*, **1981**, *3*, 29–101.
12 C. Belin, M. Tillard-Charbonnel, *Coord. Chem. Rev.*, **1998**, *178–180*, 529–560.
13 H. J. Deiseroth, E. Biehl, H. Noglik, *Solid State Ionics*, **1997**, *101–103*, 1305–1308.
14 Ch. Druska, P. Böttcher, *Z. Anorg. Allg. Chem.*, **1994**, *620*, 1845–1849.
15 Ch. Druska, Th. Doert, P. Böttcher, *Z. Anorg. Allg. Chem.*, **1996**, *622*, 401–404.
16 H. J. Flad, F. Schautz, Y. Wang, M. Dolg, A. Savin, *Eur. Phys. J.*, **1999**, *6*, 243–254.
17 A. L. Wessels, W. Jeitschko, M. H.

Möller, *Z. Naturforsch.*, **1996**, *52b*, 469–473.
18 X. Li, A. E. Kuznetsov, H. F. Zhang, A. I. Boldyrev, L. S. Wang, *Science*, **2001**, *291*, 859–861.
19 H. J. Deiseroth, A. Stupperich, A. Pankaluoto, N. E. Christensen, *Z. Anorg. Allg. Chem.*, **1991**, *597*, 41–50.
20 A. V. Mudring, M. Jansen, J. Daniels, S. Kremer, M. Mehring, J. P. P. Ramalho, A. H. Romero, M. Parrinello, *Angew. Chem.*, **2002**, *114*, 128–132.
21 H. Otterbach, H. J. Deiseroth, to be published.
22 R. Ferro, *Acta Crystallogr.*, **1954**, *7*, 781.
23 A. Simon, in *Solid State Chemistry Compounds*, A. K. Cheetham, P. Day, eds., Clarendon Press, Oxford, **1992**, p. 112–161.
24 E. Biehl, H. J. Deiseroth, *Z. Anorg. Allg. Chem.*, **1999**, *625*, 1073–1080.
25 I. Hwang, T. Drews, K. Seppelt, *J. Am. Chem. Soc.*, **2000**, *122*, 8486–8489.
26 W. Carrillo-Carera, N. Caroca-Canales, K. Peters, H. G. von Schnering, *Z. Anorg. Allg. Chem.*, **1993**, *619*, 1556–1563.
27 S. C. Sevov, J. D. Corbett, *Inorg. Chem.*, **1993**, *32*, 1612–1615.
28 G. Cordier, V. Müller, *Z. Naturforsch.*, **1993**, 1035–1040.
29 H. J. Deiseroth, A. Strunck, W. Bauhofer, *Z. Anorg. Allg. Chem.*, **1988**, *558*, 128–136.

2.5
Molecular Cages and Clusters of the Heavier Group 14 Elements (E = Si, Ge, Sn or Pb) of Formula E_nR_m ($n \geq m$)

Nils Wiberg and Philip P. Power

2.5.1
Introduction

Stable cages and clusters of the heavier group 14 elements Si–Pb (tetrels) encompass several compound classes. These include the Zintl anions, for example M_5^{2-} or M_9^{n-} (M = Ge, Sn or Pb, $n = 2$, 3 or 4), which can be isolated with alkali-metal-cryptand cations, or M_9^{4-} (M = Si–Pb) anions that are also stable as neat salts [1]. There are also larger clusters found in ternary compounds such as $Ba_{16}Na_{204}Sn_{310}$, that contain $[Ba_4@Sn_{56}]^{36-}$ anions in which the Sn_{56} cage is stabilized by internal barium cations [2]. Related to the Zintl phases of the tetrels are clathrates which were originally obtained as metastable phases during thermal decomposition of a simple Zintl phase such as NaSi. They were termed clathrates due to their similarity to clathrate hydrates. Numerous structural types are known [3], however, they are not discrete clusters as suggested by formulae such as Na_8Si_{46} [4] or $Cs_8Na_{16}Ge_{136}$, [5] but are three dimensional networks of tetrahedrally coordinated tetrels (group 14 element). There also exist large numbers of organic derivatives of the heavier group 14 elements analogous to linear or cyclic alkanes of formula E_nR_{2n+2} or E_nR_{2n} (E = tetrel, R = organic or related group), however, this very large class of compounds is outside the scope of this book and this brief survey is confined to organo substituted species of formula E_nR_m ($n \geq m$) and related compounds. Many of the major advances in the area of these compounds have taken place over the last 15 years and an impressive variety of structural types have been discovered, especially among the tin derivatives. The area has been the subject of reviews which have focused on the individual elements and provided detailed information on some of the compounds in some cases up to about mid-1997 [6–9]. These earlier results and those obtained in the ensuing period, which account for almost half of the references, will now be summarized.

2.5.2
Silicon Species of Formula Si_nR_m ($n \geq m$)

2.5.2.1
Dimers and Trimers

The simplest compounds of the Si_nR_m type are the dimers Si_2R_2. These are analogous to the alkynes, but, at present, they remain unknown as well characterized, stable species in spite of several attempts to synthesize them [10–12]. Perhaps the closest such approach has involved the reduction of $(R^*_2MeSi)(Cl)Si{=}Si(Cl)(SiMeR^*_2)$ ($R^* = SiBu^t_3$) with lithium naphthalenide in tetrahydrofuran (THF) which after evaporation of all volatile products at r.t. and treating the residue with benzene leads to an orange-red solution. Chemical ionization (NH_3) mass spectra of orange crystals obtained from the latter indicated the presence of molecules with the mass of the desired disilyne $(R^*_2MeSi)Si{\equiv}Si(SiMeR^*_2)$ and that of its oxidation product [12]. Calculations have predicted that the disilyne $(R^*_2MeSi)Si{\equiv}Si(SiMeR^*_2)$ should be stable enough to isolate, and should have a short Si–Si bond length of 2.072 Å and a wide Si–Si≡Si bond angle of 148° consistent with substantial triple bonding [13]. Three membered rings of formula Si_3R_3 which have one unpaired electron are currently unknown as stable compounds, probably as a result of the instability caused by the high degree of strain in the three-membered ring as well as their radical character.

2.5.2.2
Tetramers

For tetrameric species of formula Si_4R_4 the tetrahedrane structure is the most symmetric, but since it contains four fused three-membered rings it also has a high degree of strain [14]. Calculations have indicated that for Si_4H_4 the tetrahedrane structure is indeed a local minimum [15], but the structure can easily convert into an isomer with a four-membered ring arrangement that has incipient di-radical character [16a]. Computational data also showed that the substituent at silicon is of crucial importance. Silyl substituents are the most effective at lowering strain, stabilizing the tetrahedrane structure and reducing the energy difference between the isomers [7].

The most obvious precursors for the synthesis of polyhedral species are monosubstituted silicon halides of various types (e.g., halogenated $RSiX_3$, $RSiX_2{-}SiX_2R$) with large R groups being necessary to limit the degree of oligomerization upon reduction. The reducing agent is also important and agents such as Li, Na, Na/K or $LiC_{10}H_8$, $NaSiBu^t_3$ can dehalogenate the silicon halides with the formation of the desired product [6, 16b, 16c, 17]. Magnesium metal or $Mg/MgBr_2$ have proven useful, milder reductants.

The first well characterized tetrasilatetrahedrane $\mathbf{1}_{Si}$ (cf. Scheme 2.5-1) was synthesized from R^*SiX_3 or $R^*SiX_2\text{-}SiX_2R^*$ ($R^* = SiBu^t_3$, X = halogen) and NaR^* in tetrahydrofuran (THF) [18]. It was obtained as orange crystals and has high ther-

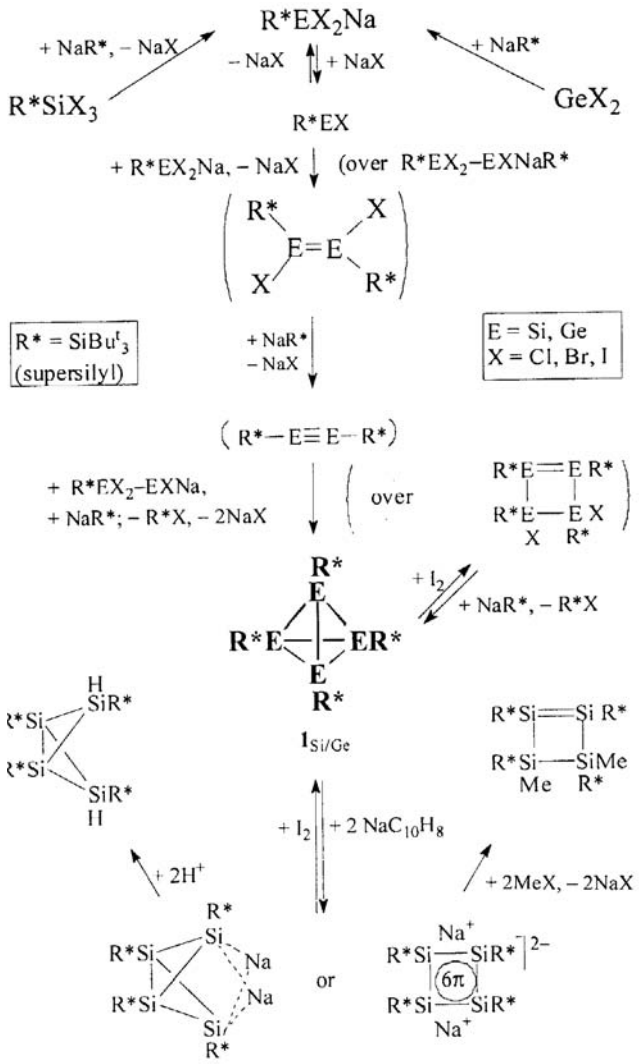

Scheme 2.5-1. Synthetic routes to the silicon or germanium clusters $\mathbf{1}_{Si}$ and $\mathbf{1}_{Ge}$; some reactions of $\mathbf{1}_{Si}$ [16a, 16b].

mal stability as well as being stable to moisture and light. Within the Si_4 tetrahedron, the endocyclic and exocyclic Si–Si bond lengths are 2.34 and 2.37 Å. The tetrahedral Si–Si bonds are marginally longer than those calculated for Si_4H_4 and the exocycli Si–Si bonds slightly longer than those in disilanes (2.34 Å) [19].

As $\mathbf{1}_{Si}$ is obtained in quantitative yields from the bromides or iodides, the pathways for the formation of **1** must be straightforward (Scheme 2.5-1). It has been found from trapping experiments [16a, 16b] that silanes R^*SiX_3 in the presence

of NaR^* in THF at −78 °C initially form the silanides R^*EX_2Na, which then add silylenes R^*SiX, generated from R^*SiX_2Na at about −50 °C, to give the disilanides R^*SiX_2-$SiXNaR^*$. For $(R^*_2MeSi)SiX_3$ the silylenes $(R^*_2MeSi)SiCl$, which are formed as intermediates, dimerize to give disilenes [12]. The disilanides, which are also formed directly from R^*SiX_2-SiX_2R^* and NaR^* in THF at −78 °C, transform, by elimination of NaX at about −30 to −10 °C, first into reactive disilene intermediates $R^*XSi{=}SiXR^*$, and then, probably, into the reactive disilyne intermediate $R^*Si{\equiv}SiR^*$ which, with R^*SiX_2-$SiXNaR^*$ (see above) and NaR^*, gives, via isolable cyclotetrasilenes $R^*_4Si_4X_2$, finally the tetrahedrane $\mathbf{1}_{Si}$ (cf. Scheme 2.5-1).

The reaction of $Si_4R^*_4$ with I_2 in 1:1, 1:3, and 1:4 molar ratios affords the species $R^*_4Si_4I_2$ (cf. Scheme 2.5-1), $R^*_3Si_4I_5$ and $R^*_2Si_4I_6$ [20, 21]. Oxygen reacts with solid $Si_4R^*_4$ very slowly, but with $Si_4R^*_4$ in solution, the tetrahedrane oxides $R^*_4Si_4O_2$, $R^*_4Si_4O_4$ and $R^*_4Si_4O_6$ [16b] were formed ($R^*_4Si_4O$ is also formed by hydrolysis of the cyclotetrasilene $R^*_4Si_4I_2$). The existence of the thermolabile tetrasilanediide $Na_2Si_4R^*_4$, obtained by reaction of $\mathbf{1}_{Si}$ with $NaC_{10}H_8$ in THF at −78 °C (Scheme 2.5-1), has been elucidated by its reaction with MeOH leading to the *endo,endo-bicyclo*-tetrasilane $R^*_4Si_4H_2$. This is what is expected from the proposed structure of $\mathbf{1}_{Si}{}^{2-}$ as shown on the left hand bottom of Scheme 2.5-1. On the other hand, the formation of the cyclotetrasilene $R^*_4Si_4Me_2$ from $\mathbf{1}_{Si}{}^{2-}$ and Me_2SO_4 is in better agreement with the structure shown on the right hand bottom of Scheme 2.5-1. The $Si_4{}^{2-}$ ring also constitutes a 6π aromatic system.

In addition, R'_4Si_4 ($R' = Dis_2MeSi$ with $Dis = CH(SiMe_3)_2$ has been synthesized by reaction of $R'Br_2Si{-}SiBr_2R'$ and NaR^* in THF [17]. The tetrahedrane ($Si{-}Si_{endo}$/$Si{-}Si_{exo}$ av. 2.352/2.409 Å) reacts with KC_8 in diethyl ether by reductive cleavage of an exocyclic Si–Si bond. In the crystal, $K(18\text{-crown-6})^+R'_3Si_4{}^-$ shows a separated ion pair and the anion $R'_3Si_4{}^-$ has a significantly distorted tetrahedran skeleton.

2.5.2.3
Hexamers and Octamers

The reduction of $Ar(Cl)_2SiSi(Cl)_2Ar$ ($Ar = C_6H_3$-2,6-Pr^i_2) with $Mg/MgBr_2$ afforded the hexasilaprismatic compound Si_6Ar_6 [22]. ^1H NMR data showed that there was a large barrier to rotation of the aryl groups. The X-ray crystal structure (Figure 2.5-1) showed that there were only slight distortions in the trigonal prismatic geometry. The Si–Si bonds within the triangular units (average 2.380 Å) are slightly longer than those in the square units (2.372 Å). Both sets of distances are longer than a normal single bond length of 2.34 Å [19]. The highly crowded nature of the molecule may play a role in lengthening the bonds. On irradiation ($\lambda = 360$–380 nm) of the hexaprismane Si_6Ar_6 at −50 °C in solution, new absorption bands appeared which were assignable to the isomeric hexasila Dewar benzene Si_6Ar_6. Excitation of the bands at $\lambda > 460$ nm resulted in the immediate regeneration of the hexaprismane (the latter forms also at 0 °C with a $t_{1/2}$ of *ca.* 30 s).

The first Si_nR_n compound to be fully characterized was the octasilacubane spe-

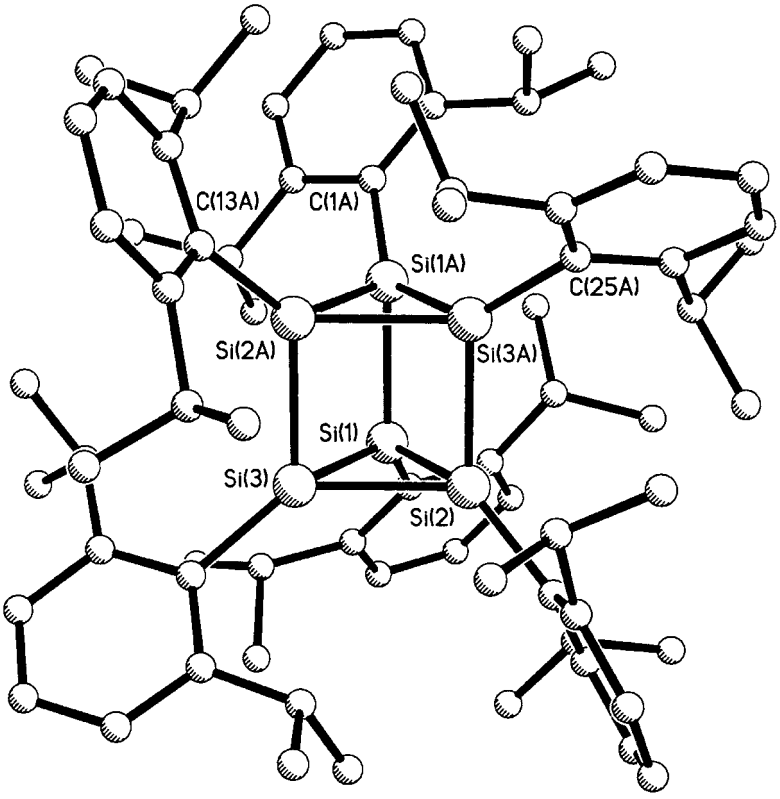

Fig. 2.5-1. X-ray crystal structure of $Si_6(C_6H_3\text{-}2,6\text{-}Pr^i_2)_6$ [22]. H atoms are not shown.

cies $Si_8(SiMe_2Bu^t)_8$ [23]. This was achieved by the reduction of $(Bu^tMe_2Si)SiBr_3$ or $(Bu^tMe_2Si)Br_2SiSiBr_2(SiMe_2Bu^t)$ with sodium. Several other octasilacubane derivatives with the substituents Bu^t [24], CMe_2CHMe_2 [25] (Figure 2.5-2), C_6H_2-2,4,6-Mes [6] and C_6H_3-2,6-Et_2 [26] have also been synthesized and structural data are available for the Bu^t, CMe_2CHMe_2 and C_6H_3-2,6-Et_2 species. They possess Si_8 cubane arrays that are slightly distorted from idealized geometry with Si–Si distances that vary from *ca.* 2.38 to 2.45 Å within the series. The bond lengths are elongated by steric effects. However, calculations showed that electronic effects can also play a role. For example, increased charge separation in the Si–C bond leads to an increase in positive charge at the skeletal atoms and a lengthening of the Si–Si bonds. The stability of the octasilacubanes depends on the steric bulk of the substituents. The silyl substituted $Si_8(SiMe_2Bu^t)_8$ is oxidized in air [23] as are the Si_8Ar_8 (Ar = Mes or C_6H_3-2,6-Et_2) whereas the more crowded $Si_8(CMe_2CHMe_2)_8$ [25] is stable in air for several weeks. However, one or two oxygens can be inserted into the octacubane framework by photolysis in the presence of DMSO in benzene solution. These products have been structurally characterized [27].

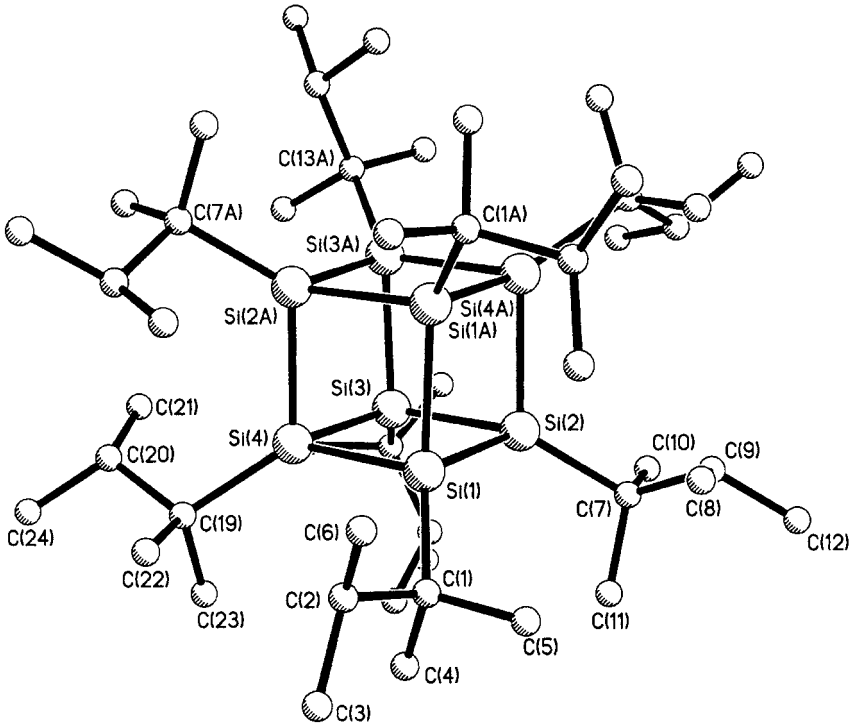

Fig. 2.5-2. X-ray crystal structure of $Si_8(CMe_2CHMe_2)_8$ [25]. H atoms are not shown.

2.5.3
Germanium Cages and Clusters Ge_nR_m ($n \geq m$)

2.5.3.1
Dimers

The recently isolated species Ar′GeGeAr′ (Ar′ = C_6H_3-2,6-$Dipp_2$; Dipp = C_6H_3-2,6-Pr^i_2) has the lowest possible $(GeR)_n$ cluster formula [28]. It was synthesized by the reduction of Ge(Cl)Ar′ with sodium or potassium. Although it corresponds to a digermanium alkyne analogue, it possesses a planar, *trans-bent* (C_{2h}) CGeGeC core geometry as a result of the presence of some non-bonding electron density at each germanium (Figure 2.5-3). The bending may be viewed as a second order Jahn-Teller distortion as a result of mixing of a Ge–Ge σ^* and π levels [29]. The Ge–Ge–C angle is 128.67(8)° and the Ge–Ge distance is 2.2850(6) Å, which is much shorter than a normal Ge–Ge single bond (ca. 2.44 Å) and lies in the lower half of the known bond length range for digermenes the germanium analogues of alkenes. The bond length and the molecular orbital bonding picture suggest that the Ge–Ge bond order is approximately two, which is consistent with bond order calculations [30]. The related "digermyne" Ar*GeGeAr* (Ar* = C_6H_3-2,6-$Trip_2$;

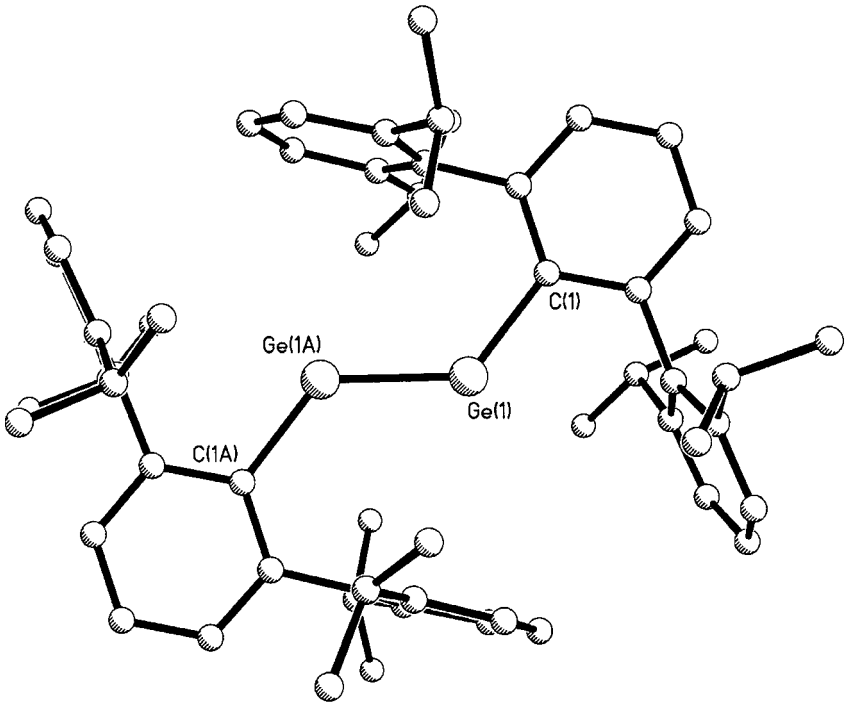

Fig. 2.5-3. X-ray crystal structure of Ar′GeGeAr′, Ar′ = C_6H_3-2,6-$Dipp_2$ [28]. H atoms are not shown.

Trip = C_6H_2-2,4,6-*i*-Pr_3), which has two "extra" Pr^i groups on the flanking aryl rings, has been characterized by a derivatization reaction with 2,3-dimethyl-1,3-butadiene [31]. Earlier work had shown that stirring Ar*GeCl with sodium for extended periods gave the reduced compound Na_2{Ar*GeGeAr*} [32]. This compound also featured a central *trans-bent* CGeGeC array with a Ge–Ge distance of 2.394(1) Å and a Ge–Ge–C angle of 102.37(8)°. In addition, the two sodium ions are complexed by the *ortho*-Trip rings of the Ar* substituents. It seems likely that the presence of such ions are essential for the stability of the putative dianion $[Ar^*GeGeAr^*]^{2-}$. Since it is isolectronic with the corresponding neutral Ar*AsAsAr* compound, it is probable that the Ge–Ge bond is formally a double one, even though it is only slightly shorter than a Ge–Ge single bond (Ge–Ge = 2.44 Å). The lengthening can be accounted for in terms of increased Coulombic repulsions owing to the 2− charge.

2.5.3.2
Germanium Trimers

Cyclic, trimeric germanium compounds containing the unit Ge_3R_3 are of two types: the cationic $(GeR)_3^+$ [33] species and the neutral radical $(GeR)_3$ [34]. The

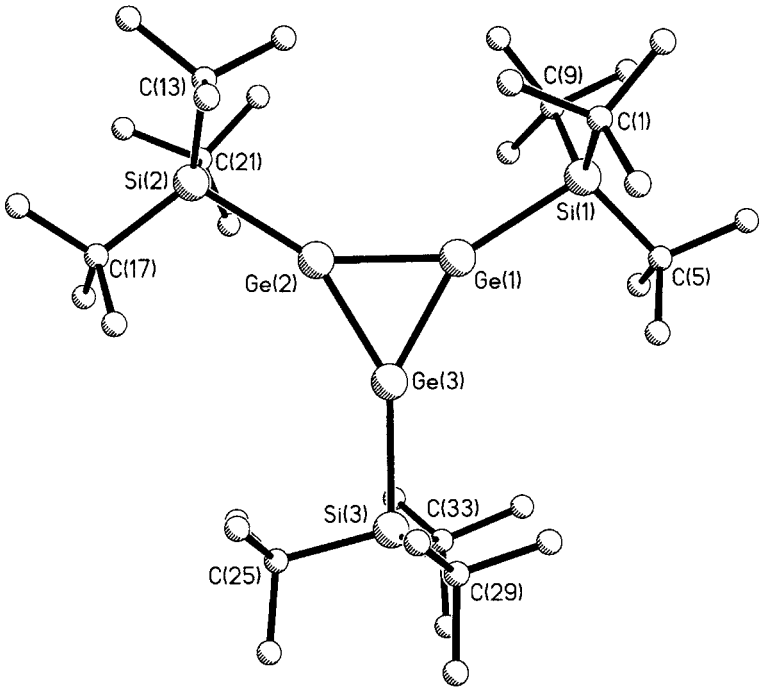

Fig. 2.5-4. X-ray crystal structure of the $[Ge_3R^*_3]^+$ cation in $[Ge_3R^*_3][BPh_4]$, ($R^* = SiBu^t_3$) [33]. H atoms are not shown.

former species was obtained via the reaction of $Ge_3R^*_4$ with $[CPh_3][BPh_4]$ in benzene that produced $[Ge_3R^*_3]^+[BPh_4]^-$, which was isolated as yellow crystals. It featured a free cyclotrigermenium cation with a trigonal planar skeleton and Ge–Ge bonds that have an average distance of 2.326(4) Å (Figure 2.5-4). The Ge–Ge distance indicated considerable multiple character, which was consistent with the presence of a doubly occupied π-level delocalized over the three germaniums. The ring is thus aromatic and is analogous to the cyclopropenium cation. Reduction of the ArGeCl ($Ar = C_6H_3$-2,6-Mes_2; $Mes = C_6H_2$-2,4,6-Me_3) with KC_8 afforded the cyclotrigermenyl radical Ge_3Ar_3 as dark blue crystals [34]. An X-ray crystal structure (Figure 2.5-5) showed that it has a three-membered Ge_3 ring in which the average Ge–Ge distance is 2.35(7) Å. Unfortunately, the structure displayed disorder involving the important core germaniums. The disorder was consistent with the location of the unpaired electron at a single germanium with a double bond between the remaining two germaniums of the ring. The molecule may adopt three different orientations with equal probability in the crystal since the periphery of the molecule is hardly affected by the core arrangements. This model of the bonding is supported by EPR studies which indicated that hyperfine coupling occurred to a single ^{73}Ge ($I = \frac{9}{2}$, 7.8%) nucleus. The coupling constant of 16 G is consistent with the location of the unpaired electron in an orbital of π-symmetry

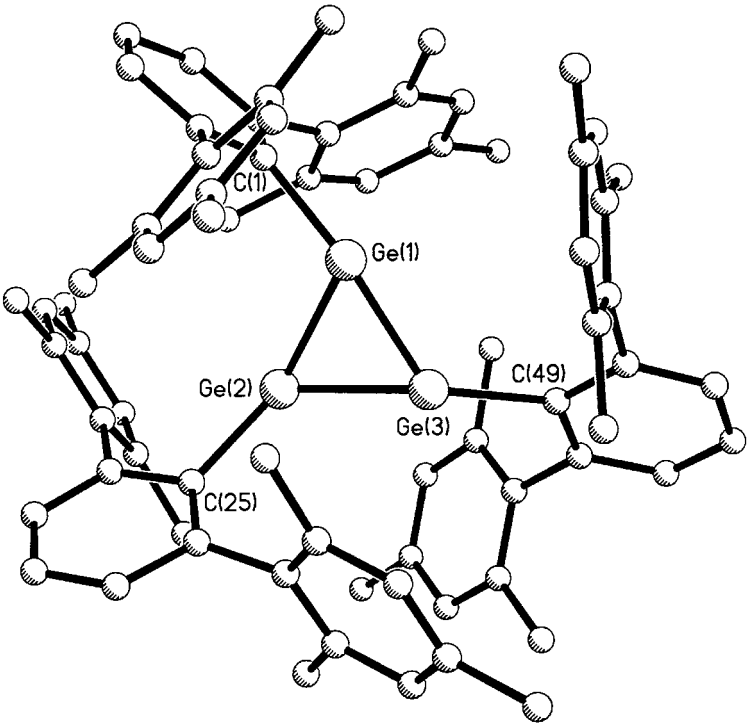

Fig. 2.5-5. X-ray crystal structure of the radical Ge_3Ar_3, Ar = C_6H_3-2,6-Mes_2 [34]. H atoms are not shown.

indicating planar or near planar geometry at the germanium. Further reduction afforded the green salt $LiGe_3Ar_3$ (Ar = C_6H_3-2,6-Mes_2) which features the trigermenyl allyl anion analogue [34].

2.5.3.3 Germanium Tetramers

Like the corresponding silicon compounds, the tetragermatetrahedrane $Ge_4R^*_4$ ($\mathbf{1}_{Ge}$, Scheme 2.5-1) can be obtained in low yield by the reaction of $R^*(Cl)_2$-$GeGe(Cl)_2R^*$ with NaR^* or in better yield by the reaction of $GeCl_2$ with NaR^* [35]. The cluster was obtained as deep red crystals whose X-ray crystal structure (Figure 2.5-6) revealed a regular Ge_4 tetrahedral array with average Ge–Ge and Ge–Si distances of 2.44 and 2.38 Å. These values are typical for single bonding between these elements [19, 36]. The formation of $\mathbf{1}_{Ge}$ from $GeCl_2$ and NaR^* in THF obviously proceeds in an analogous manner to the formation of $\mathbf{1}_{Si}$ from R^*SiX_3 and the first reaction intermediates formed, namely R^*SiX_2Na and R^*GeCl_2Na (cf. Scheme 2.5-1), are comparable.

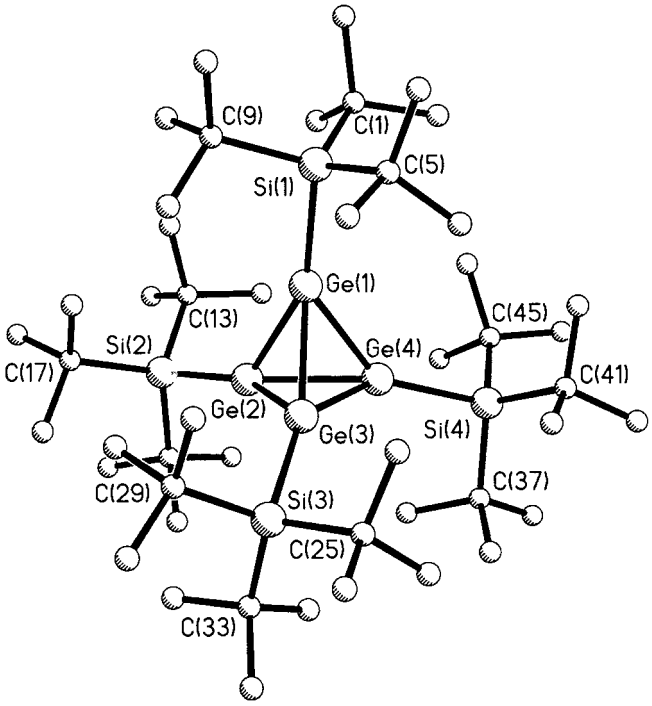

Fig. 2.5-6. X-ray crystal structure of $Ge_4R^*_4$, $R^* = SiBu^t_3$ [35]. H atoms are not shown.

2.5.3.4

Germanium Hexamers, Octamers and Decamers

The first $(GeR)_n$ compound to be isolated and structurally characterized was the hexagermaprismane $Ge_6\{CH(SiMe_3)_2\}_6$ which was synthesized by the reduction of $(Me_3Si)_2CHGeCl_3$ with magnesium metal [37]. It was isolated as orange-yellow crystals in about 28% yield. An X-ray crystal structure showed (Figure 2.5-7) that within the Ge_3 triangles and the Ge_4 rectangles the Ge–Ge distances, which averaged 2.580 and 2.522 Å, were considerably longer than normal Ge–Ge single bonds, presumably as a result of the crowding induced by the six $-CH(SiMe_3)_2$ ligands. The reaction between magnesium and 2,6-Pr^i_2-$H_3C_6GeCl_3$ also yielded a hexagermaprismane $Ge_6\{C_6H_3$-2,6-$Pr^i_2\}_6$ [22]. In the Ge_6 core the triangular Ge_3 units have an average Ge–Ge bond length of 2.503 Å and in the Ge_4 rectangles it is 2.468 Å. Clearly the distances are significantly shorter than those in the $-CH(SiMe_3)_2$ substituted analogue. These differences are also reflected in the UV–visible spectra, which exhibit a red shift for the $-CH(SiMe_3)_2$ derivative owing to the weaker Ge–Ge bonds.

The testing of germanium halide derivatives of other bulky substituents such as Bu^t did not afford $(GeBu^t)_n$ species. Instead, a variety of polygermane species with interesting structures were isolated [38]. The use of the more bulky $-CMeEt_2$

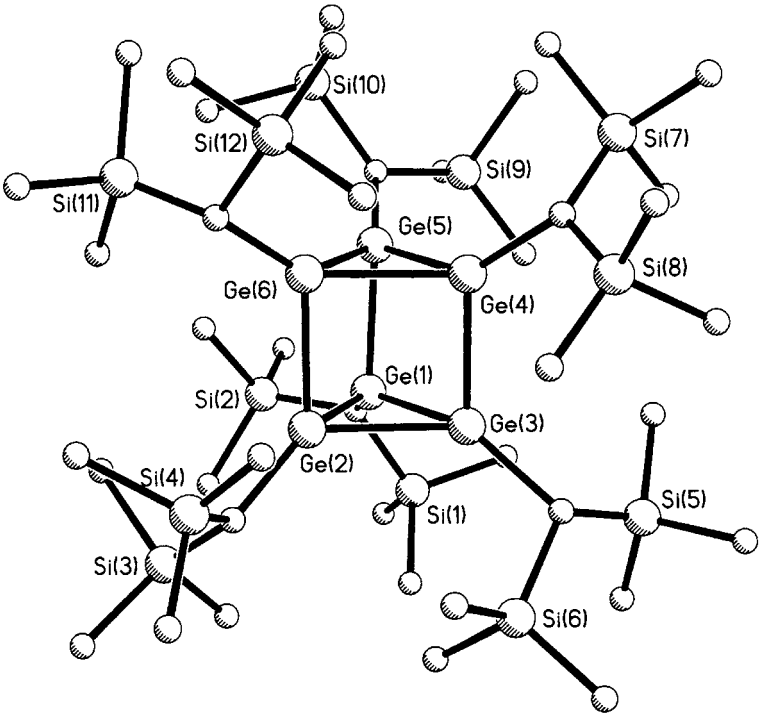

Fig. 2.5-7. X-ray crystal structure of $Ge_6\{CH(SiMe_3)_2\}_6$ [37]. H atoms are not shown.

substituent [39] led to the octacubane species $Ge_8\{CMeEt_2\}_8$ in about 16% yield, via the reduction of a tetrahalocyclotetragermane c–$Ge_4Cl_4\{CMeEt_2\}_4$ with Mg/$MgBr_2$. The cluster $Ge_8\{CMeEt_2\}_8$ can also be synthesized in 3% yield by reduction of $(Et_2MeC)GeCl_3$. A complete X-ray structure was not obtainable owing to disorder problems. However, the data showed that the cubane skeleton was regular and the Ge–Ge bond length averaged 2.534 Å [6]. X-ray data for $Ge_8(C_6H_3\text{-}2,6\text{-}Et_2)_8$ also showed a regular Ge_8 cubane array with an average Ge–Ge bond length of 2.490 Å [40]. The difference between the Ge–Ge distances, which are both longer than a Ge–Ge single bond, is due to the different steric requirements of the substituents.

Recent developments [40] have involved further reactions of the $[Ge_3R^*{}_3]$-$[B(C_6F_5)_4]$ ($R^* = SiBu^t{}_3$) salt, which when reacted with KI afforded $Ge_3R^*{}_3I$. Heating of this species in PhMe at 50 °C for 1 week afforded the novel aggregate $[Ge_{10}R^*{}_6I][B(C_6F_5)_4]$ as shown in Figure 2.5-8. It features a triangular array of three unsubstituted germaniums sandwiched between two $Ge_3R^*{}_6$ moieties, one of which is capped by GeI. The interatomic distances between the unsubstituted germaniums are ca. 3.26 Å and are much longer than a single bond. The remaining Ge–Ge distances range between 2.489 and 2.545 Å similar to the lower clusters. These results suggest that other higher molecular clusters of germanium can also be synthesized by similar routes.

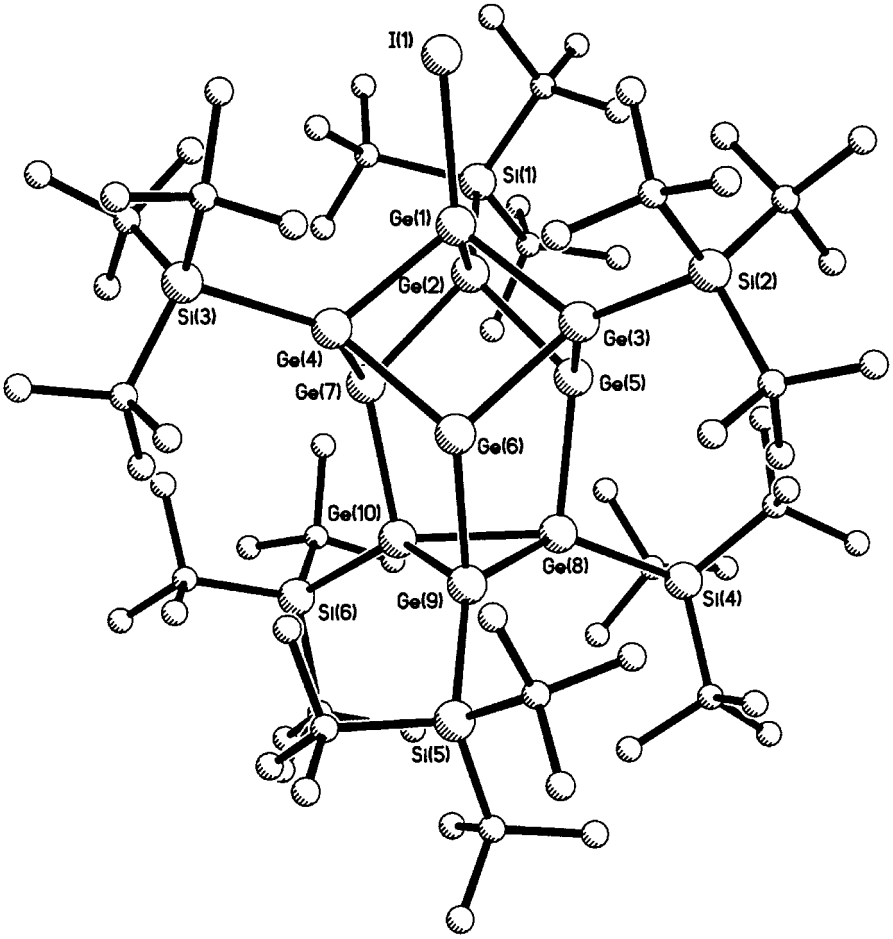

Fig. 2.5-8. X-ray crystal structure of the $[Ge_{10}R^*_6I]^+$ cation in $[Ge_{10}R^*_6I][B(C_6F_5)_4]$ ($R^* = SiBu^t_3$) [40]. H atoms are not shown.

2.5.4
Tin Cages and Clusters and Sn_nR_m ($n \geq m$)

2.5.4.1
Dimers, Trimers and Tetramers

The radius of tin (ca. 1.4 Å) is substantially greater than that of silicon (1.17 Å) or germanium (1.22 Å) [41]. As a result, steric protection of tin to the same degree as either silicon or germanium requires substantially larger substituents. Accordingly, it is more difficult to stabilize the lower aggregate tin clusters even with very large

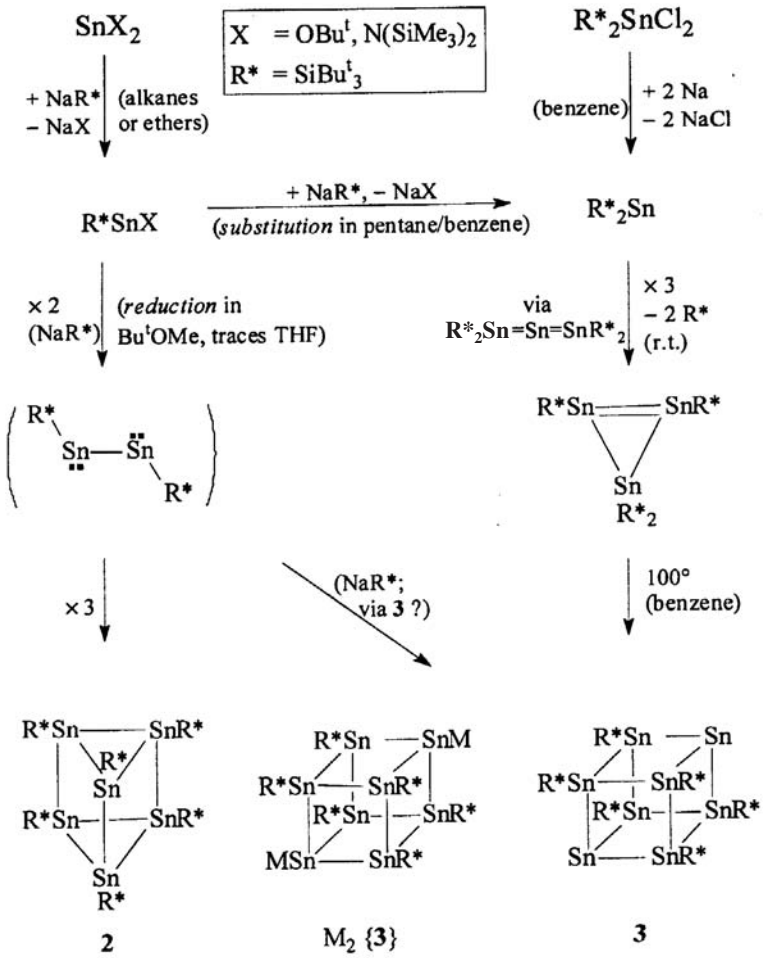

Scheme 2.5-2. Synthetic routes to the cages and clusters **2**, **3**, and M_2{**3**} [M = Na(THF)$_2$] [42–44].

substituents. This difficulty is reflected in the fact that no stable Sn_3R_3 or Sn_4R_4 clusters are currently known. Nonetheless, the related red-brown tetrasupersilyltristannacyclopropene $Sn_3R_4^*$ can be formed, according to Scheme 2.5-2, from $R^*_2SnCl_2$ and Na in benzene at room temperature, or from SnX_2 [X = OBu^t, N(SiMe$_3$)$_2$] and NaR* in pentane/benzene at −78 °C via the stannylene SnR_2^* and the dark violet tristannaallen $R^*_2Sn{=}Sn{=}SnR_2^*$ which, with a half-life of 9.8 h, isomerizes into $Sn_3R^*_4$. It is notable because it contains the shortest known Sn–Sn double bond distance of 2.59 Å [42].

Attempts to prepare the lower aggregates have led either to higher aggregates or to disproportionated products. Nonetheless, use of the extremely bulky terphenyl ligand Ar′ = C_6H_3-2,6-Dipp$_2$ allowed the first dimer of the type Ar′SnSnAr′ to be

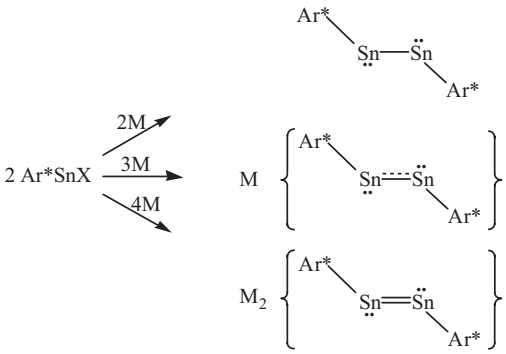

Scheme 2.5-3. Reduced salts of diaryltin species (Ar*=C_6H_3-2,6-$Trip_2$; Trip=C_6H_2-2,4,6-*i*-Pr_3).

isolated upon reduction of Sn(Cl)Ar′ with potassium [45]. Like its germanium counterpart [28], it is the first stable tin analogue of an alkyne and it possesses a planar *trans-bent* Sn_2C_2 core structure with an Sn–Sn bond length of 2.6675(4) Å. It is probable that the bonding is similar to that in Ar′GeGeAr′ discussed earlier. It is also possible to obtain reduced salts of diarylditin species as shown by Scheme 2.5-3.

These could be isolated as both singly and doubly reduced species. The singly reduced species $[K(THF)_6][Ar^*SnSnAr^*]$ [46] or $(THF)_3Na\{Ar^*SnSnAr^*\}$ [47] are radicals and display EPR signals which indicate that the unpaired electron could be located in a π orbital lying perpendicular to the *trans-bent* CSnSnC core. The Sn–Sn distances are close to 2.81 Å and there is a narrow Sn–Sn–C angle of around 95°. The addition of a second electron by potassium reduction results in $K_2\{Ar^*SnSnAr^*\}$ which displays a shortening of the Sn–Sn bond to 2.7763(9) Å [32]. Both these distances are distinctly longer than the 2.6675(4) Å found in Ar′SnSnAr′, which underlines the multiplicity of the Sn–Sn bond in this compound.

2.5.4.2
Hexamers, Octamers and Decamers

Thermolysis of the cyclotristannane $\{Sn(C_6H_3\text{-}2,6\text{-}Et_2)_2\}_3$, under different conditions, yielded a variety of clusters as indicated by Scheme 2.5-4 (cf. thermolysis of the tristannaallene, Scheme 2.5-2). By heating at 200 °C in naphthalene the perstanna [1.1.1] propellanes **4** [48] and **5** [49] could be isolated. It was also discovered that these products could be obtained by reaction of the cyclotristannane with lithium in THF. Although **4** and **5** do not strictly lie within the scope of this discussion, the ratio of Sn:R approaches 1:1. Also, the fact that they were obtained from a common starting material under slightly different conditions suggests a close relationship in the mechanisms whereby the Sn_n frameworks are assembled. They are of further interest owing to the fact that their frameworks are formally electron

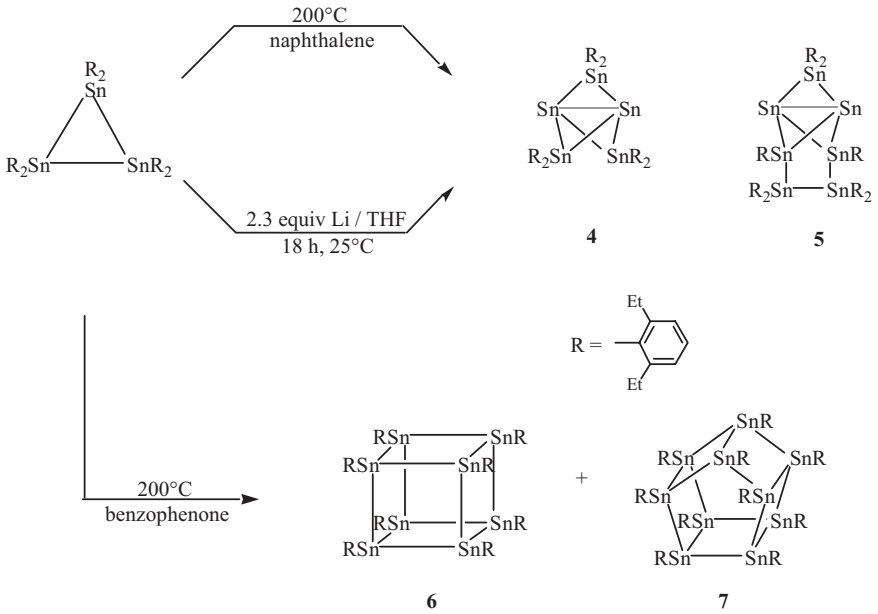

Scheme 2.5-4. Synthetic routes to the tin cages clusters **4**–**7** [9].

deficient (e.g., 10 framework electrons in the case of **4**). The structures of all the compounds presented in Scheme 2.5-4 were established by X-ray crystallography and ^{119}Sn NMR spectroscopy. In the cubane compound $Sn_8(C_6H_3\text{-}2,6\text{-}Et_2)_8$, **6**, which was obtained by the thermolysis of the cyclotristannane at 200 °C in benzophenone [50], the Sn_8 cube has a regular geometry with an average Sn–Sn bond length of 2.854 Å. This bond length is just slightly shorter than that predicted for the parent Sn_8H_8 system [14, 51] so that it can be assumed that steric effects do not play an important role in determining the Sn–Sn distances in this compound. This view is supported by the structure of the unique decastannaprismane, **7** [52], in which the average Sn–Sn distance is very similar at 2.856 Å (Figure 2.5-9). Both sets of Sn–Sn bond lengths are ca. 0.05 Å longer than the Sn–Sn distance in grey tin.

The trigonal prismatic compound $Sn_6R^*_6$, **2**, can be formed according to Scheme 2.5-2 as dark violet crystals by the reaction of the amide $Sn\{N(SiMe_3)_2\}_2$ with two equivalents of NaR^* in Bu^tOMe [43]. The structure of $Sn_6R^*_6$ has an almost equilateral Sn_6 trigonal prismane framework with slight deviations from regularity. The Sn–Sn distance within the Sn_3 triangular faces is 2.91 Å, whereas there is a small variation, 2.91–2.94 Å, in the Sn–Sn bonds between the triangles. The Sn_6 core is electron precise in that the Sn–Sn bonds may be regarded as two-electron, two-center bonds. Its structure thus differs from that of the Zintl ion $[Sn_6\{Cr(CO)_5\}_6]^{2-}$ which (Figure 2.5-10) has an octahedral array of atoms [53]. In this compound the Sn–Sn distances range from 2.90 to 2.93 Å. The Sn_6^{2-} array

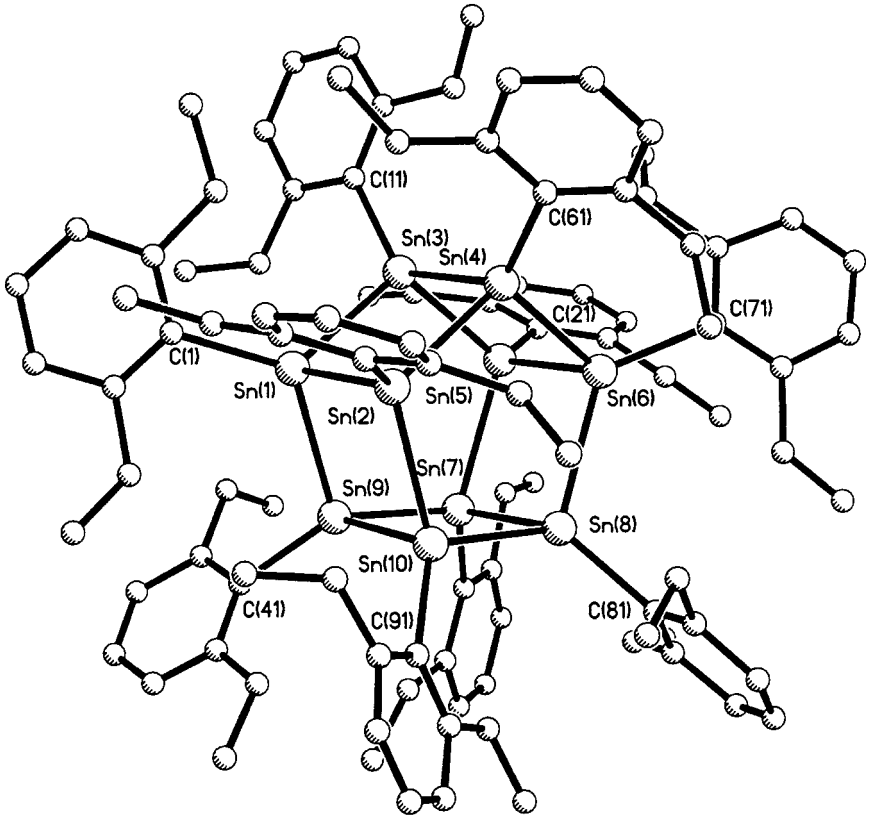

Fig. 2.5-9. X-ray crystal structure of $Sn_{10}(C_6H_3\text{-}2,6\text{-}Et_2)_{10}$ [52]. H atoms are not shown.

has 14 electrons available for cage bonding and each tin lone pair coordinates a $Cr(CO)_5$ moiety.

Thermolysis of $Sn_3R^*_4$ in benzene at 100 °C led to the species $Sn_8R^*_6$ **7** (Scheme 2.5-2) which has a cubane structure in which two diagonally opposed tins carry no substituent [44]. Full details of the structure could not be given owing to disorder problems. However, according to Scheme 2.5-2 the related species $[\{(THF)_2Na\}_2Sn_8R^*_6]$ ($M_2\{\mathbf{3}\}$) could be obtained as black crystals by the reaction of NaR^* with $Sn\{N(SiMe_3)_2\}_2$ in Bu^tOMe at ca. −78 °C [44]. This compound also features a nearly regular cubane Sn_8 framework with tin–tin distances in the range 2.871(2)–2.908(2) Å, which are somewhat longer than the 2.80 Å found in gray tin [41]. Diagonally opposed tins carry the sodium substituents with an Na–Sn distance of 3.099(7) Å. The ^{119}Sn NMR displays two high field tin signals at δ −767 (6 SnR^*) and at −2045.1 (2 SnNa). The formation of $M_2\{\mathbf{3}\}$, as well as the trigonal prismatic **2**, probably results from the reduction of initially obtained R^*SnX by NaR^* via the bisstannylene R^*SnSnR^* which trimerizes into **2**, or tetramerizes with

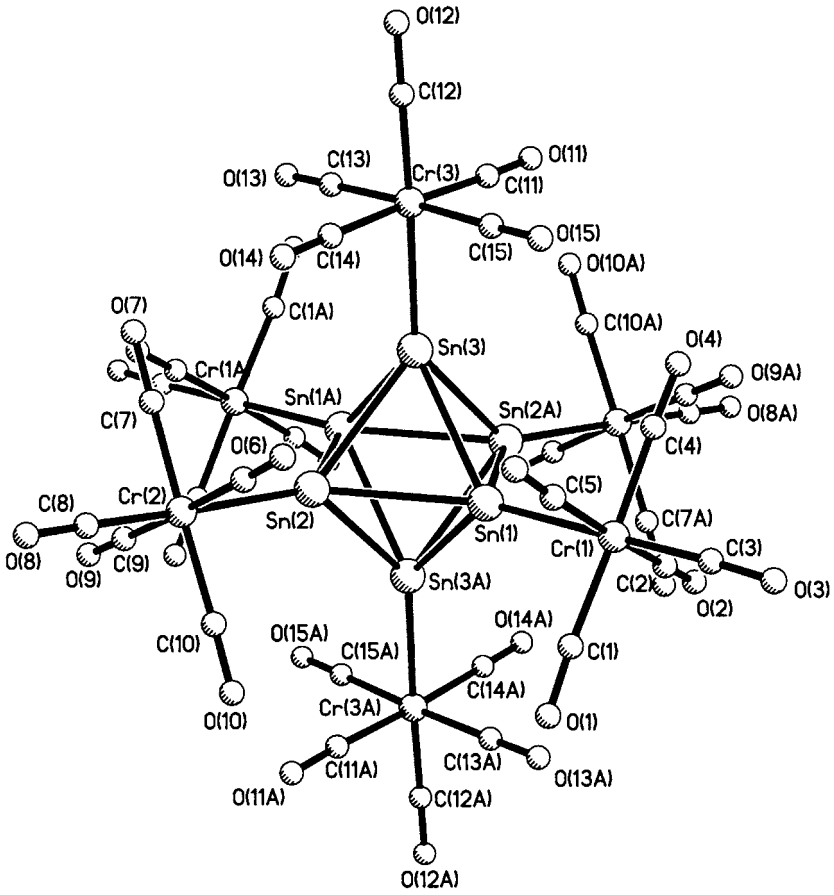

Fig. 2.5-10. X-ray crystal structure of the anion in the salt [K(2.2.2-cryptand)]2[$Sn_6\{Cr(CO)_5\}_6$] [53].

the loss of two R* groups into **3** whereupon **3** is reduced by NaR* to $M_2\{\mathbf{3}\}$ (Scheme 2.5-1).

The reduction of 2,6-$Mes_2H_3C_6SnCl$ with potassium produced a different type of Sn_8 cluster in the form of $Sn_8(C_6H_3\text{-}2,6\text{-}Mes_2)_4$ [54] (Figure 2.5-11). This product may be contrasted with the dimer Ar′SnSnAr′ discussed earlier which was produced by reduction of the more crowded Ar′SnCl precursor. The X-ray crystal structure shows that the Sn_8 core is arranged as a rhombic prism with possible transannular Sn–Sn [3.107(2) Å] interactions as illustrated. The Sn–Sn edges have bond lengths in the range 2.853(2)–3.023(2) Å. The bonding can be considered in a number of ways. One possibility is that it consists of a central Sn_4 core, with single Sn–Sn bonds and a lone pair at each tin that carries no organic substituents and which is complexed by two *cis*-alkyne analogue 2,6-$Mes_2H_3C_6SnSnC_6H_3$-2,6-Mes_2

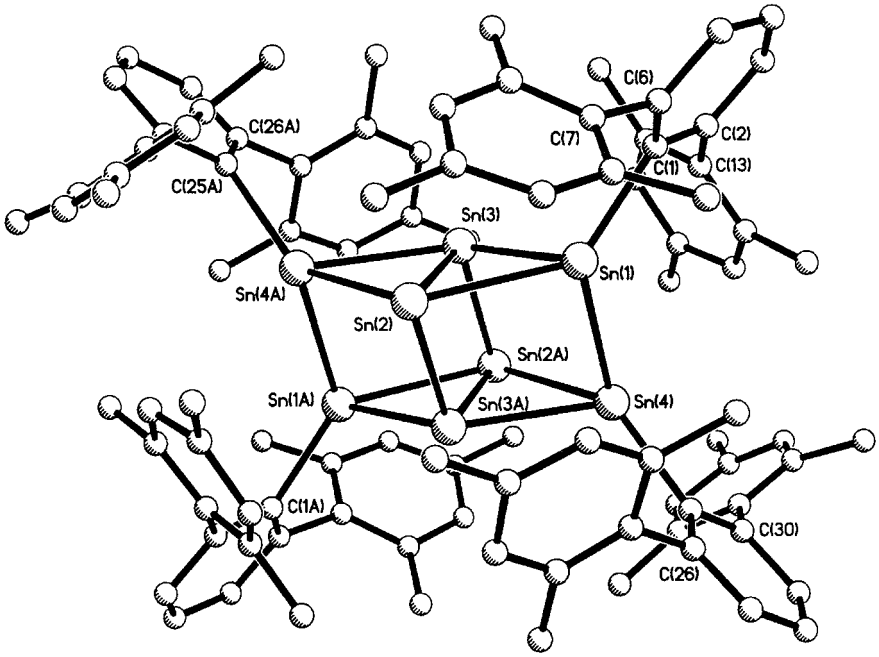

Fig. 2.5-11. X-ray crystal structure of $Sn_8(C_6H_3\text{-}2,6\text{-}Mes_2)_4$ [54]. H atoms are not shown.

fragments. However, the ''alkyne'' Sn–Sn bonds show no evidence of shortening [Sn–Sn = 2.971(2) Å] and there is a large torsion angle between the Sn–C bonds. Assuming that the four unsubstituted tins supply two electrons each for framework bonding and the four substituted tins each supply three electrons, there are 20 electrons available so that the Sn_8 moiety is electron deficient, which is probably the source of the observed structural distortions. The ^{119}Sn NMR displays two Sn signals at δ 751.7 and 483.1. The lower field signal was assigned to the substituted tins. ^{119}Sn NMR spectroscopy of the crude reaction mixture displayed several other peaks indicating that other species are present in solution.

2.5.5 Lead Clusters Pb_nR_n

At present, lead clusters of the formula Pb_nR_n are limited to one stable species. This is the recently reported dimer 2,6-$Trip_2H_3C_6PbPbC_6H_3$-2,6-$Trip_2$ (Trip = C_6H_2-2,4,6-Pr^i_3) [55]. Although it is formally an alkyne analogue (a ''diplumbyne''), the X-ray crystal structure showed that the planar CPbPbC core is *trans-bent* with a narrow CPbPb angle of 94.26(4)° and a Pb–Pb distance of 3.181(1) Å. The long Pb–Pb bond (compared with the 2.9 Å for Pb–Pb single bonds in diplumbanes [41]) and the near right angle at lead suggests that each lead atom bonds

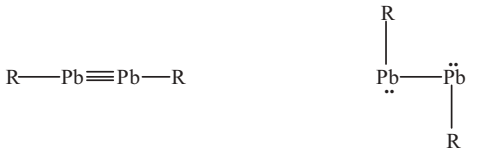

diplumbyne diplumbylene

Scheme 2.5-5. Structure of lead dimmers.

through one of their 6p orbitals, leaving a lone pair at each lead that is mainly 6s in character. The structure is therefore a diplumbylene rather than a diplumbyne as illustrated by Scheme 2.5-5.

The structure is a manifestation of the decreased hybridization in the heavier main group elements, which in the case of lead is further diminished by relativistic effects. Nonetheless calculations on the model species 2,6-$Ph_2H_3C_6PbPbC_6H_2$-2,6-Ph_2 have indicated that the very bulky terphenyl ligands stabilize the strongly *trans-bent* structure with a long Pb–Pb bond [56]. With less bulky phenyl substituents a wider Pb–Pb–C angle with a shorter Pb–Pb bond or even a phenyl bridged structure is predicted to be more stable.

2.5.6 Conclusion

Molecular cages and clusters of the formula Tt_nR_n ($n \geq m$) are known for all the heavier main group 14 elements. At present, the only stable examples known for lead is a dimeric Pb_2R_2 species. It seems probable that a much greater range of lead clusters can be synthesized since lead clusters in the form of Zintl anions, for example Pb_5^{2-} or Pb_9^{3-} [1], have been reported. For silicon, germanium and tin, the E_nR_n compounds are limited to a maximum value of $n = 10$. However, it may be possible to increase this number especially in the case of the related Tt_nR_m ($n > m$) species. Although only a handful of these are known, and none has an n value > 10, in the neighboring triel (group 13) elements clusters with as much as 84 triel atoms have been isolated and characterized [57]. The synthesis of related clusters of the tetrels, which may have important electronic or optical properties, can be anticipated.

References

1 J. D. Corbett, *Angew. Chem., Int. Ed. Engl.*, **2000**, *39*, 670–690.
2 S. Bobev, S. C. Sevov, *J. Am. Chem. Soc.*, **2002**, *124*, 3359–3365.
3 S. Bobev, S. C. Sevov, *J. Solid State Chem.*, **2000**, *153*, 92–105.
4 J. S. Kasper, P. Hagenmuller, M. Pouchard, C. Cros, *Science*, **1965**, *150*, 1713–1714.
5 S. Bobev, S. C. Sevov, *J. Am. Chem. Soc.*, **2001**, *123*, 3389–3390.
6 A. Sekiguchi, H. Sakurai, *Adv.*

Organomet. Chem., **1995**, *37*, 1–38.

7 A. Sekiguchi, S. Nagase, *The Chemistry of Organic Silicon Compounds*, Vol. 2, Part. 1, Z. Rappoport, Y. Apeloig, eds., Wiley, Chichester, 1998, Ch. 3, pp. 119–152.

8 L. R. Sita, *Acc. Chem. Res.*, **1994**, *27*, 191–197.

9 L. R. Sita, *Adv. Organomet. Chem.*, **1995**, *38*, 187–243.

10 R. Pietschnig, R. West, D. R. Powell, *Organometallics*, **2000**, *19*, 2724–2729.

11 N. Wiberg, W. Niedermayer, H. Nöth, M. Warchold, *Z. Anorg. Allg. Chem.*, **2001**, *627*, 1717–1722.

12 N. Wiberg, W. Niedermayer, G. Fischer, H. Nöth, M. Suter, *Eur. J. Inorg. Chem.*, **2002**, 1066–1070, and N. Wiberg, S.-K. Vasiskt, G. Fischer, M. Veith, to be published.

13 N. Takagi, S. Nagase, *Eur. J. Inorg. Chem.*, **2002**, *11*, 2775–2778.

14 S. Nagase, *Acc. Chem. Res.*, **1995**, *28*, 469–476.

15 D. A. Clabo, Jr., H. F. Schaeffer, III, *J. Am. Chem. Soc.*, **1986**, *108*, 4344–4349.

16 (a) S. Nagase, M. Nakano, *Angew. Chem., Int. Ed. Engl.*, **1988**, *27*, 1081–1083. (b) N. Wiberg, W. Niedermayer, *Z. Naturforsch.*, **2000**, *55b*, 406–416. (c) N. Wiberg, H. Auner, S. Wagner, K. Polborn, G. Kramer, *J. Organomet. Chem.*, **2001**, *619*, 110–131.

17 M. Ichinohe, M. Tovoshima, R. Kinjo, A. Sekiguchi, *J. Am. Chem. Soc.* **2003**, in press.

18 N. Wiberg, C. M. M. Finger, K. Polborn, *Angew. Chem., Int. Ed. Engl.*, **1993**, *32*, 1054–1056; N. Wiberg, C. M. M. Finger, H. Auner, K. Polborn, *J. Organomet. Chem.*, **1996**, *521*, 377–386.

19 E. Lukevics, O. Pudova, *Main Group Met. Chem.*, **1998**, *21*, 123–183.

20 N. Wiberg, H. Auer, H. Nöth, J. Knizek, K. Polborn, *Angew. Chem., Int. Ed. Engl.*, **1998**, *37*, 2869–2872.

21 N. Wiberg, H. Auer, K. Polborn, M. Veith, V. Huch, *Organosilicon Chemistry IV: From Molecules to Materials*, N. Auner, J. Weis, eds., Wiley-VCH, Weinheim, **2000**, pp. 124–126.

22 A. Sekiguchi, T. Yatabe, C. Kabuto, H. Sakurai, *J. Am. Chem. Soc.*, **1993**, *115*, 5853–5854.

23 H. Matsumoto, K. Higuchi, Y. Hoshino, H. Koike, Y. Naoi, Y. Nagai, *Chem. Commun.*, **1988**, 1083–1084.

24 K. Furukawa, M. Fujino, N. Matsumoto, *Appl. Phys. Lett.*, **1992**, *60*, 2744–2745; K. Furukawa, M. Fujino, N. Matsumoto, *J. Organomet. Chem.*, **1996**, *515*, 37; H. Tachibana, M. Goto, M. Matsumoto, H. Kishida, Y. Tokada, *Appl. Phys. Lett.*, **1994**, *64*, 2509–2510; K. Furukawa, M. Fujino, N. Matsumoto, *Appl. Phys. Lett.*, **1995**, *66*, 1291; H. Tachibana, M. Goto, M. Matsumoto, H. Kishida, Y. Tokuna, *Appl. Phys. Lett.*, **1995**, *66*, 1292–1293.

25 H. Matsumoto, K. Higuchi, S. Kyushin, M. Goto, *Angew. Chem., Int. Ed. Engl.*, **1992**, *31*, 1354–1356.

26 A. Sekiguchi, T. Yatabe, H. Kamatani, C. Kabuto, H. Sakurai, *J. Am. Chem. Soc.*, **1992**, *114*, 6260.

27 M. Unno, T. Yokota, H. Matsumoto, *J. Organomet. Chem.*, **1996**, *521*, 409–411.

28 M. Stender, A. D. Phillips, R. J. Wright, P. P. Power, *Angew. Chem., Int. Ed. Engl.*, **2002**, *41*, 1785–1787.

29 R. S. Grev, *Adv. Organomet. Chem.*, **1991**, *33*, 125–170.

30 T. L. Allen, W. H. Fink, P. P. Power, *Dalton Trans.*, **2000**, 407–412.

31 M. Stender, A. D. Phillips, P. P. Power, *Chem. Commun.*, **2002**, 1312–1313.

32 L. Pu, M. O. Senge, M. M. Olmstead, P. P. Power, *J. Am. Chem. Soc.*, **1998**, *120*, 12682–12683.

33 A. Sekiguchi, M. Tsukamoto, M. Ichinoke, *Science* **1997**, *275*, 60–61; M. Ichinoke, N. Fukaya, A. Sekiguchi, *Chem. Lett.*, **1998**, 1045–1046; A. Sekiguchi, N. Fukaya, M. Ichinoke, Y. Ishida, *Eur. J. Inorg. Chem.*, **2000**, 1155–1159.

34 M. M. Olmstead, L. Pu, R. S. Simons, P. P. Power, *Chem. Commun.*, **1997**, 1595–1596.

35 N. Wiberg, W. Hochmuth, H. Nöth, A. Appel, M. Schmidt-Amelunxen, *Angew. Chem., Int. Ed. Engl.*, **1996**, *35*, 1333–1334.

36 C. E. Holloway, M. Melnik, *Main Group Met. Chem.*, **2002**, *25*, 185–266.

37 A. Sekiguchi, C. Kabuto, H. Sakurai, *Angew. Chem. Int. Ed. Engl.*, **1989**, *28*, 55–56.

38 A. Sekiguchi, H. Naito, C. Kabuto, H. Sakurai, *J. Chem. Soc. Jpn., Chem. Ind.*, **1994**, 248–252.

39 A. Sekiguchi, T. Yatabe, C. Kabuto, H. Sakurai, *J. Am. Chem. Soc.*, **1992**, *114*, 6260–6262.

40 A. Sekiguchi, Y. Ishida, Y. Kabe, M. Ichinoke, *J. Am. Chem. Soc.*, **2002**, *124*, 8776–8777.

41 A. F. Wells, *Structural Inorganic Chemistry*, 5th edn., Clarendon, Oxford, 1984, p. 1279.

42 N. Wiberg, H.-W. Lerner, S.-K. Vasisht, S. Wagner, K. Karaghiosoff, H. Nöth, W. Ponikwar, *Eur. J. Inorg. Chem.*, **1999**, 1211–1218.

43 N. Wiberg, H.-W. Lerner, H. Nöth, W. Ponikwar, *Angew. Chem., Int. Ed. Engl.*, **1999**, *38*, 1103–1105.

44 N. Wiberg, H.-W. Lerner, S. Wagner, H. Nöth, T. Seifert, *Z. Naturforsch.*, **1999**, *54B*, 877–880.

45 A. D. Phillips, R. J. Wright, M. M. Olmstead, P. P. Power, *J. Am. Chem. Soc.*, **2002**, *124*, 5931–5932.

46 M. M. Olmstead, R. S. Simons, P. P. Power, *J. Am. Chem. Soc.*, **1997**, *119*, 11705–11706.

47 L. Pu, S. T. Haubrich, P. P. Power, *J. Organomet. Chem.*, **1999**, *582*, 100–102.

48 L. R. Sita, R. D. Bickerstaff, *J. Am. Chem. Soc.*, **1989**, *111*, 6454–6456.

49 L. R. Sita, I. Kinoshita, *J. Am. Chem. Soc.*, **1992**, *114*, 7024–7029.

50 L. R. Sita, I. Kenoshita, *Organometallics*, **1990**, *9*, 2865.

51 S. Nagase, *Angew. Chem., Int. Ed. Engl.*, **1989**, *28*, 329–330.

52 L. R. Sita, I. Kenoshita, *J. Am. Chem. Soc.*, **1991**, *113*, 1856–1857.

53 B. Schiemenz, G. Huttner, *Angew. Chem., Int. Ed. Engl.*, **1993**, *32*, 297–298.

54 B. E. Eichler, P. P. Power, *Angew. Chem., Int. Ed. Engl.*, **2001**, *40*, 796–797.

55 L. Pu, B. Twamley, P. P. Power, *J. Am. Chem. Soc.*, **2000**, *122*, 3524–3525.

56 Y. Chen, M. Hartmann, M. Diedenhofer, G. Frenking, *Angew. Chem., Int. Ed. Engl.*, **2001**, *40*, 2052–2055.

57 H. Schnöckel, A. Schnepf, *Adv. Organomet. Chem.* **2001**, *47*, 235–281.

2.6
Homoatomic Cages and Clusters of the Heavier Group 15 Elements: Neutral Species and Cations

Ingo Krossing

In this chapter an account of isolated cationic and neutral homoatomic heavier group 15 cages and clusters is given, that is, charged or non-charged assemblies of two or more elemental atoms E (E = P, As, Sb, Bi) without stabilizing (bulky) ligands. In the context of this discussion we differentiate between cages and clusters. Cages comprise an electron precise three dimensional arrangement of atoms in which the edges of the polyhedron are best described as localized 2e2c bonds. Most of the neutral polyphosphorus species and polyphosphides fall into this category. By contrast, the bonding within a cluster is electron deficient and totally delocalized. Therefore, the edges of a cluster-polyhedron have only a topological but not necessarily a bonding implication. All heavier group 15 cations as well as neutral E_4 (E = P–Bi) are clusters according to this definition. The focus of the chapter is on the recent developments in the condensed as well as the gas phase and only key references predating 1985 are given.

2.6.1
Introduction

Homoatomic heavier group 15 elemental cages and clusters have a long standing history, and tetrahedral white phosphorus P_4 was the first representative discovered by H. Brandt as early as 1669. Since 1844 this pyrophoric molecule has been manufactured industrially for match production on the ton scale by A. Albright in England. Nevertheless, the number of stable isolated homoatomic heavier group 15 cages and clusters remains low and is dominated in numbers by Zintl-type polyphosphides and its arsenic and antimony homologues, which are often structurally related to the Hittorf allotrope of phosphorus. The structural chemistry of such polyatomic cage anions is well understood, well documented and therefore only of partial interest for this chapter [1, 2]. In contrast, very few neutral group 15 cages are known and only bismuth has a well developed chemistry of electron deficient polyatomic cluster cations in the condensed phase. Our knowledge on such rare species and the reasons for the discrepancy between cation/neutral/anion sta-

Tab. 2.6-1. Experimentally determined fundamental properties of group 15 elements and small elemental rings, cages and clusters E_2 to E_5. Values given in italics are less certain [6].

Property	*P*	*As*	*Sb*	*Bi*
χ(Allred-Rochow)	2.06	2.20	1.82	1.67
d(E–E) in E_4 (pm)	221	243	287[a)]	312[a)]
d(E≡E) in E_2 (pm)	189.3	210.3	234.2	266.0
$r_{cov.}(E^{III})$ (pm)	110	121	141	152
BE(E–E) (kJ mol^{-1})	201	146	121	–
$D^\circ_{298}(E_2)$ (kJ mol^{-1})	490	382	299	200
IE(E) [EA(E)] (eV)	10.49 (0.75–0.77)	9.82 (0.81)	8.64 (1.05–1.07)	7.29 (0.95)
IE(E_2) [EA(E_2)] (eV)	10.53 (0.59–0.63)	10.0 (0.74)	≤8.43 (1.28)	≤7.34 (1.27)
IE(E_3) [EA(E_3)] (eV)	7.9 (1.67)	*8.1* (1.45)	*7.5* (1.85)	*8.8* (1.60)
IE(E_4) [EA(E_4)] (eV)	9.25–9.34 (1.35)	9.1–9.3 (*<0.8*)	7.4–7.8 (*<1.0*)	7.3–7.6 (1.05)
IE(E_5) [EA(E_5)] (eV)	7.04[b)] (3.88[c)])	7.9 (3.5[c)])	–(3.46[c)])	–(2.87[c)])
$\Delta H_f^\circ(E_{2,g})$ (kJ mol^{-1})	144	222	236	220
$\Delta H_f^\circ(E_{4,g})$ (kJ mol^{-1})	59	–	–	–

[a)] Calculated multi reference CI value [9]. [b)] Calculated DFT value [8].
[c)] Adiabatic detachment energy [7]. Abbreviations used: $r_{cov.}(E^{III})$ = covalent radius of element E in a trivalent compound; BE(E–E) = bond enthalpy of a single E–E bond; $D^\circ_{298}(E_2)$ = dissociation enthalpy of the E_2 molecule at standard conditions; IE = ionization enthalpy; EA = electron affinity; $\Delta H_f^\circ(E_{2,g})$ = standard enthalpy of formation of the gaseous E_2 molecule.

bilities are summarized in this chapter. Questions raised are, for example: why is it that P and As cations are unknown, but structurally characterized homopolyatomic cations of the more electronegative and thus seemingly, for cation formation, less favorable nitrogen and chalcogens are abundant [3–5].

The trend for anion formation for P but cation formation for Bi clearly becomes evident from the fundamental properties of the elements and their small elemental rings, cages and clusters E to E_5 collected in Table 2.6-1. While P clearly is a nonmetal with comparatively high P–P single bond energies, high ionization energies and a higher electronegativity χ, the situation gradually changes on going down to the metallic element Bi with low single bond energies, low ionization energies and a lower electronegativity. Electron affinities (EA) vary only slightly throughout the group, but one notes that the EA reaches a maximum for the E_5 molecule and is highest for E = P. The electronegativity, the ionization potential and bond energies of Bi are similar to those of group 13 and heavier group 14 elements and, therefore, the cationic cluster chemistry of Bi is closely related to that of the isoelectronic Ge, Sn, Pb as well as In and Tl clusters. An example [10] is the similar structure of the isoelectronic trigonal bipyramidal pair E_5^{2-} (E = Sn, Pb) and Bi_5^{3+}. From Table 2.6-1 one also notes that the uneven open shell E_3 and E_5 molecules have lower ionization energies and higher electron affinities than the even members, which is due to the higher stability of the closed shell $E_3^{+/-}$ and $E_5^{+/-}$ species.

2.6.2 Neutral Homonuclear Pnicogen Clusters

In the light of several allotropic modifications known for phosphorus, the relatively high single bond energies and the tendency of phosphorus to catenate it remains mysterious, and that apart from P_4 and As_4 only very scarce information on isolated E_n cluster molecules is available from hard experimental data. In contrast, a vast amount of solid theoretical work has been performed [11].

2.6.2.1 Structures of the Tetrahedral E_4 Cages

Only the molecular structures of P_4 and As_4 were determined and show the E_4 cages to have a regular tetrahedral structure of T_d symmetry. For P_4 both, X-ray and gas phase electron diffraction (GED) data are available and indicate a P–P bond length of about 221 pm. Crystalline yellow As is very sensitive to light and also decomposes in the X-ray beam and therefore only its GED structure is known [d(As–As) = 243 pm]. However, vibrational spectroscopy indicated that solid yellow As also consists of regular As_4 molecules [12]. The yellow form of Sb, which is also thought to be built from isolated Sb_4 tetrahedra [13], is even more sensitive to temperature and light and transforms to gray Sb readily at −90 °C. No structural data are, therefore, available for Sb_4 as well as Bi_4 [14] but (relativistically adjusted) high level CI calculations [15] give the Sb–Sb and Bi–Bi bond lengths as 287 and 312 pm, respectively. However, from mass spectrometric studies it is clear that Sb evaporates preferentially as Sb_4, while the Bi_4 concentration above solid Bi is low. The most abundant species is Bi_2 with a small amount of Bi_3 [16–18].

2.6.2.2 Bonding in P_4

From first principles it is clear that the bonding in the E_4 molecules with the very acute E–E–E bond angle of 60° but still strong E–E bonds reflects a special electronic situation. All classical bonding possibilities, that is a situation similar to tetrahedrane C_4H_4 with sp^3 hybridized P atoms (ideal bond angle: 109.5°) or a full s–p separation and only p orbital contributions to the cage bonding (ideal bond angle: 90°), would imply that the P_4 molecule with only 60° bond angles includes a high strain energy. In contrast to C_4H_4 tetrahedrane, which has a strain energy [19] in the order of 500 kJ mol^{-1}, this is not the case and the P_4 molecule is virtually unstrained (65 kJ mol^{-1}) [19–21]. From the photoelectron spectrum of P_4, it followed that the highest occupied orbitals have 3p character. Putting these two facts together one would anticipate a hypothetical and yet unknown cubic P_8 molecule (only 90° bond angles, no strain) to be more stable than the tetrahedral P_4 molecule. However, this is clearly not the case (see Section 2.6.2.3). The calculated valence molecular orbitals of the P_4 molecules are presented in Figure 2.6-1

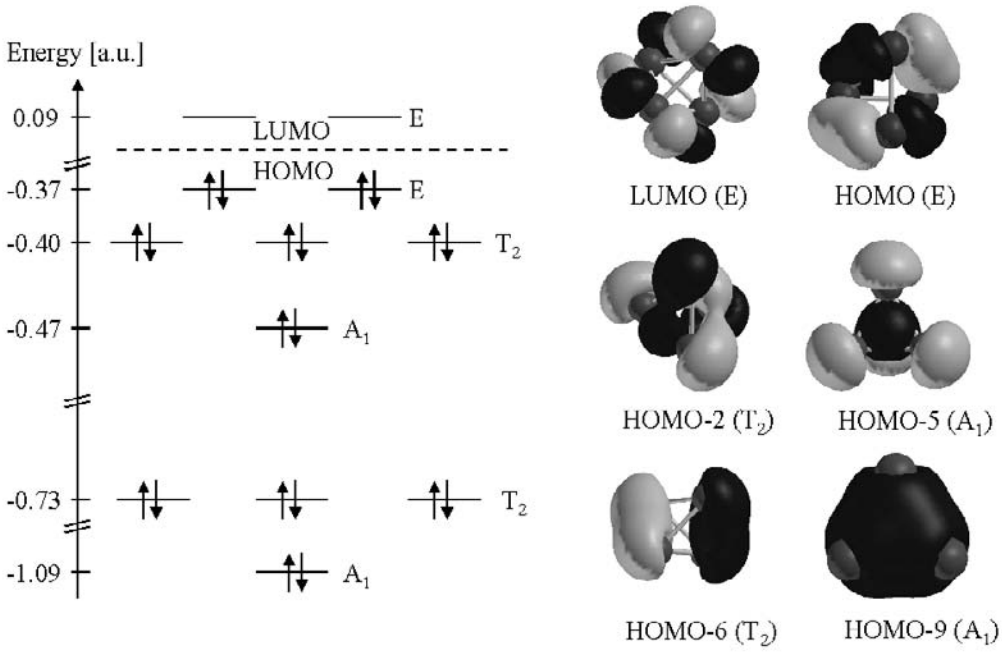

Fig. 2.6-1. Calculated valence molecular orbitals of tetrahedral P_4 (isodensity surface drawn at a cut off of 0.05 a.u.). Only one representation of the similar degenerate MOs is given.

[22, 23]. Twenty valence electrons, 8s and 12p electrons, have to be accommodated in the molecular orbitals of P_4. The 8s electrons are well separated from the p electrons and occupy the lowest four MOs of A_1 and T_2 symmetry. Overall, the 12 P–P bonding and 12 P–P antibonding interactions in these orbitals cancel and therefore these four MOs in Figure 2.6-1 have $3s^2$ lone pair character. From this assignment follows it that the P–P bonding is due to the strongly bonding P–P interactions in the upper set of occupied A_1, T_2 and E MOs formed by the 3p atomic orbitals. The graphic representation of these orbitals in Figure 2.6-1 shows the strongly delocalized ("cluster-like") bonding of the 3p electrons. The A_1 upper orbital may be constructed from four 3p atomic orbitals centered at the P atoms and pointing with lobes of the same symmetry to the center of the P_4 cage. This interaction leads to a strongly P–P bonding cluster-MO. According to the model of the spherical electron gas [22, 24], this A_1 orbital is a cluster π-orbital and inorganic cage molecules such as E_4 (E = P–Bi) or isoelectronic E_4^{4-} (E = Si–Pb) are "spherically aromatic" [22]. In the T_2 set of orbitals two pairs of collinear 3p atomic orbitals combine with two orthogonal P–P σ bonding MOs, which include additional three center interactions through the triangular faces of the tetrahedron; see Figure 2.6-2.

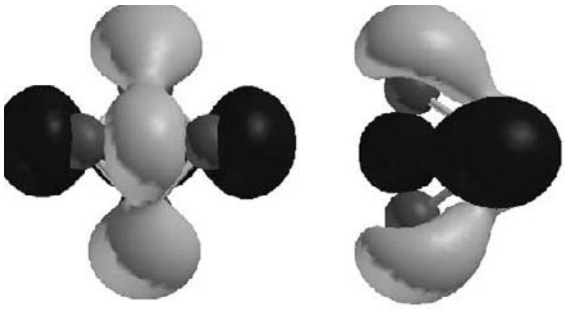

Fig. 2.6-2. Two additional views of the upper degenerate T_2 MOs in P_4.

The three upper degenerate T_2 MOs are highly delocalized and represent clearly 4c6e bonding MOs. Note that upon bond formation almost no strain results for the parent 3p atomic orbitals. The last set of degenerate MOs of *E* symmetry are the HOMOs, which can be constructed from four radially arranged 3p atomic orbitals (see Figure 2.6-3). Also in the HOMOs, the total number of P–P bonding interactions of 4 exceeds that of the antibonding interactions of 2 and, therefore, they are overall P–P bonding with no strain imposed on the constituting 3p atomic orbitals. Pauling has already suggested that bent "banana"-bonds account for the low strain in P_4 and the *E* orbital in Figure 2.6-3 may be viewed as an MO representation thereof. Since the HOMOs of P_4 are centered on the P–P edges, electrophiles should first attack the P–P edges based on frontier orbital arguments. Only recently could the primary steps of the reaction of P_4 with electrophiles be studied, and the preferential attack of the P–P edge of P_4 by H^+ and Ag^+ was verified experimentally. Indeed, gaseous H^+ affords the C_{2v} symmetrical HP_4^+ ion with an

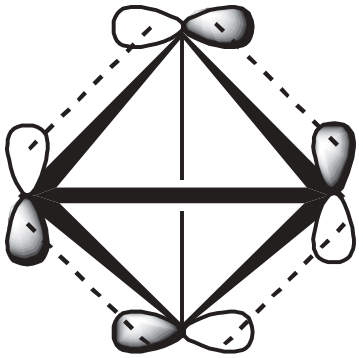

Fig. 2.6-3. Schematic representation of one of the P_4 HOMOs of *E* symmetry constructed from four radially arranged 3p atomic orbitals. The degenerate HOMO is similar and, therefore, omitted.

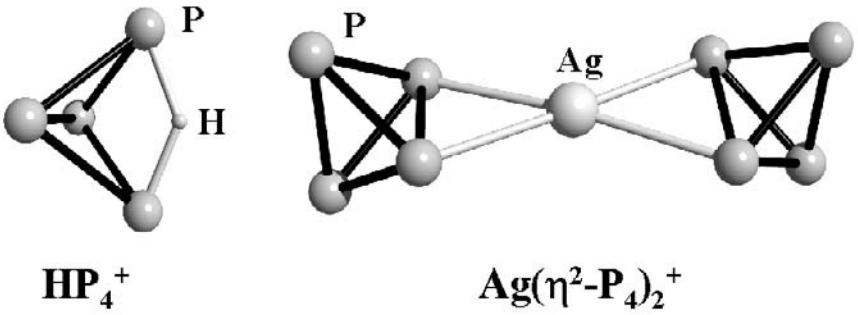

Fig. 2.6-4. Structures of HP_4^+ in the gas phase [25] and $Ag(\eta^2\text{-}P_4)_2^+$ in the crystal [26].

edge bridging 3c2e P–H–P bond [25] while reaction of P_4 with Ag^+ leads to the $Ag(\eta^2\text{-}P_4)_2^+$ cation in which Ag^+ ions coordinate to one P–P edge of each P_4 molecule (Figure 2.6-4) (see also Section 2.6.3.6) [26].

2.6.2.3 Larger P_n Cages ($n > 4$)

Although no E_n cluster molecules with $n > 4$ are known in the condensed phase, it has been shown [27] that neutral P_6 can be generated in the gas phase by neutralization-reionization mass spectrometry with $cp^*{}_2P_6$ as a precursor [$cp^* = C_5(CH_3)_5$] [28]. Since the $cp^*{}_2P_6$ precursor molecule already has a hetero-benzvalene P_6 skeleton, it was inferred that the neutral P_6 molecule should have the benzvalene structure as shown in Figure 2.6-5. This is in agreement with a multitude of quantum chemical calculations [8, 11, 27, 29–32]. Note that the handle of the basket of P_6 includes two dicoordinate P atoms linked by a P=P double bond (cf.: R-P=P-R: ≈203 pm [33]).

Much controversy arose over the prediction of the most stable P_8 structure. It was anticipated that a P_8 molecule should "naturally" possess a cubic structure with O_h symmetry. This geometry would ideally suit the formation of σ-MOs from the 3p atomic orbitals so that a cubic P_8 would have no strain and should be at least close in energy to twice that of P_4 [34]. However, paradoxically it is now firmly established by theory that the most stable P_8 geometry is the cuneane structure shown on the right in Figure 2.6-5 [8, 11, 19, 29–32].

The dimerization of 2 molecules of P_4 giving P_8 cuneane is endergonic at 298 K by 123.2 kJ mol^{-1} [11]. Structural rules for possible isomers of larger P_n molecules were developed [31] and some of these are more stable relative to gaseous P_4. For instance, the gaseous P_{18} isomer shown in Figure 2.6-6 is more stable by 36 kJ mol^{-1} than 4.5 molecules P_4 (free energy at 298 K) [11].

This P_{18} isomer contains two P_8 cuneane moieties linked through a P_2 bridge and resembles one of the structural motifs of Hittorf phosphorus shown in Figure

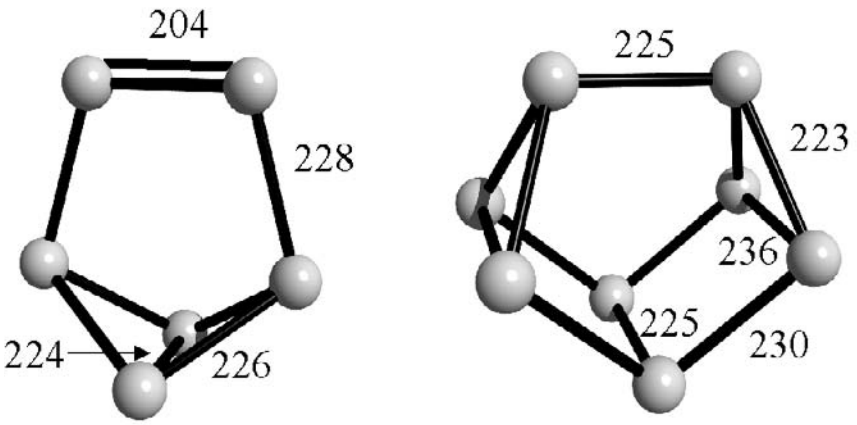

Fig. 2.6-5. Calculated structures of the most stable P_6 and P_8 isomers [8, 11]. Note that P_6 includes a double bond. Bond lengths were obtained at the BP86/SVP level [23]. For comparison: at the same level the P–P bond length of P_4 is 223 pm and close to the experimental value of 221 pm [35].

2.6-7. This structural similarity clearly points to the difficulties in obtaining pure samples of larger isolated P_n cages on a preparative scale: white phosphorus P_4 is only stable at room temperature because an aggregation is a symmetry forbidden process. Once the oligomerization process has started, it is difficult to stop at an intermediate molecular stage. Therefore, the product usually obtained is amorphous red phosphorus, which is thought to be built from long helical tubes of structural building blocks similar to those shown in the P_{18} structure, or that of Hittorf phosphorus shown in Figure 2.6-7 [36].

In addition to the P_8 cuneane building block, Hittorf phosphorus contains a P_9 unit which serves to cross link the long tubular strands $(P_8–P_2–P_9)_x$ in three di-

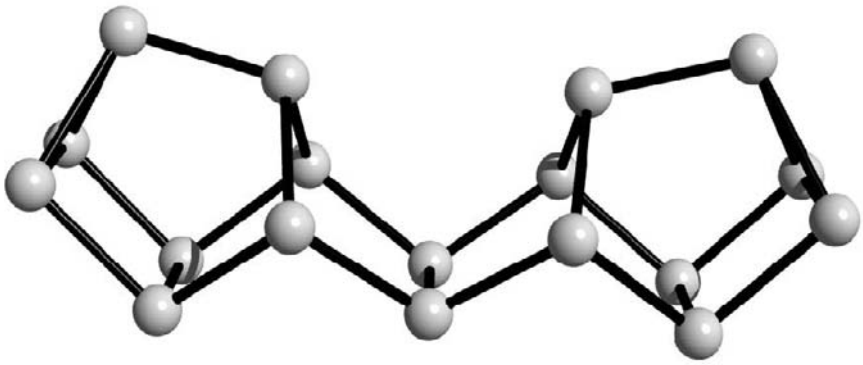

Fig. 2.6-6. Calculated structure of a P_{18} isomer more stable than 4.5 P_4 [11].

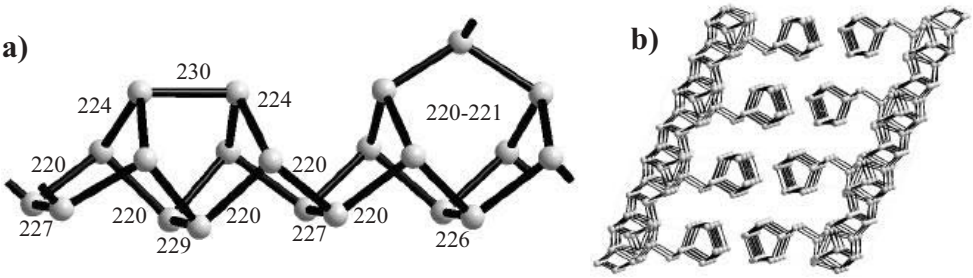

Fig. 2.6-7. (a) Structural motifs of Hittorf phosphorus in the crystal $(P_8{-}P_2{-}P_9)_x$, (b) packing diagram of Hittorf phosphorus.

mensions (Figure 2.6-7b). One possible reason for the non-crystallinity of red phosphorus is its apparently helical structure, which may not be efficiently packed [2, 37]. A possible synthetic pathway to overcome this deficiency is the use of copper(I) halides as flexible matrices in which the P_n-units are embedded, delivering the crystalline material. Spectacular examples for the validity of this approach were recently presented: neutral all phosphorus tubes and helices included in $(CuI)_3P_{12}$, $(CuI)_8P_{12}$ and $(CuI)_2P_{14}$ [37–39]. Some low charged polymeric polyphosphides should also be noted in this context: $(CuI)_2CuP_{15}$ and $(CuBr)_{10}Cu_2P_{20}$ [40].

As a final comment on the structure and bonding of the increasingly larger clusters starting from P_4, one should note the following: (1) in the small elemental cluster P_4 a delocalized bonding situation accounts for the high relative stability of this molecule; (2) slightly larger clusters P_n ($n > 12$) were found to be more stable than P_4 at 298 K, however, until now it has proven impossible to prepare isolated clusters of this type on a preparative scale; (3) in the larger aggregates and solid allotropes the P–P–P bond angles are close to the optimal orbital requirements for classical localized 2c2e bonds and thus there is no need to form non-classical cluster type orbitals such as those shown for P_4 above. Therefore, with the exception of semiconducting cubic black phosphorus, the solid allotropes of P are covalently bonded insulating polymers with localized 2e2c bonds.

2.6.3 Cationic Homonuclear Pnicogen Clusters

2.6.3.1 Overview

Despite many synthetic efforts no P- or As-cluster cations have been characterized in condensed phases to date, although their existence in the gas phase is well established by mass spectrometry and photoionization in combination with quantum chemical calculations (see below). Only one antimony cation is claimed in con-

densed phases based on an elemental analysis and physical measurements, but without a solid state structure determination [44]. This may be contrasted with the total of five different types of structurally characterized polyatomic bismuth cations collected in Table 2.6-2 and Figure 2.6-8. Note that also for homopolyatomic chalcogen and halogen cations the structural wealth is larger for the heaviest and least electronegative members Te and I [3]. At this point the recent synthesis and structural characterization of several C_{2v}-symmetric angular N_5^+ salts should be mentioned [5], which leaves P and As as the only elements in group 15 for which homopolyatomic elemental cations remain unknown in condensed phases. However, to date cage or cluster compounds N_x^{n+} or N_y^{m-} are still non-existent.

2.6.3.2
Reaction Media and Environment for Bi Cluster Syntheses

The Bi cluster cations, and more particularly their lighter congeners, are highly electrophilic species that require a very weakly basic environment to be stable in condensed phases. In this respect the prerequisite for stabilizing these clusters is to provide a weakly basic environment for the cluster cations. In other words, cation–anion or cation–solvent interactions have to be minimized by using weakly basic counterions [41] such as $AlCl_4^-$, AsF_6^- or the more complex halogenobismutates(III) as well as weakly basic solvents such as acidic $NaAlCl_4$ and Bi halide melts, benzene, SO_2.

2.6.3.3
Structurally Characterized Bi Cations [42]

The first known Bi cations [43] were synthesized in acidic $NaAlCl_4/AlCl_3$ melts by reaction of Bi metal and $BiCl_3$ with $AlCl_3$ as the chloride acceptor or by direct fusion of Bi metal and $BiCl_3$ as shown in Eqs. 1–3:

$$11\ Bi + 7\ BiCl_3 \xrightarrow[350\ ^\circ C]{BiCl_3} 3\ Bi_6Cl_7\ [= 0.75\{(Bi_9^{5+})_2(BiCl_5^{2-})_4(Bi_2Cl_8^{2-})\}] \quad (1)$$

$$22\ Bi + 2\ BiCl_3 + 6\ AlCl_3 \xrightarrow[350\ ^\circ C]{NaAlCl_4} 3\ Bi_8[AlCl_4]_2 \quad (2)$$

$$4\ Bi + BiCl_3 + 3\ AlCl_3 \xrightarrow[350\ ^\circ C]{NaAlCl_4} Bi_5[AlCl_4]_3 \quad (3)$$

Later it was found that no solvent (i.e., molten $NaAlCl_4$) is necessary for the high temperature synthesis and that the chloride acceptor $AlCl_3$ may be replaced by GaX_3, $HfCl_4$ or ZrX_4 (X = Cl, Br, see Table 2.6-3). The use of a mixture of 3Ga-7($SbCl_3$-4$GaCl_3$) tempered at 80 °C gave a dark material which supposedly is $Sb_5[GaCl_4]_3$ [44]. Bi_5^{3+} and Bi_8^{2+} salts may also be prepared using SO_2 as a solvent and the pentafluorides EF_5 (E = As, Sb) as an oxidant (Eq. 4) [45].

$$10\ Bi + 9\ AsF_5 \xrightarrow{SO_2} 2\ Bi_5[AsF_6]_3.(SO_2)_2 + 3\ AsF_3 \quad (4)$$

Only recently [42a, 46, 47] it was found that the presence of an electron rich transition metal such as Ir in melts of BiX_3 (X = Cl, Br) and Bi metal leads to the formation of large isolated and weakly coordinating cluster anions of type $[IrBi_6X_{12}]^-$ and $[IrBi_6X_{13}]^{2-}$ that stabilize the smaller hitherto unknown Bi_5^+ and Bi_6^{2+} in the interstices of the anion lattice (Eq. 5).

$$65\ Bi + 37\ BiBr_3 + 3\ Ir \xrightarrow{1000\ ^\circ C} 3\ Bi_{34}Ir_3Br_{37} \qquad (5)$$

The intriguing structure of the $[IrBi_6X_{12}]^-$ and $[IrBi_6X_{13}]^{2-}$ anions formed deserves a description: they contain octahedrally coordinated Ir atoms that are bound to six Bi atoms which bear a total of 12 or 13 halogen atoms and Ir may be replaced by Rh. The low overall charge, the surface made from halogen atoms and their spherical structure makes them a novel type of weakly coordinating anions [41, 48]. The structures of all currently characterized group 15 cluster cations are collected in Figure 2.6-8 and a summary, including other characterizations and references, is given in Table 2.6-2.

A closely related heteronuclear cation in this context is the $Bi_8Si_2^{3+}$ cation found in the phase $Bi_{14}Si_2MI_{12}$ (M = Rh, Ir) together with the $[MBi_6I_{12}]^{3-}$ counterion [64]. For other related species see Refs. [65–68].

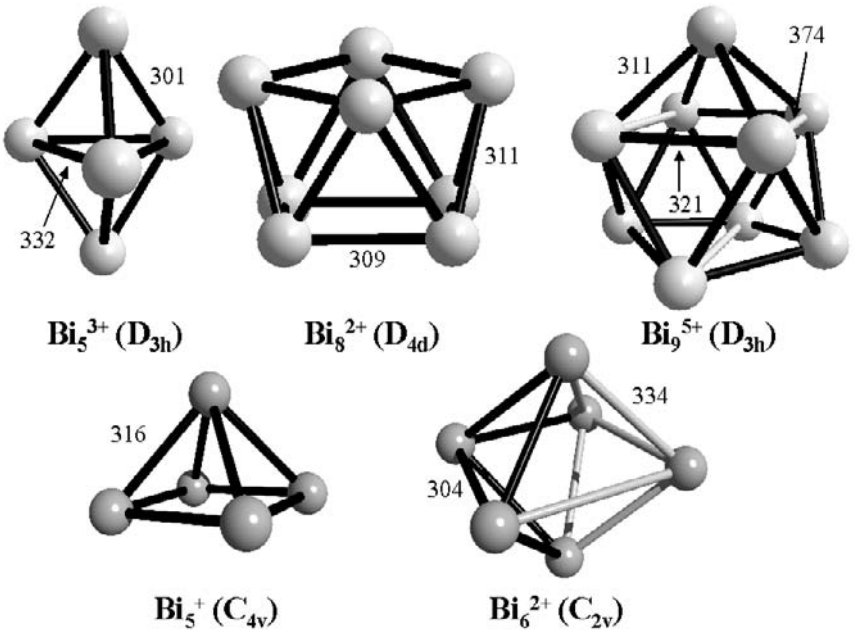

Fig. 2.6-8. Structurally characterized polybismuth cations and their basic (averaged) structural parameters. Gray bonds indicate long interatomic separations still below the sum of the van der Waals radii and symmetries given are idealized.

Tab. 2.6-2. Summary of the known "naked" group 15 cluster cations.

	X-ray diffraction analysis	*IR and/or Raman*	*Other characterizations*	*Theory*
Bi_5^+	$Bi_{34}Ir_3Br_{37}$ [46], $Bi_{12-x}MX_{13-x}$ (M = Ir, Rh, X = Cl, Br, $x < 1$) [47]	–	electrical conductivity and magnetic properties: [47]	[49]
Bi_5^{3+}	$Bi_5[AlCl_4]_3$ [50, 51[a)]]; $Bi_5[GaCl_4]_3$ [44]; $Bi_5[GaBr_4]_3$ [52]	[45, 53]	UV: [45, 53–55] LXS, NMR: [53]	[44, 49, 54]
Bi_6^{2+}	$Bi_{34}Ir_3Br_{37}$ [46], $Bi_{12-x}MX_{13-x}$ (M = Ir, Rh, X = Cl, Br, $x < 1$) [47]	–	electrical conductivity and magnetic properties: [47]	[49]
Bi_8^{2+}	$Bi_8[AlCl_4]_2$ [50a, 56, 57]; $Bi_8[GaBr_4]_2$ [52]; $Bi_8[InBr_4]_2$ [58]		UV: [54, 55]	[49, 54]
Bi_9^{5+}	Bi_6Cl_7 [43, 57], Bi_6Br_7 [59], $Bi_{10}M_3Cl_{18}$ ($=(Bi_9^{5+})(Bi^+)[MCl_6^{3-}]_3$) M = Hf [60], Zr [61], $Bi_{37}InBr_{48} = (Bi_9^{5+})_3(InBr_5^{2-})\cdot(Bi_3Br_{13}^{4-})(Bi_7Br_{30}^{9-})$ [62]	[63]	UV: [54, 55]; solid state conductivity: [57, 59]	[49, 54]; [57][b)]; [62][c)]
Sb_5^{3+}	powder data of $Sb_5[GaCl_4]_3$ [44]	[44]	elemental analysis: [44]	[44]

[a)] Neutron diffraction of liquid $Bi_5[AlCl_4]_3$ [51]. [b)] Bi_6X_7 band structure.
[c)] $Bi_{37}InBr_{48}$ band structure.

It was shown that the positive charges within the cationic Bi clusters are delocalized almost evenly over all atoms. This also suggested a delocalized bonding situation. In agreement with this notion, the structures of the Bi cations were shown to follow the rules developed by Rudolph, Williams, Wade and Mingos (in the following abbreviated to Wade rules) [69] to describe electron deficient cluster compounds such as the polyboranes. Instead of the available 5 valence electrons (VE) only 3 VE count per Bi atom due to the relativistically contracted inert $6s^2$ pair of electrons of Bi. The structure of Bi_5^{3+} with 12 electrons may be understood as a *closo* cluster built from a closed deltahedron with $n = 5$ corners, that is a trigonal bipyramid, and $n + 1 = 6$ skeletal electron pairs (SEPs). Clearly the Bi_5^{+} structure is related to that of Bi_5^{3+} in that it has one SEP more and with 5 corners ($n = 5$) it therefore is an $n + 2 = 7$ SEPs *nido* type cluster. The parent closed deltahedron is an octahedron where one cap is omitted leading to the observed square pyramidal structure. The Bi_8^{2+} structure is an *arachno* type cluster with $n + 3 = 11$ SEPs derived from a bicapped square antiprism by removing two opposite caps. For Bi_6^{2+} the situation is a little more subtle since it forms, approximately, an octahedron ($n = 6$) and thus a *closo* type arrangement of the Bi atoms. However, an electron count reveals 8 SEPs and thus ($n + 2$) SEPs corresponding to a *nido* structure. Closer inspection of the Bi_6^{2+} structure shows that the octahedron is indeed distorted and the best description may be derived starting from a pentagonal bipyramid, as the corresponding parent deltahedron (7 corners) from which one atom of the equatorial belt was removed. The resulting C_{2v} structure is then further distorted by solid state effects. Note that in Bi_5^{+} as well as in Bi_6^{2+} the cation–anion contacts are stronger than in other Bi cluster cations and, therefore, solid state effects may distort the expected geometry more effectively than with other less basic anions [46, 47].

Bi_9^{5+} presents another problem case in that it is a *nido* cluster with $n + 2 = 11$ SEPs. Therefore, one would expect a capped square antiprism (C_{4v} symmetry) to be the ground state structure. In several solid state structures of Bi_9^{5+} the geometry of this ion is close to a tricapped trigonal prism with idealized D_{3h} symmetry. However, this is a closed deltahedron and would correspond to a *closo* structure with two skeletal electrons less. Recently it was shown by relativistically adjusted *ab initio* calculations [49] that the most stable gaseous Bi_9^{5+} structure is in fact the expected C_{4v} symmetric capped square antiprism. However, the energetic differences between the D_{3h} and C_{4v} structures are only 3–9 kJ mol^{-1} [49]. Therefore, and due to the easily interchangeable structures of D_{3h} and C_{4v} Bi_9^{5+}, it is mainly the subtle cation–anion interactions that seem to be responsible for this difference. It was shown by DFT calculations that the Bi_9^{5+} cluster cation is spherically aromatic in both its D_{3h} and C_{4v} form [22, 24]. A recent investigation [49] examined the bonding in a series of known and hypothetical Bi_m^{n+} cations. It was found that, with very few exceptions, the Wade rules are applicable to Bi polycations. Based on natural bond orbital (NBO) and electron localization function (ELF) arguments it was concluded that the electrons involved in the cluster bonding are found both as localized in bonds and delocalized over larger regions. The localized bonds are predominantly found around the four-membered rings (see for example

Bi_8^{2+}) and these in turn are kept together by delocalized electrons between the four-membered rings.

2.6.3.4 What About Gaseous P_n^+ and As_n^+ Cations?

Although polyatomic P cations remain unknown in condensed phases, Martin [70] discovered larger gaseous P_n^+ cations ($n = 2$–24) in 1986 by mass spectrometric investigations of He beam quenched vapors above solid red phosphorus. Subsequently several groups [71, 72] embarked on the journey to prepare the largest P_n^+ cations and the current world record appears to be $n = 91$ [72]. From the spectra it was noted that the intensities of the closed shell uneven P_n^+ cations with $n = 3, 5, 7, 9 \ldots$ were higher than that of the open shell even members. The higher stability of uneven P_n^+ cations was also shown by the systematic calculation of a series of P_n and P_n^+ clusters using an MD-DFT approach and simulated annealing (MD = molecular dynamics) [8]. The calculated adiabatic ionization potentials of P_n clusters with $n = 2$–11 are shown in Figure 2.6-9.

Uneven open shell P_n clusters are easier to ionize than even closed shell ones and the stability of the closed shell uneven P_n^+ cluster cations is higher. For very large P_n^+ cations with $n = 25 + 8x$ ($x = 0, 1, 2, \ldots 8$) islands of stability were observed in the time of flight mass spectrum (TOF-MS) obtained by laser ablation of red phosphorus, suggesting that the more stable P clusters have connections with units of eight P atoms [71d]. A lot of effort has been put into the calculation of the most stable P_n^+ cation structures. The respective global minimum structures of the more stable uneven P_3^+, P_5^+, P_7^+ and P_9^+ cluster cations are shown in Figure 2.6-10 [73, 74].

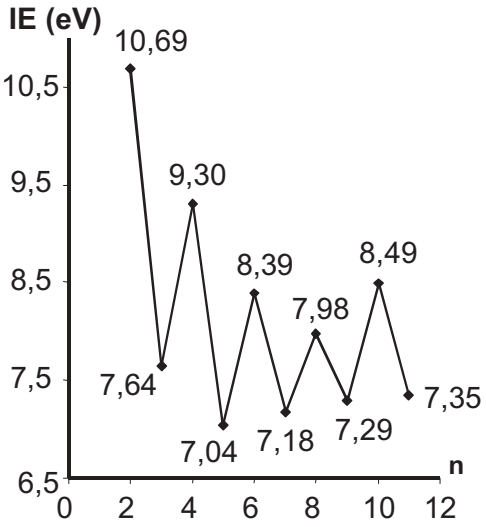

Fig. 2.6-9. The calculated adiabatic ionization potentials of P_n clusters with $n = 2$–11 [8].

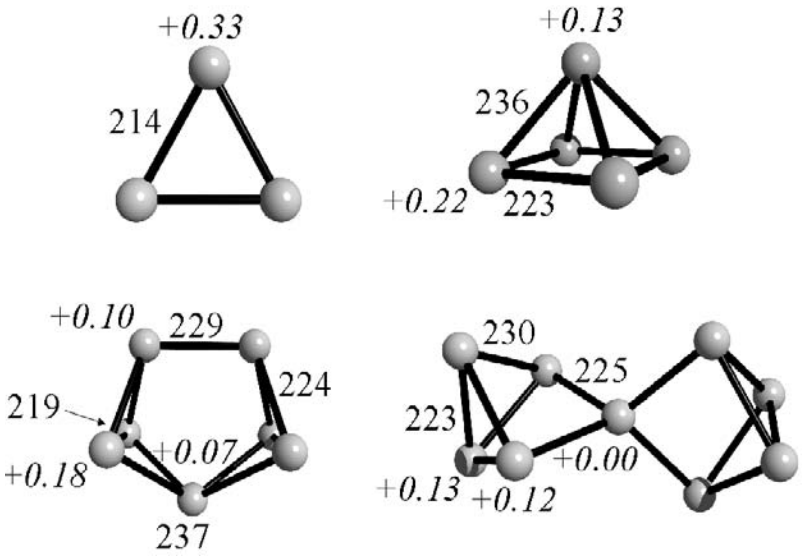

Fig. 2.6-10. The calculated global minimum structures of the more stable uneven P_3^+, P_5^+, P_7^+ and P_9^+ cluster cations [8, 73]. Bond lengths and Mulliken charges (in italics) were obtained at the BP86/SVP level [23]. For comparison: at the same level the P–P bond length is 223 pm and close to the experimental value of 221 pm [35].

P_3^+ is best described as a $C_3H_3^+$ cyclopropenium analogue with one π bond delocalized over the three P atoms and a 9 pm shortened P–P bond length. It was shown for the larger cations that one tetracoordinate phosphorus atom is always included in the minimum structures while all other P atoms are tricoordinate [8, 73]. The positive charges are delocalized over (almost) the entire cations with the odd exception of the tetracoordinate P atoms, and thus formal phosphonium centers, which bear the lowest charges. The structures of P_5^+ and P_7^+ can be understood according to the Wade rules as electron deficient *nido*- (P_5^+, square pyramid) and *arachno*-type (P_7^+, capped trigonal prism) clusters. Until recently P_9^+ was also thought to be a C_{3v} symmetrical *hypho* cluster [8], however, in an extensive investigation of 25 possible isomers of P_9^+ the tubular D_{2d} structure depicted in Figure 2.6-10 emerged as the most stable geometry [73a]. This is in line with the experimental and computational results [11], since larger charged or uncharged P clusters tend to form tubular structures with the extreme being the Hittorf allotrope of elemental phosphorus [36] (see earlier). Recently the structures of P_n^+ cluster cations as large as $n = 49$ were assessed by DFT calculations [71d]. Less work was dedicated to the calculation of As cluster cations, however, it seems clear from the calculations available [8, 32] that the global minimum structures appear to be the same for P_n^+ and As_n^+ with a uniform expansion of the E–E bond lengths by about 10% in going from phosphorus to arsenic. The structures of gaseous Sb_n^+ and Bi_n^+ cations [16] also appear to follow the Wade rules [17]. Very large ag-

gregates of $(Sb_4)_x^+$ (x can be up to several hundred) can be vaporized and subsequently ionized in TOF-MS experiments [18]. In contrast, Bi vapor shows no preferential formation of $(Bi_4)_x^+$ cations but form evenly distributed Bi_n^+ cations [18].

2.6.3.5 The Stability of Hypothetical P_n^+ and As_n^+ Cations in Condensed Phases

The recent report on the successful synthesis of N_5^+ salts [5] raised the question of whether one could also prepare their P and As analogues. In fact, the high ionization energy of N_2 of 15.58 eV compared with that of P_2 (10.53 eV) and As_2 (10.0 eV) would suggest that P and As are easier to oxidize and that P_5^+ and As_5^+ cations should be more stable in condensed phases than N_5^+. Solid N_5^+ salts contain fluorometallate anions such as MF_6^- (M = As, Sb) and $Sb_2F_{11}^-$ [5]; it seems clear that the stability of the E_5^+ cation (E = N, P, As) is connected to the counterion. It appears that the hypothetical or existing $E_5^+[A]^-$ salts ($A^- = MF_6^-$, $Sb_2F_{11}^-$, $AlCl_4^-$) decompose with the formation of EX_3 (X = F, Cl) and that the tendency to decompose increases according to $N \ll P \approx As$. The reasons for this trend seem to arise from the mean E–F and E–Cl bond enthalpies of the EX_3 (X = F, Cl) molecules [75] within group 15 (Table 2.6-3).

The Bi–Cl bond enthalpy is the lowest E–Cl bond energy in the series. Therefore, chlorometallate based counteranions such as $AlCl_4^-$ stabilize Bi_n^{m+} cations but may decompose in the presence of the more electrophilic P_n^+ and As_n^+ cations. One also notes from Table 2.6-3 that the P–F and As–F bond enthalpy are extraordinarily high compared with those of N and Bi. This rationalizes the fact that the fluorometallate based anions MF_6^- (M = As, Sb) and $Sb_2F_{11}^-$ may be used to stabilize N_5^+ [5] and Bi_n^{m+} cations [45], but all attempts to prepare P_n^{m+} or As_n^{m+} cations led to immediate decomposition of the fluorometallate anions and formation of PF_3 and MF_3. Since the enthalpies of formation ΔH_f of $P_5^+{}_{(g)}$ [76], $AsF_6^-{}_{(g)}$ [3], $PF_{3(g)}$ [6], $AsF_{3(l)}$ [6] and $P_{4(s)}$ [6] are known, this qualitative picture was quantified for the in condensed phases unknown P_5^+ cation in a hypothetical $P_5^+[AsF_6]^-$ salt (see Scheme 2.6-1). The lattice potential enthalpy $\Delta H_{latt.}$ of $P_5^+[AsF_6]^-$ was estimated using Jenkins' and Passmore's [77, 78] volume based equation. According to Scheme 2.6-1 the decomposition of solid $P_5^+[AsF_6]^-$ giving PF_3 gas, liquid AsF_3 and solid P_4 is highly exothermic by 288 kJ mol^{-1}. The free energy ΔG for this process will be even larger, since the formation of gaseous PF_3

Tab. 2.6-3. Mean E–F and E–Cl bond enthalpies (BE) of the EX_3 (X = F, Cl) molecules for group 15 elements [75].

E=	*N*	*P*	*As*	*Sb*	*Bi*
BE(E–F) (kJ mol^{-1})	283	490	484	440	393
BE(E–Cl) (kJ mol^{-1})	313	326	321	315	274

$$\begin{array}{rccc} & P_5^{+}{}_{(g)} + AsF_6^{-}{}_{(g)} & \xrightarrow{\Delta_{Latt.}H(P_5^{+}[AsF_6^{-}])} & P_5^{+}[AsF_6^{-}]_{(s)} \\ \Delta_fH = & +913 \quad -1919 & = -485 & \end{array}$$

$$\Rightarrow \Delta_f\mathbf{H(P_5^{+}[AsF_6^{-}])} = 913 + (-1919) + (-485) = \mathbf{-1491}$$

$$\begin{array}{rcl} & P_5^{+}[AsF_6^{-}]_{(s)} & \longrightarrow \quad PF_{3\,(g)} + AsF_{3\,(s)} + P_{4\,(s)} \\ \Delta_fH = & -1491 & \Delta_fH = \quad -958 \quad -821 \quad 0 \end{array}$$

$$\Rightarrow \Delta_r\mathbf{H} = (-958) + (-821) + 0 - (-1491) = \mathbf{-288}$$

Scheme 2.6-1. Scheme used to establish the enthalpy of reaction for a decomposition of solid $P_5^{+}[AsF_6]^{-}$ giving PF_3 gas, liquid AsF_3 and solid P_4. All quantities are given in kJ mol^{-1}.

increases the entropy of the system and thus the reaction will be more exergonic than 288 kJ mol^{-1}. Using a similar approach to Scheme 2.6-1 and the known [79] enthalpies of formation as well as the estimated lattice potential enthalpies [77, 78], one can assess similar decomposition reactions of $E_5^{+}[A]^{-}$ salts (E = N, P; $A^{-} = SbF_6^{-}$, $Sb_2F_{11}^{-}$) as summarized in Table 2.6-4.

From the enthalpies of the decomposition reactions collected in Table 2.6-4 one can assume that even with the most stable anion considered ($Sb_2F_{11}^{-}$) a decomposition of the hypothetical $P_5^{+}[Sb_2F_{11}]^{-}$ salt would be exothermic by at least −197 kJ mol^{-1} [80]. According to Scheme 2.6-1 the reason for this instability is found in the thermodynamically controlled formation of PF_3. Similar arguments hold for the arsenic cations. In contrast, all $N_5^{+}[A]^{-}$ decompositions are endothermic by 32 to 108 kJ mol^{-1}. Nevertheless, since two moles of N_2 gas are formed during the decomposition, entropy favors the right hand side. This is in agreement with the observation that $N_5^{+}[AsF_6]^{-}$ is only marginally stable at room temperature while $N_5^{+}[Sb_2F_{11}]^{-}$ remains unchanged up to 70 °C [5].

Tab. 2.6-4. Enthalpies ΔH_r of the decomposition-reactions for a series of hypothetical (E = P) and known (E = N) $E_5^{+}[A]^{-}$ salts (kJ mol^{-1}).

	ΔH_r
$P_5^{+}[AsF_6]^{-}{}_{(s)} \rightarrow PF_{3(g)} + AsF_{3(l)} + P_{4(s)}$	**−288**
$P_5^{+}[SbF_6]^{-}{}_{(s)} \rightarrow PF_{3(g)} + SbF_{3(s)} + P_{4(s)}$	**−208**
$P_5^{+}[Sb_2F_{11}]^{-}{}_{(s)} \rightarrow PF_{3(g)} + SbF_{3(s)} + SbF_{5(l)} + P_{4(s)}$	**>−197**
$N_5^{+}[AsF_6]^{-}{}_{(s)} \rightarrow NF_{3(g)} + AsF_{3(l)} + 2\ N_{2(g)}$	**+32**
$N_5^{+}[SbF_6]^{-}{}_{(s)} \rightarrow NF_{3(g)} + SbF_{3(s)} + 2\ N_{2(g)}$	**+108**
$N_5^{+}[Sb_2F_{11}]^{-}{}_{(s)} \rightarrow NF_{3(g)} + SbF_{3(s)} + SbF_{5(l)} + 2\ N_{2(g)}$	**>+100**

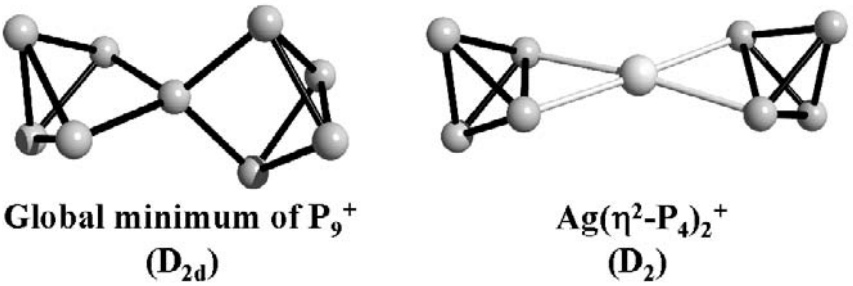

Fig. 2.6-11. Comparison of the experimental structure of $Ag(\eta^2\text{-}P_4)_2^+$ [26] versus that of the calculated global minimum of P_9^+ [73a]. Ag–P bonds are drawn in white.

2.6.4 Outlook

From the preceding section it seems clear that fluorometallate anions are not capable of stabilizing P_n^+ or As_n^+ cations in condensed phases. According to gas phase investigations and quantum chemical calculations, the P_5^+ cation is the most stable P_n^+ species ($n < 11$). As shown in Table 2.6-4 the P_5^+ cation would decompose the $Sb_2F_{11}^-$ anion, which is one of the most stable anions currently known. Therefore, preparation of P_n^+ and As_n^+ cations has to circumvent anion decomposition by using extremely robust and weakly coordinating anions [41]. Recently the new robust $Al(OR)_4^-$ anion [$R = C(CF_3)_3$] [81] was used in studies intended to prepare "naked" P_n^+ cations [76, 82]. However, reacting $Ag[Al(OR)_4]$ with 1.25 P_4 did not lead to the desired oxidation and formation of $P_5^+[Al(OR)_4]^-$ and solid silver. Instead the $Ag(\eta^2\text{-}P_4)_2^+[Al(OR)_4]^-$ salt was isolated in which two molecules of P_4 are coordinated to an Ag^+ ion. Nevertheless, the homoleptic $Ag(\eta^2\text{-}P_4)_2^+$ cation is conceptually very close to a homopolyatomic P_n^+ cation. The similarity of the experimental $Ag(\eta^2\text{-}P_4)_2^+$ structure (almost D_2 symmetry) [26] and that of the calculated [73a] global minimum of P_9^+ (D_{2d} symmetry) should be noted (see Figure 2.6-11).

To enforce an oxidation, $Ag(\eta^2\text{-}P_4)_2^+[Al(OR)_4]^-$ was reacted with I_2. Solid AgI precipitated immediately at −78 °C and the novel $P_5I_2^+[Al(OR)_4]^-$ and $P_3I_6^+[Al(OR)_4]^-$ salts formed with the possible intermediate participation of the P_5^+ cation (Figure 2.6-12) [76, 83].

Acknowledgement

This work was supported by the *Fonds der Chemischen Industrie* and the *Deutsche Forschungsgemeinschaft*. Professor J. Passmore (UNB, Canada) is thanked for helpful comments and Professor M. Ruck (TU Dresden, Germany) is gratefully acknowledged for making papers available to the author prior to publication.

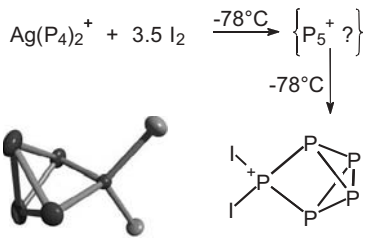

Fig. 2.6-12. Formation of $P_5I_2^+[Al(OR)_4]^-$ by reaction of $Ag(\eta^2\text{-}P_4)_2^+[Al(OR)_4]^-$ with I_2 [76]. Structure of the related almost C_{2v}-symmetrical $P_5Br_2^+$ cation in the crystal [83].

References

1 (a) H. G. v. Schnering, W. Hönle, *Chem. Rev.*, **1988**, *88*, 243; (b) A. Cowley (ed.) *Rings, Clusters and Polymers of the Main Group Elements*, ACS Symposium Series No. 232, Washington D.C., **1983**; (c) M. Baudler, *Angew. Chem., Int. Ed. Engl.*, **1982**, *21*, 492; (d) M. Baudler, *Angew. Chem., Int. Ed. Engl.*, **1987**, *26*, 419; (e) H. G. v. Schnering, *Encycl. Inorg. Chem.*, **1994**, *6*, 3106.

2 A. Pfitzner, *Chem. Eur. J.*, **2000**, *6*, 1891.

3 S. Brownridge, H. D. B. Jenkins, I. Krossing, J. Passmore, H. K. Roobottom, *Coord. Chem. Rev.*, **2000**, *197*, 397 and references cited therein.

4 This discrepancy may be ascribed to the differing electronic situation of both groups in that the chalcogens bear an additional occupied p-type lone pair orbital, which can be used to delocalize the positive charge over all atoms. A similar stabilization is impossible for the group 15 cations and may account for their rare occurrence as compounds in the bottle.

5 (a) K. O. Christe, W. W. Wilson, J. A. Sheehy, J. A. Boaty, *Angew. Chem.*, **1999**, *111*, 2112; (b) A. Vij, W. W. Wlison, V. Vij, F. S. Tham, J. A. Sheehy, K. O. Christe, *J. Am. Chem. Soc.*, **2001**, *123*, 6308.

6 All values, except those indicated, were taken from the Standard Reference Database (release 69, July 2001) of the National Institute of Standards and Technology (NIST) at www.webbook.nist.gov/chemistry/. If no generally recommended value was suggested, a range of the most reliable values is given in Table 2.6-1.

7 H.-J. Zhai, L.-S. Wang, A. E. Kuznetsov, A. I. Boldyrev, *J. Phys. Chem., A* **2002**, *106*, 5600.

8 R. O. Jones, G. Seifert, *J. Phys. Chem.*, **1992**, *96*, 7564.

9 H. Zhang, K. Balasubramaniani, *J. Chem. Phys.*, **1992**, *97*, 3437.

10 (a) P. A. Edwards, J. D. Corbett, *Inorg. Chem.*, **1977**, *16*, 903; (b) J. D. Corbett, P. A. Edwards, *J. Am. Chem. Soc.*, **1977**, *99*, 3313.

11 (a) M. Häser, U. Schneider, R. Ahlrichs, *J. Am. Chem. Soc.*, **1992**, *114*, 9551; (b) M. Häser, O. Treutler, *J. Chem. Phys.*, **1995**, *102*, 3703.

12 K. Manzel, W. Schulze, V. Wolfel, R. Minkwitz, *Z. Naturforsch.*, **1982**, *37b*, 1127.

13 H. Sontag, R. Weber, *Chem. Phys.*, **1982**, *70*, 23.

14 However, matrix isolation studies on tetrahedral Bi_4 are available: V. E. Bondybey, J. H. English, *J. Chem. Phys.*, **1980**, *73*, 42.

15 H. Zhang, K. Balasubramanian, *J. Chem. Phys.*, **1992**, *97*, 3437.

16 (a) M. E. Geusic, R. R. Freeman, *J. Chem. Phys.*, **1988**, *88*, 163; (b) T. M. Bernhardt, B. Kaiser, K. Rademann, B. Stegemann, J. Opitz, *Phys. Rev. Lett.*, **1999**, *83*, 2918; (c) R. E. Walstedt, R. F. Bell, *J. Chem. Phys.*, **1987**, *87*, 1423.

17 (a) T. M. Bernhardt, B. Kaiser, K. Rademann, *Z. Phys. D*, **1997**, *40*, 327; (b) M. E. Geusic, R. R. Freeman, *J. Chem. Phys.*, **1988**, *89*, 223.

18 (a) C. Brechignac, Ph. Cahuzac, F. Carlier, M. de Frutos, J. Ph. Roux, *J. Chem. Phys.*, **1995**, *102*, 763; (b) D. Rayane, P. Melinon, B. Tribollet, B. Cabauud, A. Hareau, M. Broyer, *J. Chem. Phys.*, **1989**, *91*, 3100.

19 B. M. Gimarc, D. S. Warren, *Inorg. Chem.*, **1993**, *32*, 1850.

20 The strain energy of P_4 was established by an isodesmotic reaction: $P_4 + 6P_2H_4 \rightarrow 4P(PH_2)_3$. If P_4 were to be totally unstrained, the reaction enthalpy for this process would be zero, since the number and type of P–P and P–H bonds is kept constant (bond additivity model [21]).

21 P. George, M. Trachtmann, C. W. Bock, A. M. Brett, *Tetrahedron*, **1976**, *32*, 317.

22 A. Hirsch, Z. Chen, H. Jiao, *Angew. Chem.*, **2001**, *113*, 2916.

23 I. Krossing, unpublished results.

24 A. Hirsch, *Top. Curr. Chem.*, **1999**, *199*, 1.

25 J. L. Abboud, M. Herreros, R. Notario, M. Esseffar, O. Mo, M. Yáñez, *J. Am. Chem. Soc.*, **1996**, *118*, 1126; see also gaseous $Li^+(P_4)$: J. L. Abboud, I. Alkorta, J. L. Davalos, J.-F. Gal, M. Herreros, P.-C. Maria, O. Mo, M. T. Molina, R. Notario, M. Yáñez, *J. Am. Chem. Soc.*, **2000**, *122*, 4451.

26 (a) I. Krossing, *J. Am. Chem. Soc.*, **2001**, *123*, 4603; (b) I. Krossing, L. van Wüllen, *Chem. Eur. J.*, **2002**, *8*, 700.

27 D. Schröder, H. Schwarz, M. Wulf, H. Sievers, P. Jutzi, M. Reiher, *Angew. Chem.*, **1999**, *111*, 3723.

28 P. Jutzi, R. Kroos, A. Müller, M. Penk, *Angew. Chem.*, **1989**, *101*, 628.

29 R. Janoschek, *Chem. Ber.*, **1992**, *125*, 2687.

30 R. O. Jones, D. Hohl, *J. Chem. Phys.*, **1990**, *92*, 6710.

31 M. Häser, *J. Am. Chem. Soc.*, **1994**, *116*, 6925.

32 P. Ballone, R. O. Jones, *J. Chem. Phys.*, **1994**, *100*, 4941.

33 (a) M. Yoshifuji, I. Shima, N. Inamoto, *J. Am. Chem. Soc.*, **1981**, *103*, 4587; (b) E. Niecke, O. Altmeyer, M. Nieger, *Angew. Chem.*, **1991**, *103*, 1158.

34 (a) K. Raghavachari, R. C. Haddon, J. S. Binley, *Chem. Phys. Lett.*, **1985**, *122*, 219; (b) G. Trinquillier, J.-P. Daudey, N. Komiha, *J. Am. Chem. Soc.*, **1985**, *107*, 7210; (c) R. Ahlrichs, S. Brode, C. Ehrhardt, *J. Am. Chem. Soc.*, **1985**, *107*, 7260; (d) E. A. Halevi, H. Bock, B. Roth, *Inorg. Chem.*, **1984**, *23*, 4376.

35 (a) L. R. Maxwell, S. B. Hendrichs, V. Mosley, *J. Chem. Phys.*, **1935**, *3*, 699; (b) A. Simon, H. Borrmann, H. Craubner, *Phosphorus Sulphur*, **1987**, *30*, 507.

36 H. von Thurn, H. Krebs, *Acta Crystallogr.*, **1969**, *B25*, 125.

37 A. Pfitzner, E. Freudenthaler, *Angew. Chem.*, **1995**, *107*, 1784.

38 M. H. Möller, W. Jeitschko, *J. Solid. State Chem.*, **1986**, *65*, 187.

39 A. Pfitzner, E. Freudenthaler, *Z. Naturforsch. Sect. B*, **1997**, *52*, 199.

40 (a) A. Pfitzner, E. Freudenthaler, *Z. Kristallogr.*, **1995**, *210*, 59; (b) A. Pfitzner, E. Freudenthaler, *Z. Kristallogr.*, **1997**, *212*, 103.

41 For reviews on weakly coordinating anions see: a) C. Reed, *Acc. Chem. Res.*, **1998**, *31*, 133; (b) S. H. Strauss, *Chem. Rev.*, **1993**, *93*, 927; (c) E. Y.-X. Chen, T. J. Marks, *Chem. Rev.*, **2000**, *100*, 1391.

42 For recent review articles see: (a) Bi_5^+ and Bi_6^{2+}: M. Ruck, *Angew. Chem.*, **2001**, *113*, 1222; (b) Sb_5^{3+}, Bi_5^{3+}, Bi_8^{2+} and Bi_9^{5+}: S. Ulvenlund, L. Bengtsson-Kloo, in *Metal Clusters in Chemistry I*, P. Braunstein, L. A. Oro, P. R. Raithby, eds., Wiley-VCH, Weinheim, Germany, **1999**, 561.

43 (a) A. Hershaft, J. D. Corbett, *Inorg. Chem.*, **1963**, *2*, 979; (b) R. M. Friedman, J. D. Corbett, *Inorg. Chim. Acta*, **1973**, 7.

44 S. Ulvenlund, K. Stahl, L. Bengtson-Kloo, *Inorg. Chem.*, **1996**, *35*, 223.

45 R. C. Burns, R. J. Gillespie, W.-C. Luk, *Inorg. Chem.*, **1978**, *17*, 3596.

46 M. Ruck, *Z. Anorg. Allg. Chem.*, **1998**, *624*, 521.

47 M. Ruck, S. Hampel, *Polyhedron*, **2002**, *21*, 651.

48 At this point the related isolated molecular cluster $RhBi_7Br_8$ should be mentioned: M. Ruck, *Angew. Chem.*, **1997**, *109*, 2059.

49 A. N. Kuznetsov, L. Kloo, M. Lindsjöö, J. Rosdahl, H. Stoll, *Chem. Eur. J.*, **2001**, *7*, 2821.

50 (a) J. D. Corbett, *Inorg. Chem.*, **1968**, *7*, 198; (b) B. Krebs, M. Mummert, C. Brendel, *J. Less-Common. Met.*, **1986**, *116*, 159.

51 K. Ichikawa, T. Yamanaka, A. Takamuku, R. Glaser, *Inorg. Chem.*, **1997**, *36*, 5284.

52 Unpublished work by A. N. Kouznetsov, L. Bengtson-Kloo, B. A. Popovkin cited as reference 59 in the review article [42b].

53 (a) S. Ulvenlund, K. Stahl, L. Bengtson-Kloo, *J. Chem. Soc., Faraday Trans.*, **1995**, *91*, 4223; (b) S. Ulvenlund, A. Wheatley, L. Bengtson-Kloo, *Chem. Commun.*, **1995**, 59.

54 G. Day, R. Glaser, N. Shimomura, A. Takamuka, K. Ichikawa, *Chem. Eur. J.*, **2000**, *6*, 1078.

55 L. Heerman, W. D'Olieslager, *J. Electrochem. Soc.*, **1991**, *138*, 1372.

56 B. Krebs, M. Mucke, C. Brendel, *Angew. Chem.*, **1982**, *94*, 453; *Angew. Chem., Int. Ed. Engl.*, **1982**, *21*, 445.

57 J. Beck, C. J. Brendel, L. Bengtsson-Kll, B. Krebs, M. Mummert, A. Stankowski, S. Uvenlund, *Chem. Ber.*, **1996**, *129*, 1219.

58 A. N. Kusnetsov, B. P. Popovkin, *Z. Anorg. Allg. Chem.*, **2002**, *628*, 2178.

59 H. von Benda, A. Simon, W. Bauhofer, *Z. Anorg. Allg. Chem.*, **1978**, *438*, 37.

60 R. M. Friedman, J. D. Corbett, *Inorg. Chem.*, **1973**, *12*, 1134.

61 A. N. Kuznetsov, A. V. Shevel'kov, S. I. Troyanov, B. A. Popovkin, *Zh. Neorg. Khim.*, **1996**, *41*, 958; *Russ. J. Inorg. Chem.*, **1996**, *41*, 920.

62 V. Dubenskii, M. Ruck, submitted to *Z. Anorg. Allg. Chem.* **2003**, *629*, 375.

63 K. Ichikawa, K. Fukushi, *J. Raman Spectrosc.*, **1987**, *17*, 139.

64 M. Ruck, *Z. Anorg. Allg. Chem.*, **2000**, *626*, 14.

65 An increasingly larger number of Bi rich binary and ternary subhalides with isolated to 1D-, 2D- and 3D structures was prepared [42a, 66]. Another related cation is the hetero-cubane $Bi_4Te_4^{4+}$ [67]. Also some related organometallic subvalent poly-bismuth species should be noted: R_4Bi_4 and R_6Bi_8 (R = bulky organometallic ligand) [68].

66 (a) M. Ruck, M. Heich, *Z. Anorg. Allg. Chem.*, **2000**, *626*, 2449 and references cited therein; (b) M. Ruck, *Solid State. Sci.*, **2000**, *3*, 369 and references cited therein; (c) E. V. Dikarev, B. A. Popovkin, A. V. Shevelkov, *Z. Anorg. Allg. Chem.*, **1992**, *612*, 118 and references cited therein.

67 J. Beck, M. Dolg, S. Schlüter, *Angew. Chem.*, **2001**, *113*, 2347; *Angew. Chem., Int. Ed. Engl.*, **2001**, *40*, 2287.

68 (a) G. Linti, W. Köstler, *Z. Anorg. Allg. Chem.*, **2002**, *628*, 63; (b) H. J. Breunig, R. Rösler, E. Lork, *Angew. Chem.*, **1998**, *110*, 3361.

69 (a) K. Wade, *Adv. Inorg. Chem. Radiochem.*, **1976**, *18*, 1; (b) R. W. Rudolph, *Acc. Chem. Res.*, **1976**, *9*, 447; (c) D. M. P. Mingos, *Acc. Chem. Res.*, **1984**, *17*, 1984.

70 T. P. Martin, *Z. Phys. D*, **1986**, *3*, 211.

71 (a) R. Huang, H. Li, Z. Lin, S. Yang, *J. Phys. Chem.*, **1995**, *99*, 1418; (b) R. B. Huang, H. D. Li, Z. Y. Lin, S. H. Yang, *Surf. Rev. Lett.*, **1996**, *3 (1)*, 167; (c) Z. Y. Liu, R. B. Huang, L. S. Zheng, *Z. Phys. D*, **1996**, *38*, 171; (d) M. D. Chen, J. T. Li, R. B. Huang, L. S. Zheng, C. T. Au, *Chem. Phys. Lett.*, **1999**, *305*, 439.

72 A. V. Bulgakov, O. F. Bobrenok,

V. I. Kosyakov, *Chem. Phys. Lett.*, **2000**, *320*, 19.

73 (a) M. D. Chen, R. B. Huang, L. S. Zheng, Q. E. Zhang, C. T. Au, *Chem. Phys. Lett.*, **2000**, *325*, 22; (b) M. D. Chen, R. B. Huang, L. S. Zheng, C. T. Au, *Main Group Metal Chem.*, **1999**, *14*, 479; (c) M. D. Chen, J. T. Li, R. B. Huang, L. S. Zheng, C. T. Au, *Chin. J. Chem. Phys.*, **1999**, *12*, 395; (d) M. D. Chen, *J. Mol Struct. (Theochem)*, **2000**, *499*, 195.

74 J. N. Feng, M. Cui, X. R. Huang, P. Otto, F. L. Gu, *J. Mol Struct. (Theochem)*, **1998**, *425*, 201.

75 J. Huheey, E. Keiter, R. Keiter, *Anorganische Chemie*, 2nd Edn., W. de Gruyter, Berlin, New York, **1995**, p. 1165.

76 I. Krossing, *J. Chem. Soc., Dalton Trans.*, **2002**, 500.

77 The thermochemical volumes of AsF_6^- (110 Å^3), SbF_6^- (121 Å^3) and $Sb_2F_{11}^-$ (227 Å^3) were taken from the literature [78]. The volume of $N_5^+[Sb_2F_{11}]^-$ (278 Å^3) is known [5] giving the thermochemical volume of N_5^+ as 51 Å^3. The thermochemical volume of P_5^+ (5 atoms) was estimated to be similar to that of $AsCl_4^+$ (5 atoms) of 124 Å^3. Using these parameters in the volume based equation in [78] gave the lattice potential enthalpies of $P_5^+[AsF_6]^-$ (485 kJ mol^{-1}), $P_5^+[SbF_6]^-$ (479 kJ mol^{-1}), $P_5^+[Sb_2F_{11}]^-$ (436 kJ mol^{-1}), $N_5^+[AsF_6]^-$ (535 kJ mol^{-1}), $N_5^+[SbF_6]^-$ (525 kJ mol^{-1}) and $N_5^+[Sb_2F_{11}]^-$ (463 kJ mol^{-1}).

78 H. K. Roobottom, H. D. B. Jenkins, J. Passmore, L. Glasser, *Inorg. Chem.*, **1999**, *38*, 3609.

79 The enthalpies of formation used to assess the decomposition reactions in Table 2.6-4: $N_5^+{}_{(g)}$ (+1469 kJ mol^{-1}) [5], $NF_{3(g)}$ (−132 kJ mol^{-1}) [6], $SbF_{3(s)}$ (−916 kJ mol^{-1}) [6], $SbF_{5(l)}$ (−1328 kJ mol^{-1}) [6], $SbF_6^-{}_{(g)}$ (−2100 kJ mol^{-1}) [3], $Sb_2F_{11}^-{}_{(g)}$ (<−3482 kJ mol^{-1}) [3].

80 The actual value will be even more exothermic, since SbF_3 and SbF_5 form stable crystalline adducts of type $SbF_3.SbF_5$ etc.

81 I. Krossing, *Chem. Eur., J.* **2001**, *7*, 490.

82 (a) I. Krossing, *J. Am. Chem. Soc.*, **2001**, *123*, 4603; (b) I. Krossing, *Chem. Eur. J.*, **2002**, *8*, 700.

83 (a) I. Krossing, I. Raabe, *Angew. Chem.*, **2001**, *113*, 4544; (b) M. Gonsior, I. Krossing, L. Müller, I. Raabe, M. Jansen, L. van Wüllen, *Chem. Eur. J.*, **2002**, *8*, 3386.

2.7
Cages and Clusters of the Chalcogens

William S. Sheldrick

2.7.1
The Elements

In stark constrast to oxygen, for which only two allotropes (O_2, O_3), one homopolyatomic cation (O_2^+) and di- and trinuclear homopolyatomic anions (O_2^{2-}, O_2^- and O_3^-) are known, sulfur exhibits a strong tendency to catenate. This ability manifests itself, in particular, in the formation of homocyclic S_n rings ($n = 6$–26) of which no less than 17 allotropic modifications ($n = 6$, 7, 8, 10–14, 18, 20) have been structurally characterized in the solid state [1–3]. Selective oxidation of elemental sulfur by increasing quantities of the powerful oxidants AsF_5, SbF_5 and $S_2O_6F_2$ in solvents of low basicity, such as liquid HF or SO_2 yields homopolyatomic dications in the order S_{19}^{2+}, S_8^{2+} and S_4^{2+} [4–6]. The pronounced catenation proclivity of elemental sulfur is also apparent in its chain-like homopolyatomic anions S_n^{2-}. Heating aqueous sulfide solutions with sulfur affords both S_3^{2-} and S_4^{2-} and although polysulfide anions in the range $n = 2$–5 are the only significant stable species in solution, S_n^{2-} anions with $n = 2$–8 have been crystallized in the presence of large cations (e.g., Cs^+, R_3NH^+).

Both selenium and tellurium exhibit unbranched infinite helical chains in their, respectively, grey and silvery-white stable elemental forms. Although the ability of these heavier group 16 elements to catenate is less pronounced than for sulfur, metastable allotropic modifications of selenium containing Se_6 and Se_8 rings (three polymorphs) are known and isolated crown-shaped Te_8 rings have been found in Cs_3Te_{22} [7] and Cs_4Te_{28} [8]. Despite its more limited tendency to form large homocyclic rings, tellurium does, in fact, exhibit a much richer homopolyatomic anion and cation chemistry than its lighter homologues. This is due to the increasing importance of both hypervalent bonding and weak $np^2 \rightarrow n\sigma^*$ interactions ($n \geq 3$) on going down group 16. In its polyanions Te_n^{x-}, tellurium can extend its coordination number to 3 (T-shaped $TeTe_3^{4-}$ units) or 4 (square-planar $TeTe_4^{6-}$ units) by participating in linear 3-center 4-electron bonds with a formal bond order of 0.5 [Figure 2.7-1(a)]. The energy difference between occupied np^2 lone pair orbitals and antibonding $n\sigma^*$ orbitals decreases with increasing n, thereby making intra- and intermolecular $np^2 \rightarrow n\sigma^*$ bonding more favorable, in particular

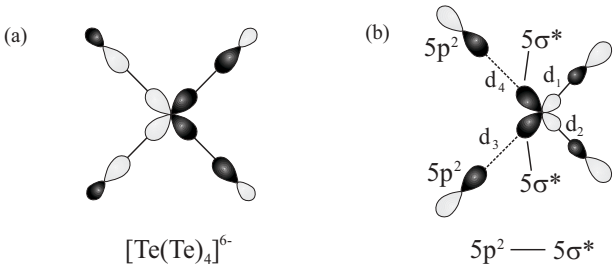

Fig. 2.7-1. (a) 3-center 4-electron bonding and (b) $5p^2 \rightarrow 5\sigma^*$ secondary bonding in polytellurides.

for the relatively diffuse Te $5p^2$ and $5\sigma^*$ orbitals [Figure 2.7-1(b)]. Such versatile secondary bonding can enable the formation of different structures of similar energy.

For example, no less than 12 different formula types are now known for the alkali metal tellurides M_xTe_y [9, 10]. As the total bond order for Te–Te bonds and their opposite secondary Te···Te interactions must remain constant at 1.0, distances d_1/d_2 will increase in logarithmic dependence on their individual bond order as d_3/d_4 shorten. Values of d_1/d_2 can range from those of typical single bonds (269–287 pm [10]) to 304 ± 9 pm for symmetrical and modestly distorted 3-center 4-electron interactions.

On applying the Gillespie-Nyholm concept [11], the atoms of the $TeTe_3^{4-}$ and $TeTe_4^{6-}$ units can be described as, respectively, ψ-trigonal bipyramidal and ψ-octahedral. The central Te atoms carry formal charges of −1 and −2 and can be regarded as being isoelectronic to iodine and xenon. In accordance with the Zintl concept, two Te atoms in valence precise homopolyatomic cations Te_n^{2+} must be assigned a formal charge of +1 and will be expected to exhibit a pyramidal (ψ-tetrahedral) coordination environment. This arrangement with its Te–Te–Te angles of around 100° enables not only the formation of valence precise cages but also of electron-deficient cluster structures by homopolyatomic tellurium cations such as Te_6^{4+}, Te_6^{2+} and Te_8^{4+}. In its valence precise Te_n^{2+} cations, the trivalent Te atoms are formally isoelectronic to the group 15 neighbor Bi, a fact that is underlined by the recently prepared $[Bi_4Te_4]^{4+}$ cation in $[Bi_4Te_4](AlCl_4)_4$ in which pyramidal Bi and Te atoms are sited at alternating corners of a regular cube [12]. Many of the structures of the homopolyatomic chalcogen cations cannot, however, be explained in detail by adopting a classical electron precise Lewis approach. Recent good quality quantum chemical calculations [13] indicate that positive charge is delocalized over many atoms so as to minimize electrostatic repulsion. This charge dilution can be achieved by np_π–np_π, π^*–π^*, and $np^2 \rightarrow n\sigma^*$ interactions or combinations thereof and is often reflected in characteristic bond length alternations.

As will be discussed in Section 2.7.3.1, a number of cluster-like non-valence precise Te_n moieties ($n = 4, 6$) have also been identified in alkali metal tellurides but these alleviate their electron surplus by participating in asymmetric linear 3-

Tab. 2.7-1. Known polyatomic chalcogen cations.

	Nuclearity[a)]					
Chalcogen	***4***	***6***	***8***	***10***	***>10***	***∞***
S	S_4^{2+}		S_8^{2+}		S_{19}^{2+}	
S/Te		$Te_3S_3^{2+}$				
Se	Se_4^{2+}		Se_8^{2+}	Se_{10}^{2+}	Se_{17}^{2+}	
Se/Te	$Te_xSe_y^{2+}$ [b)]	$Te_2Se_4^{2+}$	$Te_2Se_6^{2+}$	$Te_2Se_8^{2+}$		$^1_\infty[Te_3Se_4^{2+}]$
						$^1_\infty[Te_{3.15}Se_{4.85}^{2+}]$
Te	Te_4^{2+}	Te_6^{2+}	Te_8^{2+} (3)			$^1_\infty[Te_4^{2+}]$, $^1_\infty[Te_7^{2+}]$ (3)
		Te_6^{4+}	Te_8^{4+}			$^1_\infty[Te_8^{2+}]$, $^1_\infty[Te_{10}^{2+}]$

[a)] The number of isomeric forms is given in parentheses.
[b)] $x = 2,\ y = 2;\ x = 3,\ y = 1$.

center 4-electron $np^2 \rightarrow n\sigma^*$ bonds to neighboring Te units so as to afford polymeric networks.

2.7.2 Homopolyatomic Cations

Although it had been known since the early 19th century that elemental sulfur, selenium and tellurium dissolve in oleum to afford intensively colored solutions, it was not until the 1960s that the structures of the responsible homopolyatomic cations began to be elucidated in detail.

The first chalcogen polycation to be fully characterized was O_2^+ in $O_2(PtF_6)$, which was prepared in 1962 by Bartlett from oxygen and PtF_6 [14]. Subsequently Gillespie demonstrated that the homopolyatomic cations E_4^{2+} (E = S, Se, Te), Te_6^{4+}, E_8^{2+} (E = S, Se), Se_{10}^{2+} and S_{19}^{2+} can be obtained by oxidizing the elements under highly acid conditions and stabilizing the resulting naked E_n^{2+} moieties with anions such as AsF_6^-, SO_3F^- moieties and $AlCl_4^-$, as weak conjugate bases of very strong Lewis acids [15–17]. This list was extended in the 1990s by a further selenium (Se_{17}^{2+}) and 11 new tellurium polycations (see Table 2.7-1), most of which were prepared by Beck and co-workers by element oxidation with transition metal halides under chemical vapor transport conditions [18, 19].

The major synthetic strategies for preparing homopolyatomic cations of group 16 elements can be summarized as follows:

- Oxidation of the elements in acidic media (e.g., H_2SO_4, HSO_3F or anhydrous HF) or in liquid SO_2. Suitable oxidants are provided by $S_2O_8^{2-}$, $S_2O_6F_2$ or MF_5 (M = As, Sb):

$$8Se + 3AsF_5 \xrightarrow{SO_2} Se_8(AsF_6)_2 + AsF_3 \quad (1)$$

$$4Se + S_2O_6F_2 \xrightarrow{HSO_3F} Se_4(SO_3F)_2 \quad (2)$$

- Synproportionation reactions of elements and their higher halides in the presence of a strong halide acceptor:

$$15Se + SeCl_4 + 4AlCl_3 \xrightarrow{250\ ^\circ C} 2Se_8(AlCl_4)_2 \quad (3)$$

- Chemical transport reactions involving the element and/or an elemental subhalide and a transition metal halide/oxyhalide. The components are heated in evacuated sealed glass tubes at 100–300 °C for a period of days to weeks. Applying a small temperature gradient (10–20 °C) leads to gas phase transport and crystallization at the cooler end of the ampoule [19].

$$8Te + 2WCl_6 \xrightarrow{150\ ^\circ C} {Te_8}^{2+}({WCl_6}^-)_2 \quad (4)$$

$$2Te + 2Te_3Cl_2 + 2VOCl_2 \xrightarrow{270\ ^\circ C} {Te_8}^{4+}({VOCl_4}^{2-})_2 \quad (5)$$

Solovothermal techniques have also recently been employed. For instance, the reactions of Te with WCl_6 and of Te, $TeCl_4$ and $NbCl_5$ in $SnCl_4$ at 150 °C afford the compounds $[Te_6][Te_8](MCl_6)_4$ (M = W, Nb) [19] with boat shaped ${Te_6}^{2+}$and ${Te_8}^{2+}$ in a bicyclo[2.2.2]octane geometry.

The structures of individual polychalcogen cations and theoretically based interpretations of their bonding will now be discussed in order of increasing nuclearity $n = 4$–19. For more details, the reader is referred to the excellent recent review articles of Beck [19] (structures) and Passmore [13] (bonding and energetics).

2.7.2.1 The 6π Aromatic Cations ${E_4}^{2+}$

The tetraatomic cations ${Se_4}^{2+}$ and ${Te_4}^{2+}$ were structurally characterized in the early 1970s in $Se_4(HS_2O_7)_2$ [20] and $Te_4(AlCl_4)_2$ [21]. Numerous examples of salts containing these square planar cations and the analogous ${Se_4}^{2+}$ moiety are now known with the most recent representatives being provided by $Se_4(Bi_4Cl_{14})$ [22] and $Se_4(ReCl_6)_2$ [23]. In contrast to ${O_2}^+$, radical cations ${E_2}^+$ (E = S, Se, Te) dimerize in solution and in the solid state to form these 6π aromatic species, whose participating π-orbitals [24, 25] are illustrated schematically in Figure 2.7-2. The occupied A_{2u} and E_g orbitals are, respectively, bonding and nonbonding leading to an overall formal bond order of 1.25 for a π-bond delocalized over all four ring atoms.

In accordance with this bonding description, the Se–Se distance of 228 pm in $Se_4(HS_2O_7)$ is significantly shortened relative to that in α-Se_8 (234 pm) as is the average Te–Te distance of 267 pm in $Te_4(AlCl_4)_2$ relative to that in the discrete Te_8 rings of Cs_3Te_{22} (280 pm).

Ab initio calculations [25] show that the planar D_{2h} geometry is also energetically favorable for ${E_4}^{2+}$ in the gas phase over the alternative C_{2v} butterfly shaped structure, namely by +155, +115 and +86 kJ·mol^{-1} for, respectively, E = S, Se, Te. Although no example is known with the latter geometry, the alternative chain-like valence precise cation ${}^1_\infty[{Te_4}^{2+}]$ [Figure. 2.7-2(b)] is found in $[Te_4][Te_{10}](Bi_2Cl_8)$

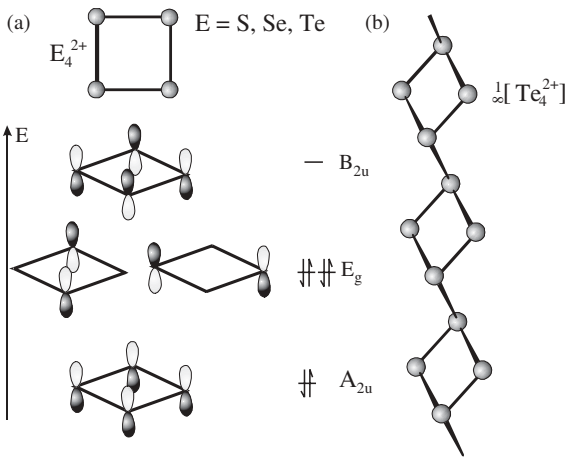

Fig. 2.7-2. (a) π-orbitals in E_4^{2+} cations and (b) the polymeric structure of $^1_\infty[Te_4^{2+}]$ in $[Te_4][Te_{10}](Bi_2Cl_8)_2$.

[19]. Donation of electron density from the $5p^2$ lone pairs of the dicoordinated ring atoms into the empty vicinal $5\sigma^*$ orbitals of the tricoordinated Te atoms [compare with the A_{2u} orbital of Figure 2.7-2(a)] enables a degree of delocalization of the latter's formal positive charge. This $5p^2 \rightarrow 5\sigma^*$ interaction of π-symmetry is reflected in the lengthening of the exocyclic Te–Te bond to 298 pm in comparison with typical single bond distances of 275–281 pm within the planar rings.

It is interesting to note that both Te_4^{2+} and neutral Te_4 rings have been characterized as ligands, namely in the respective complexes $[Te_4\{Nb_3OI_6(Te_2)_2\}]$ [26] and $[Te_4\{Cr(CO)_5\}_4]$ [27]. As we will see in Section 2.7.3, effectively isolated Te_4^- rings are present in the anionic network of Cs_4Te_{28} [8].

2.7.2.2
Bonding in Hexanuclear Te_6^{4+} and Te_6^{2+}

The trigonal prismatic cation Te_6^{4+} [Figure 2.7-3(a)] was first prepared as $Te_6(AsF_6)_4 \cdot 2AsF_3$ in 1979 [28] and is also present in $[Te_6][Se_8](AsF_6)_6SO_2$ [29]. Formal addition of two electrons affords the boat shaped cations of Te_6^{2+} [Figure 2.7-3(b)], which have been found in both $Te_6(WOCl_4)_2$ [30] and $Te_6(NbOCl_4)_2$ [31]. Neither of these hexanuclear cations can be described by a classical Lewis struc-

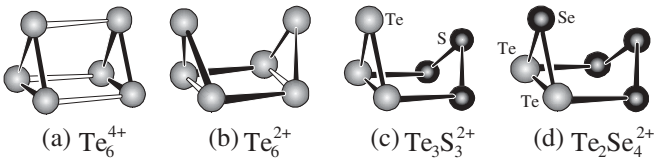

Fig. 2.7-3. Molecular structures of the hexanuclear cations Te_6^{4+}, Te_6^{2+}, $Te_3S_3^{2+}$ and $Te_2Se_4^{2+}$.

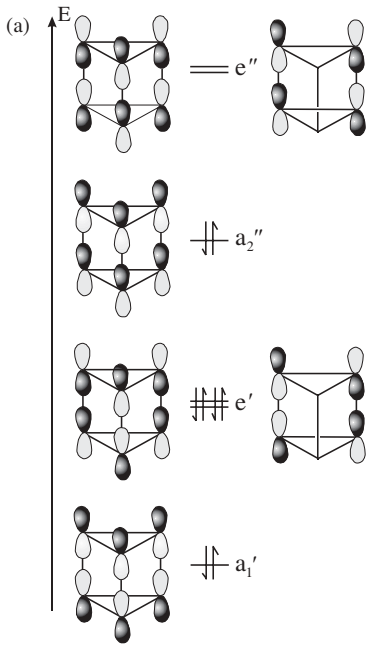

Fig. 2.7-4. Molecular orbitals of the Te_6^{4+} cation.

ture, in contrast to the mixed polycations $Te_3S_3^{2+}$ [32] and $Te_2Se_4^{2+}$ [33] in which the positive charges are clearly located on the heavier tricoordinated tellurium atoms [Figure 3(c) and (d)].

Te_6^{4+} can be rationalized as a dimer of Te_3^{2+} units that interact through a π^*–π^* 6-center 4-electron bond [34]. Only eight electrons reside in the six molecular orbitals of a_1', a_2'', e' and e'' symmetry obtained by combining the tellurium 5_{p_z} orbitals (Figure 2.7-4). The e' orbitals are nonbonding within the individual Te_3^{2+} rings but bonding between such units, and will represent their overall interaction as the a_1' contribution is cancelled by the a_2'' orbital. This description assigns a formal bond order of 2/3 to the longer sides of the trigonal prisms in accordance with their average length of 313 pm in $Te_6(AsF_6)_4 \cdot 2AsF_3$ as opposed to 268 pm within the triangular faces. Although isolated Te_3^{2+} cations have not been obtained, such a triangular species has been characterized as a facial tridentate ligand with average Te–Te distances of 273 pm in the complex $[W(CO)_4(Te_4)](SbF_6)_2$ [35].

A valence precise boat shaped Te_6^{2+} cation should contain just one transannular Te–Te bond as in $Te_3S_3^{2+}$ and $Te_2Se_4^{2+}$. In fact, two albeit rather weak transannular interactions (average $d_2 = 329$ pm) are present in the hexanuclear cations of $Te_6(MOCl_4)_2$ (M = W, Nb), thereby indicating that the two positive charges must be delocalized over all four Te atoms of the rectangular face. Two bonding and two antibonding molecular orbitals can be constructed from the $5p^2$ lone pair orbitals [Figure 2.7-5(a)] and will contain a total of six electrons [13].

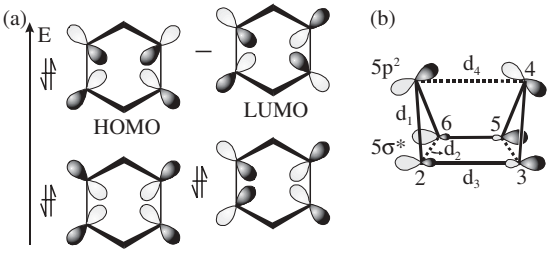

Fig. 2.7-5. (a) $5p_\pi$–$5p_\pi$ bonding of the central four atoms in Te_6^{2+} and (b) $5p^2 \rightarrow 5\sigma^*$ interactions in Te_6^{2+}.

This leads to a net gain of one $5p_\pi$–$5p_\pi$ bond which should shorten the central Te–Te bonds. Furthermore, the molecular orbitals exhibit non-cancelled transannular contributions and can therefore be regarded as representing a 4-center 2-electron π^*–π^* bond in addition to the $5p_\pi$–$5p_\pi$ bond. Interestingly the average d_3 distances of the rectangular face (274 pm) are somewhat longer than the d_1 values of the triangular faces (average 271 pm).

An explanation can be sought in $5p^2 \rightarrow 5\sigma^*$ interactions [Figure 2.7-5(b)] between the occupied $5p^2$ lone pair orbitals of Te1 and Te4 and the empty vicinal Te2–Te3 and Te5–Te6 $5\sigma^*$ orbitals [13]. This transfer of electron density will shorten the bonds to the apical atoms Te1 and Te4 whilst lengthening the central Te–Te bonds in the boat shaped cations. The experimental distances for d_1 and d_3 suggest that the $5p^2 \rightarrow 5p\sigma^*$ interactions must serve to counteract most of the bond shortening in Te2–Te3 and Te5–Te6 due to $5p_\pi$–$5p_\pi$ bonding. Te1 and Te4 are at a distance d_4 (average) of 367 pm from one another.

Rationalization of the cluster-like geometries of the cations E_4^{2+}, Te_6^{4+} and Te_6^{2+} in terms of the Wade-Mingos rules is also possible if the stereochemically inert ns^2 electrons are ignored [36]. On counting their 14 p-type valence electrons, E_4^{2+} squares contain seven skeletal electron pairs (SEPs) and therefore represent an $n + 2$ (*arachno*) cluster. Their structure is derived from an octahedron (six corners) by removing two opposite corners [Figure 2.7-6(a)]. Using an analogous counting scheme, Te_6^{2+} (11 SEPs) and Te_6^{4+} (ten SEPs) can be regarded as, respectively, $n + 4$ and $n + 3$ (*hypho*) clusters [13]. The boat shaped structure Te_6^{2+} cations can be derived from a bicapped square antiprism [minus two caps and two corners, Figure 2.7-6(b)] and the elongated trigonal prism of Te_6^{4+} from a tricapped trigonal prism [minus the three caps, Figure 2.7-6(c)].

The rationale behind the applicability of the Wade-Mingos concept lies in the goal of charge repulsion minimization. As a result of positive charge delocalization through np_π–np_π, π^*–π^* and $5p^2 \rightarrow 5\sigma^*$ interactions, each of the polychalcogen clusters can be regarded as an assembly of nearly similarly charged atoms. By occupying positions on the surface of a regular polyhedron, distances between partially charged atoms can be maximized so as to reduce Coulomb repulsion.

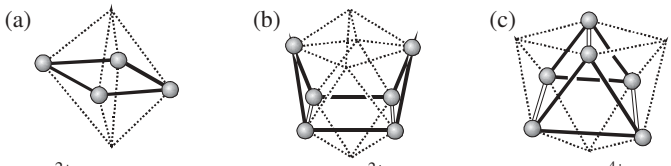

Fig. 2.7-6. Application of the Wade-Mingos rules to the cluster cations E_4^{2+}, Te_6^{2+} and Te_6^{4+}.

2.7.2.3 Molecular Structures of Te_8^{4+} and E_8^{2+}

Heating tellurium and $VOCl_3$ to 200 °C affords green $VOCl_2$ and silvery Te_3Cl_2, which then react at 270 °C together with Te to give $Te_8(VOCl_4)_2$ with the Te_8^{4+} cation [37]. As depicted in Figure 2.7-7(d), the cage-like structure of Te_8^{4+} is formally valence precise and can be regarded as resulting from the dimerization of two Te_4^{2+} species. However, the two central Te–Te bonds are markedly longer (average 301 pm) than those in the Te_4 rings (274–277 pm), which lie in the range for typical Te–Te single bonds. These differences in bond strength can once again be explained (as for Te_6^{2+}) by assuming intramolecular $5p^2 \rightarrow 5\sigma^*$ interactions between the occupied $5p^2$ lone pairs of the dicoordinated Te atoms and the empty vicinal $5\sigma^*$ orbitals of the central Te–Te bonds [13].

The S_8^{2+} and Se_8^{2+} cations in their AsF_6^- [36] and $AlCl_4^-$ [38] salts are very similar to Te_8^{2+} in $Te_8(ReCl_6)_2$ [39] as depicted in Figure 2.7-7(a). Their bicyclic structures can be regarded as being derived from the crown shaped rings of neutral E_8 molecules by flipping one atom from an *exo* to an *endo* position, and participation of the formally positively charged atoms in a central weak transannular

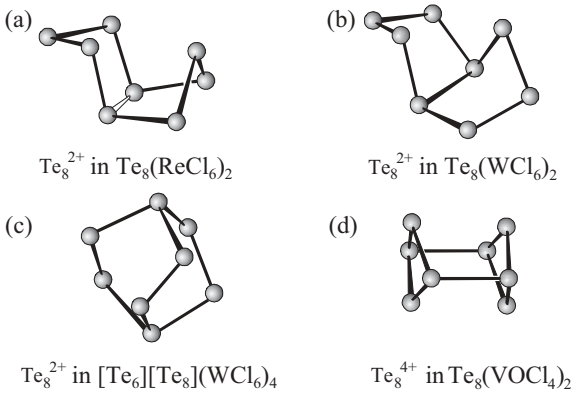

Fig. 2.7-7. Molecular structures of the octanuclear cations Te_8^{4+} and Te_8^{2+} (three isomers).

interaction, whose relative strength increases on going down the group (S_8^{2+} 286, Se_8^{2+} 284, Te_8^{2+} 315 pm). As for boat shaped Te_6^{2+}, the bonding in E_8^{2+} can be understood in terms of a σ-bonded cyclic framework with additional charge delocalization (over six atoms) by np_π–np_π ($n = 3$–5), transannular π^*–π^* and $np^2 \rightarrow n\sigma^*$ bonding. The cross-ring interactions (e.g., 300, 286, 296 in S_8^{2+}, 366, 315 and 390 pm in Te_8^{2+}) can thereby be rationalized as resulting from a 6-center 2-electron π^*–π^* bond of the six atoms residing on opposite sides of the ring.

A closely related second isomer of Te_8^{2+} can be prepared by the one electron oxidation of the element with WCl_6 [40] and exhibits a bicyclic geometry with a shorter transannular Te–Te distance of 299 pm [Figure 2.7-7(b)]. Two valence precise isomers are also known. In the mixed salt $[Te_6][Te_8](MCl_6)_4$ (M = W, Nb) [19], Te_8^{2+} exhibits a bicyclo[2.2.2]octane geometry [Figure 2.7-7(c)] as is also found for the heteropolyatomic cation $Te_2Se_6^{2+}$ of $[Te_2Se_6][Te_2Se_8](AsF_6)_4$ [41]. Boat shaped Te_6 rings are linked by Te_2 dumbbells into polymeric $^1_\infty[Te_8^{2-}]$ chains in the recently reported compounds $Te_8(Bi_4Cl_{14})$ [42] [Figure 2.7-8(c)] and $Te_8(U_2Br_{10})$ [43].

2.7.2.4 Larger Polycations and Polymers

Although discrete heptanuclear chalcogen cations are unknown, three polymeric $^1_\infty[Te_7^{2+}]$ dications with strikingly different structural motifs have been characterized. $Te_7(AsF_6)_2$ was isolated from the reaction of $Te_4(AsF_6)_2$ with $[Fe(CO)_5]$ in liquid SO_2 [44], in which the iron carbonyl is presumably responsible for the reduction of Te_4^{2+} to Te_7^{2+}. Its chair shaped Te_6 rings are linked through bridging Te atoms into infinite chains [Figure 2.7-8(a)].

A number of valence precise polymeric chalcogen cations with similar building units, namely 4 to 6 membered rings and 1 to 3 membered connecting chains are now known. The mixed $^1_\infty[Te_3Se_4^{2+}]$ cation of $[Te_3Se_4](WOCl_4)_2$ contains four membered Te_2Se_2 rings bridged by SeTeSe chains, the disordered $^1_\infty[Te_{3.15}Se_{4.85}^{2+}]$

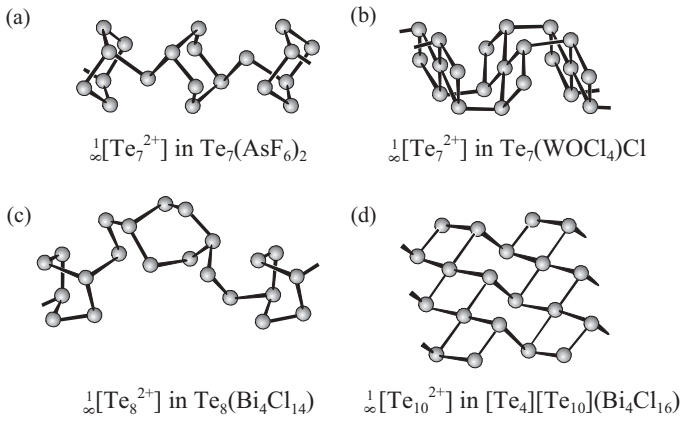

$^1_\infty[Te_7^{2+}]$ in $Te_7(AsF_6)_2$ $^1_\infty[Te_7^{2+}]$ in $Te_7(WOCl_4)Cl$

$^1_\infty[Te_8^{2+}]$ in $Te_8(Bi_4Cl_{14})$ $^1_\infty[Te_{10}^{2+}]$ in $[Te_4][Te_{10}](Bi_4Cl_{16})$

Fig. 2.7-8. Structures of polymeric tellurium cations.

cation of $[Te_{3.15}Se_{4.85}](WOCl_4)_2$ five membered rings and three membered chains [19]. In $Te_8(Bi_4Cl_{14})$, boat shaped Te_6 rings are connected through bridging Te_2 units [Figure 2.7-7(c)].

A very different type of polymeric chain [Figure 2.7-8(b)] is observed for the $^1_\infty[Te_7{}^{2+}]$ cations of $Te_7(MOX_4)X$ (M = W, Nb; X = Cl, Br) [45–47]. Its structure can be regarded as being composed of bicyclic $Te_7{}^{2-}$ anions (see Section 2.7.3) linked together into a folded band by four Te–Te bonds. An electron precise description can be achieved by assigning a formal charge of −2 to the central hypervalent Te atom with its square planar (ψ octahedral) environment and +1 to the four tricoordinated Te atoms [18]. The Te–Te distances of the $TeTe_4$ unit are relatively long (292–297 pm) as expected for 3-center 4-electron bonding [Figure 2.7-1(a)]. All the occupied $5_{p_z}{}^2$ lone pairs of the di- and tetracoordinated Te atoms can donate electron density into the empty antibonding $5\sigma^*$ orbitals of connecting Te–Te bonds [see Figure 2.7-5(b) for the analogous interactions in $Te_6{}^{2+}$]. As a result, the bonds between the tricoordinated Te atoms (288 pm) are again significantly lengthened with respect to those involving the neighboring dicoordinated atoms ($\bar{d}$ = 276 pm). A similar connectivity pattern is exhibited by the polymeric $^1_\infty[Te_7{}^{2+}]$ cations of $Te_7(Be_2Cl_6)$ [48]. However, in this case, the bicyclic Te_7 units are sited *trans* to one another with respect to the connecting Te–Te bonds. A closely related polymeric structure is observed for $^1_\infty[Te_{10}{}^{2+}]$ in $[Te_4][Te_{10}](Bi_2Cl_8)_2$ [48], which can be rationalized as containing tricyclic $Te_{10}{}^{4-}$ connected by six bonds between tricoordinated Te atoms with a formal charge of +1. Interestingly such polytelluride anions are unknown as isolated species.

Discrete homopolyatomic cations with more than eight atoms have only been obtained for S and Se and in their constituent 6–8 membered rings (Figure 2.7-9) clearly reflecting the greater tendency of the lighter group 16 elements to catenate. Whereas $Se_{10}{}^{2+}$, $Te_2Se_8{}^{2+}$ and $Se_{19}{}^{2+}$ were all characterized more than two decades ago as their $MF_6{}^-$ salts (M = As, Sb), [49,50,4, respectively] $Se_{17}{}^{2+}$ was first reported in 1995 as $Se_{17}(WCl_6)$ prepared by the chemical vapor transport reaction between Se and WCl_6 [51]. The homopolyatomic cations of Figure 2.7-9 all exhibit pronounced bond length alternation, with the bonds to the tricoordinated chal-

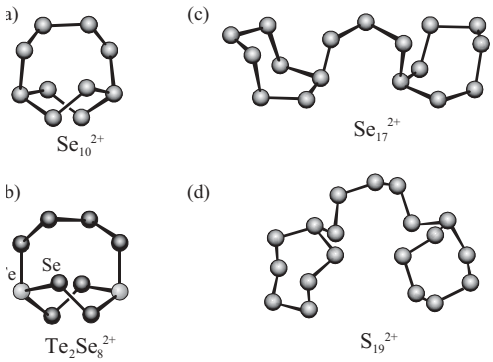

Fig. 2.7-9. Molecular structures of polychalcogen cations with ten or more atoms.

cogen atoms being on average significantly longer than those between dicoordinated atoms. For instance in $Se_{17}(WCl_6)$ values for the former bond lie in the range 235–249 pm, those for the latter Se–Se distances between 226 and 237 pm. $4p^2 \rightarrow 4\sigma^*$ electron density donation from the occupied $4p^2$ lone pair orbitals of vicinal dicoordinated Se atoms into empty antibonding $4\sigma^*$ orbitals of the bonds around the tricoordinated Se atoms must presumably be responsible for this bond lengthening.

2.7.3 Polychalcogenide Anions

Polychalcogenide dianions E_n^{2-} are known for $n = 2$–8 in the case of sulfur, $n = 2$–11 for selenium and $n = 2$–8, 12 and 13 for tellurium [10]. All known polysulfides exhibit discrete chain-like structures and on ignoring weak $4p^2 \rightarrow 4\sigma^*$ secondary interactions this is also the case for polyselenides Se_n^{2-} of nuclearity $n = 2$–9. Hypervalent 3-center 4-electron bonding leads to the formation of bicyclic structures by the larger Se_{10}^{2-} dianion [Figure 2.7-10(c)] in $[Ph_3PNPPh_3]_2Se_{10}\cdot DMF$ [52] and Se_{11}^{2-} [Figure 2.7-10(d)] in $[PPh_4]_2Se_{11}$ and $[NPr_4]_2Se_{11}$ [53, 54]. However, these interactions are strongly asymmetric in Se_{10}^{2-} and the spirobicyclic dianion of $[NPr_4]_2Se_{11}$ as evidenced by opposite d_1/d_2 distances of 276/257 pm at the ψ-trigonal bipyramidal atoms of the former and 277/256 pm at the central ψ-octahedral Se atom of the latter polyselenide. The fact that similar opposite bond lengths of 268 and 266 pm are found in $[Ph_3PNPPh_3]_2Se_{10}\cdot DMF$ indicates that the energy hypersurface for distortion of chalcogen E–E–E 3-center 4-electron bonds must indeed be very flat. Packing factors involving the structure-directing counter cations will, therefore, play an important role in determining the extent of any coordination sphere distortion. The increased tendency of tellurium to participate in intra- and intermolecular $np^2 \rightarrow n\sigma^*$ bonding leads to the presence of distorted linear Te–Te$\cdots$Te units in many polytellurides. As a consequence, their classification as discrete or as polymeric chains

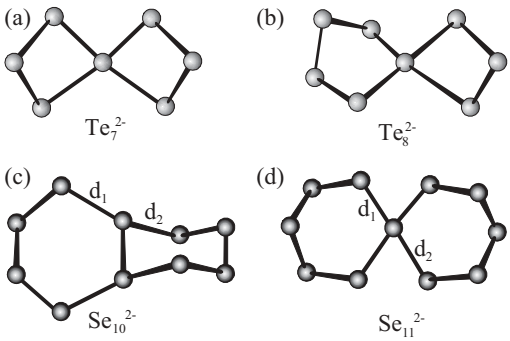

Fig. 2.7-10. Molecular structures of the discrete polyanions Te_7^{2-}, Te_8^{2-}, Se_{10}^{2-} and Se_{11}^{2-}.

or sheets may often be relatively arbitrary [10]. When only the stronger Te–Te bonds are taken into account (i.e., $d < 3.13$ Å), isolated chains Te_n^{2-} can, however be recognized for dianions with $n = 2$–6, 12 and 13. $[Re_6Te_8]Te_7$ features a butterfly-like Te_7^{2-} anion [Figure 2.7-10(a)] [55] and $[K(15\text{-crown-5})]_2Te_8$ a likewise bicyclic anion [Figure 2.7-10(b)] with a central square-planar $TeTe_4$ unit [56].

Only species Te_n^{2-} with short chains ($n = 2$–4) are present in polytelluride solutions [57]. Despite this fact many Zintl-type valence precise tellurium dianions of higher nuclearity have been isolated in the solid state in the presence of suitable counter cations. The three general synthetic routes to such polytelluride anions can be summarized with representative examples as follows:

- High temperature fusion (500–700 °C) of alkali or alkaline earth metals with tellurium, e.g., M_2Te_3 (M = K, Rb, Cs), $CsTe_4$, MTe_2 (M = Mg, Ba).
- Reaction of alkali metals with tellurium in liquid ammonia at temperatures between −78 °C and 220 °C (supercritical at 100 bar), e.g., M_2Te (M = Li, Na, K), M_2Te_2, (M = K, Rb, Cs), M_2Te_5 (M = Rb, Cs).
- Extraction of binary and tertiary tellurium alloys (M = alkali or alkaline earth metal) in basic solution (e.g., en, DMF) in the presence of an encapsulating agent or a large non-coordinating organic cation, e.g., $[(Ba(en)_3]Te_3$, $[K(15\text{-crown-5})]_2Te_8$, $[Ph_3PNPPh_3]_2Te_5 \cdot 2DMF$.

More details on the preparation and structures of these valence precise dianions are given in a recent review article by Smith and Ibers [10].

2.7.3.1 Polytelluride Anions With Cluster-like Building Units

The lamellar polytellurides $RbTe_6$ [58], $CsTe_{28}$ [8] and Cs_3Te_{22} [7] can be prepared under mild methanolothermal conditions (160–195 °C) [59] by reaction of M_2CO_3 (M = Rb, Cs) with a suitable tellurium source such as Ge/Te for $RbTe_6$ or As_2Te_3 for the cesium tellurides. As their anionic substructures contain characteristic ring shaped $Te_6^{\bullet -}$ and $Te_4^{\bullet -}$ units with a degree of radical character and cannot be described in terms of classical Lewis formulations, they will now be discussed in more detail together with the radical anion $S_6^{\bullet -}$ [60].

A trapped $S_3^{\bullet -}$ radical anion is responsible for the bright blue color of *Lapis lazuli* [61] and is also present together with other radical anions in solutions of polysulfides in organic solvents. In contrast to likewise blue $S_5^{\bullet +}$ and other radical cations that are produced in oleum solutions of the element, one radical anion $S_6^{\bullet -}$ has indeed been successfully characterized in the solid state. $[Ph_4P]S_6$ was prepared by treating $[Ph_4P]N_3$ with H_2S in the presence of Me_3SiN_3 [60]. Its discrete six membered rings exhibit a chair conformation in which two S_3 units with typical S–S single bonds ($\bar{d} = 206$ pm) are connected by two very long S–S interactions (263 pm). Molecular orbital calculations indicate that these can be rationalized as resulting from weak 4-center 3-electron bonding. A similar bond length pattern is also observed in the likewise chair shaped $Te_6^{\bullet -}$ rings of $RbTe_6$ [58], which are

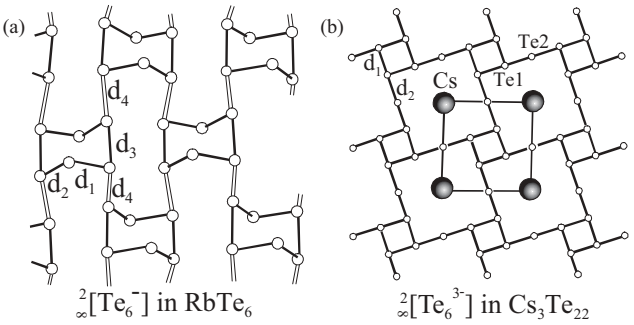

Fig. 2.7-11. The anion sheets (a) $^2_\infty[Te_6^-]$ in $RbTe_6$ and (b) $^2_\infty[Te_6^{3-}]$ in Cs_3Te_{22}.

linked through weak secondary interactions ($d_4 = 321$ pm) into corrugated $^2_\infty[Te_6^-]$ sheets [Figure 2.7-11(a)]. Bonding within the six membered rings can presumably once again be described in terms of weak 4-center 3-electron bonds ($d_3 = 320$ pm) between two singly bonded triatomic units ($d_1 = 279$, $d_2 = 278$ pm).

The resulting pronounced bond length alternation within the anion sheets of $RbTe_6$ is in stark contrast to the relatively modest differences between the Te–Te distances ($d_1 = 300$, $d_2 = 308$ pm) belonging to the planar thinned 4^4 nets (4^4 = network of Te_4 squares with 4-coordinated Te nodes and shared sides) of Cs_3Te_{22} in Figure 2.7-11(b). This tellurium-rich cesium telluride was prepared by the reaction of Cs_2CO_3 with As_2Te_3 at 195 °C and also contains effectively neutral crown shaped Te_8 rings [7] in addition to the planar $^2_\infty[Te_6^{3-}]$ anions. These contrasting substructures may be regarded as reflecting the non-metallic and metallic sides of tellurium chemistry and are stabilized by the presence of Cs^+ counter cations sited between two Te_8 rings at the centers of the large Te_{12} squares of $^2_\infty[Te_6^{3-}]$. Extended Hückel calculations [62, 63] have yielded charges of −0.22 for Te1 of the smaller Te_4 squares and −1.06 for the linear coordinated Te2 atoms. Neither of these tellurium atoms therefore achieve the maximal formal charges of, respectively, −1 and −2 that their hypervalent ψ-trigonal bipyrimidal geometries would allow. These results suggest that the $^2_\infty[Te_6^{3-}]$ layer can be described in a very simplified manner as a series of $Te_4^{\bullet -}$ anions coupled through Te^- spacers. Eight filled σ-bonding bands (for the 8 Te–Te σ-bonds per Te_6^{3-} unit), six π-type bands (for the six perpendicular $5p_z$ orbitals) and two bands associated with the in-plane $5p^2$ lone pairs of linear coordinated Te2 will account for 32 of the 39 available valence electrons per unit cell [Figure 2.7-11(b)]. The remaining seven electrons must be housed in a block of eight σ^* antibonding bands and will be more heavily associated with the weaker Te1–Te2 bonds. As its uppermost band is half-filled and exhibits a sizeable dispersion of 1.3 eV, Cs_3Te_{22} could exhibit metallic properties although this possibility has yet to be experimentally confirmed.

The template-controlled formation of the Te_8 crowns and $^2_\infty[Te_6^{3-}]$ nets in Cs_3Te_{22} can be mechanistically explained on the basis of two further cesium tellurides formed under similar conditions at lower temperatures [64]. Cs_2Te_{13} can

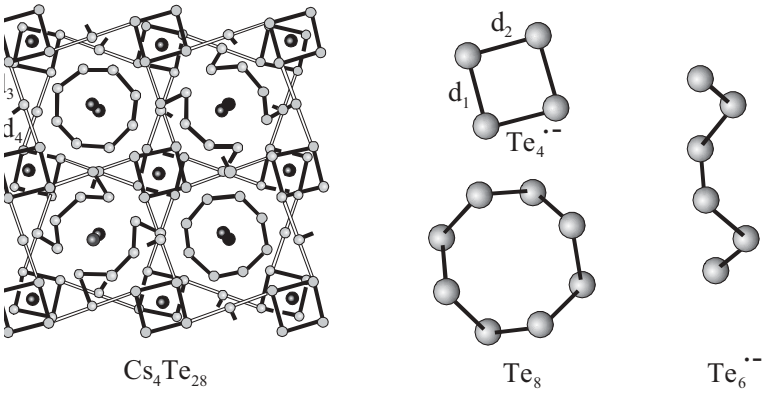

Fig. 2.7-12. Structure of Cs_4Te_{28} and its formal individual components, neutral Te_8 crowns and weakly linked $Te_4^{\bullet -}$ rings and $Te_6^{\bullet -}$ chains.

be isolated at 160 °C [8] and contains valence precise Te_{13}^{2-} chains that connect through weak $5p^2 \rightarrow 5\sigma^*$ interactions into sheets. On heating to 180 °C, Te addition and structural rearrangement leads to Cs_4Te_{28} [8], in whose three-dimensional framework neutral discrete Te_8 rings and weakly linked Te_4 rings ($d_1 = 291$, $d_2 = 295$ pm) and Te_6 chains can be identified.

On ignoring interactions between the latter units ($d_3 = 319$, $d_4 = 315$ pm), the $^3_\infty[Te_{20}^{4-}]$ anionic framework of Cs_4Te_{28} (Figure 2.7-12) can be rationalized in a simple approach as being composed of non-valence precise $Te_4^{\bullet -}$ cluster anions coupled through $Te_6^{\bullet -}$ chains, both of which with a degree of radical character. Extended Hückel calculations [62] are in basic agreement with such a formal charge assignment. A further structural rearrangement of the Te building units within Cs_4Te_{28} leads to production of Cs_3Te_{22} at 195 °C.

2.7.4 Summary and Outlook

The homopolyatomic cations of the group 16 elements and in particular those of tellurium adopt structures that enable effective positive charge delocalization through np_π–np_π, π^*–π^* and $np^2 \rightarrow n\sigma^*$ bonding. For the smaller polychalcogen cations E_4^{2+}, Te_6^{4+}, Te_6^{2+} and E_8^{2+}, this leads to cluster-like geometries whose atom arrangements can be rationalized in terms of the Wade-Mingos rules. Polymeric structures are observed for Te_n^{2+} cations of higher nuclearity ($n = 7$, 8, 10) but not for the lighter group 16 elements. This is also the case for polytelluride anions in which hypervalent linear 3-center 4-electron bonding and weaker $5p^2 \rightarrow 5\sigma^*$ interactions favor negative charge delocalization within polymeric networks. The relatively flat energy hypersurface for this type of bonding leads to the observation of a wide range of Te–Te distances (304–360 pm) and the possibility of net-

work distortions in which Te_n^{x-} substructures temporarily adopt a more isolated character (e.g., as $Te_4^{\bullet-}$ rings within the anionic network of Cs_3Te_{22}) by strengthening "intramolecular" and weakening "intermolecular" Te–Te bonds. Such rapid structural modulations should favor the development of charge density waves (CDWs) and are typical for low-dimensional metals. Interestingly the quaternary telluride $K_{0.33}Ba_{0.67}AgTe_2$ contains square planar 4^4 Te nets that already display semiconductivity at room temperature owing to CDWs resulting from structural instabilities of this type [65]. This finding points to the considerable potential of polymeric tellurium-rich ions in the search for materials with tailored structural and electronic properties [62].

References

1 R. Steudel, *Sulphur Homocycles*, in I. Haiduc, D. B. Sowerby (eds.), *The Chemistry of Inorganic Homo- and Heterocycles*, Vol. 2, Academic Press, London, **1987**, p. 737.
2 R. Steudel, O. Schuhmann, J. Buschmann, P. Luger, *Angew. Chem., Int. Ed. Engl.*, **1998**, *37*, 2377.
3 R. S. Laitinen, P. Pekonen, R. J. Suontamo, *Coord. Chem. Rev.*, **1994**, *130*, 1.
4 R. C. Burns, R. J. Gillespie, J. F. Sawyer, *Inorg. Chem.*, **1980**, *19*, 1423.
5 R. J. Gillespie, J. Passmore, P. K. Ummat, O. C. Vaidya, *Inorg. Chem.*, **1971**, *10*, 1327.
6 J. Passmore, G. Sutherland, P. S. White, *J. Chem. Soc., Chem. Commun.*, **1980**, 289.
7 W. S. Sheldrick, M. Wachhold, *Angew. Chem., Int. Ed. Engl.*, **1995**, *34*, 450.
8 W. S. Sheldrick, M. Wachhold, *J. Chem. Soc., Chem. Commun.*, **1996**, 607.
9 P. Böttcher, *Angew. Chem., Int. Ed. Engl.*, **1988**, *27*, 759.
10 D. M. Smith, I. A. Ibers, *Coord. Chem. Rev.*, **2000**, *200*, 187 and references cited therein.
11 R. J. Gillespie, *Chem. Soc. Rev.*, **1992**, *21*, 59.
12 J. Beck, M. Dolg, S. Schlüter, *Angew. Chem., Int. Ed. Engl.*, **2001**, *40*, 2287.
13 S. Brownridge, I. Crossing, J. Passmore, H. D. B. Jenkins, H. K. Roobottom, *Coord. Chem. Rev.*, **2000**, *197*, 397 and references cited therein.
14 N. Bartlett, D. H. Lohmann, *J. Chem. Soc.*, **1962**, 5253.
15 R. J. Gillespie, *J. Chem. Soc. Rev.*, **1979**, *8*, 315.
16 N. Burford, J. Passmore, J. C. P. Sanders, in J. F. Liebman, A. Greenberg (eds.), *From Atoms to Polymers, Isoelectronic Analogies*, **1989**, p. 53.
17 J. Passmore, *The Chemistry of Inorganic Ring Systems*, in R. Steudel (ed.), *Studies in Inorganic Chemistry*, **1992**, *14*, 373.
18 J. Beck, *Angew. Chem., Int. Ed. Engl.*, **1994**, *33*, 163.
19 J. Beck, *Coord. Chem. Rev.*, **1997**, *163*, 55 and references cited therein.
20 I. D. Brown, D. B. Crump, R. J. Gillespie, *Inorg. Chem.*, **1971**, *10*, 23.
21 D. J. Prince, J. D. Corbett, B. Garbisch, *Inorg. Chem.*, **1970**, *9*, 2731.
22 J. Beck, T. Hilbert, *Z. Anorg. Allg. Chem.*, **2000**, *626*, 837.
23 J. Beck, A. Desgroseilliers, K. Müller-Buschbaum, K. J. Schlitt, *Z. Anorg. Allg. Chem.*, **2002**, *628*, 1145.
24 L. J. Saethre, O. Gropen, *Can. J. Chem.*, **1992**, *70*, 348.
25 I. Krossing, J. Passmore, *Inorg. Chem.*, **1999**, *38*, 5203.
26 W. Tremel, *J. Chem. Soc., Chem. Commun.*, **1992**, 126.
27 O. Blacque, H. Brunner, M. M. Kubicki, B. Nuber, B. Stubenhofer,

J. Wachter, B. Wrackmeyer, *Angew. Chem., Int. Ed. Engl.*, **1997**, *36*, 352.
28 R. C. Burns, R. J. Gillespie, W.-C. Luk, D. R. Slim, *Inorg. Chem.*, **1997**, *11*, 3086.
29 M. J. Collins, R. J. Gillespie, J. F. Sawyer, *Acta Crystallogr. C*, **1988**, *44*, 405.
30 J. Beck, *Chem. Ber.*, **1995**, *128*, 23.
31 J. Beck, G. Bock, *Z. Anorg. Allg. Chem.*, **1996**, *126*, 823.
32 R. J. Gillespie, W. Luk, W. Mararagh, D. R. Slim, *Inorg. Chem.*, **1977**, *16*, 892.
33 R. C. Burns, M. J. Collins, S. M. Eicher, R. J. Gillespie, J. F. Sawyer, *Inorg. Chem.*, **1988**, *27*, 1807.
34 P. D. Lyne, D. M. P. Mingos, T. Ziegler, *J. Chem. Soc., Dalton Trans.*, **1992**, 2743.
35 R. Faggiani, R. J. Gillespie, C. Campana, J. W. Kolis, *J. Chem. Soc., Chem. Commun.*, **1987**, 485.
36 T. S. Cameron, R. J. Deeth, I. Dionne, H. D. B. Jenkins, I. Krossing, J. Passmore, H. K. Roobottom, *Inorg. Chem.*, **2000**, *39*, 5614.
37 J. Beck, G. Bock, *Angew. Chem., Int. Ed. Engl.*, **1995**, *34*, 2559.
38 R. K. McMullen, D. J. Prince, J. D. Corbett, *Inorg. Chem.*, **1971**, *10*, 1749.
39 J. Beck, K. Müller-Buschbaum, *Z. Anorg. Allg. Chem.*, **1997**, *623*, 409.
40 J. Beck, *Angew. Chem., Int. Ed. Engl.*, **1990**, *29*, 293.
41 M. J. Collins, R. J. Gillespie, J. F. Sawyer, *Inorg. Chem.*, **1987**, *26*, 1476.
42 J. Beck, A. Stankowski, *Z. Naturforsch.*, **2001**, *56b*, 453.
43 J. Beck, A. Fischer, *Z. Anorg. Allg. Chem.*, **2002**, *628*, 369.
44 G. W. Drake, G. L. Schimek, J. W. Kolis, *Inorg. Chem.*, **1996**, *35*, 1740.
45 J. Beck, *Angew. Chem., Int. Ed. Engl.*, **1991**, *30*, 1128.
46 J. Beck, *Z. Anorg. Allg. Chem.*, **1993**, *619*, 237.
47 J. Beck, G. Bock, *Z. Anorg. Allg. Chem.*, **1994**, *620*, 1971.
48 J. Beck, A. Fischer, A. Stankowski, *Z. Anorg. Allg. Chem.*, **2002**, *628*, 2542.
49 R. C. Burns, W.-L. Chan, R. J. Gillespie, W.-C. Luk, J. F. Sawyer, D. R. Slim, *Inorg. Chem.*, **1980**, *19*, 1432.
50 P. Boldrini, I. D. Brown, R. J. Gillespie, P. R. Ireland, W. Luk, D. R. Slim, J. E. Vekris, *Inorg. Chem.*, **1976**, *15*, 765.
51 J. Beck, J. Wetterau, *Inorg. Chem.*, **1995**, *34*, 6202.
52 D. Fenske, G. Kräuter, K. Dehnicke, *Angew. Chem., Int. Ed. Engl.*, **1990**, *29*, 390.
53 M. G. Kanatzidis, S. P. Huang, *Inorg. Chem.*, **1989**, *28*, 4667.
54 J. Dietz, U. Müller, V. Müller, K. Dehnicke, *Z. Naturforsch.*, **1991**, *46b*, 1293.
55 F. Kaiber, W. Petter, F. Hulliger, *J. Solid State Chem.*, **1983**, *46*, 112.
56 B. Schreiner, K. Dehnicke, K. Maczek, D. Fenske, *Z. Anorg. Allg. Chem.*, **1993**, *619*, 1414.
57 M. Björgvinsson, J. F. Sawyer, G. J. Schrobilgen, *Inorg. Chem.*, **1991**, *30*, 4238.
58 W. S. Sheldrick, B. Schaaf, *Z. Naturforsch.*, **1994**, *49b*, 993.
59 W. S. Sheldrick, M. Wachhold, *Angew. Chem., Int. Ed. Engl.*, **1997**, *36*, 206.
60 B. Neumüller, F. Schmock, R. Kirmse, A. Voigt, A. Diefenbach, F. M. Bickelhaupt, K. Dehnicke, *Angew. Chem., Int. Ed. Engl.*, **2000**, *39*, 4753.
61 E. Gaumann, R. Huter, W. Keller-Schierlein, L. Neipp, V. Prelog, H. Zahner, *Helv. Chim. Acta*, **1960**, *43*, 601.
62 W. S. Sheldrick, M. Wachhold, S. Jobic, R. Brec, E. Canadell, *Adv. Mater.*, **1997**, *9*, 669.
63 Q. Liu, N. Goldberg, R. Hoffmann, *Chem. Eur. J.*, **1996**, *2*, 390.
64 W. S. Sheldrick, *J. Chem. Soc., Dalton Trans.*, **2000**, 3041.
65 X. Zhang, J. Li, B. Foran, S. Lee, H.-Y. Guo, T. Hogan, C. R. Kannewurf, M. G. Kanatzidis, *J. Am. Chem. Soc.*, **1995**, *117*, 10513.

3.1
Alkali and Alkaline Earth Metal Suboxides and Subnitrides

Arndt Simon

3.1.1
Introduction

Compounds with metal–metal bonding occur frequently throughout the Periodic Table. The trivial but necessary condition for covalent M–M bonding is a low oxidation state which leaves valence electrons with the metal atom. This condition, however, is not sufficient. Compounds need to be metal-rich to allow for sufficiently close contacts between metal atoms, and the extension of the valence electron orbitals in space must be large in order to provide good overlap. Hence, it is no surprise that M–M bonding and cluster formation dominates with the heavier elements in the Periodic Table, involving s, p, d, and even f electrons.

There has been early evidence for the formation of metal-rich oxides, so called suboxides, of the heavy alkali metals rubidium and cesium [1, 2]. With alkaline earth metals several stable subnitrides are known [3–7], and the reaction of nitrogen with barium dissolved in liquid sodium indicated the formation of even more metal-rich subnitrides and Ba_xN clusters in the melt [8, 9]. Based on specially developed methods of preparation and crystal growth together with structural investigations we could clarify the nature of these remarkable suboxides [10] and numerous new subnitrides were discovered [11–18]. All structures of group 1 metal suboxides and of group 2 metal subnitrides contain clusters formed from an octahedral M_6 unit which is centered by an oxygen or nitrogen atom. Such M_6X octahedra are linked via common faces and edges, respectively, resulting in discrete clusters or one- and two-dimensional structural units. Bonding in these compounds is unique, however when analyzing it in the context of general developments of cluster chemistry within the Periodic Table it represents only one extreme [19, 20].

The chemistry of octahedral metal clusters culminates in the center of the Periodic Table with the heavy transition metals Nb, Ta, Mo, W, and Re. There is a plethora of clusters where the M–M bonded core is surrounded (and shielded) by non-metal ligands. When moving to the left of the Periodic Table the decrease in valence electron concentration calls for a stabilization through incorporation of interstitial atoms into the cluster core. Actually, the stabilization of the cluster occurs

through formation of strong heteronuclear bonds to the interstitials but at the expense of weak M–M bonding. The chemistry of zirconium halides such as $Zr_6I_{12}C$ serves as a good example [21]. It is interesting to note that the number of electrons available for M–M bonding also decreases when moving to the right-hand side of the Periodic Table, with somewhat similar consequences.

Of course, valence electron concentration is not only related to the metal atoms but also to the number and valence of the ligands. Ligand deficiency creates vacant coordination sites at metal atoms and results in cluster condensation, which is the fusion of clusters via short M–M contacts into larger units ranging from zero- to three-dimensional. The chemistry of metal-rich halides of rare earth metals comprises both principles, incorporation of interstitial atoms and cluster condensation, with a vast number of examples [22, 23].

When it comes to metal-rich compounds of the alkaline earth and alkali metals with their pronounced valence electron deficiencies it is no surprise that both principles play a dominant role. In addition, there is no capability for bonding of a ligand shell around the cluster cores. The discrete and condensed clusters of group 1 and 2 metals therefore are bare, a fact which leads to extended inter-cluster bonding and results in electronic delocalization and metallic properties for all known compounds.

The alkali metal suboxides are well understood in terms of formation, structure, and properties, yet we still face some unsolved problems that will also be addressed in the following. In contrast, the first suboxide of barium came to light only recently [24], and one has to see whether this compound is the tip of another iceberg, as turned out to be the case with the subnitrides of alkaline earth metals.

Table 3.1-1 summarizes the crystallographically characterized group 1 metal suboxides, and group 2 metal subnitrides, the latter containing additional alkali or other metals [25].

3.1.2 Alkali Metal Suboxides

Within the group of alkali metals the reactivity towards oxygen increases dramatically in the case of Rb and Cs. For safety reasons, and in order to avoid vaporization of the metal which results in undefined sample compositions, the oxidation process has to be very carefully controlled. The metals Rb and Cs exhibit a distinctly different oxidation behavior compared with the lighter homologues. The oxygen dissolves homogeneously as evidenced by a gradual change of color. The molten metal darkens with increasing oxygen content from the native golden color of Cs via bronze to violet, and bronze-colored Cs_7O or permanganate-colored $Cs_{11}O_3$ crystallize upon cooling. Silvery Rb changes into brass-colored Rb_6O and copper-red Rb_9O_2. These suboxides are stable compounds in the $M–M_2O$ systems and can be prepared from the elements as well as by reacting the necessary amounts of the metal with the corresponding higher oxides, M_2O, M_2O_2 or MO_2.

Once in a while the question is discussed as to whether the golden color of ce-

Tab. 3.1-1. Structurally characterized suboxides and subnitrides of alkali and alkaline earth metals, respectively, *Z* refers to the structural formula.

Compound	*Structural formula*	*Unit cell (at T/°C)*	*Ref.*
Rb_9O_2	$[Rb_9O_2]$	$P\,2_1/m$, $Z = 2$, $a = 832.3$, $b = 1398.6$, $c = 1165.4$ pm $\beta = 104.39°$ (−50)	26
Rb_6O	$[Rb_9O_2]Rb_3$	$P\,6_3/m$, $Z = 2$, $a = 839.3$, $c = 3046.7$ pm (−50)	27
$Cs_{11}O_3$	$[Cs_{11}O_3]$	$P\,2_1/c$, $Z = 4$, $a = 1761.0$, $b = 921.8$, $c = 2404.7$ pm $\beta = 100.14°$ (20)	28
Cs_4O	$[Cs_{11}O_3]Cs$	$Pna2_1$, $Z = 4$, $a = 1682.3$, $b = 2052.5$, $c = 1237.2$ pm (−100)	29
Cs_7O	$[Cs_{11}O_3]Cs_{10}$	P-6m2, $Z = 1$, $a = 1630.9$, $c = 915.4$ pm (−50)	30
$Cs_{11}O_3Rb$	$[Cs_{11}O_3]Rb$	$Pmn2_1$, $Z = 2$, $a = 1648.4$, $b = 1371.3$, $c = 913$ pm (−50)	31
$Cs_{11}O_3Rb_2$	$[Cs_{11}O_3]Rb_2$	$P\,2_1/c$, $Z = 8$, $a = 4231.1$, $b = 919.4$, $c = 2415.6$ pm $\beta = 108.94°$ (−50)	10
$Cs_{11}O_3Rb_7$	$[Cs_{11}O_3]Rb_7$	$P\,2_12_12_1$, $Z = 4$, $a = 3228.1$, $b = 2187.7$, $c = 902.5$ pm (−90)	32
Ba_2ONa	$[Ba_{4/2}O]Na$	$Cmma$, $Z = 4$, $a = 659.1$, $b = 1532.7$, $c = 693.9$ pm (20)	24
Ba_6NNa_{16}	$[Ba_6N]Na_{16}$	Im-3m, $Z = 2$, $a = 1252.7$ pm (20)	12
$Ba_{14}CaN_6Na_7$	$[Ba_{14}CaN_6]Na_7$	R-3c, $Z = 6$, $a = 1136.0$, $c = 6306.1$ pm (20)	18
$Ba_{14}CaN_6Na_8$	$[Ba_{14}CaN_6]Na_8$	$P\,6_3/m$, $Z = 2$, $a = 1141.9$, $c = 2154.3$ pm (20)	17
$Ba_{14}CaN_6Na_{14}$	$[Ba_{14}CaN_6]Na_{14}$	Fm-3m, $Z = 8$, $a = 1789.5$ pm (20)	14, 15
$Ba_{14}CaN_6Na_{17}$	$[Ba_{14}CaN_6]Na_{17}$	P-1, $Z = 1$, $a = 1114.2$, $b = 1206.5$, $c = 1372.5$ pm $\alpha = 66.65°$, $\beta = 67.79°$, $\gamma = 78.88°$ (20)	15
$Ba_{14}CaN_6Na_{21}$	$[Ba_{14}CaN_6]Na_{21}$	$C\,2/m$, $Z = 2$, $a = 2150.0$, $b = 1266.4$, $c = 1629.5$ pm $\beta = 129.48°$ (20)	15
$Ba_{14}CaN_6Na_{22}$	$[Ba_{14}CaN_6]Na_{22}$	$P\,6_3/mmc$, $Z = 1$, $a = 1266.6$, $c = 1263.5$ pm (20)	15, 33
Ba_3N	$[Ba_{6/2}N]$	$P\,6_3/mcm$, $Z = 2$, $a = 764.2$, $c = 705.0$ pm (20)	16
Ba_3NNa	$[Ba_{6/2}N]Na$	$P\,6_3/mmc$, $Z = 2$, $a = 844.1$, $c = 698.2$ pm (20)	11
Ba_3NNa_5	$[Ba_{6/2}N]Na_5$	$Pnma$, $Z = 4$, $a = 1189.7$, $b = 705.6$, $c = 1780.1$ pm (20)	13
Ba_2N	$[Ba_{6/3}N]$	R-3m, $Z = 3$, $a = 403.1$, $c = 2253.2$ pm (20)	7
Ca_2N	$[Ca_{6/3}N]$	R-3m, $Z = 3$, $a = 362.7$, $c = 1897.2$ pm (20)	4
Sr_2N	$[Sr_{6/3}N]$	R-3m, $Z = 3$, $a = 385.7$, $c = 2069.6$ pm (20)	6
Sr_4N_3	$[Sr_{6/3}N]_4N_2$	$C\,2/m$, $Z = 1$, $a = 670.7$, $b = 382.8$, $c = 1376.3$ pm $\beta = 96.52°$ (25)	34
Ba_6NGa_5	$[Ba_6N][Ga_5]$	R-3c, $Z = 6$, $a = 790.5$, $c = 4196.5$ pm (20)	35
Ca_6NAg_{16}	$[Ca_6N]Ag_{16}$	Im-3m, $Z = 2$, $a = 978.5$ pm (20)	12
Ca_3NAu	$[Ca_{6/2}N]Au$	Fm-3m, $Z = 4$, $a = 1474.4$ pm (20)	36
Ca_4NIn_2	$[Ca_{4/2}Ca_2N][In_2]$	$I\,4_1/amd$, $Z = 4$, $a = 491.5$, c = 2910.2 pm (20)	37
$Ca_{19}N_7Ag_8$	$[Ca_{19}N_7][Ag_4]_2$	Fm-3m, $Z = 4$, $a = 1474.4$ pm (22)	38
$Ca_{18.5}N_7Ga_8$	$[Ca_{18.5}N_7][Ga_4]_2$	Fm-3m, $Z = 4$, $a = 1440.9$ pm (20)	39
$Ca_{18.5}N_7In_8$	$[Ca_{18.5}N_7][In_4]_2$	Fm-3m, $Z = 4$, $a = 1474.7$ pm (20)	39
Sr_6NGa_5	$[Sr_6N][Ga_5]$	R-3c, $Z = 6$, $a = 758.0$, $c = 4041.3$ pm (20)	35
Sr_4NIn_2	$[Sr_{4/2}Sr_2N][In_2]$	$I\,4_1/amd$, $Z = 4$, $a = 524.0$, $c = 3067.0$ pm (20)	37

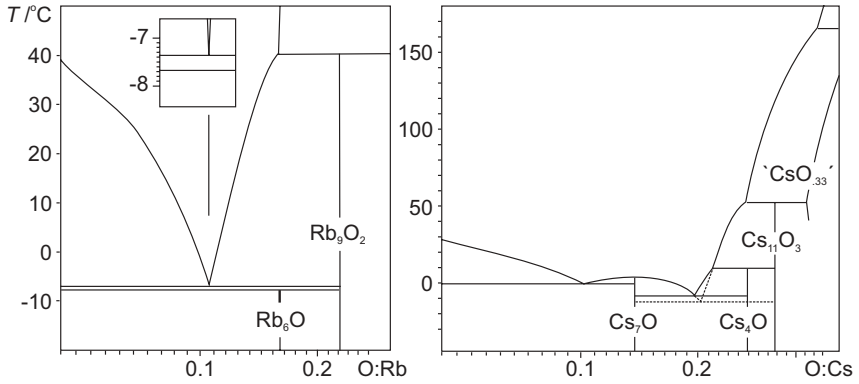

Fig. 3.1-1. Phase diagrams for the Rb and Cs suboxides.

sium is that of the pure element or rather that of a spuriously oxidized metal contaminated by suboxide. Detailed investigations [40] clearly show the color to be an intrinsic property as traces of 0.5 ppm oxygen can be detected by a characteristic change of the melting behavior. Oxygen contents higher by several orders of magnitude are necessary to observe a slight change of the color.

Thermal analyses combined with X-ray studies of single- and poly-crystalline samples have resulted in the phase diagrams shown in Figure 3.1-1 [40] partly corroborating earlier results for the binary systems [1, 2, 41], however, with corrections to compound compositions. Several compounds occur, and as can be seen in Figure 3.1-1 most of them do not exist at room temperature, in particular, when also taking the Rb–Cs mixed compounds into account. The amount of melting point depression for the metals upon oxidation gives evidence for a clustering of oxygen atoms in the liquid, however, without being conclusive in what type of clusters are formed. The phase diagrams shown in Figure 3.1-1 reveal other features that are typical for the alkali metal suboxides. As indicated by the dashed lines in the Cs–Cs_2O diagram the formation of one particular phase, Cs_4O, is kinetically hindered, and it may happen that it simply does not crystallize in spite of extended annealing at appropriate temperatures and compositions.

Such kinetic hindrance can be used on purpose to "fool" the system, as in the case of the Rb–Rb_2O system (Figure 3.1-1). Rb_6O should be formed via the reaction of both solid Rb and Rb_9O_2 at a temperature which is 0.3 °C below the eutectic melting, but it does not. Quenching of a melt to −30 °C, thus avoiding primary crystallization of Rb_9O_2, allows the reproducible preparation of Rb_6O. However, one must avoid quenching to liquid nitrogen temperature, otherwise Rb_9O_2 forms out of the amorphous state via a metastable crystalline phase [42]. These few experimental details might explain why there are still open questions, and particularly the following observation still waits for a definite explanation. Additional irreproducible thermal effects in the narrow temperature gap of 0.3 °C between the decomposition of Rb_6O into Rb and Rb_9O_2 and the eutectic melting of the latter

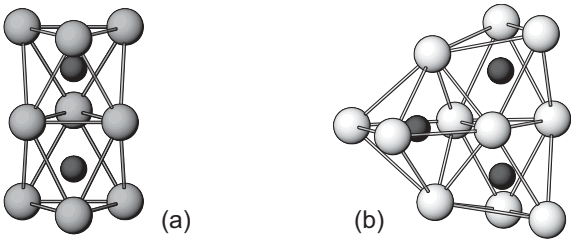

Fig. 3.1-2. Cluster (a) $[Rb_9O_2]$ and (b) $[Cs_{11}O_3]$. O atoms drawn as small spheres, for clarity only M–M contacts in the clusters outlined.

two seem to indicate the existence of still more metal-rich oxides than just Rb_6O, and the clue could lie in the specific crystal structure of Rb_6O discussed below.

Except for the range of homogeneity of "Cs_3O" the binary suboxides are strictly stoichiometric according to thermoanalytical and X-ray data. Their structures were determined from single crystals which were grown *in situ* in capillaries. Again with the exception of "Cs_3O" the alkali metal suboxides are structurally closely related. The essential units are Rb_9O_2 and $Cs_{11}O_3$ clusters formed from two and three face-sharing M_6O octahedra, respectively, as shown in Figure 3.1-2. Most probably the cause of the different sizes of clusters lies in the different atomic sizes of Rb and Cs. The oxygen atoms interact repulsively, and they are shifted towards the cluster periphery as one would expect as a consequence of Coulomb repulsion between O^{2-} ions. The description of bonding for these ion clusters as $[Rb^{+}{}_9O_2{}^{2-}]^{5+}\cdot 5e^-$ and $[Cs^{+}{}_{11}O_3{}^{2-}]^{5+}\cdot 5e^-$ is quite realistic and has been proven quantitatively, both for the ionic part through Raman spectroscopy [43] and for the electronic part through various measurements of the free electron concentrations, as will be discussed briefly in Section 3.1.5.

As shown in Figure 3.1-3(a) and (b) the crystal structures of the compounds Rb_9O_2 and $Cs_{11}O_3$ represent close packing of the respective clusters. The arrangement of Rb atoms in the $[Rb_9O_2]$ cluster corresponds to a fragment of hexagonal close packing (hcp), hence the structure of the compound can be described as an hcp metal with part of the octahedral voids being filled by oxygen atoms. The arrangement of $[Cs_{11}O_3]$ clusters in the compound with this composition is more complicated.

At first glance the structures seem to be those of molecular crystals with short M–M distances within the clusters, $350\ \text{pm} \leq d_{Rb-Rb} \leq 410\ \text{pm}$, $365\ \text{pm} \leq d_{Cs-Cs} \leq 435\ \text{pm}$, and large distances between them, most of the nearest neighbor contacts exceeding 500 pm and 550 pm for Rb and Cs, respectively. However, these distance ranges actually reflect the ionic bonding within the clusters and the metallic bonding between them. Because there are no counterbalancing anions outside the clusters but only their mutual repulsion inside, very short distances of around 265 pm between oxygen atoms and the metal atoms in the cluster periphery occur both for Rb and Cs. These distances are 10–15% shorter than the values calculated as a sum of the ionic radii.

The compounds correspond to "super-heavy" alkali metals, where the single atoms in the elemental metals have been replaced by large clusters with more than 9 and 11 times the mass of the single atom of Rb and Cs, respectively. This analogy is supported by specific heat measurements, which revealed the expected low frequency phonons of the heavy clusters [44]. One should not, however, overestimate this view too much in terms of chemistry. The clusters are only stable in the presence of an excess of electrons, and attempts to dissolve them as complex ions, for example in liquid ammonia lead to a spontaneous decomposition with the formation of hydroxide and amide. Simple Born-Mayer type calculations indeed reveal that the fully charged clusters lose alkali metal atoms and need to be stabilized by a partial shielding of the positive charges [43]. On the other hand, the analogy holds for the reaction of Rb_9O_2 and $Cs_{11}O_3$ with an excess of alkali metal, resulting in "intermetallic phases of cluster metals" that resemble intermetallic phases between the pure alkali metals.

A compilation of the structures of compounds formed by Rb_9O_2 and $Cs_{11}O_3$ with additional alkali metal is presented in Figures 3.1-3(c)–(e) and 3.1-4. The additional alkali metal atoms have no coordination to the oxygen atoms but only form metallic bonds to the clusters and between themselves.

The single alkali metals differ greatly in this type of chemistry, much more than we are used to in their normal valence compound chemistry. Rubidium forms the $[Rb_9O_2]$ cluster, cesium prefers the $[Cs_{11}O_3]$ cluster. No suboxides are known to exist with the lighter homologues. When oxygen is offered to an alloy of Rb and Cs, the $[Cs_{11}O_3]$ type cluster is formed with the possibility of a limited substitution of Cs by Rb atoms [45]. However, when the ratio Cs:O = 11:3 is reached all Rb collects in the region between the clusters, which then contain Cs only. Hence, these metals, which are so similar in aqueous solution, can be entirely separated in their suboxide structures. In an extension of such investigations to the lighter homologues clear evidence has been found for the formation of mixed suboxides of Cs and K, most probably of the type $[Cs_{11}O_3]K_x$. As these polycrystalline phases decompose at approximately -60 °C with deposition of K_2O they can not as yet be characterized.

Taking into account the differences between Rb and Cs the obvious differences in compound composition between binary and ternary phases do not come as a surprise, and even with an identical oxygen to metal ratio the structures vary, as in the case of $[Cs_{11}O_3]Cs$ and $[Cs_{11}O_3]Rb$. The structure of Rb_6O, which has to be described as $[Rb_9O_2]Rb_3$ deserves special mention. It contains alternating layers of Rb and $[Rb_9O_2]$ clusters, respectively, structural features that are mixed on an atomic scale and which change into a macroscopic scale when the compound decomposes into the eutectic mixture of Rb and Rb_9O_2 [Figure 3.1-3(c)]. The structure easily allows for a variation of the layer ratio, and such compositional variation might be the origin of the earlier mentioned additional thermal effects between the decomposition temperature of Rb_6O and the eutectic melting.

Another open question concerns the phase "Cs_3O". An early X-ray investigation [46] revealed an anti-TiI_3 structure, i.e., a hexagonal rod packing of $[Cs_{6/2}O]$ chains formed from *trans* face sharing $[Cs_6O]$ octahedra. Such $[M_3X]$ chains were also

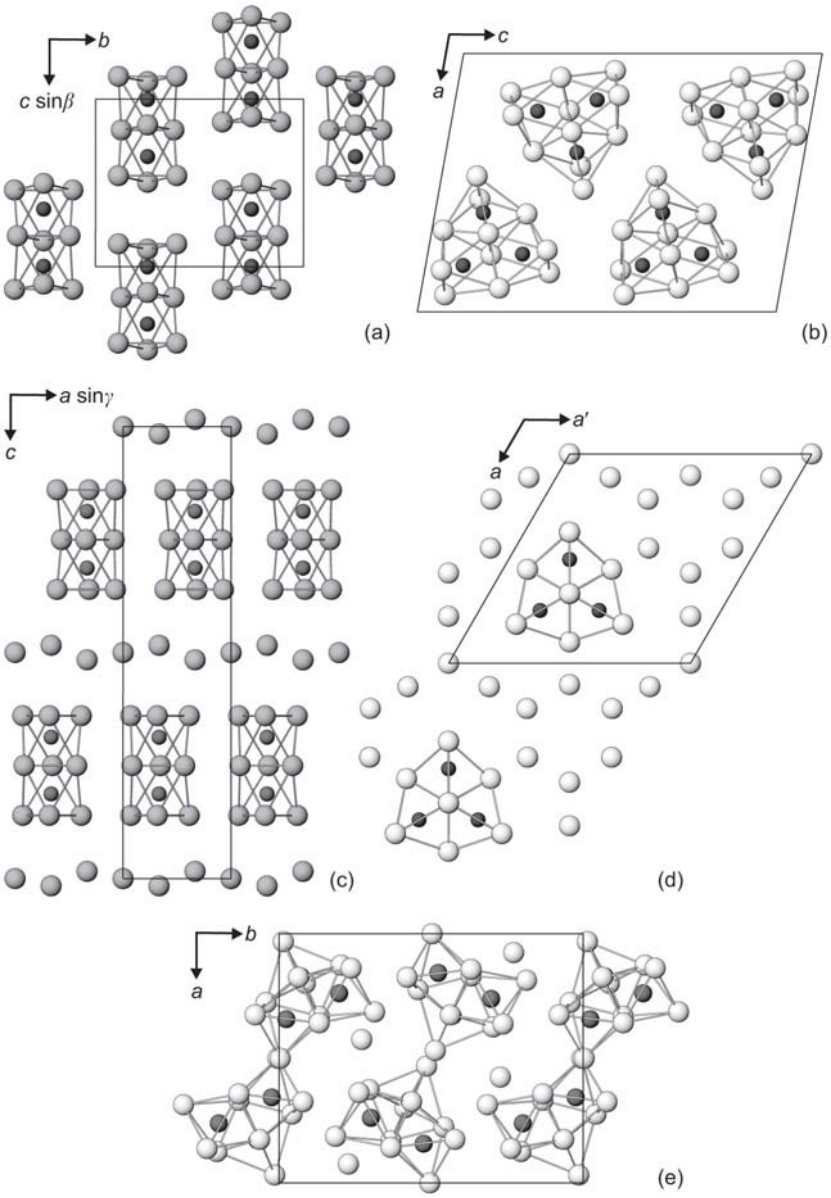

Fig. 3.1-3. Crystal structures of the binary alkali metal suboxides: (a) $[Rb_9O_2]$, (b) $[Cs_{11}O_3]$, (c) $[Rb_9O_2]Rb_3(Rb_6O)$, (d) $[Cs_{11}O_3]Cs_{10}(Cs_7O)$, and (e) $[Cs_{11}O_3]Cs(Cs_4O)$. O atoms drawn as small spheres, for clarity only M–M contacts in the clusters outlined.

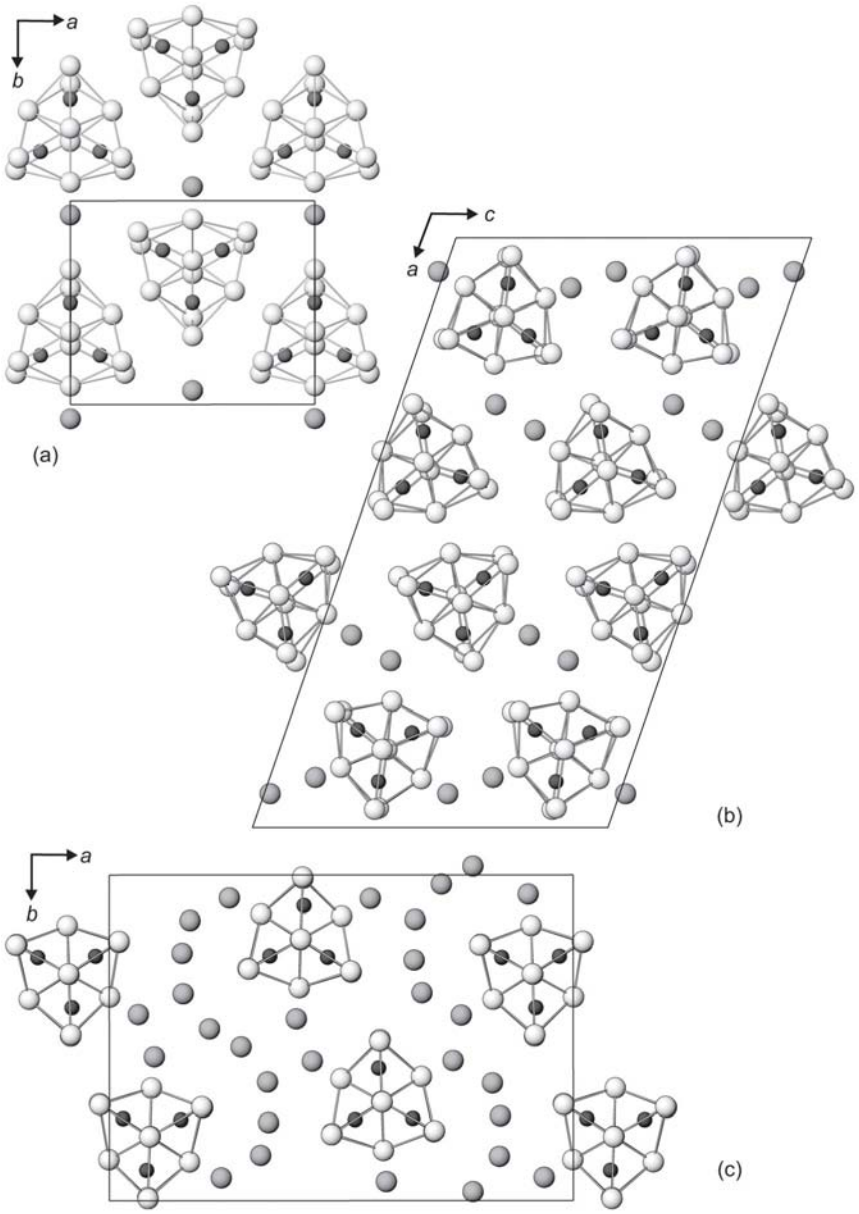

Fig. 3.1-4. Crystal structures of the ternary alkali metal suboxides: (a) $[Cs_{11}O_3]Rb$, (b) $[Cs_{11}O_3]Rb_2$, (c) $[Cs_{11}O_3]Rb_7$. O atoms drawn as small spheres, for clarity only M–M contacts in the clusters outlined.

observed repeatedly in the structures of Ba subnitrides (*vide infra.*). However, the phase exhibits a broad range of homogeneity to both sides of the assumed composition Cs_3O, and, whereas the proposed structure refines convincingly for the measured sharp Bragg reflections, extensive diffuse scattering indicates local order together with a specific low-dimensional disorder, which still needs to be understood even with respect to the chemical species involved.

3.1.3
Barium Suboxides

In early publications the existence of brownish-red Ba_2O was claimed [47], but it turned out that the color is only due to doping BaO with small amounts of Ba [48]. Similar observations hold for Ca and Sr. The discovery of Ba_2ONa [24] might be a first step towards the preparation of a binary Ba_2O as well as other closely related suboxides. Ba_2ONa forms by reacting Ba together with BaO_2 in a K–Na melt as well as by moderately heating an appropriate mixture of the intermetallic compound BaNa with Na_2O. So far, the Ba_2ONa forming large single crystals has to be selected manually from multiphase reaction products.

The structure of Ba_2ONa is shown in Figure 3.1-5. It has certain features in common with the alkali metal suboxides whereas others are distinctly different. The similarity lies in the spatial separation of metallic and ionic bonding, and the difference is due to the replacement of the characteristic octahedral M_6O unit by a tetrahedral $[M_4O]$ unit, which forms $[Ba_{4/2}O]$ chains through *trans* edge sharing. The Ba–O distance, 252 pm, is significantly shorter than the distance in BaO, 277 pm, for similar reasons as discussed with alkali metal suboxides. The Ba–Na distances, 421 to 433 pm, compare favorably with those in the binary intermetallic phases BaNa and $BaNa_2$, 427 and 432 pm, respectively. Yet, the structure is fairly well expanded with respect to the volume sum for BaO and BaNa.

The structural principle of combining salt-like bonded units with stoichiometric amounts of alkali metal in the structure of Ba_2ONa is equivalent to that which characterizes the alkali metal suboxides as well as the subnitrides of alkaline earth metals, such that a variation at least according to a general formula $[Ba_2O]Na_x$ can be expected. Indeed, there are indications of the existence of further suboxides in

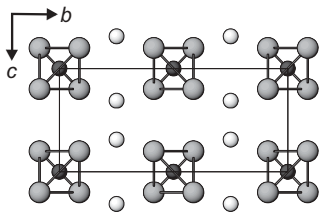

Fig. 3.1-5. Crystal structure of $[Ba_2O]Na$ viewed along chains of *trans* edge sharing $[Ba_{4/2}O]$ tetrahedra. Ba–Ba contacts outlined, Na light shading.

the Ba–Na system. On the other hand, the comparatively weak Ba–Na bonding compared with the strong Ba–O bonding might offer a chance to release the sodium from the structure and to prepare the binary Ba_2O. For other Ba suboxides formed together with Ga, In, Si, and Ge see the next section.

3.1.4
Alkaline Earth Metal Subnitrides

The structural principle of alkali metal suboxides has been unique for many years. Early attempts to synthesize cluster-type subnitrides of Ba resulted in the only compound, Ba_2N, that is isotypic with Ca_2N. Beyond these, the Sr analogue Sr_2N, and most recently Sr_4N_3 [34], have been characterized.

When reacting Ba dissolved in liquid Na with nitrogen at temperatures not too far from the melting point of the solvent, there was evidence for the formation of Ba-rich nitride clusters prior to the deposition of solid Ba_2N [8]. Using both Na as well as a K–Na alloy as solvents, an extensive class of new subnitrides can be prepared. They contain $[M_6N]$ octahedra, either discrete or condensed into finite clusters and infinite arrays, respectively.

Discrete $[Ba_6N]$ clusters are present in the subnitride $[Ba_6N]Na_{16}$ whose structure is depicted in Figure 3.1-6. It marks one end in the spectrum of known suboxides and subnitrides both with respect to the occurrence of single $[M_6N]$ units as well as to the large metal to non-metal ratio. The nitrogen acts rather as an "impurity", which stabilizes the structure. This view must be kept in mind when investigating binary systems of electropositive metals. The compound "Ag_8Ca_3" [49] has the same metal atom arrangement as $[Ba_6N]Na_{16}$ and, in fact, it can only be prepared in the presence of nitrogen. It is actually a subnitride, $[Ca_6N]Ag_{16}$. This result is reminiscent of similar findings, where the intermetallic phases "M_3E" with M = Ca, Sr, Ba, E = Sn, Pb turned out to have the compositions M_3OE [50] and Ca_4Sb_2 actually proved to be Ca_4Sb_2O [51]. These compositions seem to describe suboxides, however, the bonding actually corresponds to oxide, stannide, plumbide and antimonide, respectively, with no free electrons left, in contrast to

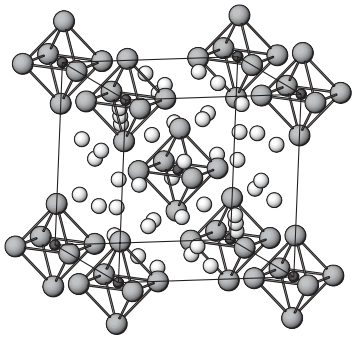

Fig. 3.1-6. Unit cell of $[Ba_6N]Na_{16}$. Ba–Ba contacts outlined, Na light shading.

the auride nitride Ca_3AuN [36]. Reports on new ternary suboxides of Ba, for example "$E_2Ba_{21}O_5$" (E = Si, Ge) [52] or "$E_3Ba_{20}O_5$" (E = Ga, In) [53] have to be revised [54]. They contain a sufficient amount of (hydridic) hydrogen to make them normal valence compounds with no excess electrons.

The observation of alkaline earth metal subnitrides in the Ba–Na and Ca–Ag systems as well as in combination with other metals raises the general question as to which metals can be combined. Good arguments towards an answer come from Miedema's rules for alloying [55], because the bonding between the metals must be similar to that in the respective pure intermetallic phases. Hence, miscibility and/or compound formation in the binary systems is a prerequisite for the metals to combine in such suboxides and subnitrides, but the interaction should be weak enough to avoid the formation of the binary intermetallic phase together with the normal oxides or nitrides. Na mixes with Ba forming several compounds whereas K (as well as the higher homologues) does not. On the other hand, Na mixes with K and forms the compound KNa_2. When using K–Na alloy as the solvent for Ba, bonding of K to Na but not K to Ba is expected to occur in possible new subnitrides. However, the K–Na alloys turned out to be very interesting solvents, which gave access to numerous new cluster subnitrides.

The discovery of a cluster of six face-sharing $[M_6N]$ octahedra, shown in Figure 3.1-7, in a compound that contained 14 additional Na atoms per cluster, seemed to violate the validity of Miedema's rule, because the central atom refined perfectly as K in the X-ray structure determination.

However, this atom was finally recognized as Ca which was incorporated into the solid from traces that were present in the barium metal used. Once recognized, the compound $[Ba_{14}CaN_6]Na_{14}$ could be prepared in large amounts. The Na content in this type of compound can be varied systematically by varying the K–Na ratio of the solvent, the subnitrides becoming more metal-rich with the increasing Na content of the solvent. Figure 3.1-8 covers the structures of the known compounds $[Ba_{14}CaN_6]Na_x$ with $x = 7, 8, 14, 17, 21, 22$. No evidence for an incorporation of K in the solid subnitrides was found, neither in the clusters nor even in the partial structures of Na. On the other hand, a substitution of Ca by Sr is possible [15]. It should be mentioned that the cluster $[Ba_8Ba_6CaN_6]$ represents the anti-type of the well known transition metal cluster $[M_6X_8X_6]$, which in the case of electron

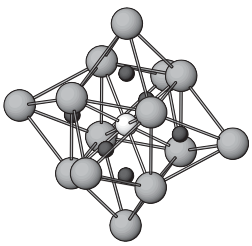

Fig. 3.1-7. $[Ba_{14}CaN_6]$ cluster formed from six $[M_6N]$ octahedra. Only Ba–Ba contacts outlined, central atom Ca, N atoms drawn as dark small spheres.

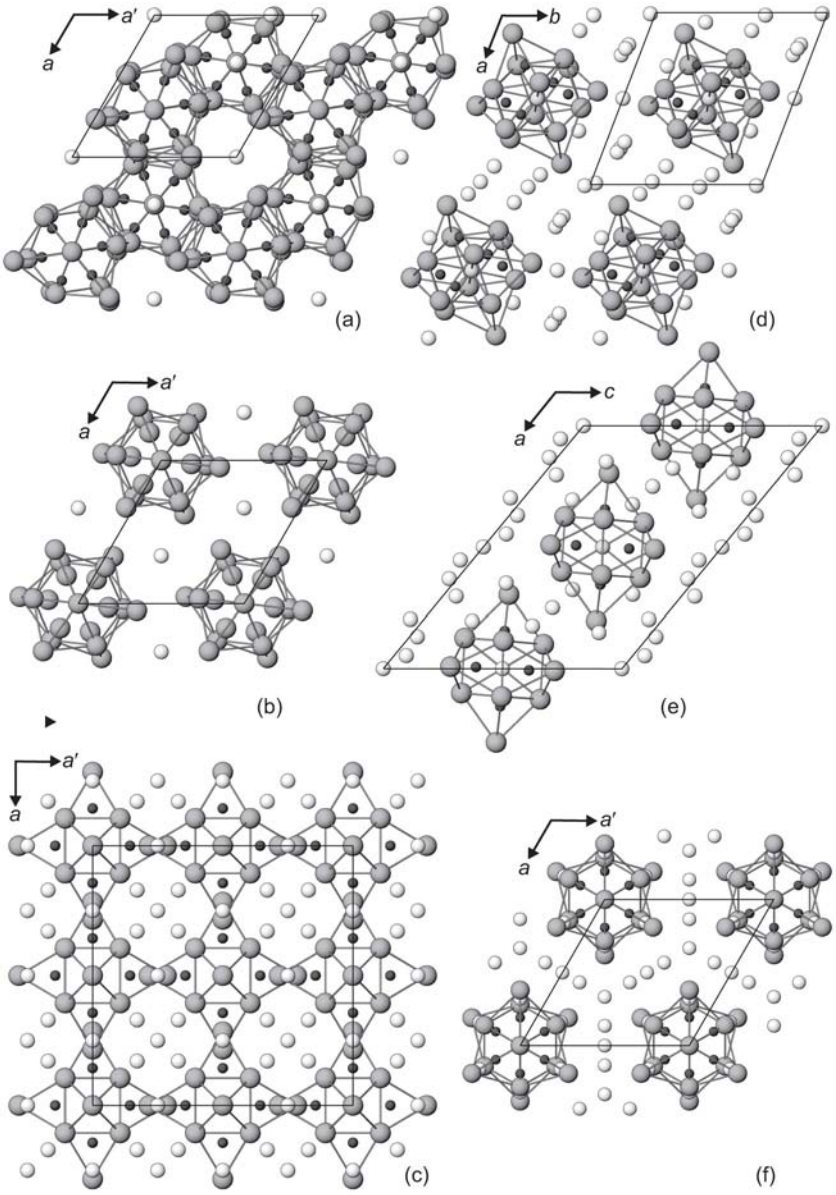

Fig. 3.1-8. Crystal structures of the compounds $[Ba_{14}CaN_6]Na_x$: (a) $x = 7$, (b) $x = 8$, (c) $x = 14$, (d) $x = 17$, (e) $x = 21$, (f) $x = 22$. Na light shading, only Ba–Ba contacts outlined, central atom Ca, N atoms drawn as dark small spheres.

deficiency may contain an additional atom in the center as shown for the compound $Nb_6I_8HI_{6/2}$ [56]. It is interesting to note that the analogous anti-type of the $[M_6X_{12}X_6]$ cluster centered by an additional atom, as is frequently found for M = Zr [21], is also known from the $[Ca_{12}Ca_6CaN_6]$ arrangement in the structure of $Ca_{19}N_7Ag_8$ [38] and the phases $Ca_{18.5}N_7E_8$ (E = Ga, In) that are probably isotypic [39].

The cluster in all these subnitrides is a rigid unit which exhibits only marginal geometric variations in different Na_x matrices. This rigidity is reflected in another common feature of all structures, namely the occurrence of large cavities in the Na sublattice. These are large enough to accommodate impurities, particularly "invisible" hydrogen atoms. As such contamination has been ruled out experimentally [15] one has to search for another origin of the cavities, and the most straightforward explanation is based on the misfit in a packing of rigid clusters and a malleable Na_x matrix. The latter part is a compromise in a way in that the volume increment per Na atom stays fairly constant throughout the whole series of compounds, 38.5 Å^3 as compared with 39.5 Å^3 in elemental Na, thus compensating for the cavities in a subtle adjustment. This adjustment of the matrix has an influence back on the arrangement of clusters and in the case of $[Ba_{14}CaN_6]Na_{22}$ leads to a remarkable disorder phenomenon [33]. In the structure of this compound, clusters alternate with small sections of metallic Na to form rods with a periodicity in diameter as well as a stiffness along their axes. Such rods are embedded in a honeycomb lattice of Na atoms as depicted in Figure 3.1-8(f), and they are shifted relative to each other by half of their periodicity length in order to optimize the packing. Denoting these positions as A and B, respectively, in each triangle of rods only two can take the optimal relative positions A, B, whereas the third is frustrated as it has to take position A or B, both resulting in unfavorable A, A or B, B type neighborhoods. The frustrated rod packing shows up in diffuse X-ray scattering. It is interesting to note that this disorder phenomenon is a structural analogue of the famous frustrated antiferromagnetism in a triangular Ising net [57].

The structures of all suboxides and subnitrides introduced so far were discussed in terms of ionic clusters with additional metallic bonding in their periphery, to adjacent clusters and alkali metal between the clusters. The structures of $[Ba_{14}CaN_6]Na_x$ provide particularly visual examples of this view. The formula can be divided into an intermetallic part Ba_6Na_x and the central part of the cluster, $[Ba_8CaN_6]$, which is electroneutral according to $Ba^{2+}{}_8Ca^{2+}N_6{}^{3-}$ and hence represents a tiny ionic unit. In fact the latter has the atomic arrangement of a single unit cell of an anti-perovskite as shown in Figure 3.1-9. Thus, the structures of $[Ba_{14}CaN_6]Na_x$ may be discussed in terms of nano-dispersions (or rather subnano-dispersions) of a salt in a metal. Electronic consequences of this remarkable separation in space will be analyzed in the next section.

Finally, another class of subnitrides has to be discussed. In early investigations of the system Ba–Na–N [8, 9], X-ray diagrams had been interpreted as being due to "Ba_4N". We know now that these diagrams result from a mixtures of Ba_2N and a new subnitride, Ba_3NNa_5. The latter crystallizes as a single phase from a dilute solution of Ba in Na, which was reacted with nitrogen in the exact Ba to N ratio

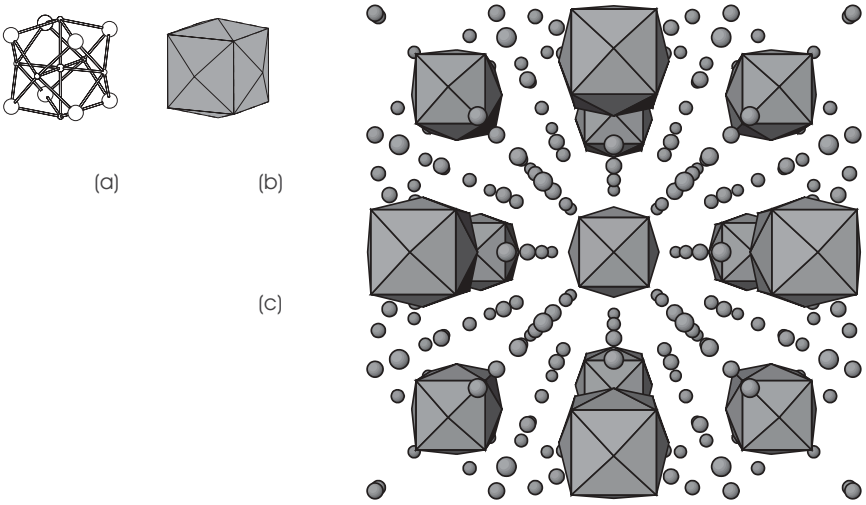

Fig. 3.1-9. Structure of $[Ba_{14}CaN_6]Na_{14}$ represented as a dispersion of a salt in a metal: (a) $[Ba_8CaN_6]$ unit corresponding to one anti-perovskite unit cell, N, Ca and Ba atoms drawn with increasing size, (b) schematic drawing of the same unit and (c) structure with Ba_6Na_{14} part drawn as spheres.

and slowly cooled. Above 133 °C another compound, Ba_3NNa, separates in large black needles when nitrogen is absorbed by a concentrated solution of Ba in Na. Interestingly Ba_3NNa_5 transforms into Ba_3NNa when treated with K forming liquid K–Na alloy. All these subnitrides are thermodynamically stable phases which are accessible via different preparative routes, using the elements, intermetallic phases such as NaBa or Na_2Ba, other Ba nitrides or NaN_3 as starting materials.

The structures of $[Ba_3N]Na$ and $[Ba_3N]Na_5$ are characterized by parallel chains of *trans* face sharing Ba_6N octahedra projected along the chain direction in Figure 3.1-10(a) and (b). Except for the one-dimensionality of the nitride unit the bonding principle closely follows that of the cluster compounds discussed earlier. The $[Rb_9O_2]$ cluster may be referred to as the first step in condensation of $[M_6X]$ octahedra towards the infinite $[M_{6/2}X]$ chain.

In context the of the structure of $[Ba_2O]Na$, it was speculated that the Na atoms could possibly be removed in order to prepare the binary suboxide, Ba_2O. For the case of the subnitrides the feasibility of such a reaction has been demonstrated. When $[Ba_3N]Na$ is heated under high vacuum it looses Na above 225 °C, and polycrystalline Ba_3N is formed, which retains the parallel $[Ba_3N]$ chains in its structure shown in Figure 3.1-10(c). In contrast to "Cs_3O" the subnitride Ba_3N does not exhibit any detectable range of homogeneity. Of course, diffuse reflections would hardly be detectable in X-ray powder diagrams. However, as the phases $[Ba_3N]Na_x$ with the same structural element of the $[Ba_3N]$ chain show no diffuse scattering in single crystal investigations, this fact, together with the stoichiometric

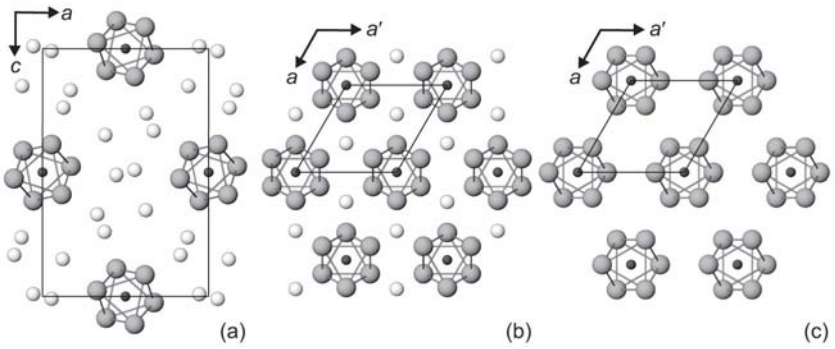

Fig. 3.1-10. Crystal structures of (a) $[Ba_3N]Na_5$, (b) $[Ba_3N]Na$ and (c) $[Ba_3N]$ viewed along the chains of condensed $[Ba_{6/2}N]$ octahedra. Ba–Ba contacts outlined, Na light shading.

nature of Ba_3N, allows its exact description in the anti-TiI_3 structure type, the Ba atoms occupying the I positions and the N atoms fhose of Ti.

Nevertheless, there is a puzzling feature with the structure of Ba_3N. Whereas the distances between the chains in TiI_3 closely correspond to twice the van der Waals radius of I, the corresponding Ba–Ba distances in Ba_3N are extremely long, 487 and 496 pm, hence exceeding by far the sum of metallic radii, 448 pm.

A similar result holds for the last subnitride to be discussed, Ba_2N, whose structure is shown in Figure 3.1-11. Layers of $[Ba_6N]$ octahedra are condensed via edges and stacked in an anti-$CdCl_2$ type fashion with Ba–N distances of 276 pm as expected, but inter-layer Ba–Ba distances of 511 pm, even longer than in Ba_3N. These very much expanded metal–metal contacts are difficult to understand and possibly reflect a fairly fundamental phenomenon. One may speculate that the

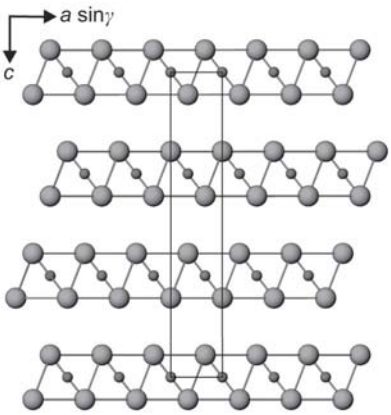

Fig. 3.1-11. Crystal structure of $[Ba_2N]$ viewed along the layers of edge-condensed $[Ba_{6/3}N]$ octahedra which are outlined.

unusual confinement of the conduction electrons in these compounds, which will be discussed in the next section, gives rise to the remarkable expansion.

3.1.5 Chemical Bonding and Physical Properties

All suboxides and subnitrides described in the preceding sections are metallic. In the case of the alkali metal suboxides this property has been demonstrated by measurements of the electrical conductivity [58]. Cs_7O, for example, exhibits a free electron like behavior in the temperature dependence of its resistivity rather similar to the element Cs itself. The characteristic colors of the alkali metal suboxides have been mentioned before, and spectroscopic investigations to be discussed in the following provide a more quantitative access to the metallic properties and the underlying chemical bonding.

Figure 3.1-12 shows reflectivity data measured on single crystals of Rb and Cs together with some selected suboxides [59]. All samples exhibit the characteristics of metals, namely high reflectivity at low energy, a well developed plasma edge and additional weak structures at high energy above the edge. Whereas the high energy structures are generally due to excitations of bound electrons, the position of the plasma edge is determined by the concentration of free electrons. The plasma edge shifts to lower energies upon oxidation, and it is obvious, without any sophisticated analysis, that the color changes from silvery Rb to copper-red Rb_9O_2, and from golden Cs via violet $Cs_{11}O_3$ to bluish-black "Cs_3O" are simply caused by shifts of the plasma edges. Each O atom removes two electrons from the conduction band,

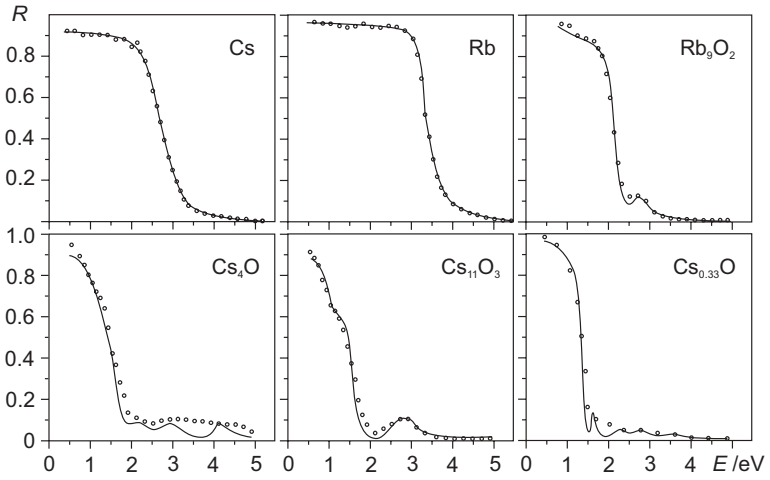

Fig. 3.1-12. Single crystal reflectivities *R* of the alkali metals Rb, Cs and some of their suboxides (points) together with the Drude-Lorentz fits (lines).

and the decrease of the concentration of free electrons is only slightly counterbalanced by the volume shrinkage upon oxidation.

The measured data are reasonably well represented by Drude-Lorentz fits taking into account additional oscillators. As such, excitations from the O 2p band into the conduction band and collective excitations of the conduction electrons (surface plasmons) can be identified. There are indications of yet one more rather unusual origin of energy loss that is closely related to the general structural principle of these suboxides and subnitrides. As explained for the phases $[Ba_{14}CaN_6]Na_x$ their structures exhibit regions of metallic and ionic bonding which are well separated in space. They represent a type of ''void metal'', where, due to the accumulation of the negative charges of O^{2-} and N^{3-} ions in the clusters, the conduction electrons can not enter the cluster centers (electronic voids) and are confined to the region between the clusters, avoiding the Coulomb repulsion of the cluster interior. The reflectance data of Rb_9O_2 strongly support the model of a void metal. The data of Cs suboxides present some ambiguity, and the expected void metal character is not obvious from de Haas van Alphen measurements [60] on $[Ba_3N]Na$, however, there is further evidence from photo electron spectra measured by excitation with the UV light of a HeI lamp (UPS).

The valence band spectra [61] of the subnitrides Ba_2N, Ba_3N, Ba_3NNa, Ba_3NNa_5 and $Ba_{14}SrN_6Na_{22}$ show finite density of states at the Fermi level giving evidence for the metallic character of all samples. Photoemission from the N 2p bands at very low energies, 2.1 to 2.4 eV, as well as LMTO (linear muffin tin orbital) band structure calculations support the view of N^{3-} ions being weakly stabilized by the Coulomb field of the surrounding partly oxidized metal atoms. The observed bands are slightly broadened, and the calculations indeed result in small dispersions of the N 2p bands.

The HeI spectra of Cs and its suboxides seen in Figure 3.1-13 allow a detailed analysis of chemical bonding [62]. Photoemission shows a clearly developed Fermi level, evidencing metallic bonding and a narrow O 2p band at the lowest known binding energy of all oxides, 2.7 eV, indicating purely ionic O^{2-}. The additional structures at the low kinetic energy side (appearing at higher binding energy) are caused by energy losses due to excitation of surface plasmons discussed earlier, and they allow a quantitative determination of the concentrations of free electrons in very good agreement with the view of $Cs_{11}O_3$ as a cluster, which provides five free electrons for alkali metal like bonding between the clusters. The spin orbit split Cs 6p level has an unusual shift to a lower binding energy in $Cs_{11}O_3$, and for $[Cs_{11}O_3]Cs_{10}$ the 6p structure imposes the impression of a heterogeneous mixture of Cs and $Cs_{11}O_3$. However, this structure is an intrinsic feature of the homogeneous compound, as indicated by the single plasmon peak in the same spectrum and by yet another important feature in the spectra, namely the gap between the energy of incident light, 21.2 eV, and the threshold for photoelectrons. This gap corresponds to the work function, which is the energy of the electrons necessary to escape the metal or, more precisely, the energy difference between the Fermi level and the vacuum level. The spectra clearly show that the work function value drastically decreases when Cs is oxidized to $Cs_{11}O_3$ and takes an intermediate value for

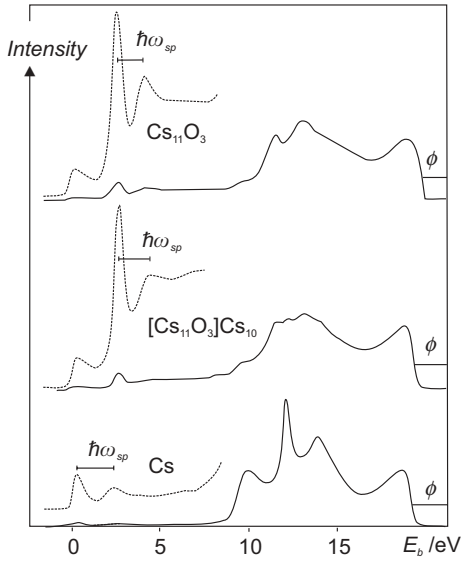

Fig. 3.1-13. HeI photoelectron spectra of Cs and its suboxides (intensities in arbitrary units, dashed curves magnified by a factor of 10), surface plasmon loss ($\hbar w_{sp}$) and work function (Φ) indicated.

$[Cs_{11}O_3]Cs_{10}$. Unfortunately, no well defined cut-off from secondary electrons can be measured with the subnitrides whose work function values therefore remain unknown.

The decrease of the work function of Rb and Cs upon oxidation is also seen in quite different experiments. The wetting properties of liquid He on the metal surfaces is critically dependent on the mutual interaction, which is determined by the work function [63, 64]. Discrete He droplets are stable to higher temperature on Cs than on Rb, the latter in this property coming close to Cs upon oxidation.

Model calculations for the Cs suboxides in comparison with elemental Cs have shown that the decrease in the work function that corresponds to an increase in the Fermi level with respect to the vacuum level can be explained semiquantitatively with the assumption of a void metal [65]. The Coulomb repulsion of the conduction electrons by the cluster centers results in an electronic confinement and a raising of the Fermi energy due to a quantum size effect.

This fundamental effect bears some relevance for applications. The electropositive metal Cs is marked by the lowest value of the work function for all elements, 2 eV, making the metal an important photocathode material. Partly oxidized Cs films have been used for decades in image converters (night vision devices) based on their photoemission in the near IR region. The low energy photoemission has been explained in terms of hetero-junction models assuming layers of semiconducting Cs_2O topped by Cs layers [66]. This assumption, however, does

not hold as it can be shown by UPS investigations of *in situ* prepared photocathodes that such layers react with each other to form suboxides [67]. The work function value for $Cs_{11}O_3$ is 0.7 eV less than for elemental Cs, and it decreases further towards "Cs_3O". Indeed, the spectral response of so-called S1 cathodes matches the values of the work function and the surface plasmon energy of these compounds.

Again, because of their low work function alkali metal suboxides might play a role in quite a different field. Spin-polarized ^3He turns out to be of interest as a very efficient polarization filter for neutrons [68], as well as a medium to image body cavities via NMR tomography [69]. One problem lies in the fast deactivation of the gas due to interaction with the container wall, and coating of the wall with Cs helps to increase the lifetime of the excited state [70]. It has been observed that the lifetime gets longer with repeated filling of the containers, until they finally loose their quality. One may speculate that the formation of suboxides from accidental contamination of the gas results in a decrease in the work function of the metal film, until the normal inactive oxide Cs_2O is formed.

The physical measurements on the group 1 suboxides and group 2 subnitrides have revealed unusual properties based on the peculiar type of bonding. Particularly in the case of the suboxides, experimental evidence seems sufficient to describe them as void metals, and this description suggests an interesting differentiation within the entire class of compounds. Those phases which contain discrete clusters represent systems with zero-dimensional voids, where the forbidden regions for conduction electrons are discrete and have no infinite extension in any direction of space. The chain-type compounds $[Ba_3N]Na_x$ offer one-dimensional voids to the conduction electrons. In terms of the conduction electron distribution, one may view them as metals which are drilled on an atomic scale and thus represent the first examples of an anti-type of long-known one-dimensional metals. Finally, the layer compound Ba_2N is a type of sliced metal and as such a new variant in the large class of two-dimensional metals.

References

1 E. Rengade, *Bull. Soc. Chim. France, [4]* **1909**, *5*, 994.
2 E. Rengade, *C.R. Acad. Sci. Paris*, **1909**, *148*, 1199.
3 E. T. Keve, A. C. Skapski, *Inorg. Chem.*, **1968**, *7*, 1757.
4 C. F. Baker, M. G. Barker, A. J. Blake, *Acta Crystallogr E.*, **2001**, *57*, i6.
5 J. Gaude, P. L'Haridon, Y. Laurent, J. Lang, *Bull. Soc. Fr. Mineral. Crystallogr.*, **1972**, *95*, 56.
6 N. E. Brese, M. O'Keeffe, *J. Solid State Chem.*, **1990**, *87*, 134.
7 H.-T. Künzel, *Thesis*, University Stuttgart, **1980**.
8 C. C. Addison, R. J. Pulham, E. A. Trevillion, *J. Chem Soc., Dalton Trans.*, **1975**, *20*, 2082.
9 C. C. Addison, *The Chemistry of the Liquid Alkali Metals*, Wiley & Sons, Chichester, **1984**.
10 A. Simon, *Struct. Bonding*, **1979**, *36*, 81.
11 P. E. Rauch, A. Simon, *Angew. Chem., Int. Ed. Engl.*, **1992**, *31*, 1519.
12 G. J. Snyder, A. Simon, *Angew. Chem., Int. Ed. Engl.*, **1994**, *33*, 689.

13 G. J. Snyder, A. Simon, *J. Am. Chem. Soc.*, **1995**, *117*, 1996.
14 U. Steinbrenner, A. Simon, *Angew. Chem., Int. Ed. Engl.*, **1996**, *35*, 552.
15 A. Simon, U. Steinbrenner, *J. Chem. Soc., Faraday Trans.*, **1996**, *92*, 2117.
16 U. Steinbrenner, A. Simon, *Z. Anorg. Allg. Chem.*, **1998**, *624*, 228.
17 G. V. Vajenine, U. Steinbrenner, A. Simon, *C.R. Acad. Sci. Paris, Série IIc*, **1999**, 583.
18 G. V. Vajenine, A. Simon, *Eur. J. Inorg. Chem.*, **2001**, 1189.
19 A. Simon, *Angew. Chem., Int. Ed. Engl.*, **1988**, *27*, 159.
20 A. Simon, in *Clusters and Colloids, from Theory to Application*, G. Schmid, ed., VCh Weinheim, New York, Basel, Cambridge, Tokyo, **1994**, p. 373.
21 R. P. Ziebarth, J. D. Corbett, *Acc. Chem. Res.*, **1989**, *22*, 256.
22 G. Meyer, *Chem. Rev.*, **1988**, *88*, 93.
23 A. Simon, Hj. Mattausch, G. J. Miller, W. Bauhofer, R. K. Kremer, in *Handbook on the Physics and Chemistry of Rare Earths*, Vol. 15, K. A. Gschneidner, Jr., L. Eyring, eds., North Holland, Amsterdam, London, New York, Tokyo, **1991**, p. 191.
24 G. V. Vajenine, A. Simon, *Angew. Chem., Int. Ed. Engl.*, **2001**, *40*, 4222.
25 O. Reckeweg, F. J. DiSalvo, *Solid State Sci.*, **2002**, *4*, 575.
26 A. Simon, *Z. Anorg. Allg. Chem.*, **1977**, *431*, 5.
27 A. Simon, H.-J. Deiseroth, *Rev. Chim. Miner.*, **1976**, *13*, 98.
28 A. Simon, E. Westerbeck, *Z. Anorg. Allg. Chem.*, **1977**, *428*, 187.
29 A. Simon, H.-J. Deiseroth, E. Westerbeck, B. Hillenkötter, *Z. Anorg. Allg. Chem.*, **1976**, *423*, 203.
30 A. Simon, *Z. Anorg. Allg. Chem.*, **1976**, *422*, 208.
31 H.-J. Deiseroth, A. Simon, *Z. Anorg. Allg. Chem.*, **1980**, *463*, 14.
32 A. Simon, W. Brämer, H.-J. Deiseroth, *Inorg. Chem.*, **1978**, *17*, 875.
33 U. Steinbrenner, A. Simon, *Z. Kristallogr.*, **1997**, *212*, 428.
34 Y. Prots, G. Auffermann, M. Tovar, R. Kniep, *Angew. Chem., Int. Ed. Engl.*, **2002**, *41*, 2288.
35 G. Cordier, M. Ludwig, D. Stahl, P. C. Schmidt, R. Kniep, *Angew. Chem., Int. Ed. Engl.*, **1995**, *34*, 1761.
36 J. Jäger, D. Stahl, P. C. Schmidt, R. Kniep, *Angew. Chem., Int. Ed. Engl.*, **1993**, *32*, 709.
37 G. Cordier, S. Rönninger, *Z. Naturforsch.*, **1987**, *42b*, 825.
38 O. Reckeweg, T. P. Braun, F. J. DiSalvo, H.-J. Meyer, *Z. Anorg. Allg. Chem.*, **2000**, *626*, 62.
39 G. Cordier, S. Rönninger, *Z. Kristallogr.*, **1988**, *182*, 60.
40 A. Simon, *Z. Anorg. Allg. Chem.*, **1973**, *395*, 301.
41 P. Touzain, M. Caillet, *Rev. Chim. Minér.*, **1971**, *8*, 277.
42 H.-J. Deiseroth, A. Simon, *Z. Naturforsch.*, **1978**, *33b*, 714.
43 T. P. Martin, H.-J. Stolz, G. Ebbinghaus, A. Simon, *J. Chem. Phys.*, **1979**, *70*, 1096.
44 E. Gmelin, A. Simon, W. Brämer, R. Villar, *J. Chem. Phys.*, **1982**, *76*, 6256.
45 H.-J. Deiseroth, A. Simon, *Rev. Chim. Minér.*, **1983**, *20*, 475.
46 K.-R. Tsai, P. M. Harris, E. N. Lassettre, *J. Phys. Chem.*, **1956**, *60*, 345.
47 A. Guntz, F. Benoit, *Bull. Soc. Chim. France [4]*, **1924**, *35*, 718.
48 M. Schriel, *Z. Anorg. Chem.*, **1937**, *231*, 313.
49 L. D. Calvert, C. Rand, *Acta Crystallogr.*, **1964**, *17*, 1175.
50 A. Widera, H. Schäfer, *Mat. Res. Bull.*, **1980**, *15*, 1805.
51 B. Eisenmann, H. Limartha, H. Schäfer, H. A. Graf, *Z. Naturforsch.*, **1980**, *35b*, 1518.
52 C. Röhr, *Z. Anorg. Allg. Chem.*, **1995**, *621*, 1496.
53 C. Röhr, *Z. Kristallogr. Suppl.*, **1995**, *9*, 24.
54 B. Huang, J. D. Corbett, *Inorg. Chem.*, **1998**, *37*, 1892.
55 A. Simon, *Z. Anorg. Allg. Chem.*, **1967**, *355*, 311.
56 A. R. Miedema, R. Boom, F. R. de Boer, in *Crystal Structure and Chemical Bonding in Inorganic Chemistry*, C. J. M. Rooymans, A. Rabenau, eds., North Holland –

American. Elsevier, Amsterdam, Oxford, New York **1975**, p. 163.
57 G. H. Wannier, *Phys. Rev. B*, **1973**, *7*, 5017.
58 W. Bauhofer, A. Simon, *Z. Anorg. Allg. Chem.*, **1978**, *447*, 29.
59 G. Metsch, W. Bauhofer, A. Simon, *Z. Naturforsch.*, **1985**, *40a*, 303.
60 H. Weiss, G. V. Vajenine, U. Steinbrenner, A. Simon, E. Balthes, P. Wyder, *Phys. Rev. B*, **2001**, *63*, 115104-1-8.
61 U. Steinbrenner, P. Adler, W. Hölle, A. Simon, *J. Phys. Chem. Solids*, **1998**, *59*, 1527.
62 G. Ebbinghaus, A. Simon, *J. Chem. Phys.*, **1979**, *43*, 117, 1979.
63 J. Dupont-Roc, G. Misguich, L. Girlanda, *Czech. J. Phys.*, **1996**, *46 (S1)*, 419.
64 B. Demolder, J. Dupont-Roc, *J. Low Temp. Phys.*, **1996**, *104*, 1.
65 M. G. Burt, V. Heine, *J. Phys. C*, **1978**, *11*, 961.
66 A. H. Sommer, *Photoemissive Materials*, Wiley, New York, **1968**.
67 G. Ebbinghaus, W. Braun, A. Simon, K. Berresheim, *Phys. Rev. Lett.*, **1976**, *37*, 1770.
68 J. Kulda, A. Wildes, A. Martin-Martin, W. Müller, W. Heil, H. Humblot, F. Tasset, *Physica B*, **1998**, *241*, 136.
69 M. Ebert, T. Grossmann, W. Heil, E. Otten, S. Surkau, M. Leduc, P. Bachert, M. V. Knopp, L. R. Schad, M. Thelen, *The Lancet* **1996**, *347*, 1297.
70 W. Heil, H. Humblot, E. Otten, M. Schafer, R. Sarkau, M. Leduc, *Phys. Lett. A*, **1995**, *201*, 337.

3.2
Carboranes: From Small Organoboranes to Clusters

Armin Berndt, Matthias Hofmann, Walter Siebert and Bernd Wrackmeyer

3.2.1
Introduction and Background

This chapter summarizes recent developments in the expanding field of electron-deficient compounds having from three up to 13 skeletal boron and carbon atoms. In particular, the focus will be on the transition of classical organoboranes into non-classical compounds. Therefore, we first want to briefly review electron counting rules and bonding characteristics of these classes. For a more thorough discussion see Chapter 1 by King and Schleyer.

Williams [1] has given an excellent review on ''Early Carboranes and Their Structural Legacy'' and he defines carboranes as follows: ''Carboranes are mixed hydrides of carbon and boron in which atoms of both elements feature in the electron-deficient polyhedral molecular skeleton''. According to the electron counting rules [2] for *closo*- ($2n + 2$ SE), *nido*- ($2n + 4$ SE) and *arachno*-clusters ($2n + 6$ SE; SE = skeletal electrons, n = number of framework atoms) and the $4n + 2$ π electron Hückel rule, small compounds with skeletal carbon and boron atoms may have an electron count for carboranes *and* for aromatics (see Chapters 1.1.2 and 1.1.3).

For instance, borirene (boracyclopropene, C_2BH_3) has the required eight skeletal electrons to be classified as a *closo*-cluster and two π electrons as an aromatic system. In analogy, the folded 1,3-dihydro-1,3-diborete $C_2B_2H_4$ with 10 SE is a *closo*-carborane (**J**, Figure 3.2-1) *and* an aromatic compound (as shown in Figure 3.2-3). However, in the absence of a molecular plane, its four-center (4c) bonding HOMO is not strictly π (but distorted towards σ, see below). $C_2B_2H_4$ (**J**) as well as the isoelectronic species $C_4H_4^{2+}$ (**G**) and $B_4H_4^{2-}$ (**Q**) may be regarded as aromatic three dimensional systems.

Multicenter bonding is the key to understanding carboranes. *Classical* multicenter π bonding gives rise to electron-precise structures characteristic of Hückel aromatics, which are planar and have $4n + 2$ π electrons. Clusters are defined here as ''ensembles of atoms connected by *non-classical* multicenter bonding'', i.e., all

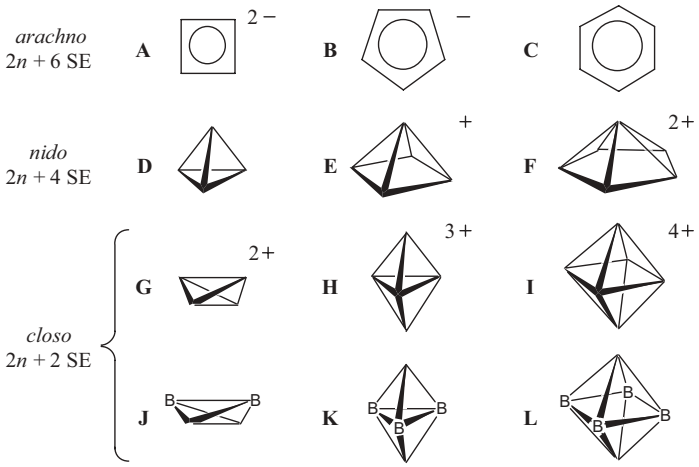

Fig. 3.2-1. Electron-rich (**A**, **B**) and electron-precise (**C**) planar aromatics as well as three dimensional structures **D**–**L** as a result of less skeletal electrons (SE). Lines in electron-deficient com-pounds indicate connectivities not 2c2e bonds.

types of multicenter bonding except pure π. Thus, the skeleton atoms may employ multicenter σ bonding (as in the cluster archetype H_3^+), or multicenter σ and π bonding, or "π,σ-distorted" multicenter bonding (see below).

In order to define a borderline between classical and non-classical structures we introduce the following criteria: compounds are classified as non-classical if their framework atoms employ multicenter σ, or multicenter σ and π, or "π,σ-distorted" multicenter bonding to cope with electron deficiency.

Classical aromatics like the electron-rich, cyclobutadiene dianion **A** or cyclopentadienyl anion **B** and electron-precise hydrocarbons (e.g., benzene **C**, Figure 3.2-1) have pure π multicenter bonds and therefore are generally not regarded as clusters.

Removal of two electrons from **B** or **C**, however, generates electron deficiency that is compensated by enhanced multicenter bonding. In order to allow more next neighbor interactions, structures become more spherical: **B** → **E**, **C** → **F**. Removal of two electrons from **A** leads to electron precise C_4H_4, which is known as a planar ring (cyclobutadiene) and as a three-dimensional structure (tetrahedrane) **D**. Further two electron oxidation leads to the dication $C_4H_4^{2+}$, **G**, which can be regarded as a folded ring as well as a distorted tetrahedron. Typically, polyhedral cluster compounds incorporate hypercoordinate atoms, which are involved in more connections than are possible by two-center, two-electron (2c2e) bonds, e.g., more than four connections to one carbon or to one boron atom. The apical carbon atoms in **E** and in **F**, for example, have connectivities of five and six, respectively, including the terminal 2c2e bond. Small clusters with only three or four cluster atoms, however, do not allow for coordination numbers larger than four. In these cases, only hydrogen atoms in 3c2e bonds are hypercoordinated.

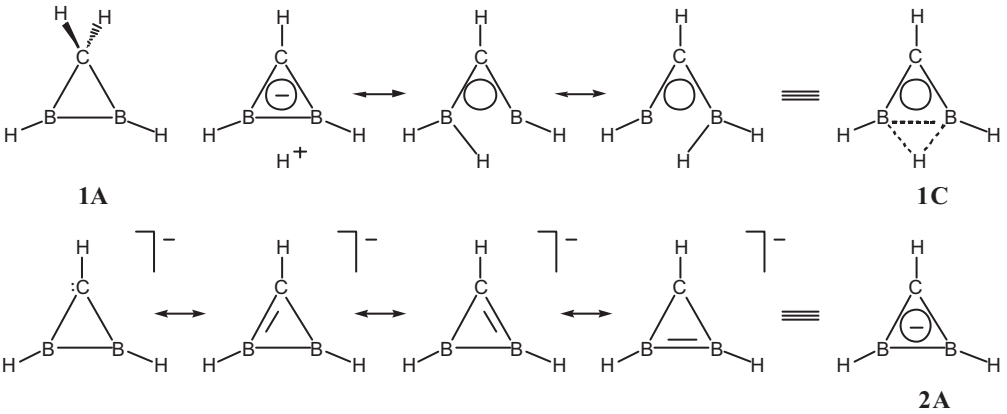

Scheme 3.2-1. Classical diboracyclopropane **1A**, the corresponding global minimum **1C** [3, 4] with a BHB bridge and anion **2A**, common to both. The CB bridged isomer **1B** is shown in Scheme 3.2-2. No single mesomeric formula provides a satisfactory description of **1C** and **2A**, respectively. The dashed triangle symbolizes a 3c2e σ bond, the circle a 3c2e π bond.

Diboracyclopropane **1A** may serve as an example to illustrate the principles discussed above. With the carbon atom tetrahedrally coordinated by two hydrogen and two boron atoms its classical structure is well described by the Lewis formula in Scheme 3.2-1. Hyperconjugation between the CH bonds and the formally empty p orbitals at the boron atoms leads to only a relatively minor reorganization of electron density compared with that suggested by the Lewis formula.

Removal of one of the methylene protons generates a carbanionic center, but the corresponding single Lewis formula is a poor description of the electronic structure. More mesomeric forms of **2A** may be written to give a more adequate fomulation. Alternatively, a circle may be drawn to symbolize the 3c2e π bond in **2A**, resulting from overlapping p orbitals *perpendicular* to the plane of atoms involved.

The multicenter bonding interaction in **2A** is classic in a sense that it results in a well known Hückel aromatic, which is planar with cyclic delocalized $4n + 2$ π electrons (no hyper-coordinate atoms). The most favorable site for a proton to bind to **2A** is not the carbon atom, but the B–B edge. The non-classical **1C** is 47.6 kcal mol^{-1} more stable than the classical structure **1A** [5].

Protonation transforms the 2c2e BB bond into a 3c2e BHB bond. Both the 2c (BB) and 3c interactions (BHB) are due to orbital overlap *in* the molecular plane and are therefore classified as *sigma*. The hydrogen atom is hypercoordinate as it is equally bound to both boron atoms. Hence, **1C** is a non-classical, delocalized and electron-deficient compound having eight skeletal electrons (SE) and therefore belongs to the class of *closo*-carboranes according to the $2n + 2$ SE rule [2].

Next, let us have a closer look at the 3c2e BBB bond in the series of triborirane dianion [6] and its homo forms [7]. The parent, cyclic $B_3H_3^{2-}$, **M**, has a true π MO occupied by two electrons and composed of pure p orbitals from the three boron atoms (see Figure 3.2-2). Inserting a methylene group into one 2c2e BB

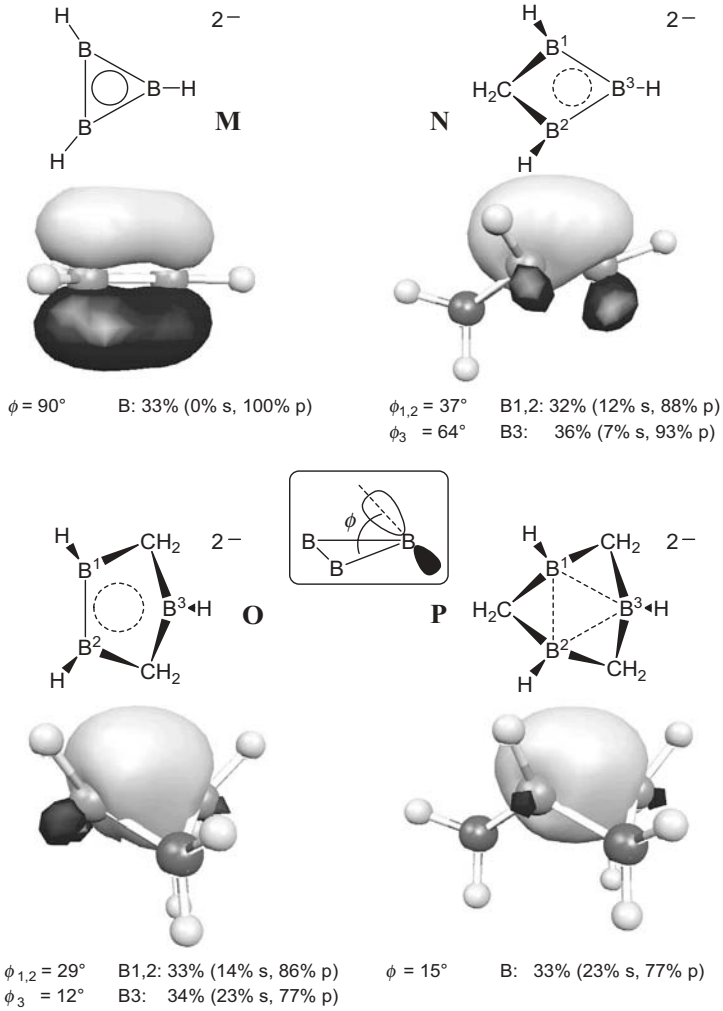

Fig. 3.2-2. Molecular formula (top view) and plot [9a] of the 3c BBB natural bonding orbital (NBO) [9b] (side view) for the triborirane dianion (**M**) as well as homo- (**N**), bishomo- (**O**) and trishomo-derivatives (**P**). The orientation (in terms of ϕ) and the s,p-character of the contributing hybrid orbitals is also given.

bond, i.e., replacing a 2c2e σ bond by a methylene bridge, gives the corresponding homoaromatic species, **N**, which is not planar. There is still a 3c2e BBB bond, but the contributing hybrid orbitals have considerable s-character. This rehybridization results in polarization (one lobe is bigger than the other), which allows for better overlap of the reoriented hybrid orbitals (which are not perpendicular to the BBB plane, see Figure 3.2-2) on one side of the BBB ring. The extent of the described changes is larger for those boron atoms which are directly connected to the homo

bridge. The presence of two (**O**) or three CH_2 bridges (**P**) changes the 3c bonding further. In derivative **P** the 3c2e BBB bond is made by almost perfect sp^3 hybrids. The latter include an angle of only 15° with the BBB plane. This is much closer to σ (0°) than to π (90°) bonding. As it is arbitrary where to draw a line we will call intermediate bonding situations (between pure π and pure σ) as "π,σ-distorted" and indicate the distorted π bond in **N** and in **O** as dashed circles. In the trishomotriborirane dianion **P** a dashed triangle is used for the 3c2e bond, which is essentially σ in character. The effect of homo bridges on the multicenter bonding is of course similar to isoelectronic molecules, e.g., cyclopropenium cation [8b,c]. Connections of atoms by both σ- and π-multicenter bonding are described as "double aromaticty" [8a,d], which is a combination of "in-plane and perpendicular aromaticty" (see Chapter 1).

Distorted π MOs can also be found in 4c2e bonding. Expanding **2A** by a CH^+ unit leads to the non-planar π,σ-distorted aromatic $C_2B_2H_4$ **J**, isoelectronic with the $(CH)_4^{2+}$ dication [11] **G** and the $B_4H_4^{2-}$ dianion **Q**, which all can be considered as distorted tetrahedra as well as folded rings. All have ten SE and classify as *closo*-clusters as shown for **G** and **J** in Figure 3.2-1.

Isoelectronic $C_4H_4^{2+}$ (**G**), 1,3-$C_2B_2H_4$ (**J**) and $B_4H_4^{2-}$ (**Q**) have one four-center, two-electron bond, each. A planar ring conformation exhibits one bonding π molecular orbital (Figure 3.2-3, left). However, in the most stable conformation, the ring is not planar, but puckered to allow for enhanced 1,3-overlap of orbitals at the cost of reduced 1,2-overlap. The former is more stabilizing due to a more favorable orientation of pairs of orbitals directed towards each other. Hence, this type of interaction is not strictly of pure π type anymore, as the overlapping atomic orbitals are not parallel. But, it is not strictly σ, either, as the orbitals do not point directly to the midpoint of the centers involved. This intermediate 4c bonding situation can be described as π,σ-distorted.

When some boron atoms in non-classical boranes are exchanged by isolobal C^+ units, the multicenter bonding MOs look qualitatively the same, but the contribution of carbon hybrid orbitals is larger than those from boron atoms [compare Figures 3.2-3(b) and (c)]. This polarization is due to the higher electronegativity of carbon versus boron atoms.

With more electron deficient centers the bonding situation becomes even less classical. In analogy with 1,3-$C_2B_2H_4$, a $C_2B_3H_5$ ring can be expected to be at least non-planar (see above). On the other hand, distortion to a spherical structure actually allows all atoms to be engaged in multicenter bonding. For the resulting trigonal bipyramid a classical Lewis structure may be drawn. However, this picture with localized CB bonds and empty p orbitals at tricoordinate B atoms is only a poor description of the real delocalized electronic structure (at least in the absence of π-donors at B, see Chapter 3.2.3.4, Ref. [53]).

Mesomeric formula involving 3c2e bonds on the delta faces are more realistic. For higher members of the dicarborane family localized descriptions are not possible [12a–d]. They are best understood in terms of one totally symmetric bonding orbital composed of radial hybrid orbitals pointing towards the cluster center, plus a set of filled bonding MOs resulting from tangential orbitals overlapping along

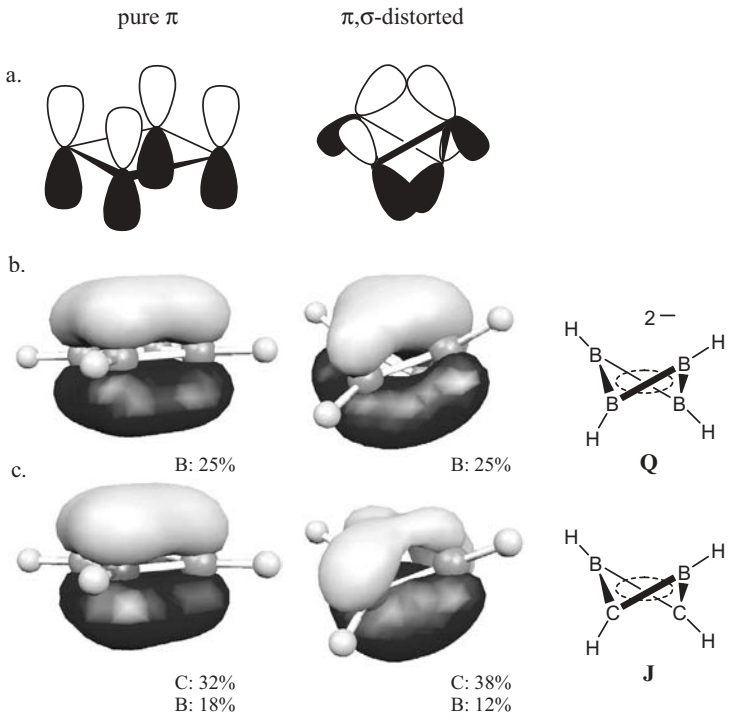

Fig. 3.2-3. The 4c bonding MO of four-membered rings in planar (left) and folded conformations (right): schematic representation (a) and plot [9a] of NLMOs (natural localized molecular orbitals) [9b] for $B_4H_4^{2-}$, **Q**, (b) and 1,3-$C_2B_2H_4$ [10], **J**, (c). Percentages refer to the individual orbital contributions (%) of carbon and boron atoms.

the sphere's surface (see also Chapter 1 for a more exhaustive discussion). In this way, *closo*-borane dianions and *closo*-carboranes resemble three dimensional analogues of three-membered rings, e.g., cyclopropane [12e] (see Figure 3.2-4), which are sigma aromatic due to one 3c2e sigma bond (radial) plus a filled set of sigma MOs (tangential) bonding along the perimeter. Hence, *closo*-borane dianions (e.g., $B_6H_6^{2-}$, Figure 3.2-4) and *closo*-carboranes can be regarded as three dimensional σ aromatics. In contrast, fullerenes are three dimensional π aromatics as their multicenter bonding arises from side-on overlap of orbitals perpendicular to the sphere's surface.

Finally, we want to point out that no sharp borderlines exist for the concepts outlined above, which are relevant for the hydrocarbon/organoborane/carborane/boron hydride continuum.

For example, both Hückel aromatics **B** and **C** conform to the Wade-Mingos electron counting rules [2] (see Chapter 1.1.2) and to the structural systematics developed for boranes and heteroboranes [1]: the hexagonal bipyramid with the apices removed is in agreement with an *arachno* electron count of 18 SE for $(CH)_6$ [2].

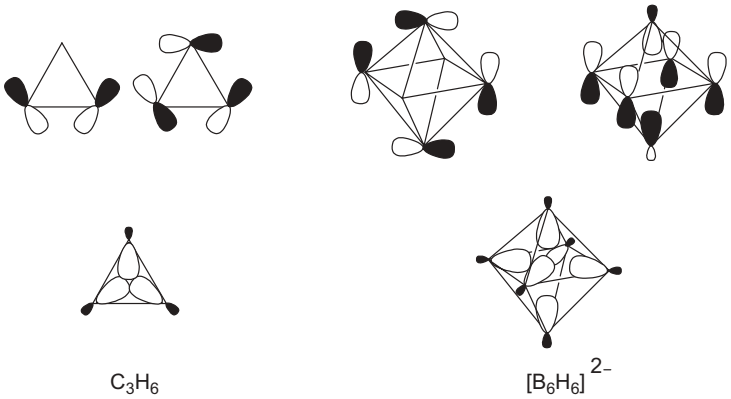

Fig. 3.2-4. Radial (bottom) and tangential (top) bonding molecular orbitals for cyclopropane [12e] (left) and hexaborane(6) dianion (right) illustrating the planar and three dimensional σ aromaticity, respectively. Tangential orbitals of $[B_6H_6]^{2-}$ are triply degenerate.

Similarly, the classical tetrahedrane **D** with six 2c2e bonds may be classified as a *nido*-cluster having $2n + 4$ SE. It is derived from the *closo*-structure (trigonal-bipyramid), with one apical vertex missing.

3.2.2 Monocarbaboranes

The monoboron compounds of the formula $RC(BR')_nH$ $(n = 1)$ are methyleneboranes [13], they do not meet the criteria of non-classical organoboranes.

3.2.2.1 Non-classical Diboriranes

As discussed in the introduction (Section 3.2.1), derivatives of the diboracyclopropane **1C** are non-classical organoboranes having 8 SE, and according to the $2n + 2$ SE rule may be classified as the simplest *closo*-carboranes of the series $CH(BH)_nH$ $(n = 2)$. Compounds **1B** and **1C** have been computed [5] to be 17.5 and 47.6 kcal mol^{-1} lower in energy, respectively, than the classical diboracyclopropane **1A**. They are 2e aromatics and possess planar-tetracoordinate centers: in **1B** this unusual geometry is found at the carbon and one boron atom, in **1C** at both boron atoms (Scheme 3.2-2).

Experimentally, derivatives of **1C** such as **1a–c** [14–16] as well as of the anion **2A**, the corresponding base [17, 18] common to compounds of type **1B** and **1C**, were obtained by various routes.

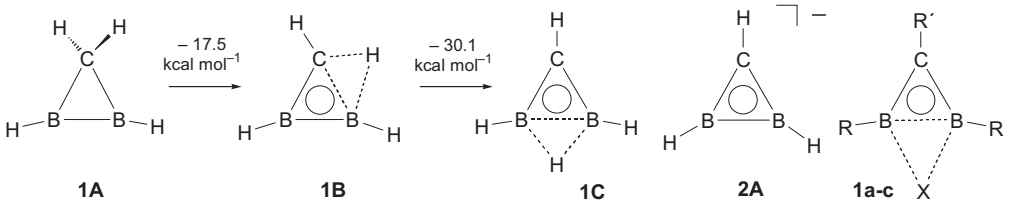

Scheme 3.2-2. 2e aromatic diboriranes **1B** and **1C** are stabilized to a considerable extent compared with classical **1A**. **1a–c** are experimentally known derivatives of **1C**. [**a**: R′ = X = 2,4,6-trimethylphenyl(mesityl), R = Bu^t, **b**: R′ = $(Me_3Si)_2CBEt_2$, R = 2,3,5,6-tetramethyl-phenyl(duryl), X = H, **c**: R′ = $(Me_3Si)_2CH$, R = Bu^t, X = H].

Reaction of **2a** with $Cl_2BCH_2SiMe_3$ yields the compound **3a** [18]. When the symmetrically substituted **3a** is reacted with lithium in diethyl ether, the unsymmetrically substituted folded **4b** [18] is obtained (Scheme 3.2-3). Formation of **4b** can be explained by a rapid isomerization of the first formed **4a** via the distorted tetrahedral transition state **5a**.

4b is strongly folded (59°) as expected for a 4c2e aromatic: its skeleton is isoelectronic with those of $C_4H_4^{2+}$ and $C_2B_2H_4$ (Figure 3.2-3). Planarization (Scheme 3.2-4, top) requires 13 kcal mol^{-1} as deduced from the temperature dependence of the line widths of the NMR signals of the diastereotopic methylene protons of its CH_2SiMe_3 substituent and of the B–Dur moieties [18]. The line shape analysis

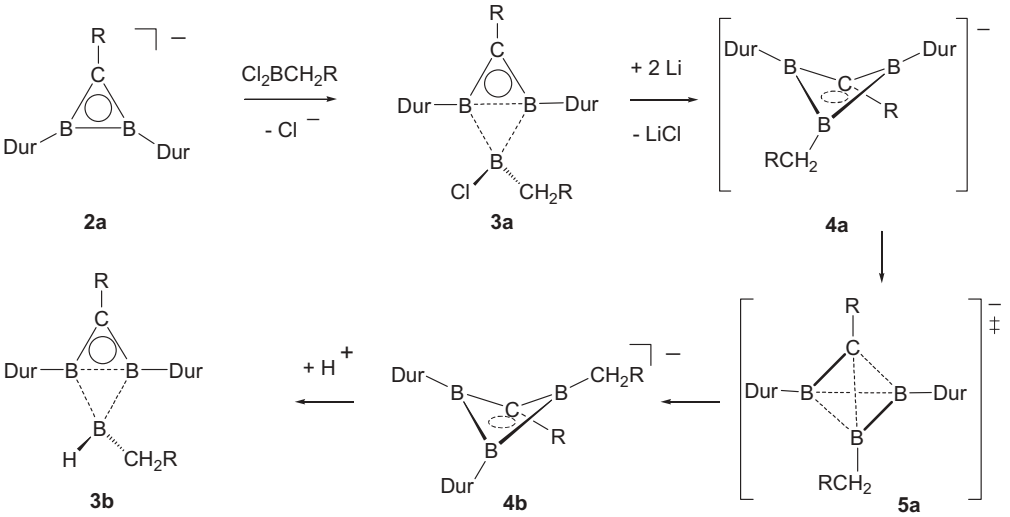

Scheme 3.2-3. Reactions with conservation of 2e aromaticity. It is the sigma skeleton which is changed, namely from classical in **2a** via partially non-classical in **3a** and classical in **4b** to partially non-classical again in **3b**. **4b** has a 4c2e non-planar π bond distorted towards σ. The four dashed lines in the transition state **5a** represent six electrons (R = $SiMe_3$, Dur = 2,3,5,6-tetramethylphenyl).

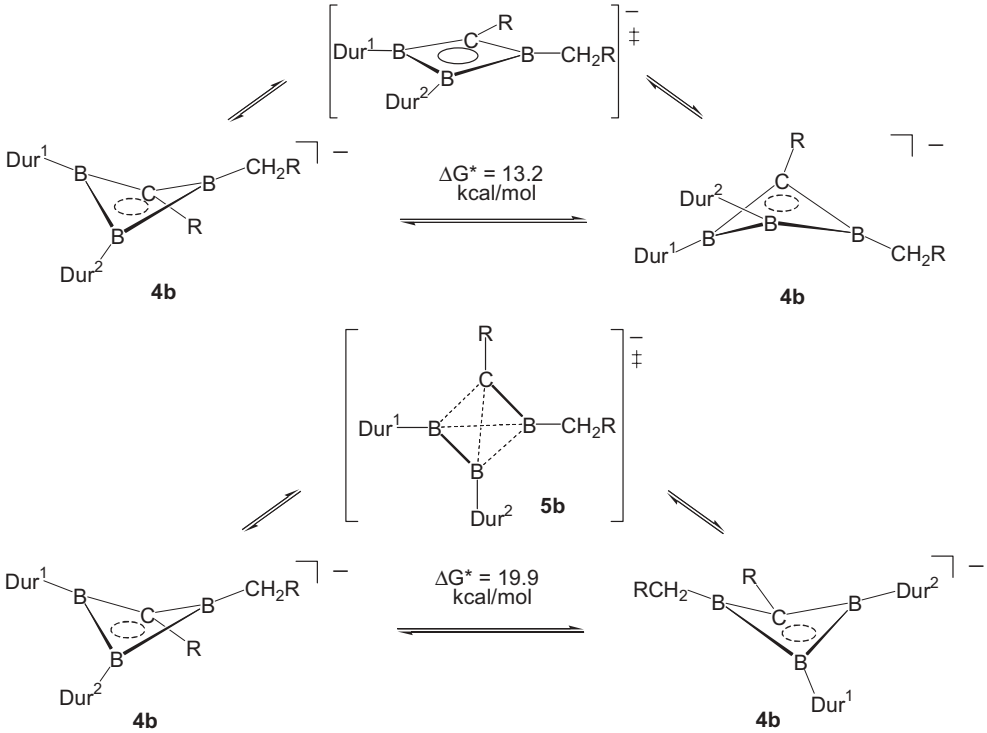

Scheme 3.2-4. Enantiomerizations of folded **4b** via two different transition states: with ring inversion (top) and without ring inversion but with exchange of the B–Dur moieties via the distorted tetrahedrane **5b** (bottom) (R = $SiMe_3$, Dur = 2,3,5,6-tetramethylphenyl).

of the temperature dependent NMR spectra of the latter allows a barrier of 19.9 kcal mol^{-1} to be deduced for the enantiomerization of **4b** via transition state **5b** (Scheme 3.2-4, bottom). Note that this stereoisomerization includes an exchange (topomerization) of the B-duryl moieties and thus a fluctuation of the skeleton bonds of **4b**. A fluctuation barrier of 17 kcal mol^{-1} is obtained by computations for a model with CH_3 and SiH_3 substituents at the ring boron and carbon atoms, respectively. Anion **4b** is the first folded 2e aromatic with fluxional skeletal bonds, its π system is π,σ-distorted.

Protonation of **4b** leads to the symmetrically substituted **3b** (Scheme 3.2-3) and methylation of **4b** at temperatures higher than −60 °C gives **3c** (Scheme 3.2-5) [19]. In the latter reaction, **6a** can be identified as an intermediate at −80 °C by ^{13}C NMR spectroscopy [19]. Its planar-tetracoordinate carbon atom is strongly deshielded (δ $^{13}C = 144$ ppm) as compared with tetrahedrally-coordinated carbon atoms connected to three boron and one silicon center (δ $^{13}C = 70$–100 ppm). Computations for the model compounds **6A** and **6B** give 144 and 104 ppm, re-

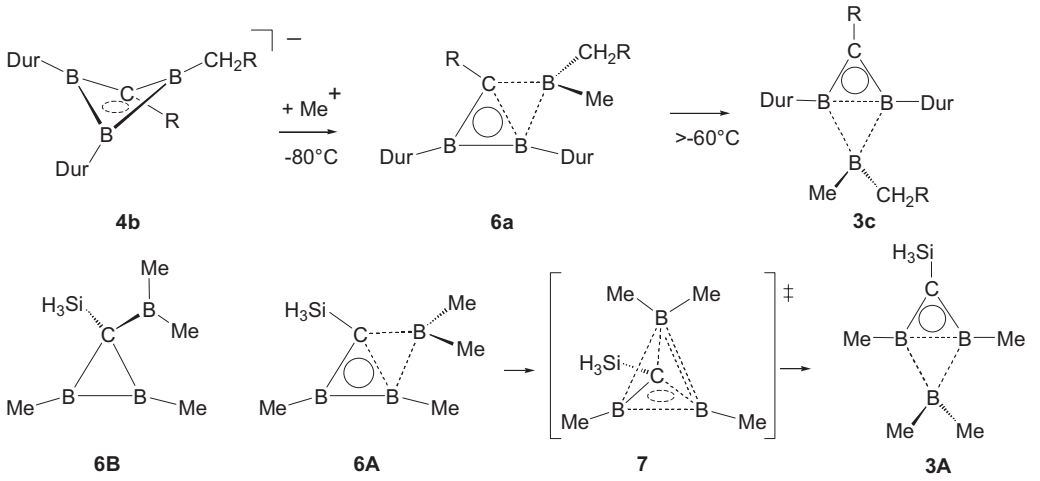

Scheme 3.2-5. Transformations with conservation of 2e aromaticity. **6a** is a derivative of **1B** (Scheme 3.2-2) and has a planar tetracoordinate carbon atom. The dashed lines of the transition state **7** represent two 3c2e bonds (BBB and CBB).

spectively. They also show that isomerization of **6A** to **3A** via transition state **7** is exothermic (by 11.6 kcal mol^{-1}) and involves a barrier of only 20.6 kcal mol^{-1} (Scheme 3.2-5) [19].

Boryl bridged **6a** is the first derivative of **1B** (Scheme 3.2-2). A corresponding replacement of the H bridge in **1C** by a boryl group is realized in compounds **3a–c** (Schemes 3.2-3 and 3.2-5).

3.2.2.2 Non-classical Triboretanes

Computations reveal the unsubstituted triboretane CB_3H_5 to be the homo form of triborirane B_3H_3. Both classical forms, **8A** and **10A** (Scheme 3.2-6), are no minima and are considerably higher in energy than the non-classical forms **8B** [6] and **10B**, respectively, as well as the H-bridged isomers of these, **9A** [6] and **11A** [20].

The stabilization of **10B** versus **10A** of 38.1 kcal mol^{-1} is remarkably large for an uncharged homoaromatic. This demonstrates the power of 2e aromaticity: **8B** is 61.6 kcal mol^{-1} lower in energy than **8A**. Less repulsion between the σ skeleton electrons, the number of which is reduced by two in the 2π electron aromatics as compared with the classical isomers, certainly contributes to the huge energy differences. The additional stabilization by formation of BHB bridges is, however, of minor importance. Note that classical σ skeletons are to be expected only for $\mathbf{8A}^{2-}$ and $\mathbf{10A}^{2-}$ [6, 20] (Scheme 3.2-6), the 2e reduction products of triborirane and triboretane.

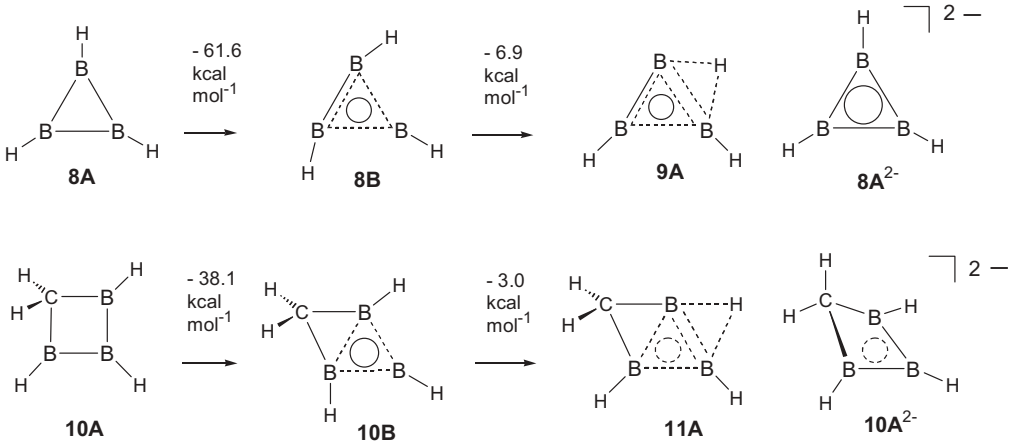

Scheme 3.2-6. Non-classical 2e aromatic triboretanes **10B** and **11A** are the homo forms of the corresponding triboriranes **8B** and **9A**, according to computations.

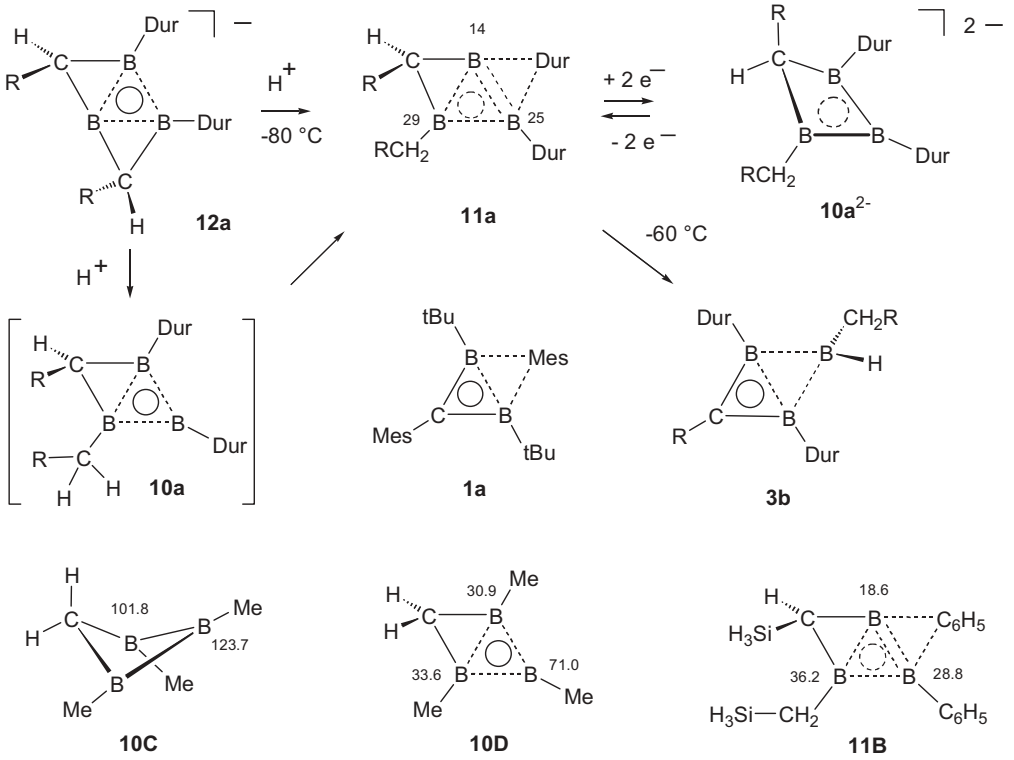

Scheme 3.2-7. Generation of the triboretane **11a** from **12a** and **10a**$^{2-}$, both with conservation of 2e aromaticity. Chemical shifts of the boron atoms of **11a** are similar to those of model **11B**, but considerably different from those of classical **10C** and non-classical **10D** (R = $SiMe_3$, Dur = 2,3,5,6-tetramethylphenyl, Mes = 2,4,6-trime-thylphenyl).

Protonation of the borenate **12a** [22] (Scheme 3.2-7) at −80 °C and stabilizing the highly reactive **11a** [20] as $\mathbf{10a}^{2-}$ by reduction with lithium naphthalenide at −100 °C gives the first derivatives of **11A** and of $\mathbf{10A}^{2-}$. When **11a** is allowed to warm to −60 °C, it rearranges into **3b** within 40 min [20]. During this process a C–H as well as a C–B bond have to be activated, i.e., cleaved under remarkably mild conditions. Oxidation of purified $\mathbf{10a}^{2-}$ with 1,2-dibromoethane at −90 °C regenerates **11a**, which can be characterized by ^{13}C and ^{11}B NMR spectroscopy when the oxidation is performed in an NMR tube at −100 °C. For the bridging duryl substituent of **11a**, shielded and deshielded carbon centers are observed at positions corresponding to those found for the bridging mesityl substituent of **1a**. Comparision of ^{11}B NMR chemical shifts of **11a** with those computed with the GIAO (gauge invariant atomic orbitals) method for models **10C**, **10D** and **11B** clearly indicates that the aromatic structure computed for bridged **11A** and **11B** is realized in **11a**. The ^{11}B chemical shifts of **11a** are remarkably similar to those of **12a** [20 and 24 ppm (2B)] which is a two-electron bis-homoaromatic containing a non-classical σ skeleton (a double aromatic with σ and π aromaticity). Replacing the classical homo bridge $CHSiMe_3$ of **12a** by the "non-classical homo bridge" [7] duryl formally leads to the skeleton of **11a**.

3.2.2.3 Non-classical Bicyclo[1.1.0]triboretanes

Isomeric with non-classical triboretanes of type **3** (Schemes 3.2-3 and 3.2-5) are tribora*bi*cyclo[1.1.0]butanes of type **13** (Scheme 3.2-8). The first derivative **13a** was obtained when **4b** was reacted with dichloro(trimethylsilylmethyl)borane [19].

The bonding situation in compounds of type **13** may be understood in relationship to that of **4**. The boron center with an additional exocyclic ligand employs two sp^2 hybrids for exo bonding and contributes only two orbitals for ring bonding: The p orbital is involved in an open 3c2e bond to the other two ring boron atoms (**14** in Figure 3.2-5, bottom) and the sp^2 hybrid takes part in four center bonding (**14** in Figure 3.2-5, top). As the latter has predominantly transannular bonding character it may also be regarded as a strongly bent transannular C–B bond, which hyperconjugates with the formally empty p orbitals of the tricoordinate boron centers of the ring. A strong π acceptor as an additional ligand (e.g., a boryl group) interacts with the open 3c2e BBB bond to give a second, three-dimensional 4c2e

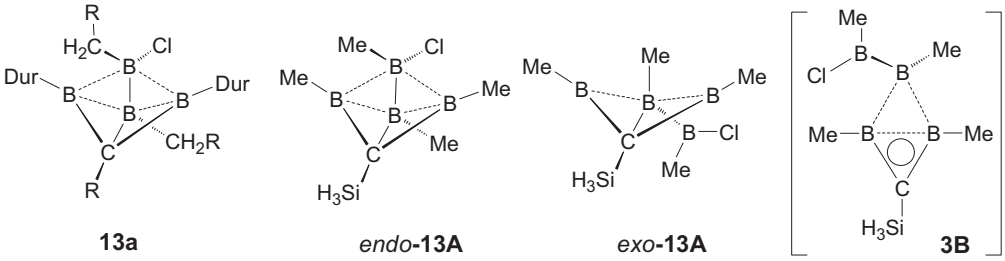

13a *endo*-**13A** *exo*-**13A** **3B**

Scheme 3.2-8. Triborabicyclo[1.1.0]butanes **13** and non-classical **3B** isomeric with **13A**.

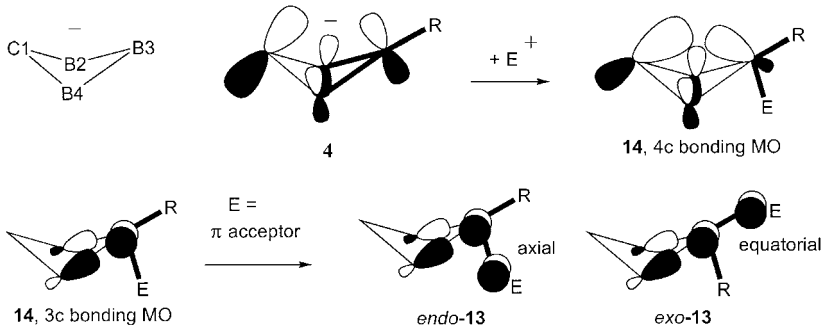

Fig. 3.2-5. The π,σ-distorted 4c bonding of **4** (MO shown) is not destroyed but retained (see **14**, 4c bonding MO) after reaction with the electrophile E^+. To allow for the new 2c2e exocyclic bond to E, B3 binds to B2 and B4 via one open 3c2e bond in **14** (see **14**, 3c bonding MO) rather than via two 2c2e σ bonds in **4**. When E is a π acceptor, the 3c bond expands to a three- or two-dimensional 4c bond like in *endo*-**13** and *exo*-**13**, respectively. Bold lines indicate 2c2e bonds involving sp^2 hybrids from B3.

bond with better overlap resulting from an axial position (*endo*-**13**, Figure 3.2-5). Overlap with the boryl group in the equatorial position in *exo*-**13** leads to a considerably less effective two-dimensional 4c2e bond. The model *exo*-**13A** with an equatorial boryl substituent and an axial methyl group at the pentacoordinate boron center is computed to be not even an energy minimum and 22 kcal mol^{-1} higher in energy than *endo*-**13A**. The latter is 11 kcal mol^{-1} more stable than the 2e aromatic **3B** (see Scheme 3.2-8).

Compounds of type **13** are species at the borderline between classical aromatics and three-dimensional σ-aromatic clusters (see also Section 3.2.2.4).

3.2.2.4
Derivatives of 1-Carba-*closo*-oligoborate Ions $[CH(BH)_n]^-$

Reaction of **13a** with elemental Li in Et_2O yields **15a**, the first derivative of the simplest polyhedral *closo*-carborane of the anionic series $[CH(BH)_n]^-$ $(n = 4)$ (Scheme 3.2-9). Polyhedral members with $n = 3$ are transition states of type **5** as shown in Section 3.2.2.1.

The geometry of **15a** is similar to that of the isoelectronic dicarbapentaboranes discussed in Section 3.2.3.4. Three-dimensional aromaticity of the prototype $CB_4H_5^-$ was established by computations of aromatic stabilization energies, nucleus independent chemical shifts (NICS) and magnetic susceptibilities(χ) [12a]. Thus, **15a** has one of the simplest skeletons with three-dimensional σ aromaticity. The aromatic stabilization energy (ASE) of the prototype $CB_4H_5^-$ (**15A**) can be estimated by averaging the ASE's of the isoelectronic three-dimensional aromatics $B_5H_5^{2-}$ and $C_2B_3H_5$ to be 27 kcal mol^{-1} (see Section 3.2.3.4, Ref. [54]).

Oxidation of the anion **15a** with C_2Cl_6 leads to the blue radical **15a**$^{\bullet}$ characterized by $g = 2.0039$, which is reminiscent of the blue radical $CB_{11}Me_{12}^{\bullet}$ ($g = 2.0037$) obtained by oxidation of the corresponding anion $CB_{11}Me_{12}^-$ [23].

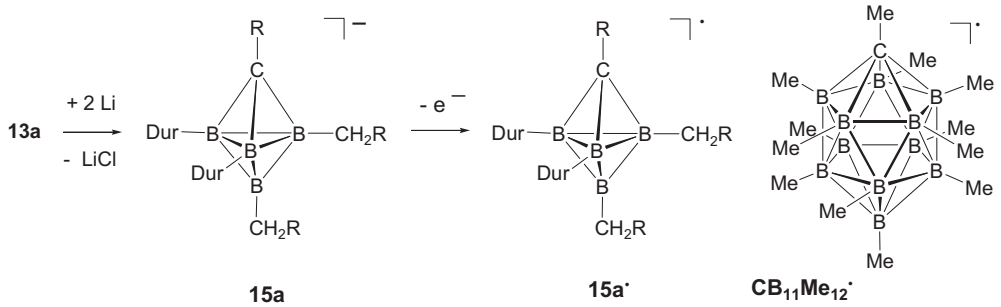

Scheme 3.2-9. Synthesis of the simplest monocarba-*closo*-borane anion **15a** starting from triborabicyclo[1.1.0]butane **13a**, and the one-electron oxidation product of **15a**.

The larger 1-carba-*closo*-oligoborates $[CB_5H_6]^-$ [24], $[CB_7H_8]^-$, $[CB_8H_9]^-$, $[CB_{11}Me_{12}]^-$ [23] and, recently, [*closo*-2-$CB_6H_7]^-$ [25] and $[PhCB_6H_6]^-$ [26] have been described. The icosahedral-shaped anions $[HCB_{11}H_5X_6]^-$ and $[HCB_{11}Me_5X_6]^-$ (X = Cl, Br) are the most inert, least nucleophilic anions, which allow for the isolation of protonated benzene [27a] $[C_6H_7]^+$ and protonated fullerene [27b] $[C_{60}H]^+$.

3.2.2.5 Carba-*nido*-tetraboranes(7)

The first derivative of carba-*nido*-tetraboranes(7), **16a**, was prepared by reaction of anionic **17** with iodomethane and characterized by NMR spectroscopy and by model computations (Scheme 3.2-10) [28]. The structurally analyzed **16b** is obtained by deuteration of the dianion **10a**$^{2-}$ [20] mentioned in Section 3.2.2.2. The results of an X-ray structural analysis of its dilithium salt are discussed in Section 3.2.8.3. The lithium cations are coordinated side-on to the B–B 2c2e bonds just as predicted for the aromatic $Li_2B_3H_3$ [6]. Obviously, $(Li^+)_2$**10a**$^{2-}$ is a 2e homoaromatic. Since the positions of the lithium cations resemble those of the deuter-

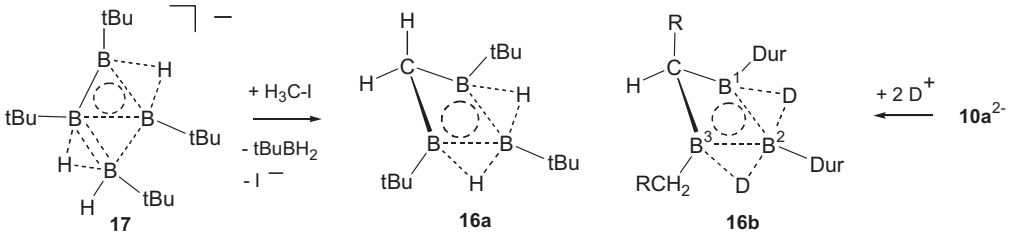

Scheme 3.2-10. Methylation of **17** [28] to **16a** and deuteration of **10a**$^{2-}$ to **16b**: transformations with conservation of 2e aromaticity.

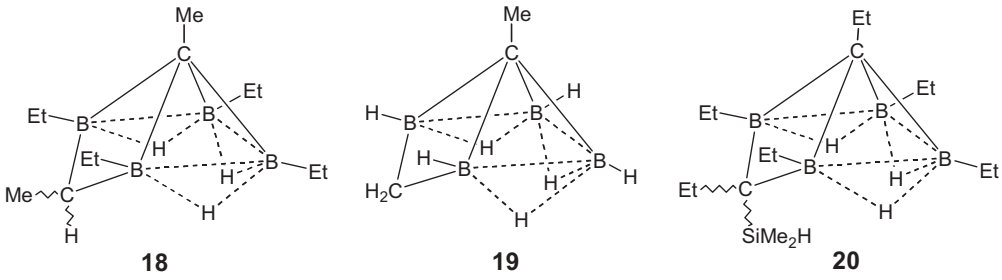

Scheme 3.2-11. Carboranes with an *arachno*-CB_4 skeleton.

ium atoms in **16b**, $(Li^+)_2$**10a**$^{2-}$ may also be regarded as a dilithio-carba-*nido*-tetraborane; *vice versa*, **16b** may be classified as an uncharged 2e homoaromatic. From this point of view, the two BDB bridges are non-classical homo bridges [7], having a similar influence on the BBB 3c bonding MO as classical methylene bridges.

3.2.2.6
1-Carba-*arachno*-pentaboranes(10)

Carbaboranes with an *arachno*-CB_4 skeleton, that is derivatives of 1-carba-*arachno*-pentaborane(10), were identified as side products (Scheme 3.2-11): **18** in the reaction of dichloroethylborane with elemental Li [29], and **19** was obtained from propyne and tetraborane(10) [30]. The reaction of dimethyl(dipropyn-1-yl)silane with a large excess of tetraethyldiborane(6) ["hydride bath" which contains $Et_2BH_2BEt_2$, other ethyldiboranes(6) and triethylborane] [31, 32] resulted in the formation of **20** in good yield [33].

Replacement of the chloro substituents and hydroboration of the benzoannelated diborafulvene **21** with $LiBH_4$ leads to an anionic product, which after protonation affords the 1-carbapentaborane(10) **22** in 36% yield (Scheme 3.2-12) [34].

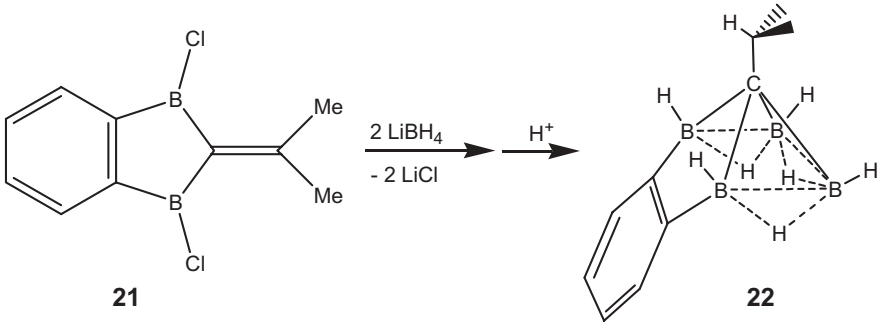

Scheme 3.2-12. Exchange of chlorine for hydrogen with $LiBH_4$ in the diborabenzofulvene **21** followed by hydroboration and coordination with BH_3 as well as protonation to give 1-carba-*arachno*-pentaborane(10) **22**.

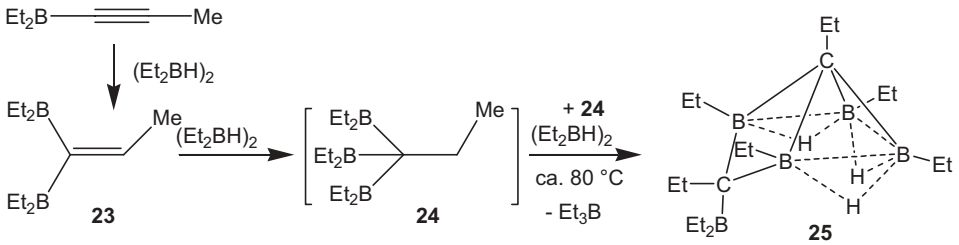

Scheme 3.2-13. Hydroboration of diethyl(propyn-1-yl)borane in the "hydride bath" via **23** and **24**, followed by Et_2BH-catalyzed condensation and self-assembly, leads to the 1-carba-*arachno*-pentaborane(10) **25**, having the Et_2B substituent at the exopolyhedral carbon atom.

The reaction leading to **20** was used to prepare **25** (Scheme 3.2-13) [35], starting from diethyl(propyn-1-yl)borane which served as a versatile reagent for the synthesis of other carboranes (*vide infra*). 1,1-Bis(diethyl-boryl)propene **23** can be detected and isolated, whereas it was not possible to identify 1,1,1-tris(diethylboryl)propane **24** in the reaction mixture.

It turned out that the [B–H]-catalyzed condensation of two molecules of the intermediate **24** proceeds slowly with elimination of BEt_3, when compared with bis(diethylboryl)-substituted hydrocarbons. Thus, a route to the *arachno*-carboranes **27** is provided [36] by heating the *in situ* formed **24** and **26** in the "hydride bath". The carboranes **27** were obtained as mixtures of isomers (Scheme 3.2-14).

3.2.3 Dicarbaboranes

In the late 1950s the first carboranes, the *closo*-carboranes 1,5-$C_2B_3H_5$, 1,2-$C_2B_4H_6$, 1,6-$C_2B_4H_6$ and $C_2B_5H_7$ were obtained by Williams and his group. However, the

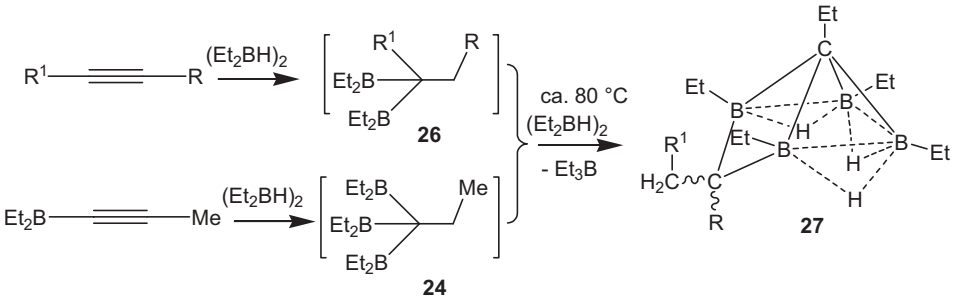

Scheme 3.2-14. Combined hydroboration of alkynes and diethyl(propyn-1-yl)borane in the "hydride bath" (**24** and **26**), followed by Et_2BH-catalyzed condensation and self-assembly, provides a general route to the 1-carba-*arachno*-pentaborane(10) derivatives **27** (R = Me, Bu, Ph, R^1 = H, $SiMe_3$).

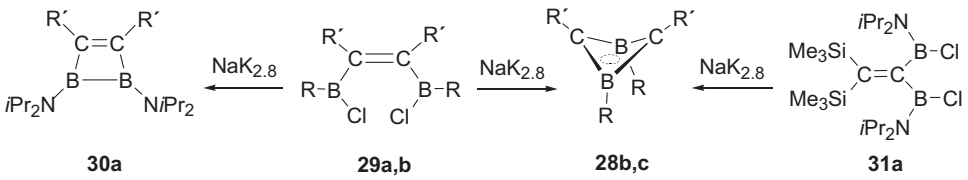

Scheme 3.2-15. Formation of 1,2- and 1,3-dihydro-diboretes **30** and **28**. **30a**: R′ = H, **29a**: R′ = H, R = NPr^i_2, **b**: R′ = CMe_3, R = NMe_2, **28a**: R′ = H, R = NPr^i_2, **b**: R′ = CMe_3, R = NMe_2, **c**: R′ = $SiMe_3$, R = NPr^i_2.

very low yields of the carboranes from thermal reactions of B_2H_6 and ethyne did not allow their fascinating chemistry to be explored [1].

3.2.3.1
Non-classical 1,3-Dihydro-1,3-diboretes

As discussed in the introduction (Section 3.2.1) the 1,3-dihydro-1,3-diborete $C_2B_2H_4$ (**28A** = **J** in Figure 3.2-3) is puckered, and its 4c2e π MO is distorted towards σ. Derivatives of **28A** may be regarded as the smallest dicarba-*closo*-boranes (see **J** in Figure 3.2-1) of the series $(CH)_2(BH)_n$. The energy of planarization of **28A** has been computed to 16.9 kcal mol^{-1} [37].

The $(Bu^tC)_2(BMe)_2$ derivative of **28A** was reported to be formed from $Bu^t{}_2C_2$, $MeBBr_2$ and C_8K. However, the product could not be separated from the borirene byproduct [38], and attempts for reproducing these results were not successful [39]. Dehalogenations of **29b** and **31a** yield directly **28b** [40] and **28c** [41], respectively (Scheme 3.2-15). Their X-ray structure analyses confirmed the results of *ab initio* computations [10].

Planar **30a** is obtained by dehalogenation of **29a** [42]. Upon heating, **30a** rearranges to the folded 1,3-diborete **28a**. Its X-ray structure analysis revealed the shortest transannular C–C distance (174 pm) in 1,3-dihydro-1,3-diboretes [43].

3.2.3.2
Non-classical 1,2-Diboretanylidenes (Boriranylideneboranes)

Computations show that carbene **32A** as well as its homo and bishomo forms **33A** and **34A**, respectively, do not correspond to electronic ground states. Promoting the non-bonded electron pair of the carbene center in **32A** from σ to p, allows for double 3c CBB bonding: a 3c2e σ bond originates from the empty in plane hybrid orbital at carbon together with the 2c2e B–B bond and a 3c2e π bond employs the three p orbitals and the promoted electron pair. In this way, carbene centers are strongly stabilized by adjacent B–B moieties through the formation of double aromatics [4, 44] such as **32B**, **33B** and **34B**, each having one σ-aromatic and one π-aromatic system (Scheme 3.2-16).

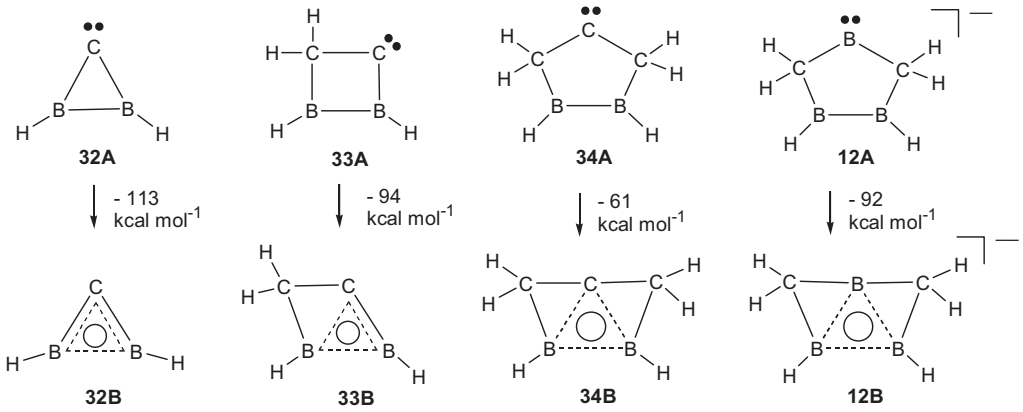

Scheme 3.2-16. Double aromatic prototypes **32B**, **33B** and **34B** with σ- and π-aromaticity: according to computations, carbenes **32A**, **33A** and **34A** are strongly stabilized by adjacent B–B moieties. Derivatives of **12B**, isoelectronic with **34B**, are known experimentally [22, 44].

Experimentally, derivatives **33b–d** were synthesized and fully characterized [13]. These planar non-classical organoboranes exhibit a unique chemistry [13]. We first described **33b–d** as valence-isomeric boriranylideneboranes **33′b–d** until their electronic structure was understood during the theoretical analysis of the electronic structure of **12a** [44] (Scheme 3.2-17). The synthesis of derivatives of **34B**, which is isoelectronic with **12B**, remains a challenge.

3.2.3.3
Non-classical 1,2-Diboretanes

The classical form **35A** of 1,2-diboretane is 34.5 kcal mol^{-1} higher in energy than the non-classical, homoaromatic isomer **36A** [46]. However, the planar C_{2v} form **35A** is not a local minimum. This is reminiscent of the corresponding results for diborirane (see Section 3.2.2.1). The classical minimum is the C_1 symmetric,

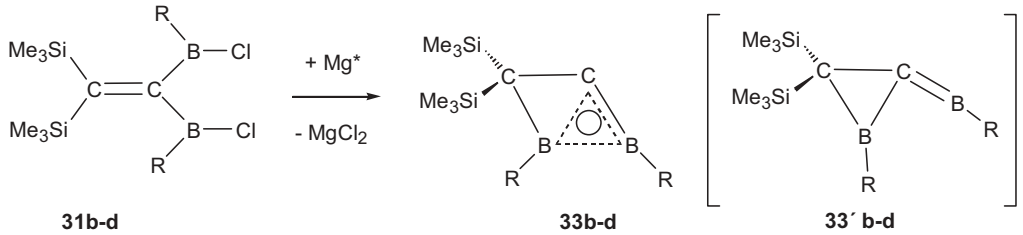

Scheme 3.2-17. Compounds **33b–d** are experimentally fully characterized derivatives of **33B**. (**b**: R = Bu^t, **c**: R = 2,4,6-trimethylphenyl, **d**: R = 2,3,5,6-tetramethylphenyl).

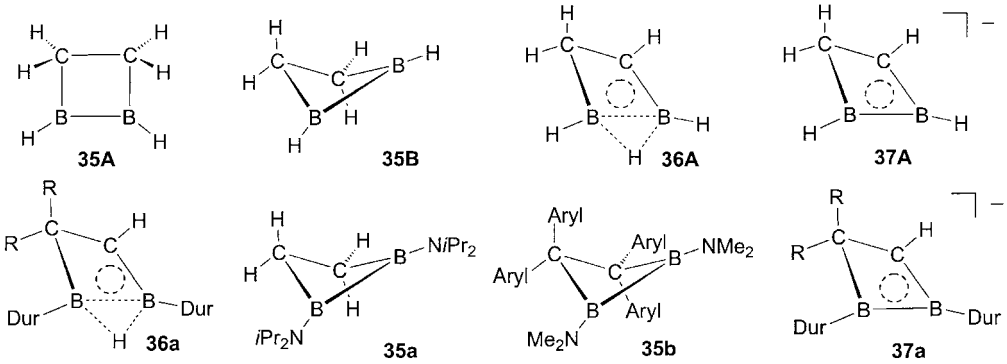

Scheme 3.2-18. Molecules **35A–37A** and compounds **35a–37a** ($(Aryl)_2C$ = fluorenylidene, R = $SiMe_3$).

folded **35B** which benefits from hyperconjugation: **35B** is 9.6 kcal mol^{-1} lower in energy than **35A**. Two derivatives of **35B** are known, experimentally, **35a** [47] and **35b** [48] (Scheme 3.2-18), both carrying amino substituents at their boron centers. **35a** was shown to be folded by 28°, **35b** to rearrange at 65 °C into its 1,3-isomer. Several derivatives of **36A** like **36a** [46] have been described. **37a**, a derivative of **37A**, which can be expected to result from deprotonation of **36a**, has also been also synthesized [21].

3.2.3.4
Dicarba-*closo*-pentaboranes

The *closo*-carboranes with a C_2B_3 skeleton are of particular interest because their structure and bonding have been described as classical and non-classical. Köster et al. [49] reported the preparation of pentaalkyl-1,5-dicarba-*closo*-pentaboranes by hydroboration of dialkyl(1-alkynyl)boranes with tetraalkyl-diboranes(6) $(R_2BH)_2$. By using a large excess of $(Et_2BH)_2$ as a "hydride bath" the route to pentaethyl-1,5-dicarba-*closo*-pentaborane(5) was found to proceed via the 1-carba-*arachno*-pentaborane(10) [50] (see also Section 3.2.2.4 [33]).

Heating of the dicarba-*nido*-hexaborane(8) **38** at 120 °C leads to elimination of $EtBH_2$ (Scheme 3.2-19) and quantitatively gives pentaethyl-1,5-dicarba-*closo*-

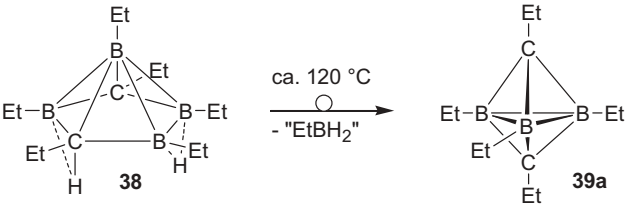

Scheme 3.2-19. Conversion of the *nido*-C_2B_4 cluster **38** into the *closo*-C_2B_3 carborane **39a** with elimination of ethylborane.

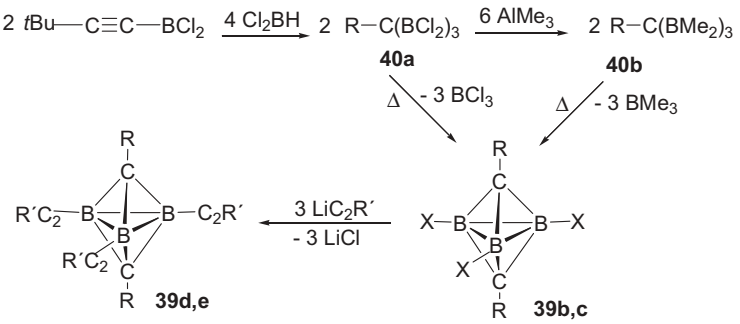

Scheme 3.2-20. Formation of 1,5-dicarba-*closo*-pentaborane derivatives **39** ($R = CH_2CMe_3$) via hydroboration of a borylalkyne with $HBCl_2$ to give **40a**, which on heating yields the chloro derivative **39c**. Its methylation leads to **39b**, and reaction with RC_2Li to **39d,e** (**b**: X = Me; **c**: X = Cl, **d**: $R' = CMe_3$; **e**: $R' = Ph$).

pentaborane(5) **39a** [50]. Its structure follows from ^{11}B [51] and ^{13}C NMR data [52], and deformation electron density data obtained by refinement of the X-ray diffraction data [53], indicate unambiguously the presence of multicenter bonding in **39a**. Decisive evidence for non-classical bonding in five-vertex *closo*-heteroboranes and *closo*-pentaborates $[X_2(BH)_3]$ (X = N, CH, BH^-) follows from NLMO analyses [54].

A different route (Scheme 3.2-20) to *closo*-$C_3B_2R_5$ derivatives **39** starts with the synthesis of 1,1,1-tris(dichloroboryl)-3,3-dimethylbutane **40a**. Lithiation of 3,3-dimethyl-1-butyne with BuLi, followed by salt-metathesis reaction with BCl_3 and double hydroboration of the borylalkyne with $HBCl_2$ leads to **40a**, which upon heating to 170 °C yields the trichloro derivative **39c** [55]. Its high reactivity is demonstrated in reactions with $AlMe_3$, MeLi, RC_2Li ($R = C_6H_5$, CMe_3) and Me_3SiNMe_2 to give the corresponding derivatives in good yields. **39b** is also formed from **40b**.

The molecular structures of **39c**,**e** in the crystals show that the B–B and B–C distances of the C_2B_3 frameworks are considerably shorter than those of boron-amino-substituted derivatives [56], which are described as *bicyclo*-organoboranes.

The non-classical 1,2-diboretane **36b** eliminates $HSiMe_3$ upon heating to form the dicarba-*closo*-pentaborane **39f**. Its Pr^i_2N substituent may be replaced by OMe using MeOH/HCl and the latter by Cl upon reaction with BCl_3. Thermal isomerization of **41g**,**h** leads to **39g**,**h** (Scheme 3.2-21). Derivative **39g** is also obtained from **28c**$^{2-}$ and duryldifluoroborane. The *closo*-carboranes **39h**,**i** are transformed into the antiaromatic dianions **42h**,**i** upon 2e reduction with K/Na alloy [57]. These dianions are stabilized strongly by one alkali cation, which is in η^5 contact with the C_2B_3 ring.

Thermal elimination of Me_3SiH transforms **1b** (8 SE) into the folded 1,3-dihydro-1,3-diborete **28g** (10 SE), which undergoes cluster expansion to give the dicarba-*closo*-pentaborane(5) **39j** (12 SE) (Scheme 3.2-22). Note that one of the duryl substituents bound to boron in **1b** and **28g** is attached to carbon in **39j**. This describes

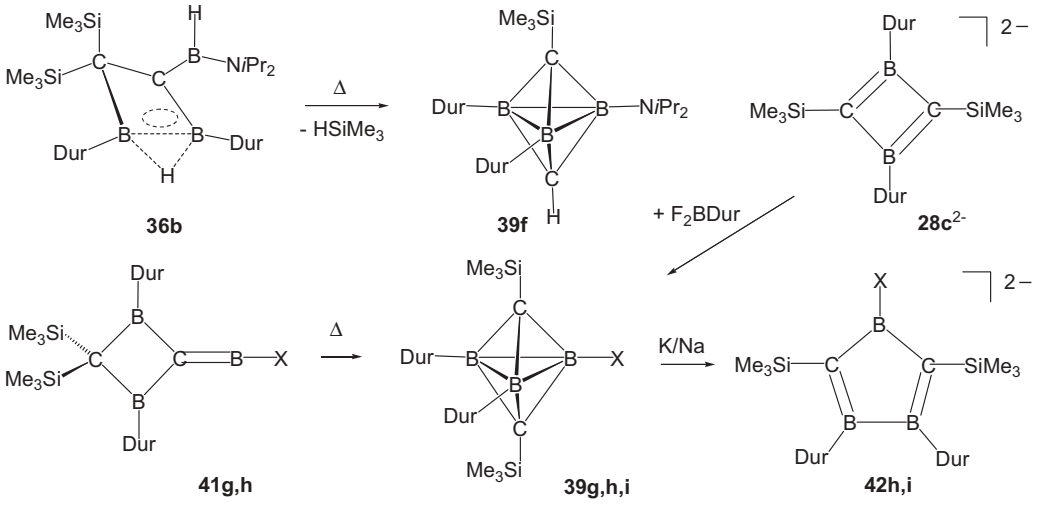

Scheme 3.2-21. Various routes to 1,5-dicarba-*closo*-pentaboranes **39f–i**. 2e reduction of **39h,i** furnishes **42h,i** (X = Dur, NR_2).

an intramolecular incorporation of two exo atoms of **1b** into the framework to give the *closo*-cluster **39j**.

3.2.3.5

Dicarba-*arachno*-pentaborane-dianions

In Section 3.2.1 the prototype **O** of the bishomo form of the triborirane dianion was discussed (see Figure 3.2-2). Experimentally, bishomotriborirane dianions were obtained by reduction of 1,2,4-triboracyclopentanes or by addition of nucleophiles to **12a** (see Scheme 3.2-7) [22]. However, these species do not exist as free dianions, but as contact ion pairs and will be presented together with derivatives of **N** and **P** (see Figure 3.2-2) in Section 3.3.8.

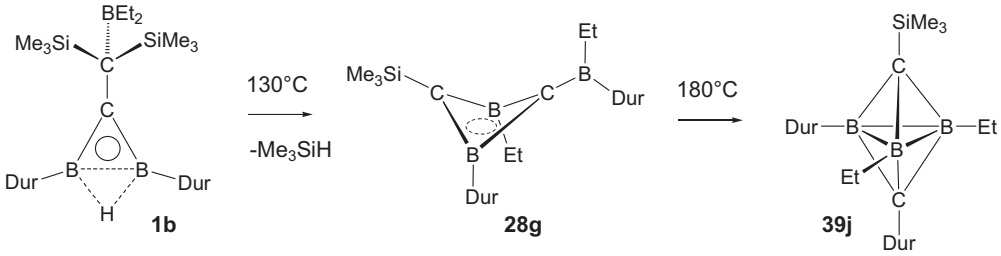

Scheme 3.2-22. Conversion of the three-center two-dimensional 2e π-aromatic **1b** into the five-center three-dimensional σ-aromatic **39j** via the four-center folded 2e aromatic **28g** with σ-type overlap of p-type orbitals.

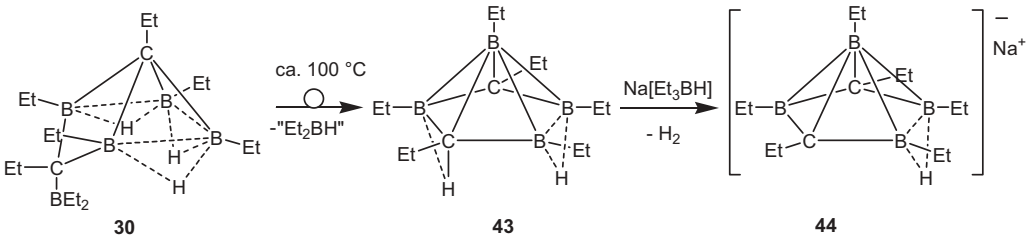

Scheme 3.2-23. Conversion of the 1-carba-*arachno*-pentaborane(10) **30** into the 2,4-dicarba-*nido*-hexaborane(8) **43**, followed by deprotonation yields borate **44**.

3.2.3.6

Dicarba-*nido*-hexaboranes and Dicarba-*closo*-boranes

In the framework of the 1-carba-*arachno*-pentaborane(10) derivatives (Section 3.2.2.6), the carbon atom occupies the apical position, which has the highest connectivity, and is therefore an unfavorable position for carbon. Hence, rearrangements to more stable structures with *nido*- or even *closo*-frameworks can be expected. Upon heating to 100 °C, the *arachno*-carborane **30** looses Et_2BH to give the 2,4-dicarba-*nido*-hexaborane(8) derivative **43** (Scheme 3.2-23) [45, 58]. One of the carbon atoms in the cluster of **43** bears an endohedral hydrogen atom which is supposed to have a weak 3c2e interaction with an adjacent boron atom (indicated by a dashed line in Scheme 3.2-23).

Many derivatives of isomeric 2,3-dicarba-*nido*-hexaborane(8) are known, available from the reaction of pentaborane(9) with alkynes [59, 60]. In contrast, the carboranes of type **43** with non-adjacent carbon atoms are rare.

The endohedral hydrogen atom in **43** is readily removed as a proton by strong bases to give the carbaborate **44**, structurally characterized as its sodium salt [45]. Treatment of **44** with CH_3OH or CH_3OD reforms the carborane **43** with an endohedral C–H or C–D bond, respectively.

The reactions of **44** with various electrophiles (e.g., MeI, Me_3SiCl, Et_2BCl, I_2) afford hexaethyl-1,5-dicarba-*closo*-hexaborane(6) **45** in low to moderate yields as the only identified product. When **44** is reacted with BBr_3, **45** and a mixture of the 2,4-dicarba-*closo*-heptaborane(7) derivatives **46** and **47** are formed (Scheme 3.2-24) [61]. The electron count of the borate anion **44** indicates the analogy with the cyclopentadienyl anion. It proved possible to prepare and characterize the ferrocene-like sandwich complex **48** [Fe(**44**)$_2$] [61]. In solution the ^{1}H NMR signal of the bridging hydrogen atoms in **48** is at low frequency (δ −6.17), indicating close Fe–H contacts.

Although legions of icosahedral carboranes **49** are known, the formation of supra-icosahedral boron-containing clusters was restricted to metal carboranes ($M_xC_2B_{10}$ or $M_xC_4B_8$, $x = 1, 2$) [62, 63].

Recently, Welch et al. [64] have shown that it is possible to expand icosahedral carborane to yield the new C_2B_{11} framework. This was achieved by reacting the dianion [7,8-μ-{$C_6H_4(CH_2)_2$}-7,8-*nido*-$C_2B_{10}H_{10}$]$^{2-}$ **50** [65] with $PhBCl_2$ to form the 13-vertex carborane **51** 1,2-μ-[$C_6H_4(CH_2)_2$]-3-Ph-1,2-$C_2B_{11}H_{10}$ (Scheme 3.2-25). The shape of the cluster is that of a henicosahedron.

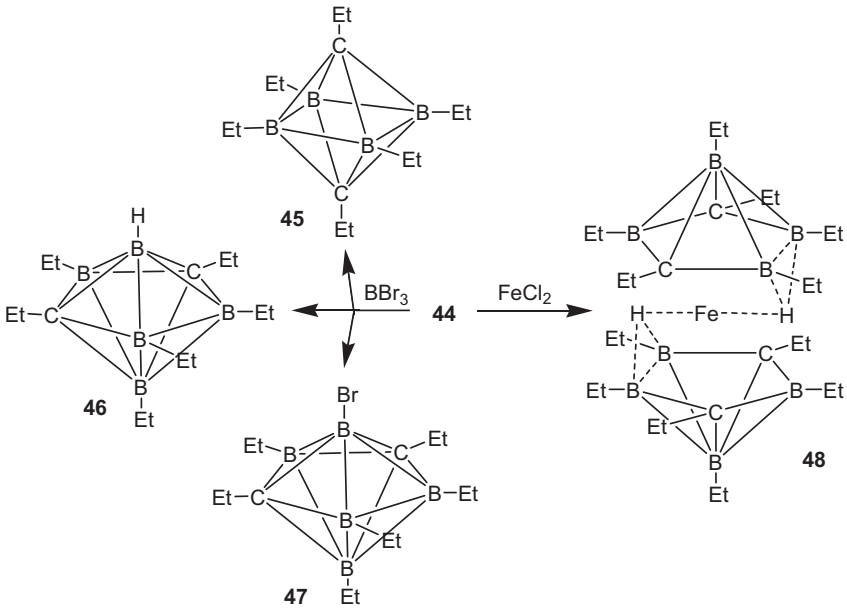

Scheme 3.2-24. Reaction of **44** with BBr_3 gives a mixture of *closo*-carboranes **45**, **46** and **47**, and with $FeCl_2$ the metallacarborane/sandwich complex **48**.

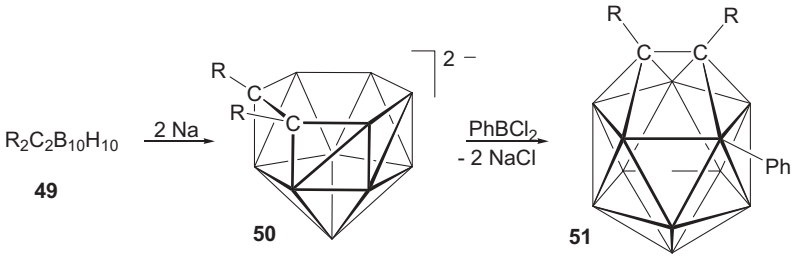

Scheme 3.2-25. Two electron reduction of 1,2-μ-$\{C_6H_4(CH_2)_2\}$-1,2-*closo*-$C_2B_{10}H_{10}$ **49** (R_2 = 1,2-μ-$\{C_6H_4(CH_2)_2\}$) with sodium yields [7,8-μ-$\{C_6H_4(CH_2)_2\}$-7,8-*nido*-$C_2B_{10}H_{10}]^{2-}$ which reacts with $PhBCl_2$ to give the 13-vertex carborane **51**.

3.2.4
Tricarbahexaborane

3.2.4.1
2,3,5-Tricarba-*nido*-hexaboranes(7)

Derivatives of 2,3,4-tricarba-*nido*-hexaborane(7) are well known [66]. The first derivatives of the 2,3,5-isomer **55** were obtained in a series of 2,3,5-tricarbahexabor-

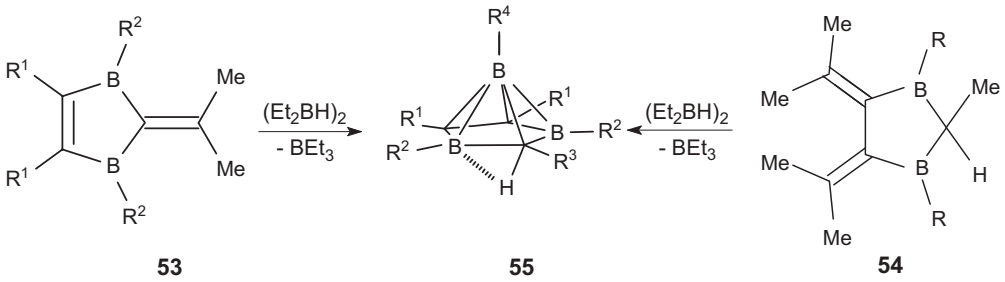

53 55 54

Scheme 3.2-26. Hydroboration of 1,3-dihydro-1,3-diboraful-venes **53** and of 4,5-diisopropylidene-1,3-diborolanes **54** with $(Et_2BH)_2$ results in the formation of *nido*-2,3,5-tricarbahexa-boranes(7) **55**.

anylnickel complexes [67]. Designed syntheses for derivatives of the 2,3,5-tricarba-hexaborane **55** are the double hydroboration of 1,3-dihydro-1,3-diborafulvenes **53** as well as 4,5-diisopropylidene-1,3-diborolanes **54** with $(Et_2BH)_2$ as shown in Scheme 3.2-26 [68]. The stability of the liquid carboranes depends on the substituents R at carbon and boron. The axial (endo) hydrogen atom is acidic and involved in 3c2e bonding to one of the basal boron atoms. In the ^1H NMR it exhibits a high field shift near $\delta = -1.4$. Deprotonation of **55** with potassium or Bu^tLi leads to the anion (**55**-H)$^-$, which is isolobal with $C_5H_5^-$. Reactions of **55** and (**55**-H)$^-$ with appropriate metal complexes lead to metallacarboranes with sandwich structures [67, 69].

The promising aspects of the condensation route to carbaboranes, starting from simple organoboranes in the ''hydride bath'' $(Et_2BH)_2$, prompted the search for a new method to obtain derivatives of **55**. As shown in Scheme 3.2-27, treatment of 1,2-bis(diethylboryl)alkenes and diethyl(propyn-1-yl)borane in the ''hydride bath'' affords a mixture of carboranes. The tetracarba-*nido*-hexaboranes(6) **56** (*vide infra*) are side products, while the tricarba-*nido*-hexaboranes(7) **55e**,**f** and **55g** (see also Section 3.2.7) are the main products. The endohedral hydrogen in 55e,f can be removed by treatment with strong bases to give the corresponding carbaborate (**55**-H)$^-$, isolated as sodium or potassium salt. Protonation with methanol leads back to the carboranes **55e**,**f** [70]. The carbaborates (**55**-H)$^-$ are versatile reagents; e.g., its reaction with Ph_3P-Au-Cl leads to **57** [71a].

Two other well defined carboranes **55g** and **76** (*vide infra*, Section 3.2.7) are present in the reaction mixture containing **64c** (*vide infra*, Scheme 3.2-35). Although pure **55g** could not be isolated, its solution-state structure follows from a complete set of NMR spectra [71b]. This unusual carborane is a spiro derivative without precedence and belongs to the family of 2,3,5-tricarba-*nido*-hexaboranes(7). *Ab initio* MO calculations and NMR data indicate that the boron atom linked to the C_3B_3-framework by an endohedral C–B bond takes part in the cluster bonding [71b] (similar to an endohedral C–H bond in the other carboranes **55**).

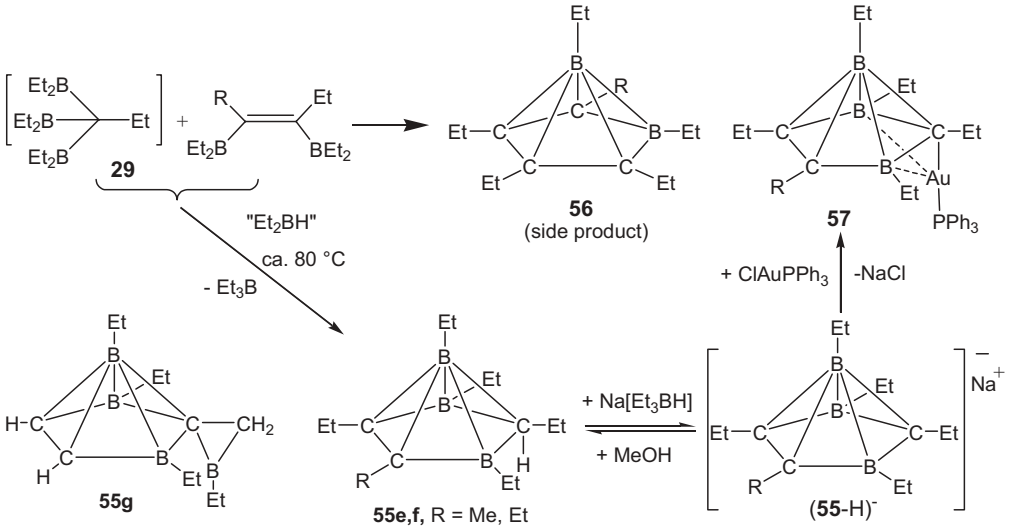

Scheme 3.2-27. Combined hydroboration and Et_2BH-catalyzed condensation of diethyl(propyn-1-yl)borane (via **29**) and (*Z*)-bis(diethylboryl)alkenes lead to the 2,3,5-tricarba-*nido*-hexaborane(7) derivatives **55** which can be deprotonated to give $(\mathbf{55}\text{-H})^-$, another cyclopentadienyl anion analogue. **55g** is formed by a different route (see Scheme 3.2-39).

3.2.4.2 Dianions of 2,4,6-Tricarba-*hypho*-hexaborane

In Section 3.2.1 the 3c2e BBB bonds in the series of triborirane dianions (**M**) and its homo forms **N**, **O** and **P** were described and the NBOs (natural bonding orbitals) are displayed in Figure 3.2-2. The chemistry of derivatives of **N** (**10A**$^{2-}$ in Scheme 3.2-6) was reported in Section 3.2.2 (non-classical triboretanes), and several derivatives of the bishomotriborirane dianion (**O**) are known [22] (see Section 3.2.8).

Derivatives of the trishomotriborirane dianion **P** are formed when alkali metals react in donor solvents with 1,3,5-triboracyclohexane derivatives. The dianion $[(CHMe)_3(MeB)_3]^{2-}$ has 20 SE and according to the cluster rules classifies as 2,4,6-tricarba-*hypho*-hexaborane-diid. However, the compounds exist as contact ion pairs, and are therefore regarded as heterocarboranes (see Section 3.2.8).

$[(BH)_3]^{2-}$	$[CH_2(BH)_3]^{2-}$	$[(CH_2)_2(BH)_3]^{2-}$	$[(CH_2)_3(BH)_3]^{2-}$
M	**N**	**O**	**P**

Scheme 3.2-28. Formulae of **M**–**P**.

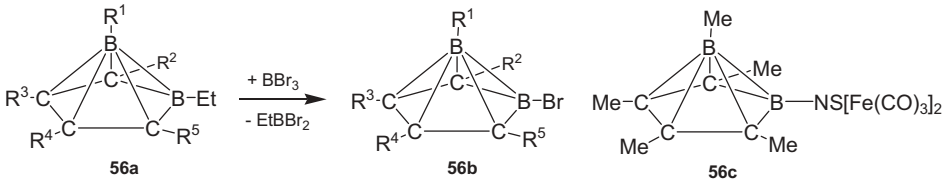

Scheme 3.2-29. Hexaalkyl-2,3,4,5-tetracarba-*nido*-hexaboranes(6) **56a** (R^1–R^5 = Me, Et) react in boiling BBr_3 by Et/Br exchange, selectively at the 6-position. The products **56b** can be used to combine carboranes with transition metal clusters as shown in the case of **56c**.

3.2.5 Tetracarba-*nido*-boranes

3.2.5.1 Tetracarba-*nido*-hexaboranes

Peralkylated tetracarba-*nido*-hexaboranes(6) **56** [72] are extremely stable, and almost inert in air and stable towards H_2O, in contrast with the parent carbaborane [73]. $^{11}B/^{11}B$ magnetization transfer experiments performed at 140 °C for the perethyl derivative show that exchange reactions between boron atoms in positions 1 and 6 are very slow.

Heating peralkylated derivatives **56a** in BBr_3 leads selectively to the 6-bromo derivatives **56b** via Br/alkyl exchange [74]. Among other transformations, the reaction of **56b** with the sodium salt of a thioazadiiron cluster is an example of combining main group and transition metal clusters in one molecule (**56c**), which provided crystals for structural characterization (Scheme 3.2-29) [75].

2,3,4,5-Tetraalkyl-1,6-dihalogeno-2,3,4,5-tetracarba-*nido*-hexaboranes(6) **56d** were obtained in high yield by another route (Scheme 3.2-30), taking advantage of the exchange reactions of the spirotin compounds **57** with boron halides.

The halogeno derivatives **56b** and **56d** are excellent candidates for the synthesis of other derivatives of the *nido*-C_4B_2 cluster series bearing functional groups either in the 6- or the 1,6-positions. With few exceptions, the reactions of **56d** with nu-

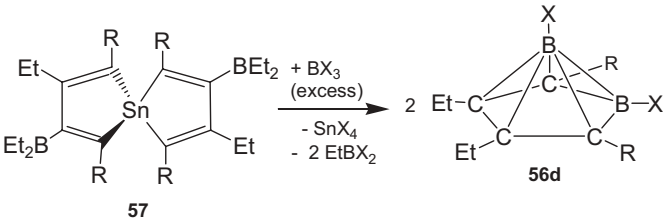

Scheme 3.2-30. Classical spirotin compounds **57** react with boron trihalides to give the 1,6-dihalogeno-substituted *nido*-C_4B_2 clusters **56d** (X = Cl, Br, I; R = Et, Bu).

cleophiles proceed selectively via substitution at atom B6. The ligand exchange reaction of the B–Br function in **56d** with hydride ($Li[Et_3BH]$) led at first to the monohydride (H–B6), but also to the dihydride with H–B6 and H–B1 moieties [76]. These derivatives are thermally much less stable when compared with the peralkylated carboranes. In addition to substitution of **56b** or **56d** at the B6 atom with organo groups (alkyl, phenyl, vinyl, alkynyl) numerous other functional groups were introduced, e.g., phosphanyl [77], stannyl [78], alkoxy groups and fluorine. In all cases the *nido*-C_4B_2 framework was not affected.

The most intriguing substituent at the boron atom(s) of the *nido*-C_4B_2 framework is the amino group NR_2 because of potential (N=B6)π interactions which may weaken the B–B bonding in the cluster, because $NPr^i{}_2$ groups enforce a classical bicyclic structure **60** [79].

Alkyl groups in 2,3,4,5-positions may have a different influence. Thus, the 1,6-dibromocarboranes of type **56d** were treated with one or two equivalents of lithium amides. The resulting B6-dialkylamino-substituted carboranes **56e** rearrange slowly in solution at room temperature (in contrast with *N*-trimethylsilylamino or *N*-pyrrolyl derivatives) into the B1-dialkylamino derivatives **56f** (Scheme 3.2-31). Apparently, the B6-dialkylamino group weakens the B1–B6 bonding, the cluster is opened to a square face which closes again to trigonal faces with the B-dialkylamino group in the 1-position. This is an example of the DSD (diamond-square-diamond) mechanism [80]. The carboranes **56f** with the B1-dialkylamino group now have a Br–B6 functionality, ready for further substitution reactions. Introduction of a second dialkylamino group in the 6-position finally causes the carborane framework to change into a classic structure **58**, in contrast to **60**.

The bicyclic compound **58** was found to be extremely reactive towards traces of H-acidic reagents. Even secondary amines, e.g., Et_2NH react with **58** by ring-

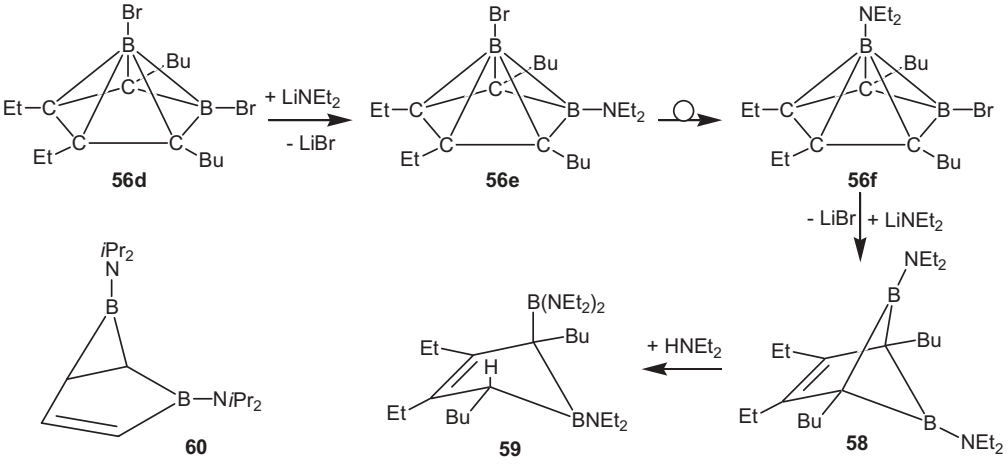

Scheme 3.2-31. The framework atoms C_4B_2 prefer classical structures (e.g., **58** or **60**) if dialkylamino groups are linked to both boron atoms. Note also the rearrangement of the C_4B_2 framework in **56e** to **56f**, which can be understood as an example of the diamand-square-diamond skeletal rearrangement [80].

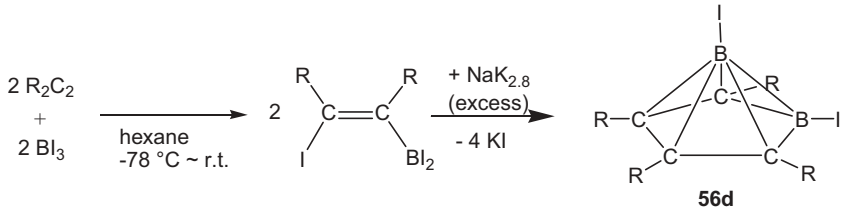

Scheme 3.2-32. A one pot route to 1,6-diiodo-*nido*-C_4B_2 carboranes **56d** (R = Me, Et, Ph).

opening to give **59**. Some results of the influence of diethylamino groups are shown in Scheme 3.2-31.

A one pot route to *nido*-1,6-diiodo-tetracarba-*nido*-hexaborane derivatives is depicted in Scheme 3.2-32. After iodoboration of the alkynes with BI_3 the dehalogenation of the alkenyl derivatives presumably leads to dimerization and rearrangement to give structurally characterized 1,6-diiodo-*nido*-carboranes **56d** [81].

Reductive opening of a tetracarba-*nido*-hexaborane cluster to an *arachno*-dianion was described for **56g**, which is accessible by thermal elimination of bis(trimethylsilyl)ethyne from the bridged bishomoborirene **61** [82]. Reaction of **56g** with elemental lithium in THF gives $[(Li{\cdot}thf)_2]$1,3-diboratabenzene **62**, its reoxidation to **56g** requires boiling 1,2-dibromoethane (Scheme 3.2-33).

3.2.5.2
Tetracarba-*nido*-octaboranes

In the dicarbaboranes $C_2B_3R_5$ and tetracarbaboranes $C_4B_2R_6$ the carbon atoms have the classical connectivity of four, whereas in $C_3B_3R_6H$ **55** the carbon atom C5 is pentacoordinated because of the extra hydrogen in the axial (endo) position (Scheme 3.2-26). In *nido*-$C_4B_4R_8$ carboranes **64** all framework carbon atoms are four-coordinated and located at the rim of the hexagonal, boat-like *nido*-opening of the cluster. Several approaches to derivatives of $C_4B_4H_8$ (**64**) have been reported [83, 84], the organoborane routes are described below.

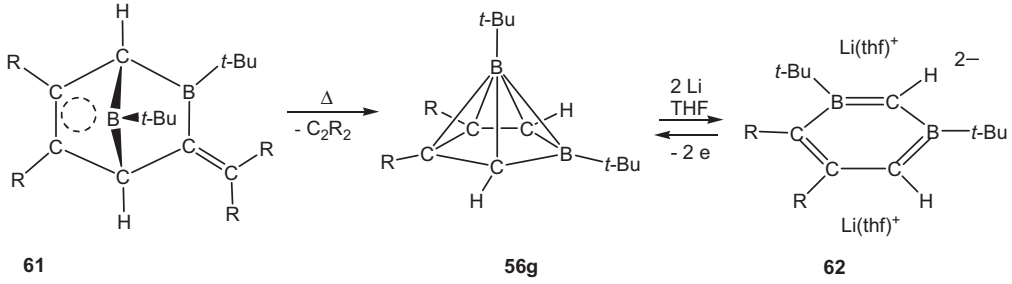

Scheme 3.2-33. 2e reductive opening of the *nido*-carborane **56g** to the *arachno*-dianion **62** (R = $SiMe_3$) and the reverse reaction by 2e oxidation.

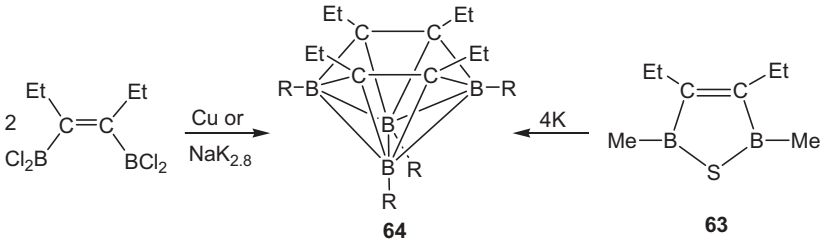

Scheme 3.2-34. Dehalogenations of *Z*-3,4-bis(dichloroboryl)-hexene with Cu vapour or sodium potassium alloy give crystalline **64b**, R = Cl. Reaction of **63** with potassium yields **64a**, R = Me.

Reaction of the 1-thia-2,5-diborole **63** with potassium leads to liquid **64a** [85], and dehalogenation of (*Z*)-2,3-bis(dichloroboryl)hexene with copper vapor or Na/K alloy results in the formation of crystalline **64b** [86], both in low yields (Scheme 3.2-34).

Considering the success of the condensation route to carboranes in the "hydride bath" (*vide supra*), other alkynylboranes than diethyl(propyn-1-yl)borane might be equally suitable. By heating a mixture of bis(diethylboryl) ethyne (**65**) and excess of $(Et_2BH)_2$ ("hydride bath") at 110–120 °C, 1,2,3,4-tetraethyl-5,6,7,8-tetracarba-*nido*-octaborane(8) **64c** was obtained by distillation in ca. 20% yield as a colorless liquid, stable to air and H_2O (Scheme 3.2-35) [87]. Possible intermediates in this reaction can be proposed as **67** and **68**, where **67** results from double hydroboration of bis(diethylboryl)ethyne (**65**), which "dimerizes" to **68** and finally yields the carborane **64c** by elimination of Et_3B.

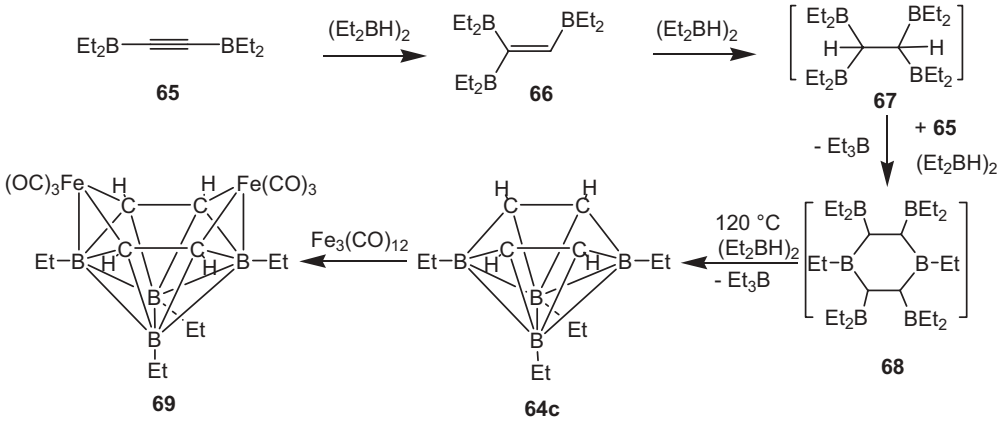

Scheme 3.2-35. Hydroboration of bis(diethylboryl)ethyne **65** in the "hydride bath" to **66** and **67**, followed by Et_2BH-catalyzed condensation to **68** and self-assembly to give the *nido*-C_4B_4 carborane derivative **64c**. The hexagonal open face in **64c** is ready for further transformations as shown by the synthesis of **69** (formation of **64a**,**b** see Scheme 3.2-34).

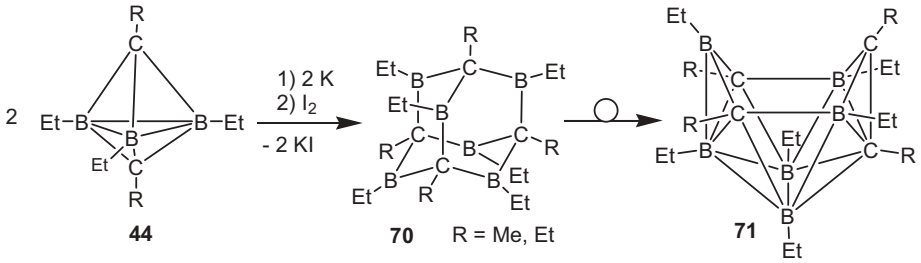

44 **70** **71**

Scheme 3.2-36. From non-classical **44** to classical **70** and again to non-classical bonding in **71**: oxidative fusion of two opened C_2B_3 fragments and irreversible rearrangment of the classical hexaboraadamantane cage **70** (R = Me, Et) into the *nido*-C_4B_6 carborane cluster **71**, which possess a fluxional C_4B_6 framework structure.

The carborane **64c** was characterized by a consistent set of NMR data, *ab initio* MO calculations, and by X-ray structure analysis [88]. The synthetic potential of **64c** is indicated by its reaction with $Fe(CO)_3$ fragments to give **69** [87]. The diferracarborane **69** is isostructural with *nido*-decaborane(14), because two BH and four BH(H) fragments were replaced by two isolobal $Fe(CO)_3$ and four CH fragments, respectively.

3.2.5.3
Tetracarba-*nido*-decaboranes

Reduction of the pentaalkyl-1,5-dicarba-*closo*-pentaboranes(5) **44** with elemental K opens the cluster and subsequent reaction with I_2 enforces oxidative fusion of two C_2B_3 units to give a C_4B_6 cage (Scheme 3.2-36). The peralkylated hexaboraadamantane derivatives **70** (R = Me, Et; X-ray structure analysis for R = Me [89]) rearrange irreversibly into the carboranes **71** with a *nido*-C_4B_6 framework [89] (X-ray structural analysis for R = Et [90]). The structure of the *nido*-C_4B_6 cluster is fluxional in solution [91].

Only three of the four carbon atoms occupy positions at the hexagonal open face in **71**. NMR spectroscopic data of the parent compound suggest a different structure with all four carbon atoms at the hexagonal open face.

3.2.6
Pentacarba-*nido*-hexaboranes

Carboranes with five carbon atoms are rare. In the uncomplexed form the *nido*-1-boranediyl-2,3,4,5,6-pentamethyl-2,3,4,5,6-pentacarbahexaborane(6) **72** is not known, its stabilization is possible with Lewis acidic species such as Br^+, $Fe(CO)_4$, BCl_3, and BCl_2R (Scheme 3.2-37).

Cleavage of Me_5C_5-$GeMe_3$ with excess of BBr_3 yields the cation **72a** [92], stabilized with the anion BBr_4^- or $AlBr_4^-$ [obtained in the reaction [93] of $[(Me_5C_5)Al]_4$

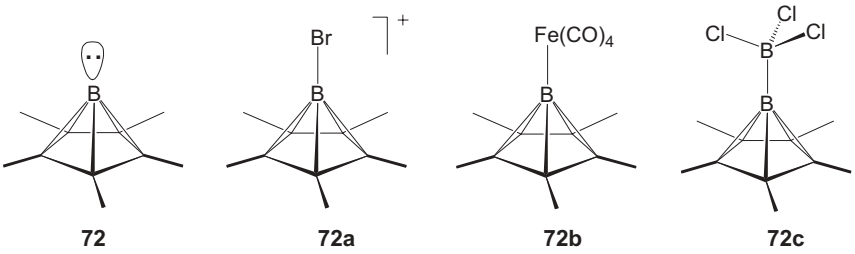

72 **72a** **72b** **72c**

Scheme 3.2-37. Pentacarba-*nido* hexaboranes **72–72c**

with BBr_3]. C_5Me_5-BCl_2 and $Na_2[Fe(CO)_4]$ react to give **72b**, [94] which has been studied theoretically and by X-ray structure analysis [95]. When B_2Cl_4 and (η^5-$C_5Me_5)_2Si$ are reacted in hexane at low temperature a complex mixture is formed, of which $(C_5Me_5)B \rightarrow BCl_2$-$SiCl_2C_5Me_5$ and $(C_5Me_5)B \rightarrow BCl_2$-$Si(C_5Me_5)_2Cl$ were isolated [96]. **72c** is obtained in 53% yield by replacement of one chlorine in B_2Cl_4 with C_5Me_5 and rearrangement of the diborane(4) derivative to give the boranediyl-trichloroborane adduct (Scheme 3.2-38). It exhibits a short B1–B2 bond (168.1 pm) and an unusual stability towards substitution of chlorine and replacement of the Lewis acid BCl_3, which is supported by a recent MO study [97].

3.2.7 Hexacarbaboranes

Two other well defined carboranes **55g** and **76** (*vide infra*) are present in the reaction mixture containing **66** (in Scheme 3.2-39). In the case of **55g** it is conceivable that hydroboration of bis(diethylboryl)ethyne does not lead selectively to **67** but also to **74**. After its condensation with **67** to yield **75**, it rearranges to give **55g** (Scheme 3.2-39). This unusual carborane is a spiro derivative without precedence and belongs to the family of *nido*-C_3B_3-carboranes (not to tricarbaheptaboranes). *Ab initio* MO calculations and NMR data [71b] indicate that the boron atom linked to the C_3B_3-cluster by an endohedral C–B bond takes part in the cluster bonding ($EtB{-}CH_2$ supplies one electron to the C_3B_3 cluster bonding as the endohedral hydrogen in $C_3B_3R_6H$ **55** does).

The hexacarbaborane **76** (Scheme 3.2-40) has a drum-shaped *arachno*-C_6B_6 structure, according to NMR data and MO calculations. It is assumed that **76** results from further condensation of **67** with **68** to give the intermediate **77**. Interestingly, the compound **78** is the parent compound of **76**, however, they have different structures. **78** is a C_4B_6-cluster having a classical C_2H_2 handle [98].

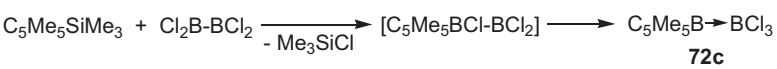

Scheme 3.2-38. Reaction of B_2Cl_4 with pentamethylcyclopentadienyl-trimethylsilane gives the *nido*-C_5B-cluster **72c**.

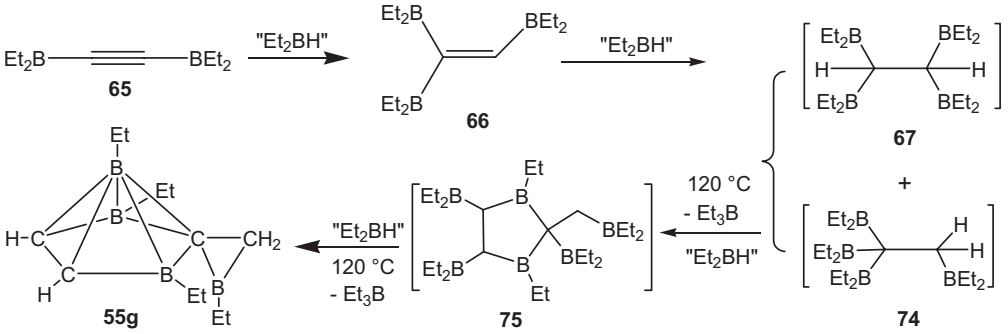

Scheme 3.2-39. The spirocarbaborane **55g** is formed as one component (see Scheme 3.2-27) in the "hydride bath" starting from bis(diethylboryl)ethyne as the result of hydroboration and Et_2BH-catalyzed condensations.

3.2.8
Heterocarboranes

Parent carboranes are composed of carbon, boron and hydrogen atoms. Whenever a hydrogen bridge occurs (BHB or CHB), the electron of the bridging hydrogen atom is needed for the framework bonding of the cluster. Replacement of the

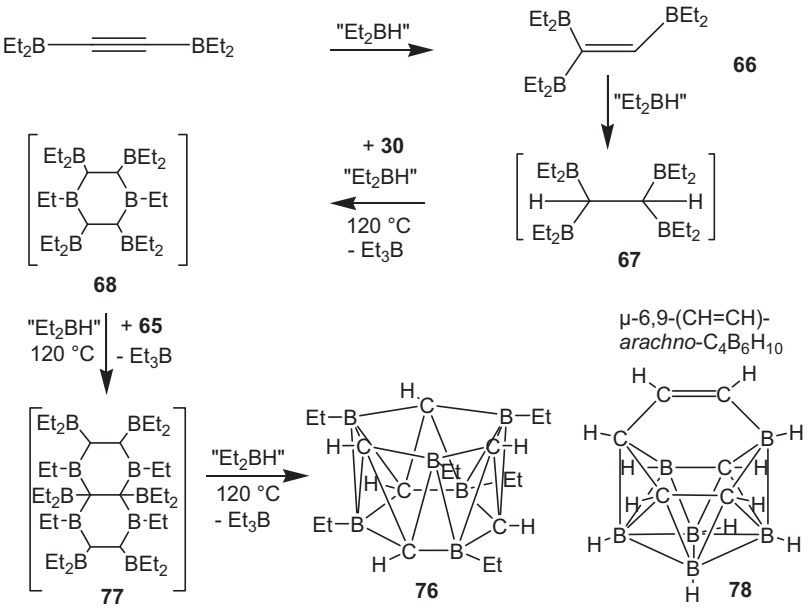

Scheme 3.2-40. Et_2BH-catalyzed condensation reactions of three borylated C_2-units (see **77**) in the "hydride bath", starts from bis-(diethylboryl)ethyne and **67**, leading to the *arachno*-C_6B_6 carborane derivative **76**, of which the structure differs greatly from that of the parent compound $C_6B_6H_{12}$ **78**.

bridging hydrogen by other elements or groups (e.g., BR_2 see Section 3.2.6, or AlR_2, or C_6H_5) the new bridging moiety also supplies only one electron. A bridging hydrogen as well as a bridging homo- (C and B) or heteroatom does not occupy a position of a framework atom, it only participates with one electron/one orbital in bonding. However, the heteroatoms of the heterocarboranes described in this chapter occupy a vertex of the cluster and may supply 2–4 electrons and three orbitals for bonding.

3.2.8.1
2,4,5-Azadicarba-*nido*-hexaboranes

The 1,2,5-azadiborolane **79** is obtained in good yields, when the corresponding 3,4-diborylhexadiene derivative is reacted with heptamethyldisilazane. Upon hydroboration of **79** with $H_3B{\cdot}$thf two products are formed depending on the amount of borane used. A 1:1 ratio ($n = 1$) yields the azadicarbahexaborane **80**, characterized by spectroscopic and structural data [99]. When a large excess of diborane is applied the main product of the reaction is the heterocycle **81** (Scheme 3.2-41). Its formation occurs formally by 1,4-addition of hydrogen to the isopropylidene groups of **79**, thereby forming the 1,2,5-azadiborole [100].

3.2.8.2
2,4,5-Thiadicarba-*nido*-hexaborane

Analogously to compound **79** the thiadiborolane **82** is formed from a 3,4-diborylhexadiene and $(Me_3Si)_2S$. The very air and moisture sensitive **82** reacts with an excess of $BH_3{\cdot}$thf to yield the *nido*-thiacarborane [100, 101] **83** and very little of the 1,2,5-thiadiborole **84**. In addition to **83** and **84** the thiacarborane $S(CPr^i)_2(BH)_6$ (**85**) was identified by GC-MS and ^{11}B NMR. **85** has 22 SE for a *nido*-framework, which is supported by computed IGLO ^{11}B NMR shifts [101].

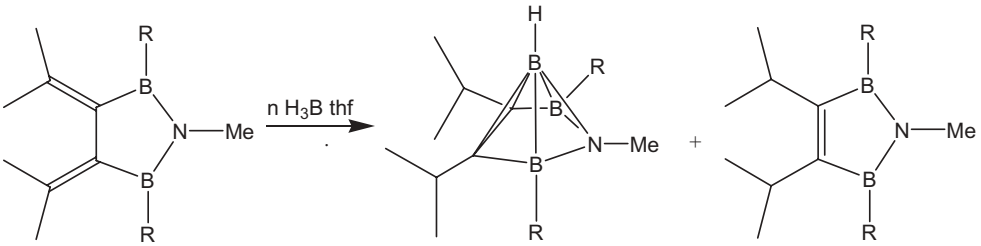

79 **80** **81**

Scheme 3.2-41. Hydroboration of 3,4-diisopropylidene-1-aza-2,5-diborolane **79** (R = C_6Me_4H) with thf·BH_3 yields the 2-aza-4,5-dicarba-*nido*-hexaborane **80** (R = C_6Me_4H) and the azadiborole **81**.

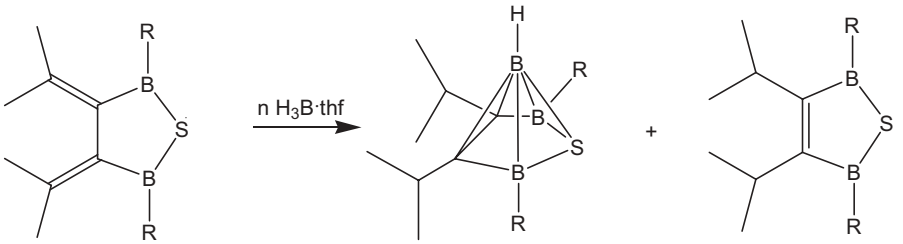

82 **83** **84**

Scheme 3.2-42. Hydroboration of 3,4-diisopropylidene-1-thia-2,5-diborolane **82** with thf·BH_3 forms the 2-thia-4,5-dicarba-*nido*-hexaborane **83** and small amounts of the thiadiborole **84**.

3.2.8.3 *Nido*- and *Hypho*-lithiacarboranes

Reduction of the triboracyclobutane **11a**, (Scheme 3.2-7), the 1,2,4-triboracyclopentane **86a**, and the 1,3,5-triboracyclohexane **87** with elemental Li gives the lithium salts of the corresponding dianions $\mathbf{10a}^{2-}$, $\mathbf{86a}^{2-}$ and $\mathbf{87}^{2-}$, respectively [20, 22, 102]. The dianion $\mathbf{86b}^{2-}$ is obtained by addition of phenyllithium to the anion of **12b** (Scheme 3.2-43) [44].

Crystal structures show that the new Li compounds are contact ion pairs. Lithium cations are coordinated side-on to B–B σ bonds in compounds containing such building blocks, i.e., in contact ion triples of $\mathbf{10a}^{2-}$ and $\mathbf{86a,b}^{2-}$ (Figure 3.2-6). B–B moieties involved in π bonding and carrying a partial negative charge are strong donor ligands: side-on coordination of lithium cations has been computed to be strongly preferred over a sandwich type coordination in the prototypical dilithium salt of $(BH)_3^{2-}$ (**M** in Figure 3.2-2) [6]. In the absence of noncoordinated B–B σ bonds, lithium cations coordinate to C–B σ bonds, as seen in $\mathbf{86a,b}^{2-}$ [22] and $\mathbf{87}^{2-}$ [103].

In salts of dianions containing bulky substituents, the coordination sphere at the lithium cations is completed by THF solvent molecules. However, dianions without sterically demanding substituents are much stronger ligands than ether molecules, as indicated by the tetrameric structure of the dilithium salts of $\mathbf{87}^{2-}$. Depending on the donor ligands {tetrahydropyrane (thp), [12]crown-4([12]cr-4)} the crystalline tetrameric cluster compounds $[Li(thp)_2Li\mathbf{87}]_4$ and $\{Li[12]cr\text{-}4\}_4(Li\mathbf{87})_4$ are obtained. X-ray structure analyses [103] of the latter prove the presence of tetrameric aggregates in which four $[(MeCH)_3(BMe)_3]^{2-}$ clusters (20 SE, *hypho*) are bridged by four Li cations. In $[Li(thp)_2Li\mathbf{87}]_4$ each unit has one terminal lithium ion coordinated by two thp donors. Figure 3.2-6 shows the molecular structure of the tetrameric aggregates in which each of the four bridging lithium centers connect two C_2B faces. The B_3 ring exhibits different BB bond lengths. Attempts to prepare the monomeric unit $[(MeCH)_3(BMe)_3Li_3(thp)_6]^+$ with the expected *hypho* structure have failed [103].

Besides the tetrameric aggregates with lithium ions, a polymeric meander-like

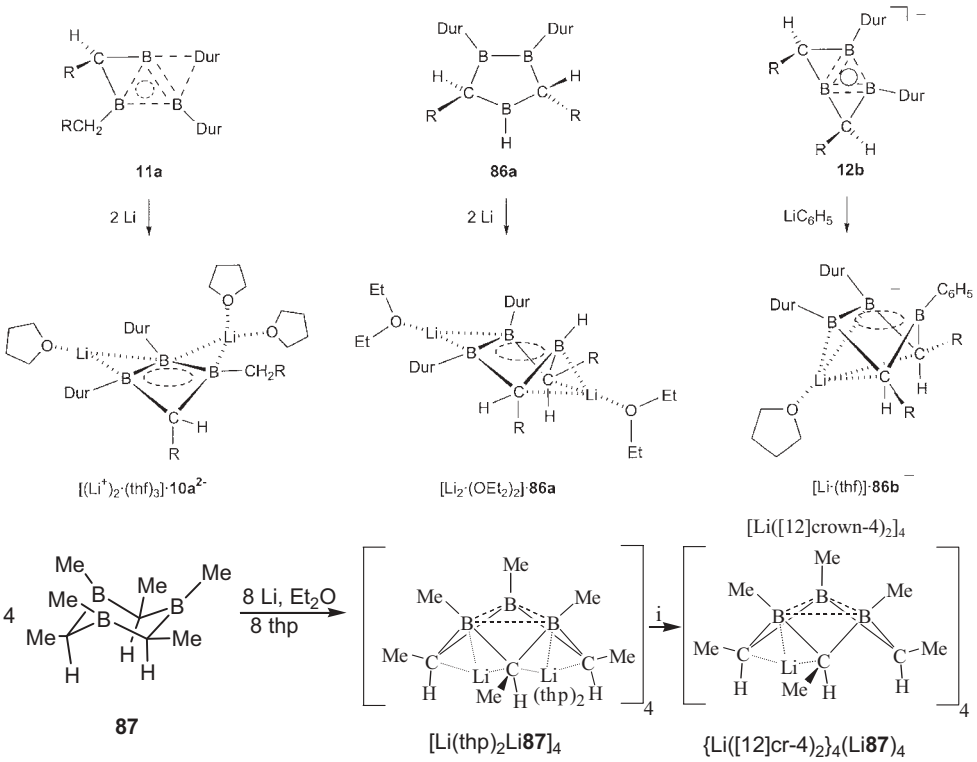

Scheme 3.2-43. Reactions of lithium in donor solvents with **11a**, **86a**, and the 1,3,5-triboracyclohexane **87** lead to the formation of mono-, bis-, and trishomoaromatic contact ion triples $(Li^+)_2(thf)_3$ $\mathbf{10a}^{2-}$, $[Li_2(OEt_2)_2]\mathbf{86a}$, and tetrameric $[Li(thp)_2Li\mathbf{87}]_4$, respectively. The latter reacts with crown ether (i = [12]cr-4) to give $\{Li([12]cr\text{-}4)_2\}_4(Li\mathbf{87})]_4$. $[Li(thf)]\mathbf{86b}^-$ is obtained from **12b** and PhLi.

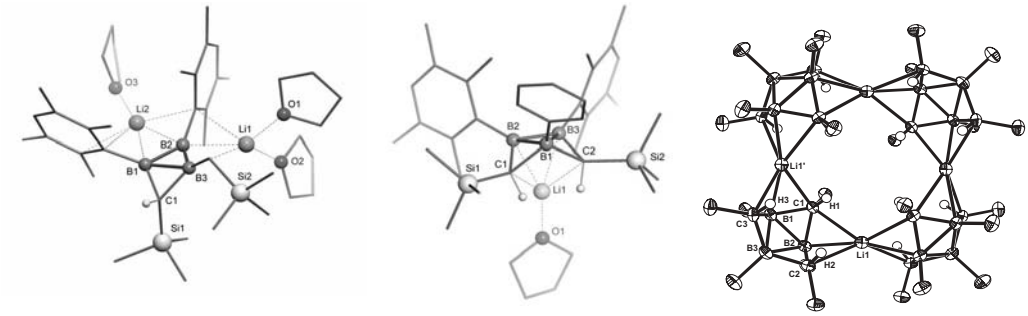

$[(Li^+)_2(thf)_3]\mathbf{10a}^{2-}$ $[Li(thf)]\mathbf{86b}^-$ $\{[Li\mathbf{87}]_4\}^{4-}$

Fig. 3.2-6. Structures of the mono- and bishomoaromatics, $[(Li^+)_2(thf)_3]\mathbf{10a}^{2-}$, $[Li(thf)]\mathbf{86b}^-$, and tetrameric trishomoaromatic $\{[Li\mathbf{87}]_4\}^{4-}$.

chain or a complex tetramer with sodium, and a zigzag-chain polymer with potassium are established by X-ray diffraction analyses. The set of dianions shows characteristic NMR chemical shifts (^{1}H, ^{11}B, ^{13}C) in the low frequency region. The computed nucleus-independent chemical shift (NICS) values prove the homoaromatic character of the reduced triboraheterocycles, which show remarkable stabilization energy towards the corresponding, nonaromatic species [103]. Interestingly, the homoaromatic character in reduced **87** is based on the overlap of three almost sp^3 hybrid orbitals, resulting in three-center π,σ-distorted bonding (see also Figure 3.2-2).

On the other hand, the mono-, bis- and trishomoaromatic (**N**, **O**, **P**) species are formally derived from the triborirane dianion **M** by successive incorporation of methylene bridges into the ring.

With an increasing number of methylene bridges the p character of the 3c2e bond hybrids decreases from 100% in **M** to 76% in **P** with increasing s character (24% in **P**), the accompanying change of π bonding distorted towards σ is symbolized in **M** → **P** by a full circle → dashed circle → dashed triangle) (Figure 3.2-7). The alternative cluster description of the dianions **M** to **P** indicates the changes in the number of SE (skeletal electrons) and structures from **M** (8 SE, *closo*) to **N** (12 SE, *nido*) to **O** (16 SE, *arachno*) and to **P** (20 SE, *hypho*).

The influence of the lithium ions on the structures and bonding of the above discussed compounds is shown in Scheme 3.2-43 and Figure 3.2-6.

As the lithium ions in $[(Li^+)_2(thf)_3\mathbf{10a}^{2-}]$ bridge two B–B edges they do not occupy vertices, the ion pair and its dianion $\mathbf{10a}^{2-}$ have similar (12 SE) *nido* structures. For $[Li_2(OEt_2)_2\mathbf{86a}]$ and $[Li(thf)\mathbf{86b}^-]$ one would expect *arachno* structures (16 SE, compare **O**). Although the X-ray diffraction studies exhibit different structures as a consequence of the coordinating ligands (Et_2O, THF) at lithium, both clusters incorporate one lithium cation into the framework having 16 SE. This increases the number of vertices to $n = 6$ and classifies both derivatives as *nido* and not as *arachno* clusters based on **O** (Figure 3.2-7).

Insertion of a third methylene bridge into **M** leads to *hypho* **P** with 20 SE. The tetrameric species $[Li(thp)_2Li\mathbf{87}]_4$ and $\{Li([12]cr\text{-}4)_2\}_4(Li\mathbf{87})_4$ suggest that one Li^+ has to be assigned to each $[(MeCH)_3BMe]_3{}^{2-}$ *arachno* cluster. The former is coordinated by two C–B bonds of the neighboring cluster [103]. This increases the total

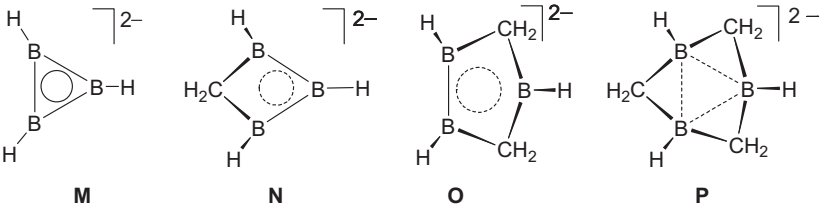

Fig. 3.2-7. The different types of 3c bonding in the dianions $[(BH)_3]^{2-}$ (**M**), $[CH_2(BH)_3]^{2-}$ (**N**), $[(CH_2)_2(BH)_3]^{2-}$ (**O**), and $[(CH_2)_3(BH)_3)]^{2-}$ (**P**) are symbolized by a full circle (pure π, **M**), a dashed circle (π,σ-distorted, **N** and **O**) or a dashed triangle (essentially σ, **P**).

number of SE from 20 to 22 (and the skeletal atoms from six to seven) suggesting a *hypho* species ($2n + 8$ SE). Incorporation of $[Li(thp)_2]^+$ into $(Li\mathbf{87})^-$ increases the number of SE to 24 and that of cluster atoms n to eight, resulting in a *hypho* structure. As a consequence these bis- and trishomoaromatics are described in this chapter as heteroatom-carboranes. However, as discussed in Section 3.2.2.5 and above, the monohomoaromatics are not lithiacarboranes but dilithio bridged carboranes.

3.2.9 Conclusions

Multicenter bonding is the key to understanding carboranes. The series $[CB_nH_{n+1}]^-$ and $C_2B_nH_{n+2}$ (Schemes 3.2-44) contain mainly polyhedral clusters (trigonal bipyramids **15** and **39**, octahedral $[CB_5H_6]^-$ and $C_2B_4H_6$, icosahedra $[CB_{11}H_{12}]^-$ and $C_2B_{10}H_{12}$) which are three-dimensional σ aromatics, however, the series start with two-dimensional π aromatics (diboriranide **2** and borirene C_2BH_3). The border between these areas is occupied by the puckered four-membered compounds **3** and **28**, which may be described as non-planer aromatics having π,σ-distorted 4c bonding as well as clusters with distorted *closo*-tetrahedrane structures.

The power of 2e aromaticity explains why non-classical structures such as **1c**, **3**, **6**, **11**, **33** and **36** are strongly preferred over their classical, nonaromatic forms (Scheme 3.2-44).

Carboranes containing one, two or more carbon and up to six boron atoms have been shown to be much more stable with organyl groups than with hydrogen substituents. In particular B–ethyl groups stabilize carboranes kinetically with re-

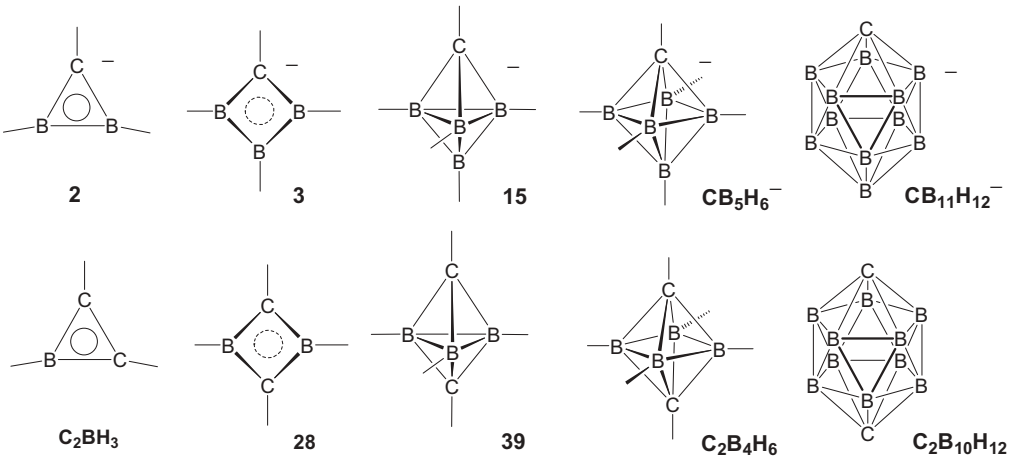

Scheme 3.2-44. From two-dimensional π aromatics (planar **2**, **C_2BH_3**) to three-dimensional σ aromatics (polyhedral **15**, **39** and higher members of the series) via folded aromatics (**3**, **28**) connecting both classes.

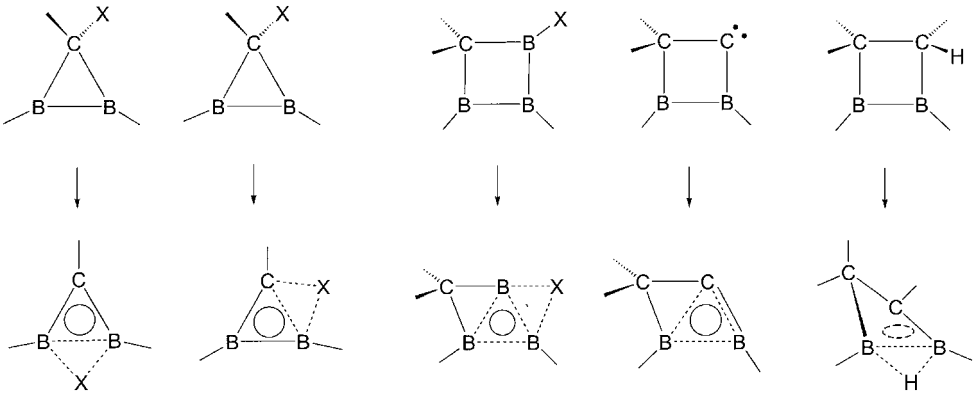

Scheme 3.2-45. Non-classical 2e aromatic structures (bottom) are preferred over classical structures (top). Full circles represent two π electrons, the dashed triangles symbolize 3c2e σ bonds and the dashed circle depicts the intermediate situation of a π,σ-distorted 3c2e bond.

spect to further rearrangements and potential degradation of the carborane cluster. Ethyl substituents at boron appear to offer a two-fold advantage: (1) dehydroboration, leading to B–H units and ethene, is not to be expected at temperatures below 250 °C (in strong contrast with propyl or butyl groups), and (2) ethyl groups are of the appropriate size (better than methyl groups) to protect the boron atoms against most intra- or intermolecular reactions. Exceptions are hydride-catalyzed processes. The formation of carboranes in the ''hydride bath'' takes advantage of these properties of B–ethyl groups. The steric demand of the ethyl groups prevent a strong association in the diborane(6) derivatives via B–H–B bonds and allows for B–H catalyzed exchange processes, which finally leads to self-assembling of organoboranes to carboranes. Apparently, compounds or intermediates with two and three diethylboryl groups attached to one carbon atom can readily rearrange, under the influence of the ''hydride bath'', into carboranes containing one, two, three, four or six carbon atoms in various vertex positions. The presence of B–ethyl and often also of C–alkyl groups may lead to structures of carboranes which do not always follow the empirical rules that were established for the parent compounds (Scheme 3.2-46).

Dehalogenation of unsaturated organohalogenoboranes also leads to *nido*-C_4B_2 and *nido*-C_4B_4 carboranes. The *nido*-C_5B cluster's apex boron forms very strong bonds with Lewis acids BX_3.

Hydroboration of unsaturated diboraheterocycles have been used to prepare *nido*-C_3B_3(7) carboranes (**55**) and hydroboration of diboraheterocycles (X = NMe, S) allowed the formation of the corresponding *nido*-heterocarboranes with the XC_2B_3 frameworks (Scheme 3.2-47).

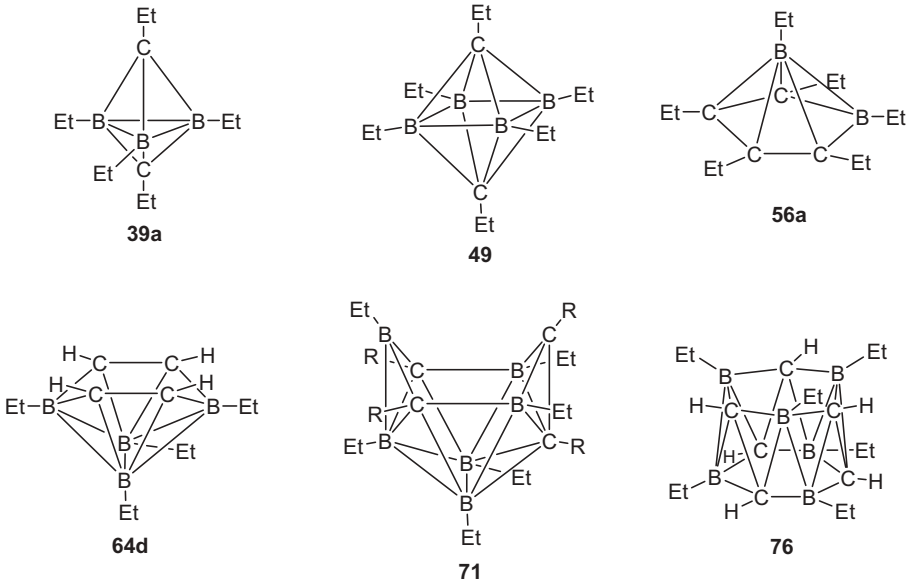

Scheme 3.2-46. *Closo*- (**39a**, **49**) and *nido*-carboranes (**56a**, **64d**, **71**) and drum-like **76**, an *arachno*-carborane.

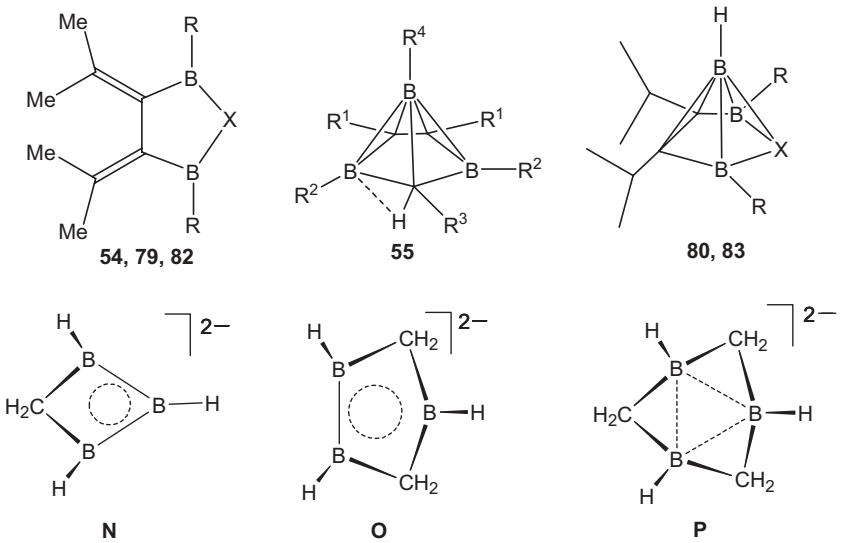

Scheme 3.2-47. Transformation of boron heterocycles (**54**, **79**, **82**, X = CHR, NR, S) to *nido*-carboranes **55**, **80** (X = NR) and **83** (X = S). Mono-, bis-, and trishomoaromatics **N**, **O**, and **P**.

Lithiacarboranes are obtained when 1,2,4-triboracyclopentanes and 1,3,5-triboracyclohexanes are reacted with elemental Li in donor solvents. In the contact ion pairs Li ions coordinate to B–B and B–C bonds depending on the number of methylene bridges in bis- and trishomoaromatic species (**O**, **P**). The 3c2e bonds in **N**, **O** are described as π,σ-distorted (indicated as dashed circles) and the overlapping sp^3 hybrid orbitals in **P** practically yield σ bonding (dashed triangle). Derivatives of **N**, **O**, and **P** fully characterized by X-ray structure analyses, are presented.

References

1 R. E. Williams, *Early Carboranes and Their Structural Legacy*, in *Adv. Organomet. Chem.*, **1994**, *36*, 1–55.

2 K. Wade, *Chem. Commun.*, **1971**, 792; K. Wade, *Adv. Inorg. Chem. Radiochem.*, **1976**, *18*, 1; D. M. P. Mingos, *Nature Phys. Sci.*, **1972**, *99*, 236; D. M. P. Mingos, *Adv. Organomet. Chem.*, **1977**, *15*, 1.

3 R. E. Williams, *Adv. Inorg. Chem. Radiochem.*, **1976**, *18*, 67; K. Krogh-Jespersen, D. Cremer, D. Poppinger, J. A. Pople, P. von R. Schleyer, J. Chandrasekhar, *J. Am. Chem. Soc.*, **1979**, *101*, 4843.

4 A. Berndt, D. Steiner, D. Schweikart, C. Balzereit, M. Menzel, H.-J. Winkler, S. Mehle, M. Unverzagt, T. Happel, P. von R. Schleyer, G. Subramanian, M. Hofmann, in *Advances in Boron Chemistry*, W. Siebert, ed., Royal Society of Chemistry, Cambridge, **1997**, p. 61.

5 K. Sorger, P. von R. Schleyer, *THEOCHEM*, **1995**, *338*, 317 and literature cited therein; S. Fau, G. Frenking, *THEOCHEM*, **1995**, *338*, 117.

6 A. A. Korkin, P. v. R. Schleyer, M. L. McKee, *Inorg. Chem.*, **1995**, *34*, 961.

7 M. Hofmann, D. Scheschkewitz, A. Ghaffari, G. Geiseler, W. Massa, H. F. Schaefer III, A. Berndt, *J. Mol. Model.*, **2000**, *6*, 257–271.

8 (a) J. Chandrasekhar, E. D. Jemmis, P. v. R. Schleyer, *Tetrahedron Lett.*, **1979**, 3707–3710. (b) A. B. McEwen, P. v. R. Schleyer, *J. Org. Chem.*, **1986**, *51*, 4357–4368. (c) P. v. R. Schleyer, A. H. Otto, J. Gauss, F. Reichel, D. Cremer, *J. Phys. Org. Chem.*, **1993**, *6*, 445–464. (d) P. v. R. Schleyer, H. Jiao, M. N. Glukhovtsev, J. Chandrasekhar, E. Kraka, *J. Am. Chem. Soc.*, **1994**, *116*, 10129–10134.

9 (a) MOLEKEL 4.0, P. Flükiger, H. P. Lüthi, S. Portmann, J. Weber, Swiss Center for Scientific Computing, Manno (Switzerland), **2000**. (b) A. E. Reed, L. A. Curtiss, F. Weinhold, *Chem. Rev.*, **1988**, *88*, 899–926.

10 K. Krogh-Jespersen, D. Cremer, J. D. Dill, J. A. Pople, P. v. R. Schleyer, *J. Am. Chem. Soc.*, **1981**, *103*, 2589.

11 M. Bremer, P. von R. Schleyer, U. Fleischer, *J. Am. Chem. Soc.*, **1989**, *111*, 1147, and literature cited therein.

12 (a) H. M. Budzelaar, K. Krogh-Jespersen, T. Clark, P. v. R. Schleyer, *J. Am. Chem. Soc.*, **1985**, *107*, 2773. (b) P. v. R. Schleyer, K. Najafian, *Inorg. Chem.*, **1998**, *37*, 3454, and literature cited therein. (c) A. A. Fokin, B. Kiran, M. Bremer, X. Yang, H. Jiao, P. v. R. Schleyer, P. R. Schreiner, *Chem. Eur. J.*, **2000**, *6*, 1615–1628. (d) R. B. King, P. v. R. Schleyer, Chapter 1 of this book. (e) D. Cremer, J. Gauss, *J. Am. Chem. Soc.*, **1986**, *108*, 7467–7477; D. Cremer, *Tetrahedron*, **1988**, *44*, 7427–7454.

13 A. Berndt, *Angew. Chem.*, **1993**, *105*, 1034; *Angew. Chem., Int. Ed. Engl.*, **1993**, *32*, 985, and literature cited therein.

14 M. Pilz, J. Allwohn, W. Massa, A. Berndt, *Angew. Chem.*, **1990**, *102*, 436; *Angew. Chem. Int., Ed. Engl.*,

1990, *29*, 399; M. Menzel, H.-J. Winkler, T. Ablelom, D. Steiner, S. Fau, G. Frenking, W. Massa, A. Berndt, *Angew. Chem.*, **1995**, *107*, 1476; *Angew. Chem., Int. Ed. Engl.*, **1995**, *34*, 1340.

15 M. Menzel, D. Steiner, H.-J. Winkler, D. Schweikart, S. Mehle, S. Fau, G. Frenking, W. Massa, A. Berndt, *Angew. Chem.*, **1995**, *107*, 368; *Angew. Chem., Int. Ed. Engl.*, **1995**, *34*, 327.

16 R. Wehrmann, H. Meyer, A. Berndt, *Angew. Chem.*, **1985**, *97*, 779; *Angew. Chem., Int. Ed. Engl.*, **1985**, *24*, 788, and literature cited therein.

17 H. Meyer, G. Schmidt-Lukasch, G. Baum, W. Massa, A. Berndt, *Z. Naturforsch.*, **1988**, *43b*, 801.

18 Y. Sahin, C. Präsang, P. Amseis, M. Hofmann, G. Geiseler, W. Massa, A. Berndt, *Angew. Chem.*, **2003**, *115*, 693; *Angew. Chem., Int. Ed. Engl.*, **2003**, *42*, 669.

19 Y. Sahin, C. Präsang, M. Hofmann, G. Subramanian, G. Geiseler, W. Massa, A. Berndt, *Angew. Chem.*, **2003**, *115*, 695; *Angew. Chem., Int. Ed. Engl.*, **2003**, *42*, 671.

20 P. Amseis, W. Mesbah, C. Präsang, M. Hofmann, G. Geiseler, W. Massa, A. Berndt, *Organometallics*, **2003**, *22*, 1594.

21 D. Steiner, H.-J. Winkler, C. Balzereit, T. Happel, M. Hofmann, G. Subramanian, P. v. R. Schleyer, W. Massa, A. Berndt, *Angew. Chem.*, **1996**, *108*, 2123; *Angew. Chem., Int. Ed. Engl.*, **1996**, *35*, 1990.

22 D. Scheschkewitz, A. Ghaffari, P. Amseis, M. Unverzagt, G. Subramanian, M. Hofmann, P. v. R. Schleyer, H. F. Schaefer III, G. Geiseler, W. Massa, A. Berndt, *Angew. Chem.*, **2000**, *112*, 1329; *Angew. Chem., Int. Ed. Engl.*, **2000**, *39*, 1272.

23 B. T. King, B. C. Noll, A. J. McKinley, J. Michl, *J. Am. Chem. Soc.*, **1996**, *118*, 10902.

24 J. Jaballas, T. Onak, *J. Organomet. Chem.* **1998**, *550*, 101 and references cited therein.

25 B. Stibr, O. L. Tok, W. Milius, M. Barkardjiev, J. Holub, D. Hnyk, B. Wrackmeyer, *Angew. Chem.*, **2002**, *114*, 2230; *Angew. Chem., Int. Ed. Engl.*, **2002**, *41*, 2126 are literature cited therein.

26 A. Franken, D. L. Ormsby, C. A. Kilner, W. Clegg, M. Thornton-Pett, J. D. Kennedy, *J. Chem. Soc., Dalton Trans.*, **2002**, 2807.

27 (a) D. Stasko, C. A. Reed, *J. Am. Chem. Soc.*, **2002**, *124*, 1148–1149. (b) C. A. Reed, K.-C. Kim, R. D. Bolskar, L. Mueller, *Science*, **2000**, *289*, 101–104.

28 A. Neu, K. Radacki, P. Paetzold, *Angew. Chem.*, **1999**, *111*, 1358; *Angew. Chem., Int. Ed. Engl.*, **1999**, *38*, 1281.

29 R. Köster, G. Benedikt, M. A. Grassberger, *Justus Liebigs Ann. Chem.*, **1968**, *719*, 187–209.

30 M. A. Fox, R. Greatrex, M. Hofmann, P. v. R. Schleyer, *Angew. Chem.*, **1994**, *106*, 2384–2386; *Angew. Chem., Int. Ed. Engl.*, **1994**, *33*, 2298–2300.

31 R. Köster, G. Bruno, P. Binger, *Liebigs Ann. Chem.* **1961**, *644*, 1.

32 B. Wrackmeyer, H.-J. Schanz, W. Schüßler, R. Köster, *Fresenius' J. Anal. Chem.*, **1998**, *362*, 378–381.

33 R. Köster, G. Seidel, B. Wrackmeyer, *Angew. Chem.*, **1994**, *106*, 2380; *Angew. Chem., Int. Ed. Engl.*, **1994**, *33*, 2294.

34 B. Gangnus, H. Stock, W. Siebert, M. Hofmann, P. v. R. Schleyer, *Angew. Chem.*, **1994**, *106*, 2383–2384; *Angew. Chem., Int. Ed. Engl.*, **1994**, *33*, 2296–2298.

35 R. Köster, R. Boese, B. Wrackmeyer, H.-J. Schanz, *Chem. Commun.*, **1995**, 1691.

36 B. Wrackmeyer, H.-J. Schanz, *Collect. Czech. Chem. Commun.*, **1997**, *62*, 1254.

37 M. McKee, *Inorg. Chem.*, **2000**, *39*, 4206 and literature cited therein.

38 S. M. van der Kerk, P. H. M. Budzelaar, A. van der Kerk-van Hoof, G. J. M. van der Kerk, P. v. R. Schleyer, *Angew. Chem.*, **1983**, *95*, 61; *Angew. Chem., Int. Ed. Engl.*, **1983**, *22*, 48.

39 B. Wrackmeyer, G. Kehr, *Polyhedron*, **1991**, *10*, 1497–1506.

40 M. Hildenbrand, H. Pritzkow, U. Zenneck, W. Siebert, *Angew. Chem.*, **1984**, *96*, 371–372; *Angew. Chem., Int. Ed. Engl.*, **1984**, *23*, 371.

41 P. Hornbach, M. Hildenbrand, H. Pritzkow, W. Siebert, *Angew. Chem.*, **1986**, *98*, 1121; *Angew. Chem., Int. Ed. Engl.*, **1986**, *25*, 1112.

42 M. Hildenbrand, H. Pritzkow, W. Siebert, *Angew. Chem.*, **1985**, *97*, 769; *Angew. Chem., Int. Ed. Engl.*, **1985**, *24*, 759.

43 H. Irngartinger, J. Hauck, W. Siebert, M. Hildenbrand, *Z. Naturforsch.*, **1991**, *46b*, 152–155.

44 M. Unverzagt, G. Subramanian, M. Hofmann, P. von R. Schleyer, S. Berger, K. Harms, W. Massa, A. Berndt, *Angew. Chem.*, **1997**, *109*, 1567; *Angew. Chem., Int. Ed. Engl.*, **1997**, *36*, 1469.

45 B. Wrackmeyer, H.-J. Schanz, W. Milius, *Angew. Chem.*, **1997**, *109*, 98–99; *Angew. Chem., Int. Ed. Engl.*, **1997**, *36*, 75.

46 D. Steiner, C. Balzereit, H.-J. Winkler, N. Stamatis, M. Hofmann, P. v. R. Schleyer, W. Massa, A. Berndt, *Angew. Chem.*, **1994**, *106*, 2391; *Angew. Chem., Int. Ed. Engl.*, **1994**, *33*, 2303.

47 A. Krämer, J.-K. Uhm, S. E. Garner, W. Pritzkow, W. Siebert, *Z. Naturforsch.*, **1990**, *45b*, 1017.

48 R. Littger, H. Nöth, M. Thomann, M. Wagner, *Angew. Chem.*, **1993**, *105*, 275; *Angew. Chem., Int. Ed. Engl.*, **1993**, *32*, 295.

49 R. Köster, H.-J. Horstschäfer, P. Binger, P. K. Mattschei, *Justus Liebigs Ann. Chem.*, **1975**, 1339–1356; R. Köster, G. W. Rotermund, *Tetrahedron Lett.*, **1964**, 1667.

50 R. Köster, R. Boese, B. Wrackmeyer, H.-J. Schanz, *J. Chem. Soc., Chem. Commun.*, **1995**, 1691–1692.

51 H. Nöth, B. Wrackmeyer, *Nuclear Magnetic Resonance Spectroscopy of Boron Compounds*, in *NMR – Basic Principles and Progress*, P. Diehl, E. Fluck, R. Kosfeld, eds., Vol. 14, Springer Verlag, Berlin-Heidelberg-New York, **1978**.

52 R. Köster, B. Wrackmeyer, *Z. Naturforsch.*, **1981**, *36b*, 704.

53 M. Antipin, R. Boese, D. Blaeser, A. Maulitz, *J. Am. Chem. Soc.*, **1997**, *119*, 326–333.

54 P. v. R. Schleyer, G. Subramanian, A. Dransfeld, *J. Am. Chem. Soc.*, **1996**, *118*, 9988–9989.

55 M. J. Bayer, H. Pritzkow, W. Siebert, *Eur. J. Inorg. Chem.*, **2002**, 1293–1300.

56 D. Bromm, U. Seebold, M. Noltemeyer, A. Meller, *Chem. Ber.*, **1991**, *124*, 2645–2649; W. Maringgele, H. Knop, D. Bromm, A. Meller, S. Dielkus, R. Herbst-Irmer, G. M. Sheldrick, *Chem. Ber.*, **1992**, *125*, 1807–1813.

57 M. Unverzagt, H.-J. Winkler, M. Brock, M. Hofmann, P. R. Schleyer, W. Massa, A. Berndt, *Angew. Chem.*, **1997**, *109*, 879; *Angew. Chem., Int. Ed. Engl.*, **1997**, *36*, 853.

58 M. Hofmann, M. A. Fox, R. Greatrex, R. E. Williams, P. v. R. Schleyer, *J. Organomet. Chem.*, **1998**, *550*, 331.

59 R. B. Maynard, L. Borodinsky, R. N. Grimes, *Inorg. Synth.*, **1983**, *22*, 211; R. N. Grimes, *Collect. Czech. Chem. Commun.*, **2002**, *67*, 679–727.

60 N. S. Hosmane, J. A. Maguire, *J. Cluster Sci.*, **1993**, *4*, 297; A. K. Saxena, J. A. Maguire, N. S. Hosmane, *Chem. Rev.*, **1997**, *97*, 2421.

61 B. Wrackmeyer, H.-J. Schanz, W. Milius, C. McCammon, *Collect. Czech. Chem. Commun.*, **1999**, *64*, 977.

62 R. N. Grimes, C. L. Bramlett, N. L. Vance, *Inorg. Chem.*, **1968**, *7*, 1066.

63 M. A. Fox, R. Greatrex, A. Nikrahi, *Chem. Soc. Commun.*, **1996**, 175.

64 A. Burke, D. Ellis, B. T. Giles, B. E. Hodson, S. A. Macgregor, G. M. Rosair, A. J. Welch, *Angew. Chem.*, **2003**, *115*, 235–238; *Angew. Chem., Int. Ed. Engl.*, **2003**.

65 G. Zi, H. W. Li, Z. Xie, *J. Chem. Soc., Chem. Commun.*, **2001**, 1110.

66 R. N. Grimes, C. L. Bramlett, N. L. Vance, *Inorg. Chem.*, **1968**, *7*, 1066.

67 J. Zwecker, Th. Kuhlmann, H. Pritzkow, W. Siebert, U. Zenneck, *Organometallics* **1988**, *7*, 2316; Th. Kuhlmann, H. Pritzkow, U. Zenneck, W. Siebert, *Angew. Chem.*, **1984**, *96*, 994; *Angew. Chem., Int. Ed. Engl.*, **1984**, *23*, 965.

68 A. Feßenbecker, A. Hergel, R. Hettrich, V. Schäfer, W. Siebert, *Chem. Ber.*, **1993**, *126*, 2205.

69 W. Siebert, R. Hettrich, H. Pritzkow, *Angew. Chem.*, **1994**, *106*, 215; *Angew. Chem., Ind. Ed. Engl.*, **1993**, *33*, 203.

70 B. Wrackmeyer, H.-J. Schanz, *Main Group. Met. Chem.*, **1998**, *21*, 29.

71 (a) H.-J. Schanz, Dissertation, Universität Bayreuth, 1997. (b) B. Wrackmeyer, H.-J. Schanz, M. Hofmann, P. v. R. Schleyer, *Angew. Chem.*, **1998**, *108*, 1329–1331; *Angew. Chem., Int. Ed. Engl.*, **1998**, *37*, 1245.

72 (a) P. Binger, *Tetrahedron Lett.*, **1966**, 2675. (b) R. Köster, M. A. Grassberger, *Angew. Chem.*, **1967**, *79*, 197; *Angew. Chem., Int. Ed. Engl.*, **1967**, *6*, 218.

73 T. Onak, G. T. F. Wong, *J. Am. Chem. Soc.*, **1970**, *92*, 5226.

74 B. Wrackmeyer, A. Glöckle, *Z. Naturforsch. Teil B*, **1996**, *51*, 859.

75 M. Herberhold, U. Bertholdt, W. Milius, A. Glöckle, B. Wrackmeyer, *Chem. Commun.* **1996**, 1219–1220.

76 B. Wrackmeyer, G. Kehr, *J. Organomet. Chem.*, **1995**, *501*, 87.

77 B. Wrackmeyer, A. Glöckle, G. Kehr, *Phosphorus, Sulfur, Silicon*, **1997**, *131*, 25.

78 B. Wrackmeyer, A. Glöckle, *Main Group. Met. Chem.*, **1997**, *20*, 181.

79 G. E. Herberich, H. Ohst, H. Meyer, *Angew. Chem.*, **1984**, *96*, 975; *Angew. Chem., Int. Ed. Engl.*, **1984**, *23*, 969.

80 W. N. Lipscomb, *Science*, **1966**, *153*, 373.

81 Y. Nie, S. Schwiegk, H. Pritzkow, W. Siebert, *Eur. J. Inorg. Chem.*, **2003**, in press.

82 C. Balzereit, H.-J. Winkler, W. Massa, A. Berndt, *Angew. Chem.*, **1994**, *106*, 2394; *Angew. Chem., Int. Ed. Engl.*, **1994**, *33*, 2306.

83 T. P. Fehlner, *J. Am. Chem. Soc.*, **1977**, *99*, 8355; *ibid* **1986**, *102*, 3426.

84 M. G. L. Mirabelli, L. G. Sneddon, *Organometallics*, **1986**, *5*, 1510.

85 W. Siebert, M. El Din, M. Essawi, *Chem. Ber.*, **1979**, *112*, 1480.

86 W. Siebert, A. Maier, unpublished.

87 B. Wrackmeyer, H.-J. Schanz, W. Milius, *Angew. Chem.*, **1997**, *109*, 1145; *Angew. Chem., Int. Ed. Engl.*, **1997**, *36*, 1117.

88 B. Wrackmeyer, H.-J. Schanz, M. Hofmann, P. v. R. Schleyer, R. Boese, *Eur. J. Inorg. Chem.*, **1999**, 533.

89 R. Köster, G. Seidel, B. Wrackmeyer, D. Bläser, R. Boese, M. Bühl, P. v. R. Schleyer, *Chem. Ber.*, **1991**, *124*, 2715.

90 B. Stibr, T. Jelinek, E. Drdakova, S. Hermanek, J. Plesek, *Polyhedron*, **1988**, *7*, 669–670.

91 R. Köster, G. Seidel, B. Wrackmeyer, *Angew. Chem.*, **1984**, *96*, 520; *Angew. Chem., Int. Ed. Engl.*, **1984**, *23*, 512; R. Köster, G. Seidel, B. Wrackmeyer, *Angew. Chem.*, **1985**, *97*, 317; *Angew. Chem., Int. Ed. Engl.*, **1985**, *24*, 326.

92 P. Jutzi, A. Seufert, W. Buchner, *Chem. Ber.*, **1979**, *112*, 2488.

93 C. Dohmeier, R. Köppe, Ch. Robl, H. Schnöckel, *J. Organomet. Chem.*, **1995**, *487*, 127.

94 A. H. Cowley, V. Lomeli, A. Voigt, *J. Am. Chem. Soc.*, **1998**, *120*, 6401.

95 Ch. L. B. Macdonald, A. H. Cowley, *J. Am. Chem. Soc.*, **1999**, *121*, 12113.

96 P. Greiwe, A. Bethäuser, H. Pritzkow, Th. Kühler, P. Jutzi, W. Siebert, *Eur. J. Inorg. Chem.*, **2000**, 1927.

97 A. Y. Timoshkin, G. Frenking, *J. Am. Chem. Soc.*, **2002**, *124*, 7240.

98 B. Grüner, T. Jelinek, Z. Plzak, J. D. Kennedy, D. L. Ormsby, R. Greatrex, B. Stibr, *Angew. Chem.*, **1999**, *111*, 1922; *Angew. Chem., Int. Ed. Engl.*, **1999**, *38*, 1806.

99 P. Greiwe, V. Beez, H. Pritzkow, W. Siebert, *Eur. J. Inorg. Chem.*, **2001**, 381.

100 P. Greiwe, H. Pritzkow, W. Siebert, *Eur. J. Inorg. Chem.*, **2001**, 1599.

101 V. Beez, P. Greiwe, H. Pritzkow, M. Hofmann, P. v. R. Schleyer, W. Siebert, *Eur. J. Inorg. Chem.*, **1998**, 1775.

102 W. Lößlein, H. Pritzkow, P. v. R. Schleyer, L. R. Schmitz, W. Siebert, *Angew. Chem.*, **2000**, *112*, 1333.

103 W. Lößlein, H. Pritzkow, P. v. R. Schleyer, L. R. Schmitz, W. Siebert, *Eur. J. Inorg. Chem.*, **2001**, 1949.

3.3
Heteropolyboranes With the Heavier Group 14 Elements

Lars Wesemann and Narayan S. Hosmane

3.3.1
Introduction

This chapter will cover the compounds in which a group 14 element (E = Si, Ge, Sn, Pb) is incorporated into the polyhedral borane cage. Specifically, it will cover only those compounds in which a main group element is incorporated into the cage structure. Compounds in which the element is involved in an *exo*-polyhedral group bonded to the cage by standard 2c2e bonds or where the heteroatom is in a bridging group linking several polyhedra together will not be included.

Boranes are hydrides in which the boron atoms are incorporated into electron deficient polyhedral cages (see Chapter 2.1). A large number of main group elements have been incorporated into these polyhedral cages. Since most of the elements to be discussed are metals or metalloids, a vast majority of the compounds will be metallaboranes, in which the main group element functions as a capping group. Much of the insight into the bonding and reactivity of main group heteroboranes has been derived directly from structural data, mainly solid state X-ray diffraction analyses, thus, a great deal of emphasis will be placed on the results of structural studies. There have been a large number of reviews and monographs that cover earlier work on these compounds [1], and such work will be discussed only as background to current results or for the purposes of comparison. The cage geometries can range from closed polyhedra (*closo*-), to more open ones, derived by removing one (*nido*-), two (*arachno*-), or more vertices from the closed structures. The structures of heteroboranes composed of fused deltahedra can be predicted from the number of electron pairs involved in cage bonding, using a set of rules embodied in the Polyhedral Skeletal Electron Pair Theory [2a–c] (see Chapter 1.1.2). The number of electrons involved in cage bonding can be obtained by assuming that one valence electron of each cage hetero or boron atom is involved in a classical two-center two-electron bond with an *exo*-polyhedral hydrogen atom (or other group), leaving the remaining valence electrons (3 from each group 14 hetero atom and 2 from each boron atom) for cage bonding. In the case of a hetero atom carrying no substituent, two electrons for an *exo*-polyhedral electron pair have to be subtracted from the number of valence electrons contributed to cage bonding. The respective isolobal pairs are shown in Figure 3.3-1.

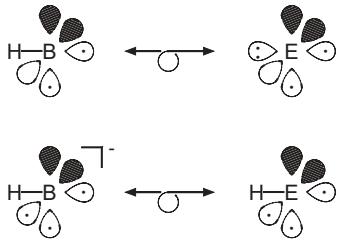

Fig. 3.3-1. Isolobal pairs between BH and group 14 element fragments.

In addition to the cage and terminal atoms, bridged hydrogens can also be present, which will each contribute one electron to the cage. If the cluster is anionic, the electrons imparting the overall charge to the cage are also assumed to be involved in cage bonding. These cage electrons are delocalized in a set of molecular orbitals (MOs) constructed from three atom based orbitals of each cage atom, one radially directed into the center of the cluster and the other two tangentially oriented. Using such rules, a borane of the formula $[(BH)_nH_b]^{c-}$ or a heteroborane with the general formula $[(EH)_a(BH)_{n-a}H_b]^{c-}$ having n vertices and b bridged hydrogens would have, respectively, $1/2[2n + b + c]$ or $1/2[2n + a + b + c]$ skeletal electron pairs (P). If $P = n + 1$, a *closo*-structure is expected, when $P = n + 2$ a *nido*-structure should be the most stable, $P = n + 3$, an *arachno*-structure, etc., can be predicted [2]. Thus, *closo*-boranes will have the general formula $[B_nH_n]^{2-}$ according to Wade's rules [2a]. Following the isolobal replacement of BH-units by the respective group 14 fragment, as shown in Figure 3.3-1, *closo*-heteroboranes are, for example, of the formula $[EB_nH_n]^{2-}$ (without a substituent on E) or $[(EH)_2B_nH_n]$. It should be noted that the replacement of a vertex by an isolobal and isoelectronic moiety should not materially affect intracage bonding or cluster geometry. In addition, the *exo*-polyhedral hydrogens could be replaced by any single bonding group without changing any of the above arguments. Using such isolobal and isoelectronic arguments, the electron counting rules can be extended to heteroboranes and to other clusters, including transition metal clusters [2d].

3.3.2
Syntheses of Heteropolyboranes With Heavier Group 14 Elements

The general structural trends in the group 14 heteroboranes can be understood in terms of a substitution of a $[B–H]^-$ group in a borane cage with the isoelectronic and isolobal E–R moiety (E = group 14 element, R = H or an *exo*-polyhedral group) (Figure 3.3-1). The net result of such a substitution in a borane would be a cage of similar structure but with one less negative charge. However, the substitution of a [BH] group against an isolobal unsubstituted hetero atom E results in no change of the charge. The vast majority of heteroboranes known belong to the group of 12 vertex *closo* and 11 vertex *nido*-clusters. So far smaller silaboranes have only been investigated theoretically [3].

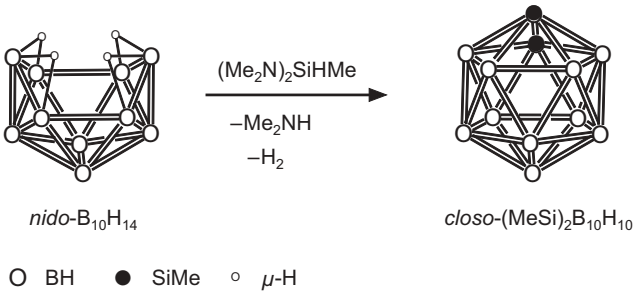

Scheme 3.3-1. Formation of 1,2-dimethyl-1,2-disila-*closo*-dodecaborane.

3.3.2.1

Twelve Vertex *Closo*-heteroboranes

Seyferth, and co-workers reported the synthesis of the disilaborane, 1,2-Me_2-*closo*-1,2-$Si_2B_{10}H_{10}$, in 15% yield, from the reaction of $B_{10}H_{14}$ and $Me(H)Si(NMe_2)_2$ in refluxing toluene (Scheme 3.3-1) [4, 5].

This disilaborane was an unexpected co-product in the synthesis of decaborane-alkylamine polymers. The Si_2B_{10} cluster core consists of a distorted icosahedron in which the two silicon atoms occupy adjacent positions. The Si–Si interatomic distance is 2.308(2) Å, which is slightly less than the Si–Si distance in organodisilanes (2.35 Å) and the Si–B distances [2.017(3) to 2.116(3) Å] are very close to the sum of the covalent radii of the two atoms (2.07 Å). Further derivatives with disilaborane cluster geometry are known for the phenyl substituted compounds 1,2-Ph_2-*closo*-1,2-$Si_2B_{10}H_{10}$ and 1-Me-2-Ph-*closo*-1,2-$Si_2B_{10}H_{10}$ [6, 7]. In addition to these disila-*closo*-dodecaborane clusters one example with two different group 14 elements as a part of the cluster core is known. In Scheme 3.3-2 the synthesis of this sila-stanna-*closo*-dodecaborate is shown. The structure of this heteroborate was determined in the solid state and the Si–Sn distance is 2.608(4) Å (Scheme 3.3-2) [8].

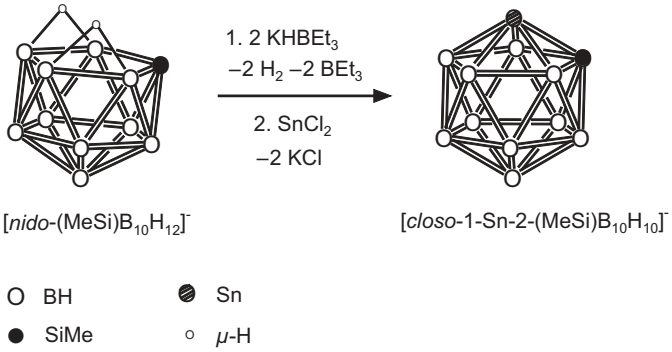

Scheme 3.3-2. Transformation of sila-*nido*-undecaborate into sila-stanna-*closo*-dodecaborate.

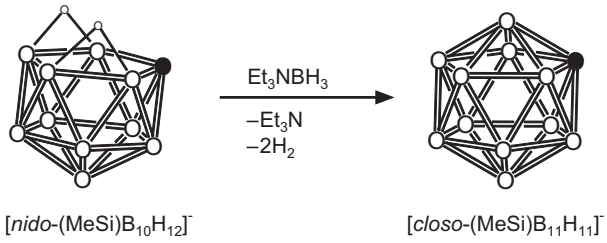

Scheme 3.3-3. Synthesis of sila-*closo*-dodecaborate.

Besides incorporation of other main group metals into the silaborate framework, the *nido*-borate $[MeSiB_{10}H_{12}]^-$ is also a versatile ligand towards transition metals. So far, four different coordination modes of the pentagonal open face have been reported [9–12]. Twelve vertex clusters with only one group 14 element in the cluster framework are known for the complete series of elements from carbon to lead. The monocarbon carborane was described over 30 years ago [13], while the monosilaborate $[1\text{-Me-}closo\text{-}1\text{-Si-}B_{11}H_{11}]^-$ has been synthesized more recently. Reaction of the *nido*-silaborate $[MeSiB_{10}H_{12}]^-$, with Et_3NBH_3 leads to the *closo*-monosilaborate $[1\text{-Me-}closo\text{-}1\text{-}SiB_{11}H_{11}]^-$ [14], which is the only reported synthesis of a *closo*-monosilaborane (Scheme 3.3-3).

This *closo*-silaborate could also be synthesized by the two atom cage expansion of the siladecaborane, $MeSiB_9H_{12}(NHMe_2)$ depicted in Scheme 3.3-4 [15, 16].

Salt elimination reactions proved to be very effective for the synthesis of *closo*-heteroborates with the heavy elements of this group. Todd and co-workers prepared for the first time the lead, tin and germanium cluster dianions $[EB_{11}H_{11}]^{2-}$ as shown in Scheme 3.3-5 [17].

These stanna- and germapolyboranes were found to react with MeI to give the $[closo\text{-}MeEB_{11}H_{11}]^-$ products, whose geometry was confirmed by the X-ray crys-

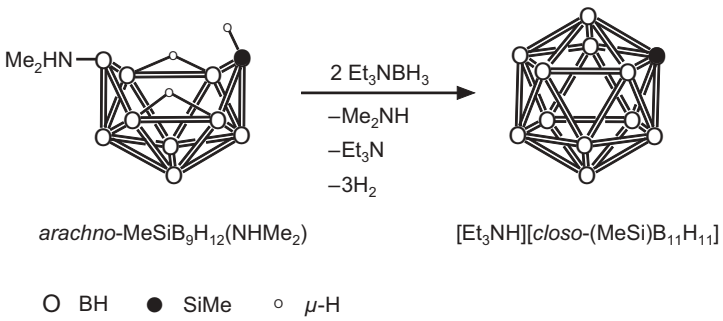

Scheme 3.3-4. Boron insertion into the siladecaborane skeleton.

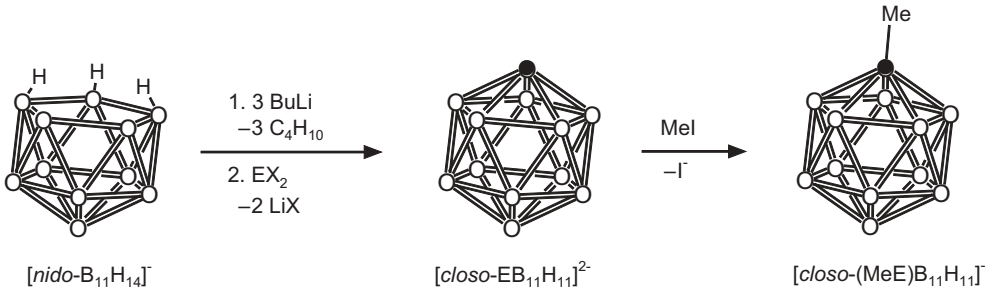

Scheme 3.3-5. Synthesis of hetero-*closo*-dodecaborates (Ge, Sn, Pb) and methylation reactions at the heteroatoms germanium and tin.

tallographic characterization of the respective methylstannaborate [17]. According to its ^{119}Sn Mössbauer spectrum the tin atom in $[MeSnB_{11}H_{11}]^-$ is in oxidation state +4. The methylation reactions (Scheme 3.3-5) are of interest, since these findings are an indicator for the nucleophilicity of the heteroatoms in the clusters $[closo\text{-}EB_{11}H_{11}]^{2-}$. This is in marked contrast to the corresponding stannacarboranes, 1,2,3-Sn$(CMe)_2B_9H_9$ and 1,2,3-Sn$(CSiMe_3)_2B_4H_4$, which have chemically inactive lone pairs at the Sn atoms [18, 19]. Apparently, stanna-*closo*-dodecaborate $[SnB_{11}H_{11}]^{2-}$ is strong enough in nucleophilicity to react with a variety of transition metal halides affording new derivatives with tin–metal bonds. Thus, the nucleophilic substitution of the chloride ions in (dppp)$PtCl_2$ leads to [(dppp)-Pt$(SnB_{11}H_{11})_2]^{2-}$ (Scheme 3.3-6). Furthermore the coordinated tinborate serves as a ligand in other platinum complexes which promote octene hydroformylation [20, 21, 22].

3.3.2.2
Eleven Vertex *Nido*-heteroboranes

Some 30 years ago, Loffredo and Norman reported the low yield preparation of $Me_2MB_{10}H_{12}$ (M = Ge, Sn) from the reaction of $NaB_{10}H_{13}$ with the alkyl halides, Me_2MCl_2 (M = Ge, Sn) [23]. Somewhat later the corresponding silicon compound, $Me_2SiB_{10}H_{12}$, was reported by the same authors [24] (Scheme 3.3-7). The silaborane was found to be less susceptible to Me_2M removal than either the Ge or the Sn analogues. The ^{11}B NMR spectra of the compounds were consistent with a structure in which the Me_2M moiety occupies a position on the open face of an 11-vertex *nido* structure, as shown in Scheme 3.3-7.

$Me_2SnB_{10}H_{12}$ was found to undergo cleavage reactions with molecular halogens to give Me_2SnX_2 and $B_{10}H_{12}X_2$ (X = Br_2 and I_2) [25]. Greenwood and Youll re-

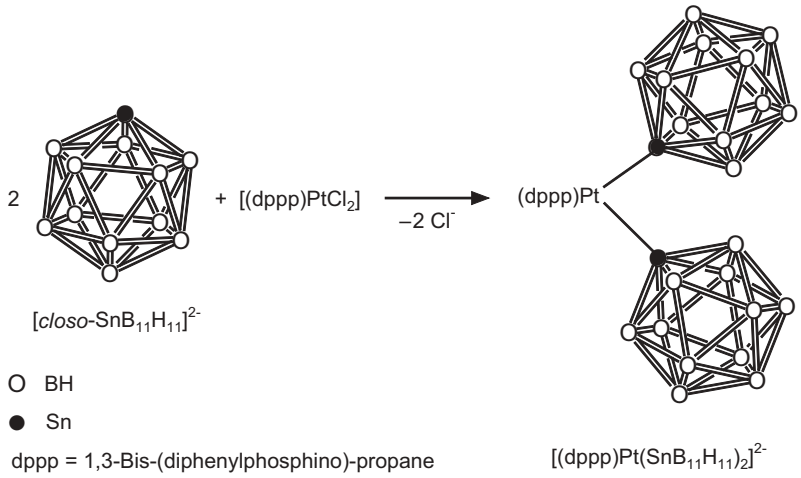

Scheme 3.3-6. Stanna-*closo*-dodecaborate coordination at platinum centers.

ported the synthesis of the corresponding dihalostannaborate, $[B_{10}H_{12}SnCl_2]^{2-}$ from the reaction of the $[Ph_4As]^+$ and $[Ph_3MeP]^+$ salt of $[B_{10}H_{12}]^{2-}$ with $SnCl_2$ [26]. The reaction of $SnCl_2$ with $Na_2[B_{10}H_{12}]$ proved ineffective, but weak coordinating cations, such as $[Ph_4As]^+$ and $[Ph_3MeP]^+$ increase polyborate reactivity. The ^{119}Sn Mössbauer spectrum of the resulting $[B_{10}H_{12}SnCl_2]^{2-}$ revealed the presence of a tin atom in the oxidation state +2. Reaction of either the quaternary arsonium or phosphonium salt of $[B_{10}H_{12}]^{2-}$ with R_2SnCl_2 (R = Me, Et) produced a number of different products, among which was found the unusual $[B_{10}H_{12}R_2SnCl_2]^{2-}$ ion, whose Mössbauer and IR spectra were consistent with the presence of an Sn +4 atom [26]. More than 20 years after these first findings Gaines et al. presented a straightforward procedure for the incorporation of Si, Ge and Sn atoms into the decaborane cluster framework. Starting again from de-

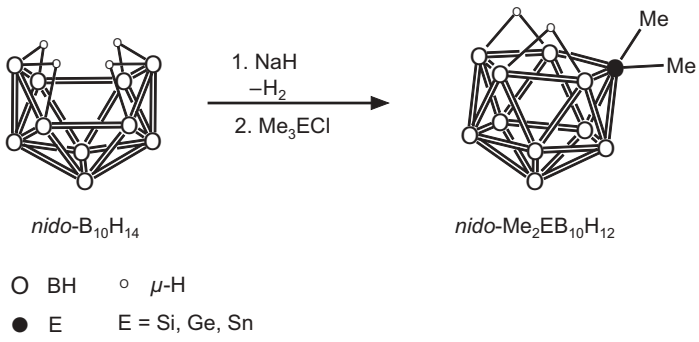

Scheme 3.3-7. Incorporation of group14 heteroatoms into the decaborane(14) framework.

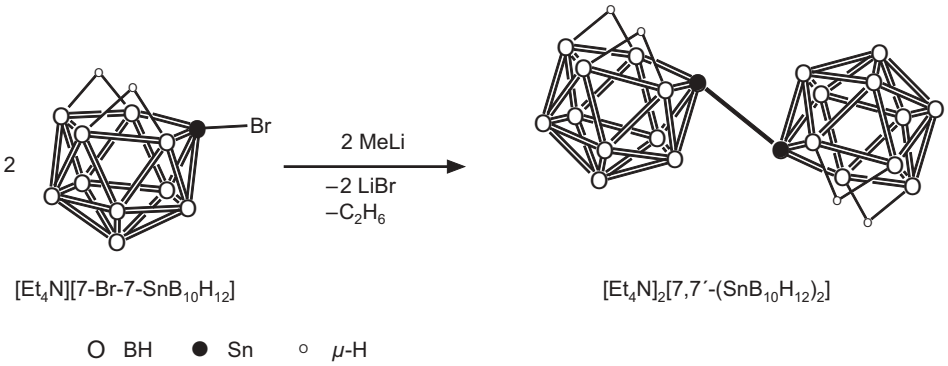

Scheme 3.3-8. Coupling reaction between two 11 vertex stannaborates.

protonated decaborane $Na_2[B_{10}H_{12}]$ the heteropolyborates $[7\text{-Me-}nido\text{-}7\text{-}SiB_{10}H_{12}]^-$, $[7\text{-I-}nido\text{-}7\text{-}GeB_{10}H_{12}]^-$ and $[7\text{-Br-}nido\text{-}7\text{-}SnB_{10}H_{12}]^-$ were isolated in 70–90% yield and characterized by NMR spectroscopy and X-ray diffraction [27, 28]. In the case of the tin derivative $[7\text{-Br-}nido\text{-}7\text{-}SnB_{10}H_{12}]^-$ an interesting coupling reaction of two *nido*-polyborate cluster frameworks via formation of an Sn–Sn bond was found (Scheme 3.3-8) [28].

Apart from incorporation of a silicon vertex into the decaborane skeleton by salt elimination reactions, the controlled nucleophilic degradation of the disilaborane $Me_2Si_2B_{10}H_{10}$ with NaOH is another versatile method for the preparation of the *nido*-silaborate, $[MeSiB_{10}H_{12}]^-$, which is depicted in Scheme 3.3-9 [29].

This latter synthesis requires the immediate precipitation of the sila-*nido*-undecaborate by using $[NMe_4]Cl$ as precipitating agent. If the monoanion remains in water for only a few minutes, further degradation occurs resulting in the complete removal of silicon [29]. As in the case of other *nido*-polyboranes and carboranes the two bridged hydrogens in $[MeSiB_{10}H_{12}]^-$ can be deprotonated. Reaction of this trianion with metal halides results in the formation of *closo*-metallasiladecaborates (Scheme 3.3-2) [8, 9].

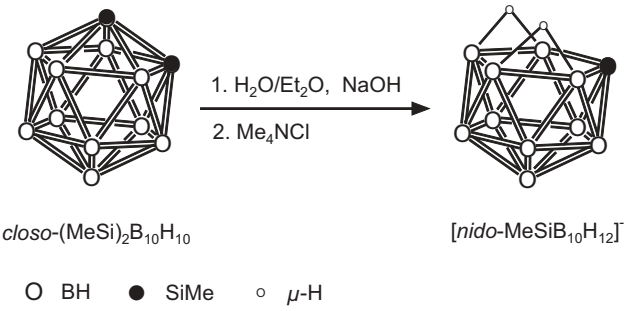

Scheme 3.3-9. Nucleophilic degradation of 1,2-dimethyl-1,2-disila-*closo*-dodecaborane.

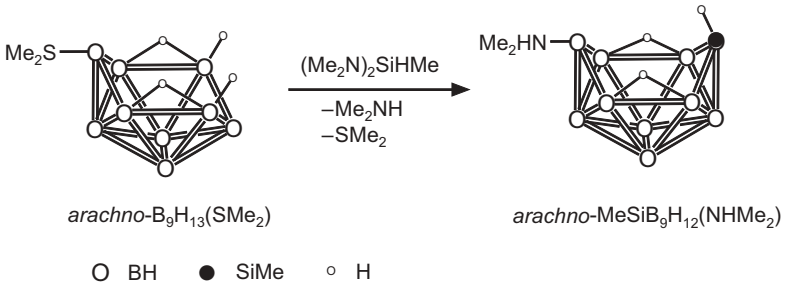

Scheme 3.3-10. The synthesis of sila-*arachno*-decaborane.

3.3.2.3
Smaller Heteropolyboranes

Surprisingly few examples are known in the field of heteroborane clusters with less than 11 vertices. The first *arachno*-silaborane, $MeSiB_9H_{12}(NHMe_2)$ was formed in 85% yield from the reaction of *arachno*-$B_9H_{13}(SMe_2)$ with $MeHSi(NMe_2)_2$ [15] (Scheme 3.3-10).

As in the latter example, the same aminosilane employed for the synthesis of the disilaborane (Scheme 3.3-1) was used to incorporate a silicon vertex into a polyborane cluster skeleton. However, attempts to use pentaborane(9) B_5H_9 for this method proved not to be successful. Instead, pentaborane(9) undergoes degradation and formation of the tetraborane derivative $[B_4H_8SiMe(NMe_2)_2BH_2]$ was observed [30].

Reactions of the group 14 metal alkyl halides R_nMX_{4-n} (M = Si, Ge, Sn, Pb; X = halogen, R = alkyl) with smaller borane cages, such as pentaborane(9), leads to bridged complexes of the general form μ-$R_3MB_5H_8$ (R = H, Me, and Et; M = Si, Ge, Sn or Pb) (Figure 3.3-2) [31, 32].

These compounds were found to isomerize in the presence of mild Lewis bases to produce isomers in which the R_3M is terminally bound to either the apical boron (1-$R_3MB_5H_8$) or to one of the basal boron atoms (2-$R_3MB_5H_8$). In most cases the 2-isomer is formed preferentially, while the 1-isomer is only accessible at elevated temperatures or in the presence of strong bases [33]. However, the stabilities can be reversed through bulky organometal groups. For example, the 1-isomer

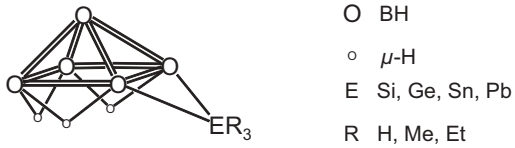

2,3-μ-$(SnPh_3)B_5H_8$

Fig. 3.3-2. Structure of pentaborane with bridging group 14 fragments.

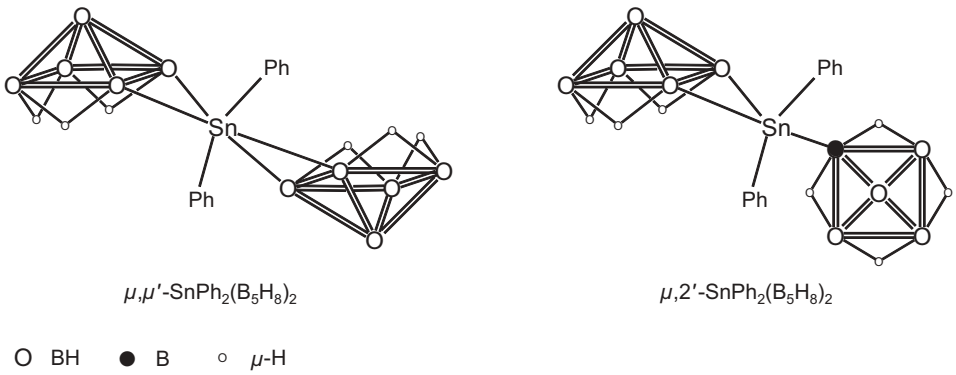

Fig. 3.3-3. Two pentaborane cages linked by a single tin atom.

seems to be the most stable product in the reaction of $K[B_5H_8]$ with $SnClPh_3$ [34], while the low temperature reaction of $K[B_5H_8]$ with $SnCl_2Ph_2$ (Ph = C_6H_5) in a molar ratio of 2:1 furnishes the bridged intermediate μ,μ'-$SnPh_2(B_5H_8)_2$, which rearranges further to $\mu,2'$-$SnPh_2(B_5H_8)_2$. In the latter compound the tin atom is bridged to one pentaborane moiety but terminally bonded to the other (Figure 3.3-3) [35].

3.3.3
Adducts of Disila-*closo*-dodecaborane

It should be noted that the degradation reaction of the disila-*closo*-dodecaborane 1,2-Me_2-*closo*-1,2-$Si_2B_{10}H_{10}$, (see Scheme 3.3-9) is quite different from its corresponding carborane analogue, *closo*-1,2-$(CR)_2B_{10}H_{10}$, which, under base hydrolysis conditions, loses a B–H vertex to give the corresponding *nido*-7,8-$(CR)_2B_9H_{11}$ [36]. Both theoretical calculations and photoelectron spectroscopy studies on disila-*closo*-dodecaborane derivatives indicate that the $B_{10}H_{10}$ moiety is extremely electron rich, leaving the two adjacent silicon atoms highly electropositive. In addition, the LUMOs of the disila-*closo*-dodecaborane are essentially concentrated on the two silicon atoms, so that they can serve as the sites of nucleophilic attack [5, 37]. These observations not only explain the course of the nucleophilic degradation (see Scheme 3.3-9), but also help to rationalize several other unusual reactions of 1,2-$(Me)_2$-*closo*-1,2-$Si_2B_{10}H_{10}$. For example, the reaction of the disila-*closo*-dodecaborane with Et_2NLi gave a product whose ^{11}B NMR spectrum was consistent with an adduct in which the ethylamido group bridges the two silicon atoms [37]. This structure was confirmed by the X-ray diffraction analysis of $[Zr(NEt_2)_3(THF)_2]^+[(Et_2N)(MeSi)_2B_{10}H_{10}]^-$. The latter compound was formed in 85% yield from the reaction of the disila-*closo*-dodecaborane with $Zr(NEt_2)_4$ in THF (Scheme 3.3-11) [37].

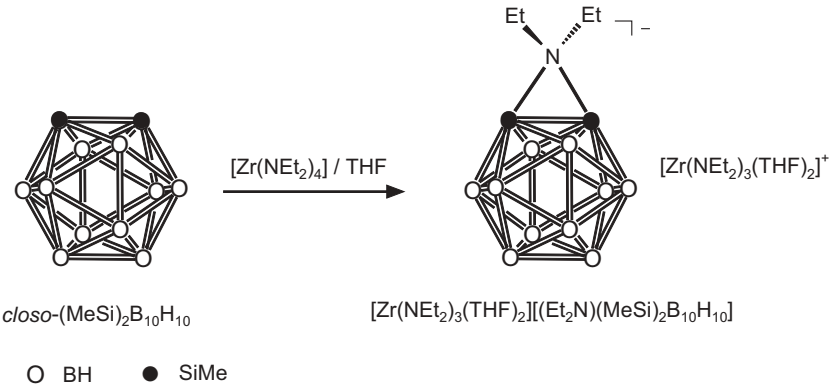

Scheme 3.3-11. Formation of an adduct between diethylamide and 1,2-dimethyl-1,2-disila-*closo*-dodecaborane.

The structure of the $[(Et_2N)(MeSi)_2B_{10}H_{10}]^-$ ion clearly shows the Si–N–Si bridge structure. The most unusual aspect is that the Si–Si distance of 2.332(1) Å is essentially the same as that in the initial 1,2-dimethyl-1,2-disila-*closo*-dodecaborane [2.308(2) Å]. This same similarity was found when comparing the B–B and B–Si bond lengths in this amino adduct $[(Et_2N)(MeSi)_2B_{10}H_{10}]^-$ with those in the starting material 1,2-Me_2-*closo*-1,2-$Si_2B_{10}H_{10}$. The major structural change was found in the C–Si–Si bond angle, which increased by 28° on complexation. The diphenyl derivative of the disila-*closo*-dodecaborane was also synthesized and structurally characterized [6]. The Si–Si bond length of 2.314(1) Å observed in this compound is very similar to that found in $Me_2Si_2B_{10}H_{10}$. The 1,2-diphenyl-1,2-disila-*closo*-dodecaborane was found to undergo the same degradation and amido addition reaction as the dimethyl derivative [6]. In contrast to the bridging dialkylamido nucleophile, alkoxides coordinate at one silicon vertex in the solid state. However, the NMR spectroscopic findings in solution do not correspond with the structure in the solid state. One resonance in the ^{13}C, ^{1}H and ^{29}Si NMR for two MeSi-units of the cluster alkoxide adduct $[(MeO)(MeSi)_2B_{10}H_{10}]^-$ is a good indicator for migration of the alkoxide from one silicon vertex to the other [38]. The disila-*closo*-dodecaboranes were also found to react with the Grignard reagents RMgBr (R = Me, Ph, benzyl, allyl, vinyl and ethynyl) [7]. In all cases the R group bonds to one of the silicon atoms to form anionic adducts with the general formula $[B_{10}H_{10}(SiR'_2)R]^-$ (R′ = Me or Ph; R = Me, Ph, benzyl, allyl, vinyl and ethynyl). A mixed Me-Ph-disila-*closo*-dodecaborane could be synthesized from the reaction of the diphenyl-*o*-disiladodecaborane with MeMgBr and Ph_3CBF_4, as outlined in Scheme 3.3-12 [7].

In comparison with the enormous number of carboranes the family of the heavier group 14 heteroborane clusters is yet very small. Most of the heteropolyborane skeletons with Si, Ge, Sn or Pb atoms belong to the group of larger sized *closo*- and *nido*-clusters and the chemistry of these heteroboranes is essentially concentrated on the heteroatoms.

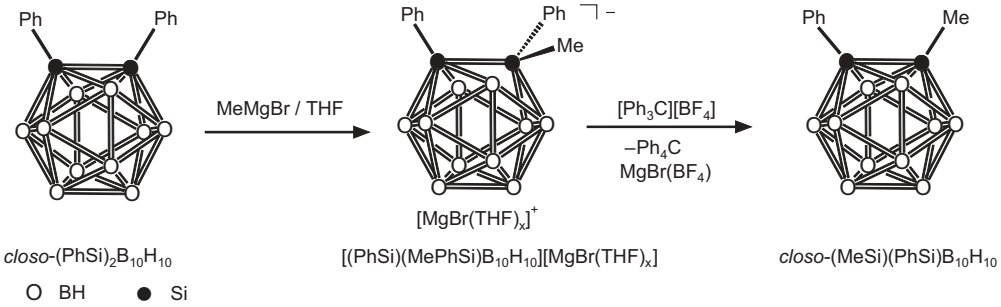

Scheme 3.3-12. Substitution of a phenyl group against a methyl group at the cluster sphere of 1,2-diphenyl-1,2-disila-*closo*-dodecaborane.

References

1 (a) E. W. Abel, F. G. A. Stone, G. Wilkinson, eds., *Comprehensive Organometallic Chemistry II*, Vol. 1, Pergamon, Oxford, **1995**, Chaps. 6–8. (b) R. N. Grimes, *Carboranes*, Academic Press, New York, **1970**. (c) N. S. Hosmane, J. A. Maguire, in *Electron-Deficient Boron and Carbon Clusters*, G. A. Olah, K. Wade, R. E. Williams, eds., Wiley, New York, **1991**, Chap. 9. (d) N. S. Hosmane, J. A. Maguire, *Adv. Organomet. Chem.*, **1989**, *30*, 99–150. (e) N. S. Hosmane, J. A. Maguire, *J. Cluster Sci.*, **1993**, *4*, 297–349. (f) A. K. Saxena, J. A. Maguire, J. J. Banewicz, N. S. Hosmane, *Main Group Chem. News*, **1993**, *1(2)*, 14. (g) N. S. Hosmane, in *Main Group Elements and Their Compounds*, V. G. Kumar Das, Narosa Publishing House/Springer-Verlag, New Delhi, India, **1996**, 299. (h) N. S. Hosmane, *Curr. Sci.*, **2000**, *78*, 452–463. (i) N. S. Hosmane, in *Contemporary Boron Chemistry*, M. Davidson, A. K. Hughes, T. B. Marder, K. Wade, eds., Royal Society of Chemistry, Cambridge, **2000**, pp. 299–307. (j) G. Rana, J. A. Maguire, N. S. Hosmane, *Main Group Met. Chem.*, **2000**, *23*, 529–549. (k) N. S. Hosmane, J. A. Maguire, *J. Organomet. Chem.*, **2000**, *614*, 10–17. (l) K. Vyakaranam, J. A. Maguire, N. S. Hosmane, *J. Organomet. Chem.*, **2002**, *646*, 21–38.

2 (a) K. Wade, *Adv. Inorg. Chem. Radiochem.*, **1976**, *18*, 1–66. (b) R. E. Williams, *Adv. Inorg. Chem. Radiochem.*, **1976**, *18*, 67–142. (c) R. W. Rudolph, *Acct. Chem. Res.*, **1976**, *9*, 446–452. (d) D. M. P. Mingos, R. L. Johnston, *Struct. Bonding*, **1987**, *68*, 29–87.

3 (a) E. D. Jemmis, G. Subramanian, M. L. McKee, *J. Phys. Chem.*, **1996**, *100*, 7014–7017. (b) E. D. Jemmis, G. Subramanian, *J. Phys. Chem.*, **1994**, *98*, 9222–9226. (c) H. Nöth, T. Habereder, W. Lippert, in *Contemporary Boron Chemistry*, M. Davidson, A. K. Hughes, T. B. Marder, K. Wade, eds., Royal Society of Chemistry, Cambridge, **2000**, pp. 386–390.

4 D. Seyferth, K. Büchner, W. S. Jr. Rees, W. M. Davis, *Angew. Chem.*, **1990**, *102*, 911–913; *Angew. Chem., Int. Ed. Engl.*, **1990**, *29*, 918–920.

5 D. Seyferth, K. Büchner, W. S. Jr. Rees, L. Wesemann, W. M. Davis, S. S. Bukalov, L. A. Leites, H. Bock, B. Solouki, *J. Am. Chem. Soc.*, **1993**, *115*, 3586–3594.

6 L. Wesemann, Y. Ramjoie, M. Trinkaus, B. Ganter, *Z. Anorg. Allg. Chem.*, **1998**, *624*, 1573–1576.

7 L. Wesemann, M. Trinkaus, U. Englert, J. Müller, *Organometallics*, **1999**, *18*, 4654–4659.

8 L. Wesemann, Y. Ramjoie, B. Ganter, H. Maisch, *Chem. Ber.*, **1996**, *129*, 837–839.

9 (a) L. Wesemann, M. Trinkaus, Y. Ramjoie, in *Contemporary Boron Chemistry*, M. Davidson, A. K. Hughes, T. B. Marder, K. Wade, eds., Royal Society of Chemistry, Cambridge, **2000**, pp. 353–359. (b) L. Wesemann, Y. Ramjoie, B. Ganter, B. Wrackmeyer, *Angew. Chem.*, **1997**, *109*, 902–904; *Angew. Chem., Int. Ed. Engl.*, **1997**, *36*, 888–890.

10 L. Wesemann, Y. Ramjoie, M. Trinkaus, B. Ganter, *Inorg. Chem.*, **1997**, *36*, 5192–5197.

11 L. Wesemann, Y. Ramjoie, M. Trinkaus, T. Spaniol, *Eur. J. Inorg. Chem.*, **1998**, 1263–1268.

12 L. Wesemann, M. Trinkaus, M. Ruck, *Angew. Chem.*, **1999**, *111*, 2518–2520; *Angew. Chem., Int. Ed. Engl.*, **1999**, *39*, 2375–2377.

13 W. H. Knoth, *J. Am. Chem. Soc.*, **1967**, *89*, 1274–1275.

14 L. Wesemann, U. Englert, *Angew. Chem.*, **1996**, *108*, 586; *Angew. Chem., Int. Ed. Engl.*, **1996**, *35*, 527.

15 L. Wesemann, B. Ganter, *Organometallics*, **1996**, *15*, 2569–2570.

16 L. Wesemann, Y. Ramjoie, M. Trinkaus, in *Advances in Boron Chemistry*, W. Siebert, ed., Royal Society of Chemistry, Cambridge, **1997**, pp. 422–425.

17 R. W. Chapman, J. G. Kester, K. Folting, W. E. Streib, L. J. Todd, *Inorg. Chem.*, **1992**, *31*, 979–983.

18 N. S. Hosmane, N. N. Sirmokadam, R. H. Herber, *Organometallics*, **1984**, *3*, 1665–1669.

19 P. Jutzi, P. Galow, S. Abu-Orabi, A. M. Arif, A. H. Cowley, N. C. Norman, *Organometallics*, **1987**, *6*, 1024–1031.

20 L. Wesemann, T. Marx, U. Englert, M. Ruck, *Eur. J. Inorg. Chem.*, **1999**, *9*, 1563–1566.

21 T. Marx, L. Wesemann, S. Dehnen, I. Pantenburg, *Chem. Eur. J.*, **2001**, *7*, 3025–3032.

22 S. Hagen, T. Marx, I. Pantenburg, L. Wesemann, M. Nobis, B. Drießen-Hölscher, *Eur. J. Inorg. Chem.*, **2002**, 2261–2265.

23 R. E. Loffredo, A. D. Norman, *J. Am Chem. Soc.*, **1971**, *93*, 5587–5588.

24 R. E. Loffredo, A. D. Norman, *Inorg. Nucl. Chem. Lett.*, **1977**, *13*, 599.

25 T. J. Dupont, R. E. Loffredo, R. C. Haltiwanger, C. A. Turner, A. D. Norman, *Inorg. Chem.*, **1978**, *17*, 2062–2067.

26 N. N. Greenwood, B. Youll, *J. Chem. Soc., Dalton Trans.*, **1975**, 158–162.

27 J. A. Dopke, A. N. Bridges, M. R. Schmidt, D. F. Gaines, *Inorg. Chem.*, **1996**, *35*, 7186–7187.

28 J. A. Dopke, D. R. Powell, R. K. Hayashi, D. F. Gaines, *Inorg. Chem.*, **1998**, 37, 4160–4161.

29 L. Wesemann, U. Englert, D. Seyferth, *Angew. Chem.*, **1995**, *107*, 2435–2436; *Angew. Chem., Int. Ed. Engl.*, **1995**, *34*, 2236–2238.

30 L. Wesemann, Y. Ramjoie, T. Wagner, *Inorg. Chem. Commun.*, **1998**, *1/11*, 443–445.

31 D. F. Gaines, T. V. Irons, *J. Am. Chem. Soc.*, **1967**, *89*, 4249–4250.

32 D. F. Gaines, T. V. Irons, *J. Am. Chem. Soc.*, **1968**, *90*, 6617–6621.

33 J. A. Heppert, D. F. Gaines, *Inorg. Chem.*, **1983**, *22*, 3155–3161.

34 K. Dileep, D. K. Srivastava, N. P. Rath, L. Barton, *Organometallics*, **1992**, *11*, 2263–2273.

35 H. Fang, D. Zhao, L. Brammer, L. Barton, *J. Chem. Soc., Chem. Commun.*, **1994**, 1531–1532.

36 M. F. Hawthorne, D. C. Young, P. M. Garrett, D. A. Owen, S. G. Schwerin, F. N. Tebbe, P. A. Wegner, *J. Am. Chem. Soc.*, **1968**, *90*, 862–868.

37 L. Wesemann, Y. Ramjoie, M. Trinkaus, B. Ganter, J. Müller, *Angew. Chem.*, **1998**, *110*, 1484–1488; *Angew. Chem., Int. Ed. Engl.*, **1998**, *37*, 1412–1416.

38 L. Wesemann, M. Trinkaus, Y. Ramjoie, B. Ganter, U. Englert, J. Müller, *Eur. J. Inorg. Chem.*, **2000**, 735–739.

3.4
Borane Clusters with Group 15 and Group 16 Heteroatoms: Survey of Compounds and Structures

Peter Paetzold

3.4.1
Introduction

The world of boron hydrides (''boranes'') is characterized by electron deficiency: more valence orbitals than valence electrons are available. Although *ab initio* calculations of the structure and properties of boranes are now more or less easily workable, it is still worth localizing the binding electrons in 2c2e and 3c2e bonds for a quick qualitative understanding, bearing in mind the experience that a borane molecule will not be stable unless it can be constructed with such a localized bond scheme. Another most useful qualitative concept is given by the Wade-Williams rules (see Chapter 1.1.2), which allow the textbook-known classification of the borane clusters, according to the number of cluster electrons, and enable the structure of the more or less open deltahedral frameworks to be deduced from a canon of closed deltahedra. The openings (''apertures'') appear as planar or non-planar tetragons, pentagons, etc., in the deltahedral framework. In order to designate a structure, we follow R. E. Williams and state first the classification symbol, cl, ni, ar, or hy for *closo*, *nido*, *arachno*, or *hypho*, respectively, followed by the cluster size (i.e., the number of vertices *n*) and then by the size of the aperture (in Roman numerals). The term ni-10⟨VI⟩, for example, symbolizes the ten-vertex *nido*-structure of decaborane(14) with its non-planar boat-type hexagonal aperture.

Heteroboranes are those in which one or more non-boron atoms replace a BH vertex, together with groups that may be attached to these heteroatoms. Boranes that contain CH vertices constitute the vast family of carbaboranes. The possibility for carbon to participate in electron-deficient frameworks contradicted the former prejudice of the always electron-precise carbon as the well-behaved brother of naughty boron. So far, most elements have been introduced as heteroatoms into borane frameworks, with the exception of the halogens and the noble gases.

In this chapter the group 15 and 16 elements are considered as hetero-elements. The first three in these groups, N, P, As and O, S, Se, respectively, are more electronegative than boron. As far as possible, these elements prefer the positions of lowest connectivity (i.e., the number of adjacent atoms in the cluster skeleton). In

the case of vertices with an *exo*-H atom (NH, PH, AsH) or vertices with an *exo*-lone pair (N, P, As, O, S, Se), positions with the connectivity three (''3k'') would allow these elements to form 2c2e bonds only and to avoid 3c2e bonds. In the case of the most electronegative element in this series, oxygen, higher connectivities than 3k have never been found in heteroborane clusters. All of the other elements in question, however, have also been found in 4k and even 5k positions, where they necessarily suffer from electron deficiency.

Whereas a BH vertex contributes two and a CH vertex three electrons to the cluster, the vertices NH, PH, AsH (and analogously NR, PR, AsR) obviously contribute four electrons, the lone-pair vertices N, P and As three and the lone-pair vertices O, S and Se four electrons.

An electron-count complication will arise, however, when groups such as NH_2 or SH are found to bridge two BH cluster vertices, similar to a bridging H atom. When the amino group carries one and the sulfanido group two lone pairs, only one electron remains as a cluster contribution. With no lone pair at nitrogen or only one lone pair at sulfur, three cluster electrons are contributed and the cluster needs be classified one category lower, towards the electron-richer side. A different way of looking at bridging NH_2 or SH groups is to make them 2k cluster vertices. The amino group would then contribute three nitrogen electrons and in addition the two electrons from an *endo*-NH bond (in analogy to *endo*-BH bonds), which means a contribution of five cluster electrons, according to the Wade-Williams formalism. The same would be true for the sulfanido group, which keeps two electrons apart from the cluster, either as an *exo*-lone-pair or as an *exo*-SH group, so that again five electrons remain for the cluster. We shall go more into detail, when discussing the ar-11 family.

In the following section, we give a survey of the known types of heteroboranes in question and discuss the structures in terms of the Wade-Williams rules. Readers, who are interested in the synthesis of heteroatom clusters, in their skeletal transformations, or in reactions at the ligand sphere, are referred to the cited literature. *conjuncto*-Boranes with heteroatoms in the skeleton are not considered in this brief discussion.

3.4.2 *Closo*-Clusters

Closed deltahedral clusters, which contain group 15 or group 16 in the skeleton, exhibit structures well-known from the borates $B_nH_n^{2-}$ (Figure 3.4-1).

3.4.2.1 The cl-5 to cl-9 Families

We do not consider hetero-cyclotriboranes EB_2H_2 to be clusters, although a *closo*-electron count could formally be applied. Extensively investigated examples of this

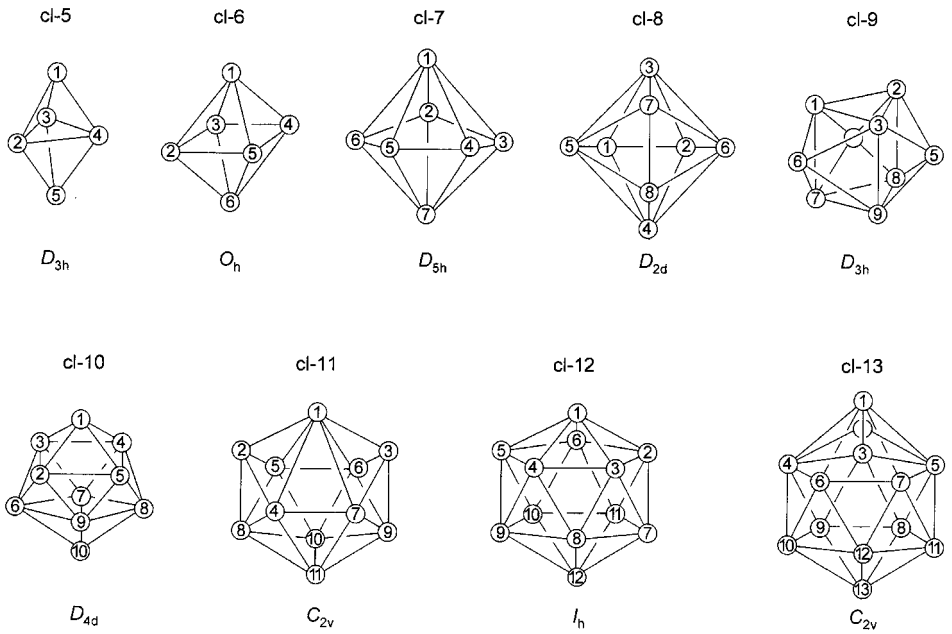

Fig. 3.4-1. Parent *closo*-$B_nH_n^{2-}$ structures ($n = 5$–13: cl-5 to cl-13); the balls represent BH vertices.

family are, e.g., the organic derivatives of OB_2H_2 [1] and $(NH)B_2H_2$ [2]. Even tetrahedral heteroboranes EB_3H_3 are not considered here. The azaborane $(NH)B_3H_3$, e.g., was shown by DFT calculations to have a potential energy minimum in its tetrahedron-type C_{3v} structure, that is by more than 200 kJ mol^{-1} higher in energy than five non-tetrahedral minimum structures [3]. Organic derivatives of $(NH)B_3H_3$ have been synthesized, which turned out to be B-boryl derivatives of a cyclotriborane [–NR–BR–B(BR_2)–] [3].

Clusters with one heteroatom E, EB_4H_4, EB_5H_5, and EB_6H_6 (E = S, NH, PH), were studied by *ab initio* methods [4, 5] and in the case of the EB_4 and EB_6 species the 1- and the 2-isomers were considered. The expected cl-5, cl-6, and cl-7 structures (Figure 3.4-1) represent the minima in energy. The isomers of the two-heteroatom clusters $E_2B_3H_3$, $E_2B_4H_4$, and $E_2B_5H_5$ (E = N, P) were also investigated by computational methods. The 1,5-isomer of $N_2B_3H_3$ is more stable then the 1,2-isomer, whereas the stability of all three isomers of $P_2B_3H_3$ is comparable. The 1,6-isomer is more stable then the 1,2-isomer with $N_2B_4H_4$, whereas the opposite is true for $P_2B_4H_4$ [6, 7]. The clusters $E_2B_3H_3$ (E = N, P) were also subjected to *ab initio* calculations in order to elucidate the nucleus-independent chemical shifts (NICS), the aromatic stabilization energies, and the magnetic susceptibility exaltations, thus relating delocalized bonding to aromaticity. The aromaticity se-

quence $BH^- > CH > N > SiH > P$ was established for E in $E_2B_3H_3$ [8]. Clusters with two different heteroatoms, NEB_3H_3, NEB_4H_4 (E = P, CH, SiH), PEB_3H_3, PEB_4H_4 (E = CH, SiH), and NPB_5H_5 have also been studied [7]. A pentagonal bipyramid with the five-membered ring (–S–BH–CH–CH–BH–) as the pentagonal basis and MCp as the axial tops (M = Fe, Co) was calculated as the theoretical basis of a broad experimental polydecker chemistry of organic derivatives of this five-membered ring [9, 10].

The amount of experimental evidence for 5- to 7-vertex hetero-clusters is not as widely spread as the theoretical insight. The octahedral clusters $P_2B_4Cl_4$, $P_2B_4Br_4$, $As_2B_4Cl_4$, and $PAsB_4Cl_4$ have been well characterized as the 1,2-isomers [11–13], and the compounds $P_4B_8Cl_6$ and $As_4B_8Cl_6$ were structurally identified as two B–B linked octahedra [12, 13]. Tripledecker structures with the cyclic thiadicarbapentaborane (–S–BMe–CEt–CEt–BMe–) (tcpb) as the central unit, doubly capped by FeCp/FeCp, NiCp/NiCp, $Mn(CO)_3/Mn(CO)_3$, $FeCp/Mn(CO)_3$, $Fe(C_6H_6)/Mn(CO)_3$, etc., are well known. Polydeckers of the type (tcpb)Co(tcpb)Co(tcpb) or CpFe(tcpb)·Fe(tcpb)FeCp or (tcpb)Co(tcpb)Fe(tcpb)Co(tcpb), etc. contain one or more cl-7 cluster units as building blocks [14–21].

Little is known about cl-8 and cl-9 hetero-borane clusters.

3.4.2.2 The cl-10 Family

After some earlier semiempirical work (e.g., on SB_9H_9 [22]), completely optimized geometries, vibrations, atomic charges, and dipole moments for 1-EB_9H_9 (E = O, S, NH, PH, BH^{2-}) became available through an SCF study [23], based on the expected cl-10 structure. The overall coordination number five of nitrogen in 1-aza-*closo*-decaborane is uncommon and promotes the strongly electronegative nitrogen to the family of elements that may suffer electron deficiency. Nitrogen cannot be incorporated into a 4k cluster position by simple 2c2e bonds. The parent molecule $(NH)B_9H_9$ has been characterized [24, 25] as well as the anion $NB_9H_9^-$ (with a lone pair at nitrogen) [24], the N-organo derivatives $(NR)B_9H_9$ [26–30], and derivatives with non-hydrogen substituents at boron, e.g., $(NR)B_9H_7I_2$ (I in pos. 6,10), $(NR)B_9H_4X_5$ (X = Br, Me, in pos. 6–10), $(NR)B_9H_4Me_4(OTrf)$ (triflate in pos. 6, Me in pos. 7–10) [28]. An azadimetalla-*closo*-decaborane, 1,6,7-$[(NEt)B_7H_7M_2]$ ($M = RhCp^*$), has also been characterized [31].

The anion $PB_9H_9^-$ [32] and the chloro-derivative $P_2B_8Cl_8$ [13] have been described. The following 1-thia-*closo*-decaboranes were characterized: SB_9H_9 [33–38], SB_9H_8X {X = 6-Hal, 10-Hal (Hal = Cl, Br, I), 10-Me, 2-$IrHCl(PPh_3)_2$ [33–35, 39, 40]}, $SB_9H_7X_2$ {X = Br, I, in pos. 6,10 [33])}, $SB_9H_6Cl_3$ {Cl in pos. 6,7,8 [39]}, $SB_9H_{9-n}R_n$ {n = 1–5; R = Me, Et, in pos. 6–10 [41]}, $SB_9H_4D_5$ {D in pos. 6–10 [39]}. B–B linked SB_9 units are present in SB_9H_8–SB_9H_8 {2,2′-, 2,6′- and 6,6′-linkage [42–44]} and in SB_9H_8–X {with $X = SB_{11}H_{10}$ (2,2′- or 2,7′-linkage), $(CH)_2B_{10}H_9$, $(CH)_2B_9H_8$ [42]}. Finally, thiametalla-*closo*-decaboranes, $[SB_8H_8M]$, should be mentioned {M = 2-$IrH(PMe_3)_2$ [45], 6-CoCp [46], 2-$Ru(C_6Me_6)$ [47]}.

3.4.2.3 The cl-11 Family

The position 1 with the extra-high connectivity 6 is reserved for transition metals in the 2,1-thiametalla-*closo*-decaboranes $[SB_9H_9M]$ {M = $IrCp^*$ [48], $Pd(PPh_3)_2$ [49], Co(tcpb)CoCp [50]} or -borates $[SB_9H_9M]^-$ {M = RhL_2, L = PPh_3, L_2 = dppe [51–53]}. In these borates, M contributes only one electron to the cluster, and the same is true for 2,1-$[SB_9H_8LM]$ {M = RhL(CO), L = PMe_2Ph, PPh_3, in pos. 3 [54]; M = Rh(dppe), L = η^1-dppe, in pos. 3 [55]} and for 2,3,1-$[S(CH)B_8H_8M]$ {M = $Rh(PPh_3)_2$ [56]}. Two $[SB_9H_8M]$ units can be connected, when the didentate ligand dppe adds to B3 of the one and to B3′ of the other unit, replacing the original H atoms {M = Rh(dppe) [55]}.

3.4.2.4 The cl-12 Family

3.4.2.4.1 Theoretical Results

Because of the importance of the dicarba-*closo*-dodecaboranes in the history of cluster chemistry, cl-12 clusters with group 15 and 16 heteroatoms aroused early interest. Earlier semiempirical studies {e.g., on $N(CH)B_{10}H_{10}$ [57], $SB_{11}H_{11}$ [22, 58], $EB_{11}H_{11}$ (E = F^+, O, NH) [59]} were followed by *ab initio* computational work on $EB_{11}H_{11}$ {E = O, S, NH, PH [23]} and $EE'B_{10}H_{10}$ {EE′ = NN, PP, AsAs, SbSb, P(CH), As(CH) [60, 61]}, revealing that the stability of the three isomers of $P_2B_{10}H_{10}$ follows that of $(CH)_2B_{10}H_{10}$ (1,12 > 1,7 > 1,2), whereas in the case of $N_2B_{10}H_{10}$, the 1,7- should be more stable than the 1,12-isomer. The molecules $FB_{11}H_{11}^+$, $OB_{11}H_{11}$, $N_2B_{10}H_{10}$ are hypothetical, but $(NH)B_{11}H_{11}$ with a skeletal N atom of connectivity five is a well characterized molecule [62] and aroused particular theoretical interest [63, 64]. Theoretical studies were accompanied by experimental work, e.g., with the electron diffraction data of $SB_{11}H_{11}$ [65] and $(NH)B_{11}H_{11}$ [66], with the vibrations of the methyl derivative $(NMe)B_{11}H_{11}$ [67], or with spectroscopic and X-ray data of the aryl derivative $(NAr)B_{11}H_{11}$ {Ar = 4-XC_6H_4, X = H, Br, BuO [68]}.

3.4.2.4.2 Group 16 Heteroatoms

The cl-12 clusters $EB_{11}H_{11}$ (E = S, Se, Te) were well characterized and a great number of reactions were investigated {E = S [34–36, 39, 40, 69, 70], Se [71–73], Te [71]}. Derivatives of the parent molecules are available: $SB_{11}H_5D_6$ and $SeB_{11}H_5D_6$ {D in pos. 7–12 [39]}, $SB_{11}H_{10}Hal$ {Hal = 12-Br [68], 6-Cl, Br, I [39]}, $SB_{11}Cl_{11}$ [12], $SB_{11}H_{10}X$ {X = SB_9H_8, 2,2′ or 7,2′ B–B linkage [42]}, $SB_{11}H_{10}M$ {M = $IrHCl(PPh_3)_2$, exo-bound to B2 [35]}.

A series of clusters $[EB_{10}H_{10}M]$ with the heteroatoms in the *ortho*-position have been synthesized. The metal vertices M = CoCp and PtL_2 (L = PEt_3, PMe_2Ph, PPh_3) are well known in clusters with E = S [46, 71, 74–76], Se [77–79] and Te [77, 80, 81]. The metal vertices can also be $RhHL_2$, $IrHL_2$ {E = S, Se, Te; L = PPh_3 [81–84]}, $RhXL_2$ {E = Te; X = PhN=CH–S^-; L = PPh_3 [85]}, RhXL {E = Se, Te;

X = S=CH–S$^-$ or S=C(NHPh)–S$^-$, both didentate via sulfur; L = PPh_3 [83, 85]}, or PdL_2 {L = PMe_2Ph, $PMePh_2$, PPh_3 [86, 87]}.

In the species [$TeB_{10}H_8F_2M$] {F in pos. 7,11; M = Mo(η^7-C_7H_7) [88]} and [$TeB_{10}H_9RM$] {R = CH=NBu^t in pos. 3; M = PdI(CNBu^t) [89]}, the metal vertex provides only one cluster electron, and the substances are paramagnetic. The cl-12 structure is preserved, in spite of the lack of cluster electrons. In [$TeB_{10}H_9LM$] {M = PdXL; L = PPh_3; X = Hal, CN, etc. [87, 90]}, the metal vertex contributes again only one cluster electron, but the replacement of an *exo*-H atom by the Lewis base L balances the *closo*-count in the right way. The telluralmetallaborate [$TeB_{10}H_9LM$]$^-$ {L = PPh_3 in pos. 7; M = PdLL′ in pos. 2; L′ = H_2O, CO, NCMe, etc. [90]} exhibits a *closo*-structure in spite of a *nido*-electron count.

Two *nido*-$EB_{10}H_{10}^{2-}$ units (E = S, Se) can be bound to the d^6 ions Fe^{2+} or Co^{3+} in a sandwich-type manner, giving [$M(EB_{10}H_{10})_2]^{n-}$ (n = 2 or 1, respectively) [77, 91–93]. In [$SeB_9H_9M_2$] (M = CoCp), the three heteroatoms occupy the positions 1, 2, 3 [94].

More complex structural arrangements, all of which with adjacent heteroatoms, are found in [$EB_{10}H_9(RhHLL')$] {E = S, Te; L = PPh_3, L′ = PPh_2(*o*-C_6H_4); one *o*-phenylene-C atom is linked to B7 and replaces H7 [95, 96]} or in [$EB_{10}H_{10}Rh$](S–CHL–S)$_2$[$RhB_{10}H_{10}E$] {E = Se, Te; L = PPh_3; each of the two monoanionic ligands $^-$S–CHL$^+$–S$^-$ acts as a didentate ligand towards one Rh vertex and as a monodentate ligand (via a second lone pair of one of the S atoms) towards the other Rh atom and *vice versa*, thus donating Rh^+ (d^8) six electrons [83, 97]}. In [{$TeB_{10}H_{10}(RhL)$}$_2$] (L = PPh_3), the two icosahedra are linked by an Rh–Rh bond (273.71 pm) and two MHB-3c2e bonds, Rh–H7′–B7′ and Rh′–H7–B7, so that each Rh vertex can contribute two electrons to the cluster [84]. Note that such an MHB-3c2e bond may also be designated as an ''MHB-hydrogen bridge'' or as a ''BH–M agostic interaction''. A metal–metal bond is also found in [$EB_{10}H_{10}(CuL)_2$] (E = Se, Te; L = PPh_3). One Cu atom acts as a vertex in pos. 2, to which L is bound as one ligand and the other CuL moiety as a second ligand; this outer Cu atom interacts with two cluster B–H bonds, giving the two 3c2e bonds Cu–H7–B7 and Cu–H11–B11 [98].

3.4.2.4.3 Group 15 Heteroatoms

Six covalent bonds from nitrogen to boron and hydrogen in (NH)$B_{11}H_{11}$ give this stable molecule a unique position in nitrogen chemistry. The icosahedral symmetry is reduced to C_{5v}. The nitrogen atom is situated closer to the cluster center than the boron atoms, and the five *ortho*-B–H bonds are shifted somewhat from the radial direction towards the N–H bond, thus leaving too little space for replacing the N-bound H atom by secondary or tertiary alkyl groups [62, 66, 99, 100]. The lone pair at nitrogen in $NB_{11}H_{11}^-$ makes this anion structurally comparable to $SB_{11}H_{11}$ [62, 101, 102]. Derivatives (NR)$B_{11}H_{11}$ are available {R = Me, Et, 4-C_6H_4X (X = H, Me, Br, OBu^t) [30, 67, 68, 100, 103], R = BH_2L (L = SMe_2) [101]}. In (NX)$B_{11}H_{10}$, the group X = BH_2–NEt_2–CH_2–CH_2 is back-bound via the terminal CH_2 group to B2, replacing H2 [101]}. Derivatives with non-hydrogen ligands at boron were also synthesized: (NR)$B_{11}H_{10}$X {R = Me, X = Br, I in pos. 12 [28]; R = Ph, 4-C_6H_4Me,

$X = CH_2CH_2SiMe_3$ in pos. 7 [104]}, $(NMe)B_{11}H_9Br_2$ {Br in pos. 7,12 [102]}, $(NMe)B_{11}H_8Br_3$ {Br in pos. 7,8,12 [102]}, $(NH)B_{11}Cl_5I_6$ {Cl in pos. 2–6 [102]}, $(NMe)B_{11}H_5Me_6$ {Me in pos. 7–12 [28]}, $(NMe)B_{11}H_5Me_5(OTrf)$ {Me in pos. 7–11, triflate in pos. 12 [28]}. The 1,2-azametallaboranes $[(NH)B_{10}H_{10}M]$ {M = $Ru(C_6H_6)$, $Ru(C_6Me_6)$, $RhCp^*$, $RhH(PPh_3)_2$, $Ni(PPh_3)_2$ [105, 106]} and the cobaltocenium analogue $[Co\{(NH)B_{10}H_{10}\}_2]^-$ [105] may complete this brief summary.

Whereas in the case of nitrogen the vertices NH or NR are present as 4e-donors, the heavier group 15 elements are incorporated into the icosahedron-type skeleton as anions E^-, yielding $EB_{11}H_{11}^-$ with an *exo*-lone pair {E = As [107–109], Sb [109, 110], Bi [109, 111]}. Replacing H by a Lewis base L gives neutral clusters, e.g., $PB_{11}H_{10}L$ {L = NMe_3 in pos. 2 [32]}. A *closo*-count is also given by the diheteroatom clusters 1,2-$E_2B_{10}H_{10}$ {E = P [32], As [107, 108, 112–114], Sb [110, 113, 114]}, $AsSbB_{10}H_{10}$ [110], 1,2-$EBiB_{10}H_{10}$ {E = P, As, Sb, Bi [111]} and by the halo-derivatives 1,7-$P_2B_{10}Cl_{10}$ [13], 1,2-$As_2B_{10}H_8I_2$ {I in pos. 4,9 or 8,9 [115]}, 1,2-$As_2B_{10}Cl_{10}$ [11, 12], $Sb_2B_{10}Cl_{10}$ [12], and $PAsB_{10}Cl_{10}$ [13]. All three isomers of the clusters $E(CH)B_{10}H_{10}$ have been synthesized {E = P, As, Sb [113, 114, 116–130]}, whereas only the 1,7- and 1,12-isomers of $As(CX)B_{10}H_{10}$ (X = HgMe) are known [131]. Heavier group 14 elements with an *exo*-lone pair are involved in the clusters $E(CH)GeB_9H_9$ {E = P, As; 1,2,3- and 1,2,7-isomers [126]} and $AsEB_{10}H_{10}^-$ {E = Sn, Pb [108]}. Four heteroatoms are present in 1,2,7,3-$As(CH)_2TlB_8H_8$. The thallium vertex with an *exo*-lone pair can contribute only one electron to the cluster; the three electrons from each of the three remaining hetero-vertices complete the 26e-shell of the *closo*-skeleton [132].

A series of arsametalla-*closo*-dodedecaboranes were investigated: 1,2-$[AsB_{10}H_{10}M]^-$ {M = CoCp [133, 134]}, 1,2,3-$[As_2B_9H_9M]$ {M = CoCp [108, 133]; $RhCp^*$, $RhH(PPh_3)_2$ [114]; NiL_2, PdL_2, PtL_2 (L = PMe_2Ph, PPh_3 [135, 136]); $Pt(PEt_3)_2$ [137]; Ni(dppe) [108]}, 1,2,3-$[As_2B_9H_8LM]^+$ {M = PdLL′; L = CN*t*Bu, L′ = PMe_2Ph, L in pos. 8 [138]}, 1,2,3-$[As_2B_9H_8LM]$ {M = NiClL, PdClL (L = PMe_2Ph, PPh_3, L in pos. 8 [135, 139])}, 1,2,3-$[As_2B_9H_8XM]$ {M = $Pd(PMe_2Ph)_2$, $Pd(PMe_2Ph)(CNBu^t)$; X = CN in pos. 5 [140]}, $[AsSbB_9H_9M]$ {M = CoCp [110]}. Moreover, the distibametalla-*closo*-dodecaborane $[Sb_2B_9H_9M]$ {M = NiL_2, PdL_2, PtL_2 (L = PMe_2Ph, PPh_3) [136]} and the arsacarbametallaborane $[As(CH)B_9H_9M]$ {M = CoCp [117]} should be mentioned.

Sandwich-type *closo*-clusters, in which two phospha- or arsa-*nido*-undecaborate moieties are linked via a common twelfth metal vertex, are also available: $[Fe\{E(CH)B_9H_9\}_2]^{2-}$ {E = P, As [141]}, $[Fe\{(PM)(CH)B_9H_9\}_2]^{2-}$ {M = $Cr(CO)_5$, $Mo(CO)_5$, $W(CO)_5$ [141]}, $[Co(AsB_{10}H_{10})_2]^{3-}$ [133, 134], and $[Co(As_2B_9H_9)_2]^-$ [133]. The heteroatoms are found in positions 1 (P, As), 2 (M), and 7 (C), respectively, of the corresponding icosahedra.

3.4.2.5 The cl-13 Family

No cl-13 representatives with group 15 or group 16 elements in the skeleton have been synthesized up to now, though carbametalla derivatives, e.g. [1,3,4-$(CH)_2B_{10}H_{10}M$] (M = CoCp), have been known for a long time [142–146], and

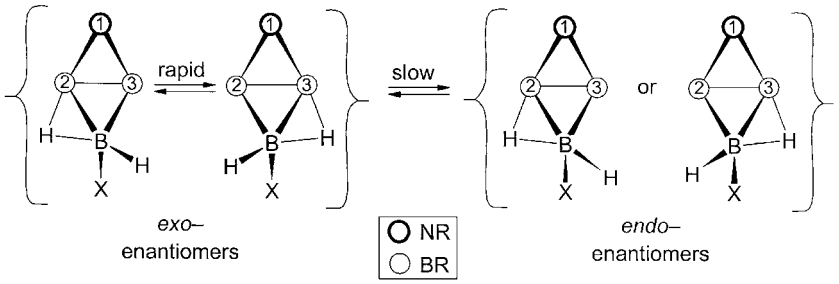

Fig. 3.4-2. The *exo*- and *endo*-enantiomers of *nido*-$(NR)B_3H_2R_3X$ and their transformation into each other ($R = Bu^t$; X = H, Cl, R′).

the closed 13-vertex species $(CH)_2SnB_{10}H_{10}$ [147] and an organic derivative of $(CH)_2B_{11}H_{11}$ [148] have been described recently.

3.4.3 *Nido*-Clusters

3.4.3.1 The ni-4 and ni-5 Family

Ab initio calculations of $OB_3H_6^+$, NB_3H_6, and $(NH)B_3H_6^+$ suggest a trigonal-pyramidal structure with the heteroatoms at the top and three BHB-3c2e bonds at the basis [149]. The experimental structure is different, however. Derivatives $(NR)B_3H_2R_2X$ of 1-aza-*nido*-tetraborane, $(NH)B_3H_5$, are well known {$R = Bu^t$; X = H, Cl, Me, Bu^s, Bu^t, CMe_2Pr^i, Ph [3, 150]}. Their NB_3 skeleton is derived from the cl-5 structure (Figure 3.4-1) by subtracting the 4k-vertex B4. An interplanar angle between the two skeletal triangles in the range 137–140°, a B2–B5 hydrogen bridge and the ligand X in pos. 5 define an *exo*/*endo*-alternative of the ligand couple H/X (Figure 3.4-2). The *exo*-isomer undergoes an enantiomerization via a transition state with two *endo*-H atoms at B5 (C_s), which is rapid enough to establish pseudo-C_s symmetry in the NMR experiment. An enantiomerization is not possible, however, for the *endo*-isomer, because a transition state with two H atoms in *exo*-position at B5 would be unfavorable. The *exo*/*endo*-isomerization is slow enough to make an equilibrium of both isomers observable by the NMR method. The computed and observed NMR shifts are in good agreement.

The hypothetical ni-5⟨IV⟩ cluster $NB_4H_8^+$, a C_{4v} analogue of B_5H_9 with a lone pair at the pyramidal apex, was studied by *ab initio* methods [151].

3.4.3.2 The ni-6 Family

The two structural alternatives, ni-6⟨V⟩ and ni-6⟨IV⟩ (Figure 3.4-3), have been discussed for 15 hypothetical species of the type $EE'B_4H_4^{n-}$ by *ab initio* methods, including the vertices E,E′ = BH, CH, NH, O, and S [152]. When at least one of the two vertices E and E′ is BH or CH, the pentagonal-pyramidal ni-6⟨V⟩ struc-

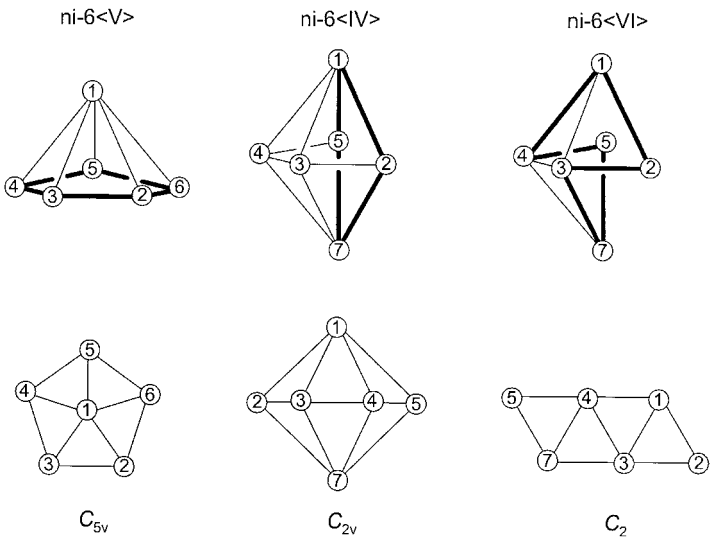

Fig. 3.4-3. Perspective and planarized representations of the ni-6⟨V⟩ (derived from cl-7 minus B7), the ni-6⟨IV⟩ (derived from cl-7 minus B6) and the ni-6⟨VI⟩ (derived from ni-6⟨IV⟩ by opening of B1–B5 and B2–B7) structures of hypothetical $B_6H_6^{4-}$ (apertures in bold lines).

ture is the better one: $B_6H_6^{4-}$, 2-$(CH)B_5H_5^{3-}$, 2,4-$(CH)_2B_4H_4^{2-}$, 2-$EB_5H_5^{2-}$, 2,4-$E(CH)B_4H_4^-$ (E = NH, O, S). Otherwise, the open bipyramidal ni-6⟨IV⟩ structure dominates: 2,5-$EE'B_4H_4$ [EE′ = $(NH)_2$, O(NH), S(NH), O_2, OS, S_2]. This is in accord with the experimental findings in the case of certain derivatives of a few of the computed parent compounds.

Pentagonal pyramidal structures with a ring sequence (–S–BH–CH–CH–BH–) as the pyramidal basis have been studied theoretically, including 2,4,5-$S(CH)_2B_3H_3$ [153], 2,4,5,1-[$S(CH)_2B_2H_2M$] {M = $Fe(CO)_3$ [154]}, [$Ni\{S(CH)_2B_2H_2\}_2$] [155], and the analogous cluster system [2,4,5,6,1-$(NH)_2(CH)_2BHM$] {M = $Cr(CO)_3$ [154]}.

The cyclic thiadicarbapentaborane (–S–BMe–CEt–CEt–BMe–) (tcpb) as the pyramidal basis plays a role in a number of metallahexaboranes with the metal as the pyramidal apex: [M(tcpb)] {M = $Cr(CO)_4$, $Mo(CO)_4$, $Fe(CO)_3$, Fe(ar) (ar = C_6H_6, C_6H_5Me, 1,4-$C_6H_4Me_2$, 1,4-$C_6H_4F_2$, 1,3,5-$C_6H_3F_3$), CoCp, NiCp, $Ni(CO)_2$ [156–160]}, [$\{Co(CO)_2(tcpb)\}_2$] [159], [$Ni(tcpb)_2]^-$ [156, 159, 160]. A benzo-group is connected to the pyramidal basis in [$Fe(CO)_3$(–S–BMe–C_6H_4–BMe–)] [161]. A variety of boron substituents are known in [$Fe(CO)_3$(–S–BX–CEt–CEt–BX′–)] {X = X′ = H, Cl, Br, I, OEt, SMe, NMe_2, Me; X/X′ = F/I, OEt/I, Me/I [162]}. Comparable non-metal ni-6⟨V⟩ clusters are the 2,4,5-thiadicarba-*nido*-hexaboranes $S(CPr^i)_2B_3HRR'$ {R/R′ in pos. 3,6: H/Pr^i, Pr^i/Pr^i, Pr^i/Ph, Pr^i/Dur, Dur/Dur (Dur = duryl, 2,3,5,6-C_6HMe_4) [153, 163]} and the analogous azadicarbahexaborane $(NMe)(CPr^i)_2B_3HR_2$ {R in pos. 3,6: H, Dur [163]}.

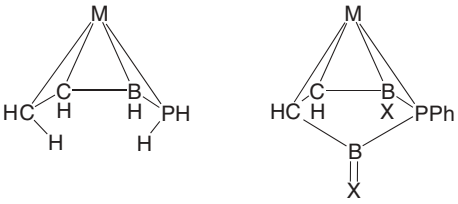

Fig. 3.4-4. The hypothetical ar-5⟨V⟩ parent molecule $[(PH_2)(CH)(CH)_2BHM]$ and its formal derivative $[(PPh)(CH)_2B_2X_2M]$.

The 2,4,5,1-phosphadicarbametallahexaborane $[(PPh)(CH)_2B_2X_2M]$ {X = NPr^i_2, M = $Fe(CO)_3$)} may be considered as a border case: One of the two expected Fe–B bonds is not present, a consequence, presumably, of a strong BN π-bonding interaction with one of the two B–X bonds. The corresponding BX moiety does not act, therefore, as a vertex in a ni-6 cluster, but either as a bridging moiety in an ar-5 cluster, which formally replaces two *exo*-H atoms in a hypothetical molecule $[(PHPh)(CH)(CH_2)BXM]$ with a 2,4,5,1-phosphadicarbametalla-ar-5⟨V⟩ structure [164] (Figure 3.4-4).

The ni-6⟨IV⟩ structure is found in hexaorganoderivatives of 1,7-diaza-*nido*-hexaborane, as expected for the parent $(NH)_2B_4H_4$ by theory [152]. Ten derivatives $(NR)_2B_4R'_2R''_2$ were described (R/R′/R″ = $Pr^i/Pr^i/Pr^i$, $Pr^i/Pr^i/Bu^t$, Bu^t/Me/Me, Bu^t/Me/Bu^t, $Bu^t/Et/Pr^i$, $Bu^t/Et/Bu^t$, $Bu^t/Et/Bu^s$, $Bu^t/Pr^i/Pr^i$, $Bu^t/Pr^i/Bu^t$, $SiMe_3/Pr^i/Bu^t$) [2, 165]. In the case of R′ ≠ R″, only the unsymmetric isomers with R′ in the 1,3- and R″ in 4,7-position are formed in a stereospecific manner as a pair of enantiomers, whereas the symmetric isomers (C_{2v}) with R′ in 1,7- and R″ in 3,4-position or *vice versa* are not present. This was interpreted as a consequence of the mechanism of the formation by dimerization from $(NR)B_2R'R''$ [166]. Another example of a ni-6⟨IV⟩ skeleton is presented by the 2,5,1,6-dithiadimetalla-*nido*-hexaborane $[S_2B_2H_2M_2]$ {M = CoCp [167, 168]}.

A particularly high sterical demand at the BN double bonds B1=N2 and B7=N5 makes a ni-6⟨VI⟩ structure stable in $(NR)_2B_4R_2R'_2$ {Figure 3.4-3; R = Bu^t, R′ = CH_2Bu^t (in pos. 3,4) [166]}.

3.4.3.3
The ni-7 Family

The 2,7,8-phosphadicarba-*nido*-heptaborane $(PR)(CH)_2B_4H_4$ [169] was suggested to exhibit an ni-7⟨V⟩ structure [170] with the three heteroatoms in the three 3k positions (Figure 3.4-5).

The compound $[(NH)_2(CH)_2(BMe)_2M]$ {M = $Cr(CO)_3$ [171]} gives formally a *nido*-count. However, the hexagonal–pyramidal structure with a benzene-analogous hexagon (=NH–NH=BMe–CH=CH–BMe=) as the pyramidal basis does not present a borane-type cluster structure. The electron-deficiency is not concentrated at boron, but at the metal.

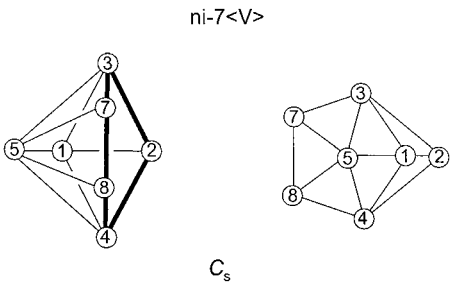

Fig. 3.4-5. Perspective and planarized representation of the ni-7⟨V⟩ structure of hypothetical $B_7H_7^{4-}$ (derived from cl-8 minus B6, aperture in bold lines).

3.4.3.4
The ni-8 Family

The ground state structures of the 12 hypothetical species EB_7H_9, $EB_7H_8^-$, $EB_7H_7^{2-}$, and $E_2B_6H_6$ (E = O, S, NH) were *ab initio* computed [172]. The ni-8⟨VI⟩ structure (Figure 3.4-6) with one or two heteroatoms in the 3k positions 3 or 3 and 5, respectively, dominates in ten species. The extra-H atom of the mono-anions bridge B5 and B6 and the two extra-H atoms of the neutral species form B5–B6 and B4–B5 bridges or (in OB_7H_9) B5–B6 and B7–B8 bridges. Exceptions from the ni-8⟨VI⟩ structure were computed for $OB_7H_7^{2-}$, whose heteroatom is found in the 3k position 5 of a ni-8⟨V⟩ structure, and for $SB_7H_7^{2-}$, whose B

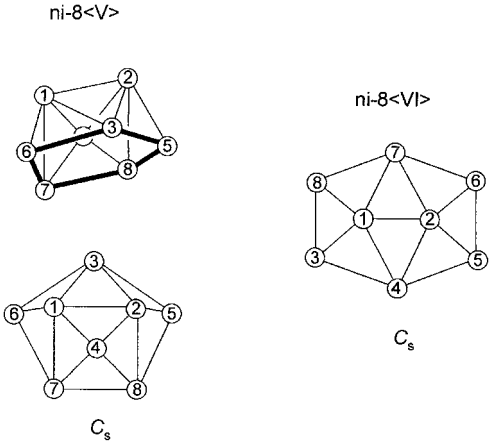

Fig. 3.4-6. Perspective and planarized representation of the ni-8⟨V⟩ (derived from cl-9 minus B9) and planarized representation of the ni-8⟨VI⟩ (derived from ni-8⟨V⟩ by opening of the B7–B8 bond; numbering taken from ar-8⟨VI⟩) structures of hypothetical $B_8H_8^{4-}$ (aperture in bold lines).

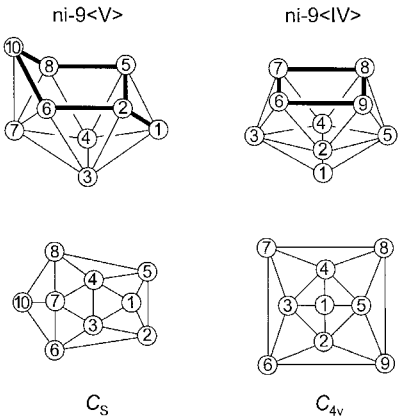

Fig. 3.4-7. Perspective and planarized representations of the ni-9⟨V⟩ (derived from cl-10 minus B9) and of the ni-9⟨IV⟩ (derived from cl-10 minus B10) structures of hypothetical $B_9H_9^{4-}$ (apertures in bold lines).

atoms are arranged in a ni-7⟨V⟩ structure (Figure 3.4-5) with sulfur capping the 3k vertices 2, 7, 8.

3.4.3.5
The ni-9 Family

The ni-9⟨V⟩ structure (Figure 3.4-7) was found with the thiaborane SB_8H_{10} (two extra-H atoms bridge B2–B6 and B5–B8), the thiaborate $SB_8H_9^-$ (μ-H bridging B2–B5) [34, 173]} and the azaborate $(NR)B_8H_9^-$ {R = Bzl, 4-XC_6H_4 (X = Cl, Me); μ-H bridges B2–B5 again [27]}. The heteroatoms E prefer the 3k position 10, which allow them classical E–B 2c2e bonds in a sulfonium- or ammonium-type structure, respectively. The same type of structure was found with the azametallaborane $[(NH)B_7H_8M]$ {M = $Ir(PMe_3)_3$ in pos. 2; μ-H bridges Ir and B5 [45]}.

Interestingly, the dithiadimetallaborane $[S_2B_5H_5M_2]$ (M = CoCp) seems to prefer the ni-9⟨IV⟩ structure with the four heteroatoms in the 4k positions 6,8,7,9 at the tetragonal aperture [174].

3.4.3.6
The ni-10 Family

There is a great deal of synthetic knowledge on *nido*-decaboranes EB_9H_{11} with one non-boron vertex in the 3k position 6 of an ni-10⟨VI⟩ structure (Figure 3.4-8): E = S [34, 37, 40, 42, 43, 46, 48, 175–186], Se [72, 179], NH [24, 101, 175, 186–188], NR {R = H, Bu, Bu^t, Bzl, CH_2Bu^t, Ph, 4-XC_6H_4 (X = Cl, Me) [26, 27, 188]}. As in decaborane(14), the two extra-H atoms bridge the 3k vertex B9 to the 4k

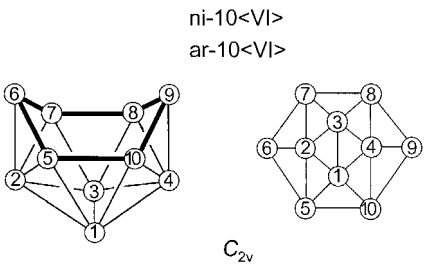

Fig. 3.4-8. Perspective and planarized representation of the ni-10⟨VI⟩ (derived from cl-11 minus B1) and of the ar-10⟨VI⟩ (derived from cl-12 minus B11, B12) structures of the hypothetical $B_{10}H_{10}^{4-}$ and $B_{10}H_{10}^{6-}$ anions (aperture in bold lines).

vertices B8 and B10. In the anions $EB_9H_{10}^-$, the remaining μ-H atom is in a rigid position, bridging B9 to B8: E = S [182, 189], NR {R = H, Bzl, Ph [29, 188]}. The N-bound proton in $(NH)B_9H_{10}^-$ does not migrate into the bridging position B9–B10 to give $NB_9H_{11}^-$. Organic derivatives are well known: $EB_9H_{10}R$ {R in pos. 9; E = S [176, 190], NR′ [29, 104]}, $SB_9H_9R_2$ (R in pos. 1,9) and $SB_9H_8R_3$ (R in pos. 1,3,9) [190]}. In SB_9H_9R with $R = CH_2NH_2Bu^t$ (in pos. 9), the anionic negative cluster charge is balanced by the positive ammonium charge of the ligand, μ-H bridging again B8–B9 [183]. The azido-derivative $(NH)B_9H_{10}(N_3)$ (N_3 in pos. 5) [187, 188] deserves no particular interest. In the amino-derivative $(NR)B_9H_{10}(NR'R'')$ {$R = 4\text{-}ClC_6H_4$; $NR'R'' = NHBu^t$, NEt_2, $NPr^i{}_2$ (in pos. 9)}, however, the amino group seems to cause some B9–N π-interaction, so that the two extra-H atoms lose their bridging function, B9–B8 and B9–B10, and move more or less into an *endo*-position at B8 and B10, respectively. In a way, the BN π-electrons increase the number of the cluster electrons and change the electron count towards an ar-10⟨VI⟩ structure, so that the bridging H atoms approach the "gunwale" positions of the boat-type aperture {7–8, 5–10; see (f) in Figure 3.4-17 [29]}.

More than one heteroatom may be incorporated into the ni-10⟨VI⟩ skeleton. We mention the 6,9-thiacarbaborate $S(CH)B_8H_8^-$ with no extra-H atom [191], the 6,8,2,7-thiacarbadimetallaborane $[S(CH)B_6H_7M_2]$ {M = IrCp*, μ-H in position 9–10 [192]}, and the 5,9,6-dithiametallaborane $[S_2B_7H_8M]$ {M = FeCp [193]}. The electronegative sulfur atom generally prefers the 3k vertex 6, but sulfur can also occupy a 4k vertex (as in the preceding example).

There is a series of metallaboranes of the type $[SB_8H_{10}M]$, $[S_2B_7H_7M]$, etc., where M seems to contribute two cluster electrons giving a *nido*-electron count. Nevertheless, these metallaboranes must be designated as *arachno*-clusters. Though the principal structure of the 10-vertex *nido*- and *arachno*-skeleton is the same, they differ structurally by the position of the bridging H atoms (which are the gunwale positions 5–10 and 7–8 in the *arachno*-case) and, moreover, in their physical properties, particularly in the sequence of the ^{11}B NMR shift values. We will discuss the ar-10 clusters with formal ni-10 electron count later.

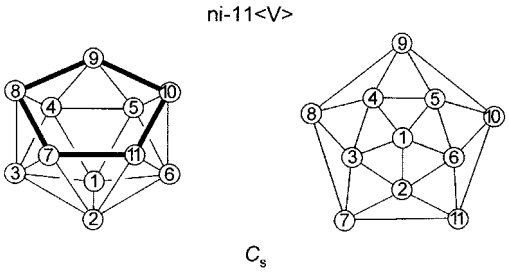

Fig. 3.4-9. Perspective and planarized representation of the ni-11⟨V⟩ structure of hypothetical $B_{11}H_{11}^{4-}$ (derived from cl-12 minus B12; aperture in bold lines).

3.4.3.7
The ni-11 Family

The ni-11⟨V⟩ clusters with their typical monocapped pentagonal-antiprismatic structure (Figure 3.4-9) have been comprehensively investigated. The group 15 and group 16 heteroatoms are generally found in the 4k positions of the pentagonal aperture.

Several theoretical studies are available, older semiempirical work as well as more recent *ab initio* computations, often directed towards the comparison of observed and computed NMR shifts. Clusters $SB_{10}H_{12}$, $(PR)B_{10}H_{12}$ with one heteroatom and the corresponding anions $SB_{10}H_{11}^-$, $(PR)B_{10}H_{11}^-$ have been investigated [58, 194]. Two heteroatoms are discussed in positions 7 and 9 {$S_2B_9H_9$ [195], $Se_2B_9H_9$ [195], $S(PR)B_9H_9$ [194]} and three heteroatoms in positions 7, 8, 9 {$S(CH)_2B_8H_8$, $(PR)(CH)_2B_8H_8$ [194]} or 7, 9, 10 {$S(CH)_2B_8H_8$ [58, 194, 196] and $(NH)(CH)_2B_8H_8$ [57, 64, 197]}.

Experimental studies include the simple species $EB_{10}H_{12}$: E = S [34, 42, 46, 58, 137, 180, 198], Se [76, 198], Te [76, 198], NR {R = H, $NB_2HBu^t_3$ [62, 199, 200]}, PR {R = Me, Ph [194, 198]}, AsR {R = Me, Ph [107, 198]}. The two extra-H atoms bridge B8–B9 and B10–B11. The corresponding anions $EB_{10}H_{11}^-$ are as well known with μ-H in the bridging position B9–B10: E = S [34, 35, 194], Se [73, 77, 78, 82, 87, 201, 202], Te [77, 82, 88, 89, 203], NH [105, 106], PR {R = Me, Ph [194]}, AsR {R = Me, Ph [107]}. The corresponding anions $(PH)B_{10}H_{11}^-$ and $(AsH)B_{10}H_{11}^-$, however, are unknown, in contrast to their isomers $PB_{10}H_{12}^-$ [204] and $AsB_{10}B_{12}^-$ [107, 108, 198]. Note the reverse situation with the azaboranes $(NH)B_{10}H_{11}^-$ and $NB_{10}H_{12}^-$, the latter being unknown, a situation, that we encountered in the ni-10 family in an analogous manner. Such a difference parallels the Brønsted acidity sequence $NH_4^+ < PH_4^+ < AsH_4^+$. Dianions $EB_{10}H_{10}^{2-}$ have also been described: E = S [205], NH [105, 106].

Two non-metallic heteroatoms are present in 7,9-$S_2B_9H_9$ [94, 195], 7,9-$Se_2B_9H_9$ [94, 175, 195, 206], 7,8-$Se_2B_9H_9$ [207, 208], 7,9-$SSeB_9H_9$ [94, 195], 7,8-$As_2B_9H_{10}^-$ [107], 7,8-$As_2B_9H_9^{2-}$ [136, 139], 7,8-$Sb_2B_9H_9^{2-}$ [136, 139], and 7,9-$S(PR)B_9H_9$ {R = Me, Ph [194]}. An additional carbon vertex is found in 7,9-$S(CH)B_9H_{10}$ [191],

7,8-E(CL)B_9H_9 {E = S, Se; L = NH_2Cy [179]}, 7,9-Se(CL)B_9H_9 {L = NMe_3) [209]}, E(CH)$B_9H_{10}^-$ {E = P, Sb (7,8-isomers [117, 204]); E = As (7,8- and 7,9-isomers) [116, 117)}, E(CH)$B_9H_9^{2-}$ {E = P (7,8-isomer), E = As (7,8- and 7,9-isomers) [127]}, and (AsMe)(CH)B_9H_{10} (both isomers) [117].

Among the 11-vertex-*nido*-clusters with three non-metallic heteroatoms, we mention first the species 7,8,11-E$As_2B_8H_8$ {E = S, Se [201, 210, 211]} and then the dicarbaboranes 7,9,10-E$(CH)_2B_8H_8$ {E = S [212–214], Se [207], NH [197, 212, 215], NR (R = Me, Bzl) [197, 215]}, 7,8,9-E$(CH)_2B_8H_9$ {E = P, As [132]}, 7,8,9-(PR)$(CH)_2B_8H_8$ {R = Me, Ph [194]} and the azadicarbaborate 7,9,10-N$(CH)_2B_8H_8^-$ [197]. A 7,8,9,11-diarsadicarba-*nido*-undecaborane, $As_2(CH)_2B_7H_7$, has also been characterized [201, 211].

In the 7,8-thiametalla-*nido*-undecaboranes [$SB_9H_{11}M$] or [$SB_9H_{10}ClM$] (Cl in pos. 9), the metal vertex contributes two electrons to the cluster: M = Ru(ar) {ar = toluene, *p*-cymene [47, 180, 216]}, $IrCp^*$ [48]. Boranes of the type 7,8-[$SB_9H_{10}M$] meet the *nido*-cluster electron count, when M contributes three electrons: M = RhL_3 {L = $P(OMe)_3$, PMe_2Ph}, $Rh(CO)(PPh_3)_2$, RhL(dppe) {L = CO, MeCN, η^1-dppe}, RhLL′ {L = η^1-dppe; L′ = η^2-dppe, $Cl_2Ru(PPh_3)$(cymene) (connected to the cluster metal atom via two Cl bridges)} [53, 54, 217–220]. A particular example is presented by 7,8-[SB_9H_9(SMe)M], where the metal vertices $Ir(PPh_3)_2$ or Rh(η^4-C_5HMe_5) can contribute only one electron [221]; the SMe ligand with a lone pair at sulfur bridges B9–B10, thus balancing the *nido*-electron count by the contribution of three electrons. Three electrons are also provided to the cluster by rhodium in 7,8-[SB_9H_9M] with M = RhL_2L' {L = PPh_3, L′ = S=CH–S^-, with one of the two sulfur atoms replacing the *exo*-H atom at B9, thus forming a five-membered ring, condensed to the cluster [96]}.

Thiametallaboranes [$SB_9H_{10}M$] can undergo a rapid skeletal enantiomerization via a transition state of C_s symmetry, including the opening of two M–B bonds and the closure of two equivalent M–B bonds {Figure 3.4-10; M = $Rh(PPh_3)_2$ [96]}.

In the dithiametallaboranes [$S_2B_8H_8M$], two isomers are possible, the 7,8,9- {M = Ru(cymene) [216]} and the 7,9,8-isomer {M = $RhH(PMe_3)_2$ [45]}. The 7,9,8-isomer is also present in [S(CH)B_8H_9M] {M = $RhH(PPh_3)_2$ [56]}. Four heteroatoms, finally, are found in the compound [$SAs_2B_7H_7M$] {M = CoCp [201, 211]}.

There are several thiametallaboranes [$SB_9H_{10}M$] (or derivatives [SB_9H_9XM] and [SB_9H_8LM] thereof) with the one-electron contributing metalla-vertex RhL_2 and an

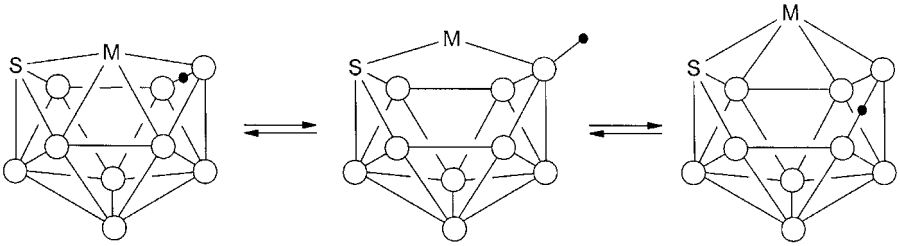

C_s

Fig. 3.4-10. Enantiomerization equilibrium of [$SB_9H_{10}M$].

apparent *closo*-count. (Note that the symbol X means an ordinary substituent and L a neutral Lewis base, which carries a positive formal charge when bound to the cluster, here and elsewhere.) Nevertheless, these clusters belong to the *nido*-family with the typical ni-11⟨V⟩ structure, the heteroatoms being found in the positions 7 and 8 and the bridging proton more or less fluctuating between the 9–10 and the 10–11 positions. The metal ligands L in these thiametallaboranes turn out to contain a phosphorus-bound phenyl group: RhL_2 = $Rh(PPh_3)_2$, Rh(dppe) [51, 53, 55, 74, 75, 96, 219, 222, 223]. As an additional result, the *nido*-cluster $[SB_9H_{10}M]$ {M = Rh(dppe)(NCMe)}, which clearly gives a *nido*-electron count, loses acetonitrile on standing, but the loss of two electrons does not alter the ni-11⟨V⟩ skeletal framework [51, 53]. Conversely, the thiametallaborane $[SB_9H_{10}M]$ {M = $Rh(PPh_3)_2$}, a *closo*-counting *nido*-species, can add CO to the metal without structural change [54]. Similarly, the *nido*-skeletal framework of $[SB_9H_{10}M]$ {M = $Rh(PPh_3)_2$} is not changed, when CS_2 is added, giving a hydroboration of a C=S bond by the B9–H9 bond and a coordination of the second S atom to the metal; the $S{=}CH{-}S^-$ anion connects M to B9 and changes the *closo*- to a *nido*-count without skeletal alteration [96]. When the *nido*-species $[SB_9H_{10}M]$ {M = Rh(dppe)} is deprotonated to give $[SB_9H_9M]^-$, however, the electron count does not change, obviously, but the cluster skeleton is transformed from the ni-11 into the cl-11 type [51, 53]. As an explanation, one of the *ortho*-C–H bonds of a sterically appropriate phenyl group had been considered. The electron pair of the C–H bond is assumed to accept the Rh atom as the third center of a 3c2e bond (agostic interaction), thus transforming the seemingly *closo*- into an actual *nido*-electron count [51, 53]. This explanation is supported by the structural analysis of $[SB_9H_{10}(RhL)]$, where the ligand L means the dppe-borane adduct $Ph_2P{-}CH_2{-}CH_2{-}PPh_2(BH_3)$: the ligand being only monodentate via phosphorus, the BH_3 moiety gives two Rh–H–B 3c2e bonds and provides the metal with three electron pairs in total, thus leading to a *nido*-electron count for the cluster [219].

3.4.3.8 The ni-12 Family

The ni-12 clusters $EB_{11}H_{12}^-$ with the hetero-vertices E = O, S, NH in the 3k position 1 were theoretically investigated by semiempirical [59, 224] as well as by *ab initio* methods [225]. The non-planar pentagonal aperture of the hypothetical $B_{12}H_{12}^{4-}$ contains a trapezoidal arrangement of B4, B5, B8 and B9, and the vertices B4 and B5 are connected by B1 above the trapezoidal plane (Figure 3.4-11).

Two of the simple anions $EB_{11}H_{12}^-$ have been synthesized: E = O [59, 224, 226–230] and E = NMe [100]. The extra-H atom bridges the two 4k vertices B8 and B9. A large number of derivatives of $(NR)B_{11}H_{12}^-$ have been characterized: $(NR)B_{11}H_{11}X^-$ {X in pos. 2; R = H, X = OMe; R = Me, X = F, Cl, OMe, OBu^t, NEt_2, NHBu, Me, Bu, $Fe(CO)_2Cp$; R = Ph, X = OH, Br, N_3, $NHBu^t$ [100, 103, 231]}, $(NR)B_{11}H_{11}L$ {L in pos. 2 or 8; R = Me, L = $NHEt_2$, NH_2Bu^t, py; R = Ph, L = NMe_3, NEt_3 [100]}, $(NPh)B_{11}H_5Me_5(OTrf)(OH)^-$ {OH in pos. 2, triflate in pos. 12, Me in the remaining 5k positions [103]}, $(NMe)B_{11}H_5Me_5(OTrf)(NEt_3)$ {NEt_3 in pos. 2, triflate and Me as before [103]}, $(NMe)B_{11}H_{10}IMe^-$ {Me in pos. 2,

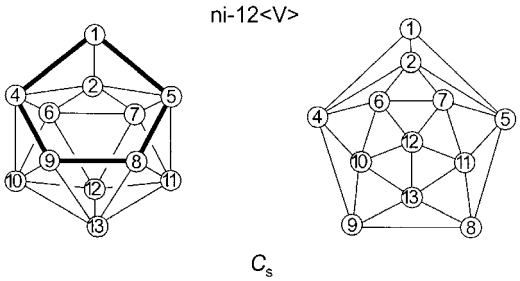

Fig. 3.4-11. Perspective and planarized representation of the ni-12⟨V⟩ structure of hypothetical $B_{12}H_{12}^{4-}$ (derived from cl-13 minus B3; aperture in bold lines).

I in pos. 12 [103]}, $(NMe)B_{11}H_{10}Hal(NEt_3)$ {NEt_3 in pos. 2, Hal = Br, I in pos. 12 [103]}.

In the phospha- and arsacarba-*nido*-dodecaborates $E(CH)B_{10}H_{10}^{2-}$ (E = P, As), the heteroatoms presumably occupy the 3k and one of the two 4k positions [121]. The same is true for the oxametallaborane $[OB_{10}H_9ClLM]$ {M = $RhCp^*$ in pos. 8; L = PMe_2Ph at B9; Cl at B5 [232, 233]}. Analogously, the group 15 elements E of $E(CMe)_2B_9H_9$ are found in pos. 1 and the two carbon vertices in pos. 8,9 {E = PCl, PPr^i, AsCl, $AsPr^i$ [234]}. In $(AsR)(CH)_2B_9H_9$ (R = Me, Bu, Ph), a similar structure might be present, although a cl-12 species has been suggested [235]. In $[E_2B_9H_9M]$, the non-metallic heteroatoms are found in the low-connectivity positions 1 and 8, the metal however in the 5k position 5, adjacent to the heteroatoms {E = S, M = Ru(cymene), CoCp, $RhCp^*$ [50, 94, 216]; E_2 = SSe, M = CoCp [94], CoXCoCp (X is the Cp-analogous 1,3,4,5-tetraethyl-2-methyl-1,3-diboracyclopentadienide(3–) anion, which makes a type of tripledecker out of the molecule) [50]; E = Se, M = CoCp [94], $IrH(PPh_3)_2$ [75]}.

We discussed $[SB_9H_9(SMe)M]$ {M = $Ir(PPh_3)_2$, etc.} as an ni-11 species, considering the SMe unit as a bridging ligand. One could write the same molecule as $[S(SMe)B_9H_9M]$, considering the SMe unit as a vertex and thus arriving at an ni-12⟨VI⟩ species with a hexagonal aperture. The structure can be derived from the common ni-12⟨V⟩ structure by opening the B1–B5 bond. The SMe group would then contribute five electrons to the cluster.

3.4.4 *Arachno*-Clusters

3.4.4.1 The ar-5 Family

Both ar-5 structures, ar-5⟨V⟩ and ar-5⟨V′⟩, were characterized in derivatives of the parent diazapentaborane $N_2B_3H_7$. The compounds $(NR)(NR'R'')B_3H_2R_2$ represent the non-planar ar-5⟨V⟩ skeleton with the group R′ in the *endo*-position {Figure 3.4-12; R = Bu^t, R′/R″ = H/Pr, H/Bu^t, Me/Me, Et/Et [150]}. The products

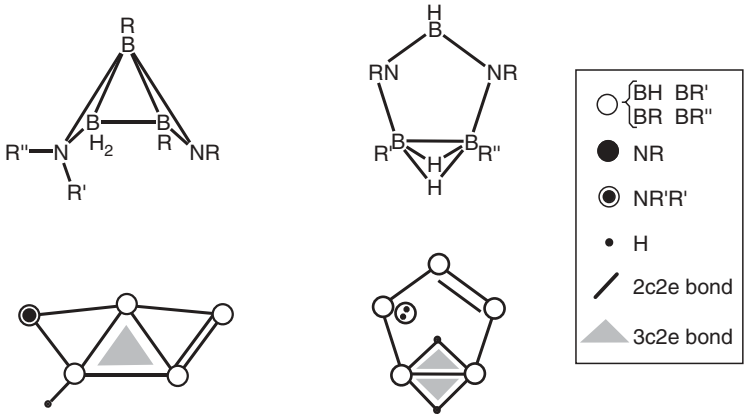

Fig. 3.4-12. Two derivatives of the hypothetical parent diaza-*arachno*-pentaborane $N_2B_3H_7$ with an ar-5⟨V⟩ and an ar-5⟨V′⟩ structure in a topological representation and in one with localized bonds.

$(NR)_2B_3H_3R'R''$ represent the planar ar-5⟨V′⟩ skeleton, in which B4 is connected to B5 via two H bridges; a lone pair at nitrogen and a BN double bond (Figure 3.4-12) perform an allyl anion-type resonance {R = Bu^t; R′ = H, R″ = H, Et, Pr, Bu, Bu^t and R′ = R″ = Et, Pr, Bu [236]}.

The ar-5⟨V⟩ structure was also found for $(SR')(NR)B_3H_2R_2$, a derivative of the parent SNB_3H_6, comparable to $N_2B_3H_7$ {R = Bu^t, R′ = Pr, Ph [237]}.

3.4.4.2
The ar-6, ar-7 and ar-8 Families

The cluster molecules and cations $OB_5H_{10}^+$, NB_5H_{10}, $(OH)B_5H_{10}^{2+}$, and $(NH)B_5H_{10}^+$ were investigated by *ab initio* computations [238]. A pentagonal pyramid with the hetero-vertex in the apical position and five hydrogen bridges along the basis (C_{5v}) was considered. A pentagonal-pyramidal skeleton can be derived from the cl-8 structure by removing B4 and B8.

There is a lack of experimental evidence for ar-6 and ar-7 clusters with group 15 and group 16 heteroatoms.

A compound $(NR)_2B_6H_2R_4$ (R = Bu^t) has been described [239], to which an ar-8 structure was attested, derived from a cl-10 skeleton by subtracting B5 and B7 and by opening the B4–B8 bond (Figure 3.4-13).

3.4.4.3
The ar-9 Family

All examples in this family, where group 15 or 16 elements replace a BH vertex, are derived from the ar-9⟨VI⟩ skeleton of *iso*-nonaborane(15) (Figure 3.4-14). The

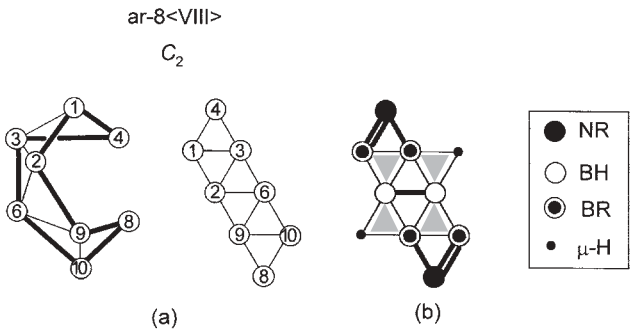

Fig. 3.4-13. (a) Perspective and planarized representation of the hypothetical ar-8⟨VIII⟩ $B_8H_8^{6-}$ structure (derived from cl-10 minus B5 and B7 and by opening of B4–B8; aperture in bold lines; numbering according to cl-10). (b) $(NR)_2B_6H_4R_4$ (R = Bu^t) in LMO presentation.

electronegative vertices E = S, Se, NH, CH^- are always found in one of the three equivalent 3k positions 4, 6, 8.

Theoretical studies have been carried out for EB_8H_{12} {E = S, NH [240]}, SEB_7H_9 {E = S, CH_2 [241]} and $S(CH_2)_2B_6H_6$ [242].

The four μ-H atoms of EB_8H_{12} {E = S [46, 76, 175, 177, 184, 186, 243–245], NH [175, 186, 246]} bridge the four B–B edges of the hexagonal aperture. Three BHB bridges are left in the anion 4-$SB_8H_{11}^-$, bridging B5–B6, B6–B7, B7–B8 in the ground state (C_1), however show fluxional behavior in solution (*pseudo*-C_s) [243, 247]. In derivatives of the type $SB_8H_{10}L$ with S in position 4, the ligand L is bound to the 3k vertex B6 in the *exo*-position, so that we have three extra-H atoms, one in the *endo*-position at B6 and two bridging H atoms (B7–B8 and B8–B9) {L = SMe_2, NMe_3, PMe_3, MeCN, py, etc. [173, 245, 248]}.

Two heteroatoms in the positions 4 and 6 are found with $S_2B_7H_9$ with hydrogen bridges in the positions B7–B8 and B8–B9 [241, 249, 250–252]. An analogous structure is found for $SSeB_7H_9$ [94], $S(CH_2)B_7H_9$ {with an *endo*-H atom at the carbon vertex [191, 241, 249, 253–255]}, and $S_2B_7H_8R$ {R = Me, Ph, CH=CH(CN)

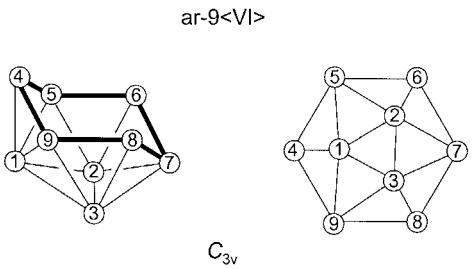

Fig. 3.4-14. Perspective and planarized representation of the ar-9⟨VI⟩ structure of hypothetical $B_9H_9^{6-}$ (derived from cl-12 minus B12 and B11; aperture in bold lines).

in pos. 8 [256–259]}. One bridging H atom in pos. 7–8 remains in the anion 4,6-$S_2B_7H_8^-$ [50] and possibly also in the short-lived anion $S(CH_2)B_7H_8^-$ [191].

An example with three heteroatoms is exhibited by $S(CH_2)_2B_6H_6$ with the heteroatoms in the three 3k positions and with two *endo*-H atoms at carbon [260].

The metal vertex in the clusters $[S_2B_6H_8M]$ {M = CoCp, $RhCp^*$, $Pd(PMe_2Ph)_2$ [46, 174, 193, 261]} and $[S(CH_2)B_6H_8M]$ {M = $RhCp^*$, $IrCp^*$ [254]} prefers the 4k position 5 between the electronegative heteroatoms in the positions 4 and 6, leaving the edges B7–B8 and B8–B9 for hydrogen bridging.

3.4.4.4
The ar-10 Family

The skeletal arrangement of the ar-10⟨VI⟩ structure, including the numbering system, is the same as for the ni-10⟨VI⟩ structure (Figure 3.4-8). An obvious difference is the position of the extra-H atoms, in the heteroborane as well as in the homoborane clusters. In the homoborane prototypes ni-$B_{10}H_{14}$ and ar-$B_{10}H_{12}L_2$, the four extra-H atoms of the *nido*-species connect the four 3k–4k edges, whereas the four extra-H atoms of the ar-species are found as two *endo*-H atoms at the 3k vertices (with L in the *exo*-position) and as two μ-H atoms connecting the 4k gunwale positions of the boat-type aperture.

The anions $EB_9H_{12}^-$ represent typical examples {(a) in Figure 3.4-15; E = S [34, 37, 47, 48, 50, 94, 182, 201, 211, 219, 243, 249, 262–268], Se [72, 211], Te [72], NR (R = H, Ph, Bzl) [24, 175, 188]}. The anions $EB_9H_{11}X^-$ belong to the same type {E = S, X = OH, CN in pos. 9 [49, 179]; E = Se, X = CN in pos. 9 [179]; E = NH, $X = N_3$ in pos. 5 [188]} and the base-borane adducts $EB_9H_{11}L$ as well [(b) in Figure 3.4-15]: E = S {L = thf, SMe_2, NH_3, NEt_3, $(CH_2)_6N_4$, py, isoquinoline, 4-picoline, 4,4′-bipyridine, PCy_2Ph, PPh_3, CNMe, $CNBu^t$, CNCy [49, 179, 186, 269–272]}, Se

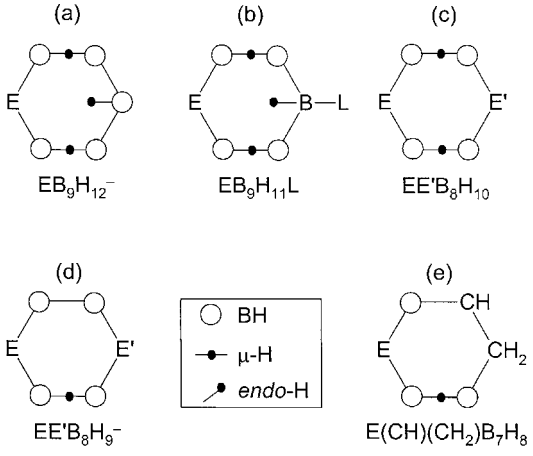

Fig. 3.4-15. The planarized hexagonal aperture of five types (a)–(e) of ar-10⟨VI⟩ heteroatom clusters.

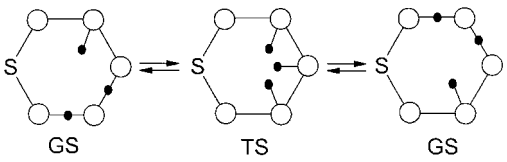

Fig. 3.4-16. The planarized hexagonal aperture of the ground state enantiomers (GS) and the transition state (TS) of the enantiomerization of $SB_9H_{12}^-$.

{L = NMe_3, NEt_3, $CNBu^t$, CNCy [72, 179]}, NH {L = SMe_2, NH_3, NEt_3, MeCN, urotropine, py, quinoline, isoquinoline, PH_3, PPh_3, CNMe, CNCy [24, 175, 186]}, NR {R = 4-C_6H_4Cl, L = NH_2Bu^t [29]}. The same is true for the adducts $(SB_9H_{11})_2$(L–L), where L–L is a didentate ligand such as urotropine [186] or [Fe{$C_5H_4(PPh_2)$}$_2$] (via phosphorus) [273].

The position of the extra-H atoms in Figure 3.4-15 follows from NMR or crystal structure analysis. The anion $SB_9H_{12}^-$ was also analyzed by a DFT calculation. Two enantiomers with two bridging and one *endo*-H atom form the ground state and are transformed into one another via a transition state with three *endo*-H atoms, 20.9 kJ mol^{-1} above the ground state (Figure 3.4-16) [247]. Averaging the calculated ^{11}B NMR shifts gave excellent agreement with the experimental data, which indicate *pseudo-*C_s symmetry.

The triazenido ligand in EB_9H_{10}(NH⋯N⋯NR) connects B4 to B9, thus forming a five-membered ring, which shares the B–B bond with the cluster. One of the three extra-H atoms is *endo*-bound to B9 {E = S, R = $SiMe_3$ [274]; E = NH, R = H, Bzl [275]}. Two heteroatoms are present in the clusters $EE'B_8H_{10}$ {(c) in Figure 3.4-14; EE′ = SeSe [72, 208, 276], $S(CH_2)$ (with a carbon-bound *endo*-H atom) [56, 58, 191, 254, 277], S(NH) [184]} and in the corresponding anions $EE'B_8H_9^-$ {(d) in Figure 3.4-15; EE′ = SeSe [276], $S(CH_2)$ [191]}. Finally, we must mention the three-heteroatom clusters $E(CH)(CH_2)B_7H_8$ {(e) in Figure 3.4-15; E = S [278], Se [208]} and [$SB_7H_7XM_2$] {S in pos. 5, M in pos. 6 and 9, X = OMe in pos. 8, μ-H in pos. 7–8; M_2 = CpRh–Cl–RhCp with the bridging Cl anion above the boat-type hexagon [279]}.

There are several metallaboranes, whose formal electron count identifies them as ni-10⟨VI⟩ clusters. According to the position of the extra-H atoms and to physical properties such as the characteristic sequence of ^{11}B NMR shifts, these clusters must be assigned as ar-10⟨VI⟩ species. Most examples are found with the type [$EB_8H_{10}(PtL_2)$] {(a) in Figure 3.4-17}: E = O {L = $PMePh_2$ [280]}, S {L = PEt_3, PMe_2Ph, PPh_3 [36, 281, 282]}, Se {L = PMe_2Ph [78]}, NH {L = PPh_3 [283, 246]}. Three heteroatoms are present in [SEB_7H_8M] {(b) in Figure 3.4-17}: E = S, M = $Rh(PPh_3)_2$ {M contributes only one electron to the cluster, balanced by the extra-H atom [252]}; E = CH, M = $Pt(PMe_2Ph)_2$ [255]. There are no extra-H atoms in [$S_2B_7H_7(PtL_2)$] {(c) in Figure 3.4-17; L = PMe_2Ph [251]}, whose *arachno*-character was concluded from the ^{11}B NMR data.

As pointed out above, clusters [$SB_9H_{10}M$] with a ni-11⟨V⟩ structure in spite of

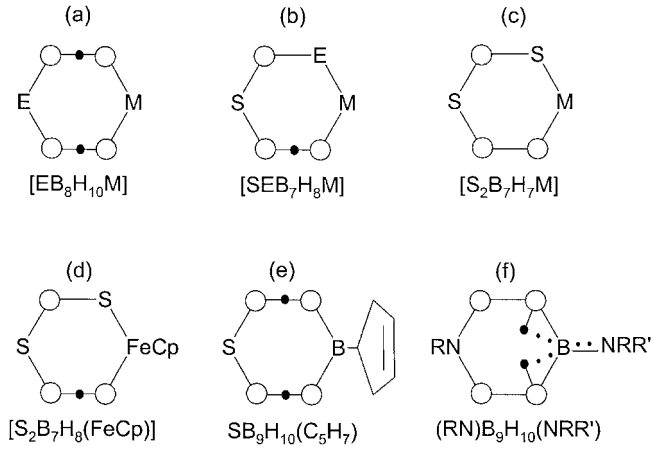

Fig. 3.4-17. The planarized hexagonal aperture of five types (a)–(e) of ar-10⟨VI⟩ heteroatom clusters and of a ni/ar-10⟨VI⟩ border-case (f).

a cl-11 cluster-electron count may obtain an additional cluster-electron pair through the agostic interaction of an *ortho*-CH bond of a phosphorus-bound phenyl group with the metal. Phosphorus-bound phenyl groups are also present in the ar-10⟨VI⟩ clusters just mentioned, so that a similar explanation for an *arachno*-electron count could come to mind. There is one example, however, $[SB_8H_{10}(PtL_2)]$ ($L = PEt_3$), where that explanation cannot apply because of the lack of Ph groups. A further example is given by the dithiaferraborane $[S_2B_7H_8(FeCp)]$ with a *nido*-count, but an *arachno*-structure {(d) in Figure 3.4-17 [193]} and, finally, by the non-metallaborane $SB_9H_{10}R$ {(e) in Figure 3.4-17; R = 3-cyclopentenyl [46]}. Are there electron contributions from the Cp group or from the C_5H_7-π-bond to the cluster skeleton? The border-case situation of the compound $(NR)B_9H_{10}(NR'R'')$ has been discussed with respect to the ni-10 family {(f) in Figure 3.4-17}.

3.4.4.5 The ar-11 Family

The ar-11⟨VI⟩ structure can formally be derived from the ni-11⟨V⟩ structure by the opening of one bond at the aperture, thus generating a VI- from a V-aperture (Figure 3.4-18). The 3k positions 9 and 10 are expected to host electronegative heteroatoms.

An example of an ar-11⟨VI⟩ cluster with one heteroatom is presented by the anion $(NH)B_{10}H_{13}^-$ with the NH moiety in position 9 {(a) in Figure 3.4-19}. The azido group of $(NH)B_{10}H_{12}(N_3)^-$ can be bound to B2 or to B8, with one of the extra-H atoms bridging B7–B8 or remaining chiefly in an *endo*-position at B7, respectively [187, 188]. Two heteroatoms in the anions $S_2B_9H_{10}^-$ {(b) in Figure 3.4-19 [50, 189, 284]}, $S(NR)B_9H_{10}^-$ and $Se(NR)B_9H_{10}^-$ {(c) in Figure 3.4-19;

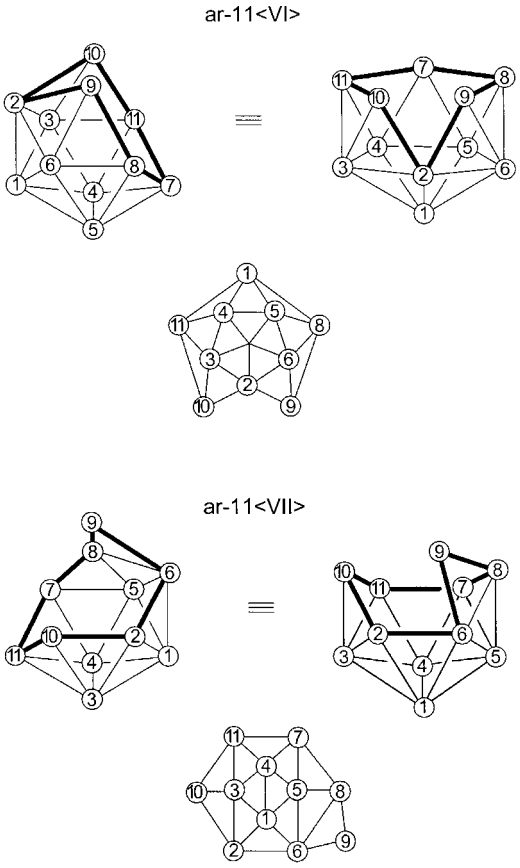

Fig. 3.4-18. Perspective and planarized representation of the ar-11⟨VI⟩ (derived from cl-13 minus B1, B5) and of the ar-11⟨VII⟩ (derived from cl-13 minus B3, B5) structures of hypothetical $B_{11}H_{11}^{6-}$ (apertures in bold lines); the numbering of ar-11⟨VII⟩ is taken from that of ar-11⟨VI⟩, which is transformed into ar-11⟨VII⟩ by opening the B2–B9 bond.

R = Ph, 4-MeC_6H_4 [188]} are found in the 3k positions 9 and 10. An additional transition metal heteroatom can be accommodated in the 5k position 2: [S(SR)B_8H_9M] {(d) in Figure 3.4-19; R = $(CH_2)_5$I, M = RhCp* [284]}; the SR vertex with an *exo*-group R contributes five cluster electrons.

An alternative ar-11⟨VII⟩ is formed from the ar-11⟨VI⟩ structure by opening of the B2–B9 bond (Figure 3.4-18). Examples with one heteroatom in the 2k position are (SMe)$B_{10}H_{13}$, (SeMe)$B_{10}H_{13}$ {(a) in Figure 3.4-20 [285]} and $(NH_2)B_{10}H_{12}(N_3)$ {(b) in Figure 3.4-20; N_3 in position 8 [187, 188, 286]}. The vertices SMe, SeMe and NH_2 in these clusters are considered to contribute five electrons to the cluster, giving an *arachno*-electron count. One could argue, that all of these clusters exhibit ni-10⟨VI⟩ structures, derived from the parent $B_{10}H_{14}$ by replacing one bridging H

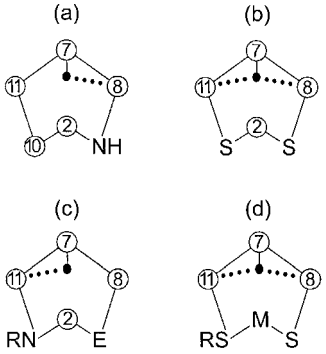

Fig. 3.4-19. The planarized hexagonal aperture of four ar-11⟨VI⟩ clusters [see text for an explanation of R and E; (a) and (b) represent anions].

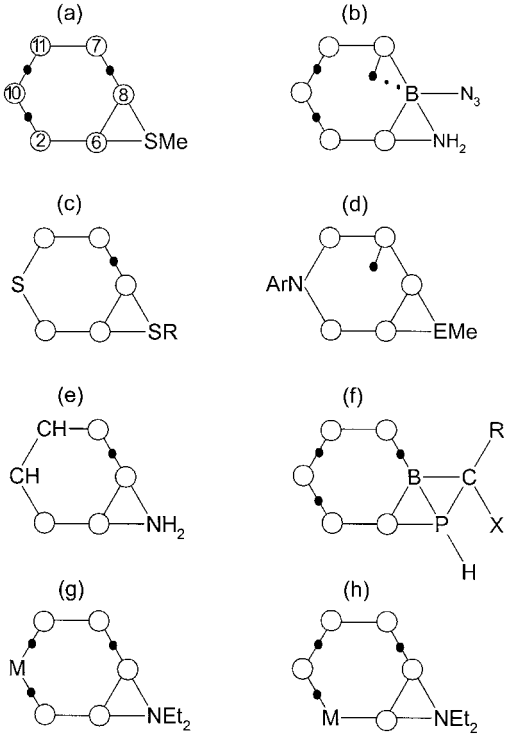

Fig. 3.4-20. The planarized heptagonal aperture of eight ar-11⟨VII⟩ clusters (see text for an explanation of R, Ar, X, E and M).

atom by the groups SMe, SeMe or NH_2 as one-electron donating moieties, with two lone pairs at sulfur or selenium and one lone pair at nitrogen. The compound $(NH_2)B_{10}H_{12}(N_3)$, however, is not only formally related to the above mentioned ar-11⟨VI⟩ anion $(NH)B_{10}H_{12}(N_3)^-$ (N_3 in position 8), but also chemically, since the anion is really formed from the neutral species by deprotonation. It does not seem reasonable that a deprotonation provokes a change in the number of cluster electrons and transforms a ni-10⟨VI⟩ into an ar-11⟨VI⟩ cluster. The same argument holds for the couple $S_2B_9H_{10}^-/S(SH)B_9H_{10}$, which can be reversibly transformed into each other by protonation or deprotonation, respectively. Analogously, $S_2B_9H_{10}^-$ can be methylated to give neutral $S(SMe)B_9H_{10}$. The neutral clusters exhibit the ar-11⟨VII⟩ and the anions the ar-11⟨VI⟩ structures {(c) in Figure 3.4-20 (R = H, Me) and (b) in Figure 3.4-19, respectively [189, 221, 285]}. A similar methylation relates $S(NR)B_9H_{10}^-$ and $Se(NR)B_9H_{10}^-$ {both ar-11⟨VI⟩; (c) in Figure 3.4-19 (E = S, Se)} to $(SMe)(NR)B_9H_{10}$ and $(SMe)(NR)B_9H_{10}$, respectively {(d) in Figure 3.4-20} [188].

An ar-11⟨VII⟩ structure could be assumed for $(NH_2)(CH)_2B_8H_9$ {(e) in Figure 3.4-20 [197, 212, 287]}. An amino bridged ni-10⟨VI⟩ structure, however, was also discussed for this heteroborane and as well for the two isomers of $[(NEt_2)B_9H_{12}M]$ {(g) and (h) in Figure 3.4-20; M = $RhCp^*$ [288]}.

Finally, the compound (–PH)$B_{10}H_{12}$(CXR–) is mentioned as a more sophisticated ar-11⟨VII⟩ example {(f) in Figure 3.4-20; CXR in pos. 8, R = Bu^t, X = $B_{10}H_{11}$(SMe) [289]}. The borane $B_{10}H_{13}(PEt_2)$ [290] seems to be a simpler example of a phosphino-bridged cluster, formally comparable to $B_{10}H_{13}$(SMe) {(a) in Figure 3.4-20}. The distance B6–B8 of 269 pm, however, no longer represents a bonding interaction, so that the phosphino group binds B6 to B8 by a covalent B6–P and a coordinative B8–P bond.

The Wade-Williams rules define a border between the electrons in the *endo*- and the *exo*-cluster sphere and relate the cluster classification to the *endo*-sphere. When this border becomes less distinct, the classification may no longer make sense. This is the case with the above mentioned ar-11⟨VII⟩ clusters, but also with the ni-10⟨VI⟩ example $(NR)B_9H_{10}(NR'R'')$ or with the above mentioned *closo*-counting ni-11⟨V⟩ examples $[SB_9H_{10}M]$. This border does not exist in *ab initio* calculations, which were described for several of the ar-11⟨VII⟩ clusters, e.g., for $(SMe)B_{10}H_{13}$ [285] or $(NH_2)(CH)_2B_8H_9$ [197], and logically cannot decide an artificial classification problem, though the classification turned out to be useful for a qualitative understanding in most cases. Physical properties such as the NMR shifts, charges, polarizabilities, etc., of the cluster vertices can be typical of the different cluster classes. A grey zone between the classes, however, will not always allow a clear classification.

3.4.5 *Hypho*-Clusters

A large number of borane clusters of the *hypho*-type are known that contain bridging groups such as CH_2, NH, S, etc. Formally, these groups could be considered to

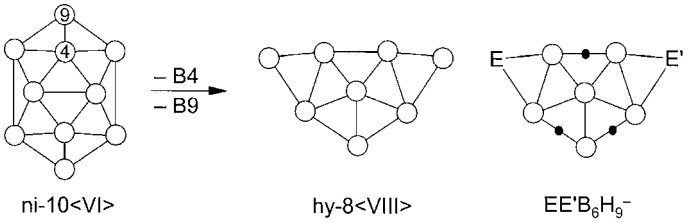

Fig. 3.4-21. The formal derivation of the hy-8⟨VII⟩ from the ni-10⟨VI⟩ skeleton and the real hy-8⟨VII⟩ anions $EE'B_6H_9^-$, all of them planarized.

be 2k vertices in a heteroborane cluster. We will discuss the situation for a few hy-8 and hy-9 clusters.

Anions $EE'B_6H_9^-$ exhibit an hy-8⟨VII⟩ structure {Figure 3.4-21; E/E′ = S/S [291–293], S/NH [184], S/CH_2 [191]} and the same is true for the neutral species $(ER)E'B_6H_9$ {ER/E′ = SMe/CH_2 [191], NH_2/S [184]}. The structure of $(SMe)_2B_6H_8$ is related to that of $EE'B_6H_9^-$ by removing the bridging H atom on the mirror plane and adding two methyl cations to sulfur [291].

Clusters with a pentagonal and a hexagonal aperture can formally be derived from $S_2B_6H_9^-$ by adding BH_2^+ {(a) in Figure 3.4-22 [193, 250, 291]}, by removing the proton on the mirror plane and adding E^{2+} {(b) in Figure 3.4-22; E = CH_2 [291], SiR_2 (R = Me, Ph) [193]}, or by adding M^+ {(c) in Figure 3.4-22; M = $Mn(CO)_4$ [193, 250], $RuCl(C_6Me_6)$ [292], $PdCl(PPh_3)_2$ [293]}. Replacement of the two μ-H atoms at B2 of $S_2B_7H_{11}$ by the 1-iminoethyl group, *endo*-bound to B2, removal of *endo*-H at B8, and addition of the imino-lone pair to B8 gives $S_2B_7H_8(CMe{=}NH)$ with a bridging CMe=NH unit [294]. In the dimeric cluster $[(S_2B_6H_8M)_2]$ {M = $Pd(PPh_3)$ [293]}, Pd is bound to S7, B2 and B3 of the one and to S9′ of the other cluster unit, and Pd′ *vice versa* to S7′, B2′, B3′ and S9 with hydrogen bridges connecting the edges 1–6, 4–5, 1′–6′, 4′–5′.

The *hypho*-electron count of the 9-vertex clusters $(NHR)B_8H_{11}(NH_2R')$ {R/R′ = Et/Et, Pr^i/Pr^i, Pr^i/Bu^t (Figure 3.4-23)} and $(NEt_2)B_8H_{11}(NHEt_2)$ [295] results from

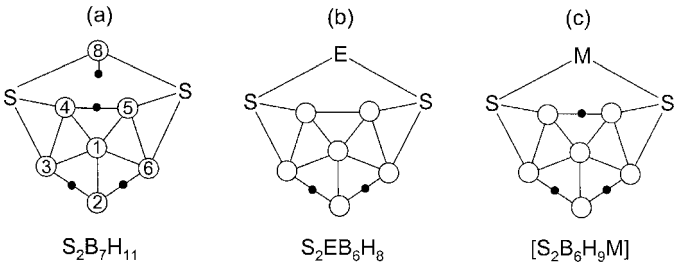

Fig. 3.4-22. Three types of planarized hy-9⟨V,VI⟩ clusters, derived from $S_2B_6H_9^-$ by adding BH_2^+ (a) or adding E^{2+} and subtracting H^+ (b) or by adding M^+ (c).

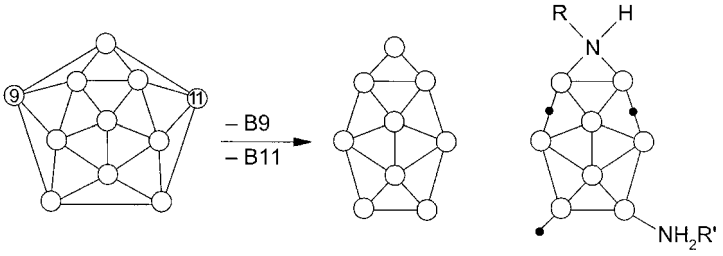

Fig. 3.4-23. The formal derivation of the hy-9⟨VII⟩ from the ni-11⟨V⟩ structure and the real hy-9⟨VII⟩ clusters $(NHR)B_8H_{11}(NH_2R')$.

the contribution of five cluster electrons of the NHR vertex including the $N–H_{endo}$ bonding electrons, i.e., three more electrons than one pair; three electrons from the extra-H atoms and two from the amine, acting as a Lewis base, give altogether eight electrons more than nine pairs.

References

1 K. Biermann, P. Paetzold, *Z. Anorg. Allg. Chem.*, **2001**, *627*, 2313.
2 M. Müller, P. Paetzold, *Coord. Chem. Rev.*, **1998**, *176*, 135.
3 M. Müller, J. Müller, P. Paetzold, K. Radacki, *Z. Anorg. Allg. Chem.*, **2000**, *626*, 1349.
4 E. D. Jemmis, G. Subramanian, B. V. Prasad, *Inorg. Chem.*, **1994**, *33*, 2046.
5 R. M. Minyaev, V. I. Minkin, T. N. Gribanova, A. G. Starikov, *Mendeleev Commun.*, **2001**, 132.
6 M. L. McKee, *J. Phys. Chem.*, **1991**, *95*, 9273.
7 E. D. Jemmis, G. Subramanian, *J. Phys. Chem.*, **1994**, *98*, 9222.
8 P. von Rague Schleyer, G. Subramanian, H. Jiao, K. Najafian, M. Hofmann, in *Advances in Boron Chemistry*, W. Siebert, ed., Royal Society of Chemistry, Cambridge, **1997**, p. 3.
9 M. C. Böhm, *Ber. Bunsenges. Phys. Chem.*, **1981**, *85*, 755.
10 H. Yu, Z. Yang, Z. Wang, Y. Zhu, *Gaodeng Xuexiao Huaxue Xuebao*, **1988**, *9*, 144.
11 R. Schäfer, W. Einholz, W. Keller, G. Eulenberger, W. Haubold, *Chem. Ber.*, **1995**, *128*, 735.
12 W. Einholz, R. Schäfer, W. Keller, B. Vogler, *Z. Naturforsch. B*, **1997**, *52*, 221.
13 W. Keller, G. Sawitzki, W. Haubold, *Z. Anorg. Allg. Chem.*, **2000**, *39*, 1282.
14 W. Siebert, K. Kinberger, *Angew. Chem.*, **1976**, *88*, 451; *Angew. Chem., Int. Ed. Engl.*, **1976**, *15*, 434.
15 W. Siebert, T. Renk, K. Kinberger, M. Bochmann, C. Krüger, *Angew. Chem.*, **1976**, *88*, 850; *Angew. Chem., Int. Ed. Engl.*, **1976**, *15*, 779.
16 W. Siebert, C. Böhle, C. Krüger, Y.-H. Tsay, *Angew. Chem.*, **1978**, *90*, 558; *Angew. Chem., Int. Ed. Engl.*, **1978**, *17*, 527.
17 J. Edwin, M. Bochmann, M. C. Böhm, D. E. Brennan, W. E. Geiger, C. Krüger, J. Pebler, H. Pritzkow, W. Siebert, W. Swiridoff, H. Wadepohl, J. Weiss, U. Zenneck, *J. Am. Chem. Soc.*, **1983**, *105*, 2582.
18 J. Edwin, W. Siebert, C. Krüger, *J. Organomet. Chem.*, **1985**, *282*, 297.

19 W. Siebert, W. Rothermel, *Angew. Chem.*, **1977**, *89*, 346; *Angew. Chem., Int. Ed. Engl.*, **1977**, *16*, 333.

20 W. Siebert, W. Rothermel, C. Böhle, C. Krüger, D. J. Brauer, *Angew. Chem.*, **1979**, *91*, 1014; *Angew. Chem., Int. Ed. Engl.*, **1979**, *18*, 949.

21 W. Siebert, C. Böhle, C. Krüger, *Angew. Chem.*, **1980**, *92*, 758; *Angew. Chem., Int. Ed. Engl.*, **1980**, *19*, 746.

22 J. MacCurtain, P. Brint, T. R. Spalding, *J. Chem. Soc., Dalton Trans.*, **1985**, 2591.

23 R. Zahradnik, V. Balaji, J. Michl, *J. Comput. Chem.*, **1991**, *12*, 1147.

24 A. Arafat, J. Baer, J. C. Huffman, L. J. Todd, *Inorg. Chem.*, **1986**, *25*, 3757.

25 L. Schneider, U. Englert, P. Paetzold, *Z. Anorg. Allg. Chem.*, **1994**, *620*, 1191.

26 F. Meyer, J. Müller, M. U. Schmidt, P. Paetzold, *Inorg. Chem.*, **1993**, *32*, 5053.

27 M. Roth, P. Paetzold, *Chem. Ber.*, **1995**, *128*, 1221.

28 P. Lomme, M. Roth, U. Englert, P. Paetzold, *Chem. Ber.*, **1996**, 1227.

29 M. Roth, F. Meyer, P. Paetzold, *Coll. Czech. Chem. Commun.*, **1997**, *62*, 1299.

30 W. Dirk, E. Leuschner, P. Roth, P. Paetzold, M. Roth, in *Advances in Boron Chemistry*, W. Siebert, ed., Royal Society of Chemistry, Cambridge, **1997**, p. 399.

31 U. Dörfler, J. D. Kennedy, L. Barton, C. M. Collins, N. P. Rath, *J. Chem. Soc., Dalton Trans.*, **1997**, 707.

32 J. L. Little, M. A. Whitesell, R. W. Chapman, J. G. Kester, J. C. Huffman, L. J. Todd, *Inorg. Chem.*, **1993**, *32*, 3369.

33 W. L. Smith, B. J. Meneghelli, N. McClure, R. W. Rudolph, *J. Am. Chem. Soc.*, **1976**, *98*, 624.

34 W. R. Pretzer, R. W. Rudolph, *J. Am. Chem. Soc.*, **1976**, *98*, 1441.

35 D. A. Thompson, W. R. Pretzer, R. W. Rudolph, *Inorg. Chem.*, **1976**, *15*, 2948.

36 T. K. Hilty, D. A. Thompson, W. M. Butler, R. W. Rudolph, *Inorg. Chem.*, **1979**, *18*, 2642.

37 R. W. Rudolph, W. R. Pretzer, *Inorg. Synth.*, **1983**, *22*, 226.

38 H. Mollendal, S. Samdal, J. Holub, D. Hnyk, *Inorg. Chem.*, **2002**, *41*, 4574.

39 W. L. Smith, B. J. Meneghelli, D. A. Thompson, P. Klymko, N. McClure, M. Bower, R. W. Rudolph, *Inorg. Chem.*, **1977**, *16*, 3008.

40 T. P. Fehlner, M. Wu, B. J. Meneghelli, R. W. Rudolph, *Inorg. Chem.*, **1980**, *19*, 49.

41 B. J. Meneghelli, R. W. Rudolph, *J. Organomet. Chem.*, **1977**, *133*, 139.

42 W. R. Pretzer, R. W. Rudolph, *Inorg. Chem.*, **1976**, *15*, 1779.

43 W. R. Pretzer, R. W. Rudolph, *J. Chem. Soc., Chem. Commun.*, **1974**, 629.

44 W. R. Pretzer, T. K. Hilty, R. W. Rudolph, *Inorg. Chem.*, **1975**, *14*, 2459.

45 J. Bould, N. P. Rath, L. Barton, *Organometallics*, **1996**, *15*, 4916.

46 S. O. Kang, P. J. Carroll, L. G. Sneddon, *Inorg. Chem.*, **1989**, *28*, 961.

47 M. Bown, X. L. R. Fontaine, N. N. Greenwood, J. D. Kennedy, *Z. Anorg. Allg. Chem.*, **1991**, *602*, 17.

48 K. Nestor, X. L. R. Fontaine, N. N. Greenwood, J. D. Kennedy, M. Thornton-Pett, *J. Chem. Soc., Dalton Trans.*, **1991**, 2657.

49 A. R. Siedle, D. McDowell, L. J. Todd, *Inorg. Chem.*, **1974**, *13*, 2735.

50 W. Weinmann, H. Pritzkow, W. Siebert, L. G. Sneddon, *Chem. Ber.*, **1997**, *130*, 329.

51 K. J. Adams, T. D. McGrath, R. L. Thomas, A. S. Weller, A. J. Welch, *J. Organomet. Chem.*, **1997**, *527*, 283.

52 K. J. Adams, T. D. McGrath, R. L. Thomas, A. S. Weller, A. J. Welch, *J. Orgamomet. Chem.*, **1997**, *534*, 249.

53 K. J. Adams, T. D. McGrath, G. M. Rosair, A. S. Weller, A. J. Welch, *J. Organomet. Chem.*, **1998**, *550*, 315.

54 S. Coughlan, T. R. Spalding, G. Ferguson, J. F. Gallagher, A. J. Lough, X. L. R. Fontaine, J. D. Kennedy, B. Stibr, *J. Chem. Soc., Dalton Trans.*, **1992**, 2865.

55 R. Macias, N. P. Rath, L. Barton, *Organometallics*, **1999**, *18*, 3637.

56 K. Nestor, J. D. Kennedy, M. Thornton-Pett, J. Holub, B. Stibr, *Inorg. Chem.*, **1992**, *31*, 3339.

57 J. Bicerano, W. N. Lipscomb, *Inorg. Chem.*, **1980**, *19*, 1825.

58 T. Vondrak, S. Hermanek, J. Plesek, *Polyhedron*, **1993**, *12*, 1301.

59 C. Serrar, A. Ouassas, A. Boutalib, E. Barday, B. Gautheron, B. Hanquet, B. Frange, *Main Group Met. Chem.*, **1997**, *20*, 247.

60 E. D. Jemmis, B. Kiran, D. Coffey Jr., *Chem. Ber.*, **1997**, *130*, 1147.

61 M. Zhang, Y. Zhao, *THEOCHEM*, **2001**, *545*, 105.

62 J. Müller, J. Runsink, P. Paetzold, *Angew. Chem.*, **1991**, *103*, 201; *Angew. Chem. Int. Ed. Engl.*, **1991**, *30*, 175.

63 W. Yu, M. Zhang, J. Sun, *Science in China B*, **1996**, 449.

64 S. P. Ionov, N. T. Kuznetsov, *Russ. J. Coord. Chem.*, **2000**, *26*, 325.

65 D. Hnyk, E. Vajda, M. Buehl, P. von Rague Schleyer, *Inorg. Chem.*, **1992**, *31*, 2464.

66 D. Hnyk, M. Bühl, P. von Rague Schleyer, H. V. Volden, S. Gundersen, J. Müller, P. Paetzold, *Inorg. Chem.*, **1993**, *32*, 2442.

67 J. Müller, P. Paetzold, B. Steuer, W. Preetz, B. Wrackmeyer, *Z. Anorg. Allg. Chem.*, **1999**, *625*, 2003.

68 W. Fendrich, J. E. Harvey, P. Kaszynski, *Inorg. Chem.*, **1999**, *38*, 408.

69 J. Plesek, S. Hermanek, *J. Chem. Soc., Chem. Commun.*, **1975**, 127.

70 J. Machacek, V. Vsetecka, D. Hnyk, S. Hermanek, in *Contemporary Boron Chemistry*, M. G. Davidson, A. K. Hughes, T. B. Marder, K. Wade, eds., Royal Society of Chemistry, Cambridge, **2000**, p. 155.

71 G. D. Friesen, L. J. Todd, *J. Chem. Soc., Chem. Commun.*, **1978**, 349.

72 G. D. Friesen, R. L. Kump, L. J. Todd, *Inorg. Chem.*, **1980**, *19*, 1485.

73 D. Reed, G. Ferguson, B. L. Ruhl, O. N. Dhubhghaill, T. R. Spalding, *Polyhedron*, **1988**, *7*, 17.

74 M. Murphy, T. R. Spalding, G. Ferguson, J. F. Gallagher, *Acta Crystallogr.*, **1992**, *C48*, 638.

75 R. Macias, J. Holub, J. D. Kennedy, B. Stibr, M. Thornton-Pett, *J. Chem. Soc., Chem. Commun.*, **1994**, 2265.

76 P. Kaur, A. Brownless, S. D. Perera, P. A. Cooke, T. Jelinek, J. D. Kennedy, B. Stibr, M. Thornton-Pett, *J. Organomet. Chem.*, **1998**, *557*, 181.

77 J. L. Little, G. D. Friesen, L. J. Todd, *Inorg. Chem.*, **1977**, *16*, 869.

78 Faridoon, O. N. Dhubhghaill, T. R. Spalding, G. Ferguson, B. Kaitner, X. L. R. Fontaine, J. D. Kennedy, *J. Chem. Soc., Dalton Trans.*, **1989**, 1657.

79 G. Ferguson, M. Parvez, J. A. MacCurtain, O. N. Dhubhghaill, T. R. Spalding, D. Reed, *J. Chem. Soc., Dalton Trans.*, **1987**, 699.

80 G. Ferguson, J. D. Kennedy, X. L. R. Fontaine, Faridoon, T. R. Spalding, *J. Chem. Soc., Dalton Trans.*, **1988**, 2555.

81 G. Ferguson, J. D. Kennedy, X. L. R. Fontaine, Faridoon, T. R. Spalding, *J. Chem. Soc., Dalton Trans.*, **1989**, 383.

82 Faridoon, O. N. Dhubhghaill, T. R. Spalding, G. Ferguson, B. Kaitner, X. L. R. Fontaine, J. D. Kennedy, *J. Chem. Soc., Dalton Trans.*, **1988**, 2739.

83 G. Ferguson, Faridoon, T. R. Spalding, *Acta Crystallogr.*, **1988**, *C44*, 1368; Faridoon, T. R. Spalding, G. Ferguson, J. D. Kennedy, X. L. R. Fontaine, *J. Chem. Soc., Chem. Commun.*, **1989**, 906.

84 G. Ferguson, A. J. Lough, Faridoon, M. N. McGrath, T. R. Spalding, J. D. Kennedy, X. L. R. Fontaine, *J. Chem. Soc., Dalton Trans.*, **1990**, 1831.

85 G. Ferguson, D. O'Connell, T. R. Spalding, *Acta Crystallogr.*, **1994**, *C50*, 1432; P. A. Mceneaney, T. R. Spalding, G. Ferguson, *Inorg. Chem.*, **1997**, *26*, 145.

86 G. Ferguson, J. F. Gallagher, J. P. Sheehan, T. R. Spalding, J. D. Kennedy, R. Macias, *J. Chem. Soc., Dalton Trans.*, **1993**, 3147.

87 G. Ferguson, J. F. Gallagher, M. McGrath, J. P. Sheehan, T. R. Spalding, J. D. Kennedy, *J. Chem. Soc., Dalton Trans.*, **1993**, 27.

88 F. di Biani, F. Laschi, P. Zanello, G. Ferguson, J. Trotter, G. M.

O'Riordan, T. R. Spalding, *J. Chem. Soc., Dalton Trans.*, **2001**, 1520.
89 G. Ferguson, J. F. Gallagher, J. P. Sheehan, T. R. Spalding, *J. Organomet. Chem.*, **1998**, *550*, 477.
90 J. P. Sheehan, T. R. Spalding, G. Ferguson, J. F. Gallagher, B. Kaitner, J. D. Kennedy, *J. Chem. Soc., Dalton Trans.*, **1993**, 35.
91 B. R. Davis, I. Bernal, *J. Cryst. Mol. Struct.*, **1972**, *2*, 261.
92 B. R. Davis, I. Bernal, J. Buttone, M. L. Good, *Moessbauer Eff. Methodol.*, **1973**, *8*, 127.
93 G. Ferguson, B. L. Ruhl, O. N. Dhubhghaill, T. R. Spalding, *Acta Crystallogr.*, **1987**, *C43*, 1250.
94 G. D. Friesen, A. Barriola, P. Daluga, P. Ragatz, J. C. Huffman, L. J. Todd, *Inorg. Chem.*, **1980**, *19*, 458.
95 G. Ferguson, Faridoon, T. R. Spalding, *Acta Crystallogr.*, **1988**, *C44*, 1371.
96 G. Ferguson, M. C. Jennings, A. J. Lough, S. Coughlan, T. R. Spalding, J. D. Kennedy, X. L. R. Fontaine, B. Stibr, *J. Chem. Soc., Chem. Commun.*, **1990**, 891.
97 M. Thornton-Pett, J. D. Kennedy, F. Spalding, T. R. Spalding, *Acta Crystallogr.*, **1995**, *C51*, 840.
98 M. Thornton-Pett, J. D. Kennedy, S. P. Breen, T. R. Spalding, *Acta Crystallogr.*, **1995**, *C51*, 1496.
99 P. Paetzold, J. Müller, F. Meyer, H.-P. Hansen, L. Schneider, *Current Topics in the Chemistry of Boron*, (G. W. Kabalka, ed., Royal Society of Chemistry, Cambridge, **1994**, p. 337.
100 P. Lomme, F. Meyer, U. Englert, P. Paetzold, *Chem. Ber.*, **1995**, *128*, 1225.
101 L. Schneider, U. Englert, P. Paetzold, *Chem. Ber.*, **1994**, *127*, 87.
102 H. Yao, P. Lomme, C. Hu, P. Paetzold, *Z. Anorg. Chem.*, **2001**, *627*, 2477.
103 P. Paetzold, P. Lomme, U. Englert, *Z. Anorg. Allg. Chem.*, **2002**, *628*, 632.
104 P. Paetzold, E. Leuschner, *Z. Anorg. Allg. Chem.*, **2002**, *628*, 658.
105 H.-P. Hansen, J. Müller, U. Englert, P. Paetzold, *Angew. Chem.*, **1991**, *103*, 1357; *Angew. Chem. Int. Ed. Engl.*, **1991**, *30*, 1377.
106 H.-P. Hansen, U. Englert, P. Paetzold, *Z. Anorg. Allg. Chem.*, **1995**, *621*, 719.
107 J. L. Little, S. S. Pao, K. K. Sugathan, *Inorg. Chem.*, **1974**, *13*, 1752.
108 T. P. Hanusa, N. Roig de Parisi, J. G. Kester, A. Arafat, L. J. Todd, *Inorg. Chem.*, **1987**, *26*, 4100.
109 A. Ouassas, C. R'Kha, H. Mongeot, B. Frange, *Inorg. Chim. Acta*, **1999**, *180*, 257.
110 J. L. Little, *Inorg. Chem.*, **1979**, *18*, 1598.
111 J. L. Little, M. A. Whitesell, J. G. Kester, K. Folting, L. G. Todd, *Inorg. Chem.*, **1990**, *29*, 804.
112 A. J. Leffler, M. N. Alexander, P. L. Sagalyn, *J. Chem. Phys.*, **1977**, *67*, 844.
113 P. Brint, B. Sangchakr, M. McGrath, T. R. Spalding, R. J. Suffolk, *Inorg. Chem.*, **1990**, *29*, 47.
114 X. L. R. Fontaine, J. D. Kennedy, M. McGrath, T. R. Spalding, *Magn. Reson. Chem.*, **1991**, *29*, 711.
115 D. O'Connell, T. R. Spalding, G. Ferguson, *Acta Crystallogr.*, **1991**, *C47*, 492.
116 L. J. Todd, A. R. Burke, H. T. Silverstein, J. L. Little, G. S. Wikholm, *J. Am. Chem. Soc.*, **1969**, *9*, 3376.
117 L. J. Todd, A. R. Burke, A. R. Garber, H. T. Silverstein, B. N. Storhoff, *Inorg. Chem.*, **1970**, *9*, 2175.
118 A. N. Echeistova, Y. K. Syrkin, V. I. Kyskin, L. I. Zakharkin, *Zh. Strukt. Khim.*, **1971**, *12*, 728.
119 L. I. Zakharkin, V. I. Kyskin, *Izv. Akad. Nauk SSSR, Ser. Khim.*, **1971**, 2052.
120 L. I. Zakharkin, V. I. Kyskin, *Izv. Akad. Nauk SSSR, Ser. Khim.*, **1971**, 2053.
121 E. A. Yakovleva, G. G. Isaeva, V. I. Kyskin, L. I. Zakharkin, A. I. Shatenshtein, *Izv. Akad. Nauk SSSR, Ser. Khim.*, **1971**, 2797.
122 L. I. Zakharkin, V. I. Kyskin, *Izv. Akad. Nauk SSSR, Ser. Khim.*, **1972**, 214.

123 V. Bryukhova, V. I. Kyskin, L. I. Zakharkin, *Izv. Akad. Nauk SSSR, Ser. Khim.*, **1972**, 532.

124 L. A. Fedorov, V. I. Kyskin, L. I. Zakharkin, *Izv. Akad. Nauk SSSR, Ser. Khim.*, **1972**, 536.

125 L. E. Vinogradova, V. I. Kyskin, L. A. Leites, L. I. Zakharkin, *Izv. Akad. Nauk SSSR, Ser. Khim.*, **1972**, *11*, 2436.

126 L. I. Kruglyak, E. S. Petrov, V. N. Kalinin, E. G. Rys, L. I. Zakharkin, A. I. Shatenshtein, *Zh. Obshch. Khim.*, **1972**, *42*, 2670.

127 D. C. Beer, L. J. Todd, *J. Organometal. Chem.*, **1973**, *50*, 93.

128 E. I. Fedin, V. A. Antonovich, E. G. Rys, V. N. Kalinin, L. I. Zakharkin, *Izv. Akad. Nauk SSSR, Ser. Khim.*, **1975**, 801.

129 V. S. Mastryukov, E. G. Atavin, L. V. Vilkov, A. V. Golubinskii, V. N. Kalinin, G. G. Zhigareva, L. I. Zakharkin, *J. Mol. Struct.*, **1979**, *56*, 139.

130 I. M. Alymov, T. L. Khotsyanova, G. K. Semin, *Yad. Kvadrupol'nyi Rezon.*, **1976**, *1*, 89.

131 L. A. Fedorov, *Zh. Strukt. Khim.*, **1976**, *17*, 247.

132 H. M. Colquhoun, T. G. Greenhough, M. G. H. Wallbridge, *J. Chem. Res.*, **1979**, 248.

133 J. L. Little, S. S. Pao, *Inorg. Chem.*, **1978**, *17*, 584.

134 W. E. Geiger, D. E. Brennan, J. L. Little, *Inorg. Chem.*, **1982**, *12*, 2529.

135 M. McGrath, T. R. Spalding, X. L. R. Fontaine, J. D. Kennedy, M. Thornton-Pett, *J. Chem. Soc. Dalton Trans.*, **1991**, 3223.

136 S. A. Jasper, Jr., S. Roach, J. N. Stipp, J. C. Huffman, L. J. Todd, in *Current Topics in the Chemistry of Boron*, G. W. Kabalka, ed., Royal Society of Chemistry, Cambridge, **1994**, p. 314.

137 D. O'Connell, J. C. Patterson, T. R. Spalding, G. Ferguson, J. F. Gallagher, Y. Li, J. D. Kennedy, R. Macias, M. Thornton-Pett, J. Holub, *J. Chem. Soc., Dalton Trans.*, **1996**, 3323.

138 G. Ferguson, Y. Li, T. R. Spalding, J. C. Patterson, *Acta Crystallogr.*, **1995**, *C51*, 1498.

139 A. Jasper, Jr., S. Roach, J. N. Stipp, J. C. Huffman, L. J. Todd, *Inorg. Chem.*, **1993**, *32*, 3072.

140 S. A. Jasper, Jr., J. C. Huffman, L. J. Todd, *Inorg. Chem.*, **1995**, *34*, 6430.

141 D. C. Beer, L. J. Todd, *J. Organomet. Chem.*, **1972**, *36*, 77.

142 G. B. Dunks, M. M. McKown, M. F. Hawthorne, *J. Am. Chem. Soc.*, **1971**, *93*, 2541.

143 E. R. Churchill, B. G. DeBoer, *Inorg. Chem.*, **1974**, *13*, 1411.

144 M. F. Hawthorne, *J. Organomet. Chem.*, **1975**, *100*, 97.

145 C. J. Salentine, M. F. Hawthorne, *Inorg. Chem.*, **1976**, *15*, 2872.

146 W. M. Maxwell, R. F. Bryan, R. N. Grimes, *J. Am. Chem. Soc.*, **1977**, *99*, 4008.

147 N. M. M. Wilson, D. Ellis, A. S. Boyd, B. T. Giles, S. A. Mcgregor, G. M. Rosair, A. J. Welch, *J. Chem. Soc., Chem. Commun.*, **2002**, 464.

148 A. Burke, D. Ellis, B. T. Giles, B. E. Hodson, S. A. Mcgregor, G. M. Rosair, A. J. Welch, *Angew. Chem.*, **2003**, *115*, 235; *Angew. Chem. Int. Ed. Engl.*, **2003**, *42*, 225.

149 H.-S. Wu, W.-L. Zhou, *Huaxue Xuebao*, **1997**, *55*, 453.

150 M. Müller, T. Wagner, U. Englert, P. Paetzold, *Chem. Ber.*, **1995**, *128*, 1.

151 H. S. Wu, X.-H. Xu, C.-J. Zhang, W.-L. Zhou, *Huaxue Xuebao*, **1997**, *55*, 1185.

152 R. E. Williams, G. Ji, J. W. Bausch, in *Contemporary Boron Chemistry*, M. G. Davidson, A. K. Hughes, T. B. Marder, K. Wade, eds., Royal Society of Chemistry, Cambridge, **2000**, 497.

153 V. Beez, P. Greiwe, H. Pritzkow, M. Hofmann, P. von Ragué Schleyer, W. Siebert, *European J. Inorg. Chem.*, **1998**, *11*, 1775.

154 T. A. Albright, R. Hoffmann, *Chem. Ber.*, **1978**, *111*, 1578.

155 M. D. Su, S. Y. Chu, *J. Phys. Chem.*, **1989**, *93*, 6043.

156 W. Siebert, R. Full, C. Krüger, Y.-H. Tsay, *Z. Naturforsch.*, **1976**, *31B*, 203.

157 K. Kinberger, W. Siebert, *Chem. Ber.*, **1978**, *111*, 356.

158 U. Zenneck, L. Suber, H. Pritzkow, W. Siebert, *Chem. Ber.*, **1986**, *119*, 971.

159 W. Siebert, H. Schmidt, R. Full, *Z. Naturforsch.*, **1980**, *35B*, 873.

160 W. Siebert, M. E. D. M. El-Essawi, R. Full, J. Heck, *Z. Naturforsch.*, **1985**, *40B*, 458.

161 W. Siebert, G. Augustin, R. Full, C. Krüger, Y.-H. Tsay, *Angew. Chem.*, **1975**, *87*, 286; *Angew. Chem. Int. Ed. Engl.*, **1975**, *14*, 262.

162 W. Siebert, R. Full, J. Edwin, K. Kinberger, C. Krüger, *J. Organomet. Chem.*, **1977**, *131*, 1; W. Siebert, R. Full, J. Edwin, K. Kinberger, *Chem. Ber.*, **1978**, *111*, 823.

163 P. Greiwe, V. Beez, H. Pritzkow, W. Siebert, *European J. Inorg. Chem.*, **2001**, *2*, 381; P. Greiwe, H. Pritzkow, W. Siebert, *Eur. J. Inorg. Chem.*, **2001**, *6*, 1599.

164 P. Frankhauser, M. Driess, H. Pritzkow, W. Siebert, *Chem. Ber.*, **1992**, *125*, 1341.

165 R. Boese, B. Kröckert, P. Paetzold, *Chem. Ber.*, **1987**, *120*, 1913.

166 S. Luckert, U. Englert, P. Paetzold, *Inorg. Chim. Acta*, **1998**, *269*, 43.

167 R. P. Micciche, P. J. Carroll, L. G. Sneddon, *Organometallics*, **1985**, *4*, 1619.

168 S. O. Kang, L. G. Sneddon, *Inorg. Chem.*, **1988**, *27*, 3769.

169 N. S. Hosmane, K.-J. Lu, A. H. Cowley, M. A. Mardones, *Inorg. Chem.*, **1991**, *30*, 1325.

170 R. E. Williams, *Chem. Rev.*, **1992**, *92*, 177.

171 W. Siebert, R. Full, H. Schmidt, J. von Seyerl, M. Halstenberg, G. Huttner, *J. Organomet. Chem.*, **1980**, *191*, 15.

172 A. J. Tebben, G. Ji, R. E. Williams, J. W. Bausch, *Inorg. Chem.*, **1998**, *37*, 2189.

173 J. Holub, J. D. Kennedy, B. Stibr, *Coll. Czech. Chem. Commun.*, **1994**, *59*, 367.

174 G. J. Zimmerman, L. G. Sneddon, *J. Am. Chem. Soc.*, **1981**, *103*, 1102.

175 K. Base, *Collect. Czech. Chem. Commun.*, **1983**, *48*, 2593.

176 B. J. Meneghelli, R. W. Rudolph, *J. Am. Chem. Soc.*, **1978**, *100*, 4626.

177 K. Base, S. Hermanek, V. Gregor, *Chem. Ind. (London)*, **1979**, 743.

178 B. J. Meneghelli, M. Bower, N. Canter, R. W. Rudolph, *J. Am. Chem. Soc.*, **1980**, *102*, 4355.

179 J. Bould, A. Brownless, C. A. Kilner, M. G. S. Londesborough, B. Stibr, J. D. Kennedy, M. Thornton-Pett, *Acta Crystallogr.*, **2001**, *C57*, 52.

180 S. O. Kang, P. J. Carroll, L. G. Sneddon, *Organometallics*, **1988**, *7*, 772.

181 M. Bown, X. L. R. Fontaine, J. D. Kennedy, *J. Chem. Soc., Dalton Trans.*, **1988**, 1467.

182 S. O. Kang, L. G. Sneddon, *Inorg. Chem.*, **1988**, *27*, 3298.

183 S. Küpper, P. J. Carroll, L. G. Sneddon, *Inorg. Chem.*, **1992**, *31*, 4921.

184 T. Jelinek, J. D. Kennedy, B. Stibr, *J. Chem. Soc., Chem. Commun.*, **1993**, 1628.

185 Y.-S. Cho, J.-J. Ko, Y. Kim, S. O. Kang, *Bull. Korean Chem. Soc.*, **1994**, *15*, 821.

186 B. Stibr, J. Holub, T. Jelinek, X. L. R. Fontaine, J. Fusek, J. D. Kennedy, M. Thornton-Pett, *J. Chem. Soc., Dalton Trans.*, **1996**, 1741.

187 J. Müller, P. Paetzold, U. Englert, J. Runsink, *Chem. Ber.*, **1992**, *125*, 97.

188 P. Paetzold, U. Englert, H.-P. Hansen, F. Meyer, E. Leuschner, *Z. Anorg. Allg. Chem.*, **2001**, *627*, 498.

189 J. Holub, A. E. Wille, B. Stibr, P. J. Carroll, L. G. Sneddon, *Inorg. Chem.*, **1994**, *33*, 4920.

190 N. Canter, C. G. Overberger, R. W. Rudolph, *Organometallics*, **1983**, *2*, 569.

191 J. Holub, J. D. Kennedy, T. Jelinek, B. Stibr, *J. Chem. Soc., Dalton Trans.*, **1994**, 1317.

192 P. A. Cooke, C. O'Dowd, M. G. S. Londesborough, J. Holub, B. Stibr, M. Thornton-Pett, W. Clegg, S. J. Teat, J. D. Kennedy, *J. Organomet. Chem.*, **2000**, 614.

193 C.-H. Kang, S.-J. Kim, J.-J. Ko, S. O. Kang, *Bull. Korean Chem. Soc.*, **1995**, *16*, 1067.

194 A. M. Shedlow, L. Sneddon, *Inorg. Chem.*, **1998**, *37*, 5269.

195 O. N. Dhubhghaill, D. Reed, T. R. Spalding, *Polyhedron*, **1993**, *12*, 1977.

196 D. Hnyk, M. Hofmann, P. von Rague Schleyer, M. Buhl, D. W. H. Rankin, *J. Phys. Chem.*, **1996**, *100*, 3435.

197 J. Plesek, B. Stibr, D. Hnyk, T. Jelinek, S. Hermanek, J. D. Kennedy, M. Hofmann, P. von Rague Schleyer, *Inorg. Chem.*, **1998**, *37*, 3902.

198 W. F. Wright, A. R. Garber, L. J. Todd, *J. Magn. Reson.*, **1978**, *30*, 595.

199 M. Müller, E. Eversheim, U. Englert, R. Boese, P. Paetzold, *Chem. Ber.*, **1995**, *128*, 99.

200 M. Müller, U. Englert, P. Paetzold, *Inorg. Chem.*, **1995**, *34*, 5925.

201 A. M. Barriola, T. P. Hanusa, L. J. Todd, *Inorg. Chem.*, **1980**, *19*, 2801.

202 G. Ferguson, M. J. Hampden-Smith, O. N. Dhubhghaill, T. R. Spalding, *Polyhedron*, **1988**, *7*, 187.

203 Faridoon, M. McGrath, T. R. Spalding, X. L. R. Fontaine, J. D. Kennedy, M. Thornton-Pett, *J. Chem. Soc., Dalton Trans.*, **1990**, 1819.

204 T. Yamamoto, L. J. Todd, *J. Organomet. Chem.*, **1974**, *67*, 75.

205 D. A. Thompson, R. W. Rudolph, *J. Chem. Soc., Chem. Commun.*, **1976**, 770.

206 G. D. Friesen, T. P. Hanusa, L. J. Todd, L. G. Sneddon, *Inorg. Synth.*, **1992**, *29*, 103.

207 K. Base, B. Stibr, *Chem. Ind. (London)*, **1977**, 919.

208 G. D. Friesen, A. Barriola, L. J. Todd, *Chem. Ind. (London)*, **1978**, 631.

209 R. V. Schultz, J. C. Huffman, L. J. Todd, *Inorg. Chem.*, **1979**, *18*, 2883.

210 A. R. Siedle, L. J. Todd, *J. Chem. Soc., Chem. Commun.*, **1973**, 914.

211 A. M. Barriola, T. P. Hanusa, L. J. Todd, *Inorg. Chem.*, **1980**, *19*, 2801.

212 V. A. Brattsev, S. P. Knyazev, G. N. Danilova, V. I. Stanko, *Zh. Obshch. Khim.*, **1975**, *45*, 1393.

213 Z. Janousek, J. Plesek, Z. Plzak, *Collect. Czech. Chem. Commun.*, **1979**, *44*, 2904.

214 J. Holub, B. Stibr, Z. Janousek, J. D. Kennedy, M. Thornton-Pett, *Inorg. Chim. Acta*, **1994**, *221*, 5.

215 J. Plesek, S. Hermanek, J. Huffman, P. Ragatz, R. Schaeffer, *J. Chem. Soc., Chem. Commun.*, **1975**, 935.

216 Y.-H. Kim, R. Greatrex, J. D. Kennedy, *Coll. Czech. Chem. Commun.*, **1997**, *62*, 1289.

217 G. Ferguson, A. J. Lough, S. Coughlan, T. R. Spalding, *Acta Crystallogr.*, **1992**, *C48*, 440.

218 K. J. Adams, T. D. McGrath, A. Welch, *Polyhedron*, **1998**, *17*, 341.

219 R. Macias, N. P. Rath, L. Barton, *Angew. Chem.*, **1999**, *111*, 203; *Angew. Chem. Int. Ed. Engl.*, **1999**, *38*, 993.

220 O. Volkov, N. P. Rath, L. Barton, *Inorg. Chem. Commun.*, **2002**, 127.

221 R. Macias, J. Holub, J. D. Kennedy, B. Stibr, M. Thornton-Pett, W. Clegg, *J. Chem. Soc., Dalton Trans.*, **1997**, *2*, 149.

222 K. J. Adams, T. D. McGrath, A. J. Welch, *Acta Crystallogr.*, **1995**, *C51*, 401.

223 G. M. Rosair, A. J. Welch, A. S. Weller, *Acta Crystallogr.*, **1996**, *C52*, 3020.

224 A. Es-sofi, C. Serrar, A. Boutalib, A. Ouassas, *THEOCHEM*, **1999**, *492*, 197.

225 X. Yang, H. Jiao, P. von Rague Schleyer, *Inorg. Chem.*, **1997**, *36*, 4897.

226 A. Ouassas, B. Fenet, H. Mongeot, B. Gautheron, E. Barday, B. Frange, *J. Chem. Soc., Chem. Commun.*, **1995**, 1663.

227 A. Ouassas, B. Fenet, H. Mongeot, B. Frange, in *Current Topics in the Chemistry of Boron*, G. W. Kabalka, ed., Royal Society of Chemistry, Cambridge, **1994**, p. 363.

228 B. Frange, J. D. Kennedy, *Main Group Met. Chem.*, **1996**, *19*, 175.

229 A. Franken, B. T. King, J. Rudolph, P. Rao, B. C. Noll, J. Michl, *Coll. Czech. Chem. Commun.*, **2001**, *66*, 1238.

230 W. Dirk, P. Paetzold, K. Radacki, *Z. Anorg. Allg. Chem.*, **2001**, *627*, 2615.

231 F. Meyer, J. Müller, P. Paetzold, R. Boese, *Angew. Chem.*, **1992**, *104*, 1221;

Angew. Chem. Int. Ed. Engl., **1992**, *31*, 1227.

232 X. L. R. Fontaine, H. Fowkes, N. N. Greenwood, J. D. Kennedy, M. Thornton-Pett, *J. Chem. Soc., Chem. Commun.*, **1985**, 1722.

233 X. L. R. Fontaine, H. Fowkes, N. N. Greenwood, J. D. Kennedy, M. Thornton-Pett, *J. Chem. Soc., Dalton Trans.*, **1987**, 2417.

234 P. Jutzi, D. Wegener, M. Hursthouse, *J. Organomet. Chem.*, **1991**, *418*, 277.

235 H. D. Smith Jr., M. F. Hawthorne, *Inorg. Chem.*, **1974**, *13*, 2312.

236 S. Küpper, U. Englert, P. Paetzold, *Heteroatom Chem.*, **1990**, *1*, 479.

237 M. Müller, U. Englert, P. Paetzold, *Chem. Ber.*, **1995**, *128*, 1105.

238 H.-S. Wu, X. Xu, C. Zhang, *Huaxue Xuebao*, **2000**, *16*, 627.

239 S. Küpper, P. Paetzold, R. Boese, *Chem. Ber.*, **1993**, *126*, 1787.

240 J. Dolansky, S. Hermanek, R. Zahradnik, *Collect. Czech. Chem. Commun.*, **1981**, *46*, 2479.

241 R. W. Rudolph, *Inorg. Chem.*, **1978**, *17*, 1097.

242 D. Hnyk, M. Hofmann, P. von Rague Schleyer, *Collect. Czech. Chem. Commun.*, **1999**, *64*, 993.

243 K. Base, M. G. H. Wallbridge, X. L. R. Fontaine, N. N. Greenwood, J. H. Jones, J. D. Kennedy, B. Stibr, *Polyhedron*, **1989**, *8*, 2089.

244 T. Jelinek, J. D. Kennedy, B. Stibr, *J. Chem. Soc., Chem. Commun.*, **1994**, 1415.

245 J. Holub, B. Stibr, J. D. Kennedy, M. Thornton-Pett, T. Jelinek, J. Plesek, *Inorg. Chem.*, **1994**, *33*, 4545.

246 K. Base, B. Stibr, I. A. Zakharova, *Synth. React. Inorg. Met.-Org. Chem.*, **1980**, *10*, 509.

247 D. E. Kadlecek, L. G. Sneddon, *Inorg. Chem.*, **2002**, *41*, 4239.

248 P. Kaur, J. Holub, N. P. Rath, J. Bould, L. Barton, B. Stibr, J. D. Kennedy, *J. Chem. Soc., Chem. Commun.*, **1996**, 273.

249 J. Plesek, S. Hermanek, Z. Janousek, *Collect. Czech. Chem. Commun.*, **1977**, *42*, 785.

250 C. H. Kang, S. J. Kim, J. J. Ko, K. B. Lee, S. O. Kang, *Bull. Korean Chem. Soc.*, **1993**, *14*, 537.

251 J. H. Jones, X. L. R. Fontaine, N. N. Greenwood, J. D. Kennedy, M. Thornton-Pett, B. Stibr, H. Langhoff, *J. Organomet. Chem.*, **1993**, *445*, C15.

252 M. P. Murphy, T. R. Spalding, C. Cowey, J. D. Kennedy, M. Thornton-Pett, J. Holub, *J. Organomet. Chem.*, **1998**, *550*, 151.

253 J. Plesek, T. Jelinek, B. Stibr, S. Hermanek, *J. Chem. Soc., Chem. Commun.*, **1988**, 348.

254 K. Nestor, J. D. Kennedy, J. Holub, B. Stibr, *Inorg. Chim. Acta*, **1993**, *214*, 17.

255 J. H. Jones, J. D. Kennedy, B. Stibr, *Inorg. Chim. Acta*, **1994**, *218*, 1.

256 H. J. Jeon, J. J. Ko, S. J. Kim, D. S. Shin, S. O. Kang, *Bull. Korean Chem. Soc.*, **1992**, *13*, 220.

257 H. J. Jeon, J. Hee, J. J. Ko, K. B. Lee, S. O. Kang, *Bull. Korean Chem. Soc.*, **1993**, *4*, 113.

258 K. Su, P. J. Carroll, L. G. Sneddon, *J. Am. Chem. Soc.*, **1993**, *115*, 10004.

259 H.-J. Jeon, S. O. Kang, in *Current Topics in the Chemistry of Boron*, G. W. Kabalka, ed., Royal Society of Chemistry, Cambridge, **1994**, p. 330.

260 K. Base, S. Hermanek, F. Hanousek, *J. Chem. Soc., Chem. Commun.*, **1984**, 299.

261 G. Ferguson, D. E. McCarthy, T. R. Spalding, J. D. Kennedy, *Acta Crystallogr.*, **1996**, *C52*, 548.

262 E. L. Muetterties, C. W. Alegranti, *J. Am. Chem. Soc.*, **1970**, *92*, 4114.

263 E. L. Muetterties, W. G. Peet, P. A. Wegner, C. W. Alegranti, *Inorg. Chem.*, **1970**, *9*, 2447.

264 E. L. Muetterties, C. W. Alegranti, *J. Am. Chem. Soc.*, **1972**, *94*, 6386.

265 A. R. Siedle, G. M. Bodner, A. R. Garber, L. J. Todd, *Inorg. Chem.*, **1974**, *13*, 1756.

266 L. J. Guggenberger, *J. Organomet. Chem.*, **1974**, *81*, 271.

267 G. Ferguson, M. F. Hawthorne, B. Kaitner, F. J. Lalor, *Acta Crystallogr.*, **1984**, *C40*, 1707.

268 V. D. Yumatov, V. V. Murakhtanov, V. V. Volkov, E. A. Il'inchik, O. V.

Volkov, *Zhurnal Neorganicheskoi Khimii*, **1998**, *43*, 1677.
269 V. V. Volkov, E. A. Il'inchik, O. V. Volkov, G. S. Voronina, *Izvest. Akad. Nauk SSSR, Ser. Khim.*, **1990**, 2113.
270 G. M. Rosair, A. J. Welch, A. S. Weller, *Acta Crystallogr.*, **1996**, *C52*, 2851.
271 P. A. Cooke, J. Holub, J. D. Kennedy, B. Stibr, M. Thornton-Pett, *Acta Crystallogr.*, **1998**, *C54*, 121.
272 T. K. Hilty, R. W. Rudolph, *Inorg. Chem.*, **1979**, *18*, 1106.
273 K. J. Donaghy, P. J. Carroll, L. G. Sneddon, *Inorg. Chem.*, **1997**, *36*, 547.
274 S. Küpper, P. J. Carroll, L. G. Sneddon, *J. Am. Chem. Soc.*, **1992**, *114*, 4914.
275 F. Meyer, P. Paetzold, U. Englert, *Chem. Ber.*, **1992**, *125*, 2025.
276 G. D. Friesen, R. L. Kump, L. J. Todd, L. G. Sneddon, *Inorg. Synth.*, **1992**, *29*, 105.
277 J. Holub, T. Jelinek, J. Plesek, B. Stibr, S. Hermanek, J. D. Kennedy, *J. Chem. Soc., Chem. Commun.*, **1991**, 1389.
278 D. Hnyk, J. Holub, *Coll. Czech. Chem. Commun.*, **2002**, *67*, 813.
279 A. Arafat, G. D. Friesen, L. J. Todd, *Inorg. Chem.*, **1983**, *22*, 3721.
280 Y.-H. Kim, A. Brownless, P. A. Cooke, J. D. Kennedy, M. Thornton-Pett, *Inorg. Chem. Commun.*, **1998**, *1*, 19.
281 D. A. Thompson, T. K. Hilty, R. W. Rudolph, *J. Am. Chem. Soc.*, **1977**, *99*, 6774.
282 G. A. Kukina, M. A. Porai-Koshits, V. S. Sergienko, Y. V. Zefirov, G. G. Sadikov, *Koord. Khim.*, **1985**, *11*, 385.
283 K. Base, B. Stibr, I. A. Zakharova, V. Petricek, *Proc. Conf. Coord. Chem.*, **1978**, 11.
284 R. Macias, S. A. Barrett, J. Bould, U. Dörfler, J. Holub, J. D. Kennedy, M. Thornton-Pett, B. Stibr, *Acta Crystallogr.*, **2001**, *C57*, 520.
285 H. Binder, S. Soylemez, R. Stöckle, A. Pfitzner, M. Hofmann, P. von Rague Schleyer, *Z. Anorg. Allg. Chem.*, **1997**, *623*, 1157.
286 J. Müller, P. Paetzold, R. Boese, *Heteroatom Chem.*, **1990**, *1*, 461.
287 J. Plesek, B. Stibr, S. Hermanek, *Chem. Ind. (London)*, **1974**, 662.
288 U. Dörfler, W. Clegg, J. D. Kennedy, M. Thornton-Pett, *J. Chem. Soc., Dalton Trans.*, **1998**, 2353.
289 F. Meyer, P. Paetzold, U. Englert, *Chem. Ber.*, **1994**, *127*, 93.
290 L. B. Friedman, D. L. Perry, *Inorg. Chem.*, **1973**, *12*, 288.
291 S. O. Kang, L. G. Sneddon, *J. Am. Chem. Soc.*, **1989**, *111*, 3281.
292 K. Mazighi, P. J. Carroll, L. G. Sneddon, *Inorg. Chem.*, **1992**, *31*, 3197.
293 M. Murphy, T. R. Spalding, J. D. Kennedy, M. Thornton-Pett, K. M. A. Malik, M. B. Hursthouse, J. Holub, *J. Chem. Soc., Chem. Commun.*, **1994**, 2403.
294 S. O. Kang, G. T. Furst, L. G. Sneddon, *Inorg. Chem.*, **1989**, *28*, 2339.
295 U. Dörfler, J. F. Kennedy, M. Thornton-Pett, *J. Chem. Soc., Dalton Trans.*, **1997**, 2547.

3.5
Heteropolyalanes, -gallanes, -indanes and -thallanes

Werner Uhl and Herbert W. Roesky

Homonuclear clusters of the heavier elements of the third main-group aluminum, gallium, indium and thallium having direct element–element interactions form a fascinating new class of compounds. As discussed in the previous Chapter 2.3, in some cases their structures resemble those known with the lightest element of that group, boron, while in other cases novel, metal-rich compounds were obtained which do not have any analogue in boron chemistry.

Some remarkable heteronuclear cluster compounds containing heteroatoms embedded in their cluster skeletons have been reported in the recent literature. Clearly, their bonding is on the borderline between the delocalized multicenter approach of the pure clusters and more localized 2c2e bonds in electron precise molecules. This chapter deals with their syntheses, structures and bonding properties. Carbaalanes are discussed that have clusters formed by carbon and aluminum atoms and which, to some extent, show similarities to the class of carbaboranes. Furthermore, some selected examples of important aluminum and gallium cage compounds with oxygen and nitrogen as skeleton atoms are considered, which clearly are electron precise and in fact do not require a delocalized bonding description.

3.5.1
Clusters Including Carbon and Silicon Atoms

3.5.1.1
Aluminum and Gallium Clusters Containing Silicon

Clusters of the elements aluminum to thallium containing only one or two carbon atoms and strong direct element–element interactions, similar to boron rich carbaboranes, have not yet been synthesized, and also the corresponding silicon derivatives are relatively rare. To the best of our knowledge only one aluminum–silicon and one gallium–silicon cluster (**1** and **2**) has been reported in the literature. The reaction of metastable aluminum(I) chloride with decamethylsilicocene or with a mixture of $SiCl_4$ and $(AlCp^*)_4$, respectively, afforded black crystals of

compound **1** in moderate yields [Eq (1)]. Its cluster consists of an inner silicon atom which is coordinated by eight aluminum atoms in a cubic arrangement. All six faces of the Al_8 cube are bridged by $Al(\eta^5\text{-}Cp^*)$ groups to give the overall formula $[SiAl_8(AlCp^*)_6]$ [1]. The Al–Al distances are rather long and show values of about 290 pm along the edges of the cube and 280 pm to the bridging aluminum atoms. The last ones are comparable to the Al–Al separations in the $Al_4Cp^*_4$ cluster (277 pm), which has a tetrahedron of monovalent aluminum atoms in the solid state [2], but dissociates into the monomers upon dissolution or in the gas phase [3]. The 40 delocalized electrons of the cluster (central Si: 4e; 8 Al atoms of the cube: 8 × 3e; six bridging $AlCp^*$ groups: 6 × 2e) give a stable Jellium state (Chapter 2.3), and indeed compound **1** is stable enough to be detected in the mass spectrum. The bonding may best be described by highly delocalized cluster orbitals.

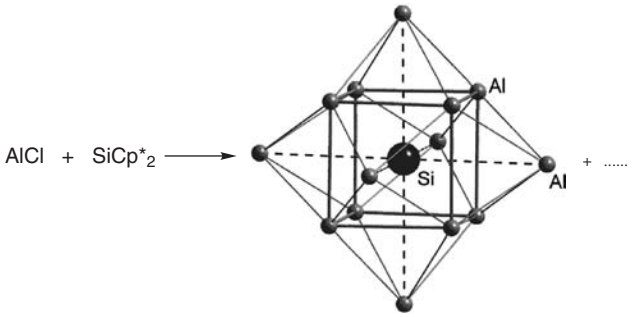

(1)

$[SiAl_8(AlCp^*)_6]$

1

The gallium silicon compound **2** possesses a tetrahedron of four gallium atoms of which one face is bridged by a silicon atom (Figure 3.5-1) [4]. A trigonal bipyramidal cluster core is formed with the silicon atom in an axial position. Each of the equatorial gallium atoms bears a terminal tris(trimethylsilyl)silyl group, while sterically less demanding trimethylsilyl groups are attached to the axial atoms. The

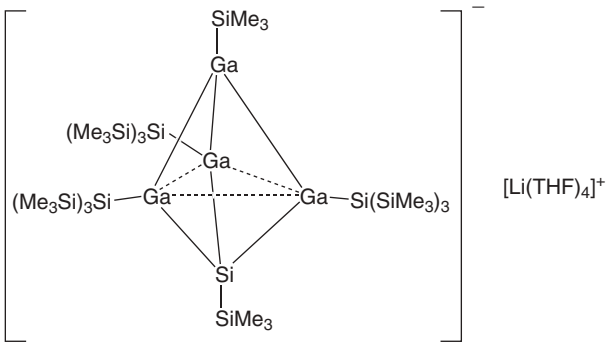

2

Fig. 3.5-1. Schematic drawing of the cluster $[SiGa_4\{Si(SiMe_3)_3\}_3(SiMe_3)_2]^-$ **2**.

negative charge is required for the complete pairing of all electrons. The Ga–Ga distances to the axial gallium atoms are short (244 pm) and correspond to Ga–Ga single bonds. Similarly, the Ga–Si distances are in the characteristic range of single bonds. At first glance, **2** may thus be described as a compound containing six localized 2c2e bonds. Relatively short equatorial Ga–Ga distances of 279 pm indicate, however, a more complex bonding situation, and quantum chemical calculations indeed verified that the complete description of the bonding requires the consideration of some multicenter interactions across the triangular faces of the cluster. Thus, **2** is isoelectronic and isostructural to the small carbaboranes $B_3C_2R_5$, for which calculations also confirm the relevance of multicenter bonding [5]. The electron count gives six electron pairs in these clusters, which in accordance with the Wade rules [6] corresponds to a *closo* configuration as the best description for these five vertex clusters. Compound **2** was obtained by the reaction of the THF adduct of $LiSi(SiMe_3)_3$ with ''GaI'' [7], which is accessible by ultrasonication of gallium in the presence of iodine and which actually seems to be a mixture of gallium subhalides. The deep violet crystals were isolated in 19% yield [4].

3.5.1.2 Carbaalanes

The carbaalanes [8, 9] possess clusters formed by aluminum and carbon atoms. They represent a new class of compounds which, in some respects, may be compared to the important class of carbaboranes. Usually, they were obtained by the reaction of aluminum alkynides with aluminum hydrides (hydroalumination) and the release of trialkylaluminum derivatives (condensation). The first carbaalane, $(AlMe)_8(CCH_2Ph)_5H$ **3** [10], was synthesized by the treatment of dimethylaluminum phenylethynide with neat dimethylaluminum hydride. The idealized stoichiometric ratio of the components is given in Eq. (2), which also shows a schematic drawing of the molecular structure. Compound **3** was isolated in the form of colorless crystals in 60% yield. While **3** is only slightly air-sensitive, the less sterically shielded propynide derivative **4**, also shown in Eq. (2), is highly pyrophoric [11].

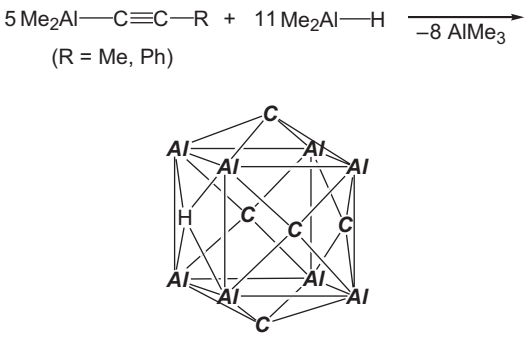

(2)

3: ***Al*** = AlMe; ***C*** = CCH_2Ph
4: ***Al*** = AlMe; ***C*** = CCH_2CH_3

Under optimized reaction conditions a large excess of the hydride was employed to isolate product **3** in reasonable yields. Smaller quantities of dimethylaluminum hydride yielded the different compound $(AlMe)_8(CCH_2Ph)_5(C{\equiv}C\text{-}Ph)$ **5** [Eq (3)] [12], that contains an alkynido group instead of the bridging hydrogen atom and which may be described as the product of an incomplete hydroalumination of the starting aluminum alkynide. While the phenylethynide derivative gives bright red crystals, the alkyl substituted compound **6** [11] is yellow.

$$10\ Me_2AlH + 6\ Me_2Al{-}C{\equiv}C{-}R \xrightarrow[-\ 8\ AlMe_3]{} \qquad (3)$$

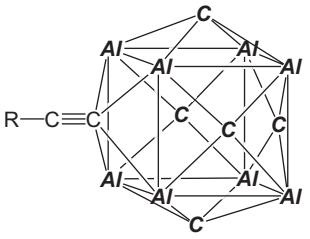

5: ***Al*** = AlMe; ***C*** = CCH_2Ph; R = Ph
6: ***Al*** = AlMe; ***C*** = CCH_2CH_3; R = Me

The structures of the compounds **3** to **6** are closely related, and that of the hydrogen bridged compound **3** is depicted in Figure 3.5-2. It may be described as a slightly distorted cube of eight aluminum atoms, five faces of which are bridged by $C{-}CH_2{-}Ph$ groups, while the remaining face is bridged by a hydrogen atom with two short and two long Al–H distances. The Al–C bond lengths to the terminal methyl or ethyl groups attached to aluminum are within the normal range of Al–C single bonds of about 195 pm, while longer distances were detected in the clusters (200 to 215 pm) in accordance with their delocalized bonding situation. The Al–Al separations vary between 260 and 280 pm, the longer ones of which were observed at the hydrogen or alkynido bridged faces. The shorter distances confirm the multicenter bonding interaction in the clusters and are in the characteristic range for 3c2e Al–H–Al or Al–C–Al bonds. Similar values were found for the compounds $[Me_2Al(\mu\text{-}H)_2AlMe_2]$ [13] and $(AlMe_3)_2$ [14] (262 pm on average). Slightly longer distances (up to 265 pm) were detected for Al–Al single bonds in organoelement compounds of the type $R_2Al{-}AlR_2$ [15]. Similar structural parameters were observed in all carbaalanes published so far and do not require further discussion here.

At first glance, electron count in these clusters gives a remarkable analogy to the carbaboranes. Each aluminum atom contributes two electrons to the cluster, three electrons are from each carbon atom, and one electron is added by the bridging hydrogen atom. A total count of 32 electrons or 16 electron pairs results, which in accordance with the Wade rules [6] gives an *arachno*-type 13-vertex cluster. Indeed,

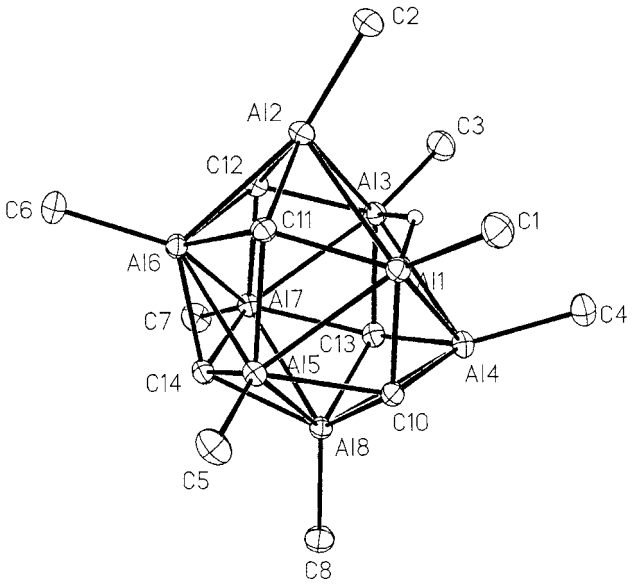

Fig. 3.5-2. Molecular structure of the carbaalane $(AlMe)_8(CCH_2C_6H_5)_5H$ **3** (phenyl groups and methyl hydrogen atoms are omitted.

the structure of these compounds (**3** to **6**) may be derived from that of the *closo*-boranate anion $[B_{15}H_{15}]^{2-}$ [16], which is known from quantum-chemical calculations only and possesses a tricapped hexagonal antiprism of boron atoms. The atom Al(8) (Figure 3.5-2) bridges a six-membered Al_3C_3 heterocycle (Al4, Al5, Al7, C10, C13, C14) at the bottom of the cluster. The next plane comprises the five atoms Al1, Al3, Al6, C11 and C12, thus one atom is missing to complete a six-membered ring and the overall hexagonal prismatic structure. The ideal *closo*-structure requires further two bridging atoms across that face, but only one atom (Al2) is present here. Thus, in accordance with an *arachno*-configuration two atoms are missing to complete a *closo*-shell. A remarkable analogy between boranes and carbaalanes may be concluded from such a description. Clearly, this analogy should not be overstressed, in particular with respect to the strongly differing atomic radii of aluminum and carbon and to the charge separation in the carbaalanes, which is caused by the considerable difference in the electronegativities of these elements.

The bridging of all six faces of the Al_8 cube by alkylidyne groups $C–CH_2R$ was observed for the carbaalanes **7** and **8** [17]. They were obtained by the reaction of the alane amine adduct $AlH_3 \cdot NMe_3$ with alkynes [Eq (4)]. Six aluminum atoms have terminally attached hydrogen atoms, while the remaining two aluminum atoms of the cluster are coordinated by a trimethylamino ligand. These clusters have a total of 36 electrons, and owing to their quite regular closed structures they do not fit at all into the concept of polyboranes or carbaboranes.

$$8\ AlH_3(NMe_3) + 6\ H{-}C{\equiv}C{-}R \xrightarrow[-6\ NMe_3]{-6\ H_2}$$

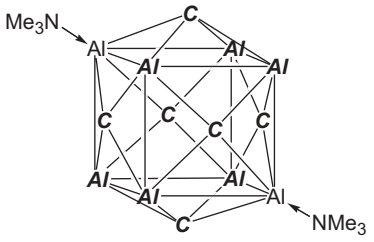

(4)

C = CCH_2R; ***Al*** = AlH
7: R = Ph
8: R = CH_2SiMe_3

One remarkable derivative of these cube-like clusters was isolated with compound **9**, in which one vertex of the Al_8 cube remained unoccupied [18]. It was obtained by a reaction similar to Eq. (2), however, a slightly better steric shielding was achieved by ethyl groups instead of methyl substituents attached to aluminum [Eq. (5)]. Orange-red crystals of **9** were isolated in 36% yield. It may be described as the product of an incomplete hydroalumination reaction and contains seven aluminum atoms, a hydrogen atom bridging only three metal atoms and two alkenyl groups with C=C double bonds that are located at the open face of the cluster. As

$$9\ Et_2AlH + 5\ Et_2Al{-}C{\equiv}C{-}R \xrightarrow[-7\ AlEt_3]{}$$

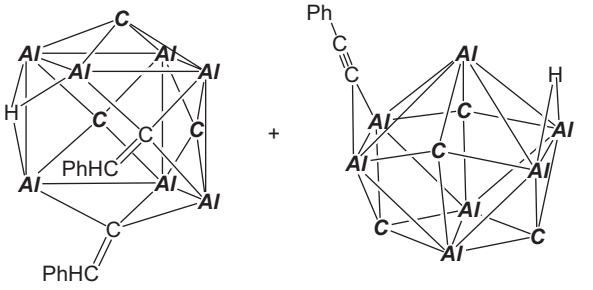

(5)

9: ***Al*** = AlEt; ***C*** = CCH_2Ph **10**: ***Al*** = AlEt; ***C*** = CCH_2Ph

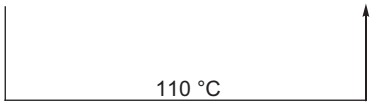

a byproduct compound **10** was isolated in 9% yield. The latter represents a novel type of cluster with a skeleton of seven aluminum and four carbon atoms. Two Al–Al edges of the cluster are bridged by a hydrogen atom and an alkynido group, respectively. Electron count yielded the figure of 12 electron pairs provided that both the bridging hydrogen atom and alkynido group were considered as *exo* ligands. For an 11-vertex cluster this gives a *closo*-configuration according to the Wade rules (see Chapter 1.1.2). Indeed, the structure of compound **10** is quite similar to that of the *closo*-borate anion $[B_{11}H_{11}]^{2-}$ [19]. It has a four-membered Al_2C_2 heterocycle at the bottom and a six-membered Al_4C_2 heterocycle in a boat conformation which is bridged by the seventh aluminum atom. Rearrangement of **9** to **10** was observed upon heating at 110 °C over a period of 1 h leading to **10** in 42% yield. The activation barrier of the rearrangement process in benzene solutions at 60 °C was estimated by ^{1}H NMR spectroscopy to about 110 kJ mol^{-1}.

A compound (**11**) similar to **10** was obtained in 63% yield by treatment of dimethylaluminum propynide with dimethylaluminum hydride [Eq. (6)] [12]. Compound **11** has two bridging hydrogen atoms across two opposite Al–Al edges of the cluster instead of one bridging hydrogen atom and one bridging alkynido group as observed in **10**. Both *closo* compounds **10** and **11** are the thermally most stable carbaalanes isolated so far, they do not decompose up to 260 °C. The other carbaalanes known undergo thermolysis within the temperature range of 100 and 200 °C.

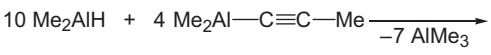

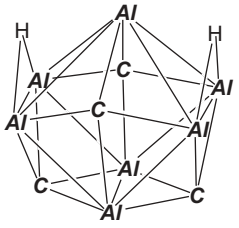

(6)

11: ***Al*** = AlMe; ***C*** = CCH_2CH_3

The bonding situation of these carbaalane clusters was investigated by quantum-chemical calculations from which two important results arose [12, 17]. Firstly, a delocalized bonding was confirmed with the expected charge separation between aluminum and the more electronegative carbon and hydrogen atoms. The orbital scheme localized on one cubic face was described as having six orbitals with a large HOMO-LUMO gap and three electron pairs in bonding orbitals. Furthermore, the topology analysis of the electron density does not provide any indication of a significant bonding interaction between any two aluminum atoms, i.e., no bond critical point was observed between aluminum atoms and direct metal–metal interactions play a minor role only. Thus, each aluminum atom is bonded to the

terminal substituent and three cluster atoms (carbon or hydrogen), while each carbon atom is bonded to four aluminum atoms as well as to the terminal substituent. For comparison, the bonding situation of the analogous boron compound $(BH)_8(CH)_5H$ was also calculated [12]. Direct boron–boron bonding in this carbon rich carbaborane cluster is also rather poor and no bond-critical point between two boron atoms was observed.

The unexpectedly high persistence of these carbaalane clusters was verified impressively by chemical reactions. Treatment of the compounds $(AlMe)_8(CCH_2Ph)_5(\mu\text{-}H)$ **3** and $(AlEt)_7(CCH_2Ph)_3(C{=}CHPh)_2(\mu\text{-}H)$ **9** with the Brönstedt acid $H[BF_4]$ resulted in the replacement of the bridging hydrogen atom by a fluorine atom [20]. The rather specific reaction of **9** is shown in Eq. (7). Surprisingly, the cleavage of the clusters by an attack of protons was not detected.

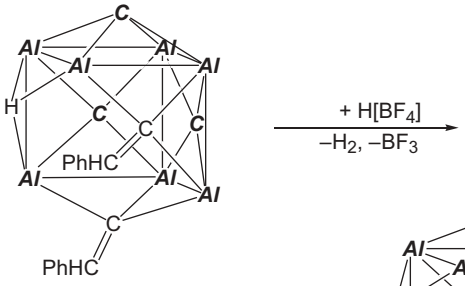

9: ***Al*** = AlEt; ***C*** = CCH_2Ph

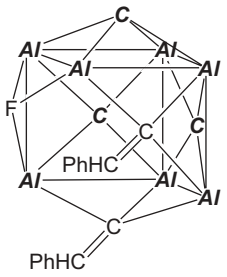

12: ***Al*** = AlEt; ***C*** = CCH_2Ph

(7)

Interestingly, HCl did not react with $(AlMe)_8(CCH_2Ph)_5(\mu\text{-}H)$ **3** by replacement of the bridging hydrogen atom. Instead the release of methane and the substitution of a terminal methyl group was observed. The attack of HCl occurred on one of those aluminum atoms which are opposite the hydrogen bridged face of the cluster (Al5 to Al8 in Figure 3.5-2) [20]. The structure of the product **13** (Figure 3.5-3) is almost identical to that of the starting compound **3**, only one terminal methyl group is replaced by a terminal chlorine atom. The carbaalane cluster also remained intact upon treatment of the closed shell compound $(AlH)_6(Al\text{-}NMe_3)_2(CCH_2CH_2SiMe_3)_6$ **8** with boron trichloride [17]. All hydrogen atoms terminally coordinated to aluminum were replaced by chlorine atoms to generate $(AlCl)_6(Al\text{-}NMe_3)_2(CCH_2CH_2SiMe_3)_6$ **14** (Figure 3.5-3). Even an excess of BCl_3 did not result in the cleavage of the cluster core, instead, in a secondary reaction one methyl group of each trimethylsilyl substituent was replaced to yield the isostructural cluster $(AlCl)_6(Al\text{-}NMe_3)_2(CCH_2CH_2SiMe_2Cl)_6$.

The syntheses of cluster or cage compounds with skeletons formed by Al and

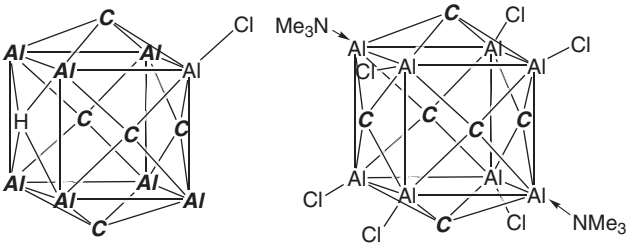

13 (***Al*** = AlMe; ***C*** = CCH_2Ph) **14**: ***C*** = $CCH_2CH_2SiMe_3$

Fig. 3.5-3. Schematic drawings of the carbaalane halides **13** and **14**.

N or Al, N and C atoms succeeded by the hydroalumination of nitriles R–C≡N or isonitriles R–N≡C. Nitriles and $AlH_3 \cdot NMe_3$ gave oligomeric amidoalanes (**15**) which possess cages of aluminum and nitrogen atoms, such as the hexagonal prism shown in Figure 3.5-4 [21]. Such compounds will be discussed in more detail below. Reaction of the alane amine adduct with *tert*-butyl isonitrile afforded the polyhedral compound $[(AlH)(CH_2NCMe_3)]_4$ **16** with a remarkable $Al_4C_4N_4$ cage [22]. It has six faces, two of which are six-membered $Al_2C_2N_2$ heterocycles in a boat conformation, while the four remaining ones are five-membered Al_2CN_2 rings.

Reactions of dialkylgallium alkynides with the corresponding dialkylgallium hydrides similar to those reported before with aluminum yielded different products that were not comparable to the carbaalanes. The starting dialkylgallium alkynides were not isolated in these cases, but synthesized *in situ* by treatment of 1-alkynes with dialkylgallium hydrides and immediately consumed by an excess of the hydrido compounds at room temperature [Eq. (8)]. Through hydrogallation and condensation heteroadamantane type compounds (**17** to **19**) resulted, which have the general formula $(GaR)_6(CCH_2R')_4$ [23]. Their cages comprise four carbon and six gallium atoms with carbon in the μ_3-bridging positions. All gallium atoms are coordinatively unsaturated, and this results in highly Lewis acidic molecular centers. In contrast to the carbaalanes discussed above, which, owing to electronic delocalization, have long Al–C distances in their clusters, the Ga–C distances of the gallium–carbon heteroadamantanes of **17** to **19** do not show a significant depen-

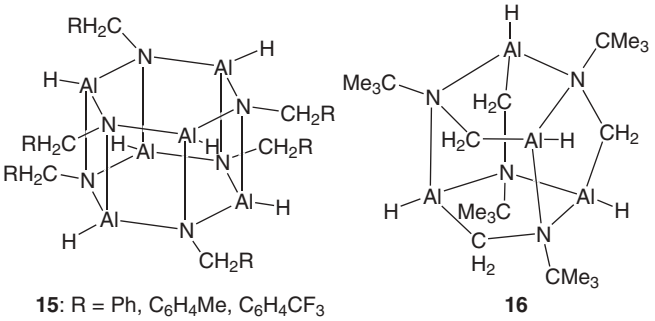

15: R = Ph, C_6H_4Me, $C_6H_4CF_3$ **16**

Fig. 3.5-4. Schematic drawings of the amidoalanes **15** and the carba-aminoalane **16**.

dence on the terminal or inner-cage arrangement. Thus, these compounds may best be described by localized 2c2e Ga–C bonds.

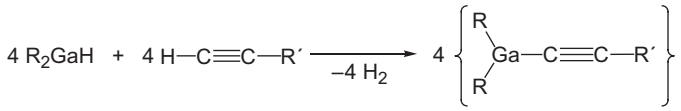

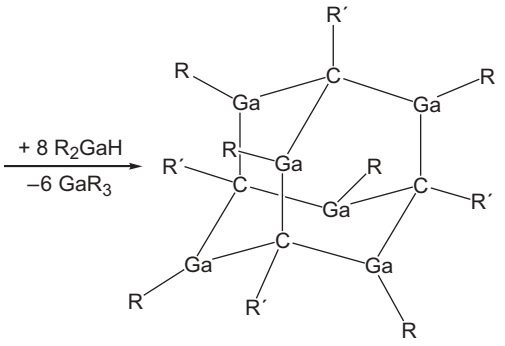

(8)

17: R = Et; R´ = Et
18: R = Et; R´ = Bu
19: R = Me R´ = Et

3.5.2
Clusters and Cages Including Pnicogen Atoms

3.5.2.1
Compounds Derived from Homonuclear Clusters

Homonuclear clusters of the elements of the third main-group such as $(AlCp^*)_4$ have often been employed for the syntheses of heteronuclear cluster or cage compounds containing phosphorus or arsenic atoms. The reaction with white phosphorus proceeded under mild conditions and gave the compound $P_4(AlCp^*)_6$ **20** in 87% yield [Eq. (9)] [24]. The structure of the P_4Al_6 cluster may be derived from two face sharing distorted cubes, of which two opposite vertices are unoccupied. The aluminum and phosphorus atoms adopt alternate positions in the cluster. A differing coordination mode was found for the Cp^* units, which are bonded in an η^1-fashion to those aluminium atoms which are coordinated by three phosphorus atoms, while they adopt a pentahapto coordination mode at the four remaining aluminum atoms, which are part of an AlP_2 unit. Quantum-chemical calculations verified some delocalization of electron density in the cluster. Each phosphorus atom bears one lone electron pair, which is mainly localized in a low lying 3s-orbital. An electron deficiency results, due to only 12 electron pairs (P: $4 \times 3e$; Al: $6 \times 2e$; $\Sigma = 24e$) forming 14 bonding interactions. This interpretation is in accordance with the values of the calculated shared electron numbers (SEN), which indicate some bonding interactions between four aluminum atoms, one across the

diagonal of the inner Al_2P_2 hetrocycle and two along diagonals of opposite outer faces of the cluster. This multicenter bonding can also be recognized by three short Al–Al distances of about 306 pm, while the remaining Al–Al contacts are much longer (386 pm). Thus, compound **20** represents a very good example of the continuous transition from electron precise cage compounds with a more localized bonding situation and 2c2e bonds to electron deficient clusters that require a delocalized, multicenter approach for a complete understanding of their bonding.

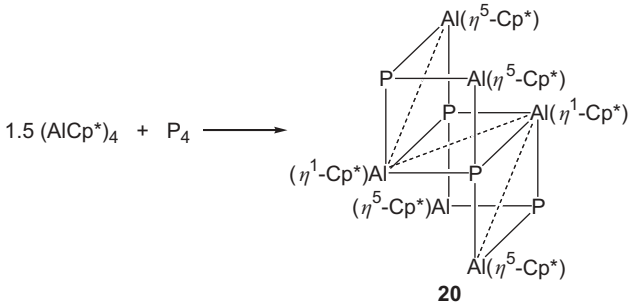

20 (9)

Treatment of $(AlCp^*)_4$ with the cyclotetraarsane $(AsCMe_3)_4$ yielded yellow crystals of the cluster $As_2(AlCp^*)_3$ **21a** in a low yield [Eq. (10)] [25]. Although the phosphorus compound $P_4(AlCp^*)_6$ **20** discussed above may just be considered as a dimer of **21a**, both compounds possess completely different molecular structures. While the cluster of **20** was derived from two face sharing cubes, the structure of the "monomeric" compound **21a** comprises a trigonal bipyramidal Al_3As_2 core in which the aluminum atoms are in the equatorial positions and are attached to pentahapto coordinated Cp^* ligands. The Al–Al distances of 283 pm are only slightly lengthened compared with those of $(AlCp^*)_4$ and indicate some attractive Al–Al interactions. Indeed, the occurrence of 3c2e Al–As–Al bonds were verified by quantum-chemical calculations. Thus, the compound may be described as a *closo*-cluster (six electron pairs, five vertices) with a delocalized electronic system. The analogous antimony compound **21b** was obtained by the reaction of $(AlCp^*)_4$ with $(SbCMe_3)_4$ [Eq. (10)] [26]. Details of its structure are not documented in literature.

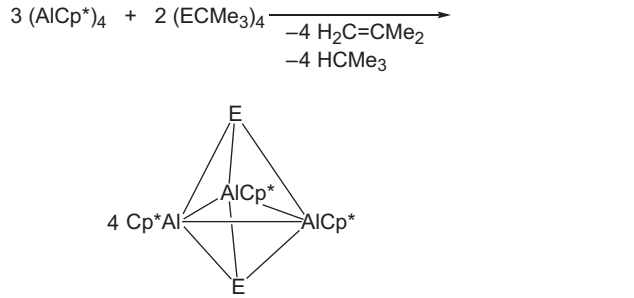

21a: E = As
21b: E = Sb

(10)

Reaction of the tetrahedral tetragallium cluster $Ga_4[C(SiMe_3)_3]_4$ with P_4 afforded the yellow cage compound $P_4[Ga\text{-}C(SiMe_3)_3]_3$ **22** in 52% yield [Eq. (11)] [27]. The mechanism of the formation of **22** may be described simply by the insertion of three monomeric GaR fragments of the Ga_4 cluster into three P–P bonds of the P_4 molecule. One triangular face of the P_4 tetrahedron remains intact. Compound **22** has three coordinatively unsaturated gallium atoms attached to one carbon and two phosphorus atoms. In accordance with long Ga–Ga separations (320 pm) delocalization is not required for a description of its bonding situation, and therefore, **22** represents an example of a typical cage compound. There are two types of chemically different phosphorus atoms in **22**, which give a doublet and quartet in the ^{31}P NMR spectrum owing to spin–spin coupling. The resonance of the single phosphorus atom at the top of the cage shows a quite unusual chemical shift of $\delta = -522$ ppm, which is at an even higher field than that observed for white phosphorus ($\delta = -488$ ppm). A similar insertion into P–P single bonds occurred on treatment of the gallium cluster with the cyclic triphosphane $(P\text{-}CMe_3)_3$, which resulted in the formation of the heterocyclic compound $(P\text{-}CMe_3)_3[Ga\text{-}C(SiMe_3)_3]$ **23** [Eq. (11)] [28].

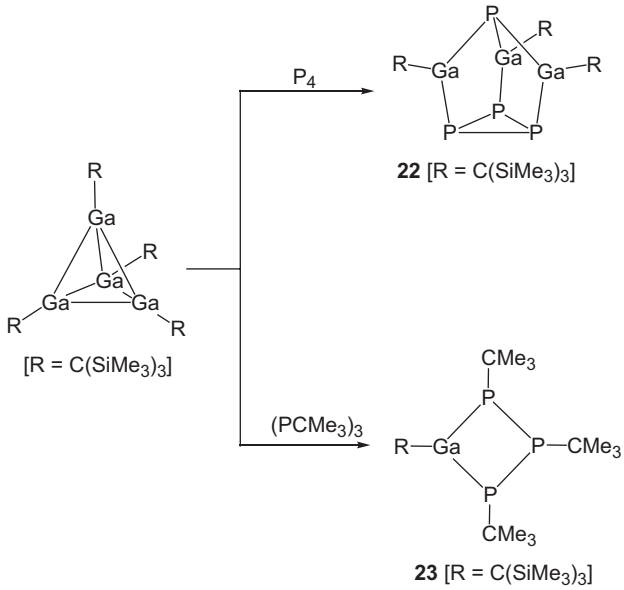

(11)

The rather complicated indium–phosphorus cluster framework **24** was obtained by the reaction of indium(III) chloride with $PhP(SiMe_3)_2$ in the presence of triethylphosphane [Eq. (12)] [29]. Apparently, a complex redox process occurred, in the course of which phosphorus atoms were oxidized by the formation of three P–P bonds, while six indium atoms were reduced from +3 to +2 accompanied by the formation of three In–In bonds. The In–In (average 274 pm) and P–P bond lengths (average 222 pm) represent localized single bonds. Other strategies for the

synthesis of III–V cluster and cage compounds are discussed in more detail in Chapter 3.6.

$$9\ InCl_3 + 3\ PEt_3 + 10\ PhP(SiMe_3)_2 \xrightarrow[-20\ Me_3SiCl]{} \quad (12)$$

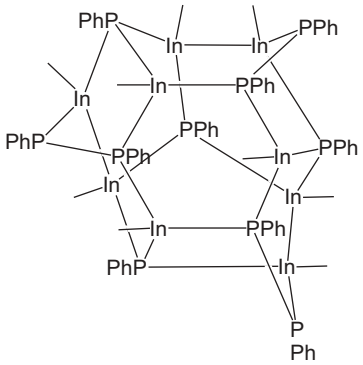

$[(InCl)_3\{(Cl)InIn(PEt_3)\}_3(PPh)_4(P_2Ph_2)_3Cl]$

24

3.5.2.2

Amino and Imino Alanes, Gallanes and Indanes

The group 13 nitrides of Al, Ga and In are of great industrial and scientific interest due to their applications in short-wavelength light-emitting diodes, laser diodes and optical storage systems, respectively [30]. These materials have excellent physical properties such as a wide direct energy band gap, strong atomic bonding and formation of a continuous range of solid solutions and superlattices. In recent years, several techniques have been used to grow expitaxial films. The deposition of group 13 nitrides by MOCVD (metal organic chemical vapor deposition) with the use of a single source precursor, having preformed metal–nitrogen bonds, is the state of the art method. Therefore, clusters of group 13 nitrides are ideal systems for this purpose and hence the motivation for their synthesis [30].

This chapter emphasizes cage and cluster compounds of aluminum, gallium and indium incorporating nitrogen atoms. A search of the literature reveals a number of monographs and reviews [31–33] as well as recent research articles available on this subject. Reactions of alanes and alanates with various amines leading to iminoalanes and aminoalanes have been well documented [21, 31, 34–36]. In summary, there are reports on the formation of iminoalanes from Eqs. (13) to (17).

$$AlH_3(NMe_3) + RNH_2 \rightarrow 1/n(HAlNR)_n + 2\ H_2 + NMe_3 \quad (13)$$

$$LiAlH_4 + RNH_2(HCl) \rightarrow 1/n(HAlNR)_n + 3\ H_2 + LiCl \quad (14)$$

$$AlH_3(NMe_3) + RCN \rightarrow 1/n(HAlNCH_2R)_n + NMe_3 \quad (15)$$

Tab. 3.5-1. Al–N bond lengths (pm) and angles (°) of various Al–N cage compounds.

Compound	*Range of Al–N bond lengths*	*Av. Al–N bond lengths*	*N–Al–N*	*Al–N–Al*	*Ref.*
$(MeAlNMes)_4$		194.8	90.1 av.	89.9 av.	36
$(MeAlNC_6F_5)_4$	191.0–196.8	193.9	87.2(2)–89.8(2)	90.4(2)–92.8(2)	37
$(Pr^iNAlH)_4$	189.7–192.3	191.4	90.1 av.	89.9 av.	38
$(Pr^iNAlMe)_4$	191.7–193.2	192.3	90.4 av.	89.6 av.	38
$(4\text{-}C_6H_4FNAlMe)_4$	192.2–195.1	193.4	89.32(10)–90.00(10)	90.00(10)–90.72(10)	39
$(PhNAlPh)_4$	190.0–193.0	191.4	90.0(0.4)	89.6(0.4)–90.0(0.4)	40
$(Pr^nNAlH)_6$	188.4–197.2	191.3	91.2–115.2 av.	88.6–124.3 av.	41
$(p\text{-}CF_3C_6H_4CH_2NAlH)_6$	188.0–198.0	191.9	90.8(4)–115.3(5)	88.1(4)–124.0(5)	21
$(PhCH_2NAlH)_6$	188.6–197.4	191.8	91.05–115.25(8)	88.57(6)–124.37(8)	21
$(PhNAlMe)_6$	190.2–195.1	192.5	90.2(2)–113.7(2)	88.9(2)–126.0(2)	42
$(MeNAlMe)_7$	181.0–197.0	191.0	86.3(13)–111.1(12)	85.9(16)–135.5(11)	43
$(1\text{-}AdCH_2NAlH)_7$	190.0–198.0	193.0	89.03(9)–115.37(9)	86.16(7)–123.70(11)	44
$(Pr^nNAlH)_8$	187.8–194.7	191.6	91.1–114.1 av.	88.8–120.8 av.	41
$(4\text{-}C_6H_4FNAlMe)_6$	190.5–195.2	191.7	90.06(11)–113.28(11)	89.11(11)–126.22(13)	39
$(Me_2NC_2H_4NAlEt)_6$	189.2–197.4	192.2	90.46(13)–114.30(14)	87.81(13)–126.1(2)	45

$$AlMe_3 + RNH_2 \rightarrow 1/4(MeAlNR)_4 + 2\ CH_4 \quad (16)$$

$$Al + RNH_2 \rightarrow 1/n(HAlNR)_n + 1/2\ H_2 \quad (17)$$

The reaction products depend to a great extent on the nature of the substituents, R, at the nitrogen atoms, the temperature and the solvent used. The isolated clusters of iminoalanes are solids. The structurally characterized compounds are listed in Table 3.5-1 with appropriate literature citations [21, 36–45]. For the preparation on a laboratory scale, the reaction in Eq. (15) is the preferred route [21]. A variety of starting materials is available on a large scale and the only volatile side product is NMe_3. Owing to the formation of a CH_2 group, which functions as a spacer between the bulky R and the nitrogen atom, the nitriles with bulky R groups can be used in this method. The reaction in Eq. (13) needs high temperatures, but many side-products are formed, while Eq. (14) yields LiCl, which is not easy to separate from the $(HAlNR)_n$ product. During the formation of aggregates as in Eqs. (13) and (15), NMe_3 is presumably replaced partly by RNH_2 and RCN, respectively. Based on the formation of hydrogenated products and an atom economical point of view, the reaction in Eq. (15) is the preferred one in this series. The transfer of the hydrogen from aluminum to carbon in forming a CH_2 group is an inter or intra molecular process. Although the structure of the monomeric RAl=NR compound is yet to be determined, an analogous compound having bulky R groups has been prepared [46] from the reaction of an aluminum(I) compound with a bulky azide and the elimination of N_2. Therefore, a short-lived monomeric RAl=NR species in solution might be a possible intermediate to these species. The degree of aggregation highly depends on the steric demand of the ligands at the nitrogen and the aluminum atoms.

In comparison with aluminum, the number of known iminogallane and iminoindane clusters is small. While the preparation of $(PhNAlPh)_4$ dates back to 1962 [34], it was structurally characterized ten years later [40], the first iminogallanes and iminoindanes were prepared in 1993 by the reaction of $C_6F_5NH_2$ with $GaMe_3$ and $InMe_3$, respectively [Eq. (18)] [47]. The four-membered intermediates, **25**, are formed in high yields and can be isolated. Further heating of **25a**,**b** without solvent results in the formation of the iminogallane **26a** and iminoindane **26b**. Methane elimination was observed between 200 and 220 °C. Therefore, using C–H instead of C–F ligands resulted in C–H activation with the formation of carbon containing heterocycles [35]. Larger substituents on the gallium atoms, such as mesityl, resulted in the monomeric species $(Mes)_2GaNHC_6F_5$ [**27**, Eq. (19)]. The conversion of **27** to the heterocubane **28** [Eq. (19)] proceeds at 200 °C.

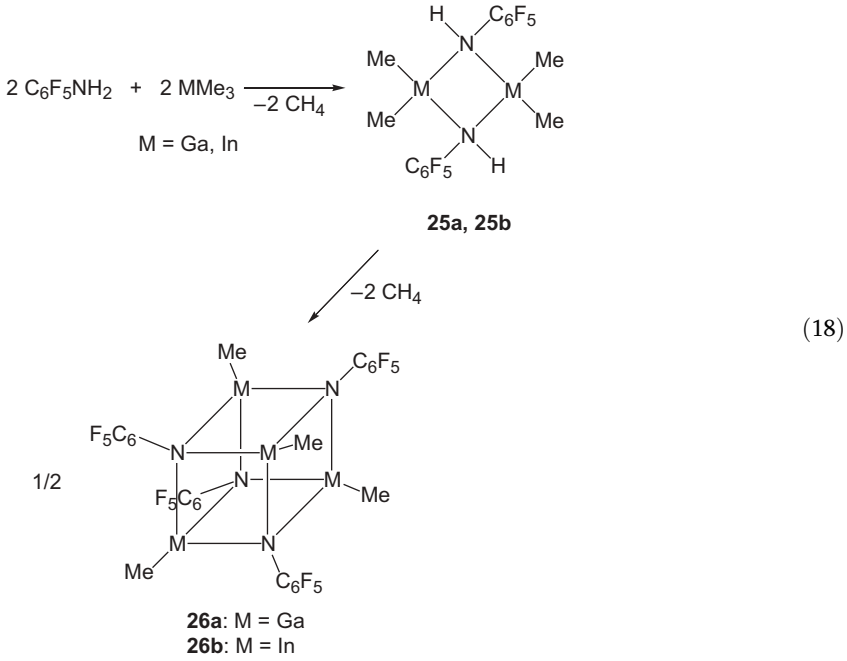

(18)

The structure of **28** consists of a Ga_4N_4 core. One of the mesityl groups on gallium in **28** was replaced by an NHC_6F_5 substituent. It is interesting to note that the reaction of 4-fluoroaniline with $AlMe_3$, $GaMe_3$ and $InMe_3$ yields iminoalanes $(4\text{-}C_6H_4FNAlMe)_4$ and $(4\text{-}C_6H_4FNAlMe)_6$, the exclusive hexagonal prismatic $(4\text{-}C_6H_4FNGaMe)_6$ [39] and a highly distorted cube consisting of In and N atoms at alternating corners, respectively. A methyl group and a THF molecule coordinate to each In atom resulting in a five-fold coordination of the In [39] in the latter case. Thus it was demonstrated that the introduction of one fluorine atom into the 4-position of the phenyl ring lowers the N–H activation barrier to yield the iminogallanes and iminoindanes. Reaction of $GaMe_3$ with phenylhydrazine yielded the

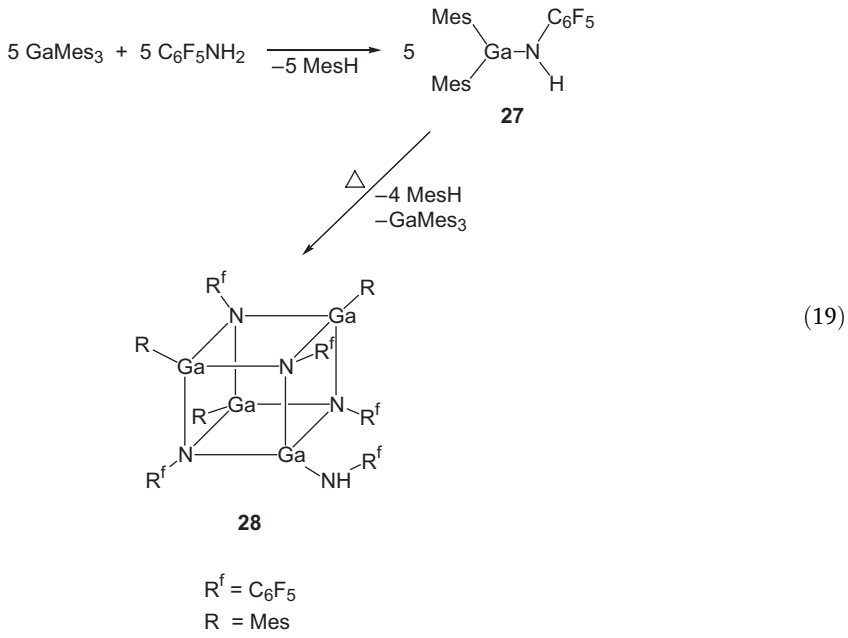

(19)

$R^f = C_6F_5$
R = Mes

colorless, heterocyclic gallium hydrazide **29** in high yield [Eq. (20)]. Upon further heating **29** undergoes a second methane elimination affording the novel Ga_4N_8 cage skeleton of **30** [Eq. (20)] [48].

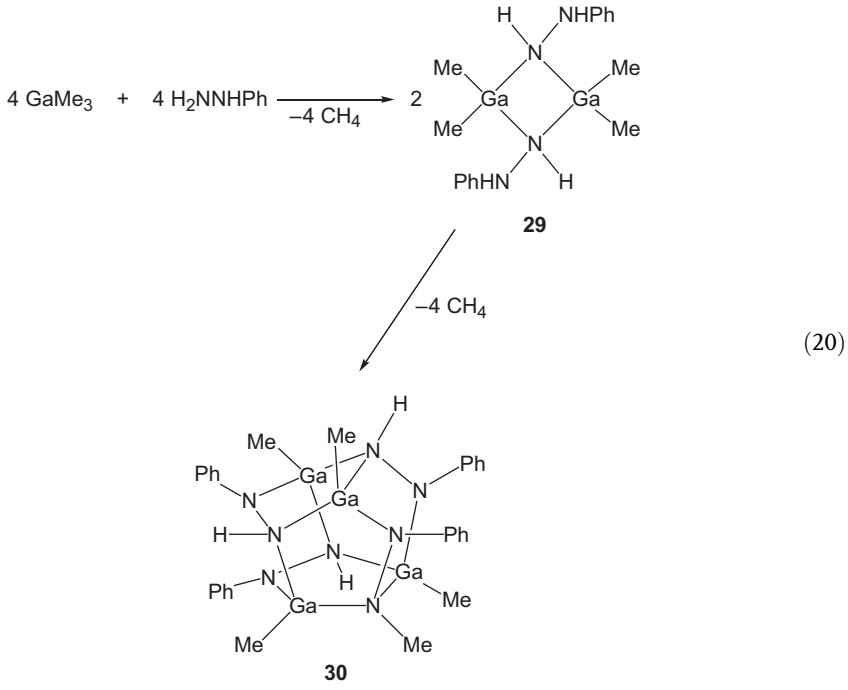

(20)

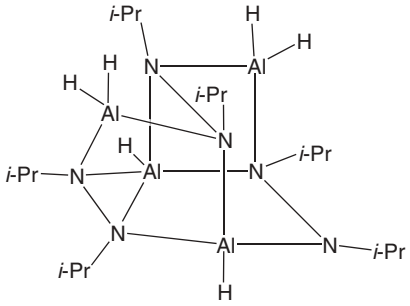

31

Fig. 3.5-5. Schematic drawing of the cage structure of the aluminum hydrazide $(AlH)_2(AlH_2)_2(N_2Pr^i_2)_3$ **31**.

Compound **30** was characterized by a single crystal X-ray structural analysis. The gallium atoms possess a distorted tetrahedral coordination sphere. The N–N distance of 148.9(3) pm is somewhat longer than predicted for a N–N single bond (145.4 pm), a result that may be attributed to the bridging nature of the hydrazido ligand in **30**. Thermolysis of the cage at 700 °C under a hydrogen atmosphere leads to the formation of hexagonal GaN [48]. A similar core structure was found for $[MeGaNHNBu^t]_4$, which was obtained from the reaction of $GaMe_3$ with H_2NNHBu^t [49]. An aluminum hydrazide with a complicated $Al_4(N_2)_3$ cage structure (**31**, Figure 3.5-5) was obtained by the reaction of $AlH_3 \cdot NMe_2Et$ with tetramethyl-2,3-diazabutadiene [50].

An In_4N_8 core structure in **32** was obtained by the reaction of $InNp_3$ (Np = neopentyl = CH_2CMe_3) with 1,2-$(NH_2)_2C_6H_4$ in a 1:1 molar ratio [Eq. (21)] [51]. The composition of **32** is $[(Np)In\{\mu\text{-}(NH)_2C_6H_4\}]_4$ with square pyramidal indium centers having an average In–N distance of 227.6 pm. All four In atoms are chemically equivalent and are pentacoordinated with the CH_2CMe_3 group occupying the fifth coordination site [51].

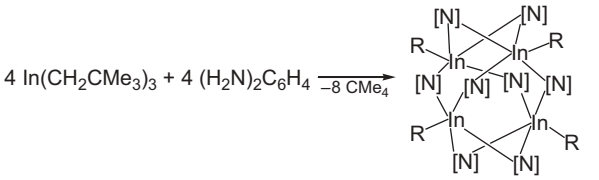

(21)

32

(R = CH_2CMe_3)
(C_6H_4 bridges not shown)

The compounds of general composition $(RAlNR')_n$ ($n = 4, 6, 7, 8$) with various R and R′ groups were characterized by single crystal X-ray analyses. The respective Al–N distances and the N–Al–N and Al–N–Al angles are listed in Table 3.5-1. The most common structural motifs are illustrated in Figure 3.5-6.

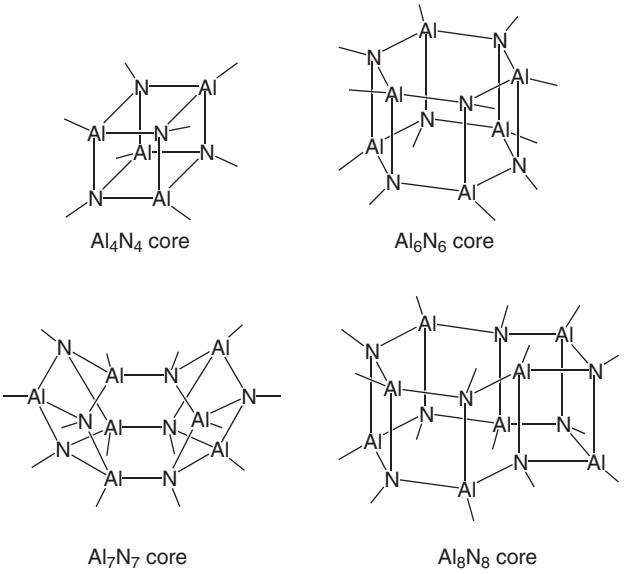

Fig. 3.5-6. Structural motifs of iminoalanes (R and R′ groups were omitted for clarity).

According to Table 3.5-1, the average Al–N bond lengths of various aggregates are almost constant. However, the range of bond lengths within the heterocubane Al_4N_4 is smaller compared with the hexagonal Al_6N_6 drum-like structure, where two six-membered Al_3N_3 rings are joined by six Al–N transverse bonds forming the six rectangular side faces of the drum. The Al–N bonds in the six-membered almost planar rings are significantly shorter than the transverse bonds joining the rings. At a first glance, the Al–N–Al and N–Al–N angles in all Al_4N_4 cubes from geometrical considerations need to be more or less 90°. The nitrogen atom can be considered to bind the three adjacent aluminum atoms through p-orbitals. Electron releasing substituents at nitrogen, as silyl groups, increase the electron density on N, resulting in a higher N···N repulsion. This demonstrates that the nitrogen atoms are located above each Al_3-triangle of the Al_4 tetrahedron, giving rise to a more acute Al–N–Al angle and a wider N–Al–N angle, respectively. Electron withdrawing substituents such as the C_6F_5 group lower the electron density at the nitrogen atoms. Therefore, N···N repulsions are less pronounced, and the nitrogen atoms are located closer to the Al_3 triangle, giving Al–N–Al angles larger than 90°. For example, in compound $(MeAlNC_6F_5)_4$ the N–Al–N angle is more acute than 90° (86–89°), while the Al–N–Al angle is wider than 90° (91–92°).

The transformation of the aminoalane $(Me_2AlNHMe)_3$ prepared from $AlMe_3$ and H_2NMe to the iminoalane $(MeAlNMe)_7$ [43] involves intermediate mixed amino-imino alanes of the type $(Me_2AlNHMe)_2(MeAlNMe)_6$ **33** (Figure 3.5-7) [52]. The analogous gallium derivative was prepared from methylamine and trimethylgallium [52]. The structures of the aluminum and gallium cages are similar. The metal and nitrogen atoms are tetracoordinated.

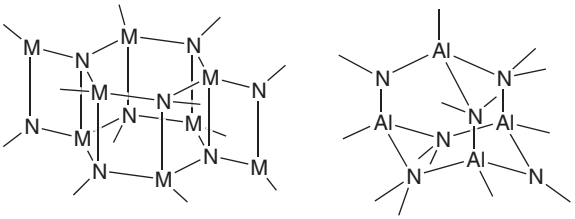

Fig. 3.5-7. Schematic drawings of the core structures of the amido-imidoalanes **33** and **34**.

Obviously, the nitrogen atoms of the two NHMe groups are part of the four-membered rings, whereas the imino nitrogen atoms form the drum. A compound of the composition $(ClAl)_4(NMe)_2(NMe_2)_4$ is a representative of an amino-iminoalane with a heteroadamantane structure (**34**, Figure 3.5-7) [53]. The molecule displays four tetrahedrally coordinated N atoms, but the other two N atoms show a trigonal planar coordination site, with an average Al–N distance of 192 pm to the four-coordinate N, and a distance of 179 pm to the three-coordinate N atoms.

3.5.3
Clusters and Cages Including Chalcogen Atoms

3.5.3.1
Compounds Derived from Homonuclear Clusters

Metal rich cluster or cage compounds formed by the earth metals and the chalcogenes are extremely rare. One example was obtained by the reaction of the tetrahedral tetraindium(I) cluster $In_4[C(SiMe_3)_3]_4$ with propylene sulfide. Under thoroughly controlled reaction conditions the transfer of only one sulfur atom to the indium cluster succeeded, and the dark red crystals of the product **35** were isolated in 44% yield [Eq. (22)] [54]. The sulfur atom occupies one face of the In_4 tetrahedron with three almost identical In–S bond lengths, so that a trigonal bipyramidal In_4S cluster with the sulfur atom in an axial position results. The In–In distances differ considerably. The shorter ones were observed along the edges of the unoccupied triangles (284 pm), while the equatorial In–In distances are elongated to 339 pm on average. The long distances are intermediate between those of the alkylindium(I) clusters In_4R_4 (300 to 314 pm) [55, 56] and those of negligible In–In bonding interactions in cyclopentadienylindium(I) derivatives (>360 pm) [57]. The cluster of compound **35** is isostructural and isoelectronic to the carbaboranes $C_2B_3R_5$ or the compounds of the heavier third main-group elements $(Cp^*Al)_3E_2$ (**21a**: E = As; **21b**: E = Sb) and to the anion $[Ga\{Si(SiMe_3)_3\}_3(GaSiMe_3)(SiSiMe_3)]^-$ **2** discussed above [4, 25, 26]. The cluster **35** may thus also be considered as a *closo*

compound (*closo*-thiapentaindane) according to the Wade rules possessing six cluster electron pairs (4 × Ga: 8e + S: 4e) and five vertices. By the addition of one sulfur atom the average oxidation state of the indium atoms was enhanced from +1 in the starting compound to +1.5 in **35**.

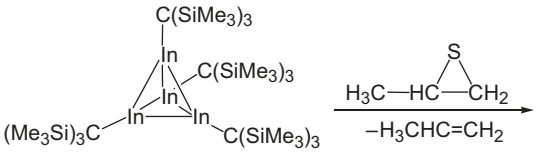

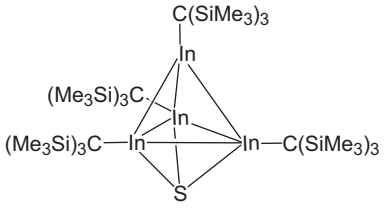

35

(22)

Complete oxidation of tetrahedral tetraelement(I) clusters (E = Al, Ga, In) by the chalcogens or chalcogen atom donors such as XPR_3 (X = S, Se, Te) afforded heterocubane type molecules $E_4X_4R_4$ (**36**, E = Al, Ga, In; X = O, S, Se, Te, Figure 3.5-8) in great number. Their formation may be described by the complete occupation of all triangular faces of the starting tetrahedra by chalcogen atoms. Some structural parameters of exclusively those compounds which were obtained by reactions of element(I) clusters are summarized in Table 3.5-2. Complete series of heterocubane derivatives with all four chalcogens are known for the clusters $Ga_4[C(SiMe_3)_3]_4$ and $In_4[C(SiMe_3)_3]_4$. As expected, the Ga–X and In–X distances increase continuously on going from oxygen to tellurium. Most heterocubanes are distorted as is evident by the E–E and X–X contact distances in Table 3.5-2. The most distorted compounds are formed with X = Te. In all gallium derivatives the Ga–Ga distances are shorter than the sum of the van der Waals radii, which for indium was observed for the oxygen derivative only. These observations confirm

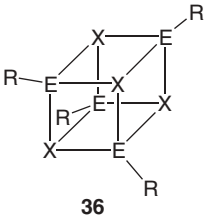

36

X = O, S, Se, Te
E = Al, Ga, In
R = Cp*, $Si(CMe_3)_3$, $C(SiMe_3)_3$

Fig. 3.5-8. Schematic drawing of the heterocubane type molecules $E_4X_4R_4$.

Tab. 3.5-2. Selected structural parameters of E_4X_4 heterocubanes obtained from organoelement(I) compounds (E = Al, Ga, In, X = O, S, Se, Te); (distances in pm; *Q* represents the ratio of the angles EXE and XEX; van der Waals radii: Ga 190, In 190, O 150, S 180, Se 190, Te 210 pm [58]).

Compound	*E–X*	*E···E*	*X···X*	*∠EXE*	*∠XEX*	*Q*	*Ref.*
$Al_4O_4[Si(CMe_3)_3]_4$	183.5	261.2	257.6	90.8	89.2	1.02	59
$Al_4Se_4Cp^*_4$	247.6	336.8	363.1	85.2	94.6	0.90	60
$Al_4Te_4Cp^*_4$	270.1	369.2	398.0	84.7	95.1	0.89	60
$Ga_4O_4[Si(CMe_3)_3]_4$	191.5	271.2	270.4	90.1	89.9	1.00	59
$Ga_4O_4[C(SiMe_3)_3]_4$	196.7	287.5	268.3	93.9	86.0	1.09	61
$Ga_4S_4[C(SiMe_3)_3]_4$	238.1	326.1	346.8	86.4	93.5	0.92	62
$Ga_4Se_4[C(SiMe_3)_3]_4$	250.1	339.1	367.2	85.4	94.5	0.90	62
$Ga_4Te_4[C(SiMe_3)_3]_4$	271.3	366.9	399.2	85.1	94.7	0.90	62
$In_4O_4[C(SiMe_3)_3]_4$	214.0	315.7	287.9	95.1	84.6	1.12	63
$In_4S_4[C(SiMe_3)_3]_4$	254.9	350.4	370.0	86.8	93.1	0.93	64
$In_4Se_4[C(SiMe_3)_3]_4$	267.1	362.1	392.1	85.4	94.4	0.90	55
$In_4Te_4[C(SiMe_3)_3]_4$	286.4	382.9	425.2	83.7	95.6	0.88	64
$In_4Se_4[Si(CMe_3)_3]_4$	267.9	355.3	400.0	82.9	96.8	0.86	59

the considerable steric stress in the Ga_4X_4 hetrocubanes, which leads to complete dissociation of the sulfur compound upon dissolution in benzene to form $Ga_2S_2R_2$ heterocyclic molecules. The extremely hygroscopic Ga_4O_4 compound has not yet been investigated with respect to its solution behavior. The most acute angles of the sulfur, selenium and tellurium cages are found at the chalcogen atoms. The distortion is inverted in the oxygen compounds in which the most acute angles are observed at the gallium or indium atoms and in which the inner cage chalcogen–chalcogen distances are shorter than the Ga–Ga or In–In separations. These findings have recently been confirmed by quantum-chemical calculations [65].

An alkoxygallium(II) compound (**37**, Figure 3.5-9) is worth mentioning, which was obtained only recently by the reaction of the dioxane adduct of Ga_2Cl_4 with potassium *tert*-butanolate [66]. Compound **37** is a *tert*-butoxy bridged dimer of the tetraalkoxydigallane(4) derivative $(Me_3CO)_2Ga\text{-}Ga(OCMe_3)_2$ and contains two Ga–Ga single bonds. The structure may be derived from a cube of four gallium and four oxygen atoms with two Ga_2O_2 heterocycles connected by two Ga–Ga bonds. The structural parameters (Ga–Ga 248 pm, Ga–O 180 and 196 pm for terminal and bridging Ga–O groups, respectively) are in accordance with an electron precise, non-delocalized bonding situation.

3.5.3.2
Oxygen Compounds of Aluminum, Gallium and Indium

The controlled hydrolysis of aluminum alkyl and aryl compounds yields oligomeric species of the formula $(RAlO)_n$. They are called alumoxanes. Alkyl substituted alu-

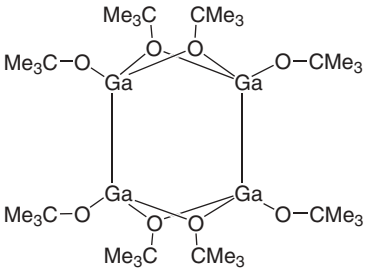

37

Fig. 3.5-9. Schematic drawing of the structure of **37**.

moxanes are active catalysts in the polymerization of epoxides, aldehydes and olefins. Methylalumoxane (MAO) is a highly active cocatalyst for group 4 metallocene catalyzed ethene and propene polymerizations. The role of the Lewis acidic MAO in polymerization reactions is proposed by abstraction of an alkyl group from the metallocene to generate a cationic metal center. Owing to the complexity of MAO, the molecular weight ranges from 900 to 1500, its structure and the mechanism of the alkyl abstraction are unknown. In contrast, well defined aggregates were obtained by selective hydrolysis of AlR_3 compounds using more bulky substituents [67, 68]. A controlled hydrolysis product of $AlMe_3$ was isolated as the lithium salt of composition $(Me_2AlOLi)_4 \cdot 7THF \cdot LiCl$. This compound represents the first isolated and structurally characterized complex of an alumoxane, which is stabilized by a separated cation and, therefore, a good model for the stabilization of catalytically active metallocene cations [69].

Generally $(RAlO)_n$ compounds are formed by hydrolysis of AlR_3 (R = organic groups) with water or hydrated salts or by the reaction with R–Si–O compounds, respectively [70]. The latter reaction is possibly due to the larger Al–O bond energy compared with that of Si–O. Usually, compounds of the composition $(RAlO)_n$ (n = 6, 7, 8, 9) form electron precise cages with the exception of $(RAlO)_4$ (R = 2,4,6-$Bu^t{}_3C_6H_2$). This compound contains a planar Al_4O_4 ring with Al–O distances in the range of 168.7 to 169.1 pm, O–Al–O angles of 117.92° and 119.85°, and Al–O–Al angles of 150.51° and 151.32°. The planarity of eight-membered rings is a rare feature usually [71]. Another noteworthy example is the $[Al_7O_6Me_{16}]^-$ anion forming a 12-membered Al_6O_6 ring capped by the seventh aluminum atom that is bonded to three alternate oxygen atoms in the ring [72].

The first step in the hydrolysis reaction is the formation of the water adduct [Eq. (23)] [69], which subsequently eliminates alkane to yield the hydroxide R_2AlOH. At elevated temperatures, further alkane elimination is observed with the formation of alkyl-alumoxane [67, 68]. Structurally characterized alumoxanes are listed in Table 3.5-3.

$$H_2O — AlR_3 \xrightarrow[-RH]{} R_2AlOH \xrightarrow[-RH]{} 1/n(RAlO)_n \qquad (23)$$

R = alkyl

Tab. 3.5-3. Structurally characterized oxygen compounds of aluminum, gallium and indium (the heterocubane type compounds have been included in Table 3.5-2).

Compound	*Bond length M–O (pm) M = Al, Ga, In*	*Ref.*
$[\{(Me_3Si)_3C\}_4Al_4(\mu\text{-}O)_2(\mu\text{-}OH)_4]$ (**38**)	179.7 av.	73
$[Bu^t{}_7Al_5(\mu_3\text{-}O)_3(\mu\text{-}OH)_2]$ (**40**)	179.3(4)–184.5(4)	68
$[Bu^t{}_6Al_6(\mu_3\text{-}O)_4(\mu\text{-}OH)_4]$ (**41**)	178–195(1)	74
$[Bu^tAl(\mu_3\text{-}O)]_6$ (**42**)	176.0(6)–190.5(5)	67
$[(Et_2O)Li]_2[Bu^t{}_6Al_6(O)_6Me_2]$ (**43**)	–[a]	75
$[\{(Me_3Si)_3C\}_4Ga_4(\mu\text{-}O)_2(\mu\text{-}OH)_4]$ (**39**)	189.5 av.	73
$[Bu^t{}_6Al_6(\mu_3\text{-}O)(\mu\text{-}OH)_2(\mu\text{-}O_2CCCl_3)_2]$ (**44**)	–[a]	76
$[Bu^t{}_6Al_6(\mu_3\text{-}O)_4(\mu\text{-}O)_2(NH_2Bu^n)]$ (**45**)	–[a]	77
$Al_5(\mu_5\text{-}O)(\mu\text{-}OBu^i)_8(OiBu)_5$ (**46**)		78
$Al_8(\mu_4\text{-}O)_2(\mu\text{-}OH)_2(\mu\text{-}OBu^i)_{10}(OBu^i)_8$ (**47**)		78
$[MesGaO]_9$ (**48**)	$(MesGaO)_3$ 191.0 av. (μ_2-MesGaO) 196.7 av.	79
$[Bu^t{}_{12}Ga_{12}(\mu_3\text{-}O)_8(\mu\text{-}O)_2(\mu\text{-}OH)_4]$ (**49**)	187.8(1)–191.1(5)	74, 75

[a] Compounds **43**, **44** and **45** are derivatives of **42** and have comparable Al–O bond lengths.

Heteroadamantane structures are known for a large variety of inorganic and organometallic compounds. This was demonstrated with the Al_4N_6 core system **34** (Figure 3.5-7). Therefore, it is quite obvious that the replacement of an NH group in Al_nN_m cages by an isoelectronic oxygen atom should not change the structural motif. However, the number of aluminum and gallium adamantane cage structures containing oxygen atoms is rare [73]. The mixed oxide-hydroxide $[\{(Me_3Si)_3C\}_4Al_4(\mu\text{-}O)_2(\mu\text{-}OH)_4]$ **38** was obtained by a selective hydrolysis of $(Me_3Si)_3CAlMe_2{\cdot}THF$. The similar, gallium-based oxide-hydroxide **39** was characterized by an X-ray crystal structure analysis (see Table 3.5-3). The average Al–O distance in **38** is shorter (179.7 pm) than the Ga–O distance in the gallium compound **39** (average 189.6 pm). This can be explained by the greater oxophilicity and Lewis acidity of aluminum compared with those of gallium [73].

Oxygen-centered organometallic heteroadamantanes are also known (Figure 3.5-10). They are formed around a four-coordinate oxygen atom, surrounded by four tetrahedrally disposed metal atoms, and this type of structure is illustrated by the organoindium hydroxo complex $[(Me_3Si)_3In]_4(\mu_4\text{-}O)(\mu\text{-}OH)_6$ [80].

The thermolysis of $[Bu^t{}_2Al(\mu\text{-}OH)]_3$ yields the pentaaluminum compound $[Bu^t{}_7Al_5(\mu_3\text{-}O)_3(\mu\text{-}OH)_2]$ **40** along with the main product, the hexamer $[Bu^tAl(\mu_3\text{-}O)]_6$ **42** [67, 68]. The core structure of **40** presumably is the result of a fusion of a six-membered Al_3O_3 ring with a four-membered Al_2O_2 ring. The Al–O distances range from 179.3 to 184.5 pm.

The most frequent structures of organo-alumoxanes are hexameric cage structures (**41**–**45**) [67] (Figure 3.5-11) (Table 3.5-3). The Al_6O_6 core can be described as a drum-like hexagonal prism with alternating Al and O atoms. The Al_3O_3 hexago-

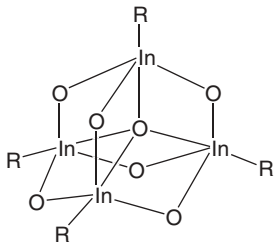

Fig. 3.5-10. Schematic drawing of the molecular structure of $[(Me_3Si)_3CIn]_4(\mu_4\text{-}O)(\mu\text{-}OH)_6$.

nal faces are essentially planar with O–Al–O and Al–O–Al angles of 113 (av.) and 126° (av.), respectively. There are two types of Al–O distances within the Al_3O_3 ring (187.7 to 190.5 pm) and those transverse of the two Al_3O_3 rings (176.0 to 179.6 pm). The oxide-hydroxide $[Bu^t{}_6Al_6(\mu_3\text{-}O)_4(\mu\text{-}OH)_4]$ **41** [74] is obtained by hydrolysis of $[Bu^tAl(\mu_3\text{-}O)]_6$. The aluminum atoms form an octahedron (Figure 3.5-11) with μ_3-O and μ_3-OH units capping the eight planes of the octahedron. The Al–O distances range from 178 to 195 pm. Compounds **43** to **45** are derivates of $[Bu^tAl(\mu_3\text{-}O)]_6$ **42** and were obtained by reacting **42** with the appropriate reagents, as shown by the formulae given in Table 3.5-3. Compounds possessing E_4O_4 heterocubanes (E = Al, Ga, In) have been discussed earlier (Table 3.5-2).

Nonameric M_9O_9 core structures (M = Al, Ga) are als konwn [67, 79]. The cage compound $[Bu^tAl(\mu_3\text{-}O)]_9$ was obtained as a side-product from the thermal treatment of $[Bu^t{}_2Al(\mu\text{-}OH)]_3$ [67], while reaction of $[Mes_2GaOH]_2{\cdot}THF$ (Mes = $Me_3C_6H_2$) at elevated temperatures yields the corresponding nonameric Ga_9O_9 skeleton in **48** [Eq. (24)]. These compounds have isostructural M_9O_9 cores. The Ga_9O_9 core can be described as having two six-membered $(MesGaO)_3$ rings connected by three μ-(MesGaO) units [79] (Figure 3.5-12).

$$9[Mes_2GaOH]_2(THF) \xrightarrow[\substack{-9\ THF\\ -18\ MesH}]{\triangle} \underset{\mathbf{48}}{2[MesGaO]_9} \qquad (24)$$

The average Ga–O distance in the two $(MesGaO)_3$ rings is 191.0 pm while the three Ga–O distances in the μ-(MesGaO) units are significantly longer (196.7 pm

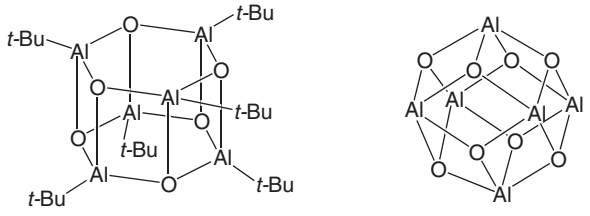

42 **41**

Fig. 3.5-11. Structures of the cage compounds **42** and **41** (core only).

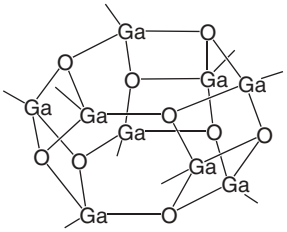

48

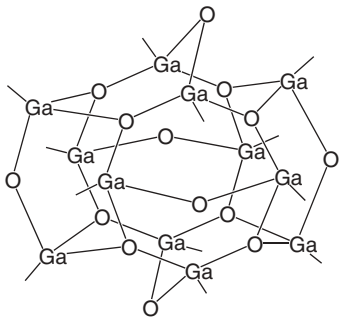

49

Fig. 3.5-12. Core structures of $Ga_9O_9Mes_9$ **48** and the dodecagallium cage **49** (Bu^t groups are omitted, and the bridging O atoms and OH groups of **49** are disordered).

av.). A dodecanuclear cage was found in $[(Bu^tGa)_{12}(\mu_3\text{-}O)_8(\mu\text{-}O)_2(\mu\text{-}OH)_7]$ **49** (Figure 3.5-12) [75]. The cage of **49** can be described as a cube of oxygen atoms in which the six planes are capped by $Bu^tGa(\mu\text{-}X)GaBu^t$ (X = O, OH) units.

3.5.4 Clusters Including Halogen Atoms

Only those compounds are considered here in which the halogen atoms are important constituents of the cluster cores. Clusters with exclusively terminally coordinated halogen atoms were described in Chapter 2.3. Reaction of the tetraalkyltetraindium(I) compound $In_4[C(SiMe_3)_3]_4$ with an equivalent quantity of the bromine donor 1,2-dibromoethane yielded the orange In_4Br_2 cluster compound **50** [Eq. (25)] by the transfer of two Br atoms [81]. Compound **50** is stable up to 164 °C in the solid state, but decomposes slowly at room temperature in solution. Its structure may be derived from that of the starting In_4 cluster. One triangular face of the In_4 tetrahedron is occupied by a μ_3-bridging bromine atom; the second bromine atom bridges an edge of that particular face in a μ_2-fashion. An average oxidation state of +1.5 at the indium atoms results. The In_4Br core structure in **50** thus resembles that of the In_4S cluster in **35**. An important difference exists with respect to the In–In distances at the bridged faces, which are much longer in **50** (361 and 407 pm) and are indicated by dashed lines in the formula given in Eq. (25). The longest In–In separation of **50** was observed along the μ_2-Br bridged site of the cluster. The In–In distances including the indium atom at the top are short (287 pm) and correspond to In–In single bonds. Thus, the bonding in the cluster may approach a more localized situation. Owing to the oxidation by bromine three electron pairs remain for the interaction between the four metal atoms, instead of four electron pairs in the starting cluster. In the case of **50** they may form three In–In single bonds to the indium atom at the top.

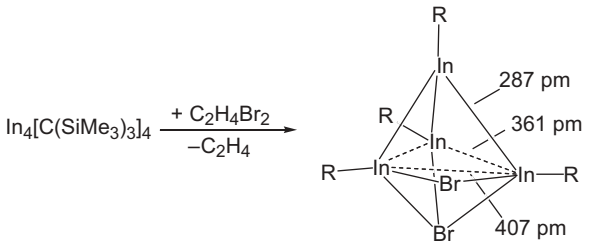

(25)

50: R = $C(SiMe_3)_3$

The related compound **51** with an average oxidation state of +1.5 at the gallium atoms was obtained in low yield by treatment of "gallium monoiodide" ("GaI", Section 3.5.1.1) with $LiSi(SiMe_3)_3$ [Eq. (26)] [82]. Further products of that reaction were two polyhedral Ga_4 and Ga_9 cluster compounds, which are discussed in more detail in Chapter 2.3. The remarkable difference with respect to the neutral In_4Br_2 derivative **50** is that an additional halide anion is present which leads to a negative charged Ga_4I_3 cluster anion. The structural parameters with short Ga–Ga distances to the gallium atom at the top of the cluster in **51** (253 pm) verify a similar bonding situation as described above for the In_4Br_2 cluster **50**.

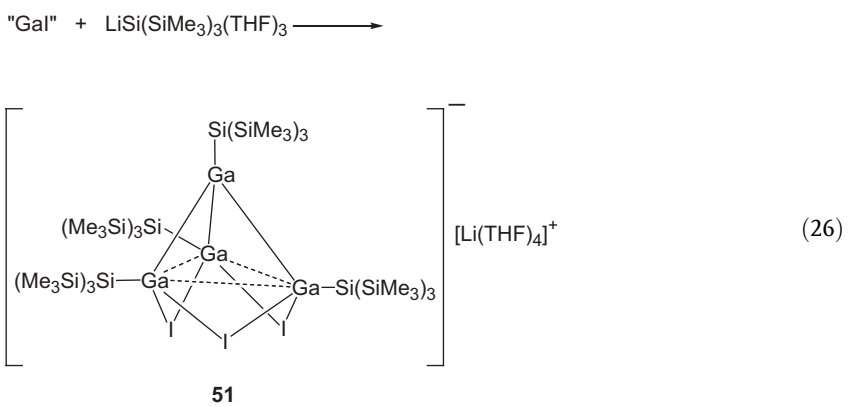

(26)

51

Both halogen cluster compounds **50** and **51** have an average oxidation state at gallium or indium of +1.5. An average number of +1.66 was achieved in the compound $In_3I_2[C(SiMe_3)_3]_3$ **52**, which was synthesized by the reaction of In_4R_4 [R = $C(SiMe_3)_3$] with a mixture of iodine and aluminum triiodide [Eq. (27)] [83]. The compound **52** has two In–In single bonds in a chain. The terminal indium atoms are bridged by two iodine atoms and are coordinatively saturated, while the inner indium atom has a coordination number of three in a planar environment. The molecular structure consists of a trigonal bipyramid in which two indium

atoms are in the axial positions, while the equatorial plane is spanned by two iodine atoms and one indium atom. The In–In bond lengths of 281 pm (av.) correspond to In–In single bonds. The intramolecular I–I and In–I contact distances are similar to the sum of the van der Waals radii and do not indicate any secondary bonding interaction. A similar compound, $[In_3Br_3\{C(SiMe_3)_3\}_3]^-$, was recently published [84]. It also possesses a chain of three indium atoms, however, the central In atom is coordinatively saturated by the formation of an adduct with a bromide ion.

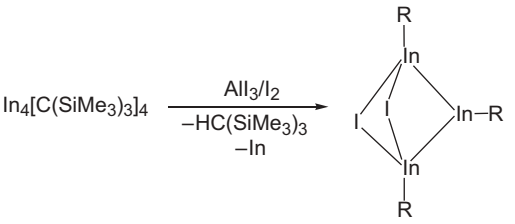

(27)

52: R = $C(SiMe_3)_3$

Enhancement of the oxidation state of the gallium or indium atoms in halogen cluster compounds to +2 gives products which contain isolated E–E single bonds. In most cases the products form dimers via halogen bridges as shown schematically in Figure 3.5-13. The compounds **53** to **56** were obtained by different routes. While the reaction of thermally labile gallium(I) bromide with $LiSi(SiMe_3)_3(THF)_3$ affords **53** [85], the reaction of the dioxane adduct of Ga_2Cl_4 with the same lithium compound gives **54** [86], and the oxidation of $In_4[C(SiMe_3)_3]_4$ with hexachloroethane or a mixture of bromine with aluminum tribromide leads to the formation of **55** and **56**, respectively [81]. An interesting alternative route for the synthesis of such element(II) halides was opened by the incomplete reduction of an organogallium dihalide with potassium, which does not yield an organogallium(I) cluster compound (Chapter 2.3), but stops at an intermediate oxidation state of +II with the formation of **57** (Figure 3.5-13) [87]. The cage structures of these dimeric sub-

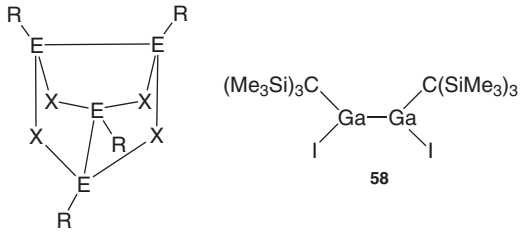

53: E = Ga; X = Br; R = $Si(SiMe_3)_3$
54: E = Ga; X = Cl; R = $Si(SiMe_3)_3$
55: E = In; X = Cl; R = $C(SiMe_3)_3$
56: E = In; X = Br; R = $C(SiMe_3)_3$
57: E = Ga; X = Cl; R = $Si(CMe_3)_3$

Fig. 3.5-13. Molecular structures of alkylelement(II) halides.

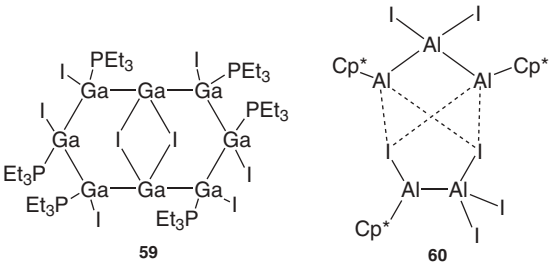

Fig. 3.5-14. Molecular structures of the alkylgallium and alkylaluminum subhalides **59** and **60**.

halides are similar to that of the mineral realgar As_4S_4. Furthermore, they may be derived from those of the tetrahedral E_4 clusters. Two opposite edges of the tetrahedron become E–E single bonds, the remaining four edges are bridged by the halogen atoms. Interestingly, the similar compound $Ga_2I_2[C(SiMe_3)_3]_2$ **58** (Figure 3.5-13) remains monomeric even in the solid state with coordinatively unsaturated gallium atoms [88]. The preference of the monomeric structure in that case may be caused by the relatively small covalent radius of the gallium atoms and the strong repulsion between the bulky $C(SiMe_3)_3$ substituents [89].

Eight gallium(I) atoms in a ring connected by Ga–Ga single bonds were observed for the compound $Ga_8I_8(PEt_6)_6$ **59** (Figure 3.5-14) [90]. Orange crystals of **59** were obtained by the reaction of "GaI" (see above) with triethylphosphane in about 65% yield. The ring is almost planar. Six gallium atoms are terminally bonded to one iodine atom and one triethylphosphane ligand, while the remaining gallium atoms in opposite positions are bridged by two iodine atoms. Treatment of aluminum triiodide with $(AlCp^*)_4$ afforded the $Cp^*_3Al_5I_6$ cluster compound **60** (Figure 3.5-14) [91] which represents another interesting aggregate with subvalent aluminum atoms. Compound **60** is labile at room temperature and was isolated in few single crystals only. Its molecular structure consists of a cage skeleton formed by five aluminum and two iodine atoms and may be described as a contact ion pair $[Cp^*_2Al_3I_2]^+$ $[Cp^*Al_2I_4]^-$ in accordance with quantum chemical calculations. Its formation may result from the insertion of three monomeric fragments $(AlCp^*)$ of the aluminum cluster $(AlCp^*)_4$ in three bridging Al–I bonds of dimeric aluminum triiodide $I_2Al(\mu\text{-}I)_2AlI_2$.

The only thallium compound to be discussed here is the $Tl_6Cl_2[Si(CMe_3)_3]_6$ cluster **61**. This remarkable compound was formed by the reaction of thallium(III) chloride with $NaSi(CMe_3)_3$ [Eq. (28)] and precipitated in the form of black crystals in 21% yield, when a solution in toluene was stored at −25 °C for six months [92]. Solutions of **61** in benzene decompose slowly at room temperature by the formation of $ClSi(CMe_3)_3$ and a black, not identified precipitate. The structure of **61** consists of two four-membered Tl_3Cl heterocycles, which are connected by one Tl–Tl and two Tl–Cl bonds. A monomeric Tl_3Cl heterocycle was isolated as a by-product in which one thallium atom was bonded to two $Si(CMe_3)_3$ substituents.

Release of silyl radicals and Tl–Tl bond formation may open the access to **61**. The Tl–Tl distances in **61** are relatively short (285 to 298 pm) and correspond to values observed in tetraorganyldithallanes $R_2Tl\text{-}TlR_2$. Accordingly, the electron count gives ten electrons available for metal–metal interactions, and the bonding in the cluster may thus be described by five Tl–Tl single bonds.

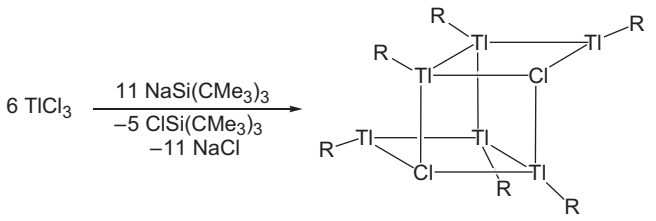

(28)

61: R = $Si(CMe_3)_3$

3.5.5
Clusters Including Hydrogen Atoms

The chemistry of hydroboranes is characterized by the occurrence of three different types of clusters which have been classified as *closo*, *nido* and *arachno* boranes. The particular structure depends on the number of cluster electrons and, related to that, on the ratio between the numbers of boron and hydrogen atoms. The enhancement of the cluster electron count results in the formation of more open clusters. The hydrogen atoms of the latter are not only in terminal positions, as in the case of the *closo* structures, but also adopt bridging positions on the open faces as essential constituents of the cluster skeletons. The most open compounds were classified as *hypho* derivatives, however, they have not yet been isolated and characterized in the form of pure homonuclear boranes. While few analogues of *closo*-borates containing heavier elements of the third main group such as aluminum or gallium are known (Chapter 2.3), *nido* and *arachno* type polyalanes or polygallanes have not been obtained so far. A single hydrogen rich oligogallane was isolated only recently, its synthesis was based on the easy availability of dialkylgallium hydrides.

The substituent exchange reaction between tri(*tert*-butyl)gallium and $GaH_3 \cdot NMe_2Et$ yielded di(*tert*-butyl)gallium hydride in about 80% yield [93]. Trimeric formula units were detected in the solid state possessing planar Ga_3H_3 heterocycles with three 3c2e Ga–H–Ga bonds. However, a temperature dependent equilibrium exists in benzene solution, and the dialkylgallium hydride partially dismutates by the formation of tri(*tert*-butyl)gallium and the novel sesquihydride $[(Me_3C)_2GaH]_2\text{-}[Me_3CGaH_2]_2$. The latter compound has an eight-membered Ga_4H_4 heterocycle with four 3c2e Ga–H–Ga bonds [93]. These mixtures are sensitive towards day light, and upon UV irradiation ($\lambda = 360$ nm) complete consumption of the starting materials was observed within 24 hours. Colorless crystals of a new compound,

$Ga_6H_6(CMe_3)_8$ **62**, precipitated in 83% yield [Eq. (29)] [94]. Compound **62** has a singular structure containing two Ga–Ga bonds with long Ga–Ga distances of 264 pm. These Ga_2 couples are connected by hydrogen bridges to give six-membered Ga_4H_2 heterocycles in a *twist* conformation. This ring is bridged by two $[H_2Ga(CMe_3)_2]^-$ ligands, each hydrogen of which is attached to one gallium atom of the heterocycle. The anions are situated below and above the average molecular plane and coordinate to opposite gallium atoms. The structure of the molecular center may be described alternatively as a distorted octahedron of six gallium atoms, two edges of which are Ga–Ga bonds, while six further edges are bridged by hydrogen atoms. Four edges remain unoccupied. The Ga–Ga distances in the 3c2e Ga–H–Ga bridges differ strongly by 292 pm in the six-membered Ga_4H_2 heterocycle and 331 pm on average for the rest. The composition of **62** is similar to that of the *hypho*-borane B_6H_{14}, which is known from quantum-chemical calculations only [95]. One of the calculated minimum structures of the boron compound is quite similar, although not identical to that of **62**, and has a six-membered B_4H_2 heterocycle in the molecular center with neighboring atoms bridged by BH_4 ligands, instead of opposite ones as observed in **62**. Clearly, compound **62** is on the borderline between compounds that require a delocalized cluster orbital scheme for the complete description of their bonding situation or which may be described sufficiently by a more localized approach. The mechanism of the unexpected formation of the Ga_6 compound **62** is not clear. The homolytic cleavage of Ga–C bonds of the starting compound may be initiated by irradiation, and the radical intermediates may dimerize via Ga–Ga bond formation.

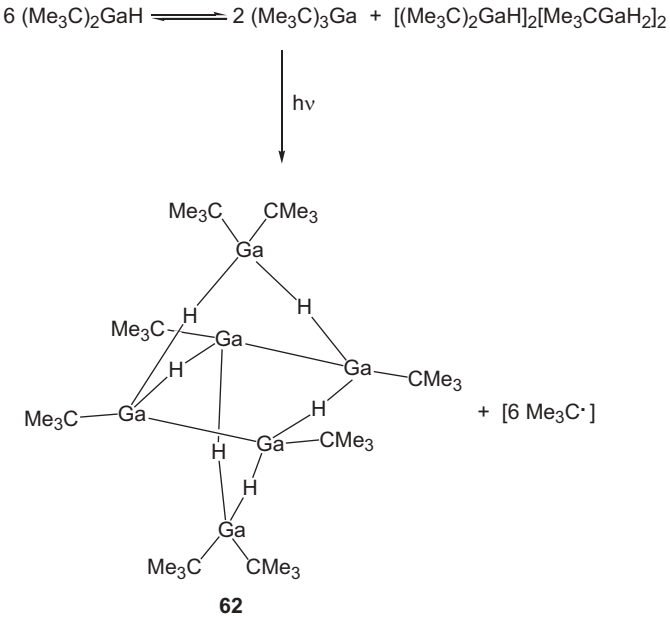

(29)

62

References

1 A. Purath, C. Dohmeier, A. Ecker, R. Köppe, H. Krautscheid, H. Schnöckel, R. Ahlrichs, C. Stoermer, J. Friedrich, P. Jutzi, *J. Am. Chem. Soc.*, **2000**, *122*, 6955–6959.

2 C. Dohmeier, C. Robl, M. Tacke, H. Schnöckel, *Angew. Chem.*, **1991**, *103*, 594–595; *Angew. Chem., Int. Ed. Engl.*, **1991**, *30*, 564–565; see also [62].

3 A. Haaland, K.-G. Martinsen, S. A. Shlykov, H. V. Volden, C. Dohmeier, H. Schnöckel, *Organometallics*, **1995**, *14*, 3116–3119; A. Haaland, K.-G. Martinsen, H. V. Volden, D. Loos, H. Schnöckel, *Acta Chem. Scand.*, **1994**, *48*, 172–174.

4 G. Linti, W. Köstler, H. Piotrowski, A. Rodig, *Angew. Chem.*, **1998**, *100*, 2331–2333; *Angew. Chem., Int. Ed. Engl.*, **1998**, *37*, 2209–2211; GaSi rings: G. Linti, W. Köstler, A. Rodig, *Eur. J. Inorg. Chem.*, **1998**, 745–749.

5 P. von Ragué Schleyer, G. Subramanian, A. Dransfeld, *J. Am. Chem. Soc.*, **1996**, *118*, 9988–9989; M. Antipin, R. Boese, D. Bläser, A. Maulitz, *J. Am. Chem. Soc.*, **1997**, *119*, 326–333.

6 K. Wade, *Adv. Inorg. Chem. Radiochem.*, **1976**, *18*, 1–66.

7 M. L. H. Green, P. Mountford, G. J. Smout, S. R. Speel, *Polyhedron*, **1990**, *9*, 2763–2765.

8 W. Uhl, F. Breher, *Eur. J. Inorg. Chem.*, **2000**, 1–11.

9 W. Uhl, *Inorganic Chemistry Highlights*, G. Meyer, D. Naumann, L. Wesemann, eds., Wiley-VCH, Weinheim, **2002**, pp. 229–243.

10 W. Uhl, F. Breher, *Angew. Chem.*, **1999**, *111*, 1578–1580; *Angew. Chem., Int. Ed. Engl.*, **1999**, *38*, 1477–1479.

11 W. Uhl, F. Breher, A. Mbonimana, J. Gauss, D. Haase, A. Lützen, W. Saak, *Eur. J. Inorg. Chem.*, **2001**, 3059–3066.

12 W. Uhl, F. Breher, J. Grunenberg, A. Lützen, W. Saak, *Organometallics*, **2000**, *19*, 4536–4543.

13 A. Almenningen, G. A. Anderson, F. R. Forgaard, A. Haaland, *Acta Chem. Scand.*, **1972**, *26*, 2315–2321.

14 R. G. Vranka, E. L. Amma, *J. Am. Chem. Soc.*, **1967**, *89*, 3121–3126; J. C. Huffman, W. E. Streib, *J. Chem. Soc., Chem. Commun.*, **1971**, 911–912.

15 W. Uhl, *Z. Naturforsch.*, **1988**, *43b*, 1113–1118; R. J. Wehmschulte, K. Ruhlandt-Senge, M. M. Olmstead, H. Hope, B. E. Sturgeon, P. P. Power, *Inorg. Chem.*, **1993**, *32*, 2983–2984.

16 J. Bicerano, D. S. Marynick, W. N. Lipscomb, *Inorg. Chem.*, **1978**, *17*, 3443–3453; M. Gielen, *Polyhedron*, **1988**, *7*, 363–368; P. von Ragué Schleyer, K. Najafian, A. M. Mebel, *Inorg. Chem.*, **1998**, *37*, 6765–6772.

17 A. Stasch, M. Ferbinteanu, J. Prust, W. Zheng, F. Cimpoesu, H. W. Roesky, J. Magull, H.-G. Schmidt, M. Noltemeyer, *J. Am. Chem. Soc.*, **2002**, *124*, 5441–5448.

18 W. Uhl, F. Breher, A. Lützen, W. Saak, *Angew. Chem.*, **2000**, *112*, 414–416; *Angew. Chem., Int. Ed. Engl.*, **2000**, *39*, 406–409.

19 E. H. Wong, L. Prasad, E. J. Gabe, M. G. Gatter, *Inorg. Chem.*, **1983**, *22*, 1143–1146; O. Volkov, W. Dirk, U. Englert, P. Paetzold, *Z. Anorg. Allg. Chem.*, **1999**, *625*, 1193–1201.

20 W. Uhl, F. Breher, B. Neumüller, A. Lützen, W. Saak, J. Grunenberg, *Organometallics*, **2001**, *20*, 5478–5484.

21 N. D. Reddy, H. W. Roesky, M. Noltemeyer, H.-G. Schmidt, *Inorg. Chem.*, **2002**, *41*, 2374–2378.

22 W. Zheng, A. Stasch, J. Prust, H. W. Roesky, F. Cimpoesu, M. Noltemeyer, H.-G. Schmidt, *Angew. Chem.*, **2001**, *113*, 3569–3572; *Angew. Chem., Int. Ed. Engl.*, **2001**, *40*, 3461–3464.

23 W. Uhl, L. Cuypers, B. Neumüller, F. Weller, *Organometallics*, **2002**, *21*, 2365–2368.

24 C. Dohmeier, H. Schnöckel, C. Robl, U. Schneider, R. Ahlrichs,

Angew. Chem., **1994**, *106*, 225–227; *Angew. Chem., Int. Ed. Engl.*, **1994**, *33*, 199–201.

25 C. K. F. von Hänisch, C. Üffing, M. A. Junker, A. Ecker, B. O. Kneisel, H. Schnöckel, *Angew. Chem.*, **1996**, *108*, 3003–3005; *Angew. Chem., Int. Ed. Engl.*, **1996**, *35*, 2875–2877.

26 S. Schulz, T. Schoop, H. W. Roesky, L. Häming, A. Steiner, R. Herbst-Irmer, *Angew. Chem.*, **1995**, *107*, 1015–1016; *Angew. Chem., Int. Ed. Engl.*, **1995**, *34*, 919–920.

27 W. Uhl, M. Benter, *Chem. Commun.*, **1999**, 771–772.

28 W. Uhl, M. Benter, *J. Chem. Soc., Dalton Trans.*, **2000**, 3133–3135.

29 C. von Hänisch, D. Fenske, M. Kattannek, R. Ahlrichs, *Angew. Chem.*, **1999**, *111*, 2900–2902; *Angew. Chem., Int. Ed. Engl.*, **1999**, *38*, 2736–2738.

30 S. J. Pearton, F. Ren, *Adv. Mater.*, **2000**, *12*, 1571; H. S. Park, S. D. Waezsada, A. H. Cowley, H. W. Roesky, *Chem. Mater.*, **1998**, *10*, 2251–2257.

31 I. Haiduc, D. B. Sowerby, eds., *The Chemistry of Inorganic Homo- and Heterocycles*, Academic Press, London, **1987**.

32 H. W. Roesky, ed., *Rings, Clusters and Polymers of Main Group and Transition Elements*, Elsevier, Amsterdam, **1989**.

33 M. Veith, *Chem. Rev.*, **1990**, *90*, 3–16.

34 F. R. R. McDonald, J. J. Jones, W. S. McDonald, *Proc. Chem. Soc.*, **1962**, 366–367.

35 K. M. Waggoner, P. P. Power, *J. Am. Chem. Soc.*, **1993**, *113*, 3385–3393.

36 G. H. Robinson, in *Coordination Chemistry of Aluminum*, G. H. Robinson, ed., VCH, New York, **1993**, Chap. 2.

37 T. Belgardt, S. D. Waezsada, H. W. Roesky, H. Gornitzka, L. Häming, D. Stalke, *Inorg. Chem.*, **1994**, *33*, 6247–6251.

38 G. DelPiero, M. Cesari, G. Perego, G. Dozzi, A. Mazzei, *J. Organomet. Chem.*, **1977**, *129*, 281–288.

39 C. Schnitter, S. D. Waezsada, H. W. Roesky, M. Teichert, I. Usón, E. Parisini, *Organometallics*, **1997**, *16*, 1197–1202.

40 T. R. R. McDonald, W. S. McDonald, *Acta Crystallogr. Sect. B*, **1972**, *28*, 1619–1622.

41 G. DelPiero, M. Cesari, G. Perego, S. Cucinella, E. Cernia, *J. Organomet. Chem.*, **1977**, *129*, 289–298.

42 A.-A. I. Al-Wassil, P. B. Hitchcock, S. Sarisaban, J. D. Smith, C. L. Wilson, *J. Chem. Soc., Dalton Trans.*, **1985**, 1929–1933.

43 P. B. Hitchcock, J. D. Smith, T. K. Mark, *J. Chem. Soc., Dalton Trans.*, **1976**, 1433–1437.

44 Y. Peng, J. Rong, D. Vidovic, H. W. Roesky, T. Labahn, J. Magull, unpublished results.

45 J. E. Park, B.-J. Bae, Y. Kim, J. T. Park, I.-H. Suh, *Organometallics*, **1999**, *18*, 1059–1067.

46 N. J. Hardman, C. Cui, H. W. Roesky, W. H. Fink, P. P. Power, *Angew. Chem.*, **2001**, *113*, 2230–2232; *Angew. Chem., Int. Ed. Engl.*, **2001**, *40*, 2172–2174.

47 T. Belgardt, H. W. Roesky, M. Noltemeyer, H.-G. Schmidt, *Angew. Chem.*, **1993**, *105*, 1101–1102; *Angew. Chem., Int. Ed. Engl.*, **1993**, *32*, 1056–1057.

48 D. W. Peters, M. P. Power, E. D. Bourret, J. Arnold, *Chem. Commun.*, **1998**, 753–754.

49 D. W. Peters, E. D. Bourret, M. P. Power, J. Arnold, *J. Organomet. Chem.*, **1999**, *582*, 108–115.

50 W. Uhl, J. Molter, B. Neumüller, *Chem. Eur. J.*, **2001**, *7*, 1510–1515.

51 H. Rahbarnoohi, R. L. Wells, A. L. Rheingold, *Chem. Commun.*, **1996**, 2661–2662.

52 S. Amirkhalili, P. B. Hitchcock, J. D. Smith, *J. Chem. Soc., Dalton Trans.*, **1979**, 1206–1212.

53 U. Thewalt, I. Kawada, *Chem. Ber.*, **1970**, *103*, 2754–2759.

54 W. Uhl, R. Graupner, W. Hiller, M. Neumayer, *Angew. Chem.*, **1997**, *109*, 62–64; *Angew. Chem., Int. Ed. Engl.*, **1997**, *36*, 62–64.

55 W. Uhl, R. Graupner, M. Layh, U. Schütz, *J. Organomet. Chem.*, **1995**, *493*, C1–C5.

56 W. Uhl, A. Jantschak, W. Saak, M. Kaupp, R. Wartchow, *Organometallics*, **1998**, *17*, 5009–5017.

57 O. T. Beachley, Jr., M. R. Churchill, J. C. Fettinger, J. C. Pazik, L. Victoriano, *J. Am. Chem. Soc.*, **1986**, *108*, 4666–4668; H. Schumann, C. Janiak, F. Görlitz, J. Loebel, A. Dietrich, *J. Organomet. Chem.*, **1989**, *363*, 243–251; H. Schumann, C. Janiak, J. Pickardt, U. Börner, *Angew. Chem.*, **1987**, *99*, 788–789; *Angew. Chem., Int. Ed. Engl.*, **1987**, *26*, 789–790.

58 J. E. Huheey, E. A. Keiter, R. L. Keiter, *Inorganic Chemistry*, 4th Edn., Harper Collins, New York, **1993**.

59 N. Wiberg, T. Blank, K. Amelunxen, H. Nöth, H. Schnöckel, E. Baum, A. Purath, D. Fenske, *Eur. J. Inorg. Chem.*, **2002**, 341–350.

60 S. Schulz, H. W. Roesky, H. J. Koch, G. M. Sheldrick, D. Stalke, A. Kuhn, *Angew. Chem.*, **1993**, *105*, 1828–1830; *Angew. Chem., Int. Ed. Engl.*, **1993**, *32*, 1729–1731.

61 W. Uhl, M. Benter, unpublished results.

62 W. Uhl, M. Benter, W. Saak, P. G. Jones, *Z. Anorg. Allg. Chem.*, **1998**, *624*, 1622–1628.

63 W. Uhl, M. Pohlmann, *Chem. Commun.*, **1998**, 451–452.

64 W. Uhl, R. Graupner, M. Pohlmann, S. Pohl, W. Saak, *Chem. Ber.*, **1996**, *129*, 143–146.

65 C. J. Bardon, P. Charbonneau, H. F. Schaefer, III, *Organometallics*, **2002**, *21*, 3605–3609.

66 G. Linti, W. Köstler, A. Rodig, *Z. Anorg. Allg. Chem.*, **2002**, *628*, 1319–1326.

67 M. R. Mason, J. M. Smith, S. G. Bott, A. R. Barron, *J. Am. Chem. Soc.*, **1993**, *115*, 4971–4984.

68 C. J. Harlan, M. R. Mason, A. R. Barron, *Organometallics*, **1994**, *13*, 2957–2969.

69 J. Storre, C. Schnitter, H. W. Roesky, H.-G. Schmidt, M. Noltemeyer, R. Fleischer, D. Stalke, *J. Am. Chem. Soc.*, **1997**, *119*, 7505–7513.

70 A. R. Barron, *Comments Inorg. Chem.*, **1993**, *14*, 123–153, and references cited therein.

71 R. J. Wehmschulte, P. P. Power, *J. Am. Chem. Soc.*, **1997**, *119*, 8387–8388.

72 J. L. Atwood, D. C. Hrncir, R. D. Priester, R. D. Rogers, *Organometallics*, **1983**, *2*, 985–989.

73 C. Schnitter, H. W. Roesky, T. Albers, H.-G. Schmidt, C. Röpken, E. Parisini, G. M. Sheldrick, *Chem. Eur. J.*, **1997**, *3*, 1783–1792.

74 C. C. Landry, C. J. Harlan, S. G. Bott, A. R. Barron, *Angew. Chem.*, **1995**, *107*, 1315–1317; *Angew. Chem., Int. Ed. Engl.*, **1995**, *34*, 1201–1203.

75 C. J. Harlan, S. G. Bott, A. R. Barron, *J. Am. Chem. Soc.*, **1995**, *117*, 6465–6474.

76 Y. Koide, S. G. Bott, A. R. Barron, *Organometallics*, **1996**, *15*, 2213–2226.

77 Y. Koide, S. G. Bott, A. R. Barron, *Organometallics*, **1996**, *15*, 5514–5518.

78 J. Abrahams, D. C. Bradley, H. Chudzynska, M. Motevalli, R. A. Sinclair, *J. Chem. Soc., Dalton Trans.*, **2002**, 259–266.

79 J. Storre, A. Klemp, H. W. Roesky, R. Fleischer, D. Stalke, *Organometallics*, **1997**, *16*, 3074–3076.

80 S. S. Al-Juaid, N. H. Buttrus, C. Eaborn, P. B. Hitchcock, A. L. Roberts, J. D. Smith, A. C. Sullivan, *J. Chem. Soc., Chem. Commun.*, **1986**, 908–909.

81 W. Uhl, S. Melle, *Chem. Eur. J.*, **2001**, *7*, 4216–4221.

82 W. Köstler, G. Linti, *Angew. Chem.*, **1997**, *109*, 2758–2760; *Angew. Chem., Int. Ed. Engl.*, **1997**, *36*, 2644–2645.

83 W. Uhl, S. Melle, G. Geiseler, K. Harms, *Organometallics*, **2001**, *20*, 3355–3357.

84 W. Uhl, F. Schmock, G. Geiseler, *Z. Anorg. Allg. Chem.*, **2002**, *628*, 1963–1966.

85 A. Schnepf, E. Weckert, G. Linti, H. Schnöckel, *Angew. Chem.*, **1999**, *111*, 3578–3581; *Angew. Chem., Int. Ed. Engl.*, **1999**, *38*, 3381–3383.

86 G. Linti, W. Köstler, *Angew. Chem.*, **1996**, *108*, 593–595; *Angew. Chem., Int. Ed. Engl.*, **1996**, *35*, 550–552.

87 N. Wiberg, T. Blank, M. Westerhausen, S. Schneiderbauer, H.

Schnöckel, I. Krossing, A. Schnepf, *Eur. J. Inorg. Chem.*, **2002**, 351.

88 W. Uhl, A. El-Hamdan, M. Prött, P. Spühler, G. Frenking, *Dalton Trans.*, **2003**, 1360–1364.

89 A similar compound not derived from a cluster has recently been published: N. J. Hardman, R. J. Wright, A. D. Phillips, P. P. Power, *Angew. Chem.*, **2002**, *114*, 2966–2968; *Angew. Chem., Int. Ed. Engl.*, **2002**, *41*, 2842–2844.

90 C. U. Doriat, M. Friesen, E. Baum, A. Ecker, H. Schnöckel, *Angew. Chem.*, **1997**, *109*, 2057–2059; *Angew. Chem., Int. Ed. Engl.*, **1997**, *36*, 1969–1971.

91 C. Üffing, E. Baum, R. Köppe, H. Schnöckel, *Angew., Chem.*, **1998**, *110*, 2488–2491; *Angew. Chem., Int. Ed. Engl.*, **1998**, *37*, 2397–2400.

92 N. Wiberg, T. Blank, H.-W. Lerner, D. Fenske, G. Linti, *Angew. Chem.*, **2001**, *113*, 1275–1278; *Angew. Chem., Int. Ed. Engl.*, **2001**, *40*, 1232–1235.

93 W. Uhl, L. Cuypers, R. Graupner, J. Molter, A. Vester, B. Neumüller, *Z. Anorg. Allg. Chem.*, **2001**, *627*, 607–614.

94 W. Uhl, L. Cuypers, G. Geiseler, K. Harms, B. Neumüller, *J. Chem. Soc., Dalton Trans.*, **2001**, 2398–2400.

95 M. L. McKee, *J. Phys. Chem.*, **1990**, *94*, 435–440; H. Horn, R. Ahlrichs, C. Kölmel, *Chem. Phys. Lett.*, **1988**, *150*, 263–268; M. Bühl, R. von Ragué Schleyer, M. L. McKee, *Heteroatom Chem.*, **1991**, *2*, 499–501; E. Fontain, *Heteroatom Chem.*, **1994**, *5*, 61–65.

3.6
Cluster Growing Through Ionic Aggregation: Synthesis and Structural Principles of Main Group Metal–Nitrogen, Phosphorus and Arsenic Rich Clusters

Matthias Driess, Robert E. Mulvey and Matthias Westerhausen

3.6.1
Fundamental Aspects of Main Group Metal–Group 15 Element Clustering

Metal-amides, -phosphanides and -arsanides (pnictides) belong to one of the important classes of key reagents in organometallic synthesis and coordination chemistry. In particular, lithium and magnesium derivatives deserve specific attention as nucleophilic and strong basic reagents in organoelement synthesis [1]. Main group metal–group 15 element bonds with strongly electropositive metals such as alkali and alkaline-earth metals possess a large proportion of ionic character because of the tremendous differences in electronegativity which favor aggregation, that is, self association of cation–anion pairs (ionic clustering). For instance, monometallated amides, phosphanides and arsanides R_2EM (R = organo group; E = N, P, As; M = Li, Na, K, Rb, Cs) aggregate voluntarily due to the high E–M bonding polarity and not least because of the presence of lone-pair electrons at the group 15 element (N, P, As) adjacent to a coordinatively unsaturated metal center. This leads to two-dimensional molecular clusters with an ionic backbone wrapped in a lipophilic shell of organo substituents. The degree of aggregation n for $(R_2EM)_n$ compounds depends on the nature of the metal (ion size, partial charge, polarizability), steric demand of the substituents, and donor solvation of the metal atom. Molecular clustering with a relatively high degree of aggregation is promoted if the metal atom is presented with an imperfectly designed ligand or ligand set. Spherical small anions such as halides, when unaccompanied by other ligands, are useless partners in this regard as their perfect symmetrical shapes complement those of the M^+/M^{2+} cations, and the electrostatic attraction between them is consummated in the form of infinite three-dimensional or two-dimensional networks. Although metal–nitrogen, –phosphorus, and –arsenic bonding is predominantly electrostatic, organosubstituted group 15 element ligands are in steric terms anisotropic, and the degree of anisotropy varies depending on the identities of the functional group (e.g., amides, amidinides, P- and As-analogs, etc.) and attached organic substituents (e.g., R in R_2N^-). Polar metal cations, being strong Lewis acids, are rarely if at all monogamous and will therefore engage with as many anions (in solvent-free structures) or combination of

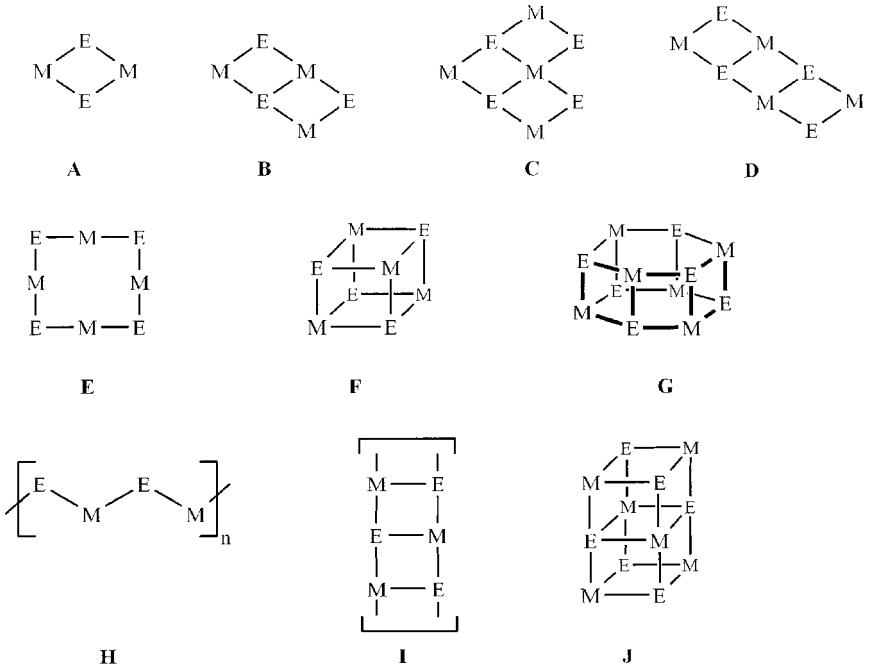

Scheme 3.6-1. Structural motifs of main group metal amides, phosphanides and arsanides (E = N, P, As).

anions and donor atoms (in solvated structures) as the steric environment of the system will allow. Ladder-like aggregation (two- and three-dimensional) is the major instrument used to achieve such coordinative saturation, as overall charge neutrality must be maintained (Scheme 3.6-1). By blocking off part of the metal's coordination sphere, anisotropic ligands make it more difficult to engineer a three-dimensional network: consequently, two- and one-dimensional polymeric, and oligomeric structures prevail more with these irregularly-shaped ligands. The most important structural motifs of two- and three-dimensional clusters of main group metal amides, phosphanides and arsanides are depicted in Scheme 3.6-1.

Lithium amides $[(R_2NLi)_n]$ represent the most studied and most utilized of all alkali metal organonitrogen compounds. The same is true for the phosphorus and arsenic homologs. Sterically demanding types of amides [most notably, lithium diisopropylamide (LDA), $Pr^i{}_2NLi$; lithium tetramethylpiperidide (LiTMP) $Me_2C(CH_2)_3C(Me)_2NLi$; lithium hexamethyldisilazide (LiHMDS), $(Me_3Si)_2NLi$] are often the reagents of choice for selective proton abstraction. However, such bulkiness generally inhibits aggregation beyond that encountered in discrete $(NLi)_n$ rings, where commonly $n = 2$ (in solvates), 3 or 4 [2, 3].

Rings with smaller amido substituents can aggregate further, though their orientations above and below the $(NLi)_n$ ring plane normally deny cluster building ("ring-stacking": vertical, face-to-face association) but allow "ring-laddering" (lat-

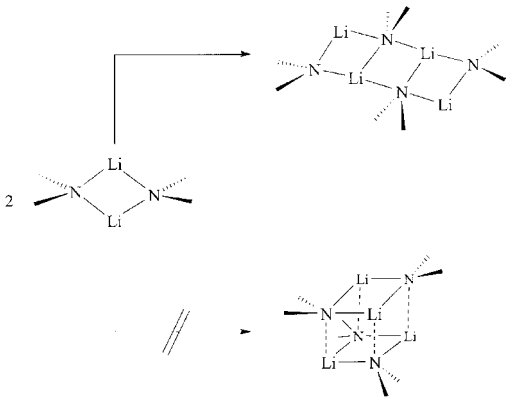

Scheme 3.6-2. Homo-aggregation of lithium amide rings showing the general preference for ladder, as opposed to stack, structures.

eral, edge-to-edge association) (Schemes 3.6-1 and 3.6-2). Conversely, other types of organonitrogen ligand have orientations more disposed towards ring-stacking: imido ($R^1R^2C{=}N^-$) ligands are exemplary examples (Scheme 3.6-3), so enabling the construction of cubane, prismatic, and other cluster types.

Alkali metal organonitrogen chemistry is a fertile field of research boasting an ever-burgeoning variety of structural types, including not just clusters in the traditional sense but also rings, ladders, chains, etc. Even to review clusters alone would be a substantial task and not feasible to complete in a chapter of this limited size. Therefore what follows in the next section is firstly an introduction to commonly observed cluster motifs in metal nitrogen compounds, chosen because they illus-

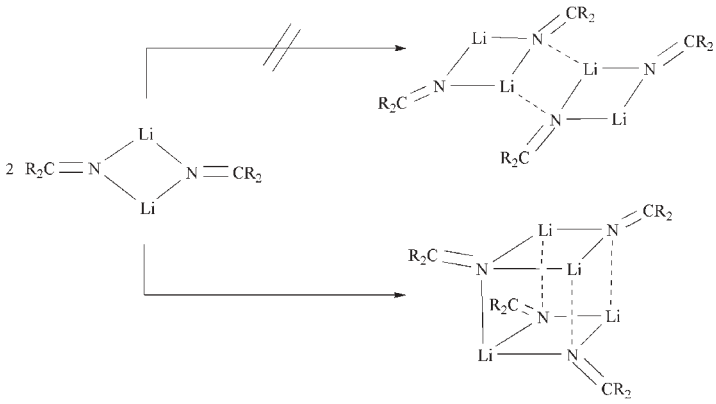

Scheme 3.6-3. Homo-aggregation of lithium ketimide rings showing the general preference for stack, as opposed to ladder, structures.

trate especially clearly the basic principles (ring-stacking in particular) that govern their construction. This section is deliberately skewed towards lithium examples, because of their pre-eminence amongst the alkali metals in terms of synthetic utility and structural diversity. A fundamentally different type of cluster is surveyed in Section 3.6.3. Templated about a central anion, these so-called "inverse crown" structures [4] owe their existence to the synergy of mixing together an alkali metal and magnesium (or zinc) in the same amido environment. Though still in its infancy, this area has already delivered exciting new chemistry which cannot be replicated by conventional homometallic amides.

3.6.2
Common Cluster Motifs in Group 1 Metal– and Group 2 Metal–Organonitrogen Chemistry

Mirroring the situation found in classical organolithium (C–Li) chemistry [5], cubane and prismatic arrangements are among the most common cluster types encountered in organonitrogen–lithium chemistry. The polyhedra are invariably distorted from the ideal due to a mismatch in ion (corner) size. Cubanes can exist solvent free as in the primary silylamidolithium tetramer $[\{(Bu^t)_2(Me)SiN(H)Li\}_4]$ **1** (Scheme 3.6-4) [6]. Dilithiated diamines can also adopt solventless cubane architectures as illustrated by the *N*,*N*′-di-*tert*-butylethylenediamine derivative $[\{Bu^tN(Li)CH_2CH_2N(Li)\text{-}Bu^t\}_2]$ **2** (Scheme 3.6-4) [7]. More often the metal corners of cubanes, if sterically accessible, welcome additional stabilization by solvent molecules. Pyridine fulfills this role in the tetrameric ketimide $[(Ph_2C{=}NLi{\cdot}PYR)_4]$ **3** (Scheme 3.6-4) [3]. The novel sodium ketimide.ketimine cubane $[(Bu^t{}_2C{=}NNa)_4{\cdot}(HN{=}C\text{-}Bu^t{}_2)_2]$ **4** [3] presents an intermediate situation in possessing two solvated and two unsolvated sodium corners. A similar hemi-solvated cubane is found for the phosphoraneiminato potassium complex $[(Cy_3P{=}NK)_4{\cdot}(O{=}PCy_3)_2]$ **5** (Scheme 3.6-4) [8]. No disruption to the cubane architecture is observed on removal of its phosphane oxide coligands, which is indicative of the diminishing importance of metal–Lewis base contacts on descending group 1. It is therefore not surprising that with the heavier alkali metal caesium both tetra-solvated $(Cy_3P{=}NCs{\cdot}O{=}PCy_3)_4]$ [8] and non-solvated $[(Ph_3P{=}NCs)_4]$ [9] analogs also display cubane structures.

Anionic ligands with ancillary Lewis base functionality can effect corner ligation without the aid of external solvent molecules. Tertiary amino groups commonly serve this purpose as exemplified by the dimethylamino-containing sidearms in the lithium ketimide cubane $[\{Me_2NCH_2CH_2N(Me)C(Ph){=}NLi\}_4]$ **6** (Scheme 3.6-4) [10]. Bromide ligands occupy the *exo* coordination site on the metal corner in the phosphoraneiminato–magnesium tetramer $[(Me_3P{=}NMgBr)_4]$ **7** [11], a rare example of an organonitrogen–magnesium cubane. The higher valency of the group 2 metal, which permits this second anionic ligation, usually mitigates against cluster formation in favor of dimeric ring motifs (either discrete or joined together in the form of a spiral chain). Introducing the powerful Lewis base HMPA

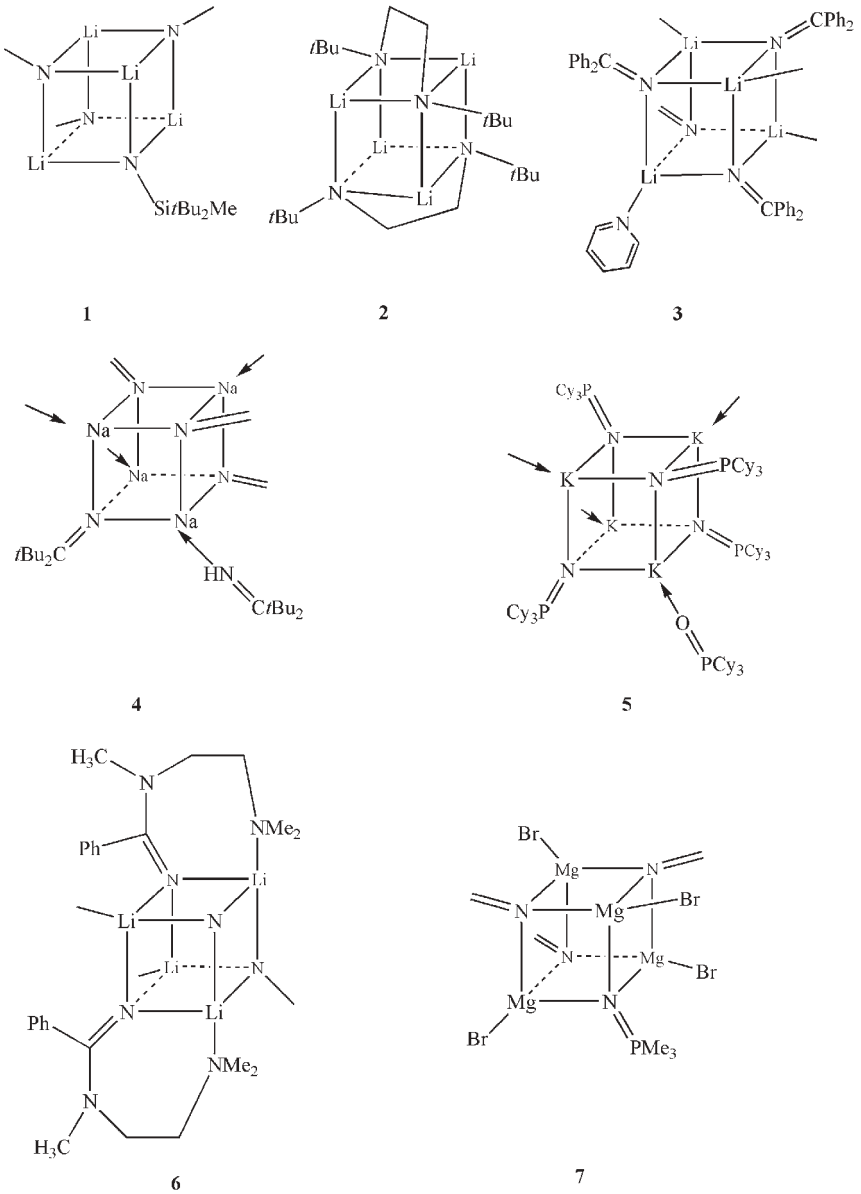

Scheme 3.6-4. Cluster structures of **1**–**7**.

(hexamethylphosphoramide) to a related phosphoraneiminatomagnesium halide yields such a discrete dimer with an $(MgN)_2$ ring in $[(Ph_3P{=}NMgCl{\cdot}HMPA)_2]$ [12].

The concept of ring-stacking emerged from the detailed analysis of a series of homeotypic lithium ketimide hexamers $[(R^1R^2C{=}NLi)_6]$ **8** (e.g., where $R^1 = Bu^t$;

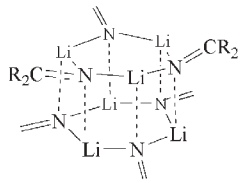

8

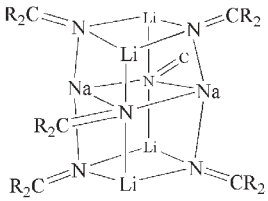

9

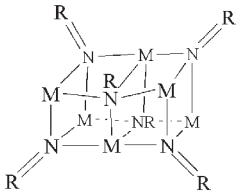

10: R = PPh_3

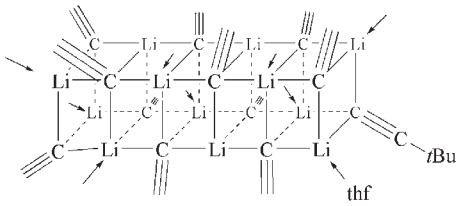

11

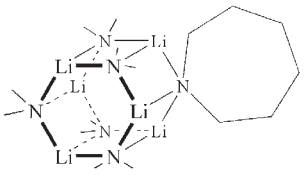

12

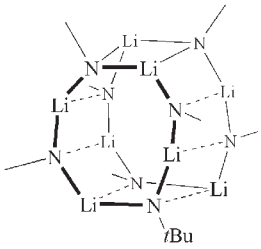

13

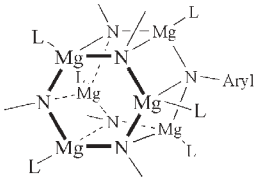

14

Scheme 3.6-5. Cluster structures of **8**–**14**.

R^2 = Ph; $R^1 = R^2 = Bu^t$) (Scheme 3.6-5) [2, 3]. Unlike the aforementioned ketimides, the latter are devoid of solvent ligands or internal complexation and therefore without competition from donor–acceptor bonds, a higher aggregation can be reached. These hexamers can be regarded as two-tier stacks, where the number of attractive $N^{\delta-}$–$Li^{\delta+}$ interactions is maximized by overlapping one $(NLi)_3$ ring on top of another in a face-to-face manner so that N centers of one ring eclipse the Li centers of the other. A basic criterion for stacking is that the organic substituents R, or more precisely their α-atoms, sit approximately in the same plane as the

$(NLi)_n$ ring to which they are attached. In theory there is no upper limit to the number of rings that might populate a stack structure. Indeed, the unsubstituted diphenyl lithium ketimide $[(Ph_2C{=}NLi)_n]$ is thought to be a polymeric stack of formula $[\{(Ph_2C{=}NLi)_3\}_\infty]$ [3], though this still requires appropriate substantiation. However, since substituents ideally must be planar or near-planar along their entire lengths to meet the steric requirements for stacking (to minimize van der Waals repulsions between substituents), most stack structures are limited to two tiers, as in the lithium ketimide hexamers. Specific circumstances may permit the construction of higher-oligomeric stacks. Fixing larger Na^+ cations into a central $(NNa)_2$ ring allows ring-stacking to operate on either side of the central ring, as demonstrated in the three-tier stack of the bimetallic ketimide $[\{Ph(Bu^t)C{=}N\}_6Li_4Na_2]$ **9** (Scheme 3.6-5) [13]. With even larger alkali metal cornerstones, the erection of related (but homometallic) three-tier stacks is made possible as inter-tier repulsions between substituents decrease sequentially as a function of increasing cation size. This point is illustrated by the phosphoraneiminato-homologs $[(Ph_3P{=}NM)_6]$ **10** (where M = K or Rb) [14]: their three-tier stack structures might alternatively be described as face-sharing double cubanes (Scheme 3.6-5). Substituents with linear bodies and tripodal-shaped tails capable of rotating to avoid interlocking with adjacent substituents should be excellent stacking ligands. Monosubstituted azo $(RN{=}N^-)$ ligands may come into this category, but for the exemplar in this connection one must look to organolithium chemistry and the alkynyl ligands in the sextuple-tier stack of dodecahedral $[(Bu^tC{\equiv}CLi)_{12}{\cdot}4THF]$ **11** (Scheme 3.6-5) [15]. As alluded to earlier, the spatial projections of R substituents in lithium amide $[(R^1R^2NLi)_n]$ structures, above and below the $(NLi)_n$ ring planes, would lead to a destabilization in a ring-stacking situation due to increased steric crowding. Self-association of lithium amide rings therefore generally proceeds through laddering not stacking. If, however, the lateral fusion of $(NLi)_n$ rings occurs exclusively in a cisoid fashion, then oligomeric ladder ends will eventually meet to form a closed cycle that masquerades as a stack. Accompanied by an increase in coordination number for both $N^{\delta-}$ and $Li^{\delta+}$ centers (compared with that in a discrete ring), this cyclical laddering action is most likely with sterically accessible amido N atoms, where, for example, both R groups are tied together and constrained within an unsubstituted cyclic amine or where one R group is a hydrogen atom. The former scenario is manifested in lithio hexamethyleneimine $[\{H_2C(CH_2)_5NLi\}_6]$ **12** [1], a cyclic ladder of six N–Li rungs [appearing like a stack of two $(NLi)_3$ rings] and the latter in the primary amide $[\{Bu^tN(H)Li\}_8]$ **13** [13], a cyclic ladder of eight N–Li rungs [appearing like a stack of two $(NLi)_4$ rings] (Scheme 3.6-5).

Organomagnesium chemistry may be the domain of ring and infinite chain aggregates, but rebellious clusters can still be assembled by choosing anionic partners of appropriate design and charge. Employing dianionic organonitrogen ligands circumvents the aforementioned numerical valency distinction and turns Mg^{2+} into a quasi alkali metal M^+ in the sense that the cation:anion stoichiometry (1:1) matches that found in monoanionic compounds of group 1 metals. This enhances significantly the opportunity for cluster growth. Resonance-stabilized geminal dianions promote the growth of hexagonal prismatic [two-tier stacks of

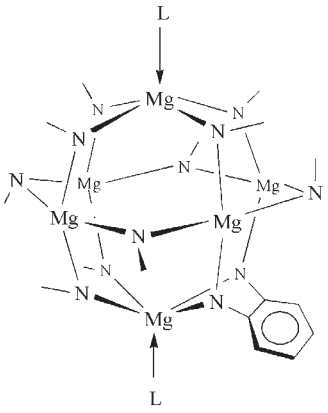

15

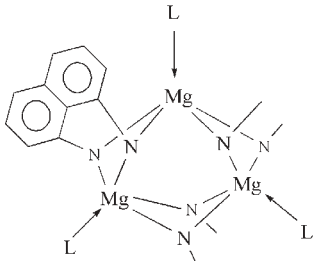

16

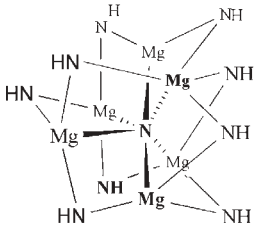

17

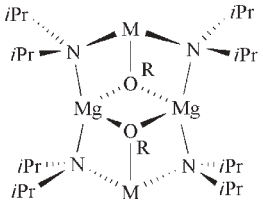

18

Scheme 3.6-6. Molecular structures of **15**–**18**.

$(MgN)_3$ rings] clusters in a series of aromatic imides $[(ArNMg{\cdot}L)_6]$ **14** (where Ar = Ph, L = HMPA or THF; Ar = 1-naphthyl, L = THF) (Scheme 3.6-5) [16]. Separating the two negative charges in diamine derivatives leads to more unusual architectures in the *o*-phenylenediamide hexamer $[\{[o\text{-}C_6H_4(NH)_2]Mg{\cdot}THF\}_6]$ **15** [17] or the 1,8-diamidonaphthalene trimer $[\{[1,8\text{-}C_{10}H_6(NH)_2]Mg{\cdot}HMPA\}_3]$ **16** [18], where an Mg_6 octahedron or Mg_3 triangle interpenetrates an N_{12} cuboctahedron or N_6 trigonal prism, respectively (Scheme 3.6-6).

3.6.3
Templation and Inverse Crown Chemistry

Having acquired the ground rules of alkali metal organonitrogen compound aggregation as outlined in the previous section, how does one begin to generate new architectures and, as structure is intimately linked to reactivity, new chemistry, i.e., how can we synthesize new metal–organonitrogen compounds which do not con-

form to these general structural patterns? One obvious approach is to build a structure around a templating seed. Growth emanating from such a ''foreign body'' may disrupt the normal directional orders of common aggregative pathways such as ring-stacking or ring-laddering. An early example from N–Mg chemistry is the nonameric *tert*-butylamide $[\{Bu^tN(H)\}_9(N)Mg_6]$ **17** [19] with its Mg_6 trigonal prism grown around a nitrido seed. If seedless, the bis-amide would be expected to follow the infinite spiral-chain aggregation well known in organomagnesium chemistry [20]. The unplanned nitride formation here from magnesium metal and *tert*-butylamine is presumably a side effect of the harsh reaction conditions employed (high temperature and pressure). This is often the case that templating seeds have not been deliberately planted but materialize fortuitously in products due to unforeseen reactions.

A second approach to developing novel structures lies within heterometallic chemistry. For decades synthetic chemists have benefited from the special deprotonating properties of mixed-metal (commonly lithium–potassium) alkide–alkoxide ''superbases'' [21]. The origin of this superbasicity, at least in part, must stem from the structural reorganization caused by the introduction (co-complexation) of a larger, more polarizable alkali metal (and its accompanying alkoxide ligand) into the molecular environment of a lithium alkylide. However, determining the crystal structure of a true experimentally-utilized (as opposed to a model) superbase, which would shed invaluable light on the black art of superbasicity, remains a ''holy grail'', though recently an illuminating structure of a related amido–alkoxo superbase, $[\{Bu^tN(H)\}_4(Bu^tO)_4Li_4K_4\cdot(C_6H_6)_3]$, has been unveiled [22]. If, rather than sharing two alkali metals, the ligand set is tempted by a mixture of an alkali metal and magnesium which offers fundamental differences in charge, electronegativity, valency, etc., then the effect on structure could be more dramatic. Both of these approaches are intertwined in the developing phenomenon of ''inverse crown'' chemistry. The name derives from the inverse topological relationship between conventional crown ether complexes and the first members of this heterobimetallic amide family (Figure 3.6-1): Lewis acidic metal sites and Lewis basic oxygen sites have been mutually interchanged. Displacements of this

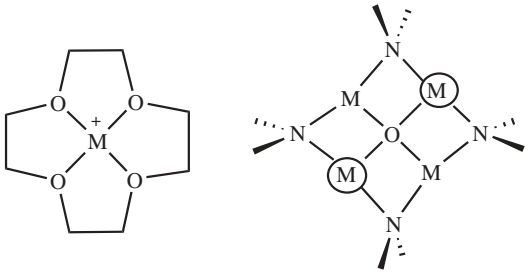

Fig. 3.6-1. Topological relationship between conventional crown ether complexes and their inverse counterparts. M denotes an alkali metal; circled M denotes Mg or Zn.

Tab. 3.6-1. Compositions of inverse crown ethers $[(M^1)_2(M^2)_2(\text{amide})_4(\text{core})]$.

Entry	*Group 1* M^1	*Group 2/12* M^2	*Amide*	*Core*[a]
(i)	Li	Mg	HMDS	O^{2-}/O_2^{2-}
(ii)	Li	Mg	TMP	O^{2-}
(iii)	Na	Mg	TMP	O^{2-}
(iv)	Na	Mg	HMDS	O^{2-}/O_2^{2-}
(v)	K	Mg	HMDS	O_2^{2-}
(vi)	Na	Zn	HMDS	O^{2-}
(vii)	K	Zn	HMDS	O^{2-}/O_2^{2-}
(viii)	Li	Mg	DPA	2*n*-OctO^-
(ix)	Na	Mg	DPA	2*n*-BuO^-
(x)	Na	Mg	DPA	2*n*-OctO^-
(xi)[b]	Na	Mg	TMP	6O
(xii)[b]	Na	Mg	DPA	6O

[a] O^{2-}/O_2^{2-} indicates a mixture of anions within the bulk crystal lattice, but not within individual molecules. [b] These compounds do not conform to the general formula for octagonal ring structures, but instead are clusters; in addition, each Na is solvated by THF.

ilk have been recognized elsewhere, most notably in mercuracarborand anti-crowns [23] and in a zinc oxime-based inverse metallacrown [24].

The first category of inverse crowns [Table 3.6-1, entries (i)–(vii)] contain octagonal rings of alternating nitrogen and metal atoms, with the latter atoms being alternately an alkali metal and magnesium [25]. Formally templating seeds, O^{2-} or O_2^{2-} anions fill their cores, though the overall compositions could be alternatively viewed as host–guest macrocycles. Permutational changes in the alkali metal (Li, Na or K), the divalent metal (Mg or Zn) or the amide (HMDS or TMP) do not alter the atom connectivities within these two-dimensional inverse crown ''ethers'', a testimony to the inherent stability of this ionic motif. Pivotal to their synthesis [Eqs. (1) and (2)] is the oxygen-scavenging ability of the synergic bulky amide mixture, whereby trace amounts of moisture (or possibly oxygen) are seized upon, attacked, and precipitated as these kinetic, oxygen-poor products (pure metal-oxide or -hydroxide products may have been expected from thermodynamics).

Utilizing diisopropylamine as the amide source, the reaction has proved extendable to straight-chain alcohols [Eq. (3)] to afford a series of composite alkali metal–magnesium–alkoxide–diisopropylamides [Table 3.6-1, entries (viii)–(x)] [26]. Lopsided (μ_3) face-capping of the top and bottom of the octagonal $(MNMgN)_2$ rings by alkoxo O atoms gives these structures (**18**) a more three-dimensional cluster appearance than their square-planar oxide counterparts. Synergic amide mixtures can also extrude O^{2-} from cleavage of THF to yield S_6-symmetrical hexagonal prismatic [two-tier stacks of $(MgO)_3$ rings] clusters with N–Na appendages [Figure 3.6-2: Table 3.6-1, entries (xi)–(xii)] [27]. The hexameric cores of these ''super'' inverse crown ethers are isostructural and isoelectronic with imides or phosphandiides such as $[(PhNMg{\cdot}THF)_6]$ [16] or $[\{(Bu^t{}_3Si)PMg\}_6]$ [28].

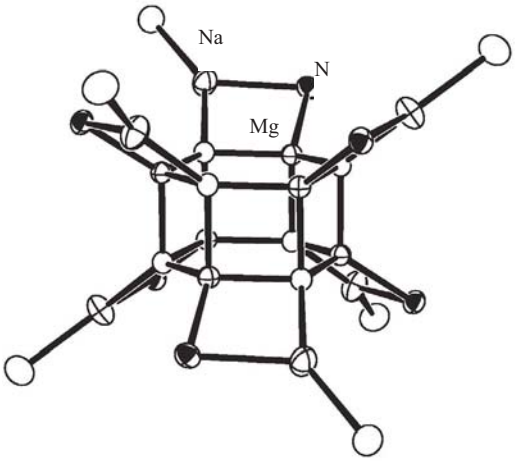

Fig. 3.6-2. Inorganic cluster core of super inverse crown ethers of general formula [{NaMg(amide)O(THF)}$_6$], where amide = TMP (2,2,6,6-tetramethylpiperidinide) or DPA (diisopropylamide).

$$n\text{BuM} + n,s\text{-Bu}_2\text{Mg} + 3\ \text{amine} \xrightarrow[-z\ \text{BuH}]{\text{trace of } H_2O/O} z[M_2Mg_2(\text{amide})_4(O_2)_xO_y] \quad (1)$$

$$\text{MHMDS} + \text{Zn(HMDS)}_2 \xrightarrow{\text{trace of } H_2O/O_2} [M_2Zn_2(\text{HMDS})_4(O_2)_xO_y] \quad (2)$$

$$n\text{BuM} + n,s\text{-Bu}_2\text{Mg} \xrightarrow[\substack{-i\text{Pr}_2\text{NH}\\ -3\ \text{BuH}}]{\substack{3\ i\text{Pr}_2\text{NH}\\ n\text{ROH}}} 0.5[M_2Mg_2(i\text{Pr}_2\text{N})_4(n\text{RO})_2] \quad (3)$$

The synergic amide effect has made its most significant impact to date in the arena of arene and metallocene metallation. For example, neither NaTMP nor Mg(TMP)$_2$ can unilaterally metallate benzene under mild conditions, but mixed together they can dimetallate it regioselectively (in the 1,4-positions) [4]. In the resulting complex [Figure 3.6-3: Table 3.6-1 entry (i)] a 12-membered polymetallic $(\text{NNaNNaNMg})_2^{2+}$ ring locks the two-fold deprotonated benzenediide into its central cavity through a combination of Mg–C σ bonds and Na–C π bonds. Toluene can be similarly transformed into an encapsulated 2,5-diide derivative [Table 3.6-2, entry (ii)]: here aromatic as opposed to alkyl deprotonation implies the synergism operates kinetically (or through a template) and not thermodynamically [4].

A spectacular ring expansion takes place on substituting sodium by potassium in these reactions [4]. Twentyfour-membered hexapotassium–hexamagnesium amide rings act as polymetallic hosts to six monodeprotonated arene anions in the products [Figure 3.6-4; Table 3.6-2 entries (iii)–(iv)]. Again the trapped arene ligands receive dual (σ and π) stabilization from the Mg and K atoms, respectively. The most remarkable demonstration yet of the deprotonating power of a synergic amide is reserved for a metallocene: ferrocene succumbs readily to losing four protons regioselectively, to leave an unprecedented 1,1′,3,3′-tetrayl residue which

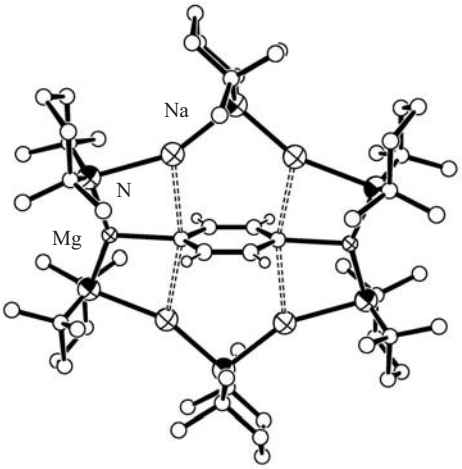

Fig. 3.6-3. Molecular structure of the super-base cluster $[Na_4Mg_2(TMP)_6(C_6H_4)]$.

is encapsulated by a 16-membered tetrasodium–tetramagnesium diisopropylamide ring [Eq. (4); Figure 3.6-5; Table 3.6-2 entry (v)] [29]. Conventional homometallic (non-synergic) bases such as Bu^nLi/TMEDA can generally only strip down ferrocene to its 1,1′-diyl form, so the promise of the synergic amide as a potent regioselective deprotonating agent is strikingly obvious.

$$Fe(C_5H_5)_2 \xrightarrow[-C_4H_{10}]{4\ BuNa/4\ Bu_2Mg/12\ iPr_2NH} [Na_4Mg_4(iPr_2N)_8\{Fe(C_5H_3)_2\}] \quad (4)$$

With understanding and rationalization of regular metal–organonitrogen structural chemistry at a well advanced level, the future prospects for this area could lie in novel multidimensional concepts, such as inverse crowns and synergic chemistry in general. These topics transcend the traditional boundaries of main group, transition metal, organometallic and organic chemistries, and in modern parlance, are perhaps best regarded as supramolecular [30]. Thus their study could lead to several promising avenues of research.

Tab. 3.6-2. Compositions of inverse crowns.[a)]

Entry	*Group 1*	*Group 2*	*Amide*	*Core*	*Host ring size*
(i)	4 Na	2 Mg	6 TMP	$C_6H_3(CH_3)^{2-}$	12
(ii)	4 Na	2 Mg	6 TMP	$C_6H_4{}^{2-}$	12
(iii)	6 K	6 Mg	12 TMP	6 $C_6H_5{}^-$	24
(iv)	6 K	6 Mg	12 TMP	6 $C_6H_4(CH_3)^-$	24
(v)	4 Na	4 Mg	8 DPA	$Fe(C_5H_3)_2{}^{4-}$	16

[a)] The "ether" designation is dropped here because these inverse crowns do not contain any oxygen-based anions.

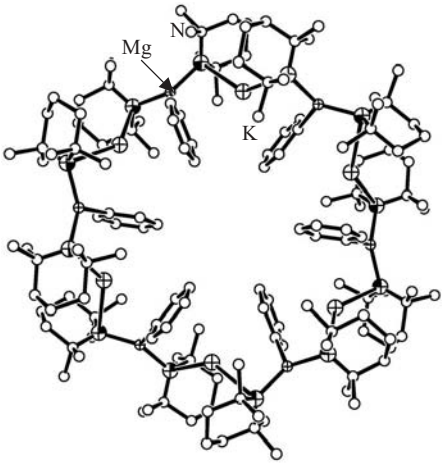

Fig. 3.6-4. Molecular structure of $[K_6Mg_6(TMP)_{12}(C_6H_5)_6]$; TMP = 2,2,6,6-tetramethylpiperidinide.

3.6.4
Alkali Metal–Phosphorus and Alkali Metal–Arsenic Clusters

3.6.4.1
Introduction

Over the past few years, a large number of novel and fascinating classes of metalated phosphanes and arsanes with group 1, 2, 3 and 4 metals have been developed. The purpose of this survey is to present the main structural features thereof.

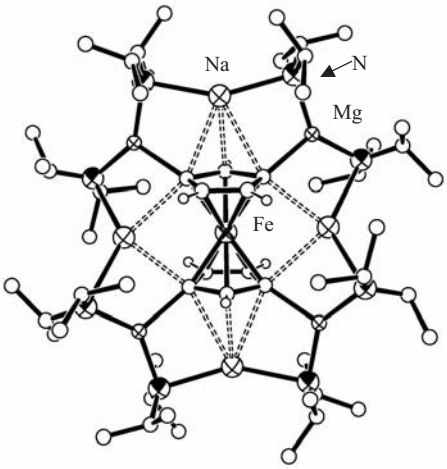

Fig. 3.6-5. Molecular structure of the heterometal cluster $[Na_4Mg_4(Pr^i{}_2N)_8\{Fe(C_5H_3)_2\}]$.

Phosphanide and arsanide clusters of the alkali metals in particular regained a high level of interest in the past decade because they represent valuable reagents for nucleophilic transfer of organophosphorus and organoarsenic building blocks. Since the hydrogen atoms of the E–H moieties (E = P, As) in primary and secondary phosphanes and arsanes are more acidic than the N–H functions in their amine homologs, metal phosphanides and arsanides are easily accessible by Bronsted acid–base reaction with metal alkylides or metal amides. Furthermore, this implied that dimetalation of primary phosphanes and arsanes succeeds more readily than for the respective primary amines. In line with this, great efforts were made to synthesize molecular dimetalated phosphandiide and arsandiide clusters. The diagonal relationship between carbon and phosphorus implies more chemical similarities of phosphanides with carbanions (alkanides) [31, 32] than with amides, although most of the structural features for metal phosphanides and amides are practically identical. Therefore, structure–reactivity relationships for nucleophilic phosphorus transfer reagents which differ from those seen in amide chemistry are of the main interest in this area. Most common examples are the phosphanide transfer to other metals (metathesis reactions), Lewis acid–base interactions (addition reactions), and transformations of the phosphanide ligands to unsaturated compounds with phosphorus–main group element multiple bonds (e.g., phosphaalkene and -alkyne synthesis via a Pederson hetero-olefination reaction). Some selected new developments in the structural chemistry of monometalated phosphanes and arsanes are discussed in the next section.

In contrast to the knowledge on monometalated phosphanides and arsanides, the state of metal-rich polyanionic phosphorus and arsenic systems is still in its infancy. For example, structural insight into the chemistry of molecular main-group dimetalated primary phosphanes (phosphandiides) and arsanes (arsandiides) was not developed until 1996, when the first structures of dilithium derivatives of silylphosphanes and silylarsanes were reported [32, 33]. One of the most striking structural features of dimetalated phosphanes and arsanes with M = Li, Na is that they can form globular, multiple-shell clusters which easily incorporate one M_2O molecule as a cluster seed in their voids. This and related structural aspects are also summarized in Section 3.6.4.2, while the following Section 3.6.5 is devoted to recent progress in metal–phosphorus and –arsenic cluster chemistry with group 2 metals and tin(+2).

3.6.4.2
Mono- and Dimetalated Phosphane and Arsane Clusters

Considering the importance of alkali metal phosphanides it is not surprising that numerous review articles have dealt with this subject [34–36]. The solid state and solution structures vary from dimers with central M_2P_2 cycles to larger rings and from chain to ladder structures as described for the lithium amides (see Sections 3.6.1 and 3.6.2). Cage compounds in the field of lithium phosphanides are unusual

and only a few examples exist, whereas different structural motifs are realized within the phosphanides and phosphanediides of the heavier alkali and alkaline-earth metals.

Oxygen and moisture has to be excluded carefully during the preparation procedures to avoid oxygen-centered cages. Then unusual metal deficient phosphanediides of lithium of the type $[(Li_2PR)_n(PR)_m]$ with $Li_{2n}P_{(n+m)}$ cages are isolated. Investigations of phosphanides of the heavier alkali metals are far less common [37].

The interconnection of two phosphanide substituents by sterically demanding RR′Si groups allows the preparation of cage compounds [38]. The two-fold lithiation of bis(phosphanyl)(alkyl)arylsilane and the dimerization of this bis(phosphanido)silane leads to the formation of **19** with a strongly distorted Li_4P_4 heterocubane structure according to Eq. (5).

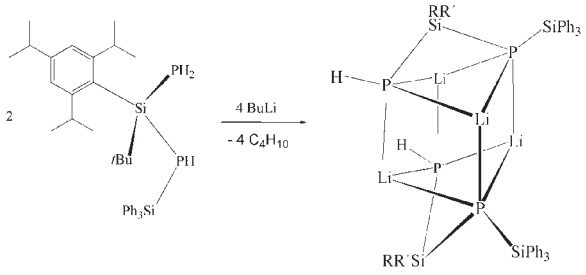

(5)

19: R = *t*Bu, R' = 2,4,6-*i*Pr$_3$C$_6$H$_2$

Furthermore, two of these cages can be interconnected by a sterically undemanding Li_2Cl_2 moiety to give **20** (Figure 3.6-6), thus forming four heterocubane moieties with common faces by the stacking of common motifs, as is also found for the lithium amides. The phosphanides of the heavier alkali metals also often crystallize with ladder motifs [39, 40]. In contrast to these favored structures, the sodiation of a tris(triisopropylsilylphosphanyl)silane gives the dimer $[(toluene)_2Na^+]_2[\{EtSi(PSiPr^i_3)_3Na_2\}^-]_2$ **21** with a hexagonal $Na_4Si_2P_6$ prism (Figure 3.6-6) [38]. The metalation of $HP(SiPr^i_3)Si(F)R_2$ with sodium bis(trimethylsilyl)amide yields the corresponding sodium phosphanide **22** [41]. Surprisingly, the reduction of the latter sodium phosphanide **22** with sodium in the presence of styrene gives the tetrasodium bis(phosphanide) **23** with a central planar subvalent Na_4^{2+} moiety according to Scheme 3.6-7 [41].

Whereas stacks of two $(RbP)_2$ cycles are found for tetrameric rubidium 2,6-dimesitylphenylphosphanide $[RbP(H)DMP]_4$ **24** to give an Rb_4P_4 heterocubane structure, an interesting and novel cage is found for a trimeric cesium 2,6-dimesitylphenylphosphanide of the type $Cs^+[Cs_2\{P(H)DMP\}_3^-]$ **25** with a trigonal Cs_2P_3 bipyramid [42], the metal atoms being in apical positions. This structural type is stabilized by additional Lewis acid/base attraction between the mesityl groups and the cesium atoms. In contrast, the Cs-analog of the (fluorosilyl)phosphanide **22** crystallizes in a unusual polymeric chain structure with strong Cs–arene π

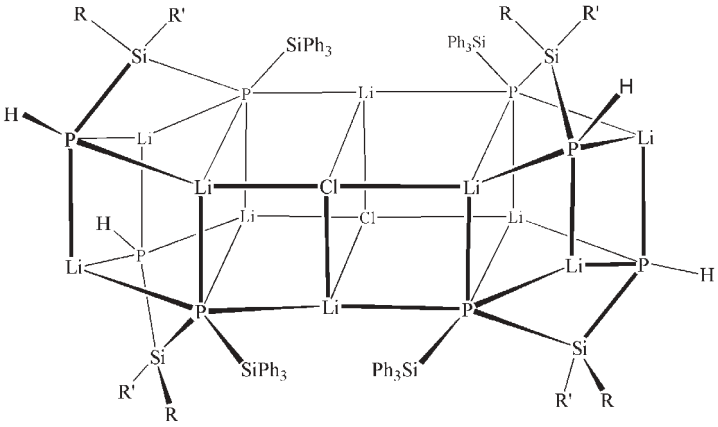

20: R = *t*Bu, R' = 2,4,6-*i*Pr$_3$C$_6$H$_2$

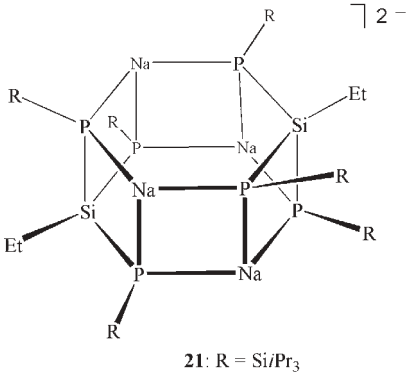

21: R = Si*i*Pr$_3$

Fig. 3.6-6. Molecular structures of the mixed lithium phosphanide–LiCl cluster **20** and the anionic cluster core in **21**.

interactions [40]. The cesiation of tri(*tert*-butyl)silylphosphane in the absence of Lewis bases yields tetrameric CsP(H)SiBu$^t_3$ with an eight-membered Cs_4P_4 cycle according to Scheme 3.6-8, which is doubly bridged by two CsN(SiMe$_3$)$_2$ molecules, giving a cage compound of formula [Cs$_6${P(H)SiBu$^t_3$}$_4${N(SiMe$_3$)$_2$}$_2$] **26**. From another point of view, the arrangement of the cesium atoms can be regarded as a greatly distorted octahedron. Two opposite planes are capped by bis(trimethylsilyl)amide groups, two other opposite planes are not capped at all. The remaining four planes are capped by the phosphanide ligands. Amide-free CsP(H)SiBu$^t_3$ **27** crystallizes from toluene as a tetramer with a Cs_4P_4 heterocubane fragment, an additional phosphane molecule is located between the cages giving a formula of [{(η^6-toluene)CsP(H)SiBu$^t_3$}$_4$·H$_2$PSiBu$^t_3$] [43].

The lithiation of both the acidic hydrogen atoms in (2,4,6-triisopropylphenyl)(2-

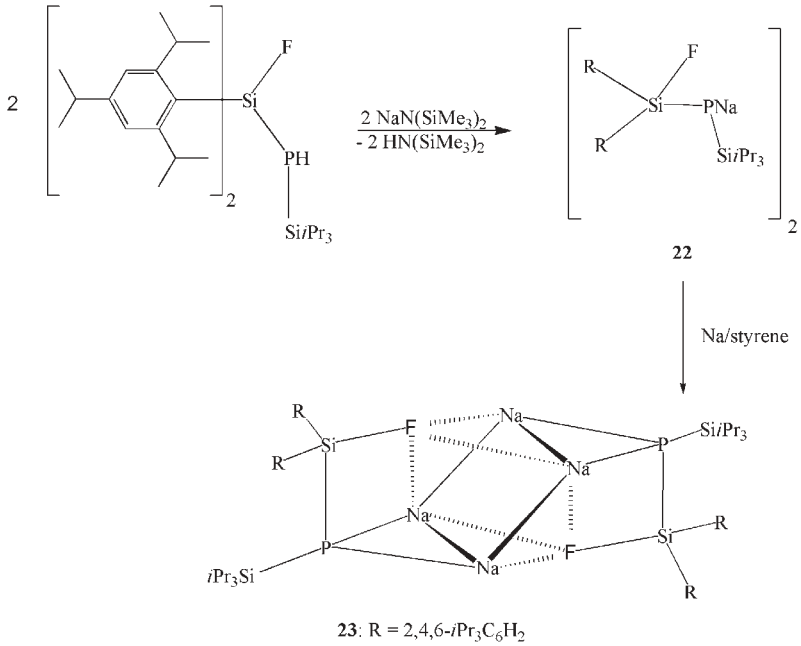

Scheme 3.6-7. Synthesis of the sodium (fluorosilyl)phosphanide clusters **22** and **23**.

hydroxycyclohexyl)phosphane yields the corresponding tetrameric dilithium salt **28** (Figure 3.6-7) [47], in which the lithium atoms form two trigonal prisms sharing a common rectangular face, while the phosphorus atoms bridge the trigonal planes, and the oxygen atoms are located above the square planes.

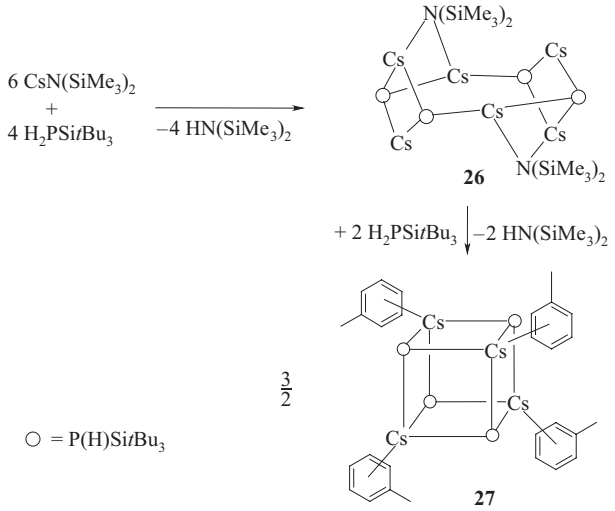

Scheme 3.6-8. Synthesis of the cesium phosphanide clusters **26** and **27**.

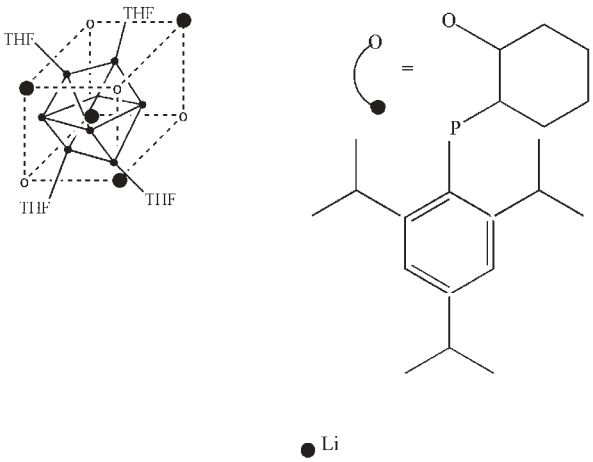

Fig. 3.6-7. Core structure of the lithium phosphanide cluster **28**. Small dark circles: lithium atoms, big dark circles: phosphorus atoms.

Whereas ring structures dominate amide and phosphanide chemistry, mainly spherical cages are found for doubly deprotonated phosphanes (phosphanediides) as well as for their heavier homologs. It has been shown that the degree of aggregation of permetallated primary phosphanes and arsanes depends on the steric demand of the organic groups around the phosphorus and arsenic atom. Thus, the dilithium diisopropyl(2,4,6-triisopropylphenyl)silylphosphandiide **29** is dimeric and consits of a distorted Li_4P_2 octahedron with the phosphorus atoms in a *trans* position (Figure 3.6-8) [44]. The structures of oligomeric $Li_2PSiBu^t_3$ remain as yet unknown, however, the hexameric disodium tri(*tert*-butyl)silylphosphandiide $[Na_2PSiBu^t_3 \cdot \frac{1}{3}THF]_6$ **30** contains a spherical $Na_{12}P_6$ cage [45]. The reaction of **30** with CuI gives $[Cu_2PSiBu^t_3]_6$ (**31**, Figure 3.6-9) where the copper atoms form a regular cuboctahedron with square Cu_4 planes capped by $PSiBu^t_3$ ligands. A larger dicopper phosphandiide cluster was isolated in the case of $[Cu_2PSiMe_2(CMe_2Pr^i)]_{12}$ **32**, the cage of which can also be deduced from a cuboctahedron (Figure 3.6-10) [46].

The lithiation of sodium triisopropylsilylphosphanide yields a solvent-separated complex best described as $(Li^+)_2 \cdot [(THF)_6Na^+]_2 \cdot [Na_{20}(PSiPr^i_3)_{12}]^{4-}$ **33** [43]. A similar structure is found for the bismuth analog of formula $[Na^+] \cdot [(THF)_4Na^+]_2 \cdot [(THF)_6Na^+] \cdot [Na_{20}(BiSiBu^t_3)_{12}]^{4-}$ **34** [48] with the THF-free sodium cation disordered in the void of the $Na_{20}Bi_{12}$-cluster. The tetraanions consist of a pentagondodecahedron of sodium atoms, the faces being capped by the phosphanediide and bismanediide substituents, respectively. The pnictogen atoms themselves form an icosahedral substructure (Figure 3.6-11).

In Table 3.6-3 the alkali metal phosphanediides and arsanediides are classified into three categories. The first type of $(M_2ER)_n$ clusters (E = P, As; R = triorganosilyl),

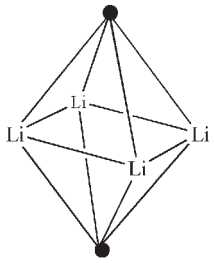

● = $PSi\mathit{i}Pr_2[C_6H_2\mathit{i}Pr_3]$ **(29)**

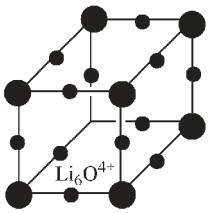

● = Li

● = $PSi\mathit{i}Pr_2(Mes)$ **(38)**

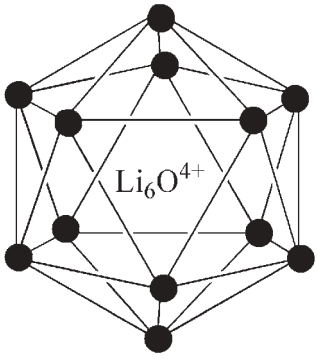

● = $ESiMe_2(CMe_2\mathit{i}Pr)$
Li above all faces
E=P **(39)**, As **(42)**

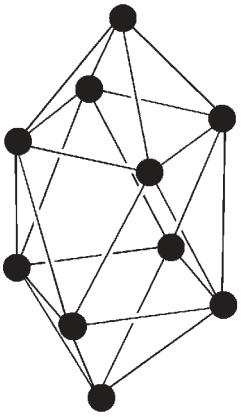

● = $PSi\mathit{i}Pr_3$ **(35)**
$AsSi\mathit{i}Pr_3$ **(36)**
Li above faces

Fig. 3.6-8. Polyhedral cluster frameworks in lithium phosphandiide chemistry. Compound **29** represents an electron-precise cluster, whereas **35** and **36** are electron-deficient, mixed-valent phosphorus and arsenic clusters with bridging lithium atoms. The clusters **38**, **39** and **42** are electron-precise and contain an Li_6O octahedron in their voids.

which could be isolated in reproducibly crystalline forms, contain one molecule M_2O (oxygen-centered mixed aggregates **38**, **39**, **42**; see Figures 3.6-8 and 3.6-12) [32]. The role of the M_2O molecule is to act as a template seed and M^+ acceptor. For example, the structures of the compounds **38** and **42** can be topologically described as ionogenic clusters which consist of three closed platonic shells. The E centers (E = P, As) in the dodecameric $(Li_2E)_{12}$ clusters (E = P, As) form a slightly distorted E_{12} icosahedron which is wrapped by a second shell (pentagondodecahedron) of 20 lithium atoms and the remaining four lithium centers are complexed by an encapsulated Li_2O molecule in the interior of the $[E_{12}Li_{20}]^{4-}$ double shell, leading to the formation of an $[Li_6O]^{4+}$ octahedral core (Figure 3.6-12).

The mixed arsanediide–iodide cluster **41** consists of an $As_{10}I_2$ icosahedron.

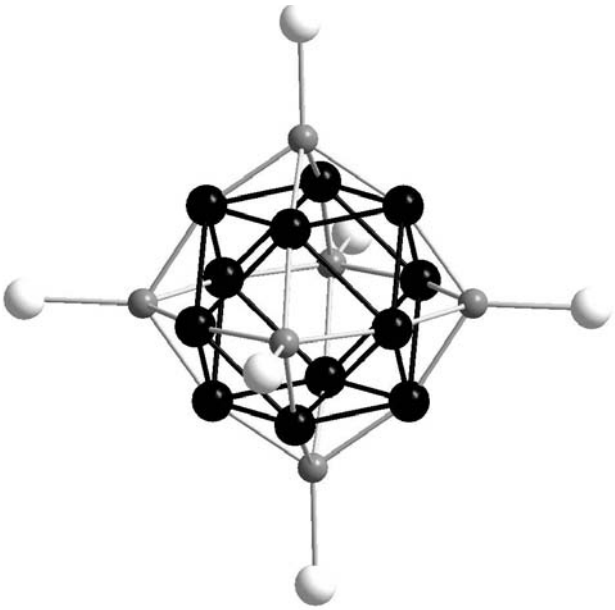

Fig. 3.6-9. Representation of the cluster core of $[Cu_2PSiBu^t_3]_6$ **31**. The black spheres (Cu atoms) form a cuboctahedron, the grey spheres (P atoms) an octahedron. The white spheres represent Si atoms.

Owing to the reduced charge as a consequence of the substitution of two RAs^{2-} fragments by two iodide anions an Li_4O^{2+} moiety is located in the center of the $As_{10}I_2$ icosahedron [32]. Because of the sensitivity of the phosphanediides and arsanediides towards moisture and the low content of oxygen within the cage, a careful exclusion of oxygen, moisture and metal hydroxides has to be maintained during the preparation in order to obtain oxygen-free clusters. In this case electron-deficient (mixed-valent) and oxygen-free cages are accessible as shown for **35** and **36** (Figure 3.6-8) [49] but, on the other hand, electron-precise and oxygen-free alkali metal phosphanediides are also known as summarized in Table 3.6-3. The structural principle for the oxygen-free systems is identical to that of the oxygen-centerd one: the pnictogen clusters adopt P_{10} **35** and As_{10} dicapped square antiprisms **36**, of which each of the 16 faces are capped by a lithium atom.

The metal to phosphorus (or arsenic) ratio varies between 1:1 (alkali metal phosphanides and arsanides) and 2:1 for bis(alkali metal) phosphanediides or arsanediides. In general, these compounds form pnictogen polyhedra with the faces being capped by monovalent metal atoms. For the alkaline-earth metal phosphorus cages, metal to phosphorus ratios between 1:2 for alkaline earth metal bis(phosphanides) and 1:1 for the phosphanediides of the divalent cations are possible.

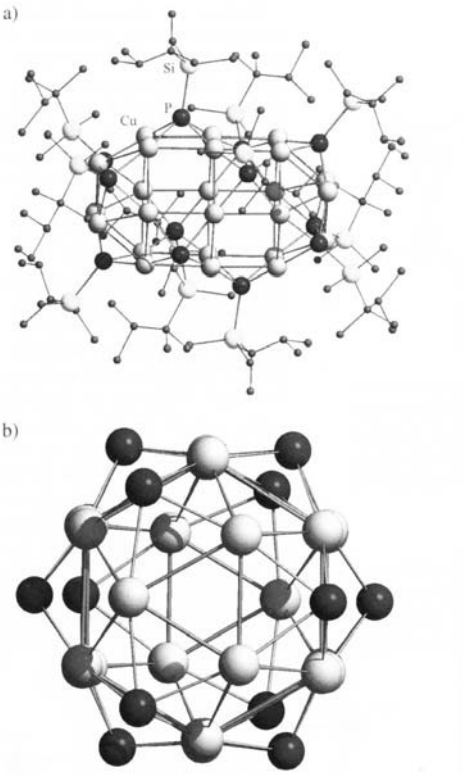

Fig. 3.6-10. (a) Molecular structure of $[Cu_2PSiMe_2(CMe_2Pr^i)]_{12}$ **32**. (b) Projection of the $Cu_{24}P_{12}$ core of **32** along the parallel Cu_3 and Cu_6 faces.

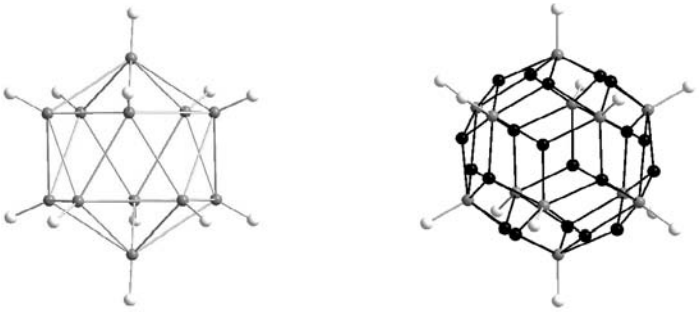

Fig. 3.6-11. Left: E_{12} icosahedron in **33** (E = P) and **34** (E = Bi). Right: Perspective drawing of the $[Na_{20}(ESiR_3)_{12}]^{4-}$ clusters in **33** and **34**. Na = black; E (P, Bi) = grey; Si = white.

Tab. 3.6-3. Overview of cage compounds of the type $[M_nO_m(REH)_x(RE)_y]$ of the monovalent atoms M (alkali metals and copper) and the pnictogen atoms E (P, As).

Comp.	*E*	*M*	*R*	*n*	*m*	*x*	*y*	*Ref.*
Electron-precise, oxygen-free								
29	P	Li	$SiPr^i_2(Pr^i_3C_6H_2)$	4	0	0	2	44
30	P	Na	$SiBu^t_3$	12	0	0	6	45
31	P	Cu	$SiBu^t_3$	12	0	0	6	45
32	P	Cu	$SiMe_2(CMe_2Pr^i)$	24	0	0	12	46
33	P	Na/Li	$SiPr^i_3$	22/2	0	0	12	43
34	Bi	Na	$SiBu^t_3$	24	0	0	12	48
Electron-deficient, oxygen-free								
35	P	Li	$SiPr^i_3$	16	0	0	10	49
36	As	Li	$SiPr^i_3$	16	0	0	10	49
Electron-precise, oxygen-centered								
37	P	Li	$SiMe_2(CMe_2Pr^i)$	20	1	6	6	49
38	P	Li	$SiPr^i_2(Mes)$	18	1	0	8	33
39	P	Li	$SiMe_2(CMe_2Pr^i)$	26	1	0	12	33
40	As	Li	$SiMe_2(CMe_2Pr^i)$	20	1	6	6	33
41	As	Li	$SiMe_2(CMe_2Pr^i)$	24	1	0	10 (+2 I)	32, 34
42	As	Li	$SiMe_2(CMe_2Pr^i)$	26	1	0	12	49
43	As	Na	$SiMe_2(CMe_2Pr^i)$	26	1	0	12	50

3.6.5
Alkaline-earth Metal– and Tin(+2)–Phosphorus and –Arsenic Clusters

In contrast to the lithium amides and phosphanides, dimeric alkaline-earth metal bis(phosphanides) of the heavier group 2 metals show bicyclic structures of the

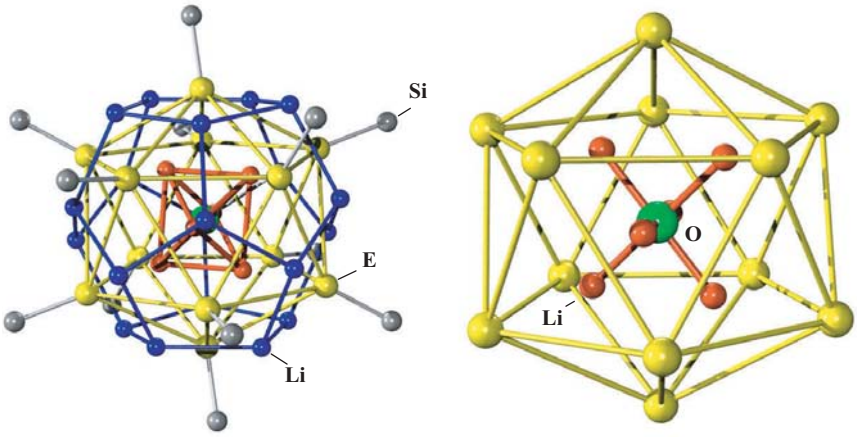

Fig. 3.6-12. Left: representation of the shell-like composition of **39** and **42**; right: connection of the $[Li_6O]^{4+}$ octahedron with the E centers (E = P, As).

general formula $[R_2P\text{-}M(\mu\text{-}PR_2)_3M]$, which are stabilized by additional neutral coligands such as THF or other ethers. This structural motif of a trigonal M_2P_3 bipyramid is very common within the phosphanides and phosphanediides of the heavy alkaline-earth metals as is shown later in this section. Homoleptic phosphanediides are only known for magnesium, whereas the compounds of the heavier group 2 metals always contain additional phosphanide ligands besides the phosphanediide substituents. In these molecules, the trigonal bipyramids are often interconnected via common faces. Starting from the hitherto unknown dimer $[MPR]_2$ all structures can be described by combining this structural moiety and the alkaline earth metal bis(phosphanides) $[M(PHR)_2]$, which are capping opposite square planes of a M_4P_4 cubane or a hexagonal M_6P_6 prism. Homoleptic alkaline-earth metal phosphanediides are available if tin(+2) atoms are incorporated into the cage compounds to give cubane structures of general formula $[M_nSn_{4-n}(PR)_4]$ with $n = 0, 1, 2$, and 3.

Alkaline-earth molecules MX_2 of the heavier alkaline earth metals show surprising and interesting structures [51] such as bent fluorides [52] and amides [53]. Dimeric molecules of the type $[MX_2]_2$ of the heavier alkaline-earth metals M tend to form polycyclic molecules (cages), such as for example the structures of the hydrides of strontium and barium (Table 3.6-4) [54]. Whereas monocyclic molecules of the type $HM(\mu\text{-}H)_2MH$ are the energy minimum structures for Mg and Ca, bicyclic structures with C_{3v} symmetry of the type $HM(\mu\text{-}H)_3M$ are calculated for Sr and Ba. The reason for these somewhat unexpected structures is a combination of the polarization of the heavy, soft metal dications by the hard anions (''reverse'' polarization) and a small but significant d-orbital participation at the metal atoms [54]. Neutral coligands such as THF should not alter the coordination geometries, but influence the bond lengths and angles [55].

In Table 3.6-4 the relative energies of coligand-free dimeric alkaline earth metal bis(phosphanides) are summarized [56, 57]. Whereas for Ca and Sr the bicyclic

Tab. 3.6-4. Relative energies obtained by *ab initio* SCF calculations of dimeric alkaline-earth metal dihydrides and bis(phosphanides) (kJ mol^{-1}).

Symmetry	*Structure*	*Mg*	*Ca*	*Sr*	*Ba*
M_2H_4					
D_{2h}	$H\text{-}M(\mu\text{-}H)_2M\text{-}H$[a]	0.0	0.0	8.4	41.0
C_{2h}	$H\text{-}M(\mu\text{-}H)_2M\text{-}H$[b]			8.4	22.2
C_{3v}	$H\text{-}M(\mu\text{-}H)_3M$	118.9	17.2	0.0	0.0
D_{4h}	$M(\mu\text{-}H)_4M$	513.7	159.5	103.0	52.8
$M_2(PH_2)_4$					
C_{2h}	$H_2P\text{-}M(\mu\text{-}PH_2)_2M\text{-}PH_2$	0.0	51.6	41.3	60.0
C_1	$H_2P\text{-}M(\mu\text{-}PH_2)_3M$	27.9	0.0	0.0	8.0
D_{4h}	$M(\mu\text{-}PH_2)_4M$	212.3	44.2	17.9	0.0

[a] Molecules contain metal atoms in a strictly planar environment.
[b] Molecules contain pyramidal coordinated metal centers.

derivatives of the type $H_2P\text{-}M(\mu\text{-}PH_2)_3M$ with C_1 symmetry are the energy minimum structures [58], for dimeric barium bis(phosphanide) even the tricyclic molecule $Ba(\mu\text{-}PH_2)_4Ba$ with a D_{4h} symmetry has to be taken into account.

The calculations predict that magnesium bis(phosphanide) should be monocyclic with a C_{2h} symmetric Mg_2P_2 cycle. Even with the sterically demanding bis(trimethylsilyl)phosphanide substituents a trimer with a structure of the type $R_2P\text{-}Mg(\mu\text{-}PR_2)_2Mg(\mu\text{-}PR_2)_2MgPR_2$ (**44**, R = $SiMe_3$) is observed in the solid state [59]. In solution or with different alkyl substituents at the silicon atoms, monocyclic dimers are observed, however, polycyclic dimeric phosphanides of magnesium are still unknown. The metalation of primary and secondary trialkylsilyl substituted phosphanes and arsanes with $M[N(SiMe_3)_2]_2$ (M = Ca, Sr, Ba) yields bicyclic dimeric phosphanides and arsanides of the type $RR'E\text{-}M(\mu\text{-}ERR')_3M$ with E = P and As as shown in Scheme 3.6-9, and the metal centers are further stabilized by neutral coligands such as THF, DME or others. In toluene or ether solutions dynamic processes lead to an exchange reaction between the terminal and bridging phosphanide substituents. For the bicyclic dimeric alkaline-earth metal bis(phosphanides) the central trigonal M_2P_3 bipyramids are characteristic structural elements. In solution the cations are shielded by solvent molecules and these mainly ionic compounds are possibly best described as $[M(L)_n]^{2+}$ $[M(PRR')_4]^{2-}$, which explains the fast exchange between terminal and bridging phosphanide substituents [60]. The steric enhancement of the trialkylsilyl substituents leads to monocyclic dimers with two terminal and two bridging phosphanide ligands as observed for $R_2P\text{-}Ba(\mu\text{-}PR_2)_2Ba\text{-}PR_2$ with R = $SiMe_2Pr^i$ [57]. Similar findings have also already been published for sterically crowded barium bis(arsanides) [61].

An equilibrium is observed between the solvated monomeric $[M\{P(H)SiR_3\}_2]$ molecules and the solvated dimeric species $[R_3Si(H)PM\{\mu\text{-}P(H)SiR_3\}_3M]$ {R = Pr^i,

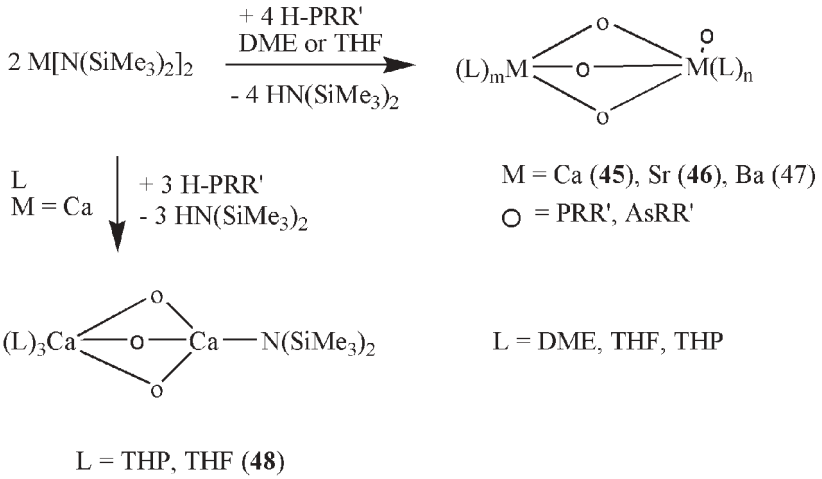

Scheme 3.6-9. Synthesis of the group 2 metal phosphaneides and arsaneides **45**–**48**.

M = Ca (**45**) [58], Sr (**46**) [62], Ba (**47**) [63, 64]} according to Eq. (6). For the dimerization process of the strontium derivative, ΔH and ΔS values of 6.6 $kJ \cdot mol^{-1}$ and 11.3 $J \cdot mol^{-1} \cdot K^{-1}$, respectively, were evaluated for a half-molar THF solution. The exchange process is prevented if one of the phosphanide ligands is substituted by an amide substituent as for example in $[(Me_3Si)_2NCa\{\mu\text{-}P(H)SiPr^i{}_3\}_3Ca(L)_3]$ (**48**, L = THF, THP; see Scheme 3.6-9). The bis(trimethylsilyl)amide group is always in a terminal position.

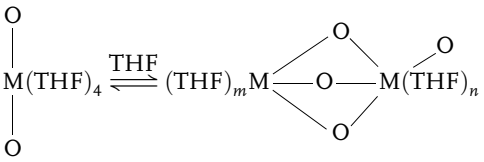

(6)

M = Ca (**45**), Sr (**46**), Ba (**47**)

O = P(H)Si*i*Pr$_3$

Table 3.6-5 gives an overall view of the homometallic compounds of the type $[M_n(L)_m(EHR)_x(ER)_y]$ with alkaline earth metal or tin(+2)–pnictogen clusters. The magnesiation of primary trialkylsilyl substituted phosphanes and arsanes in ether solvents leads to the formation of the tetramer $[(L)MgESiR_3]_4$ with an Mg_4E_4 heterocubane fragment (E = P, As; L = Et_2O, THF, DME; R = Pr*i*, Bu^t). Coligand-free cages with a central hexagonal Mg_6E_6 prismatic core are obtained via the metalation of $Bu^t{}_3SiEH_2$ [E = P (**54**), As (**60**)] in toluene. These reactions are displayed in the bottom part of Scheme 3.6-10.

In these cage compounds the size of the substituents and consequently the intramolecular strain influence the degree of oligomerization and the shape of the $(ME)_n$ polyhedra. Lowering the steric strain and variation of the stoichiometry lead to different heteroleptic complexes of magnesium which contain phosphanide and phosphanediide ligands. The magnesiation of $H_2PSiPr^i{}_3$ in toluene yields a complex of constitution $[Mg_8\{P(H)SiR_3\}_4(PSiR_3)_6]$ **58** [65] according to the upper part of Scheme 3.6-10. Surprisingly, dissolving this compound in THF leads to the complex $[\{(THF)Mg\}_4Mg_2(PSiR_3)_6]$ **55** preserving the central hexagonal Mg_6P_6 prism, the coordinated $[Mg\{P(H)SiR_3\}_2]$ molecules are substituted by neutral coligands and the formation of the above mentioned tetramer **49** is not observed. The reaction of the hexamer $[MgPSiBu^t{}_3]_6$ **54** with Lewis bases L leads to the addition of only four neutral coligands and the formation of **55** (L = THF), **56** (L = PhCN), and **57** (L = Ph-NCO). The reaction of Bu_2Mg with tri(*tert*-butyl)silylphosphane in a stoichiometric ratio of 2:3 yields $[Mg_4(PSiR_3)_2\{P(H)SiR_3\}_4]$ **53** with a central Mg_4P_2 octahedron, the Mg ··· Mg edges being bridged by the phosphanide monoanions (Scheme 3.6-10). The structural principle in that series of magnesium phosphanediides and arsanediides (Scheme 3.6-10) is the formation of a spherical polyhedron such as the Mg_4P_2 octahedron, the Mg_4P_4 heterocubane and the hex-

Tab. 3.6-5. Homometallic cage compounds of the type $[M_n(L)_m(REH)_x(RE)_y]$ of the divalent atoms M [alkaline earth metals and tin(+2)] and the pnictogen atoms E (P, As).

Comp.	*M*	*E*	*R*	*L*	*n*	*m*	*x*	*y*	*Ref.*
49	Mg	P	$SiPr^i_3$	THF	4	4	0	4	65
50	Mg	P	$SiPr^i_3$	DME	4	4	0	4	66
51	Mg	P	$SiPr^i_3$	Et_2O	4	4	0	4	35
52	Mg	P	$SiBu^t_3$	THF	4	4	0	4	67
53	Mg	P	$SiBu^t_3$	–	4	0	4	2	67
54	Mg	P	$SiBu^t_3$	–	6	0	0	6	27
55	Mg	P	$SiPr^i_3$	THF	6	4	0	6	65
56	Mg	P	$SiBu^t_3$	Ph-CN	6	4	0	6	68
57	Mg	P	$SiBu^t_3$	Ph-NCO	6	4	0	6	68
58	Mg	P	$SiPr^i_3$	–	8	0	4	6	65
59	Mg	As	$SiPr^i_3$	THF	4	4	0	4	69
60	Mg	As	$SiBu^t_3$	–	6	0	0	6	68
61	Ca	P	$SiBu^t_3$	THF	6	2	4	4	70
62	Ca	As	$SiPr^i_3$	THF	4	4	6	1	71
63	Ca	As	$SiBu^t_3$	THF	5	3	2	4	68
64	Sr	P	$SiBu^t_3$	THF	6	2	4	4	62
65	Sr	P	$SiPr^i_3$	THF	6	4	4	4	62
66	Sr	As	$SiPr^i_3$	THF	4	5	6	1	71
67	Ba	P	$SiBu^t_3$	THF	6	2	4	4	63
68	Ba	As	$SiPr^i_3$	THF	4	5	6	1	71
69	Ba	As	$SiBu^t_3$	THF	6	2	4	4	68
70	Sn	P	$SiBu^t_3$	–	4	0	0	4	72
71	Sn	P	$SiPr^i_3$	–	6	0	0	6	46
72	Sn	As	$SiPr^i_3$	–	6	0	0	6	69

agonal Mg_6P_6 prism, as is also observed for the alkali metal phosphanediides, which can be understood in terms of the diagonal relationship between Li and Mg.

The metalation of trialkylsilylphosphane and -arsane with the alkaline earth metal bis[bis(trimethylsilyl)amides] of calcium, strontium, and barium yields the mixed phosphanides and phosphanediides as well as arsanides and arsanediides depending on the stoichiometry and the demand of the trialkylsilyl substituents according to Scheme 3.6-11. The main feature is the M_2E_3 bipyramid with the metal atoms in apical positions. These cages are often interconnected via common faces (**61**, **63**, **64**, **65**, **67**, and **69**). A substitution of the phosphanide substituents by other Lewis bases such as THF or benzonitrile is not possible for these compounds and, consequently, homoleptic phosphanediides and arsanediides with inner M_4E_4 heterocubane moieties are so far unknown for M = Ca, Sr, and Ba. In all these cases a further metalation to obtain homoleptic phosphanediides failed.

Owing to the reduced reactivity of the trialkylsilylarsane compared with the isostructural phosphane, complexes with a higher arsanide content are isolated, where the trigonal bipyramids are interconnected via common corners, edges and faces (**62**, **66** and **68**).

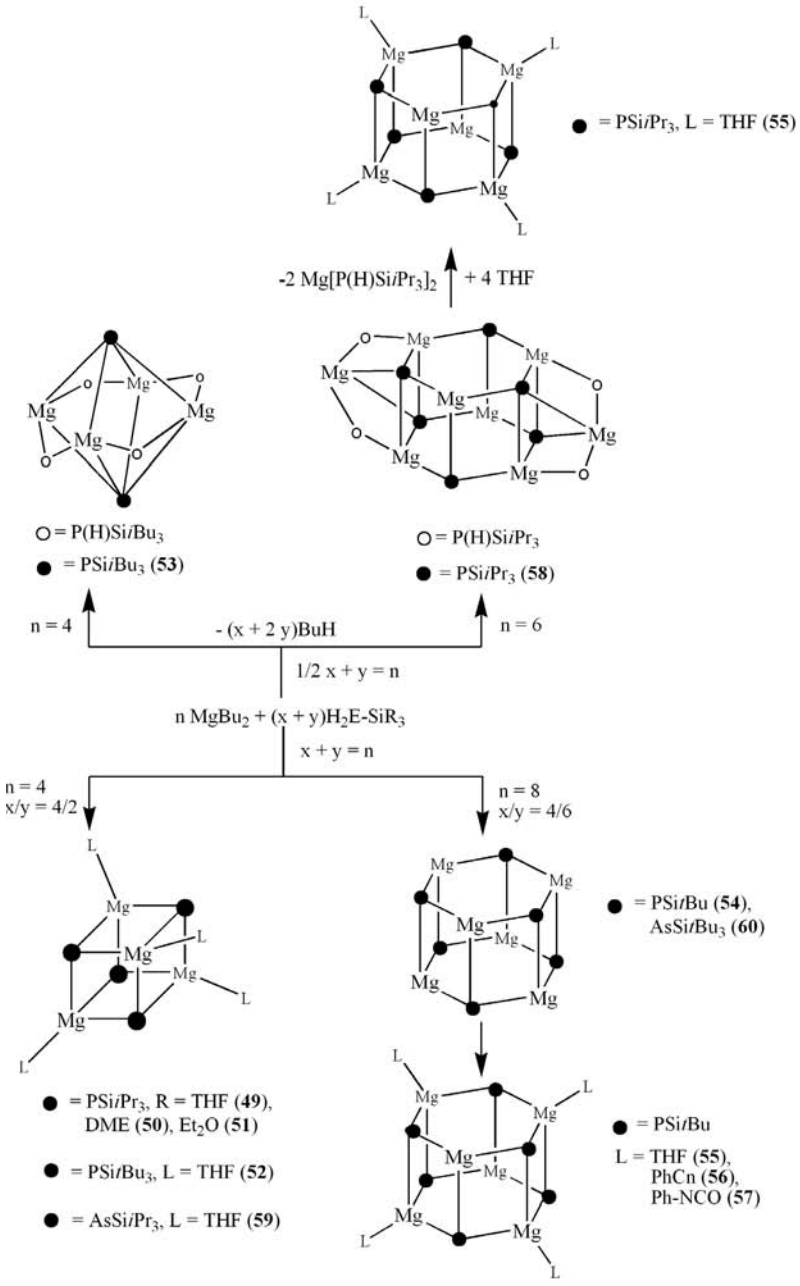

Scheme 3.6-10. Mg_nE_m cluster formation by magnesiation reactions of primary silylphosphanes and silylarsanes with Bu_2Mg.

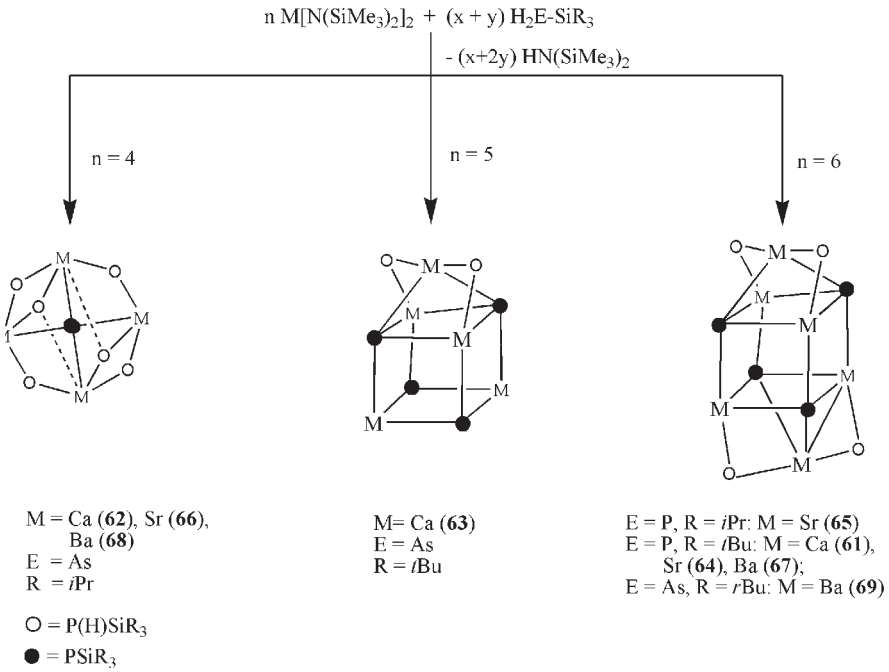

Scheme 3.6-11. Synthetic access to the Ca-, Sr- and Ba-phosphandiides and arsandiides **61**–**69**.

Homoleptic alkaline earth metal phosphanediides and arsanediides of calcium, strontium, and barium are unknown thus far, a consequence of the use of rather mild metalating reagents, because dialkylcalcium, -strontium, and -barium are at present not easily accessible [73].

The two-fold stannylation of $H_2ESiiPr_3$ (E = P, As) yields hexameric phosphandiide **71** and arsandiide **72** with hexagonal Sn_6E_6 prisms whereas the reaction of $Sn[N(SiMe_3)_2]_2$ with $H_2PSitBu_3$ gives a tetrameric molecule with a Sn_4P_4 heterocubane moiety **70** according to Scheme 3.6-12. Heteroleptic tin compounds containing phosphanide as well as phosphanediide substituents are unknown.

Oxygen-centered phosphanides are accessible by hydrolysis of the phosphanides as shown for the oxygen-centered phosphanide **73** of the formula $[Sr_4O\{P(SiMe_2Pr^i)_2\}_6]$ with an Sr_4P_6 adamantane-like structure as shown in Eq. (7) [74]. The strontium atoms are coordinatively saturated by agostic interactions to the silicon-bonded alkyl substituents.

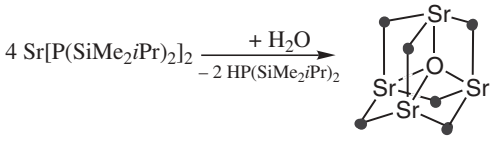

(7)

73: ● =$P(SiMe_2iPr)_2$

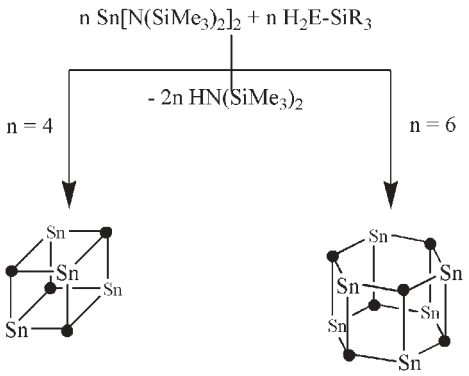

● = PSi*t*Bu$_3$ (**70**) ● = PSi*t*Bu$_3$ (**71**), AsSi*i*Pr$_3$ (**72**)

Scheme 3.6-12. Synthesis of the Sn_4P_4 and Sn_6E_6 clusters (E = P, As) **70**–**72**.

The synthesis of heterobimetallic cages which contain alkaline-earth metals and tin(+2) atoms succeeds by the metalation of trialkylsilyl substituted phosphanes with the bis(trimethylsilyl)amides of tin(+2) and of calcium, strontium, or barium according to Scheme 3.6-13. Heterobimetallic cages of tin and magnesium are unknown, instead their formation mixtures of the homometallic phosphanides are observed [75].

The heterobimetallic cage compounds of the type $[M_n(L)_mSn_l(ERR')_x(ER)_y]$ for the alkaline-earth metals M (Ca, Sr, Ba) and pnictogens E (E = P, As) are summarized in Table 3.6-6. The number y gives the size of the central phosphanediide fragment, which is a four-membered cycle [$y = 2$, M = Ca (**74**, **75**), Ba (**79**, **80**)] or a heterocubane moiety [$y = 4$, M = Ca (**76**), Sr (**77**), Ba (**81**), (**82**)].

Of special interest is the series derived from $[SnPSiBu^t_3]_4$ **70** where one, two or three tin atoms are exchanged by barium atoms. A complete substitution and the formation of a tetrameric barium tri(*tert*-butyl)silylphosphanediide is not possible either by metalating $H_2PSiBu^t_3$ with barium bis[bis(trimethylsilyl)amide] or by transmetalation of tin with distilled barium metal, even if ultrasound is applied. The substitution of the tin atoms by barium leads to a tremendous high field shift of the phosphanediide ligand bonded to three tin atoms ($\delta = -528.6$) whereas the chemical low field shift of the phosphanediide substituents increases with the number of neighboring barium atoms. These heterobimetallic species are clearly distinguishable by NMR spectroscopy due to the wide range of chemical ^{31}P shifts and the ^{31}P–^{31}P coupling pattern.

Scheme 3.6-14 gives a general overview of the observed polyhedra of alkaline earth metal rich cages and clusters. The mixed phosphanides and phosphanediides of the alkaline earth metals or tin(+2) can be described by combining only a few structural elements. On the one hand, the main fragment is the dimeric metal phosphanediide $[MPR]_2$ with a four-membered M_2P_2 cyclus which can either dimerize to heterocubane structures or trimerize to hexagonal prisms. On the other hand, there is the heteroleptic moiety of formula $[M_3(PRR')_2(PR)_2]$ with an M_3P_4

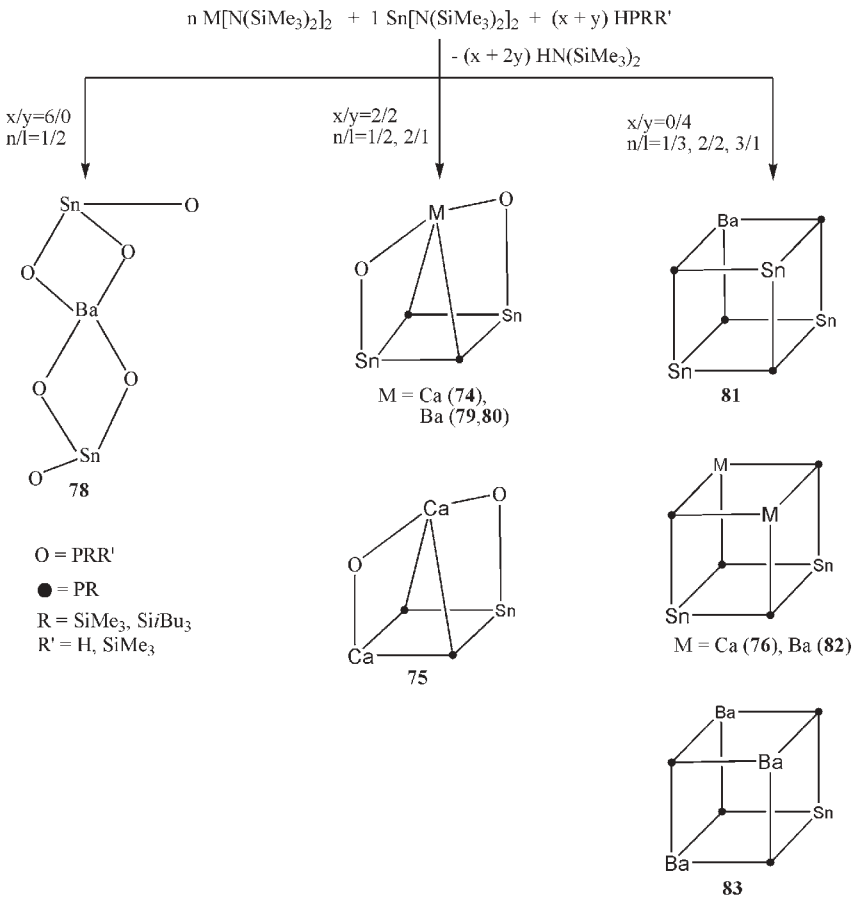

Scheme 3.6-13. Synthesis of heterobimetallic phosphanide–phosphandiide clusters.

Tab. 3.6-6. Heterometallic cage compounds of the type $[M_n(L)_mSn_l(ERR')_x(ER)_y]$ for the alkaline earth metals M (Ca, Sr, Ba).

Comp.	*M*	*E*	*R*	*R'*	*L*	*n*	*m*	*l*	*x*	*y*	*Ref.*
74	Ca	P	$SiMe_3$	$SiMe_3$	THF	1	2	2	2	2	76
75	Ca	P	$SiPr^i{}_3$	H	THF	2	5	1	2	2	58
76	Ca	P	$SiMe_3$	–	THF	2	6	2	0	4	76
77	Sr	As	$SiBu^t{}_3$	–	THF	2	5	2	0	4	68
78	Ba	P	$SiMe_3$	$SiMe_3$	THF	1	0	2	6	0	77
79	Ba	P	$SiMe_3$	$SiMe_3$	THF	1	3	2	2	2	77
80	Ba	P	$SiMe_3$	$SiMe_3$	THF	1	4	2	2	2	77
81	Ba	P	$SiBu^t{}_3$	–	Toluene	1	1	3	0	4	72
82	Ba	P	$SiBu^t{}_3$	–	THF	2	5	2	0	4	68

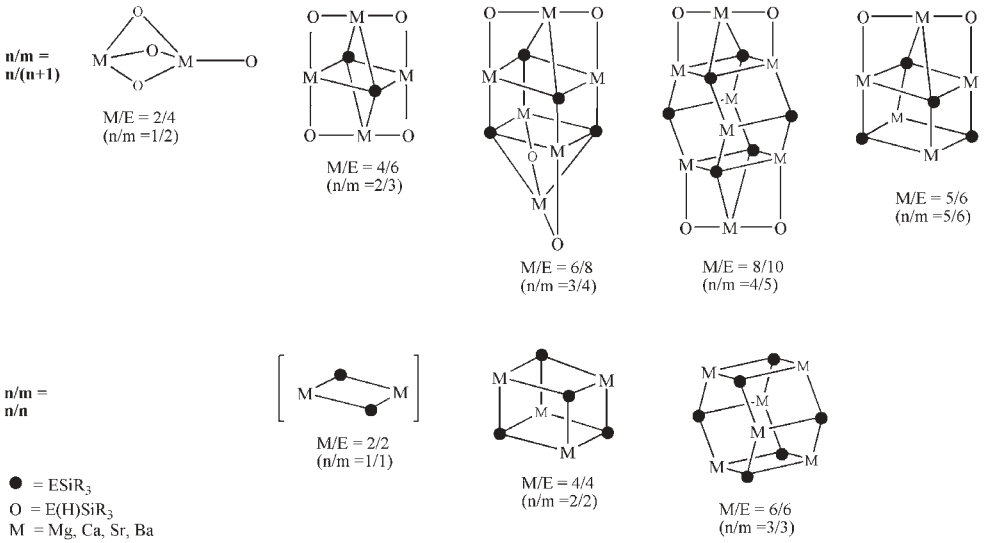

Scheme 3.6-14. Structural variety in group 2 metal and tin(+2) phosphanide (arsanide)–phosphandiide (arsandiide) cluster chemistry.

cage which consists of two trigonal bipyramids with a common face. The latter cage is only known for heterobimetallic compounds of tin(II) and the heavy alkaline earth metals whereas the homometallic alkaline earth metal derivatives crystallize as dimers.

The structural motif of a hexagonal M_6E_6 prism is also found in isoelectronic alkylaluminum triisopropylsilylphosphandiides and -arsandiides as well as in homologous gallium compounds [78–80]. This is explained by the identical size and coordination pattern of the RAl^{2+} and RGa^{2+} fragments and Mg^{2+} and $(L)Mg^{2+}$ moieties.

References

1 K. Gregory, P. v. R. Schleyer, R. Snaith, *Adv. Inorg. Chem.*, **1991**, *37*, 47.

2 F. Pauer, P. P. Power, in *Lithium Chemistry: A Theoretical and Experimental Overview*, A.-M. Sapse, P. v. R. Schleyer, eds., Wiley, New York, **1995**, p. 295.

3 R. E. Mulvey, *Chem. Soc. Rev.*, **1991**, *20*, 167.

4 R. E. Mulvey, *Chem. Commun.*, **2002**, 1049.

5 W. Setzer, P. v. R. Schleyer, *Adv. Organomet. Chem.*, **1985**, *24*, 353.

6 L. Ruwisch, U. Klingebiel, S. Rudolph, R. Herbst-Irmer, M. Noltemeyer, *Chem. Ber.*, **1996**, *129*, 823.

7 M. G. Gardiner, C. L. Raston, *Inorg. Chem.*, **1996**, *35*, 4047.

8 T. Grob, S. Chitsaz, K. Harms, K. Dehnicke, *Z. Anorg. Allg. Chem.*, **2002**, *628*, 473.

9 T. Grob, K. Harms, K. Dehnicke, *Z. Anorg. Allg. Chem.*, **2000**, *626*, 1065.

10 R. P. Davies, P. R. Raithby, G. P. Shields, R. Snaith, A. E. H. Wheatley, *Organometallics*, **1997**, *16*, 2223.

11 A. Müller, M. Krieger, B. Neumüller, K. Dehnicke, J. Magull, *Z. Anorg. Allg. Chem.*, **1997**, *623*, 1081.

12 A. S. Batsanov, P. D. Bolton, R. C. B. Copley, M. G. Davidson, J. A. K. Howard, C. Lustig, R. D. Price, *J. Organomet. Chem.*, **1998**, *550*, 445.

13 R. E. Mulvey, *Chem. Soc. Rev.*, **1998**, *27*, 339.

14 S. Chitsaz, B. Neumüller, K. Dehnicke, *Z. Anorg. Allg. Chem.*, **1999**, *625*, 9.

15 M. Geissler, J. Kopf, B. Schubert, E. Weiss, W. Neugebauer, P. v. R. Schleyer, *Angew. Chem.*, **1987**, *99*, 569; *Angew. Chem., Int. Ed. Engl.*, **1987**, *26*, 587.

16 T. Hascall, K. Ruhlandt-Senge, P. P. Power, *Angew. Chem.*, **1994**, *106*, 350; *Angew. Chem., Int. Ed. Engl.*, **1994**, *33*, 356; W. J. Grigsby, T. Hascall, J. J. Ellison, M. M. Olmstead, P. P. Power, *Inorg. Chem.*, **1996**, *35*, 3254.

17 W. Clegg, M. Frank, R. E. Mulvey, P. A. O'Neil, *J. Chem. Soc., Chem. Commun.*, **1994**, 97.

18 W. Clegg, L. Horsburgh, R. E. Mulvey, R. Rowlings, *J. Chem. Soc., Chem. Commun.*, **1996**, 1739.

19 G. Dozzi, G. Del Piero, M. Cesari, S. Cucinella, *J. Organomet. Chem.*, **1980**, *190*, 229.

20 P. R. Markies, O. S. Akkerman, F. Bickelhaupt, W. J. J. Smeets, A. L. Spek, *Adv. Organomet. Chem.*, **1991**, *32*, 147.

21 L. Lochmann, *Eur. J. Inorg. Chem.*, **2000**, 1115; M. Schlosser, *Organometallics in Synthesis*, 2nd Edn., John Wiley & Sons, Chichester, **2002**.

22 A. R. Kennedy, J. G. MacLellan, R. E. Mulvey, *Angew. Chem.*, **2000**, *113*, 3345; *Angew. Chem., Int. Ed. Engl.*, **2001**, *40*, 3245.

23 M. F. Hawthorne, Z. Zheng, *Acc. Chem. Res.*, **1997**, *30*, 267.

24 A. J. Stemmler, J. W. Kampf, V. L. Pecoraro, *Inorg. Chem.*, **1995**, *34*, 2271.

25 See Ref. 4 for a review. Note that entry (iii) is unpublished: A. R. Kennedy, J. G. MacLellan, R. E. Mulvey.

26 K. J. Drewette, K. W. Henderson, A. R. Kennedy, R. E. Mulvey, C. T. O'Hara, R. B. Rowlings, *Chem. Commun.*, **2002**, 1176.

27 A. M. Drummond, L. T. Gibson, A. R. Kennedy, R. E. Mulvey, C. T. O'Hara, R. B. Rowlings, T. Weightman, *Angew. Chem.*, **2002**, *114*, 2488; *Angew. Chem., Int. Ed. Engl.*, **2002**, *41*, 2382.

28 M. Westerhausen, M. Krofta, A. Pfitzner, *Inorg. Chem.*, **1999**, *38*, 598.

29 W. Clegg, K. W. Henderson, A. R. Kennedy, R. E. Mulvey, C. T. O'Hara, R. B. Rowlings, D. M. Tooke, *Angew. Chem.*, **2001**, *113*, 4020; *Angew. Chem., Int. Ed. Engl.*, **2001**, *40*, 3902.

30 I. Haiduc, F. T. Edelmann, *Supramolecular Organometallic Chemistry*, Wiley-VCH, Weinheim, **1999**.

31 K. B. Dillon, F. Mathey, J. F. Nixon, *Phosphorus: A Carbon Copy*, Wiley, Chichester, **1998**.

32 M. Driess, *Acc. Chem. Res.*, **1999**, *32*, 1017.

33 M. Driess, H. Pritzkow, S. Martin, S. Rell, D. Fenske, G. Baum, *Angew. Chem.*, **1996**, *108*, 1064; *Angew. Chem., Int. Ed. Engl.*, **1996**, *35*, 986.

34 K. Izod, *Adv. Inorg. Chem.*, **2000**, *50*, 33.

35 M. Driess, *Adv. Inorg. Chem.*, **2000**, *50*, 235.

36 G. Fritz, P. Scheer, *Chem. Rev.*, **2000**, *100*, 3341.

37 J. D. Smith, *Angew. Chem.*, **1998**, *110*, 2181–2183; *Angew. Chem., Int. Ed. Engl.*, **1998**, *37*, 2071.

38 M. Driess, G. Huttner, N. Knopf, H. Pritzkow, L. Zsolnai, *Angew. Chem.*, **1995**, *107*, 354; *Angew. Chem., Int. Ed. Engl.* **1995**, *34*, 316.

39 G. Rabe, H. Heise, G. P. A. Yap, L. M. Liable-Sands, I. Guzei, A. Rheingold, *Inorg. Chem.*, **1998**, *37*, 4235.

40 M. Driess, H. Pritzkow, M. Skipinski, U. Winkler, *Organometallics*, **1997**, *16*, 5108.

41 M. Driess, H. Pritzkow, M. Skipinski, U. Winkler, *J. Am. Chem. Soc.*, **1998**, *120*, 10774.

42 G. W. Rabe, S. Kheradmandan, L. M. Liable-Sands, I. A. Guzei, A. L. Rheingold, *Angew. Chem.*, **1998**, *110*, 1495; *Angew. Chem., Int. Ed. Engl.*, **1998**, *37*, 1404.

43 M. Westerhausen, S. Weinrich, B. Schmid, S. Schneiderbauer, M. Suter, H. Nöth, H. Piotrowski, *Z. Inorg. Allg. Chem.*, **2003**, *629*, 625.

44 M. Driess, S. Rell, H. Pritzkow, R. Janoschek, *Chem. Commun.*, **1996**, 305. See also for a tetrameric copper(I) phosphanide: M. Faulhaber, M. Driess, K. Merz, *Chem. Commun.*, **1998**, 1887.

45 N. Wiberg, A. Wörner, D. Fenske, H. Nöth, J. Knizek, K. Polborn, *Angew. Chem.*, **2000**, *112*, 1908; *Angew. Chem., Int. Ed. Engl.*, **2000**, *39*, 1838.

46 M. Driess, S. Martin, K. Merz, V. Pintchouk, H. Pritzkow, H. Grützmacher, M. Kaupp, *Angew. Chem.*, **1997**, *109*, 1982; *Angew. Chem., Int. Ed. Engl.* **1997**, *36*, 1894.

47 T. Koch, S. Blaurock, F. Somoza, E. Hey-Hawkins, *Eur. J. Inorg. Chem.*, **2000**, 2167.

48 G. Linti, W. Köstler, H. Pritzkow, *Eur. J. Inorg. Chem.*, **2002**, 2643.

49 M. Driess, U. Hoffmanns, S. Martin, K. Merz, H. Pritzkow, *Angew. Chem.*, **1999**, *111*, 2906; *Angew. Chem., Int. Ed. Engl.* **1999**, *38*, 2733.

50 M. Driess, T. Schaller, A. Sebald, *Solid State Nucl. Magn. Reson.*, **1997**, *9*, 219.

51 M. Kaupp, *Angew. Chem.*, **2001**, *113*, 3642; *Angew. Chem., Int. Ed. Engl.*, **2001**, *40*, 3534.

52 (a) M. Kaupp, P. v. R. Schleyer, H. Stoll, H. Preuss, *J. Am. Chem. Soc.*, **1991**, *113*, 6012. (b) L. Seijo, Z. Barandiaran, S. Huzinaga, *J. Chem. Phys.*, **1991**, *94*, 3762. For a review on metal halides see also: M. Hargittai, *Chem. Rev.*, **2000**, *100*, 2233.

53 M. Kaupp, P. v. R. Schleyer, *J. Am. Chem. Soc.*, **1992**, *114*, 491.

54 M. Kaupp, P. v. R. Schleyer, *J. Am. Chem. Soc.*, **1993**, *115*, 11202.

55 G. Mösges, F. Hampel, M. Kaupp, P. v. R. Schleyer, *J. Am. Chem. Soc.*, **1992**, *114*, 10800.

56 M. Westerhausen, *Coord. Chem. Rev.*, **1998**, *176*, 157.

57 M. Westerhausen, G. Lang, W. Schwarz, *Chem. Ber.*, **1996**, *129*, 1035.

58 M. Westerhausen, R. Löw, W. Schwarz, *J. Organomet. Chem.*, **1996**, *513*, 213.

59 M. Westerhausen, M. H. Digeser, B. Wieneke, H. Nöth, J. Knizek, *Eur. J. Inorg. Chem.*, **1998**, 517.

60 M. Westerhausen, *J. Organomet. Chem.*, **1994**, *479*, 141.

61 M. Westerhausen, M. H. Digeser, J. Knizek, W. Schwarz, *Inorg. Chem.*, **1998**, *37*, 619.

62 M. Westerhausen, C. Birg, M. Krofta, P. Mayer, T. Seifert, H. Nöth, A. Pfitzner, T. Nilges, H.-J. Deiseroth, *Z. Anorg. Allg. Chem.*, **2000**, *626*, 1073.

63 M. Westerhausen, M. H. Digeser, M. Krofta, N. Wiberg, H. Nöth, J. Knizek, W. Ponikwar, T. Seifert, *Eur. J. Inorg. Chem.*, **1999**, 743.

64 M. Westerhausen, M. Hartmann, W. Schwarz, *Inorg. Chem.*, **1996**, *35*, 2421.

65 M. Westerhausen, S. Schneiderbauer, J. Knizek, H. Nöth, A. Pfitzner, *Eur. J. Inorg. Chem.*, **1999**, 2215.

66 M. Westerhausen, C. Birg, M. Krofta, N. Makropoulos, S. Schneiderbauer, *Phosphorus Sulfur Silicon Relat. Elem.*, **2001**, *168–169*, 173.

67 M. Westerhausen, M. Krofta, P. Mayer, M. Warchhold, H. Nöth, *Inorg. Chem.*, **2000**, *39*, 4721.

68 M. Westerhausen, M. Krofta, unpublished results.

69 M. Westerhausen, N. Makropoulos, H. Piotrowski, M. Warchhold, H. Nöth, *J. Organomet. Chem.*, **2000**, *614–615*, 70.

70 M. Westerhausen, M. Krofta, P.

Mayer, *Z. Anorg. Allg. Chem.*, **2000**, *626*, 2307.

71 M. Westerhausen, C. Birg, H. Piotrowski, T. Habereder, M. Suter, H. Nöth, *Z. Anorg. Allg. Chem.*, **2001**, *627*, 882.

72 M. Westerhausen, M. Krofta, N. Wiberg, J. Knizek, H. Nöth, A. Pfitzner, *Z. Naturforsch.*, **1998**, *53b*, 1489.

73 M. Westerhausen, *Angew. Chem.*, **2001**, *113*, 3063; *Angew. Chem., Int. Ed. Engl.*, **2001**, *40*, 2975.

74 M. Westerhausen, M. H. Digeser, H. Nöth, J. Knizek, *Z. Anorg. Allg. Chem.*, **1998**, *624*, 215.

75 M. Westerhausen, M. M. Enzelberger, W. Schwarz, *J. Organomet. Chem.*, **1995**, *491*, 83.

76 M. Westerhausen, W. Schwarz, *Z. Anorg. Allg. Chem.*, **1996**, *622*, 903.

77 M. Westerhausen, H.-D. Hausen, W. Schwarz, *Z. Anorg. Allg. Chem.*, **1995**, *621*, 877.

78 M. Driess, S. Kuntz, C. Monsé, K. Merz, *Chem. Eur. J.*, **2000**, *6*, 4343.

79 M. Driess, S. Kuntz, K. Merz, H. Pritzkow, *Chem. Eur. J.*, **1998**, *4*, 1628.

80 C. von Hänisch, F. Weigend, *Z. Anorg. Allg. Chem.*, **2002**, *628*, 389.

Index